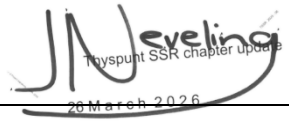
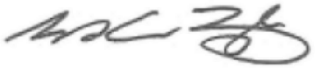
SECTION 5.13: *GEOLOGY*			
Author's declaration:	I declare that appropriate diligence and quality assurance was applied in the compilation of this report. As such I am confident in the results here described and the conclusions drawn.		
	Name: Kevin J. Coppersmith		Date: 2026-03-24
Technical Writer Review:			
	Name: Johann Neveling		Date: 2026-03-26
Project Manager Authorisation:			
	Name: Johann Neveling		Date: 2026-03-26
Eskom NSS Technical Lead Acceptance:			
	Name: M van Zyl		Date: 2026-03-27
Eskom NSS Employer's Agent Acceptance:			
	Name: F van Mosseveld		Date: 2026-03-27

© Eskom 2026/Rev 0a

AMENDMENT RECORD			
Rev	**Draft**	**Date**	**Description**
0		April 2015	New section. Thyspunt Site Safety Report compiled in support of Eskom's Nuclear Installation Site Licence for the Thyspunt site.
0a		March 2026	Section updated to comply with the updated SSR template.

© Eskom 2026/Rev 0a

EXECUTIVE SUMMARY

This section of the SSR describes the approach and results that demonstrate adequate knowledge of the geologic, geophysical, seismological, and geotechnical characteristics of the subsurface geology in the region and at the site for the purpose of assessing site suitability. The geosciences knowledge base presented in this section of the SSR provides input to the assessment of various types of geological hazards documented in other sections of the SSR, including seismic hazard analysis, geotechnical characterisation, and oceanography and coastal engineering. The main findings of this section include conclusions regarding the adequacy of the geological knowledge base, use of the geological information for seismic hazard analysis, surface faulting potential, and identification of tsunamigenic sources.

Adequacy of Geological Knowledge Base

Geological investigations that contribute to the knowledge base for the Thyspunt site have been conducted over several decades since the mid-1980s. These studies include geological mapping, onshore and offshore geophysical studies, seismicity studies, geochronological analyses, geomorphic studies, palaeoseismic studies, and geotechnical investigations. These studies were conducted as part of early screening studies to evaluate multiple nuclear sites, as well as specific studies conducted between 2003 – 2008 by the Council for Geoscience for the Thyspunt site, and geological investigations conducted specifically to address key issues related to the seismic hazard analysis from 2009 – 2012. Consistent with all existing National Nuclear Regulator (NNR) guidance and international regulatory guidance and standards, the full range of methods and tools has been applied and the investigations included the recommended increasing levels of specificity ranging from the site region, site vicinity, site area, to the site location. As is also recommended in the existing regulatory guidance, the results of the investigations conducted for the site were integrated with studies conducted by a large number of investigators within the geological community and published in the professional literature.

The net result of integrating all the geological studies is a strong, complete geological knowledge base for the site region, site vicinity, site area, and site location. Because the bulk of the studies were conducted according to international best practices for nuclear facilities in accordance with the regulatory guidance of the International Atomic Energy Agency and the United States Nuclear Regulatory Commission (U.S. NRC), the knowledge base is commensurate with that of other nuclear facilities worldwide. As a result, the subsequent disciplines that rely on the geological knowledge base as inputs to their analyses are provided with the information and data that they require.

© Eskom 2026/Rev 0a

The onshore and offshore regional geology and tectonics at the site are well understood. The shoreline and coastal plain at the site area and location represent an old and stable landscape. From an erosional point of view, the resistant rocks that establish this rugged coastline provide a stable base for the construction of nuclear installations.

Seismic Hazard Analysis

The most important potential hazard at the site for which geological information presented in this section provides input, is seismic hazard, both vibratory ground motion hazard and surface faulting hazard. As shown in a Regulatory Compliance Matrix, the development of the data, and their use in the Probabilistic Seismic Hazard Analysis (PSHA), has been conducted in compliance with NNR and methodologies that are recommended in U.S. NRC regulatory guidance. The geological data and knowledge documented in this section are the primary basis for the seismic source characterisation conducted for the PSHA. From that standpoint, the available geologic, seismologic, and geophysical data in the site region, vicinity, area, and location are sufficient and adequate for purposes of assessing both the seismic hazard at the site and the suitability of the site. The results of the PSHA are documented in Section 5.14 (Seismic Hazard Analysis) and will be used in assessing the suitability of the site from the standpoint of external events such as earthquakes (Section 6—Evaluation of External Events).

Surface Faulting Evaluation

The evaluation of the potential for surface faulting at the site is based on all the available information, including investigations conducted in the site region, vicinity, area, and location. Based on a detailed evaluation of all available data, and following the regulatory guidance provided in U.S. NRC for assessing the potential for surface faulting, it is concluded that there is no evidence for capable tectonic deformation at the Thyspunt site location and that the potential for tectonic deformation is negligible. This conclusion is based on several lines of evidence. The results of geological and seismological investigations have demonstrated that mapped faults within the site area are not capable faults. Bedrock geological mapping in the site vicinity identified no evidence for surface faulting or deformation that would suggest capable faults in the Thyspunt site area. The basis for this conclusion is the absence of geomorphic features indicative of Quaternary (the past 2.58 million years) deformation, as reported in the previous siting reports and literature, and inferred from the results of marine terrace and field studies conducted as part of the Thyspunt geological investigations programme. It is assumed that any potential deformation feature identified in site excavations during construction will be characterised to evaluate its potential for surface deformation or ground-motion generation.

© Eskom 2026/Rev 0a

Tsunamigenic Sources

This section provides a summary of the tsunamigenic sources that have the potential to affect the site. The descriptive information provided in this section is used to develop input parameters for the characterisation of tsunamigenic sources as described in Section 5.9 (Oceanography and Coastal Engineering) of this SSR. That section discusses the modelling of the size, nature, and local effects, and flooding characteristics of tsunamis at the site. The candidate potential near-field and far-field tsunamigenic sources are to be assessed according to the characteristics identified in the guidance given in U.S. NRC regulations, including earthquakes, submarine landslides, subaerial landslides, volcanic processes (e.g. pyroclastic flow and caldera collapse).

© Eskom 2026/Rev 0a

CONTENTS

EXECUTIVE SUMMARY 5.13-3

5.13 GEOLOGY 5.13-22

5.13.1 Introduction 5.13-22

5.13.2 Purpose and Scope.....5.13-23

5.13.3 Regulatory Framework.....5.13-25

5.13.4 Approach to Evaluation 5.13-29

5.13.5 Characteristics of the Regional and Site Geology 5.13-40

5.13.6 Monitoring 5.13-317

5.13.7 Management of Uncertainties 5.13-318

5.13.8 Management System 5.13-318

5.13.9 Conclusions 5.13-321

5.13.10 References.....5.13-325

© Eskom 2026/Rev 0a

TABLES

Table 5.13.1 Regulatory Compliance Matrix 5.13-26

Table 5.13.2 Geoscientific Investigations Conducted in the Thyspunt Site Region, Vicinity, Area, and Location 5.13-33

Table 5.13.3 Tectonostratigraphic Framework for the Thyspunt Site Region 5.13-70

Table 5.13.4 Summary of South African Focal Mechanism Information 5.13-93

Table 5.13.5 P-axes and T-axes for Earthquakes Having Focal Mechanisms (see *Table T-5.13.4*).....5.13-95

Table 5.13.6 Tectonic Regime Assignment (*Reference 5.13.216*) for Given Plunges of the P-, B-, and T-Axes in Degrees.....5.13-97

Table 5.13.7 Lithostratigraphic Summary of Rock Types in the Site Vicinity (*References 5.13.160* and *5.13.27*) 5.13-188

Table 5.13.8 The Four Compressional Paroxysms of the Permo-Triassic Cape Orogeny and Their Resultant Effect on Strata (Modified from *References 5.13.101*, *5.13.336*, and *5.13.337*).....5.13-226

Table 5.13.9 Summary of Joint Set Directions at the Thyspunt Site (*Reference 5.13.27*) 5.13-246

Table 5.13.10 Lithostratigraphic Summary of Rock Units Within the Site Area (8 km Radius) 5.13-263

Table 5.13.10 Maximum and Average Thicknesses of Basal Gravel Deposits Above Bedrock Stratigraphically Correlated to Either the Alexandria or Salnova Formation Within the Site Area 5.13-277

Table 5.13.12 Summary of Activities, Links, and Quality Requirements 5.13-319

FIGURES

Figure 5.13-1 (a) Locality Map Showing the 320 km Radius Site Region and 40 km Radius Site Vicinity. (b) Locality Map Showing the 40 km Radius Site Vicinity, 8 km Radius Site Area, and 1 km Radius Site Location (represented by the dot) 5.13-31

Figure 5.13-2 Physiographic Regions in Southernmost Africa.....5.13-42

© Eskom 2026/Rev 0a

Figure 5.13-3 Map of the Southern Africa Showing the Major Mesozoic Structural Elements and Sub-Basins (Modified from *Reference 5.13.74*) 5.13-44

Figure 5.13-4 Combined Bathymetry and Topography near the Thyspunt Site with Details of the Physiography Labelled (Modified from *Reference 5.13.59*) 5.13-45

Figure 5.13-5 Elevations of Marine Terraces Along the Coast of South Africa (Modified from *Reference 5.13.50*). 5.13-48

Figure 5.13-6 Regional Map of Marine Terraces (*Reference 5.13.58*).5.13-49

Figure 5.13-7 Shore-Parallel Correlation of Marine Terraces Along the Southern Coast of South Africa (*Reference 5.13.58*).....5.13-50

Figure 5.13-8 Map Showing Location of the Great Escarpment in Relation to the Cape Fold Belt and Cratons of Southern Africa (Modified from *Reference 5.13.95*).5.13-52

Figure 5.13-9 Components of the Archaean to Palaeoproterozoic Core of the Kalahari Craton Within a Gondwana Reconstruction (*Reference 5.13.98*) 5.13-55

Figure 5.13-10 The Position of the Namaqua-Natal Mobile Belt (NNMB). The Kango and Kaaimans Inliers Represent the Position of Pre-Cape Sedimentary Sequences (*Reference 5.13.112*) 5.13-57

Figure 5.13-11 Palaeogeography of the Cape Supergroup (*Reference 5.13.119*) 5.13-59

Figure 5.13-12 Map Showing the Proposed Position of the Gondwanide Mountain Chain Across the Southern Margin of Gondwana (*Reference 5.13.125*) 5.13-60

Figure 5.13-13 Map Showing the Two Structural Branches in the Cape Fold Belt (*Reference 5.13.136*) 5.13-61

Figure 5.13-14 The Development of Rift-Bounded Basins on the Agulhas Bank (AB) as a Result of Strike-Slip Motion During Gondwana Breakup. AFFZ = Agulhas-Falkland Fracture Zone; LA = Luderitz Arch; OB = Orange River Basin; WB = Walvis Basin and WS = Weddell Sea (Modified from *Reference 5.13.143*) 5.13-63

Figure 5.13-15 Plate Tectonic Reconstruction Illustrating the Likely Pre-Breakup Configuration of Late Jurassic to Early Cretaceous Rift Basins Within Southwest Gondwana (*Reference 5.13.74*).....5.13-64

Figure 5.13-16 Plate Tectonic Reconstructions Using Rotation Poles Published by König & Jokat (*Reference 5.13.148*; Modified from *Reference 5.13.77*) 5.13-66

Figure 5.13-17 Chronostratigraphic Column for the Pletmos Basin (*Reference 5.13.45*, after *Reference 5.13.72*) 5.13-68

Figure 5.13-18 Geological Map of the Onshore Site Region.....5.13-69

Figure 5.13-19 Map Showing the Distribution of the Three Groups Comprising the Cape Supergroup (*Reference 5.13.119*).....5.13-74

Figure 5.13-20 Distribution of Coastal Cenozoic Sediments in South Africa (*Reference 5.13.153*) 5.13-76

Figure 5.13-21 Generalised Composite Section for (A) Algoa Group and (B) Bredasdorp Group 5.13-77

Figure 5.13-22 Map of Sundays River to Coega River Showing Cosmogenic Nuclide (CN) Sample Sites and Burial Ages (Modified from *Reference 5.13.58*).....5.13-79

Figure 5.13-23 Dune Locations and Ages Along the Southern Coast of the Eastern Cape Province 5.13-81

Figure 5.13-24 Tectonic Setting of Africa, Including (A) Major Plate Boundaries and Motions (B) Crustal Thickness with Major Cratonic Boundaries and CMT Focal Mechanisms (Modified from *Reference 5.13.187*) 5.13-84

Figure 5.13-25 African Composite Plate, Subdivided into Smaller, Relatively Stable Blocks Separated by Seismically Active Belts (Modified from *Reference 5.13.184*) 5.13-85

Figure 5.13-26 Intraplate Indicators of Stress Regime (Indicated by Colour) and Azimuth of the Most Compressive Horizontal Principal Stress (σ1h) (*Reference 5.13.181*) 5.13-87

Figure 5.13-27 Southern Africa Stress Data from World Stress Map (*Reference 5.13.196*) 5.13-89

Figure 5.13-28 (a) Residual Velocities with Respect to a Frame Defined by All TRIGNET Stations for the 34 Best Sites. (b) Map of Principal Horizontal Strain Rate Tensors Computed for a Delaunay Triangulation of the Best TRIGNET Sites (*Reference 5.13.19)* 5.13-91

Figure 5.13-29 Stereonet Plots of P-Axes and T-Axes of the Earthquakes Having Focal Mechanisms in Table T-5.13.5. The stress tensors for the entire data set are shown with triangles for the P- and T-axes, and the B-axis is shown with a circle.....5.13-96

Figure 5.13-30 Map of African Superswell and Inferred Hotspot Tracks....5.13-

100

Figure 5.13-31 Locations of Data Points of Studies of Erosion and Uplift Rates in Southern Africa 5.13-102

Figure 5.13-32 Compilation of Basin Erosion Rates in the Southern Coastal Region of South Africa. Coloured polygons map the locations of drainage basins sampled for erosion rates (*Reference 5.13.1*) 5.13-104

Figure 5.13-33 Seismicity of Southern and Eastern Africa as Compiled in the Global Seismic Hazard Assessment (GSHAP) Regional Study (*Reference 5.13.243*). Magnitudes are expressed in terms of surface-wave magnitude, MS.....5.13-106

Figure 5.13-34 South African Seismicity for the Region South of the 28°S Parallel. The dashed circle indicates the 320 km radius around the Thyspunt site. Only events with Mw ≥ 2.0 are shown (*Reference 5.13.1*).....5.13-107

Figure 5.13-35 Seismicity for Region Surrounding the Thyspunt Site. The dashed circle indicates the 320 km radius (*Reference 5.13.1*) 5.13-109

Figure 5.13-36 South African National Gravity Data (Onshore) and GRACE Data (Offshore) with Thyspunt Site and the 320 km radius.....5.13-111

Figure 5.13-37 Distribution of the Gravity Stations, Base Stations, and Absolute Gravity Stations Used for the Collection of the National Gravity Data.....5.13-113

Figure 5.13-38 South African National Magnetic Data (Onshore) and WDMAM Data (Offshore) 5.13-114

Figure 5.13-39 Overview Map Showing the Location of Two Combined Onshore-Offshore Seismic Profiles of the Agulhas-Karoo Geoscience Transect. The dashed box shows the extent of Figure F-5.13.40 (*Reference 5.13.77*).....5.13-117

Figure 5.13-40 Detailed Map of the Onshore Geology and Structure of the Offshore Basins. The dashed line marks the position of the Agulhas-Falkland Fracture Zone (AFFZ). DMR = Diaz Marginal Ridge; MB = Mossel Bay; PB = Plettenberg Bay; PE = Port Elizabeth; SOB = Southern Outeniqua Basin (*Reference 5.13.77*).....5.13-118

Figure 5.13-41 Seismic P-Wave Velocity-Depth Model for the Eastern and Western Seismic Profiles, with the Lowermost Solid Line Representing the Moho (*Reference 5.13.77*)....5.13-119

Figure 5.13-42 Map of the Outeniqua Basin with Colour-Coded Crustal Thicknesses Along the Seismic Profiles and Average Stretching Factors. Red arrows show the approximate stress directions DMR = Diaz Marginal Ridge. SOB = Southern Outeniqua Basin

(*Reference 5.13.77*) 5.13-121

Figure 5.13-43 Geological Map Showing Location of Profile IyA-200501 (*Reference 5.13.112*) 5.13-122

Figure 5.13-44 Deep Crustal Model (*Reference 5.13.112*) 5.13-123

Figure 5.13-45 Geological Map Showing Locations of Profiles 1 and 2. The transitional zone between structural domains is indicated by orange dashed line. (Modified from *Reference 5.13.131*) 5.13-126

Figure 5.13-46 Regional Cross Sections Across the Cape Fold Belt Showing Three Stages of Deformation Across the Zone. For each section: (A) Present-day geometry with topography and structural data plotted. (B) Shows the restoration of the Cape Fold Belt through the removal of extensional faults. (C) Restored sections to pre-Cape Fold Belt deformation. (Modified from *Reference 5.13.131*).....5.13-127

Figure 5.13-47 Map Showing Major Onshore Offshore Faults in the Site Region; the Mesozoic Normal Faults Onshore Generally Dip to the South.....5.13-130

Figure 5.13-48 Sample Location Map with Minimum Limiting Ages for Pediment Samples (Green Circles) and Erosion Rates for River Samples (Yellow Boxes). TSP sample sites identified by number. BF = Baviaanskloof Fault, CF = Coega Fault, GF = Gamtoos Fault, KAF = Kango Fault, KF = Kouga Fault, PE = Plettenberg Fault, U = Uitenhage.....5.13-131

Figure 5.13-49 Map of the Outeniqua Basin Showing the Major Structural Elements and Sub-Basins and Enlargement of the Gamtoos and Algoa Basins (Modified from *Reference 5.13.144*) 5.13-135

Figure 5.13-50 Seismic Profile H-H′ and Geological Interpretation Across the Southern Gamtoos Basin (*Reference 5.13.162*) 5.13-136

Figure 5.13-51 Seismic Profile G-G′ and Geological Interpretation Across the Southern Gamtoos Basin (*Reference 5.13.162*) 5.13-137

Figure 5.13-52 Geology Along the Gamtoos Fault (Modified from *Reference 5.13.91*) 5.13-138

Figure 5.13-53 Simplified Cross Section Across the Gamtoos Horst Block in the Onshore Region (Modified from *Reference 5.13.113*) 5.13-140

Figure 5.13-54 Compilation Map Showing Generalised Quaternary Geology and Locations of Onshore and Offshore Traces of the Gamtoos and Elandsberg Faults (Modified from *Reference 5.13.58*) 5.13-141

© Eskom 2026/Rev 0a

Figure 5.13-55 Map Showing Location of Plettenberg Fault (Modified from *Reference 5.13.72*). Base topography: *Reference 5.13.279*.....5.13-144

Figure 5.13-56 Seismic Section L-L′ (Uninterpreted and Interpreted) Across the Plettenberg Fault (Offshore) (Modified from *Reference 5.13.72*).....5.13-145

Figure 5.13-57 High-Resolution Bathymetric Map Showing Geomorphology Along the Offshore Plettenberg Fault: (A) Uninterpreted (*Reference 5.13.59*; Topography from *Reference 5.13.280*). (B) with Post-Cretaceous Faults as Mapped by Roux (*Reference 5.13.45*) 5.13-147

Figure 5.13-58 Map Showing Location of the Cape St Francis Fault and Associated Fault Traces from Du Toit (*Reference 5.13.277*) 5.13-149

Figure 5.13-59 Seismic Profile Across the Cape St Francis Fault Showing No Offset Across the Cretaceous (1At1) Horizon. The location of the profile shown is highlighted in red on the map (upper left) (Modified from *Reference 5.13.142*) 5.13-150

Figure 5.13-60 Seismic Profile with Interpretation Showing Evidence of No Apparent Offset of Aptian (109.5–108 Ma) and Overlying Upper Cretaceous and Tertiary Section (*Reference 5.13.162*). The location of the profile is highlighted by the orange line in the inset map.....5.13-151

Figure 5.13-61 (A) Two-way Travel Time (TWT) Map to the Top of Synrift Deposits (1At1 Unconformity) Showing Faults That Displace the Base of Cretaceous as Seen in Seismic Data. (B) TWT Map to the Base of Tertiary (22At1 Unconformity) Showing Interpreted Post-Cretaceous Faults and Locations of Interpreted Seismic Lines Presented by Roux (*Reference 5.13.45*). The portion of Line A shown on Figure F-5.13.62 is highlighted in blue (Modified from *Reference 5.13.45*).....5.13-152

Figure 5.13-62 Upper Panel Displays Bathymetric Profile from De Wet (*Reference 5.13.59*) That Is Approximately Scaled (Horizontal Axis) to the Seismic Profile in the Lower Panel Interpreted by Roux (*Reference 5.13.45*) Across Minor Fault Within the Gamtoos Basin 5.13-153

Figure 5.13-63 Map Showing Extent of Worcester Fault (*Reference 5.13.24*) 5.13-156

Figure 5.13-64 Map Showing Worcester Fault Relative to Offshore Faults and the Syntaxis Region of the Cape Fold Belt.....5.13-157

Figure 5.13-65 Geological Map Showing Unfaulted Grahamstown Formation (Tg) Surfaces Inferred to Be Miocene in Age Mapped Across the Worcester Fault (Modified from *References 5.13.284*; *5.13.167* and *5.13.287*). Black box indicates area of *Figure F-*

5.13.68 5.13-158

Figure 5.13-66 Location of 1969 Ceres Aftershocks (Red Dashed Line) Relative to the Groenhof and Worcester Faults (Modified from *Reference 5.13.249*).....5.13-160

Figure 5.13-67 Road Cut East of Zuurbraak Showing Evidence of Neotectonic Reactivation of the Worcester Fault: (a) Mosaic Compiled by J. Viljoen in the Late 1980s. (b) Photograph of the Road Cut as Viewed by De Beer (*Reference 5.13.24*) 5.13-161

Figure 5.13-68 GoogleEarth Image Showing Unfaulted Geomorphic Surface (Pediment or Eroded Pediment) Across the Mapped Trace of the Worcester Fault (as Mapped by Theron, *Reference 5.13.284*) (Figure from *Reference 5.13.1*) 5.13-163

Figure 5.13-69 Seismic Line Across the Infanta Arch and Bredasdorp Basins (*Reference 5.13.72*) 5.13-164

Figure 5.13-70 Map of Agulhas Fracture Zone Marginal to the Southern African Continent, Illustrating Fourfold Segmentation (*Reference 5.13.68*).....5.13-166

Figure 5.13-71 Interpreted Structure of the South African Continent Margin (*Reference 5.13.69*). DMR = Diaz Marginal Ridge; AFFZ = Agulhas-Falkland Fracture Zone 5.13-167

Figure 5.13-72 Profile AWI-20050201 Showing the Shelf and Continental Shelf into Agulhas Passage. The hatched blocks show the activity levels of the various currents (*Reference 5.13.83*) 5.13-168

Figure 5.13-73 Profile AWI-20050101 Showing the Continental Rise and Agulhas Passage. The hatched blocks show the activity levels of various currents (*Reference 5.13.83*) 5.13-169

Figure 5.13-74 Alternative Western Boundary of the Kango Fault (*Reference 5.13.54*) .5.13-173

Figure 5.13-75 P-Wave Velocity Model for the Western Profile in Figure F-5.13.40. The upper panel shows just the model, the lower panel includes interpretations. Northernmost deformation of the Cape Supergroup has been marked by an arrow (PTF). Farther south, the geometry of the normal listric Kango Fault (KF; surfacing at 170 km) has been drawn. A high-velocity anomaly most likely related to the Beattie Magnetic Anomaly (BMA) has been indicated with an ellipse at a depth of ~15 km, at profile km 80 (*Reference 5.13 263*) ...5.13-174

Figure 5.13-76 Field Localities and Possible Segment Boundaries Along the Quaternary-Reactivated Kango Fault (*Reference 5.13.54* Table 7) 5.13-175

Figure 5.13-77 Digital Elevation Model of the Site Vicinity (40 km Radius) (Onshore Data from *Reference 5.13.280*; Offshore Data from *Reference 5.13.59*) 5.13-181

Figure 5.13-78 Digital Elevation Model of the Site Vicinity (40 km Radius) and Site Area (8 km Radius) and Map of Coastal Terraces.....5.13-182

Figure 5.13-79 The Landward Extent of the Transgressive Miocene Marine Planation Event Which Led to the Development of the Platform Is Marked by a Palaeosea Cliff, a Sharp Break in Slope Situated at the Southern Foot (~300 m asl) of the Interior Cape Fold Mountains, Northwest of Humansdorp near the Town of Kruisfontein.....5.13-185

Figure 5.13-80 Dunefields near the Thyspunt Site (Modified from *References 5.13.299* and *5.13.302*).....5.13-186

Figure 5.13-81 Geology of the Site Vicinity (Modified from *Reference 5.13.27*).....5.13-189

Figure 5.13-82 Approximate Thicknesses and Lithology of the Formations of the Table Mountain Group Present Within the Site Vicinity (Figure Not to Scale; Modified from *Reference 5.13.27*) 5.13-190

Figure 5.13-83 Interpreted Subsurface Occurrence of the Formations of the Table Mountain Group Beneath the Cenozoic Algoa Group Along the North-eastern Limb of the Main Cape St Francis Anticline in the Cape St Francis Area 5.13-191

Figure 5.13-84 (a) A Coastal Exposure of Competent Quartzitic Sandstone of the Peninsula Formation, Interbedded with Subordinate Dark Grey Mudrock (1.4 m in thickness) West of De Hoek. Location of Photo: 34°11′48.1″ S, 24°47′39.0″ E. (b) Soft Sediment Deformation in Quartzitic Sandstone of the Peninsula Formation Along Coastal Exposures East of Thys Bay. Location of Photo: 34°11′20.6″ S, 24°44′34.1″ E.....5.13-193

Figure 5.13-85 (a) Rarely Exposed Dark Grey to Blackish, Fine-Grained Argillaceous Cedarberg Formation Visible at the Base of a Valley, South of the Kouga Dam (33°51′44.5″ S, 24°35′42.1″ E). (b) Light Brown to Yellowish Brown Weathered Shale and Siltstone Exposure of the Cedarberg Formation Situated Within a Topographic Low Within the Landscape. Note the Elevated Quartzitic Ridge of the Peninsula Formation in the Background (33°52′13.0″ S; 24°36′35.1″ E). Photos Sourced from *Reference 5.13.27* ..5.13-194

Figure 5.13-86 The Subsurface Occurrence of the Cedarberg Formation near Cape St Francis Interpreted from Geophysical Ground Surveys (*References 5.13.42*, *5.13.306*, and *5.13.44*) and Borehole Data (*Reference 5.13.58*) 5.13-196

Figure 5.13-87 Alternating Shale and Dirty Sandstone of the Goudini Formation Seen in Borehole CSF-10 Between 40.90 m and 54.25 m Below Ground (34°11′38.2″ S, 24°49′29.3″

© Eskom 2026/Rev 0a

E). The Red Arrow Indicates the Contact Between the Cenozoic Algoa Group Sediments and the Palaeozoic Goudini Formation 5.13-197

Figure 5.13-88 Sandstone of the Goudini Formation Is Well Exposed Along the Coast Within the Huisklip Nature Reserve. Location of Photo: 34°8′25.4″ S, 24°26′30.3″ E 5.13-198

Figure 5.13-89 (a) Coastal Exposures of the Skurweberg Formation Composed of Grey to Pale Grey, Mature Quartzitic Sandstone Dipping Approximately 50° S at 34°11′23.6″ S, 24°41′54.2″ E Near Tony's Bay. (b) A Weathered Exposure of Immature Sandstone Within the Skurweberg Formation, 13 km west of Kruisfontein (33°59′40.2″ S, 24°34′50.6″ E) .5.13-199

Figure 5.13-90 (a) Immature Argillaceous Sandstone of the Baviaanskloof Formation near Sunnyside Dam, Northeast of Humansdorp (34°00′45.6″ S, 24°51′33.5″ E). (b) Along a River Section East of the Churchill Dam, the Contact Between Quartzitic Sandstone of the Skurweberg Formation (upper right) and the Immature Sandstone of the Baviaanskloof Formation (lower left) Can Be Seen (34°00′08.6″ S, 24°29′46.9″ E) 5.13-201

Figure 5.13-91 (a) Weathered Mudstone of Ceres Subgroup, Possible Gydo Formation Showing Slaty Cleavage Approximately 9 km East of the Churchill Dam (33°59′25.1″ S, 24°35′23.1″ E). (b) Bioturbated Dark Grey Shale of the Gydo Formation Along the Hankey Pass, Approximately 8 km Southwest of the Hankey (33°53′28.2″ S, 24°50′08.1″ E). The Exposure Shows Burrow Orientation Approximately Parallel to Bedding Laminations ...5.13-203

Figure 5.13-92 (a) Conglomerate and Sandstone Lenses of the Enon Formation Exposed in a Series of Benches at the Hankey Pass Quarry (33°52′ 09.6″ S, 24°51′ 12.3″ E). The Conglomerate Displays Crudely Graded Bedding. (b) Conglomerate and Pebbly Sandstone of the Enon Formation Exposed Along the Kabeljous River Showing Shallow Cave Development due to Weathering of Poorly Consolidated Conglomerate (33°58′15.2″ S, 24°54′30.1″ E) 5.13-205

Figure 5.13-93 (a) A 4 m Exposure of Grey-Weathered Normally Graded Kirkwood Formation Conglomerate, Grading Upward into Interfingering Sandstone Located Near the Gamtoos River Estuary (33°54′ 22.7″ S, 25°01′ 22.1″ E). (b) Weathered Orange-Red Mudstone and Cream-Coloured Sandstone of the Kirkwood Formation (33°54′ 17.9″ S, 25°01′ 20.9″ E) 5.13-207

Figure 5.13-94 Weathered, Pebbly, Ferruginous Silcrete of the Grahamstown Formation on the ThabaManzi Farm (33°57′44.3″ S, 24°34′17.9″ E) 5.13-208

Figure 5.13-95 Cenozoic Overburden (Algoa Group) Thicknesses in the Thyspunt, De Hoek, Cape St Francis, and St Francis Areas Within the Site Vicinity 5.13-211

Figure 5.13-96 (a) Quartzitic Sandstone of the Peninsula Formation Overlain by a Thin Discontinuous Cobble Lag of the Alexandria Formation (seen in the foreground of the photo). Location of Photo: 34°09′ 06.6″ S, 24°39′ 31.8″ E). (b) Deeply Weathered Conglomerate of the Alexandria Formation Exposed in a Quarry Located Northeast of Oyster Bay (34°07′ 48.0″ S, 24°42′ 47.4″ E) 5.13-212

Figure 5.13-97 A Partial Remnant Exposure of the Salnova Formation Located in the Interdune Areas West of Cape St Francis Below 18 m asl (34°11′34.5″ S, 24°50′ 58.6″ E). Unconsolidated and Partially Vegetated Dunes of the Schelm Hoek Formation is Seen in the Background.....5.13-215

Figure 5.13-98 (a) An Exposure of Aeolianite of the Nahoon Formation near Oyster Bay. (b) Aeolianite of the Nahoon Formation Exposed along the Western Edge of the St Francis Headland Bypass Dunefield, Mantled by Unconsolidated Mobile Sand of the Schelm Hoek Formation (34°11′31.5″ S, 24°51′10.9″ E). Photo Taken from the Database of Goedhart et al. (Reference 5.13.27) 5.13-216

Figure 5.13-99 (a) Unconsolidated Mobile Dune Sand of the Schelm Hoek Formation that Form Part of the Oyster Bay Dunefield (34°10′14.1″ S, 24°44′11.0″ E). (b) Ephemeral Wetlands are Common in the Thys Bay and Oyster Bay Dunefields, Forming in Between Dune Depressions or at the Base of Dune Slopes. Location of Photo: 34°10′20.2″ S, 24°44′16.0″ E 5.13-218

Figure 5.13-100 (a) A Coastal Inlet with Cobbles and Boulder Deposits, Near Cape St Francis. These Deposits are a Frequent Occurrence Northwest of Seal Point. (b) Stratified, Shell Rich Beach Deposits of Granule Size Exposed in a Beach Terrace, Approximately 300 m From the Coastline and 3 km Northwest of Seal Point Lighthouse (34°11′26.3″ S, 24°45′01.1″ E). (c) Unconsolidated Modern Beach Sands Deposited in an Embayment Southeast of Oyster Bay (34°10′59.7″ S, 24°41′08.4″ E) 5.13-220

Figure 5.13-101 Extensive Alluvial Deposits Along the Banks of the Lower Kromme River 5.13-222

Figure 5.13-102 A 3 m Thick Tufa Deposit West of De Hoek (34°10′59.7″ S, 24°41′08.4″ E). The Deposit is Located at the Interface Between the Palaeozoic and Cenozoic Strata 5.13-223

Figure 5.13-103 Distribution of Poles to Fault Planes Within the Site Vicinity (*Reference 5.13.27*) 5.13-225

Figure 5.13-104 Structural Interpretation of the Klippepunt Area (Modified from *Reference 5.13.27*) 5.13-228

Figure 5.13-105 (a) Overturned Convex Cross-Beds in Quartzitic Sandstone of the

Skurweberg Formation Immediately West of Klippepunt (34°11′12.3″, 24°35′45.1″). (b) Overturned Convex Shallow Channel in Sandstone of the Baviaanskloof Formation (34°11′07.2″, 24°36′21.3″) 5.13-229

Figure 5.13-106 (a) A 3 m Wide Crushed Lens of Overturned Skurweberg Formation Quartzite West of Klippepunt; View Is Eastwards (34°11′15.4″, 24°35′47.1″). (b) A View West of the Same Crushed Lens Seen in Figure (a), Showing a Yellow-Brown Mylonised Brecciated Lens (Indicated by the Yellow Line) 5.13-230

Figure 5.13-107 Intensely Fractured Skurweberg Formation Showing Pervasive Axial Planar Cleavage and Jointing Situated Between Two Adjacent Less-Fractured Beds Northwest of Klippepunt (34°11′14.8″, 24°35′44.1″) 5.13-231

Figure 5.13-108 Interpreted Location of the Tsitsikamma Thrust Fault, near the Tsitsikamma River Mouth (Modified from *Reference 5.13.27*) 5.13-234

Figure 5.13-109 A 2 m Wide Breccia Horizon, Partly Overlain by Boulders Indicating the Tsitsikamma River Mouth Fault as Viewed Due East. The Breccia Horizon Is Bounded by Tightly Folded Overturned Goudini Formation at Angles That Changes Abruptly to Open Folded East-Southeast and Southeast-Dipping Beds on the Nose of the Broad Anticline (*Reference 5.13.27*; 34°08′15.5″, 24°26′21.9″) 5.13-235

Figure 5.13-110 (a) A 4 m Exposure of the Kirkwood Formation Showing a Faulted Contact Between Orange-Red Mudstone Interbedded with Isolated Sandstone and Grey Weathering Conglomerate (33°54′22.7″, 25°01′22.1″). (b) A 3 m Exposure of the Kirkwood Formation Showing a Faulted Contact Between Orange-Red Mudstone and Tan-Coloured Sandstone (33°54′28.0″, 25°01′24.4″) 5.13-237

Figure 5.13-111 (a) Stereonet Showing Poles to Palaeozoic Bedding Within the Site Vicinity; The Folded Nature of the Bedrock Rocks Is Clearly Reflected (*Reference 5.13.27*). (b) Stereonet of Fold Axes Documented Within the Site Vicinity. A Dominant Shallow Southeast Plunge and a Subordinate Shallow Northwest Plunge Direction Is Recorded and Reflects the Presence of Double Plunging Folding (*Reference 5.13.27*) 5.13-239

Figure 5.13-112 (a) A Low-Amplitude Anticline in Incompetent Quartzitic Sandstone of the Peninsula Formation Exposed Northwest of De Hoek Along Coastal Exposures (34°11′47.1″, 24°46′35.3″). (b) An Overturned North-Verging Fold, in Sandstone of the Table Mountain Group, near Churchill Dam (34°00′02.3″, 24°29′40.3″) 5.13-240

Figure 5.13-113 (a) Slickensides Along Quartzitic Sandstone of the Peninsula Formation Bedding Planes West of Thys Bay (34°11′16.9″, 24°44′23.0″). (b) Slickensides Along Bedding Planes in Strata of the Undifferentiated Bokkeveld Group 7 km Northwest of Paradise Beach. These Slickensides Are Indicative of Movement Along Bedding Planes to

Facilitate Folding (34°04′34.9″, 24°49′19.4″).....5.13-241

Figure 5.13-114 (a) Kink Folding Observed in a Sandstone Exposure of the Goudini Formation on the Northern Flank of an Overturned North-Verging Anticline Along the Banks of the Tsitsikamma River (34°07′47.2″, 24°26′33.1″). (b) Kink Folding Observed in Coastal Quartzitic Sandstone Exposures of the Peninsula Formation Southeast of De Hoek (34°12′19.6″, 24°48′49.5″) 5.13-242

Figure 5.13-115 An Aerial View of Non-coaxial Folding Observed in Exposures of the Skurweberg Formation on the Northern Limb of the Main Cape St Francis Anticline (Modified from *Reference 5.13.27*) 5.13-243

Figure 5.13-116 The Strike Direction of Joints Recorded Within the Site Vicinity (*Reference 5.13.27*). The Main Joint Direction J1 Is Northeast-Southwest.....5.13-246

Figure 5.13-117 (a) Quartz-Filled Joints and Fractures in Quartzitic Sandstone of the Skurweberg Formation; Notice the Quartz-Filled Tension/Echelon Gashes (34°11′23.0″ 24°36′23.5″). (b) Fractures and Veins Filled with Iron Precipitate in Weathered Sandstone of the Baviaanskloof Formation.....5.13-247

Figure 5.13-118 (a) Cross-Cutting Gullies Formed Parallel and Perpendicular to Skurweberg Formation Bedding in Response to Intensely Closely Spaced Jointing in the Area Northwest of Tony's Bay (34°11′11.9″, 24°41′17.2″). (b) An Aerial View of Gully Formation Observed in the Peninsula Formation, Just East of Thys Bay. Gullies Form in Areas Where the Joint Frequency and Thus Deformation Is Greatest, Creating Zones of Weakness, Which Are Exploited by Erosional Power of Wave Action. Gully Trends Match Joint Trends Found in the Area.....5.13-248

Figure 5.13-119 A 20 m Interval DEM of the Site Area, Showing a South-North Topographical Profile Across the Onland Portion of the 8 km Radius Region 5.13-250

Figure 5.13-120 Figure Showing Bedrock Elevations Beneath Cenozoic Cover in the Thyspunt Area (Source: *Reference 5.13.58*).....5.13-251

Figure 5.13-121 Map Showing Locations of Cross Sections Based on Subsurface Boring Data at Thyspunt (Modified from *Reference 5.13.58*). Cross Sections in *Reference 5.13.58*, Appendix D 5.13-253

Figure 5.13-122 Elevation of Bedrock at the Thyspunt Site.....5.13-255

Figure 5.13-123 Detailed Maps of Elevation of Bedrock West of Thyspunt Site (see insets on Figure F-5.13.122).....5.13-256

Figure 5.13-124 Correlation of Marine Terraces near the Thyspunt Site 5.13-

257

Figure 5.13-125 Example of Marine Terrace Study Topographic Profile and Sampling Locations 5.13-258

Figure 5.13-126 Grey-Scale Offshore MBES Bathymetry Data for the 8 km Site Area (from *Reference 5.13.281*) 5.13-261

Figure 5.13-127 Offshore Topographic Profiles Developed from 1 m MBES Data DEM Through Areas of Bedrock Outcrop (from *Reference 5.13.58*).....5.13-262

Figure 5.13-128 Geology of the Site Area (Modified from *Reference 5.13.27*) 5.13-264

Figure 5.13-125 (a) Coastal Exposure of Competent Quartzitic Sandstone of the Peninsula Formation, Interbedded with Three Subordinate Dark Grey Mudrock Layers West of De Hoek. Location of photo: 34°11′48.4″ S, 24°47′38.3″ E. (b) Quartzitic Sandstone of the Peninsula Formation in Borehole NEW 30 (*Reference 5.13.61*) from 93 m to 99 m Below Ground Level, Approximately 1 km Northwest of Tony's Bay (34°11′11.5″ S, 24°41′27.7″ E) 5.13-266

Figure 5.13-130 The Medium-Grained, Pale Grey Quartzitic Sandstone with Subordinate Mudstone/Shale and Siltstone of the Goudini Formation as Observed in Borehole NEW12 (*Reference 5.13.61*) (34°11′08.3″ S, 24°42′32.4″ E) from 30.49 m to 43.34 m Below Ground Level. Bedding Is Thin and Shows Consistent Rapid Lithological Change. 5.13-268

Figure 5.13-131 (a) Coastal Exposures of the Skurweberg Formation Composed of Grey to Pale Grey Mature Quartzitic Sandstone Dipping Approximately 50° S at 34°11′23.6″ S, 24°41′54.2″ E near Tony's Bay. (b) Unweathered Quartzitic Sandstone of the Skurweberg Formation Seen in Borehole NEW 29 (*Reference 5.13.61*) from 69.43 m to 76.69 m Below Ground Level 5.13-269

Figure 5.13-132 Borehole Thickness of the Cenozoic Algoa Group Within the Site Area Plotted Against Their Distance Away from Coastal Margins. Four Thickness Zones, A to D, Can Be Identified 5.13-272

Figure 5.13-133 Cenozoic Overburden Thicknesses at Thyspunt as Derived from Borehole Data (*References 5.13.28*, *5.13.308*, *5.13.60*, *5.13.61*, *5.13.58*, and *5.13.62*). The Site Location (1 km Radius) is also indicated 5.13-273

Figure 5.13-134 Calcareous Light Grey to Greyish-Yellow Unconsolidated to Semiconsolidated Dune Sand Associated with the Nanaga Formation Observed in Borehole TS-07 (*Reference 5.13.58*) from 12.45 m to 27.15 m Below Ground Level (34°10′31.1″ S,

24°41′38.2″ E) 5.13-275

Figure 5.13-135 Unconsolidated Aeolian Dune Sands of the Schelm Hoek Formation Within the Oyster Bay Dunefield. Note the Development of Wetlands Within Dune Depressions 5.13-276

Figure 5.13-136 Nahoon Formation Palaeodune Rock Partly Overlain by Mobile Dune Sand of the Schelm Hoek Formation (34°10′31.1″ S, 24°41′38.2″ E).....5.13-276

Figure 5.13-137 Distribution of the Basal Gravel Deposits Stratigraphically Either Correlated to the Alexandria or Salnova Formation at Thyspunt as Derived from Borehole Data (*References 5.13.28*, *5.13.308*, *5.13.60*, *5.13.61*, *5.13.58*, and *5.13.62*). The Site Location (1 km Radius) is also indicated.....5.13-278

Figure 5.13-138 The Miocene to Early Pliocene Alexandria Formation or Early Quaternary Salnova Formation Conglomerate (Highlighted in White) Composed of Imbricated, Disc- to Roller-Shaped Clasts of Pebble to Cobble Size Set in a Fine- to Medium-Grained Sandy Matrix Observed in Borehole NEW12 (*Reference 5.13.61*; 34°11′08.3″ S, 24°42′32.4″ E) Between 13.50 m and 30.49 m Below Ground Level. The basal gravel deposits act as a conduit for groundwater movement in the area, which enhances in-situ weathering of the underlying bedrock, especially in bedrock topographic lows for up to as much as 30 cm. Thus, the contact zone between the basal gravel and sand deposits can be described as a weathered contact (highlighted in red).....5.13-280

Figure 5.13-139 Offshore Lithological Seabed Features (Modified from *Reference 5.13.281*) 5.13-281

Figure 5.13-131 Possible Thrust Ramps Seen in Coastal Exposures of the Peninsula Formation Quartzitic Sandstone Immediately East of Thys Bay (34°11′15.9″ S, 24° 44′21.7″ E) 5.13-284

Figure 5.13-141 Z-Shaped Folding and Overfolding Resulting in Bedding Shortening Seen in Strata of the Peninsula Formation in the Area Immediately East of Thys Bay. Overfolding May Have Been Accompanied by Thrusting Semiparallel to the Cape St Francis Fold Axis, with Folded Dismembered Fold Limb Stacked Against More Competent Beds (34°11′16.9″ S, 24°44′23.0″ E; *Reference 5.13.27*).....5.13-285

Figure 5.13-142 Small-Scale Localised Microfaults Develop Along Joint or Fracture Planes. At This Locality (34°11′26.6″ S, 24°44′52.4″ E) Along the Coast a 15 cm Displacement of a Light Green-Grey Shale Unit in the Peninsula Formation is seen5.13-286

Figure 5.13-143 Digital Elevation Model of the Site Location.....5.13-288

Figure 5.13-144 Elevation Shows a Steady Increase away from Coastal Margins

in a Northerly Direction 5.13-290

Figure 5.13-145 Geology of the Site Location (1 km Radius) (Modified from *Reference 5.13.27*) 5.13-291

Figure 5.13-146 Brown to Dark Brown, Fine-Grained Organic Sand Forms the Top Soil Within the Site Location. The Topsoil Thickness in Borehole TB32 (34°11′24.4″ S, 24°42′45.0″ E), Located Approximately 300 m from Thyspunt, Is 2.05 m (Highlighted in Green). The Topsoil Is Underlain by Undifferentiated Algoa Group Sediments 5.13-294

Figure 5.13-147 Moderately Steep Bedding Inclinations Along the Northwest-Southeast-Trending Coastline of the Site Locality 5.13-295

Figure 5.13-148 Onshore LiDAR and Offshore Bathymetric Data Presented as Hillshade DEMs (Interpreted Fault Data from *Reference 5.13.46*).....5.13-300

Figure 5.13-149 Subduction Zones and Volcanic Islands Determined to Have the Potential to Create Damaging Tsunamis in South Africa 5.13-307

Figure 5.13-150 South African Faults in the Thyspunt Site Region. Most Faults Show Evidence of Mesozoic Activity, but Only the Kango Fault Is Known to Have Evidence of Quaternary Reactivation 5.13-310

Figure 5.13-151 Rates of Terrestrial Sediment Input into the Marine System in Southern Africa (*Reference 5.13.376*) 5.13-312

Figure 5.13-152 Top: Geology from the Site Area Offshore of the Site. Bottom: Detailed Bathymetry off the Coast of the Thyspunt Site and Topographic Profile Across Features Alternatively Interpreted to Be the Result of Slumping and Erosion. Modified from *Reference 5.13.281* 5.13-314

Figure 5.13-153 Mapped Slumps along the South African Margin.....5.13-316

© Eskom 2026/Rev 0a

5.13 GEOLOGY

This section of the Site Safety Report (SSR) describes the approach and results that demonstrate adequate knowledge of the geologic, geophysical, seismological, and geotechnical characteristics of the subsurface geology in the region and at the site for purposes of assessing site suitability. In addition to demonstrating adequate levels of knowledge regarding the regional and local geological setting of the Thyspunt site, the geosciences knowledge base given in this section of the SSR provides input to the assessment of various types of geological hazards documented in other sections of the SSR, including ***Section 5.14*** (Seismic Hazard Analysis), ***Section 5.15*** (Geotechnical Characterisation) and ***Section 5.9*** (Oceanography and Coastal Engineering).

5.13.1 Introduction

As presented in Section 5.1 of this SSR, the Thyspunt site is situated about 80 km west of Port Elizabeth. In the early 1980s, the site was identified by Eskom Holdings as one of five proposed sites along the South African coast to be considered for locating future nuclear installations. As such it has been investigated by geologists and other scientists since the mid-1980s. For a selected site to be considered for investigation and development of an SSR, it will have passed a number of screening phases. See ***Section 4*** (Site Investigation Approach).

In terms of geological characterisation the following work has been carried out on or in the vicinity of the Thyspunt site:

- Desk study review of existing information such as reports, maps, air photographs and satellite imagery.
- Site reconnaissance.
- Regional and local site investigations described in ***Subsection 5.13.4.2*** (Geoscientific Investigations Performed), to understand the regional geological setting and local geological conditions and thereby contribute to the geological knowledge base. This information is used to identify geological hazards that would render the site unsatisfactory for the development of a nuclear installation. Assessment has also been made of the potential for surface faulting due to capable faults at the site location.

The results derived from the above work have been incorporated into this section. As described in ***Subsection 5.13.4*** (Approach to Evaluation), progressively more detailed regional and site geoscientific investigations have been conducted to develop a geological knowledge base and to provide input

© Eskom 2026/Rev 0a

to hazard assessments that will be used to demonstrate the suitability of the site to locate a new nuclear installation, as described in ***Section 6*** (Evaluation of External Events). As described in ***Section 5.14*** (Seismic Hazard Analysis), several geological investigations were conducted with the specific purpose of providing geologic, seismologic, and geotechnical data that were used to reduce uncertainties in the various inputs to the probabilistic seismic hazard analysis. The results of those investigations are summarised in this section and provide information regarding the capability of regional and local faults, and provide a basis for the assessment of the potential for surface faulting at the site, described in ***Subsection 5.13.5.3*** (Surface Faulting Evaluation).

This section also provides the interface with other relevant parts of the SSR, such as ***Section 5.14*** (Seismic Hazard Analysis), ***Section 5.15*** (Geotechnical Characterisation), and ***Section 5.9*** (Oceanography and Coastal Engineering).

5.13.2 Purpose and Scope

This section of the SSR describes the relevant geological, geophysical, and seismological data that demonstrate a sufficient knowledge of the site region, vicinity, and area (defined in ***Subsection 5.13.4.1***) for purposes of assessing site suitability. The geological, seismological and geophysical characteristics of a nuclear installation site and its environment must be investigated with sufficient scope and level of detail to permit evaluation of the acceptability of a proposed site for development of a new nuclear installation. Therefore this ***Section 5.13*** (Geology) and ***Section 5.14*** (Seismic Hazard Analysis) and other applicable sections of the SSR are developed in a complementary manner to provide sufficient information to support estimates of the earthquake ground motion hazard and evaluations of other earthquake-related hazards (e.g. surface faulting, liquefaction) and other geotechnical hazards (e.g., landslides), in order to permit adequate engineering solutions to be investigated to mitigate actual and potential geological and seismic effects at the proposed site, if necessary.

This section of the SSR describes the purpose and scope of the geoscientific studies, the regulatory framework (***Subsection 5.13.3***) and technical requirements for geoscientific investigations, including geological, geophysical, and seismologic characterisation data, and the results of the investigations relative to the regional and local geological conditions. It further describes the assessment of surface faulting, which is documented in ***Subsection 5.13.5.3***. It should be noted that the compilation, analysis, and use of the historical and instrumental seismicity catalogue has been documented in the probabilistic seismic hazard analysis (PSHA) report (***Reference 5.13.1***) and is summarised in ***Section 5.14*** (Seismic Hazard Analysis). It is also noted that this section includes the documentation of tsunamigenic sources, which provides input to

the tsunami hazard analysis documented in ***Section 5.9*** (Oceanography and Coastal Engineering). In aggregate and in combination with other assessments, these hazard assessments will provide inputs to the evaluation of the acceptability of the site, as described in ***Section 6*** (Evaluation of External Events).

The size of the areas to be investigated and the type of data pertinent to the investigations (and thus the type of methodologies employed) must be determined based on the geological and seismological setting of the proposed site.

In accordance with international best practice as discussed in ***Subsection 5.13.3*** (Regulatory Framework), geoscientific investigations for nuclear installations include *inter alia*:

- extensive review of existing literature, historical reports and other datasets;
- remote sensing and geophysical interpretation;
- geological, geomorphological, palaeoseismological and geophysical investigative techniques and interpretation;
- laboratory dating of geological samples.

Furthermore, the studies that are to be considered for the evaluation of the geology of a proposed site include *inter alia*:

- studies that augment and complement previous studies related to geological, geomorphic and chronostratigraphic studies of key geological surfaces, their ages and relation to faults (e.g., marine terraces, alluvial terraces);
- studies that investigate rates of uplift and deformation, such that potential capable faults can be identified or precluded within the site vicinity;
- focused tectonic geomorphic, studies of Quaternary-age fault behaviour as appropriate and fault-specific studies constraining recency, maximum earthquake magnitude (m_{max}), and slip rate.

As will be discussed in ***Subsection 5.13.4*** (Approach to Evaluation), all of the above studies have been conducted for the Thyspunt site and the results of those studies have led to the geological descriptions of the regional geology in ***Subsection 5.13.5.3*** (Surface Faulting Evaluation) and of the site geology in ***Subsection 5.13.5.4*** (Tsunamigenic sources). In addition, the scope of the

© Eskom 2026/Rev 0a

investigations and studies provided in this section includes an assessment of the potential for surface deformation (extent, amount of displacement) from tectonic surface faulting at the site location in ***Subsection 5.13***. In addition, the geological characterisation of the site region, coupled with an extensive updating and analysis of the historical and instrumental earthquake catalogue, were used as inputs to the Thyspunt PSHA (***Reference 5.13.1***).

5.13.3 Regulatory Framework

This Subsection describes the regulations and regulatory guidance that is relevant specifically to the development of geological, geophysical, seismological, and geotechnical data and information for purposes of licensing a nuclear site in South Africa. The regulatory compliance matrix is given in ***Table T-5.13.1.***

The current regulatory requirements relevant for the development of appropriate geological databases for the evaluation of external events during site characterisation for new nuclear installations are stipulated in the following document: “Regulations on Licensing of Sites for New Nuclear Installations” (***Reference 5.13.2***).

The regulations in ***Reference 5.13.2*** that make reference to the geological characteristics of the site for purposes of evaluating external events are:

“4(2) The proposed nuclear installation design(s), and the characteristics specific to the site: New nuclear installation(s) must reflect through their design, construction and operation an acceptably low probability of postulated events that could result in release of quantities of radioactive material.”

“4(5) Natural phenomena and potential man-made hazards must be appropriately accounted for in the design of the new nuclear installation(s), and that adequate emergency plans and nuclear security measures can be developed.”

“5(3) The characteristics of the site relevant to the design assessment, risk and dose calculations, including inter alia:

(a) external events”.

These high-level regulations provide only a framework for identifying the types of data that are required for characterising the geological environment of the site for purposes of evaluating the impact that external events might have on the site. More specific guidance is provided in National Nuclear Regulator position papers and regulatory guidance developed by the International Atomic

© Eskom 2026/Rev 0a

Energy Agency (IAEA) and the United States Nuclear Regulatory Commission (US NRC).

Table 5.13.1
Regulatory Compliance Matrix

Act/Regulation	Regulation	Issue	Section Where Covered
Department of Energy (2011), R.927 "Regulations on Licensing of Sites for New Nuclear Installations" (***Reference 5.13.2***)	4(2), 4(5), 5(3)(a)	Natural phenomena external events must be evaluated for design.	5.13.3
NNR Position Paper PP-0014, "Considerations of External Events for New Nuclear Installations" Draft (***Reference 5.13.3***)	Ch. 10 Sec. 10.4 Sec. 11.1 App. B App. E	Requirements for geological, seismological and geophysical information needed for seismic hazard and surface faulting assessments.	5.13.3.1
IAEA Safety Requirements NS-R-3, "Site Evaluation for Nuclear Installations" (***Reference 5.13.4***).	Sec. 2.14 Sec. 3.1 to 3.7	Requires that geological conditions be evaluated for earthquake hazards and surface faulting.	5.13.3.2
IAEA Safety Guide SSG-9 "Seismic Hazards in Site Evaluation for Nuclear Installations" (***Reference 5.13.5***).	Ch. 3	Necessary Information and Investigations: identifies the recommended elements of a geological, geophysical and geotechnical database.	5.13.3.2
IAEA Safety Guide NS-G-3.6 "Geotechnical Aspects of Site Evaluation and Foundations for Nuclear Power Plants." (***Reference 5.13.6***).	Ch. 2	Sections related to geological characterisation.	5.13.3.2
US Regulation 10 CFR Part 100, Section 100.23 (***Reference 5.13.7***)	Geological and Seismic Siting Criteria	Provides acceptance criteria for evaluating the suitability of a proposed site based on consideration of geological, geotechnical, geophysical, and seismologic characteristics of the proposed site.	5.13.3.3
US NRC Regulatory Guide 1.208, "A Performance-Based Approach to Define Site-Specific Earthquake Ground Motion" (***Reference 5.13.8***),	Sec. C.1, App. C	Recommends geological, geophysical, seismological, and geotechnical Investigations to Characterise site region, vicinity, area, and location.	5.13.3.3
US NRC Regulatory Guide 1.132, "Site Investigations for Foundations of Nuclear Power Plants" (***Reference 5.13.9***),	Sec. 2.1	Recommends geological and geophysical characterisation for evaluating site safety.	5.13.3.3

© Eskom 2026/Rev 0a

US Nuclear Standard ANSI/ANS-2.27-2008, "Criteria for Investigations of Nuclear Facility Sites for Seismic Hazard Assessments" (***Reference 5.13.10***)	Sec. 4.1, 4.2	Recommends investigations to support seismic source characterisation for PSHA and fault rupture hazard assessments.	5.13.3.3
US NRC NUREG/CR-6966, "Tsunami Hazard Assessment at Nuclear Power Plant Sites in the United States of America" (***Reference 5.13.11***)	Section 2.5 Site Investigation	Methods for identifying tsunami sources.	5.13.3.3

5.13.3.1 NNR Position Paper

The most recent and up-to-date national guidance document (albeit in draft form and out for comment with the relevant stakeholders in SA) relevant to the development of geological databases for the analysis of site specific external events is the NNR Position Paper PP-0014 on "Considerations of External Events for New Nuclear Installations" (***Reference 5.13.3***). This document outlines considerations for conducting site investigations for evaluation of hazards related to external events, including those that rely on geological, geophysical, seismological, and geotechnical databases. Applicable sections of the document are the following:

- Chapter 10 Requirements for Seismic Events. Geologic, seismic, and geophysical data needed to identify and evaluate potential seismic sources for purposes of probabilistic seismic hazard analysis and surface faulting potential are identified. IAEA regulatory guidance is indicated as being acceptable for seismic hazard evaluation.

- Section 10.4 Surface-Fault rupture and criteria for a capable tectonic source. Geological and seismologic criteria are given for evaluating whether a fault is a capable tectonic source that can generate both vibratory ground motions and tectonic surface deformation. Applicable data must be compiled and evaluated to arrive at this assessment.

- Section 11.1 Geological and geotechnical hazards. Geological and geotechnical data should be compiled that can be used to assess surface rupture due to faulting, liquefaction, collapse and slope instability due to the occurrence of an earthquake. Note that the evaluation of the data and the assessment of these hazards are given in ***Section 5.14*** (Seismic Hazard Analysis) and ***Section 5.15*** (Geotechnical Characterisation).

- Appendix B Technical Attributes for External Events. To assess seismic activity, technical characteristics and attributes should be "based on comprehensive data including geological, seismological and geophysical."

© Eskom 2026/Rev 0a

- Appendix E Capable Fault Parameters. Specifies the time period for consideration of whether or not a fault is capable, as a function of design bases and performance goals.

Although the NNR position paper promotes the compilation of geological databases and provides general guidelines for their development, detailed specification of the scope of the required investigations and their geographic extent is not provided. For that purpose, the relevant parts of international regulatory guidance documents have been used to guide the development of the geological databases, as described below in ***Subsections 5.13.3.2*** (IAEA Requirements and Guides) and ***5.13.3.3*** (US NRC Regulatory Guidance).

5.13.3.2 International Atomic Energy Agency Requirements and Guides

A source of guidance applicable to the development of geological databases is the guidance provided by the IAEA. The requirements for geological, seismological, geophysical and geotechnical characterisation studies are provided in the applicable parts of the following documents:

- IAEA Safety Requirements NS-R-3 “Site Evaluation for Nuclear Installations” (***Reference 5.13.4***). This document requires that “the seismological and geological conditions in the region and the engineering geological aspects and geotechnical aspects of the proposed site area shall be evaluated” for purposes of assessing earthquakes and surface faulting, and geotechnical hazards.

- IAEA Specific Safety Guide SSG-9 “Seismic Hazards in Site Evaluation for Nuclear Installations” (***Reference 5.13.5***). In “Chapter 3 Necessary Information and Investigations”, this document identifies the recommended elements of a geological, geophysical and geotechnical database. The elements are given as a function of distance from the site.

- IAEA Safety Guide NS-G-3.6 “Geotechnical Aspects of Site Evaluation and Foundations for Nuclear Power Plants.” (***Reference 5.13.6***). Section 2 Site Investigation discusses the investigation programme and sources of data to establish geotechnical characteristics. Note that the geological databases pertinent to geotechnical characterisation (e.g., rock types, formations, thicknesses) of the site are given in this chapter of the SSR, while the geotechnical properties related to dynamic soil properties are given in ***Section 5.14*** (Seismic Hazard Analysis), and the evaluation of geotechnical characteristics and hazards is given in ***Section 5.15*** (Geotechnical Characterisation).

© Eskom 2026/Rev 0a

5.13.3.3 US NRC Regulatory Guidance

The applicable parts of US Nuclear Regulatory Commission regulations and regulatory guidance provide recommendations to assist in the development of geological databases.

The US regulation of pertinence to the development of geological information for purposes of siting nuclear installations is 10 CFR Part 100, Section 100.23, "Geologic and Seismic Siting Criteria" (***Reference 5.13.7***), which provides acceptance criteria for evaluating the suitability of a proposed site based on consideration of geological, geotechnical, geophysical, and seismological characteristics of the proposed site. Regulatory Guide 1.208, “A Performance-Based Approach to Define Site-Specific Earthquake Ground Motion” (***Reference 5.13.8***), Section C.1 “Geological, Geophysical, Seismological, and Geotechnical Investigations” and Appendix C “Investigations to Characterize Site Geology, Seismology, and Geophysics” are applicable to this chapter of the SSR.

Regulatory Guide 1.132, "Site Investigations for Foundations of Nuclear Power Plants” (***Reference 5.13.9***), describes geological and geotechnical site investigations that enable evaluation of site safety in relation to performance of foundations and earthworks under anticipated loading conditions, including earthquakes. The discussions of geological and geophysical characterisation are applicable to ***Section 5.13*** (Geology) and the discussions of characterisation of geotechnical properties are applicable to ***Section 5.15*** (Geotechnical Characterisation) of this SSR.

The regulatory guidance of the US NRC has recently been supplemented by a set of American National Standards, including ANSI/ANS-2.27-2008 “Criteria for Investigations of Nuclear Facility Sites for Seismic Hazard Assessments” (***Reference 5.13.10***). This document describes the types of site characterisation investigations that are recommended for various types of nuclear facilities. The guidance is consistent with that given in the US NRC regulatory guides and is used as a secondary source of information beyond the regulatory guides.

The identification of potential tsunamigenic sources, both near- and far-field, is discussed in the guidance given in US NRC NUREG/CR-6966 (***Reference 5.13.11***).

5.13.4 Approach to Evaluation

This subsection presents the approach used to develop a comprehensive geological database for the Thyspunt site, consistent with the

recommendations made in the applicable regulatory guidance.

5.13.4.1 Geographical Areas of Investigation and Data Compilation

In this subsection, the term “geoscientific” is used to indicate the collection of geological, geophysical, seismological, and geotechnical data that have been compiled to form the earth science knowledge base needed to demonstrate adequate site knowledge and to provide information for use in hazard analyses. The geoscientific data have been compiled from existing studies as well as from geoscientific investigations conducted over several years within the site region for purposes of evaluating alternative sites, site characterisation for licensing, and for purposes of the seismic hazard analysis. In line with regulatory guidance, the geoscientific investigations and compilation have been carried out at different scales for the site itself and the region surrounding the site.

The investigations and compiled geoscientific data provide increasingly detailed information as they proceed from the regional level down to the site. To this effect, the following areas are defined, in accordance with the radii recommended by the US NRC in ***Reference 5.13.8***:

- **Site Region**: area within 320 km of the site.
- **Site Vicinity**: area within 40 km of the site.
- **Site Area**: area within 8 km of the site.
- **Site Location**: area within 1 km of the site.

These distances and terminology are essentially equivalent to the distances recommended in the IAEA guidance (***Reference 5.13.5***) and they are displayed for the Thyspunt site in ***Figure F-5.13.1***. The investigations compiled for these areas are summarised below in ***Subsection 5.13.4.2*** (Geoscientic Investigations Performed) and the technical findings and databases are described in more detail in *Subsection 5.13.5 (Site Region)*. The geoscientific knowledge base for the site region is summarised in ***Subsection 5.13.5.1*** (Regional Geology); for the site vicinity in ***Subsection 5.13.5.2.(a)***; for the site area in ***Subsection 5.13.5.2.(b)***; and for the site location in ***Subsection 5.13.5.2.(c)***. The detailed characterisation of the site area and site location is used to assess the potential for surface faulting beneath the proposed nuclear facility, given in ***Subsection 5.13.5.3.***

As noted above, the site region extends to a distance of 320 km from the site. However, a wider region surrounding the site was considered for the identification of potential seismic sources required to assess the vibratory

ground-motion hazard at the site. Those more distant databases are briefly summarised in ***Subsection 5.13.5*** (Site Region) and are described in more detail in ***Section 5.14*** (Seismic Hazard Analysis) and the associated PSHA report (***Reference 5.13.1***).

In addition to the areas presented above, near and distant sources that have the potential to generate tsunamis at the proposed site have also been investigated (see ***Subsection 5.13.5.4***).

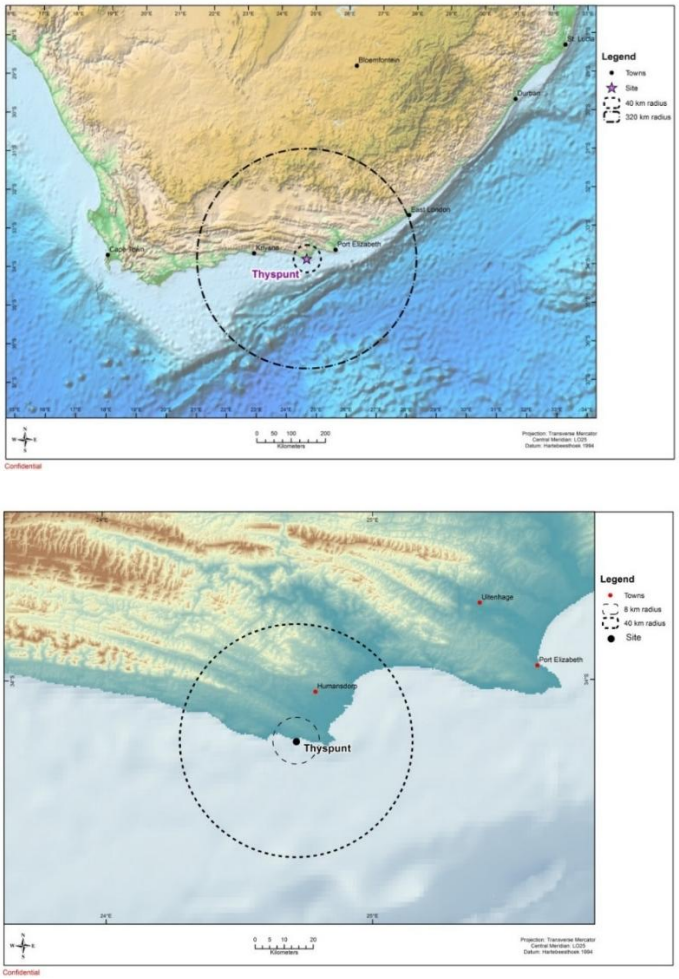


Figure 5.13-1 (a) Locality Map Showing the 320 km Radius Site Region and 40 km Radius Site Vicinity.
(b) Locality Map Showing the 40 km Radius Site Vicinity, 8 km Radius Site Area, and 1 km Radius Site Location (represented by the dot)

5.13.4.2 Geoscientific Investigations Performed

The primary objective of the geological and geophysical investigations is to support the development of an up-to-date, regional and site-specific earth science knowledge base as part of the site characterisation. The knowledge base is documented in the reports associated with the various investigations (***Table T-5.13.2***) and includes the results of both surface and subsurface investigations as recommended in the international regulatory guidance (***References 5.13.3*** and ***5.13.6***). The geoscientific disciplines that were considered and, where relevant, applied during the site investigations included: specialised aspects of geology; geophysics; seismology and geotechnical characterisation. The nature of the investigations carried out, as well as the particular techniques employed to carry out the investigation, were specific to the area being studied. For example, some techniques were applicable to the onshore region but not the offshore, and vice versa. Also, the level of detail for the geoscientific investigations and techniques employed varied as a function of whether the studies were conducted to understand the regional geological setting or to enhance the knowledge of the geological conditions within the site vicinity or site area.

The most important geoscientific investigations that contribute to the geological knowledge base for the Thyspunt site are summarised in ***Table T-5.13.2*** according to the type of investigation (geological mapping, geophysics, etc.) and the principal location of the study (site region, site vicinity, etc.).

a) Studies Conducted for Nuclear Site Investigation Programme (NSIP)

The first geological and geophysical investigations at, and in the vicinity of the Thyspunt site, were performed by the Atomic Energy Corporation (AEC, now NECSA) as part of the Nuclear Site Investigation Programme (NSIP) that first commenced in the 1980s***.*** Historical map data from the former AEC was summarised in ***Reference 5.13.21***, with more detailed maps of the site provided in ***References 5.13.22*** and ***5.13.28***. A considerable body of supporting work had been utilised in the development of these maps. This work had been conducted in preceding years (early to mid-1980's) with the focus on the Tsitsikamma coastline up to Cape St. Francis (***References 5.13.12*** and ***5.13.23***). Important sources of information include, among others, the detection of several faults in the site vicinity by geophysical investigations (***Reference 5.13.38***), geological appraisal of faulting in the project area (***Reference 5.13.23***), a preliminary rock-mass classification of the site (***Reference 5.13.29***), and detailed mineralogical studies of several selected site samples (***Reference 5.13.49***).

© Eskom 2026/Rev 0a

Table 5.13.2
Geoscientific Investigations Conducted in the Thyspunt Site Region, Vicinity, Area, and Location

Investigation[1]	Region	Vicinity	Area & Location
Geological Mapping	5.13.12 Norman, Andersen, et al. 1986 5.13.13 Goedhart 2004 5.13.14 Goedhart 2005 5.13.15 Goedhart 2006 5.13.16 De Beer 2004 5.13.17 Prasad & Claassen, 2012 5.13.18 Reddering et al., 2012 5.13.19 Mitha et al., 2013 5.13.20 McCalpin 2009	5.13.21 Van Wyk, 1987 5.13.22 Norman et al. 1987 5.13.12 Norman, Andersen, et al. 1986 5.13.23 Norman, Joubert, et al. 1986 5.13.24 De Beer 2005 5.13.25 De Beer 2006a 5.13.26 Goedhart 2007b 5.13.27 Goedhart et al., 2008	5.13.28 Raubenheimer et al. 1988 5.13.23 Norman et al., 1986b 5.13.29 (Engineering geology) Mountain & Partners 1988 5.13.30 De Beer 2000 5.13.27 Goedhart et al., 2008
Geophysics:			
Aeromagnetic		5.13.31 Anderson et al., 1986 5.13.26 Goedhart 2007b 5.13.32 Cole 2008	5.13.31 Andersen et al. 1986 5.13.33 Muller et al. 1986a 5.13.34 Muller et al. 1986b 5.13.35 Cole & Naudé 2007 5.13.36 Goedhart & Cole 2007 5.13.37 Goedhart 2007a
Gravity		5.13.38 Muller Andersen and Hennop 1986 5.13.32 Cole 2008	5.13.39 Faurie et al. 1986
Ground & marine magnetic		5.13.26 Goedhart 2007 5.13.32 Cole 2008	5.13.40 Raath & Cole 2007 5.13.41 Cole & Cole 2007 5.13.37 Goedhart 2007a
Electro-magnetic		5.13.42 Stettler et al. 2008a 5.13.43 Stettler et al. 2008b 5.13.44 Zadorozhnaya et al. 2012	
Seismic reflection	5.13.45 Roux 2011	5.13.46 Horwood 2009 5.13.45 Roux 2011	5.13.47 Fugro Survey Africa 2007b 5.13.48 Fugro Survey Africa 2007a 5.13.37 Goedhart 2007a

© Eskom 2026/Rev 0a

Investigation[1]	Region	Vicinity	Area & Location
Seismic refraction			5.13.39 Faurie et al. 1986
Mineralogy			5.13.49 Brynard et al. 1988
Geochronology	5.13.50 Roberts 2006 5.13.51 Bierman 2012a 5.13.52 Bierman 2012b 5.13.53 Forman 2012b 5.13.54 Hanson et al., 2012b	5.13.52 Bierman 2012b 5.13.55 Forman 2012a	5.13.56 Roberts 2004 5.13.57 Roberts 2005 5.13.50 Roberts 2006 5.13.52 Bierman 2012b
Geomorphology	5.13.51 Bierman 2012a 5.13.52 Bierman 2012b 5.13.54 Hanson et al., 2012b	5.13.52 Bierman 2012b 5.13.58 Hanson et al. 2012a	5.13.56 Roberts 2004 5.13.57 Roberts 2005 5.13.50 Roberts 2006 5.13.52 Bierman 2012b 5.13.58 Hanson et al. 2012a 5.13.59 De Wet, 2012 (bathymetry)
Paleoseismic	5.13.13 Goedhart 2004 5.13.14 Goedhart 2005 5.13.15 Goedhart 2006 5.13.16 De Beer 2004 5.13.54 Hanson et al. 2012b 5.13.17 Prasad & Claassen, 2012 5.13.18 Reddering et al., 2012 5.13.19 Mitha et al., 2013 5.13.20 McCalpin 2009	5.13.24 De Beer 2005 5.13.25 De Beer 2006a 5.13.58 Hanson et al. 2012a	5.13.58 Hanson et al. 2012a
Geotechnical (including borehole geology and down-hole geophysics)		5.13.31 Anderson et al., 1986	5.13.28 Raubenheimer et al. 1988 5.13.29 (Engineering geology) Mountain & Partners 1988 5.13.60 Eskom 2010a 5.13.61 Eskom 2010b 5.13.62 Engelsman, & Constable 2012 5.13.63 Park 2011 5.13.64 Rathje et al. 2012

[1] If an investigation is applicable to multiple regions, it is listed in each of the applicable regions.

© Eskom 2026/Rev 0a

In 1984 the Marine Geoscience Division of the National Research Institute for Oceanology carried out side-scan sonography and seismic profiling of an area on the Agulhas Bank to the south of the site to investigate the geology and physiography of the seafloor (***Reference 5.13.38***). The results of the investigation showed several sedimentary units separated by unconformities. Palaeozoic Table Mountain Group (TMG) rocks form the rocky inner shelf, followed seaward first by Mesozoic-age sediments (Uitenhage Group) and then by Paleogene and Neogene-age deposits towards the shelf edge. Faulting was found to be common near the Plettenberg Fault, which generally marks the Palaeozoic–Cretaceous contact.

Aeromagnetic investigations that had been carried out in the site vicinity, particularly a detailed aeromagnetic survey southward of Humansdorp, were interpreted and documented in ***Reference 5.13.31***. This resulted in improved geological maps that depicted the broader picture of the area's stratigraphy, folding and faulting. Three directions of faulting were identified, namely, north-west, north-north-east and north-east. The Bokkeveld syncline, to the north of Cape St. Francis, was seen to open towards the east, indicating that the major folds plunged eastwards.

A reconnaissance gravity survey of selected sites between Cape St. Francis and the Tsitsikamma River was performed in 1986 (***Reference 5.13.38***). Three traverses in the coastal area south of Humansdorp disclosed undulating basement topography. The main feature identified was the relatively small depressions or inlets with maximum depth of 40 m below mean sea level (mbmsl). These features are probably associated with Quaternary-age regression–transgression cycles. They are also evident at other places along the South African coast and could be attributed to differential erosion of contrasting lithologies. Older fault-controlled basins with infill of Mesozoic-age material, such as the ones that occur more than 30 km to the northeast in the Gamtoos Basin, were not found within the survey area.

A gravity and seismic refraction survey at the site, amongst others, was also completed and the results documented in ***Reference 5.13.39***. One long gravity profile was developed along the beach, whereas four seismic traverses were carried out further inland. Two control boreholes were drilled on the geophysical lines. The investigation indicated bedrock of gentle relief along the lower coastal plain. In addition, the geotechnical investigation of surficial deposits and bedrock at the site was conducted (***Reference 5.13.29***).

b) Studies Conducted by Council for Geoscience for Thyspunt Site Characterisation.

Following the work conducted in the 1980s to evaluate multiple possible sites, further studies were carried out in the 2000s under the leadership of the Council

for Geoscience (CGS). In late 2003, the need for palaeoseismic data for the Thyspunt PSHA resulted in the Council for Geoscience (CGS) being contracted to undertake Palaeoseismic-Neotectonic investigations. A summary of the knowledge of the geological and tectonic setting was provided in ***Reference 5.13.30.*** Initially, three projects were undertaken on a regional scale, namely:

- a study of coastal warping (***References 5.13.56***; ***5.13.57*** and ***5.13.50***);
- a palaeoseismic trenching study of Quaternary-age reactivation along the Ceres–Cango–Baviaanskloof–Coega fault system (***References 5.13.13*** to ***5.13.15***); and
- an investigation of the potential for neotectonic reactivation along known and newly identified faults in the intervening coastal region (***References 5.13.16***, ***5.24.24***, and ***5.13.25***).

Reference 5.13.16 provided a literature review of the available palaeoseismic-neotectonic data for the South African coastal region. Additional regional geological information and the results of reconnaissance palaeoseismic investigations were later added in ***Reference 5.13.24****.* This latter report also contains a list of potentially hazardous geological features for the site vicinity (see Table 9 of ***Reference 5.13.24***)***.*** This list served as the basis for discussions concerning the integration of Palaeoseismic-Neotectonic investigations data into assessments of seismic hazard at the site.

Technology has advanced greatly from that used in the earlier (1980's) studies, which led to improved resolution of identified features. On that basis Eskom Holdings, in late 2006, commissioned a new round of airborne, ground and marine geophysical surveys over the site. The onshore airborne magnetic surveys were supported by ground follow-up methods such as magnetics, electro-magnetics (EM34) and multi-electrode direct current profiling. The off-shore geophysical investigations included magnetic, multibeam, bathymetry, side-scan sonar and sub-bottom profiling techniques. Both the aeromagnetic and marine-magnetic surveys completely covered the 8 km Site Area and part of the 40 km site vicinity, providing very good high-resolution geophysical information (***References 5.13.47*** and ***5.13.48***).

The difficulty and danger involved with acquiring marine data in shallow water precluded coverage of a narrow 'inshore' part of the area (***Reference 5.13.47***). Since there was an indication that the Cape St. Francis Fault (see ***Section 5.13.5.1.(d) iv*** might pass along the coastline close to the site, a second marine survey was undertaken by a smaller specialised vessel over two small areas in the inshore zone to try and delineate this fault

(***Reference 5.13.48***). These surveys managed to partly extend the survey coverage into the surf zone. Details of the airborne and ground geophysical surveys are described in ***Reference 5.13.35***. Follow-up ground geophysical traverses are also outlined in ***Reference 5.13.40***. One of the more important geophysical anomalies, the northeast – southwest trending aeromagnetic lineament, termed SV1, is reviewed and discussed in ***Reference 5.13.36***. This structure, which is located 6 km northwest of the site, is considered to be an old fault related to a period of geological extension during the Cretaceous. The CGS's interpretation of Fugro's off-shore magnetic data and its overlap with the airborne geophysical survey is described in ***Reference 5.13.41***.

The above-mentioned airborne and marine geophysical data were reviewed in 2006 (***Reference 5.13.25***), from which it was concluded that while the additional work provided very useful data, it provided little insight into the timing of last movements along geological faults. Therefore, the further refining of the geological model for the area required more detailed palaeoseismic investigations within the site vicinity and the site area (***Reference 5.13.26***) and, where necessary, of faults beyond the site vicinity.

During 2008 further geological and geophysical work was conducted in the site vicinity and the site area. Existing regional gravity data (one reading about every 12 to 14 km^2) and airborne magnetic data (line spacing 1 km) were interpreted for the site vicinity. This was carried out in order to fill the missing information from the high resolution airborne magnetic survey of 2006, which only covered the area within 25 km of the proposed site location. The regional nature of the data meant that only large-scale features could be detected. The gravity data showed a broad correlation with the geological map. In addition, the magnetic data showed the continuation of magnetic lithological units of the Cape Super Group to the west (***Reference 5.13.32***).

The possible northwest extension of the Cape St. Francis off-shore fault into the Thyspunt site vicinity on-land has been investigated by a number of geophysical methods, including airborne and ground magnetic surveys, and a time-domain electromagnetic investigation. No single method could confirm the potential presence of such an extension. Recommended time-domain electro-magnetic (TDEM) studies were completed in 2008 (***Reference 5.13.42***). The results of this TDEM study suggest that three of the potential sites for the onshore extension of the fault could be discarded. Several newly-identified lineaments were also considered as potential faults qualifying as candidates for an on-land extension of the Cape St. Francis Fault. A reinterpretation of the TDEM results in conjunction with recent geological observations (***Reference 5.13.43***) indicated that there is an alternative, probably more correct model for the Cape St. Francis Fault dying out before reaching the

© Eskom 2026/Rev 0a

onshore. As will be discussed in ***Subsections 5.13.5.1.(d) iv*** and ***5.13.5.3.(b)***, lack of evidence of surface deformation in the site area and St Francis coast, including along the projected trends of the Cape St Francis Fault, indicates that even if the Mesozoic fault extends onshore, it has not displaced Quaternary deposits or geomorphic surfaces.

High resolution geophysical data gathered in the site vicinity were used in conjunction with geological information from the onshore area to develop structural interpretations of the major geological units and contacts (***Reference 5.13.46***). Extensive follow-up work was conducted in 2008, including a comprehensive review and verification of existing geological data with available geophysical and remote sensing data (***Reference 5.13.27***). Furthermore, this investigation focused on mapping areas in the vicinity of known or inferred faults, fractures and lineaments, adding detailed new information. As a result some earlier postulated north-westerly orientated 'strike faults' and several high-angle 'cross faults' could be eliminated. For instance, many linear features proved to be old joints filled with magnetic material (due to ground-water percolation). A further result of the field-verification process was a substantially 'cleaner' set of geological maps covering the Site Area and the Site Vicinity on scales of 1:5 000, 1:10 000 and 1:50 000 (***Reference 5.13.27***).

c) Studies Conducted to Support the Probabilistic Seismic Hazard Analysis (PSHA)

In light of the history of geological and geophysical investigations discussed above, a number of geological investigations were conducted in 2009 to 2012. These studies were led by the CGS, included several international geological experts, and were designed specifically to provide data to support the PSHA (***Reference 5.13.1***) and summarised in ***Section 5.14*** (Seismic Hazard Analysis) and the assessment of surface faulting (***Subsection 5.13.5.3***). The reports for each of the Geological Investigation (GI) studies are included as appendices to ***Reference 5.13.1***.

The PSHA project team conducted GI studies to evaluate potential seismic sources for the Thyspunt site as well as to define the geological and geotechnical conditions of the site location. The goal of these investigations was to collect additional data and information that would significantly reduce the epistemic uncertainties associated with the identification and characterisation of seismic sources, particularly seismogenic faults, for the Thyspunt PSHA. The GI studies included fault corridor studies along selected major faults in the Eastern Cape and marine terrace investigations. As part of the data evaluation process for the PSHA, various onshore and offshore datasets were presented and evaluated (for example, ***Reference 5.13.45***). Additionally, a new offshore bathymetry data set (***Reference 5.13.59***) was

© Eskom 2026/Rev 0a

used along with other onshore data to evaluate both seismogenic probability and slip rate for offshore fault sources. Faults evaluated in the fault corridor investigations included the Kango, Baviaanskloof, Western Coega, Eastern Coega, and Kouga fault zones. The studies included reconnaissance-level studies (***Reference 5.13.20***) followed by more detailed geological mapping (***References 5.13.17***; ***5.13.18*** and ***5.13.54***) and interpretations of the subsurface geology from borehole data (***Reference 5.13.19***). The results of the studies provided data that were used to evaluate the seismogenic probability of these faults and source characterisation parameters for identified fault sources in the seismic source characterisation (SSC) model. The only fault in the site region with evidence for Quaternary activity is the Kango Fault (discussed in ***Subsection 5.13.5.1.(d) v*** and shown in ***Figure 5.13.150*** relative to the site location) and paleoseismic investigations of the fault were conducted to assess its late-Quaternary behaviour (***Reference 5.13.54***). These studies included various types of age-dating to understand the timing of fault displacements, including cosmogenic nuclides (***Reference 5.13.51***) optically stimulated luminescence (***Reference 5.13.53***), and radiocarbon dating (***Reference 5.13.54***).

Marine terrace investigations were conducted in the Thyspunt site area and surrounding region as part of the GI programme (***Reference 5.13.58***). The objectives of the marine terrace investigations were to provide additional data to evaluate regional uplift processes and rates, to evaluate patterns of uplift to identify and characterise potential capable tectonic sources, and to document the continuity and ages of marine terraces at the Thyspunt site to evaluate the potential for surface tectonic faulting and deformation. A detailed field mapping programme was conducted in the Oyster Bay to Cape St. Francis study area. Together with new borehole and time-domain electromagnetic data, this was used to compile maps and shore-parallel profiles that show field localities, topographic profiles, top of bedrock elevations, geochronology sample locations, and correlation of terraces. Geochronology analyses included cosmogenic nuclides (***Reference 5.13.52***) and optically stimulated luminescence (***Reference 5.13.55***). The results of studies in the area that includes the Thyspunt site, address the seismogenic probability of offshore faults (i.e., the Cape St. Francis fault zone) and minor northeast-trending secondary faults documented by onshore bedrock mapping and interpretation of offshore seismic data.

In addition to the geological investigations of the fault corridors and the marine terrace sequence, extensive borehole and geophysical studies were conducted in the site area and location to further characterise the stratigraphy, layer thicknesses, and geotechnical characteristics. These studies (summarised in ***Subsections 5.13.5.2.(b)*** and ***5.13.5.2.(c)***) included geotechnical

characterisation (***References 5.13.60*** and ***5.13.61***) as well as a variety of geophysical, borehole, and laboratory studies to assess the dynamic geotechnical properties of the materials at the site for evaluating its seismic response for the PSHA (***References 5.13.62*** to ***5.13.64***). The geological results of those studies were used as input to the PSHA (***Section 5.14***) and their use along with other databases for geotechnical purposes is summarised in ***Section 5.15*** (Geotechnical Characterisation).

In association with the PSHA, a major effort was devoted to developing an earthquake catalogue that includes both historical and instrumental earthquakes. This earthquake database in discussed in detail in the PSHA report (***Reference 5.13.1***) and is summarised in ***Section 5.14*** (Seismic Hazard Analysis).

A review of near and distant potential sources of tsunami genesis along the coastline of South Africa (summarised in ***Subsection 5.13.5.4***) was also undertaken in 2008 (***References 5.13.65*** and ***5.13.66***) to inform any numerical modelling designed to predict the sources, frequency and height of tsunami that could impinge on the southern African coast.

5.13.5 Characteristics of the Regional and Site Geology

This subsection is focused on the geological characteristics of the region (***Subsection 5.13.5.1***), followed by a description of the geology of the Thyspunt site (***Subsection 5.13.5.2***), which includes the site vicinity, site area, and site location. This subsection also includes the evaluation of the potential for surface faulting at the Thyspunt site (***Subsection 5.13.5.3***) and the identification of tsunamigenic sources (***Subsection 5.13.5.4***).

5.13.5.1 Regional Geology

This subsection describes the physiography, geological history, stratigraphy, tectonic setting and structures within the Thyspunt site region (320 km radius). To provide a context and a framework for that discussion, elements of the regional geological and tectonic environment that extend beyond the 320 km radius are also discussed, where applicable.

a) Regional Physiography and Topography

This section discusses the physiographic characteristics of the site region from the offshore to onshore. The site region (320 km radius from the site; ***Figure F-5.13.1***), includes portions of the continental shelf, slope, and abyssal plain offshore, and coastal belt, Cape Fold Belt, Karoo and Great Escarpment onshore. Physiographic regions in southern Africa covered in this section are

© Eskom 2026/Rev 0a

shown on ***Figure F-5.13.2***. The south coast of southern Africa is characterised by its wide, generally flat continental shelf. Along the coast, extensive dune systems cover portions of flights of marine terraces and coastal plain. Landward of the coast, resistant units within the Cape Fold Belt form mountains. These mountains are separated from the higher elevation central portion of the continent by the Great Escarpment.

i Abyssal Plain

The abyssal plain is present in the south eastern portion of the site region. It is characterised by a fine grained sediment cover overlying oceanic crust.

ii Submarine Plateaus and Ridges

The site region includes a small corner of the Agulhas Plateau, a large igneous province formed in the Cretaceous (see ***Subsection 5.13.5.1.(b) ii*** – Mesozoic Geological History). The Agulhas Plateau rises more than 2,500 m above the surrounding seafloor and is more than 800 km long and 350 km wide at its maxima. Some locations on the plateau are coated in sediment mounds deposited by oceanic currents (***Reference 5.13.67***).

The Diaz Marginal Ridge runs parallel to the edge of the continental shelf in the zone of transition between continental and oceanic crust. The ridge is up to 350 km long and 40 km wide and in 3–4 km deep water. The ridge is formed by a series of rock outcrops (***Reference 5.13.68***) with a sediment cover of up to 500 m (***Reference 5.13.69***). The Diaz Marginal Ridge consists of sedimentary or metasedimentary rocks deformed during the breakup of Gondwana (***References 5.13.70*** and ***5.13.69***).

iii Continental Margin

The continental margin of southern Africa is characterised by its wide continental shelf (approximately 270 km wide south of Cape Agulhas) with a shelf break shoaling from 200 m off Cape Agulhas to approximately 140 m south of Port Elizabeth (***Reference 5.13.71*** and ***Figure F-5.13.2***). The origin of South Africa's continental margin is a direct consequence of the breakup and separation of western Gondwana (***References 5.13.72***, ***5.13.73***, and ***5.13.74***).

The rifting commenced in the Mesozoic, with separation (drifting) beginning in the Early Cretaceous. This created the dextral shearing of the South African margin and resulted in the formation of the Outeniqua Basin (***Reference 5.13.75***) and the Agulhas Falkland Fracture Zone (the eastern, inactive end of the Agulhas Falkland Fracture Zone is referred to as the Agulhas Fracture Zone) along the continental boundary (***Figure F-5.13.3***).

© Eskom 2026/Rev 0a

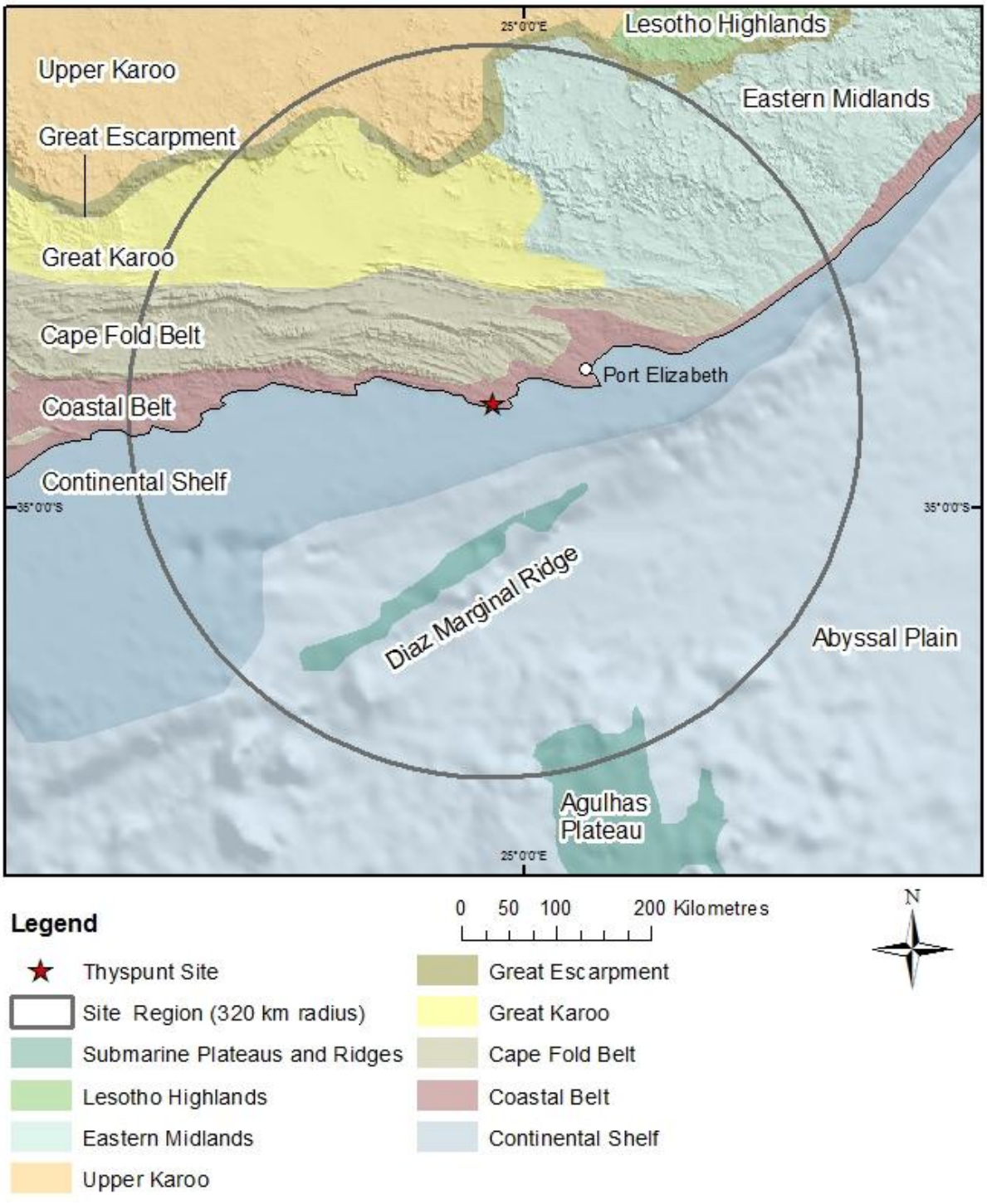


Figure 5.13-2
Physiographic Regions in Southernmost Africa

© Eskom 2026/Rev 0a

The Outeniqua Basin consists of a series of fault-bounded, sediment-filled sub-basins (the Bredasdorp, Pletmos, Gamtoos, and Algoa sub-basins) that merge into the Southern Outeniqua Basin offshore (***Figure F-5.13.3***). These sub-basins represent oblique-rift half-grabens (***References 5.13.73***, ***5.13.74*** and ***5.13.76***) and can be regarded as failed rifts that are progressively younger towards the west. Parsiegla et al. (***Reference 5.13.77***) distinguished between a northern area in the Outeniqua Basin that experienced one episode of extension, with stress directions perpendicular to the AFFZ, as a result of Gondwana rifting; and a southern area that underwent two phases of extension thinning associated with shear along the AFFZ. The division between these areas appears to correspond with the southern limit of the offshore faults in the Outeniqua Basin, as the offshore faults cannot be traced south of this line (***Reference 5.13.45***). It also corresponds roughly with the southern limit of the continental shelf (***Reference 5.13.73***). Currently, these basins are predominantly offshore but segments of the Pletmos, Gamtoos and Algoa Basins extend onshore. The modern onshore extensions of these basins are relatively flat bottomed river valleys. The Thyspunt site is located on the western flank of the Cape St. Francis Arch, which is a bedrock high between the Gamtoos and Plettenberg basins (***References 5.13.73*** and ***5.13.74***).

In general, the southern continental shelf of South Africa is characterised by a wide, flat outer shelf, a middle shelf rise at approximately 60–80 m water depth, a relatively flat inner shelf, and a narrow (approximately 2–14 km), sediment-free, rocky nearshore zone (***Figure F-5.13.4).*** No major valleys or canyons transect the south coast continental shelf (***Reference 5.13.78***).

Birch (***Reference 5.13.79***) identifies three major controlling factors of Quaternary deposition off the southern coast of South Africa: the effects of transgressive processes on the wide flat shallow shelf, a powerful littoral/longshore drift system, and coastal aeolian redistribution of bedload sediments.

The coastline is composed of a series of eastward-opening log-spiral bays (***Reference 5.13.80***). It is a high-energy coastline dominated by wave action (***Reference 5.13.81***).

© Eskom 2026/Rev 0a

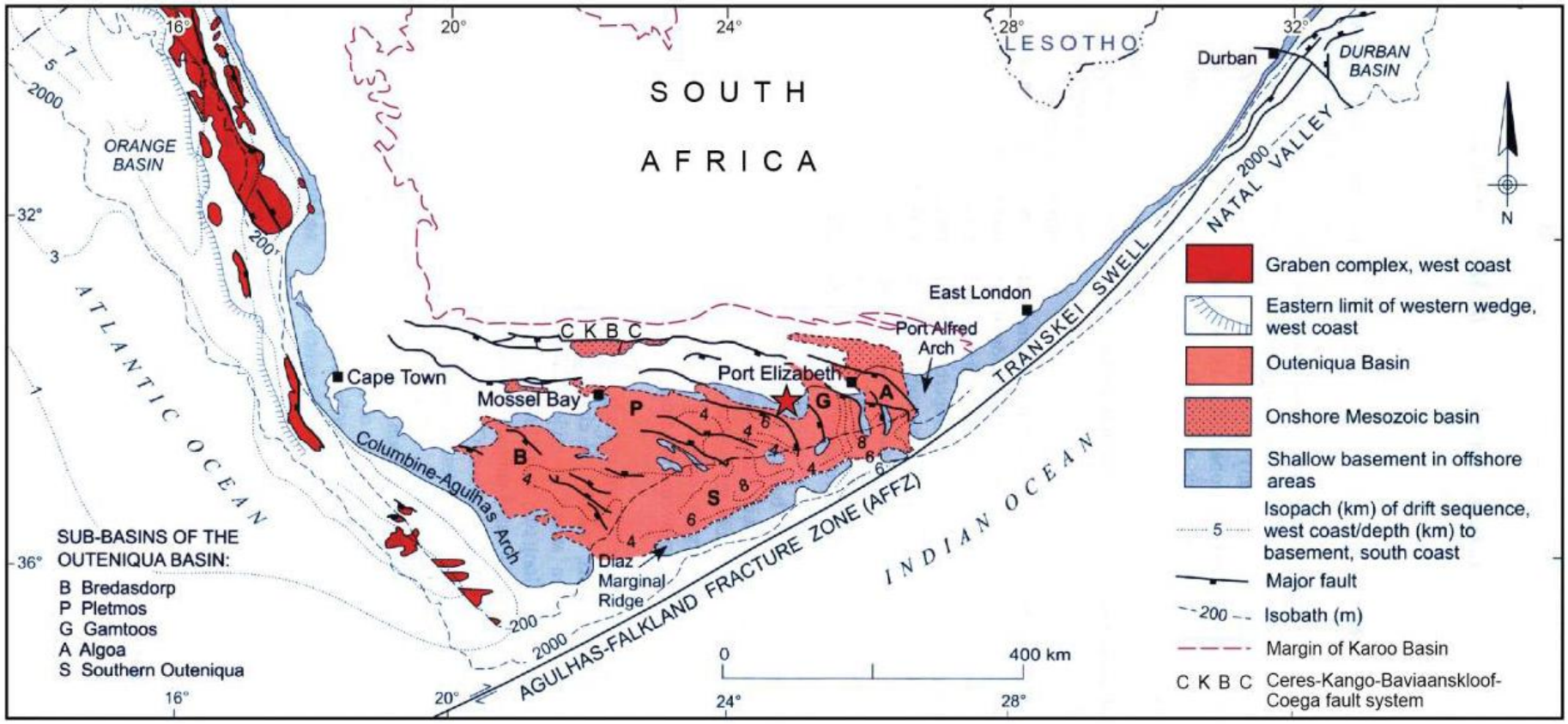


Figure 5.13-3
Map of the Southern Africa Showing the Major Mesozoic Structural Elements and Sub-Basins (Modified from *Reference 5.13.74*)

© Eskom 2026/Rev 0a

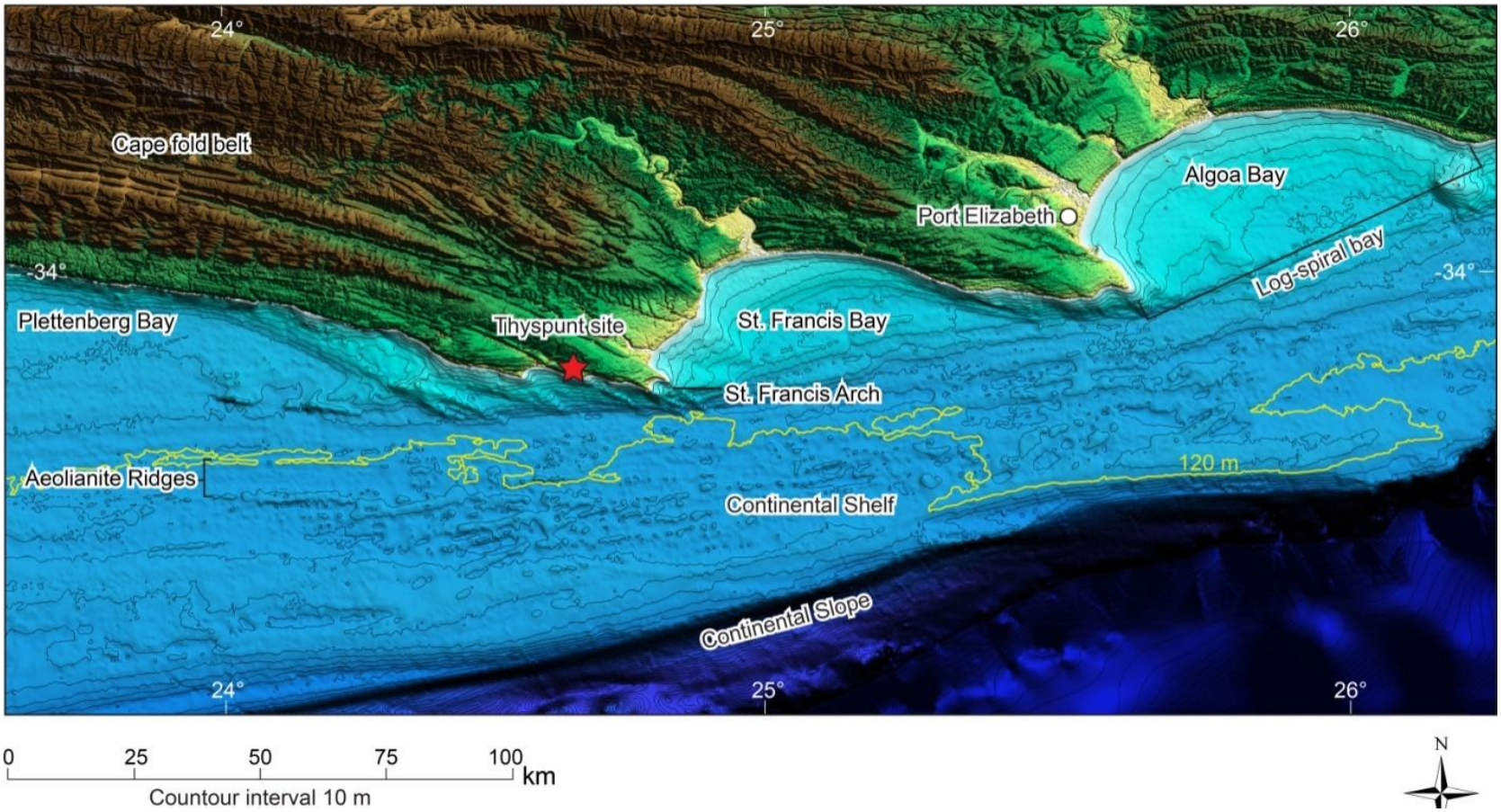


Figure 5.13-4
Combined Bathymetry and Topography near the Thyspunt Site with Details of the Physiography Labelled (Modified from *Reference 5.13.59*)

© Eskom 2026/Rev 0a

Sediments tend to shift onshore during the summer, filling coves and building beaches, whereas during the winter they are distributed seawards, exposing the gravel pavements and basement outcrop (***References 5.13.81*** and ***5.13.82***). The continental slope typically dips at 0.5°–2.5° and dips up to 8° near the Agulhas Falkland Fracture Zone (***Reference 5.13.83***).

iv Coastal Belt

The coastal belt encompasses the land surface between elevations of approximately 220 m to sea level. Partridge et al. (***Reference 5.13.84***) divide the coastal belt into the southern Coastal Platform and the Southern Coastal Lowlands. The seaward portion of the coastal belt contains active dunes and relict marine terraces. The landward portion covers silcrete coated platforms and deeply incised rivers.

Near the shore, active dunes form both dune cordons and headland bypass dune fields. Relict dunes related to Pleistocene and possibly older Pliocene sea-level fluctuations are present both on land and on the continental shelf. The major factors controlling sedimentation off the south coast of South Africa during the Quaternary are the effects of transgressive seas across a flat shallow shelf, a powerful littoral/longshore drift system and coastal aeolian transport (***Reference 5.13.79***). The Gouritz and Breede Rivers, located to the west of the site region, are the main sediment sources on the southern Cape continental shelf (***Reference 5.13.79***). It is argued, however, that a significant portion of the bedload of fluvial systems is lost through aeolian processes. For example, sands are trapped in the littoral zone by wave action resulting in the formation of extensive coastal dunefields. Nearly half of total bedload sediments off the south coast are located between Wilderness and Plettenberg Bays (***Reference 5.13.79***). Sediments are trapped in the large Wilderness embayment and the large submerged spit off Cape Seal (Robberg) on the southern edge of Plettenberg Bay (***Reference 5.13.80***). The spit defines the termination of the eastward-trending littoral drift system, associated mainly with transgressive seas, where circulation cells are recognised along the south coast (***References 5.13.79*** and ***5.13.71***).

Shoreline-parallel dune cordons are common geomorphic features along the southern coast of South Africa. Roberts et al. (***Reference 5.13.85***) discuss regional contrasts in dune system morphogenesis between the west and south coasts of South Africa, and attribute the differences between the dune plumes of the west coast and the dune cordons of the south coast to differences in climate-driven factors, chiefly differing wind regimes and rainfall patterns, which are ultimately mediated by major oceanographic systems (i.e., the cold Benguela Current and warm Agulhas Current). Inactive and lithified dunes of

© Eskom 2026/Rev 0a

various ages are present onshore and offshore (See ***Subsection 5.13.5.1.(c)*** – Regional Stratigraphy) for further discussion).

Headland-bypass dunefields are corridors of mobile transverse dunes that migrate across low-relief headlands (***Reference 5.13.86***). The coastal configuration of the south coast of the Western and Eastern Cape, South Africa, where a series of log spiral bays and associated headlands of the resistant quartzites of the Table Mountain Group are present, combined with the eastward transport of sediment due to the prevailing west-south-westerly wave and wind regime, result in the formation of headland-bypass dunefields whenever sandy beaches occur along the upwind shores of headlands. Examples of such dunefields are found at Cape Agulhas, Waenhuiskrans, Buffelsbaai, Cape St. Francis, and Cape Recife/Port Elizabeth (***Reference 5.13.86***). Hanson et al. (***Reference 5.13.58***) provide a compilation and summary of available information regarding the ages of palaeodune deposits along the coast in the site region.

Along the rocky coastline and underlying aeolian, marine and fluvial deposits, flights of marine terraces preserve the records of past sea-levels and uplift. Emergent marine terraces of various ages and elevations that occur along the entire southern African coastal belt are important geomorphic features that can be used to evaluate spatial patterns and differential rates of vertical crustal deformation or the lack thereof (***References 5.13.50*** and ***5.13.58***).

Preliminary observations have been made regarding regional patterns of marine terraces. Studies by Davies (***References 5.13.87***, ***5.13.88***, and ***5.13.89***) identified widespread evidence for past sea levels at 60, 30, 18, 9, 6, 3.5, and 1.5 m above sea level along the coastline of southern Africa (***Figures F-5.13.5***, ***F-5.13.6***, and ***F-5.13.7***). In some locations, evidence for shorelines up to 213 m above sea level were identified (***Reference 5.13.87***).

Roberts (***Reference 5.13.50***) observed staircase sequences of terraces rising from approximately 18 to 65 m on the west and southeast coasts. In addition, 90 m terrace remnants (mantled by the Pliocene Varswater and Miocene Kleinzee Formations) on the west coast appear to correlate with approximately 120 m terrace remnants (mantled by the Mio-Pliocene lower Alexandria and De Hoopvlei Formations) on the southeast coast, as indicated by comparisons of molluscan faunas (***Reference 5.13.50***). Hanson et al. (***Reference 5.13.58***) compiled available information from these earlier studies on the elevation and ages of marine terraces along the entire coastline of South Africa (***Figure F-5.13.6***). A shore-parallel profile showing the elevation of mapped terraces is presented in ***Reference 5.13.1*** Appendix 2, Plate A).

© Eskom 2026/Rev 0a

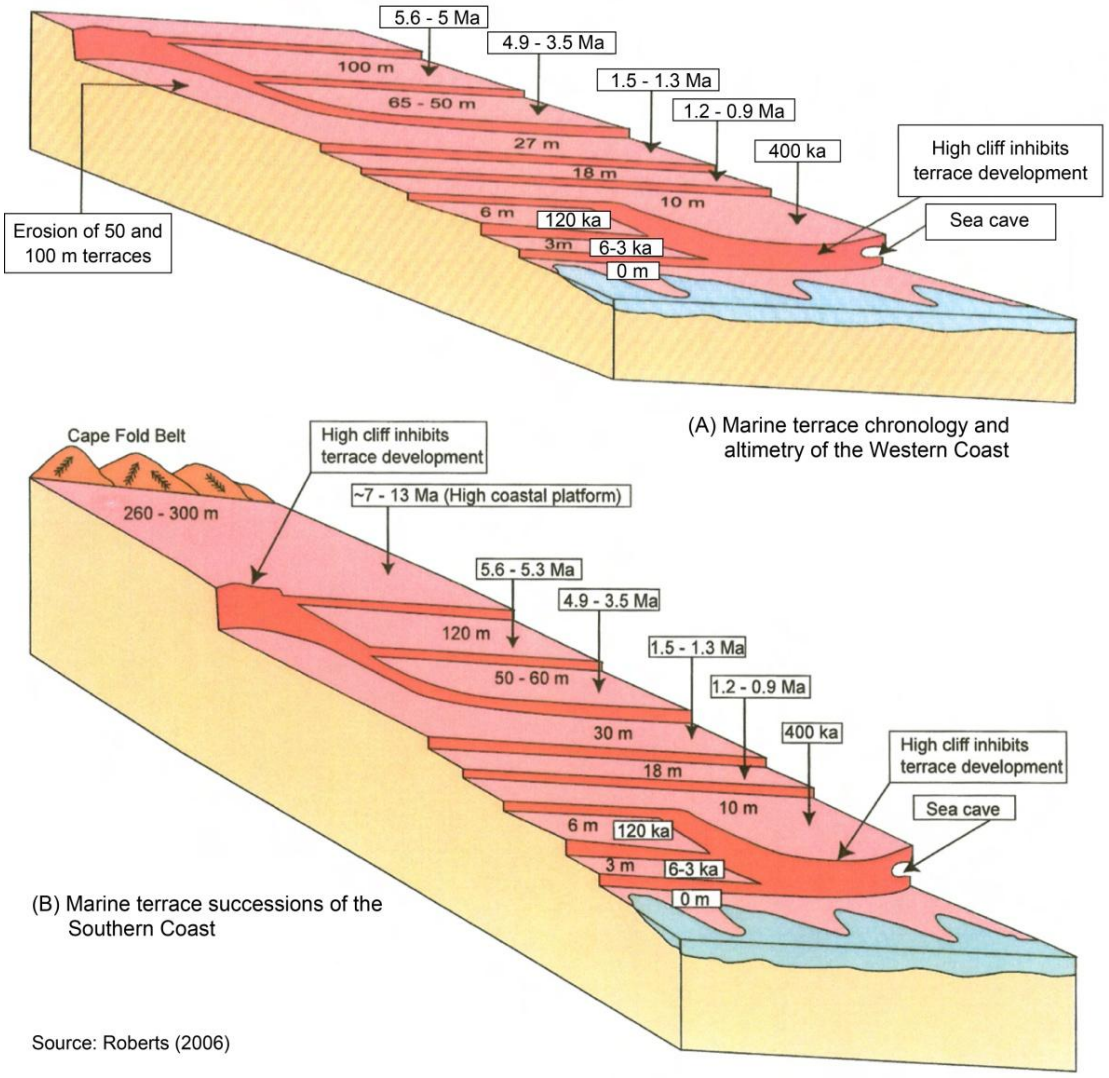


Figure 5.13-5
Elevations of Marine Terraces Along the Coast of South Africa (Modified from *Reference 5.13.50*).

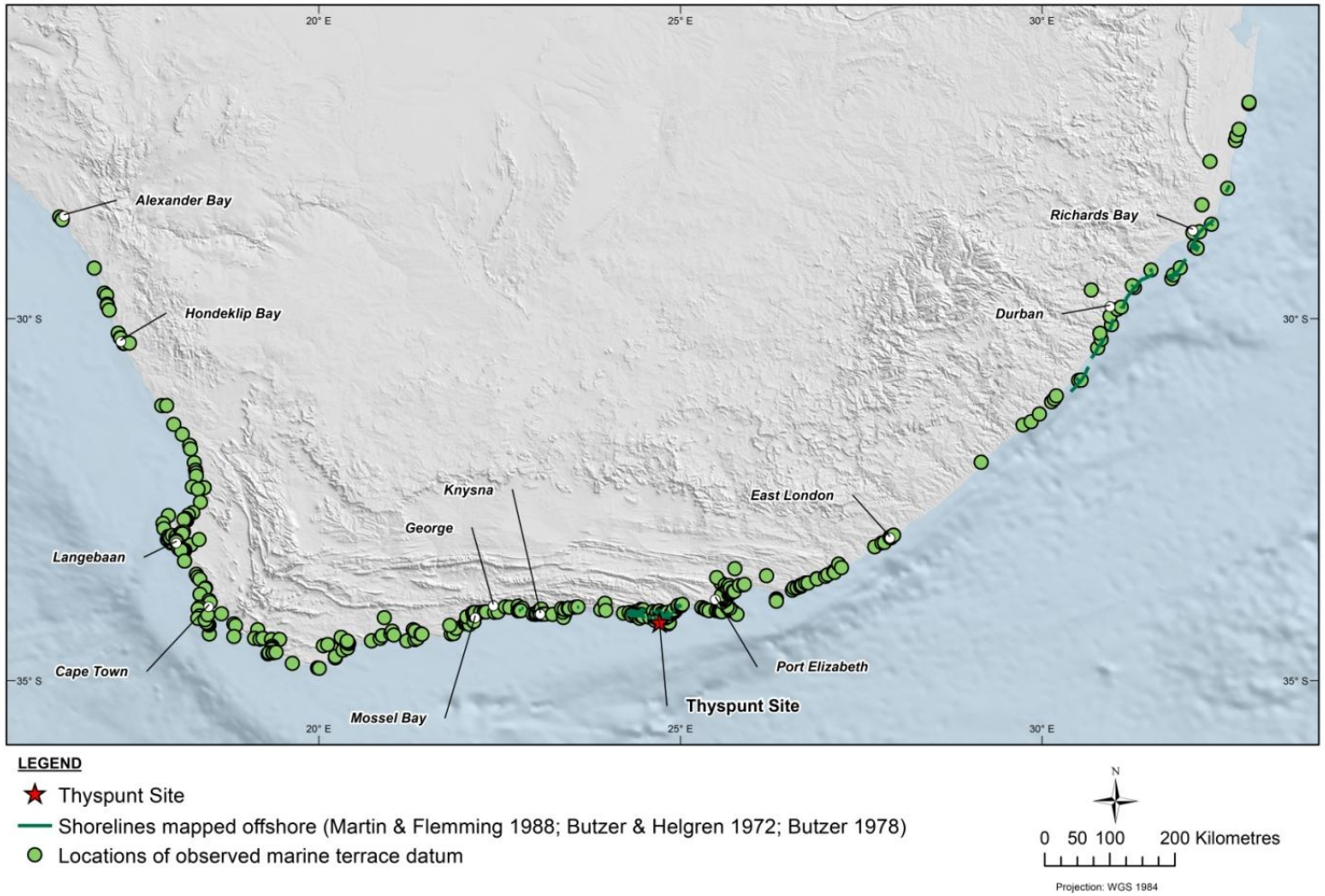


Figure 5.13-6
Regional Map of Marine Terraces (*Reference 5.13.58*)

© Eskom 2026/Rev 0a

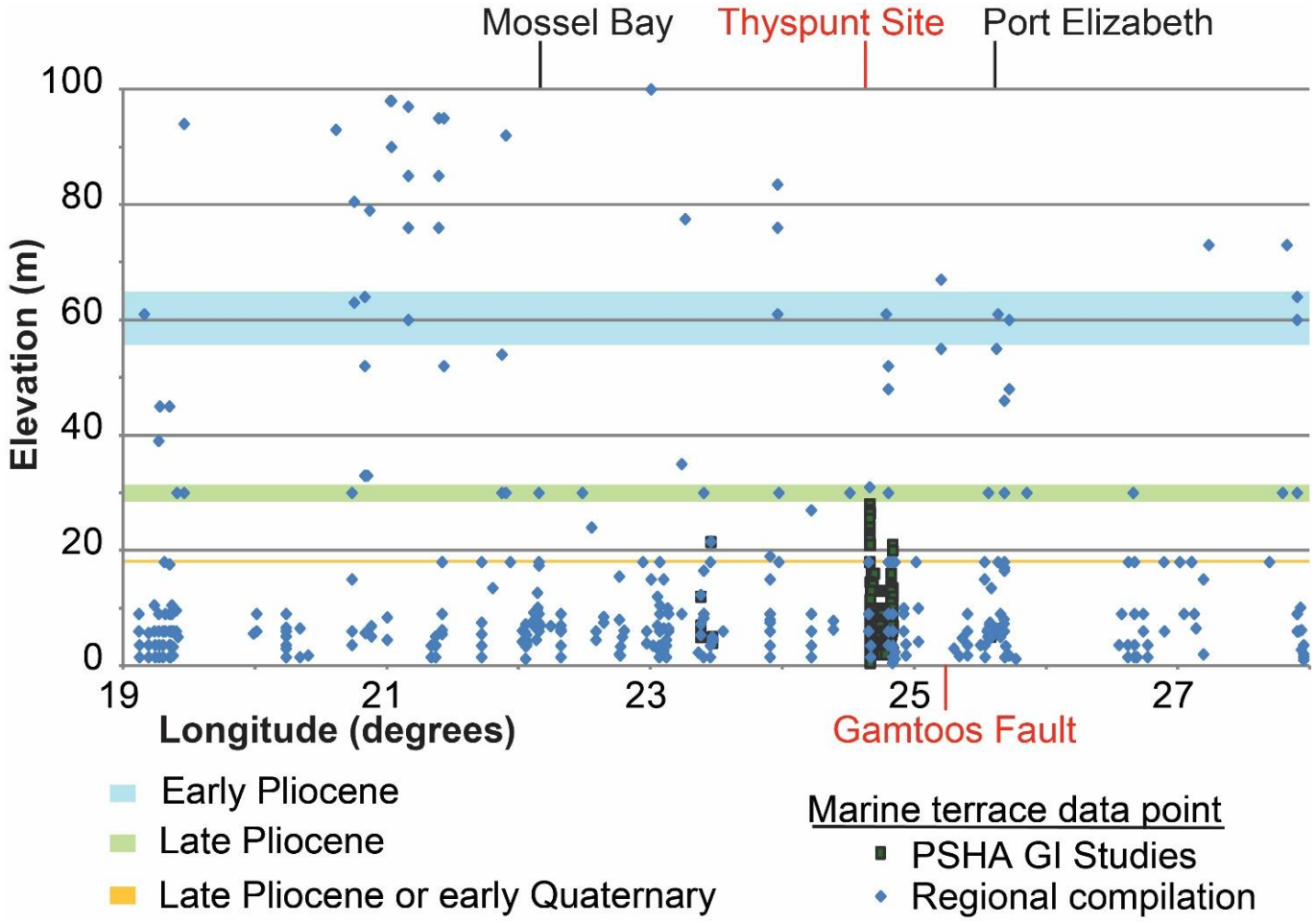


Figure 5.13-7
Shore-Parallel Correlation of Marine Terraces Along the Southern Coast of South Africa (*Reference 5.13.58*)

© Eskom 2026/Rev 0a

As shown on ***Figure F-5.13.7***, which presents a summary of the data near the Thyspunt site, terraces at elevations of 18 m, 30 m, and 60 m, are inferred to be earliest Pleistocene/late Pliocene to early Pliocene in age (***Reference 5.13.58***).

High geomorphic surfaces (possible pediments locally overlain by Grahamstown Formation [Tg]) occur landward of the coastal plain. Drainages on either side of the high geomorphic surface are incised approximately 50 m to more than 100 m below the surface. The Tg and underlying pediment surface at the bedrock alluvium contact are generally considered to be Miocene in age (***References 5.13.90*** and ***5.13.91***). Hagedorn (***Reference 5.13.92***) reports preliminary results of two electron spin resonance tests that indicated ages of 7.3 Ma and 9.4 Ma, respectively, for two samples of the silcrete caps considered to be the equivalent of the Tg surface. According to these ages, the pediments date from the upper Miocene, but they could be even older if their formation was not synchronous with the silcretisations. Bierman (***Reference 5.13.52***) concludes the surfaces are at least 1 to 4 Myr old (see ***Subsection 5.13.5.1.(d) i*** – Uplift and Denudation Rates).

v Cape Fold Belt

Late Palaeozoic compression associated with the assemblage of Pangaea resulted in the Cape Fold Belt, the dominant structural domain of the southern coast (***Reference 5.13.93*** and ***Figure F-5.13.8***). In the modern landscape, sub-parallel mountain chains consist of resistant quartz arenites of the Cape Supergroup. They are topographically the most conspicuous feature of this region, reaching elevations of between 1,000 m and 2,000 m above sea level.

Recent studies using cosmogenic nuclide analyses to measure catchment-wide and interfluve denudation rates (***References 5.13.94*** and ***5.13.51***; see ***Subsection 5.13.5.1.(d)*** -Uplift and Denudation Rates) demonstrate low rates of erosion and a topography in steady state. Scharf *et al*. (***Reference 5.13.94***) note that the alpine-like topography of the Cape Mountains in conjunction with some of the lowest denudation rates in the world is explained by the physically robust and chemically inert quartzites that make up the backbone of the mountains. Intermontane plains and valleys in the mountain chains are mostly underlain by less resistant rocks belonging to either the late Proterozoic-age basement or, more often, by argillaceous units in the early Palaeozoic Cape Supergroup (e.g., the Bokkeveld Group).

© Eskom 2026/Rev 0a

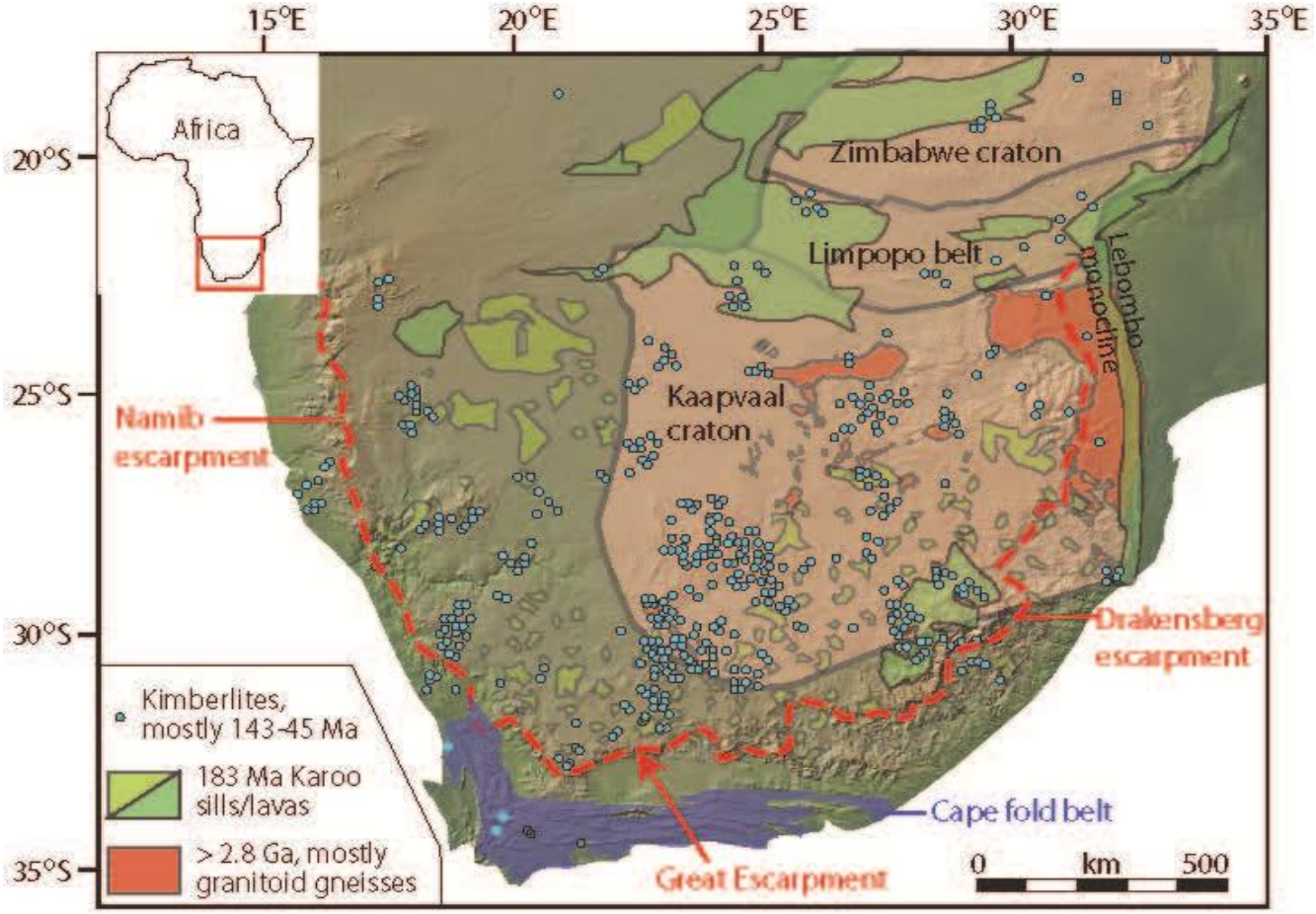


Figure 5.13-8
Map Showing Location of the Great Escarpment in Relation to the Cape Fold Belt and Cratons of Southern Africa (Modified from *Reference 5.13.95*)

© Eskom 2026/Rev 0a

vi Great Karoo

The Great Karoo is a dry, relatively flat region that extends from the Swartberg Mountains, the northernmost of the Cape Mountain ranges, to the Great Escarpment. It is underlain by the rocks of the Karoo Supergroup, which consists of gently folded to flat lying sedimentary rocks. The latter accumulated in a retroarc foreland system (***Reference 5.13.96***) during the Late Carboniferous (about 300 Ma) to Lower Jurassic as a result of subsidence related to the Cape Fold Belt orogeny to the south.

vi Eastern Midlands

The Eastern Midlands also overlies the mostly flat lying Karoo Supergroup. The region is characterised by deeply incised meandering rivers separated by relatively flat interfluves (***Reference 5.13.84***). More resistant dolerite sills cap hills in the southern portion of this region. The region has a poorly defined boundary with the Great Karoo to the west and like the Great Karoo is bounded by the Great Escarpment to the north.

vi Great Escarpment

Landward of the Cape Fold Belt, the Great Escarpment is a horseshoe-shaped scarp trending parallel to the coastline and encompassing much of southern Africa (***Figure F-5.13.8***). The escarpment separates the high topography of the central continent from lower regions near the coast. In the site region it also demarcates the boundary between the Great Karoo and upper Karoo to the north. The elevation of the Great Escarpment is generally between 1000 and 1,500 m but rises to over 2,000 m to the northeast of the site region near Lesotho.

vi Upper Karoo

The Upper Karoo is underlain mainly by the Karoo Supergroup. Dykes and sills of the Karoo Igneous Province occur more commonly than in the Great Karoo and cut through the Karoo Supergroup to form mesas and ridges due to differential erosion. Most rivers are ephemeral and occupy broad valleys (***Reference 5.13.84***).

b) Regional Geological History

The foundation of southern African geology is a core of cratonic rocks that have been subject to periods of deposition, erosion, extension, and amalgamation with other continents. The structures and features created by these events have been reactivated and have the potential to be reactivated again in later stress

regimes. The crust underlying the Thyspunt site region displays a common history and its geology can be attributed to repeated episodes of crustal compression and extension over a two-billion-year period. The rock record in the Thyspunt site region reflects the influence of five major geological events:

- The Mesoproterozoic Namaqua Orogeny that formed the Namaqua-Natal tectonic province.
- Accumulation of the Cape Supergroup in a passive margin setting (Early Ordovician to Early Carboniferous).
- Permo-Triassic Cape Orogeny that formed the Cape Fold Belt.
- Continental breakup of Gondwana during the Mesozoic.
- Late Neogene to Quaternary coastal deposition.

i Late Proterozoic and Paleozoic Geological History

The craton of southern Africa is cored by the middle Archaean (~3,700–3,100 Ma) Kaapvaal Craton (***Reference 5.13.97*** and ***Figure F-5.13.9***). During the late Archaean (3,100–2,600 Ma), the Kaapvaal Craton was sutured onto the Zimbabwe Craton along the Limpopo Belt (***Reference 5.13.97***). Prolonged crustal accretion in the Palaeoproterozoic along the northwestern margin increased the size of the combined craton, which is referred to as the Proto-Kalahari Craton. From approximately 1,400 Ma to 1,000 Ma, all margins of the Proto-Kalahari Craton recorded intense tectonic activity (***Reference 5.13.98***). Along the southern margin, the Namaqua-Natal Mobile Belt records a major arc-accretion and continent-collision event between approximately 1,100 Ma and 1,050 Ma (***Reference 5.13.99***). By approximately 1,050 Ma, the Proto-Kalahari nucleus was almost completely rimmed by voluminous Mesoproterozoic crust and became a larger entity, the Kalahari Craton (***Reference 5.13.98***). The region underwent several subsequent periods of compression and extension, including the assemblage and breakup of the supercontinents Rodinia and Pangaea (***References 5.13.100*** and ***5.13.98***). Late Palaeozoic compression associated with the assemblage of Pangaea resulted in the Cape Fold Belt, the dominant structural domain of the southern coast **(***Reference 5.13.101***).**

The Namaqua-Natal tectonic province refers to the igneous and metamorphic rocks that envelop the southern and western margins of the Kaapvaal Craton (***References 5.13.141*** and ***5.13.102***). This metamorphic belt has a complex history, having formed over a period of more than one billion years (***References 5.13.103*** and ***5.13.104***), as is reflected in its complex structure.

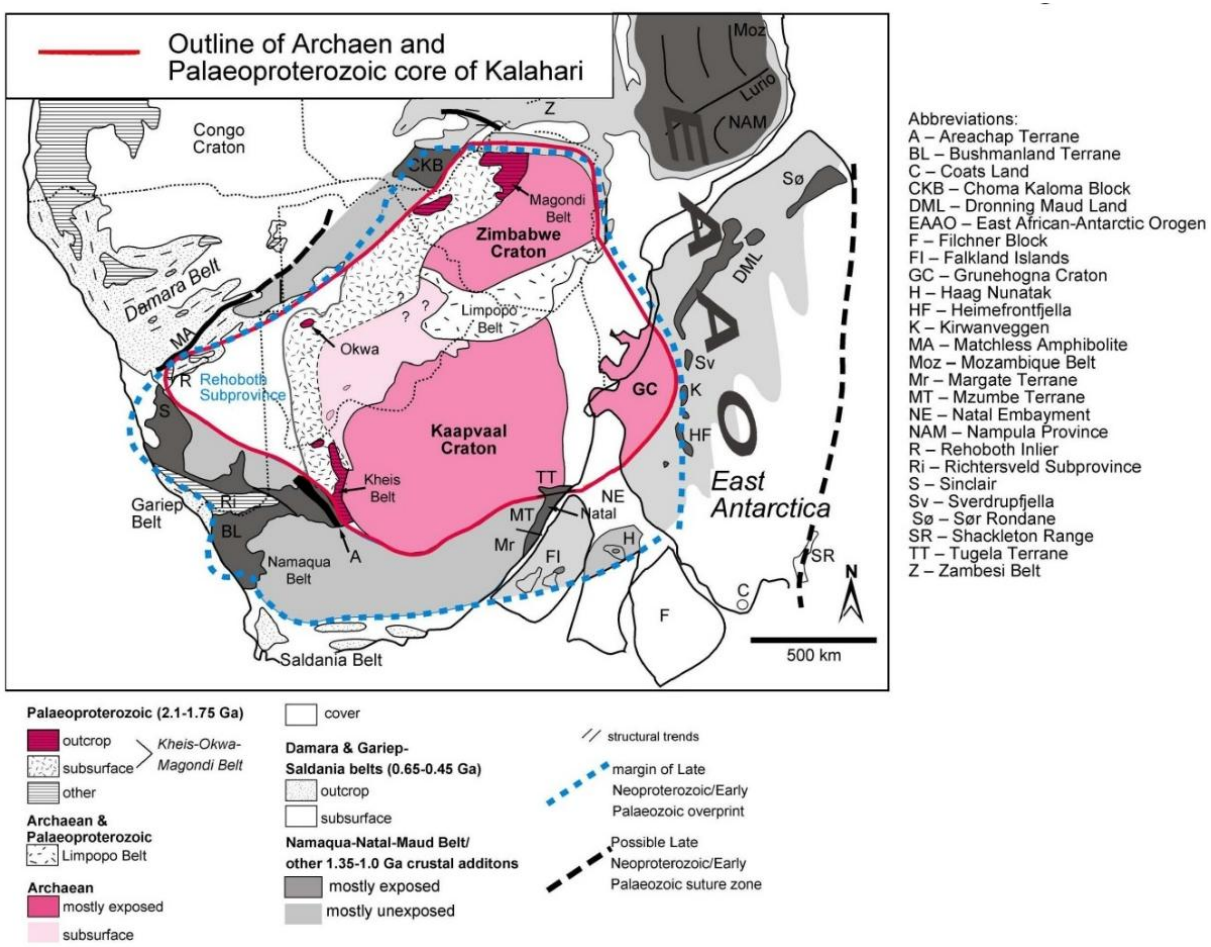


Figure 5.13-9
Components of the Archaean to Palaeoproterozoic Core of the Kalahari Craton Within a Gondwana Reconstruction (*Reference 5.13.98*)

© Eskom 2026/Rev 0a

Some of the oldest rocks of the Namaqua-Natal Mobile Belt (NNMB) accumulated as a volcano-sedimentary sequence in the Namaqua sector during 2,000–1,600 Ma, followed by the accumulation of more supracrustal sequences in rift basins during 1,600–1,350 Ma (***Reference 5.13.102***). A prolonged period of southwest-northeast-directed compression commenced at ~1,300 Ma, culminating in the main Namaqua orogenic events during 1,220–1,150 Ma that resulted in intense deformation, medium- to high-grade metamorphism and magmatic emplacement (***Reference 5.13.102***).

Following almost 100 Ma of quiescence, an oblique-slip regime was initiated that formed an array of shear zones and emplacement of granitoids (***Reference 5.13.102***), with the most intense period of metamorphism dated at ~1,030 Ma (***Reference 5.13.105***).

Whereas the northern margin of the NNMB with the Kaapvaal Craton is reasonably well-defined, the southern boundary is still subject to debate. Some workers proposed that the southern limit of the NNMB is delineated by the deep crustal Beattie geophysical anomaly and associated Southern Cape Conductive Belt (***References 5.13.106***, ***5.13.101***, ***5.13.107***, and ***5.13.108***). This anomaly has in the past been equated with the proposed contact between the NNMB and the postulated Neoproterozoic Saldania Belt (***Reference 5.13.109*** and ***Figure F-5.13.9***). However, recent geophysical studies suggest that the NNMB should be extended westward (***Reference 5.13.110***) and southward (***References 5.13.111*** and ***5.13.112***), extending below the Cape Fold Belt, probably to the continental margin (***Figure F-5.13.10***). It is therefore proposed that the NNMB forms the middle, and possibly the lower parts, of the crust below the southern Karoo Basin, Cape Fold Belt, and continental shelf of the site region (***Reference 5.13.112***).

A series of east-west-trending extensional basins developed over the NNMB between 900 Ma and 600 Ma, within which up to 3 km of the Pre-Cape Group sediments accumulated (***References 5.13.113***, ***5.13.114***, and ***5.13.115***). Today they are exposed as inliers (*i.e.*, Kango, Kaaimans, Gamtoos inliers) within the roots of large mega-anticlines in the Cape Fold Belt. These deposits underwent substantial deformation during the Pan African (600–450 Ma; ***References 5.13.116*** and ***5.13.117***) and Cape (278–230 Ma; ***Reference 5.13.118***) orogenies.

Following the Pan African orogeny, extension related to the breakup of greater proto-Gondwana formed an extensive passive margin along the southern edge of South Africa (***Reference 5.13.100***). In this continental margin setting a wedge-shaped succession of clastic, shallow-marine, deltaic and nearshore fluvial strata (*e.g.*, the Cape Supergroup) accumulated during the Early Ordovician to Early Carboniferous (***Reference 5.13.119***).

© Eskom 2026/Rev 0a

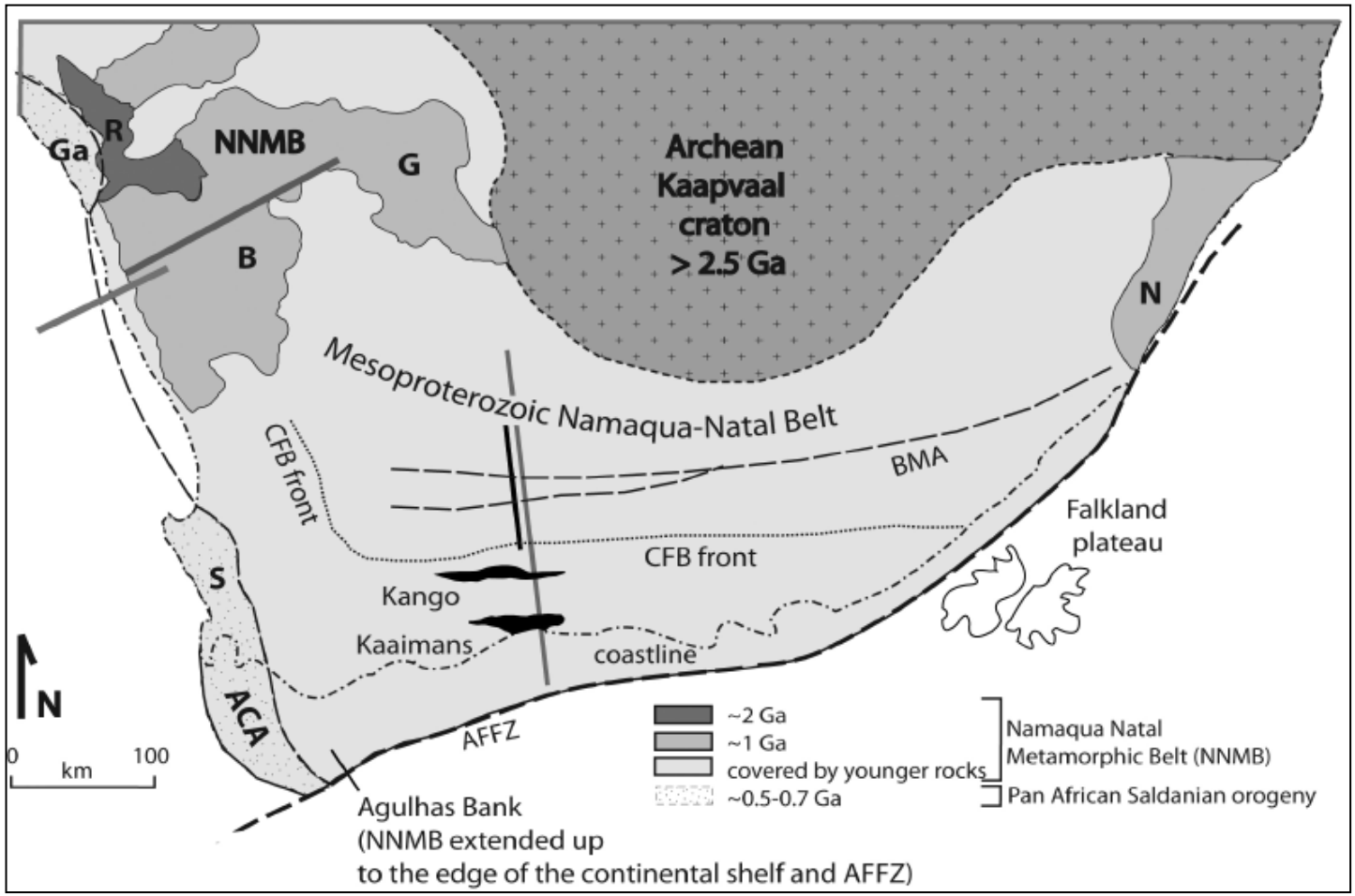


Figure 5.13-10
The Position of the Namaqua-Natal Mobile Belt (NNMB). The Kango and Kaaimans Inliers Represent the Position of Pre-Cape Sedimentary Sequences (*Reference 5.13.112*)

© Eskom 2026/Rev 0a

Palaeocurrent data, thickness changes, and grain-size variation indicate that the main source areas were located to the north and northwest of the basin (***Figure F-5.13.11***). The Cape Basin extended east–west for more than 1,000 km (***Reference 5.13.119***).

The geotectonic setting in which folding during the Permo-Triassic Cape Orogeny took place remains unresolved. Most authors favour the concept of the northward subduction of oceanic crust under the southern margin of Gondwana (***References 5.13.120***, ***5.13.121***, ***5.13.122***, ***5.13.123***, ***5.13.96***, ***5.13.124***, and ***5.13.125***; ***Figure F-5.13.12***). However, Lindeque *et al*. (***Reference 5.13.112***) pointed out that this model is not supported by deep crustal seismic data and proposed a continent-continent collision model, as did a number of earlier authors (***References 5.13.126***, ***5.13.127***, and ***5.13.128***). Hälbich (***Reference 5.13.121***) proposed that the Cape Fold Belt deformation is the result of a sub-continental convection cell or plume of limited duration.

The tectonic load of the Cape Fold Belt was responsible for the formation of a foreland basin, the Karoo Basin, to the north in which a sedimentary succession accumulated from the Late Carboniferous to the Early Jurassic. The Cape Orogeny had only a limited impact on the southernmost part of the largely flat-lying Karoo Supergroup (***References 5.13.129*** and ***5.13.130***), with intense deformation occurring to the south of the Karoo Basin where the rocks of the Cape Supergroup form the bulk of the Cape Fold Mountains (***References 5.13.129*** and ***5.13.131***).

On a regional scale, two structural branches have been recognised in the Cape Fold Belt: a north-northwest-striking western branch north of Cape Town and an east-west-trending southern branch bounding the southern margin of the continent, with the two branches coalescing in the Cape Syntaxis (***References 5.13.132***, ***5.13.133***, ***5.13.134***, ***5.13.135***, and ***5.13.136***; ***Figure F-5.13.13***).

The north-northwest-striking western branch displays relatively open, upright first-order folds, monoclines, and normal faults (***References 5.13.132*** and ***5.13.133***). In contrast, the southern branch reveals a consistent east-west structural fabric (***Reference 5.13.137***) that broadly mimics the observed orientation and structure of the Cape Basin. It displays a much higher deformational intensity, as indicated by the north-verging, recumbent first-order folds, a high incidence of second-order folds and local out-of-the-forelimb thrusting (***References 5.13.132***, ***5.13.133***, and ***5.13.138***).

© Eskom 2026/Rev 0a

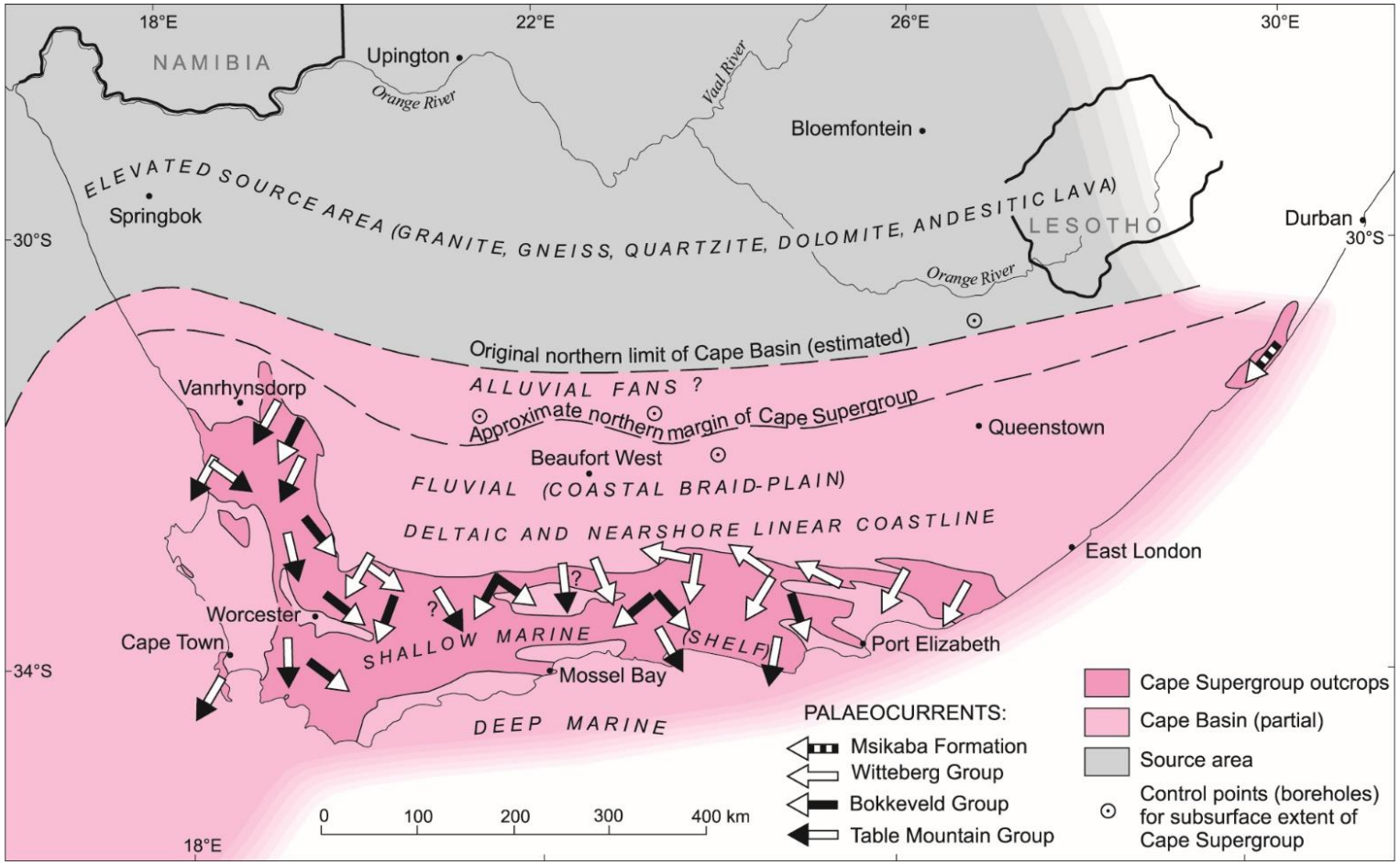


Figure 5.13-11
Palaeogeography of the Cape Supergroup (*Reference 5.13.119*)

© Eskom 2026/Rev 0a

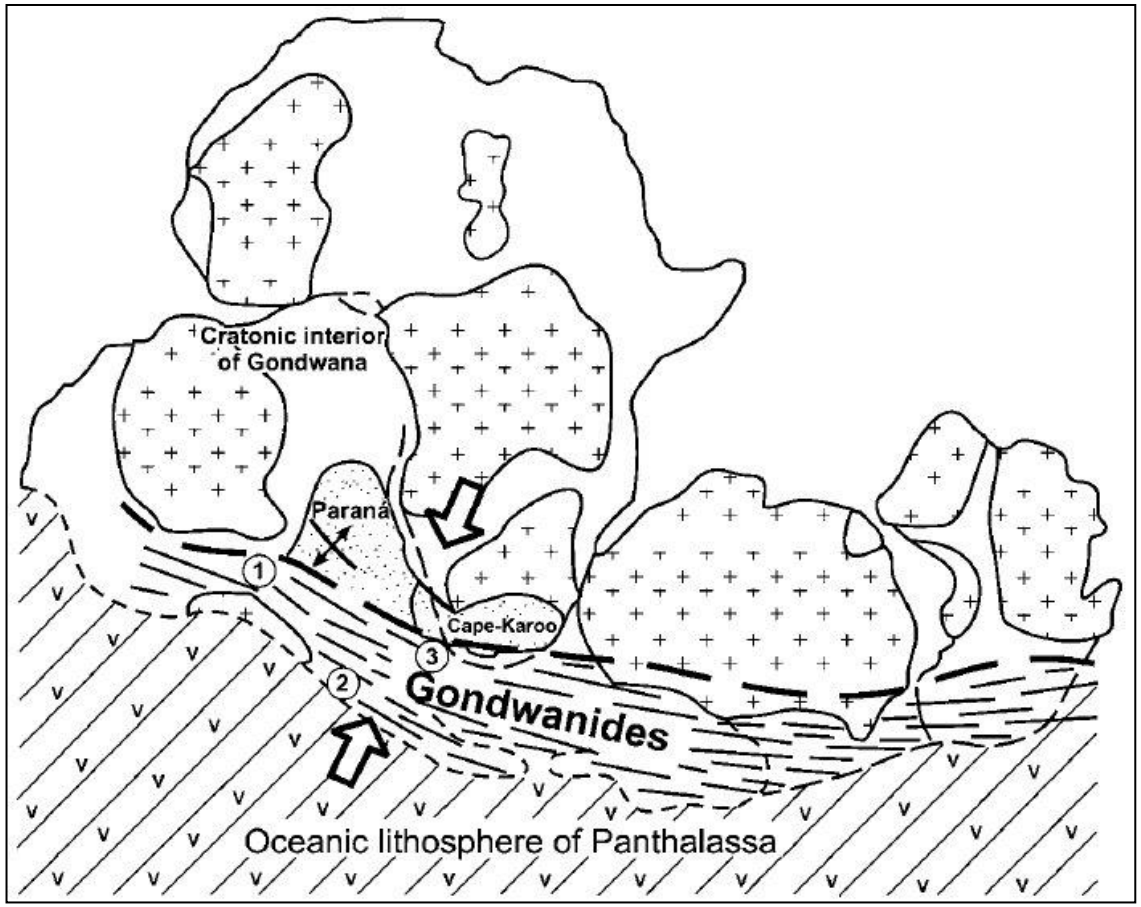


Figure 5.13-12
Map Showing the Proposed Position of the Gondwanide Mountain Chain Across the Southern Margin of Gondwana (*Reference 5.13.125*)

© Eskom 2026/Rev 0a

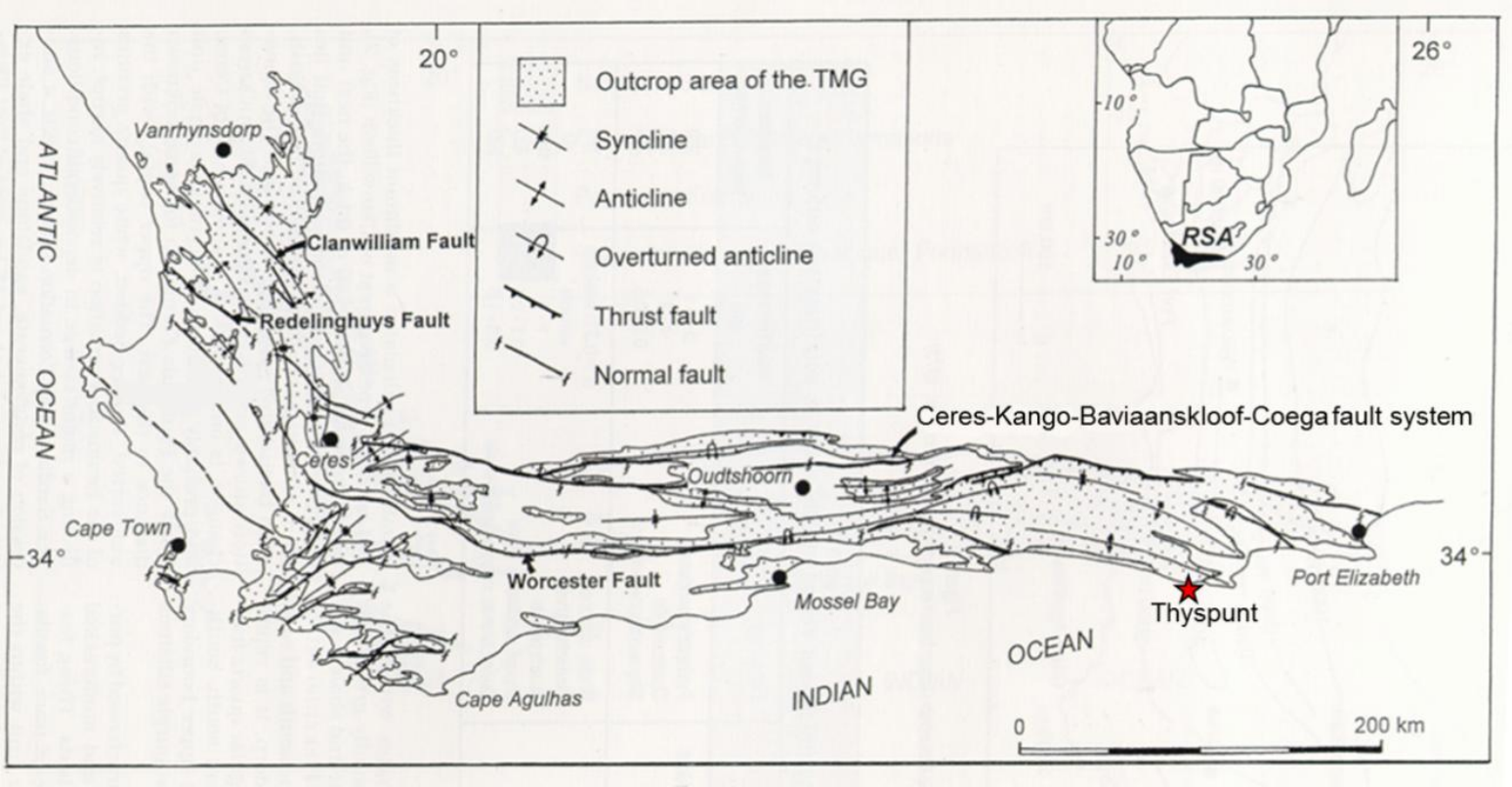


Figure 5.13-13
Map Showing the Two Structural Branches in the Cape Fold Belt (*Reference 5.13.136*)

© Eskom 2026/Rev 0a

Based on $^{40}Ar/^{39}Ar$ stepheating analyses of micas on cleavage planes (***Reference 5.13.139***), Hälbich (***Reference 5.13.118***) proposed that the Cape Fold Belt was formed during four pulses of deformation that resulted in a series of east-west-trending and south-dipping thrusts. Gresse *et al*. (***Reference 5.13.140***) recognised five episodic pulses of deformation of which three differ substantially from Hälbich (***Reference 5.13.118***). Catuneanu *et al*. (***Reference 5.13.121***) considered these to be separate events and together with an event dated at 215 Ma (considered by Hälbich *et al.* [***Reference 5.13.139***], Hälbich [***Reference 5.13.118***], and Gresse *et al*. [***Reference 5.13.140***] to reflect uplift associated with the early stages of continental breakup), proposed eight tectonic paroxysms for the Cape Fold Belt.

Gresse *et al*. (***Reference 5.13.140***) and Paton (***Reference 5.13.137***) postulated that the large compressional faults of the Cape Fold Belt represent reactivated passive margin faults that developed during the earlier deposition of the Cape Supergroup.

An eastward increase in thrust phenomena and folds intensities were noted between the Oudsthoorn area and the Baviaanskloof Mountains (***Reference 5.13.93***).

ii Mesozoic Geological History

Compression of the Cape Orogeny was followed by extension associated with the breakup of Gondwana. During this phase the Cape Fold Belt underwent negative structural inversion, resulting in the superimposition of a Mesozoic extensional system (***Figure F-5.13.3***) onto the fold belt (***References 5.13.117*** and ***5.13.142***). Continental breakup was initiated in the Early Jurassic (~180 Ma) when a general increase in tectonic activity was followed by the linkage of fracture systems across Gondwana (***Reference 5.13.143***). Buoyancy associated with mantle upwelling as a possible factor in the initiation of rifting (***Reference 5.13.149***).

The separation of the Falkland Plateau from southern and eastern Africa and movement along the Agulhas-Falkland Fracture Zone (AFFZ) (also referred to as the Agulhas-Falkland Transform) (an ultimately 1,200 km long transform fault) marked the start of a split of Western Gondwana into Africa and South America. A north-south rift, propagating northwards from the Gastre Fault–Agulhas Falkland Fracture Zone in the south Atlantic (***Figure F-5.13.14***), became the locus for seafloor spreading between Africa and South America (***Figure F-5.13.15***). The final split between the continental crusts of Africa and South America allowed for the linkage of the entire Atlantic Ocean in the Upper Cretaceous (***References 5.13.145*** and ***5.13.143***).

© Eskom 2026/Rev 0a

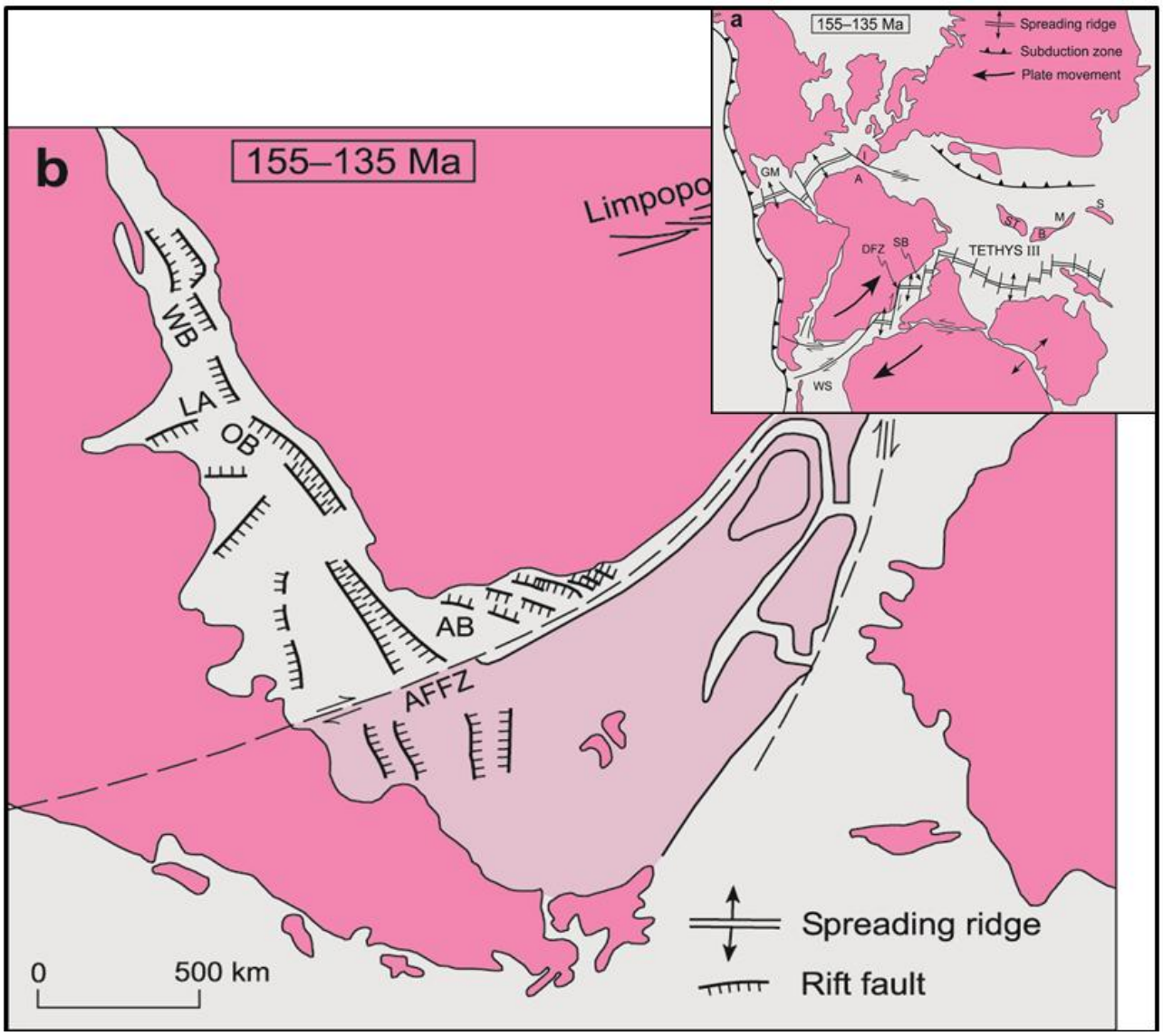


Figure 5.13-14
The Development of Rift-Bounded Basins on the Agulhas Bank (AB) as a Result of Strike-Slip Motion During Gondwana Breakup. AFFZ = Agulhas-Falkland Fracture Zone; LA = Luderitz Arch; OB = Orange River Basin; WB = Walvis Basin and WS = Weddell Sea (Modified from *Reference 5.13.143*)

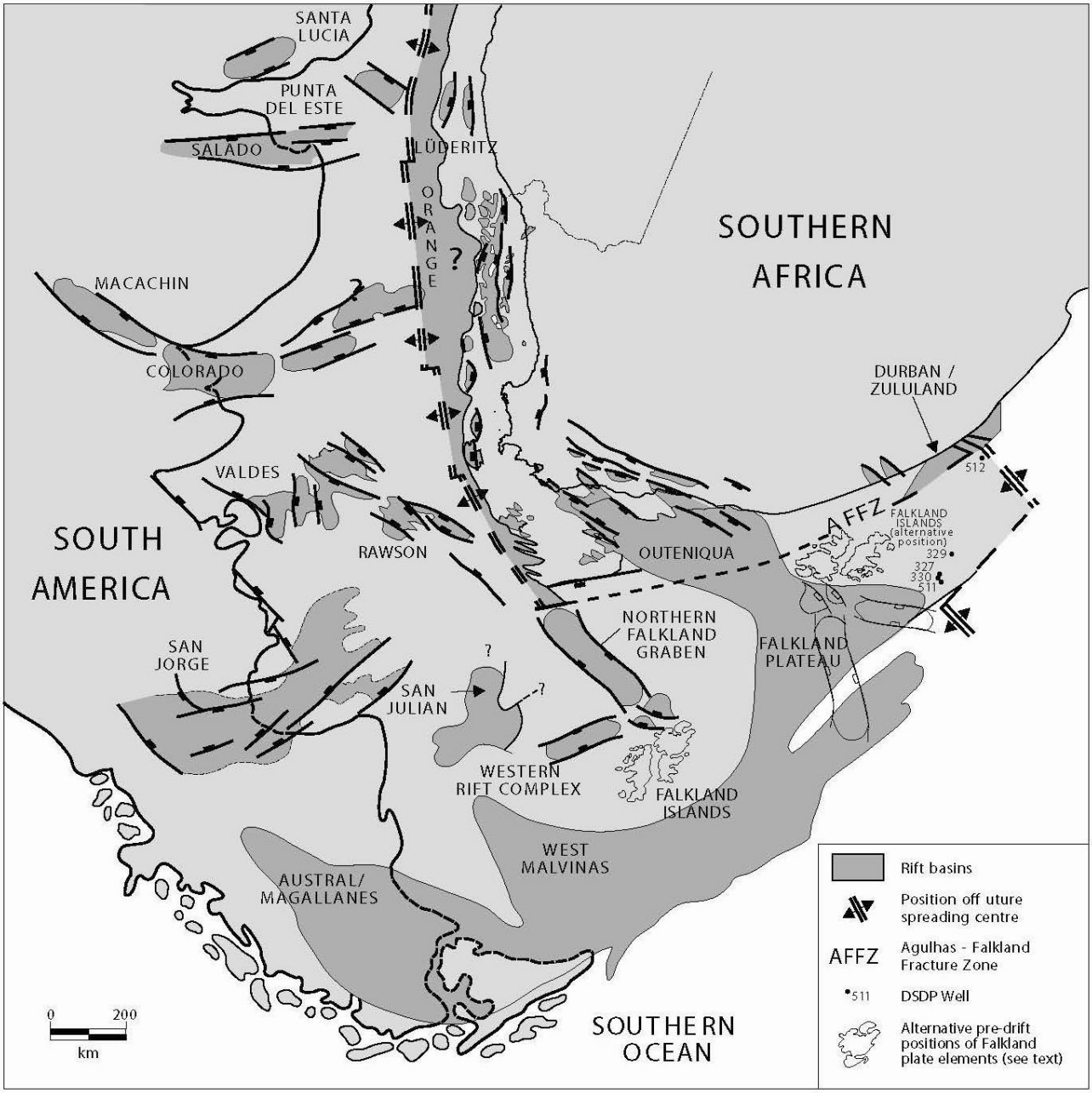


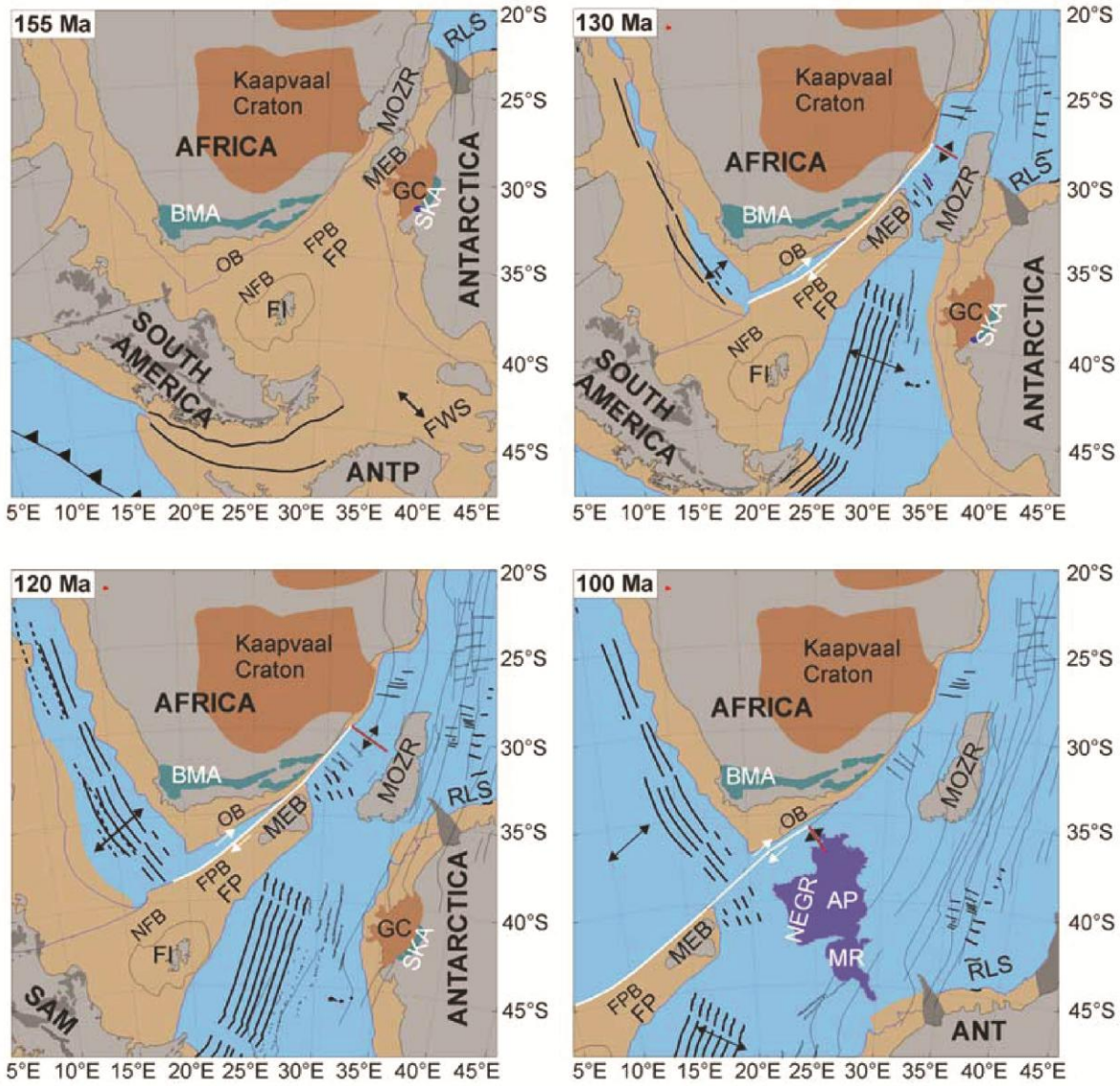
Figure 5.13-15
Plate Tectonic Reconstruction Illustrating the Likely Pre-Breakup Configuration of Late Jurassic to Early Cretaceous Rift Basins Within Southwest Gondwana (*Reference 5.13.74*)

Extension associated with rifting and the right-lateral Agulhas-Falkland Fracture Zone resulted in the reactivation of Cape Fold Belt structures as extensional faults (***References 5.13.142***, ***5.13.150***, ***5.13.140***, and ***5.13.144***). From the Late Jurassic to Early Cretaceous, extension led to the formation of a series of rift basins along the southern margin of Africa both in the onshore and offshore. These rift basins were typically graben and half-graben structural styles (***Figure F-5.13.3***). In addition to the smaller onshore basins, the large offshore Outeniqua Basin consists of a series of smaller sub-basins, including the Bredasdorp, Pletmos, Gamtoos, and Algoa sub-basins (***Figure F-5.13.15***), separated by fault-bounded basement arches composed of Cape Supergroup metasediments (***Reference 5.13.73***).

Extension associated with rifting and the right-lateral Agulhas-Falkland Fracture Zone resulted in the reactivation of Cape Fold Belt structures as extensional faults (***References 5.13.142***, ***5.13.150***, ***5.13.140***, and ***5.13.144***). From the Late Jurassic to Early Cretaceous, extension led to the formation of a series of rift basins along the southern margin of Africa both in the onshore and offshore. These rift basins were typically graben and half-graben structural styles (***Figure F-5.13.3***). In addition to the smaller onshore basins, the large offshore Outeniqua Basin consists of a series of smaller sub-basins, including the Bredasdorp, Pletmos, Gamtoos, and Algoa sub-basins (***Figure F-5.13.15***), separated by fault-bounded basement arches composed of Cape Supergroup metasediments (***Reference 5.13.73***).

The Agulhas-Falkland Fracture Zone (the eastern, inactive end of the Agulhas-Falkland Fracture Zone is referred to as the Agulhas Fracture Zone) off the coast of Africa was an active tectonic feature for about 65 Myr, from approximately 130 Ma to approximately 65 Ma, at which time the active transform was reduced to a smaller transform (~180 km ridge-ridge offset) by a ridge-jump event (***References 5.13.146*** and ***5.13.68***) and ***Figure F-5.13.16*** illustrates the history of the AFFZ using tectonic reconstructions starting at 155 Ma prior to the separation of the continents. At 130 Ma, sea floor spreading takes place in the Weddell Sea, the South Atlantic, and north of the Maurice Ewing Bank. Movement on the AFFZ was initiated at ~136 Ma (***Reference 5.13.77)***. At 120 Ma, in the later drift stage, transtension along the AFFZ is still causing crustal thinning in the southern Outeniqua Basin. At 100 Ma a large igneous province represented by the Agulhas Plateau, Maud Rise and Northeast Georgia Rise has formed after the relatively westward moving Falkland Plateau cleared southern Africa at ~105 Ma (***References 5.13.148***, ***5.13.147***, and ***5.13.77***).

© Eskom 2026/Rev 0a



AFT - Agulhas Falkland Transform (white line), ANTP - Antarctic Peninsula, AP - Agulhas Plaeau, BMA - Beatie Magnetic Anomaly, FP - Falkland Plateau, FPB - Falkland Plateau Basin, FWS - future Weddell Sea, GC - Grunehogna Craton, MEB - Maurice Ewing Bank, MOZR - Mozambique Ridge, MR - Maud Rise, NEGR - Northeast Gerorgia Rise, NFB - North Falkland Basin, OB - Outeniqua Basin, RLS - Riiser Larsen Sea, SKA - Sverdrupfjella-Kirvanveggen magnetic anomaly.

Figure 5.13-16
Plate Tectonic Reconstructions Using Rotation Poles Published by König & Jokat (*Reference 5.13.148*; Modified from *Reference 5.13.77*)

As outlined by Brown *et al.* (***Reference 5.13.72*** and ***Figure F-5.13.17***), post-rift Late Cretaceous and Cenozoic extensional stress was generated by thermally driven subsidence that initiated many shallow normal faults and locally reactivated movement along the major rift faults. High subsidence (and accommodation) rates produced well-developed aggradational sequence sets between 126 Ma and 117.5 Ma. The period following was characterised by diminished subsidence (and accommodation) rates, which resulted in extensive progradational sequences between 117.5 Ma and 112 Ma. Subsequently, with only minor perturbations, there were generally episodes of moderate subsidence (and accommodation) rates with deposition of mostly aggradational sequence sets in the periods 112–103 Ma, 103–93 Ma, and 93–80 Ma.

ii Cenozoic Geological History

The continental margin and present coastal configuration of southern Africa has been relatively stable since the Falkland Plateau cleared the continental margin in the Cretaceous (***References 5.13.151***, ***5.13.152***, and ***5.13.153***). Different rates of Cenozoic land-level change for southern Africa have been reported and multiple hypotheses have been presented to explain both the reason and the varying rates (see discussion in ***Subsection 5.13.5.1.(d) i*** – Contemporary Tectonic Setting).

The high topography of southern South Africa meant that Cenozoic deposition was largely restricted to a few river valleys and deposits along the coast. The Cenozoic coastal deposits reflect not only the relative rates of sediment supply and local subsidence, but also the major eustatic sea level fluctuations. It includes littoral marine, estuarine, fluvial, lacustrine and aeolian deposits that accumulated extensively along the coastal plains of the southern African subcontinent (***Reference 5.13.153***). Compilation and review of data regarding the position and ages of marine terraces along the coast in the Eastern Cape region confirm very low rates of uplift along the entire coast, consistent with other stable continental regions (***Reference 5.13.58***).

c) Regional Stratigraphy

The stratigraphy of the site region (320 km radius) has been compiled from a variety of sources (***Figure F-5.13.18***) and ***Table T-5.13.3*** provides a summary of the stratigraphy which also incorporates major tectonic events resulting in ‘breaks’ in the stratigraphic column ***(Reference 5.13.37***). Descriptions of the lithologic units and their depositional environments are found in the following subsections.

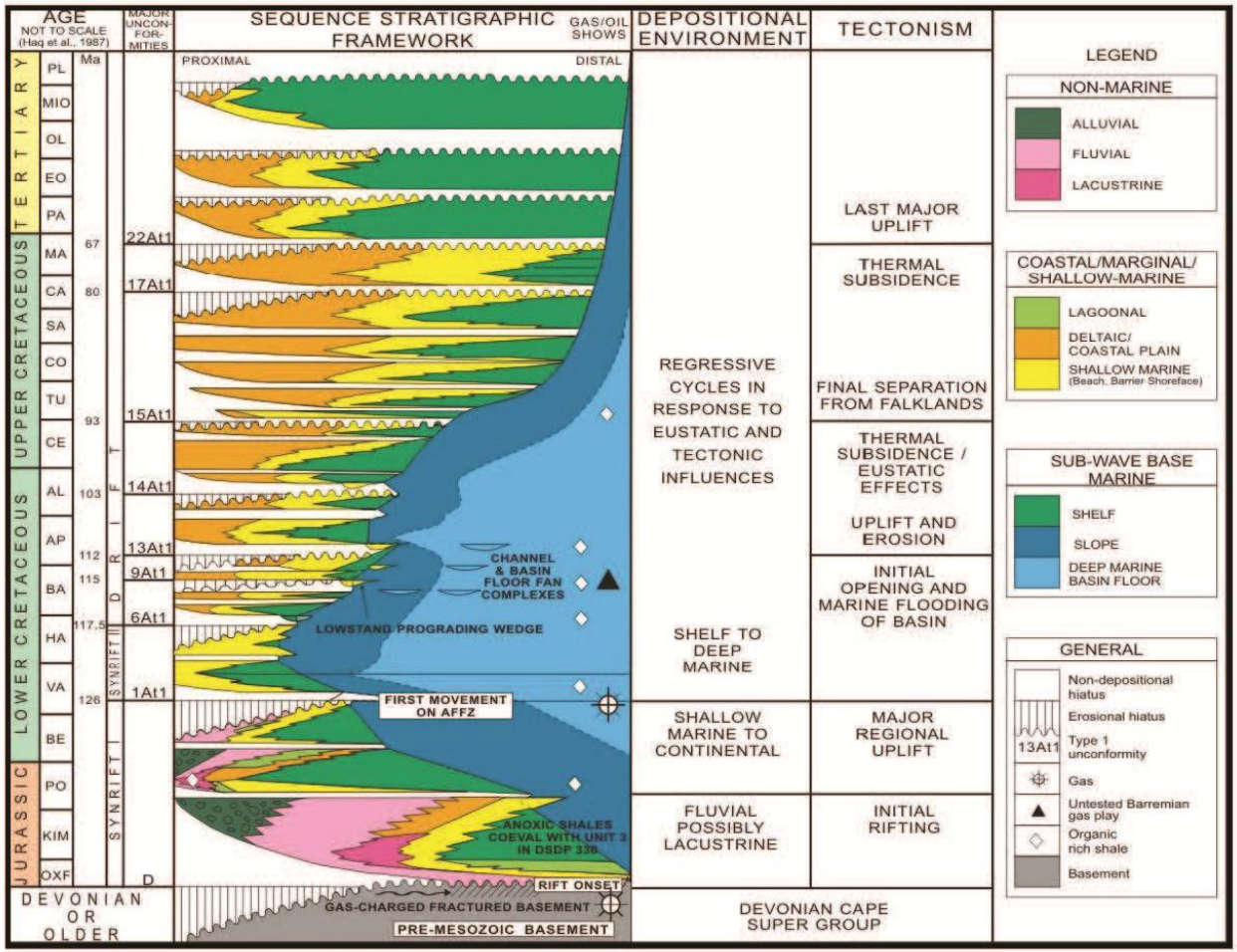


Figure 5.13-17
Chronostratigraphic Column for the Pletmos Basin (*Reference 5.13.45*, after *Reference 5.13.72*)

© Eskom 2026/Rev 0a

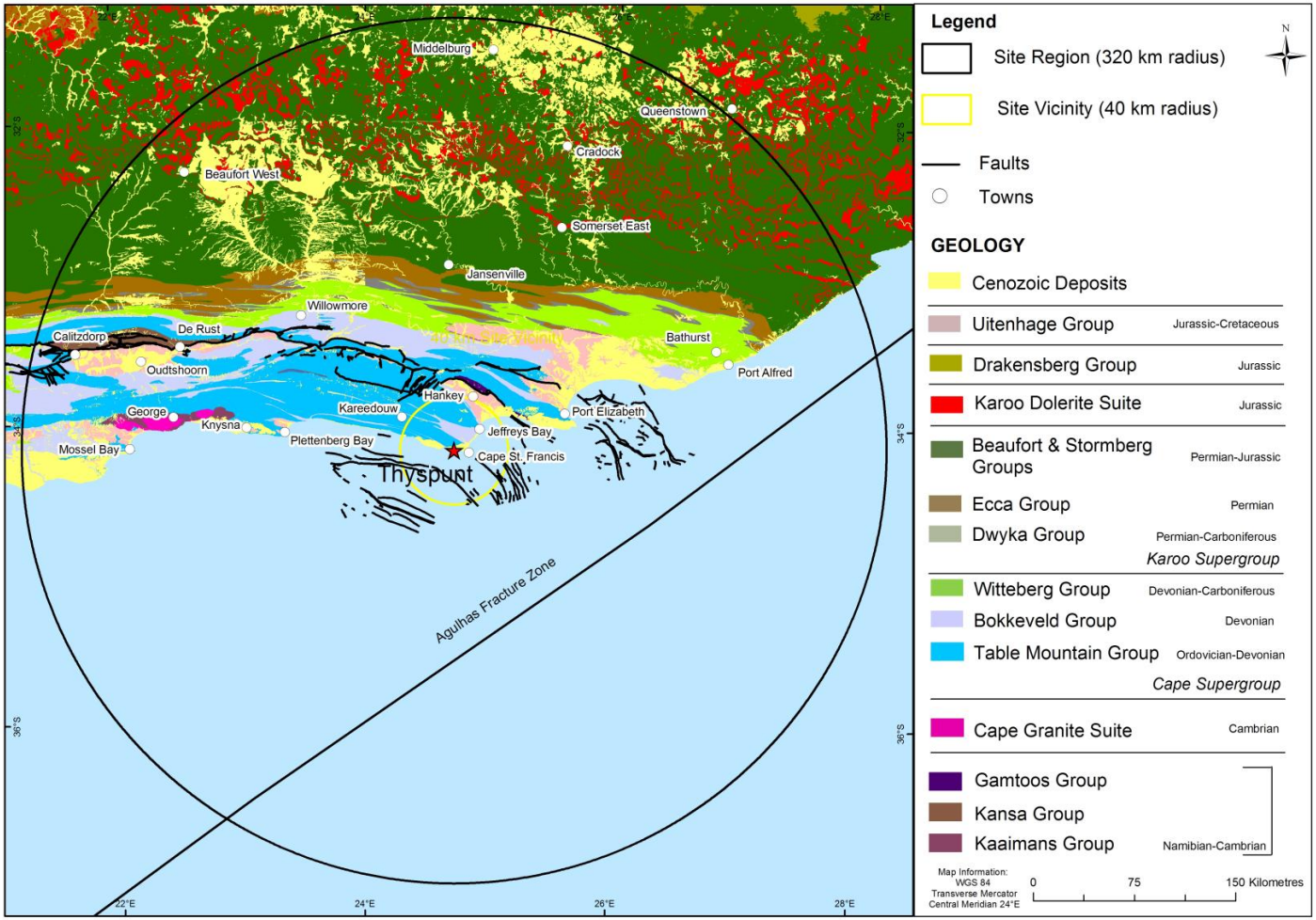


Figure 5.13-18
Geological Map of the Onshore Site Region

© Eskom 2026/Rev 0a

Table 5.13.3
Tectonostratigraphic Framework for the Thyspunt Site Region

Age	Group	Subgroup	Formation	Lithology	Origin
Holocene				Alluvium, sand, scree	Aeolian, beach, fluvial, colluvium
	Extensional reactivation of the Kango fault system; erosion of seafloor				
Pleistocene	ALGOA		Nahoon	Semi-consolidated sand	Aeolian
			Salnova	Calcarenite, coquinite	Marine
			Nanaga	Calcarenite	Aeolian
Pliocene Miocene			Alexandria	Calcarenite, coquinite	Marine and estuarine
Palaeocene			Grahamstown	Silcrete	Pedogenic
Palaeocene to Neogene	Uplift and erosion of the Cape Fold Belt and Cretaceous basins; deposition in offshore basins				
Cretaceous	UITENHAGE		Sundays River	Fossiliferous siltstone, mudrock, and sandstone with secondary limestone and gypsum	Shallow marine
			Kirkwood	Shale, mudstone, siltstone, and sandstone,	Fluvial to Upper Estuarine
Jurassic			Enon	Conglomerate	Fluvial
	SUURBERG		Mimosa, Coerney/Slagboom	Basalt, tuff, breccia	Syn-rift volcanism
Jurassic-Cretaceous	Uplift and erosion of the Cape Fold Belt, Gondwana breakup, pull-apart rift basins, marine syn-drift sedimentation in offshore basins, intrusion of mafics (diabase), extrusion of volcanics,				
Permian-Triassic	Cape orogeny: co-axial folding, thrusting, and cleavage development				
Carboniferous-Jurassic	STORMBERG			Siltstone and sandstone	Fluvial
	BEAUFORT			Siltstone and sandstone	Fluvial
	ECCA			Shale and sandstone	Marine
	DWYKA			Diamictite	Glacial
Devonian-Carboniferous	WITTEBERG			Sandstone	
Devonian	BOKKEVELD	Traka	Sandpoort	Shale	Marine, pro-delta, and delta-front
			Adolphspoort	Sandstone	
			Karies	Shale	
		Ceres	Boplaas	Sandstone	
			Tra-Tra	Shale	
			Hex River	Sandstone	
			Voorstehoek	Shale	
			Gamka	Sandstone	
			Gydo	Shale	

© Eskom 2026/Rev 0a

Age	Group	Subgroup	Formation	Lithology	Origin
Silurian	TABLE MOUNTAIN	Nardouw	Baviaanskloof	Thin-bedded, feldspathic quartz arenite	Fluvio-marine
			Skurweberg	Thick-bedded, conglomeratic, quartz arenite	Fluvial
			Goudini	Thin-bedded, feldspathic, red siltstone	Fluvio-marine
Ordovician			Cedarberg	Shale, siltstone	Post-glaciation marine
			Peninsula	Quartz arenite	Fluvio-marine
			Sardinia Bay	Phyllite, conglomerate	Tidal shelf to fan delta
Cambrian	Aborted rifting, sedimentation in rift basins, volcanism				
	CAPE GRANITE SUITE	Sardinia pluton	–	Porphyritic granite	Post-collisional
Precambrian	Pan-African orogeny: non-coaxial folding, diabase dyke intrusion, thrusting, cleavage development				
Namibian	GAMTOOS GROUP		Van Stadens	Quartzites, conglomerate, phyllite, shale, limestone	Shallow marine shelf to fan delta
			Kaan		
			Klein River		
			Lime Bank		

i Precambrian Stratigraphy

Basement in the Eastern Cape is formed by the igneous and metamorphic rocks of the Mesoproterozoic Namaqua-Natal tectonic province (***References 5.13.102*** and ***5.13.112***). The oldest rocks outcropping within the site region consist of highly deformed Neoproterozoic-age (600–700 My) phyllite, limestone, quartzite and conglomerate of the Pre-Cape Group sedimentary rocks (***Reference 5.13.115***). They include the Gamtoos Group which is exposed as inliers along a 110 km strip along the Gamtoos Fault extending from the eastern end of the Baviaanskloof towards the coast south-west of Port Elizabeth (***References 5.13.155*** and ***5.13.113***). Further west similar successions are exposed in two inliers within the roots of large mega-anticlines in the Cape Fold Belt. Two units, (Cango Caves and Kansa groups), separated by an unconformity, are exposed in the Kango inlier. Further south the Kaaimans Group crops out near the coast south of the Outeniqua range.

These Pre-Cape rocks underwent significant deformation during the Pan African (600–450 Ma; ***References 5.13.116*** and ***5.13.117***) and Cape (278-230 My; ***Reference 5.13.118***) orogenies. The Kaaimans Group is intruded by the George and Woodville plutons of the 555–515 My old Cape Granite Suite (***Reference 5.13.115***), whereas the Gamtoos Group has been intruded by

mafic dykes and, possibly, by Cape granite (***Reference 5.13.156***).

ii Stratigraphy of the Cape Super Group

The Paleozoic age Cape Supergroup is a nearly 9,000 m thick succession of sandstone, shale, and siltstone and is divided into three groups (Table Mountain, Bokkeveld and Witteberg), each comprising of several formations (***Reference 5.13.154*** and ***Figure F-5.13.19***).

Rocks of the Cape Supergroup are present over a large portion of the site region. The Cape Supergroup sediments were deposited mostly under marine conditions, in the essentially east–west striking, early Palaeozoic-age, Cape Trough.

The lowermost Table Mountain Group consists primarily of quartzitic, well-indurated sandstone and is dominated by the quartz arenites of the Peninsula Formation (***Reference 5.13.154***). In the site region the negative weathering, argillaceous Cedarberg Formation separates it from the uppermost Nardouw Subgroup (Goudini, Skurweberg, and Baviaanskloof Formations).

The greater siltstone content of the Goudini and Baviaanskloof Formations, together with the greater feldspathic content of sandstones in the latter, means that rocks of the Nardouw Subgroup are generally less resistant to weathering than the rest of the Table Mountain Group. The Table Mountain Group is overlain by shale and siltstone of the considerably less resistant Devonian-age Bokkeveld Group (about 410–380 My). The Devonian to Early Carboniferous-age (about 380–360 My) Witteberg Group is a well-bedded succession of sandstones of variable purity, and siltstone, with some shale units towards its top (***Reference 5.13.119***).

The resistance of the Table Mountain Group to erosion results in it being the dominant lithology of the Cape Fold Belt mountain ranges with the less resistant units of the Cape Supergroup occurring in valleys and on the mountain slopes. The configuration of mountain ranges and their intermontane valleys reflect, to a large extent, the mega-synclines and mega-anticlines that formed during the Cape Orogeny.

ii Stratigraphy of the Karoo Supergroup

The Karoo Supergroup outcrops to the north of the Cape Fold Belt. A maximum accumulated thickness of almost 12 km has been reported for the Karoo Supergroup (***Reference 5.13.96***), although recent work (***Reference 5.13.112***) suggested that the sequence is much thinner.

The age of the sequence ranges from the Late Carboniferous to the Jurassic and its accumulation was primarily controlled by tectonism associated with the Cape orogeny with the influence of climatic changed superimposed upon that (***Reference 5.13.96***). The climate underwent a shift from cold conditions during the Late Carboniferous–earliest Permian interval, to warmer and eventually hot climates in the Triassic and Early Jurassic, which coincided with the northward migration of the continent (***Reference 5.13.157***). This change is reflected by the lithostratigraphy, which commences with the glacial rocks of the Dwyka Group at the base, followed by the marine Ecca Group, and then the non-marine Beaufort and "Stormberg" Groups. Outcrops of the latter two show the largest aerial extent in the northern part of the site region, with the Dwyka and Ecca Groups restricted to thin ribbons along the southern edge of the Karoo Basin.

Dolerite dykes and the volcanic rocks of the Karoo Large Igneous Provence, and the equivalent intrusions elsewhere in Southern Africa extruded in the Jurassic, mark the rifting of Gondwana in South Africa (***Reference 5.13.158***).

iv Stratigraphy of the Mesozoic Basins

The breakup of the Gondwana supercontinent resulted in the formation of a number of onshore and offshore graben and half-graben rift basins (Bredasdorp, Pletmos, Gamtoos, and Algoa sub-basins) along the southern margin of South Africa that collectively make up the Outeniqua Basin. In the onshore part of the Algoa Basin, the onset of rifting is marked by a sequence of acidic tuffs and basalt flows of the Suurberg Group, which erupted along fissures confined to the northern margin of the present-day Algoa Basin to the north of Port Elizabeth (***References 5.13.91*** and ***5.13.159***).

Volcanism was followed by continued rifting and the opening of extensional half-grabens which filled with Middle Jurassic to Lower Cretaceous-age sediments of the Uitenhage Group (***Reference 5.13.160***). The oldest sediments in the Outeniqua Basin are Kimmeridgian to Portlandian in age based on sediments from cores but rocks as old as Oxfordian may exist (***Reference 5.13.74***). The basal unit of the Uitenhage Group, the Enon Formation, is conglomeratic. Upwards, the Uitenhage Group typically grades into sandstones and mudstones of the largely fluvial Kirkwood and shallow marine Sundays River Formations (***Reference 5.13.161***). Exposures of the Uitenhage Group contained in several smaller basins to the west only contain the Enon and Kirkwood Formation equivalents.

© Eskom 2026/Rev 0a

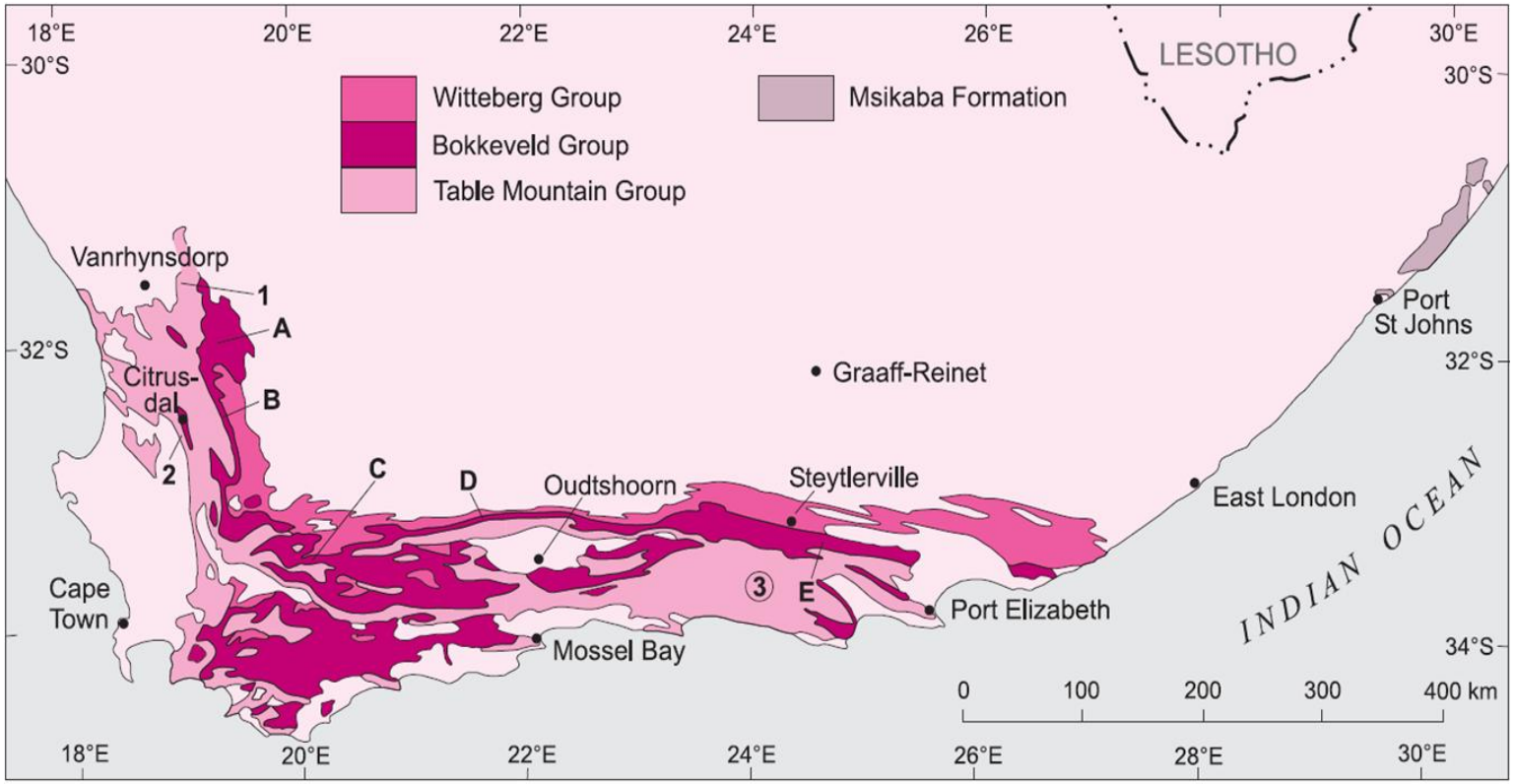


Figure 5.13-19
Map Showing the Distribution of the Three Groups Comprising the Cape Supergroup (*Reference 5.13.119*)

© Eskom 2026/Rev 0a

Offshore the stratigraphy in the Gamtoos and Pletmos basins is broken in four main sections separated by unconformities (***References 5.13.73*** and ***5.13.74***; ***Figure F-5.13.17***). The lowest unit consists of fluvial and shallow to deep marine sediments and is interpreted as synrift sedimentation. It is bounded on top by the 1At1 (early Hauterivian) unconformity which may correlate onshore to the base of the Sundays River Formation (***Reference 5.13.162***). Above the unconformity is a unit consisting of deep water claystone, anoxic shales, and rare turbidites, also interpreted as syn-rift sediments. This unit is cut by the 6At1 (late Hauterivian) unconformity. Above the 6At1 unconformity is a unit consisting of marine claystone, anoxic shales, turbidites, and prograding shelf deposits interpreted as being deposited in the transition between rift and drift. This unit is bounded on top by the 13At1 (early Aptian) unconformity. Above the 13At1 unconformity are marine claystones, prograding shelf deposits and turbidites interpreted to have been deposited during the drift phase of continental breakup.

v Cenozoic Stratigraphy

Cenozoic-age deposits along the southern African coastline can be closely linked to marine transgressions and regressions, induced both by uplift and seaward marginal tilting of the subcontinent and by glacio-isostatic sea-level changes (***Reference 5.13.153***). In the Eastern Cape, the most widespread of these deposits are those of the Algoa Group (a sequence of marine to aeolian sediments of Eocene to Late Pleistocene and Holocene age) (***References 5.13.163***; ***5.13.166*** and ***5.13.153***). Between Plettenberg and Hermanus in the Western Cape, similar deposits of Miocene to Holocene age are mapped as the Bredasdorp Group (***Figure F-5.13.20*****).** Generalised composite sections summarizing the formations and deposits within these two groups are shown on ***Figure F-5.13.21.***

Other disconnected surficial deposits of Neogene to Recent-age in the site region include fluvial terraces, calcrete, scree, alluvium and aeolian sand.

The Grahamstown Formation is a remnant pedocrete formed in high relict pediment gravel deposits (***References 5.13.160*** and ***5.13.164***). The Grahamstown Formation is widely distributed but patchy. The Grahamstown Formation is comprised of sand, and pebble- to boulder-size clasts held together by resistant siliceous cement, often referred to as the Tg silcrete surface. The Tg surface can also be cemented by ferricrete in some locations (***Reference 5.13.165***; see ***Subsection 5.13.5.2.(a) ii*** for additional discussion of the age and origin of these deposits).

© Eskom 2026/Rev 0a

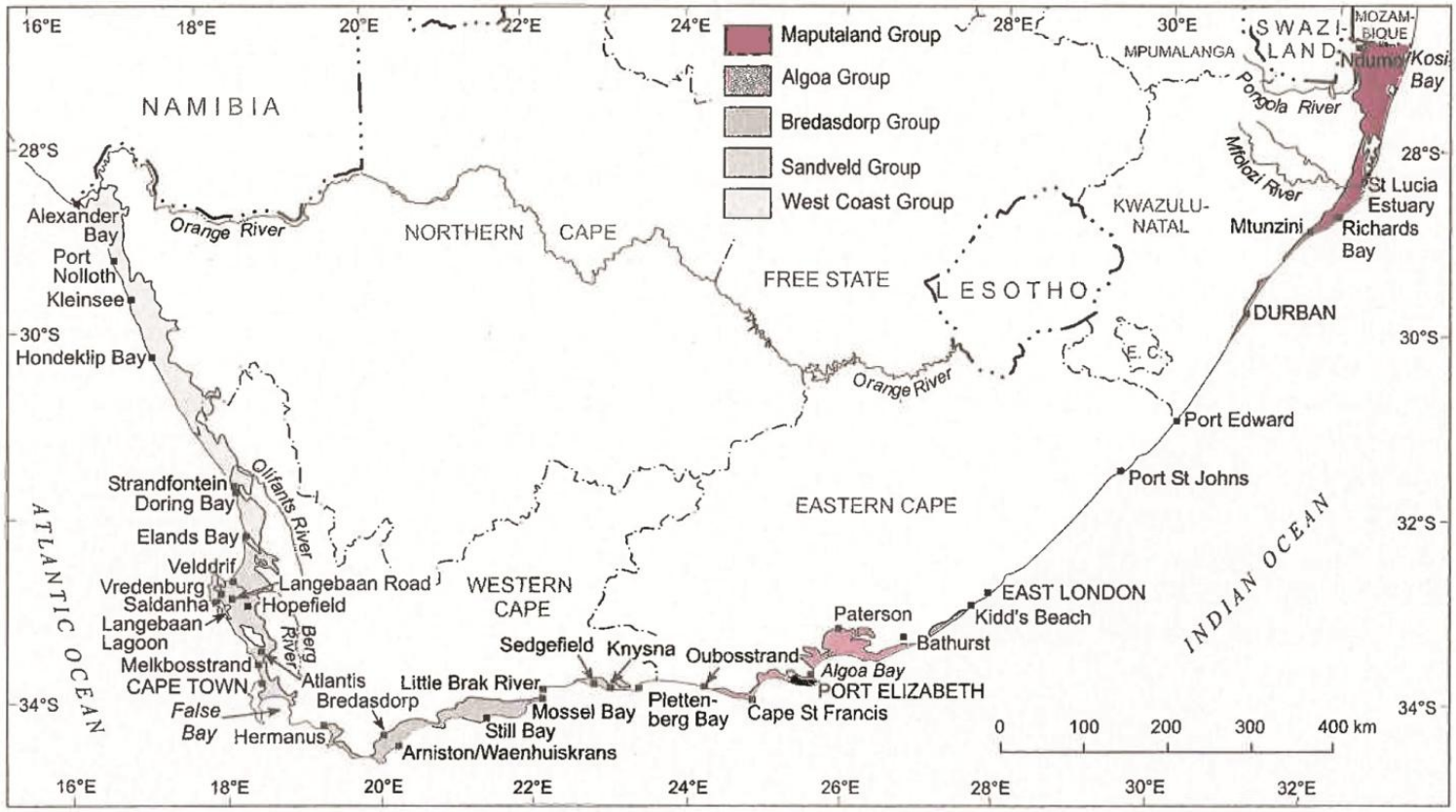
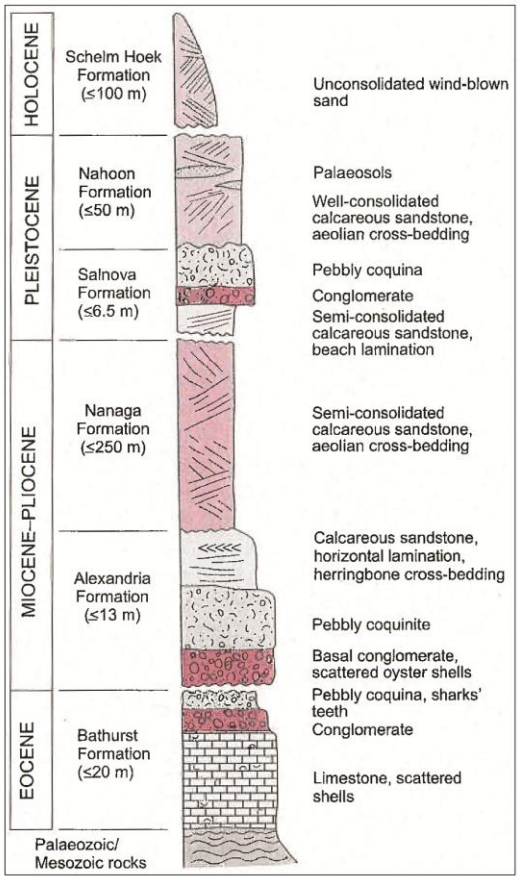
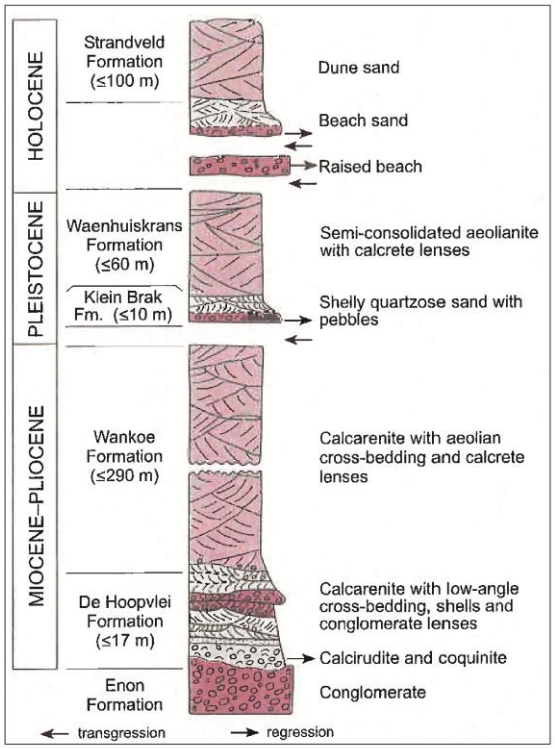


Figure 5.13-20
Distribution of Coastal Cenozoic Sediments in South Africa (*Reference 5.13.153*)

© Eskom 2026/Rev 0a



(A) Generalized composite section for the Algoa Group.



(B) Generalized composite section for the Bredasdorp Group.

Figure 5.13-21
Generalised Composite Section for (A) Algoa Group and (B) Bredasdorp Group

Along the southern coast between Knysna and Cape St. Francis the highest marine planation surface of probable Miocene age is a well-developed platform at an elevation of 200 m.

A broad 120–140 m bench is observed along the southern coast in the George-Knysna area, Natures Valley, Cape St. Francis, and between Humansdorp and the Gamtoos River (***References 5.13.167***, ***5.13.168***, and ***5.13.169***). ***Reference 5.13.167*** concludes that deposition of the De Hoopvlei Formation on this platform took place during the Pliocene regressive phase from a transgressive maximum at a present elevation of 120 m.

Several relatively long still stands occurred during the late Pliocene regression from this Pliocene transgressive maximum forming shorelines at 106 m, 90–100 m, and 84 m (***Reference 5.13.166***).

A flight of fluvial terraces along the Sundays River have been linked to marine terrace shorelines (***Figure F-5.13.22***). Le Roux (***Reference 5.13.166***) interpreted shorelines with elevations of 60 m and 52 m near the Sundays River to represent a late Pliocene transgressive maximum and stillstand, respectively.

Hattingh (***Reference 5.13.170***) mapped a flight of 13 fluvial terraces flanking the lower Sundays River valley that were divided into two groups. The Late Miocene to Late Pliocene Higher Terraces lie between 220 m and 40 m above the present riverbed with the deposits comprising mainly gravel. The Pleistocene to Holocene Lower Terraces with silt and fine-grained sand deposits occur between 25 m and 3 m above the present riverbed. Hattingh (***Reference 5.13.170***), using data extrapolated from the longitudinal profiles of the higher terraces, estimated elevations at which the palaeo-Sundays River met the Algoa Bay shoreline. Erlanger (***Reference 5.13.171***) and Erlanger et al. (***Reference 5.13.172***) sampled several fluvial terraces from the Sundays River and calculated cosmogenic nuclide (CN) burial ages using the isochron method. At a site approximately 13 km inland from the coast, CN samples collected by Erlanger (***Reference 5.13.171***) from a terrace with bedrock 53 m above the present river yielded a Pliocene age of 3.2 ± 0.486 Ma. A longitudinal profile of this fluvial terrace as mapped by Hattingh (***Reference 5.13.173***) shows this terrace to decrease to an elevation of approximately 30 m within 5 km of the coastline. An age of 4.1 ± 0.62 Ma was calculated on the next higher, 57 m bedrock strath, terrace by Erlanger (***Reference 5.13.171***).

In the vicinity of the Coega River mouth, cosmogenic geochronology investigations conducted as part of the geological investigations for the Thyspunt PSHA, included sampling of gravel lag overlying a marine terrace platform at an elevation of approximately 51.6 m in the Algoa Brick Quarry, which is east of the Coega River, approximately 6 km inland from the coast **(*Figure F-5.13.22)***. The results of the CN analysis of several clasts using the isochron method at this site (TSP-03) indicated a Pliocene age of deposition of 3.98 million years (Ma) **(*Reference 5.13.51*)**.

The isochron age and elevation of this platform above present base level suggest that the correlative fluvial terrace within the adjacent Sundays River fluvial terrace system would be the Uitkyk terrace (Terrace 7), which has a reported Pliocene isochron CN age of 4.1 ± 0.62 Ma. The palaeoshoreline elevation of the Algoa Brick Quarry terrace is not well defined. The sampling site could be close to the back edge of a terrace inset just below the 55–56 m

platform, or alternatively, these deposits may be associated with the 55–56 m terrace platform, which could extend to elevations of between 60 and 70 m, based on limited subsurface data.

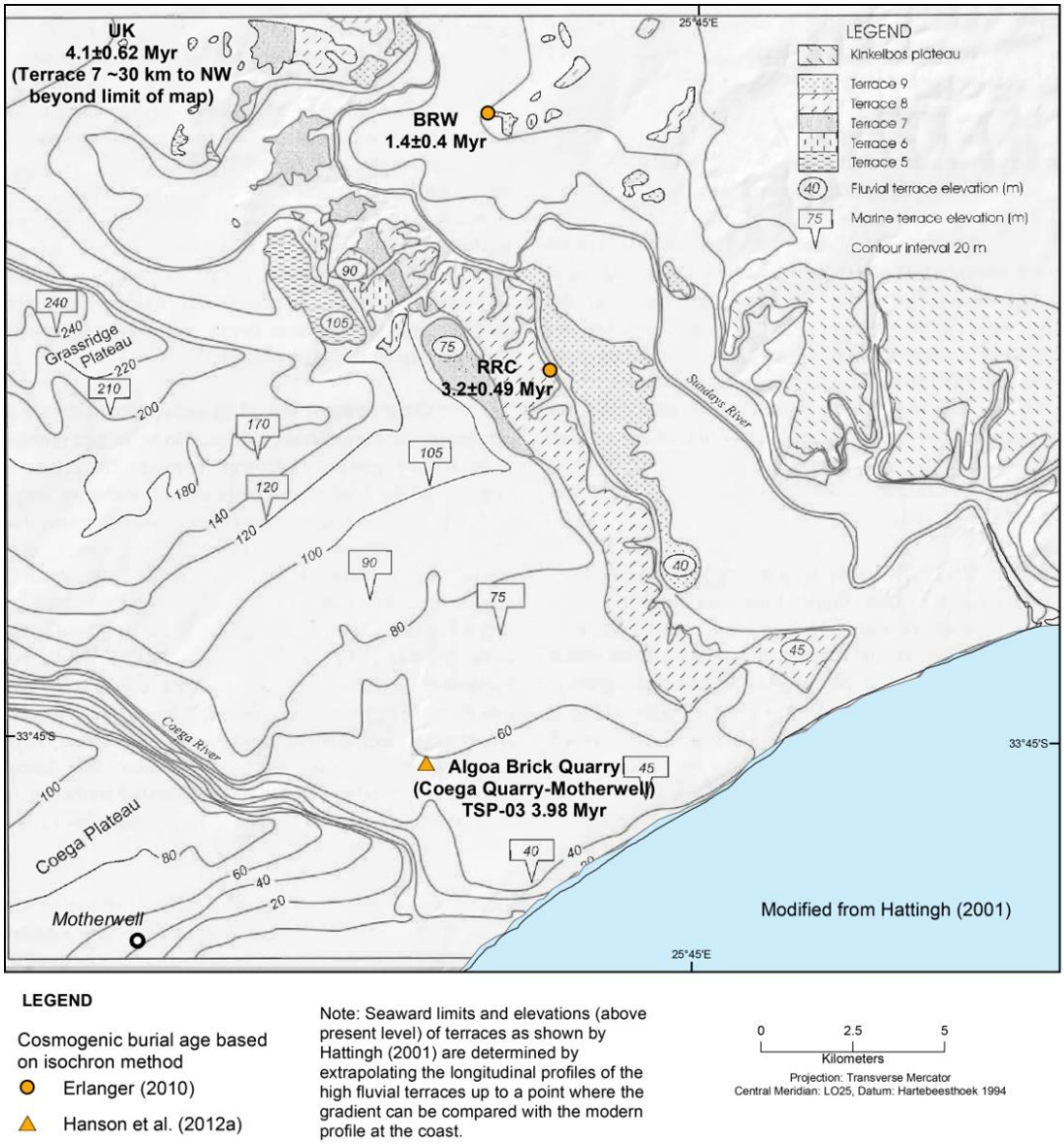


Figure 5.13-22
Map of Sundays River to Coega River Showing Cosmogenic Nuclide (CN) Sample Sites and Burial Ages (Modified from *Reference 5.13.58*)

The Quaternary Salnova Formation, which is situated on wave-cut surfaces thought to represent sea-level highstands, was deposited in an intertidal zone ranging from the sandy beach environment to a rocky shore environment (***Reference 5.13.166***). The formation reflects higher stands of sea level during Quaternary eustatic movements up to 30 m in elevation (***Reference 5.13.166***), although as noted above recent CN ages suggest that terraces at elevations of 30 m and higher are Pliocene or older. Outcrops of marine material are observed below 20 m along the rocky coast at Keurbooms, Knysna, Sedgefield, Klein Brak, and Hartenbos (***Reference 5.13.166***). These observations support the definition of the Salnova Formation to include deposits from multiple sea-level incursions (***Reference 5.13.50***). Roberts (***Reference 5.13.50***) notes that the records for the western and southern coasts of South Africa are consistent during the Pleistocene, implying tectonic stability in the recent geological past. A discussion of observations and information cited in the literature that bear on assessments of the ages and palaeo sea-levels for emergent and submerged terraces in the Thyspunt study region is provided in Hanson et al. (***Reference 5.13.58*** Appendix A).

The Nanaga, Nahoon, and Schelm Hoek Formations of the Algoa Group consist of aeolian deposits, which form well developed dune cordons along the southern coastline of the Eastern Cape (see ***Subsection 5.13.5.1.(a) iii*** – Coastal Belt). The deposits range from well consolidated to the unconsolidated Schelm Hoek Formation (***Reference 5.13.163***). Further analysis of the ages of aeolian deposits is summarised in ***Figure F-5.13.23.***

Dune cordons may have complex origins, with younger phases building on an older core, but their relative age can typically be inferred from their proximity to the coast (***References 5.13.174***, ***5.13.175***, ***5.13.85***, and ***5.13.176***). In the Wilderness area, three major dune cordons have developed.

The chronology of the landward, middle, and seaward dune cordons has been established with optically stimulated luminesce (OSL) ages (***Reference 5.13.176***), as follows:

- The landward dune cordon formed between during MIS 7 (241–221 ka) and possibly MIS 9 (334-306 ka) (***Reference 5.13.176***).

- The middle dune cordon formed in at least two phases of sea-level highstands MIS 7 (241–221 ka) and MIS 5e (144–130ka) (***Reference 5.13.176***).

- The seaward cordon developed during the transition to the last major interglacial (MIS 5e; 144–130 ka) through the Holocene (10–0 ka).

© Eskom 2026/Rev 0a

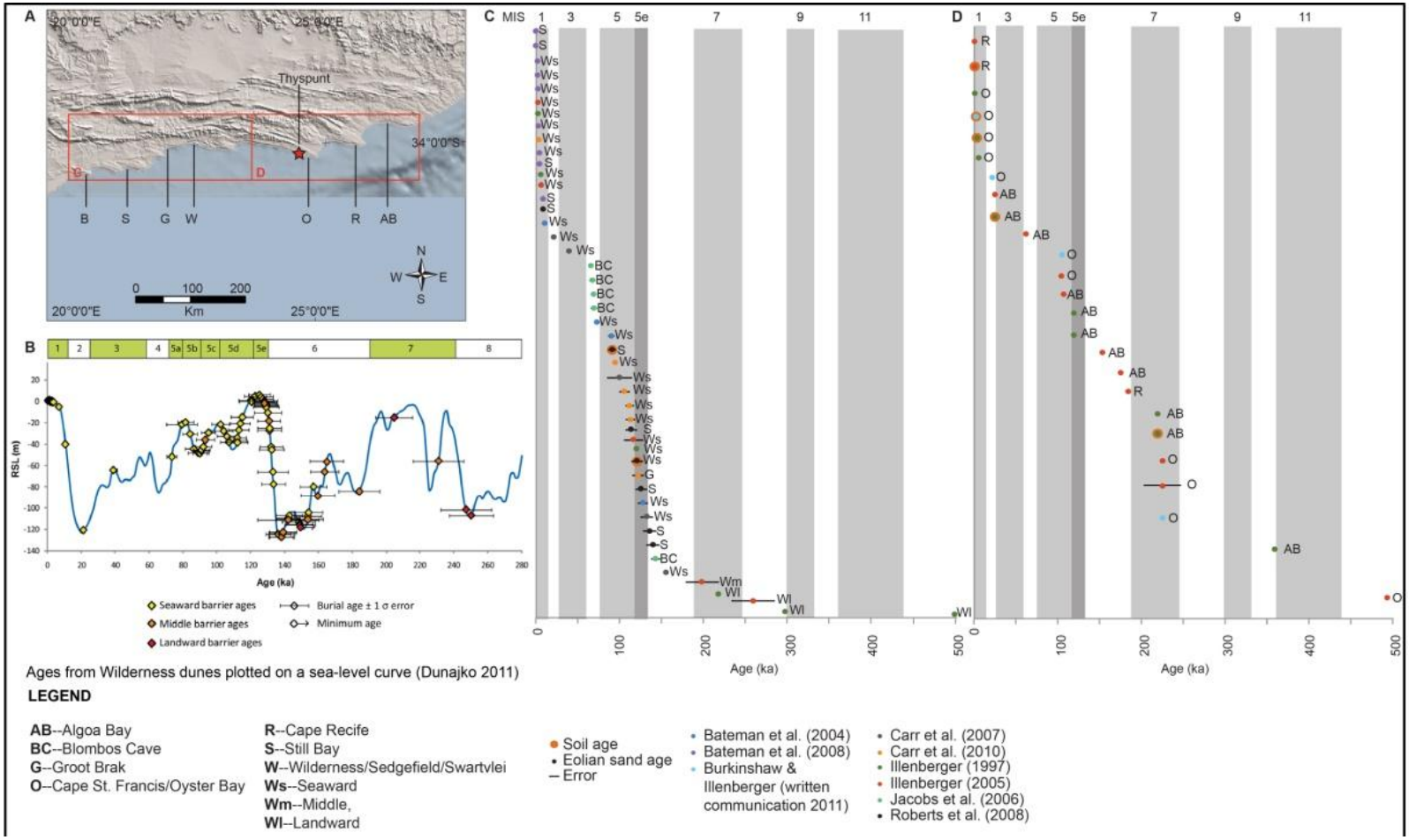


Figure 5.13-23
Dune Locations and Ages Along the Southern Coast of the Eastern Cape Province

© Eskom 2026/Rev 0a

Coalesced dune deposits lie inland of these dune cordons and are thus older—probably middle Pleistocene (~1,000 ka).

Offshore dune cordons also are recognised and are thought to have formed during the various sea-level stillstands of the Pleistocene glacial (***References 5.13.177***, ***5.13.71***, and ***5.13.174***). Martin & Flemming (***Reference 5.13.71***) recognise major shorelines at the bases of dune cordons at depths of 90–85 m, 75–65 m, 55–50 m, and 40 m, in agreement with evidence from knickpoints at depths of 100–105 m, 80–75 m, 55–50 m, and approximately 40 m. Bremner & Day (***Reference 5.13.178***) identify submerged wave-cut platforms in Algoa Bay at approximately –135 m, –116 m, –90 m, and –70 m. The deeper platforms at and below –90 m are overlain by dissected aeolianite remnants. Du Plessis & Glass (***Reference 5.13.179***) interpret a submerged, eroded aeolianite in Algoa Bay resting on a bedrock platform at approximately –23 m to be Eemian (MIS 5, 144-80 ka).

d) Regional Tectonic Setting

This subsection describes the contemporary tectonic setting of the site as well as the crustal scale properties and tectonic features of the Thyspunt site region.

i Contemporary Tectonic Setting

The seismotectonic framework of a region, which includes the basic understanding of existing tectonic features and their relationship to the contemporary stress regime and seismicity, forms the foundation for assessments of seismic sources. A conceptual neotectonic framework was developed for the Thyspunt PSHA Project (***Reference 5.13.1***) that characterises the modern tectonic setting and processes, the contemporary stress regime, and the distribution, style, and rate of active deformation in the region.

The following subsections define the region in terms of:

- Plate motions.
- Tectonic stress regime.
- Uplift and denudation rates.
- Regional and local earthquakes.

Plate Motion

The continental margins of southern Africa have been relatively stable passive margins from the time of the clearance of the Falkland Plateau from the margin in the mid-Cretaceous (***Reference 5.13.151***) until recent propagation of the East African Rift zone southwards (***Reference 5.13.180***). Propagation of the East African Rift zone is breaking apart the African continent into the Nubian (also called the African Plate) and Somalian Plates. Extension along the rift generates relative rotation between the two plates (***Reference 5.13.181***), with an Euler pole between South Africa and the southwest Indian Ridge (***Reference 5.13.182***). The exact location of the Euler pole varies depending on the model, data sampled, and number of plates used (***References 5.13.183*** and ***5.13.182***).

Modelling of plate motion data indicates that the Nubian and Somalian Plates may be separated by a smaller plate(s) or stable aseismic blocks (***References 5.13.184***, ***5.13.185***, and ***5.13.186***). Modelling of plate motions including the Lwandle, Nubian, and Somalian Plates significantly improves the fit of the model to the observations over using the Nubian and Somalian Plates alone (***Reference 5.13.186***; ***Figures F-5.13.24*** and ***F-5.13.25***).

It has been hypothesised that for the past 30 Myr, the African continent has been nearly stationary in relation to hotspot locations (***Reference 5.13.188***). Stability results in long-term interactions between upwelling in the mantle and the lithosphere (***Reference 5.13.189***) and may result in long-term impacts on topography (*e.g.*, ***Reference 5.13.190*** and ***Reference 5.13.191***). One-dimensional shear-wave velocity models of the upper mantle beneath the Kalahari Craton are similar to those of other cratons indicating a possible lower mantle source for high topography in southern Africa (***Reference 5.13.192***). Mantle upwelling may also have a role in rifting. Thin-sheet crustal modelling indicates that although buoyancy forces may advance rifting, buoyancy forces are not great enough to initiate rifting (***Reference 5.13.187***).

Mantle convection and its influence on the topography in South Africa are further described below (see discussion in ***Subsection 5.13.5.1.(d) i*** – Uplift and Denudation Rates).

© Eskom 2026/Rev 0a

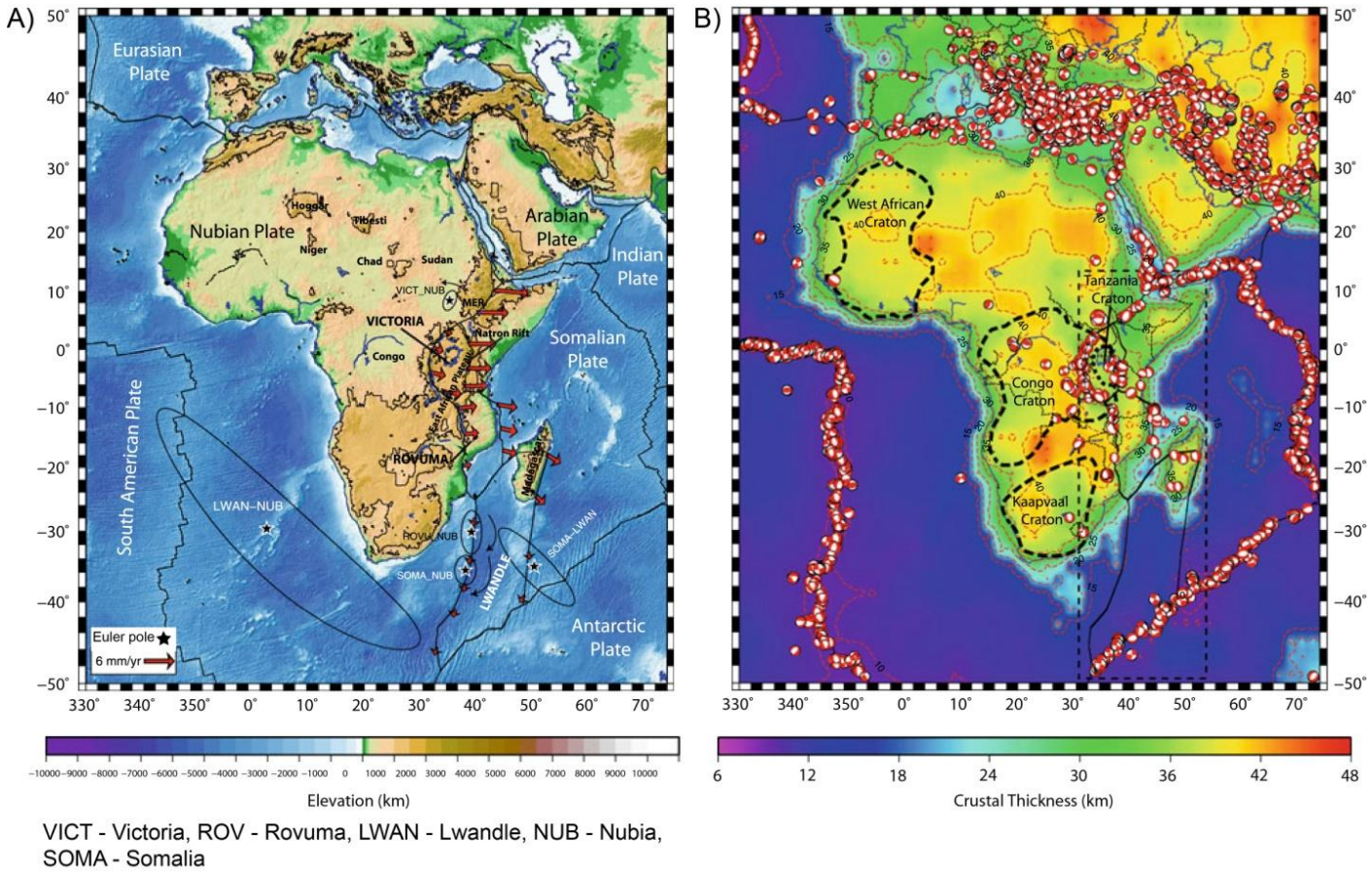
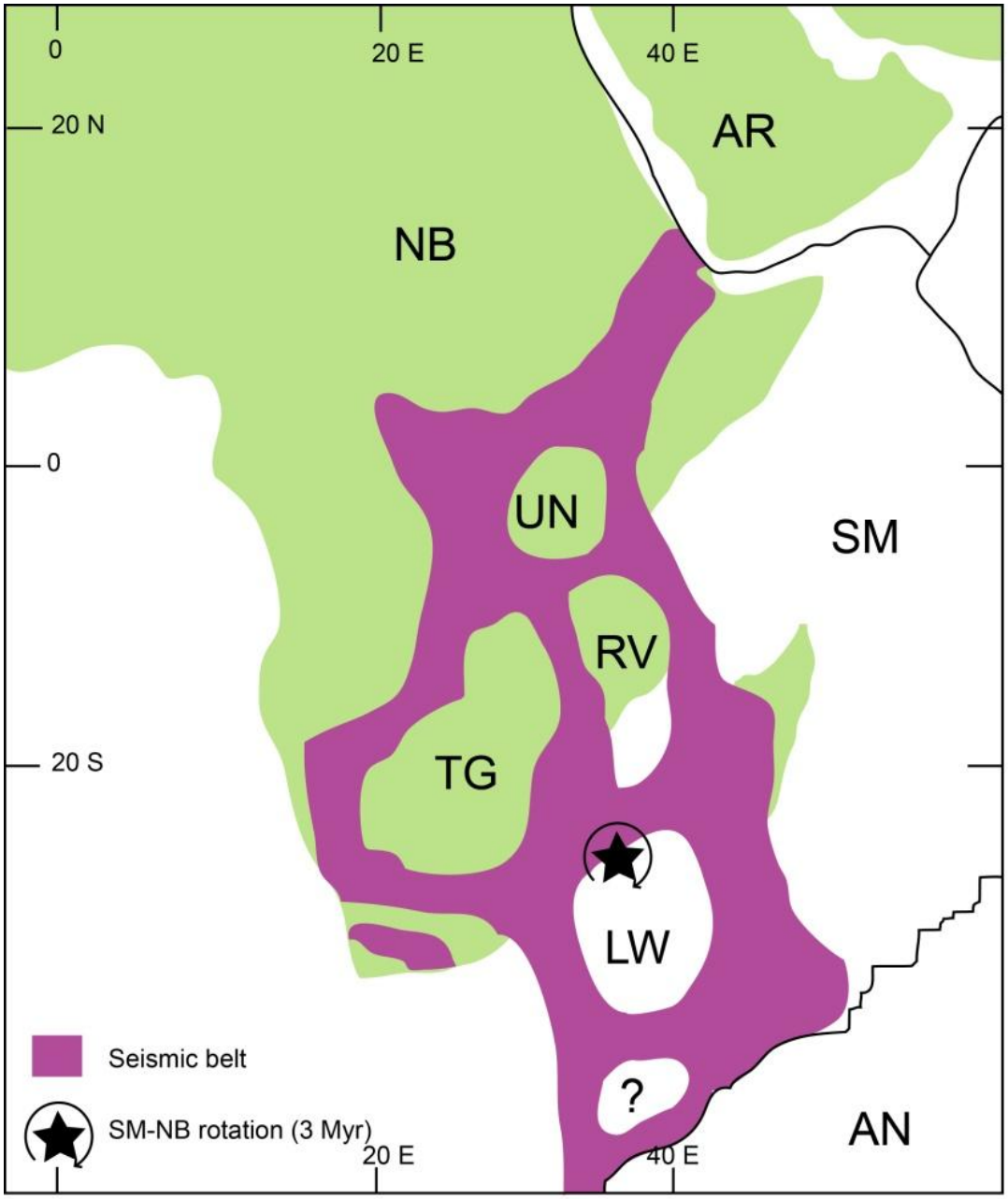


Figure 5.13-24
Tectonic Setting of Africa, Including (A) Major Plate Boundaries and Motions (B) Crustal Thickness with Major Cratonic Boundaries and CMT Focal Mechanisms (Modified from *Reference 5.13.187*)

© Eskom 2026/Rev 0a



AN - Anarctica, AR - Arabia, NB - Nubia, LW - Lwandle, RV - Rovume, SM - Somalia, TG - Transgariep, UN - Ukerewe Nyana

Figure 5.13-25
African Composite Plate, Subdivided into Smaller, Relatively Stable Blocks Separated by Seismically Active Belts (Modified from *Reference 5.13.184*)

Evidence for recent fault rupture, together with the historical earthquake catalogue in southern Africa (described below in ***Subsection 5.13.5.1.(d) i*** – Regional and Local Earthquakes and ***Section 5.14*** – Seismic Hazard Analysis), indicates ongoing seismic activity.

Low earthquake recurrence rates and a short instrumentation history inhibit the study of the modern stress regime. Recent studies have begun to analyse the modern stress regime using modern seismic events, GPS, and geological strain indicators, such as jointing, in conjunction with stress field modelling. Some models assume that crustal thinning in the East African Rift zone is due to far-field forces resulting in extension. Field evidence, however, suggests that volcanism has been coincident with rift onset and that border faults are not active early in the rifting process (***Reference 5.13.193***). This indicates that forces other than simple extension are at work. Stamps *et al.* (***Reference 5.13.187***) used the CRUST 2.0 model to simulate vertically averaged deviatoric stresses in the East African Rift zone.

The results showed that lateral crustal density variations were necessary to achieve the dynamic topography of southern Africa. Further, the results indicated that deviatoric stress alone cannot overcome the strength of the lithosphere and that either magma injection or mantle flow may assist rifting. Deep mantle convection may also be a primary driver of plate motions (***References 5.13.194*** and ***5.13.192***).

Tectonic Stress Regime

Low earthquake recurrence rates and a short instrumentation history inhibit the study of the modern stress regime. Recent studies have begun to analyse the modern stress regime using modern seismic events, Global Positioning System (GPS) data, and geological strain indicators, such as jointing, in conjunction with stress field modeling.

Bird et al. (***Reference 5.13.181***) evaluated a province of northwest-southeast-directed, most compressive horizontal principal stress along the western edge of southern Africa referred to as the Wegener stress anomaly (***Figure F-5.13.26***). Bird et al. (***Reference 5.13.181***) constrained thin-shelled finite-element modeling with data from the 2004 World Stress Map (***Reference 5.13.195***)[1] and 17 additional Holocene stress markers (based on overcoring, borehole breakout, and geological fault-slip orientation data).

[1] The updated version of this map is from *Reference 5.13.196*; see *Figure F-5.13.57*

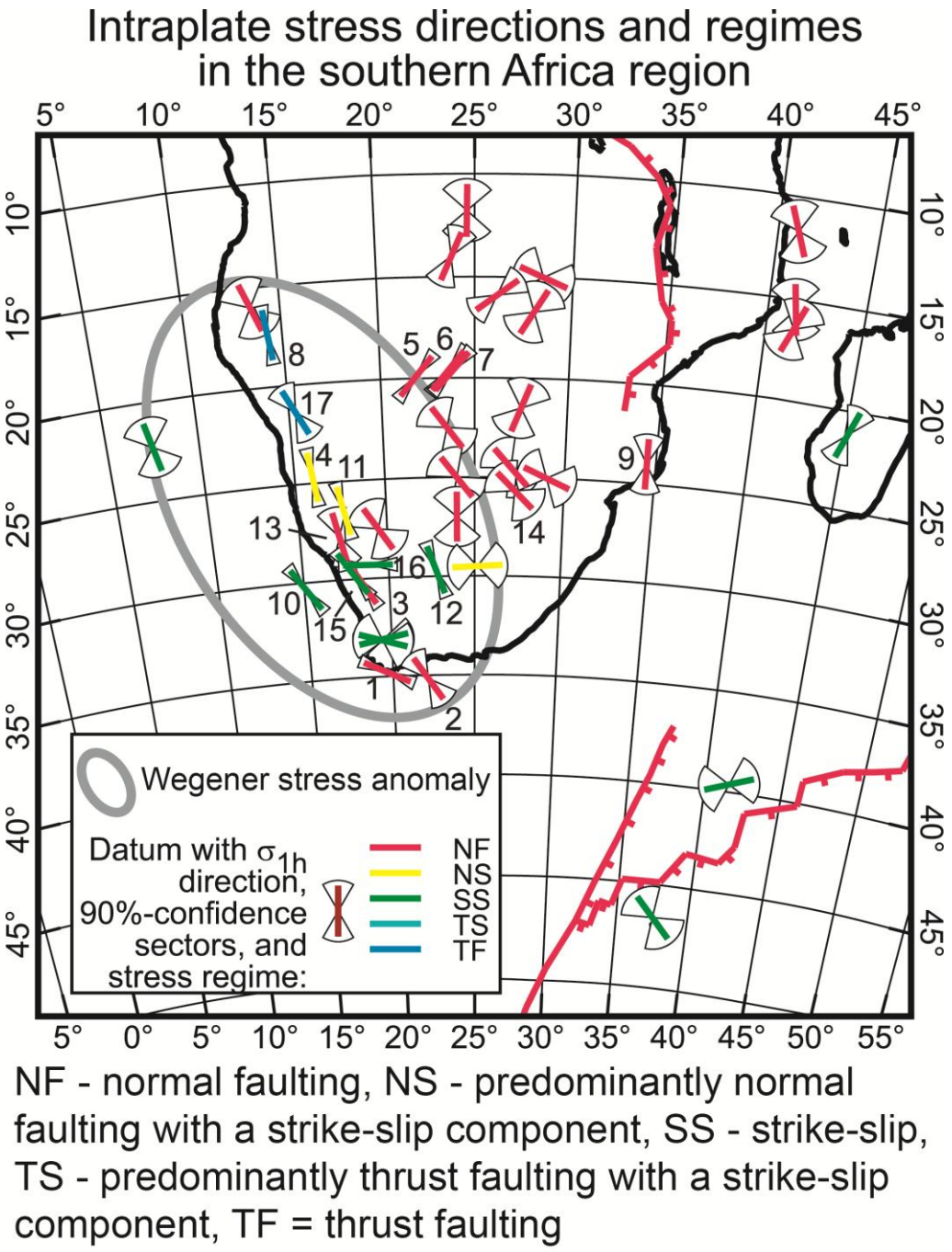


Figure 5.13-26
Intraplate Indicators of Stress Regime (Indicated by Colour) and Azimuth of the Most Compressive Horizontal Principal Stress (σ1h) (*Reference 5.13.181*)

The portion of the updated version of the World Stress Map (***Reference 5.13.196***) that covers southern Africa is shown on (***Figure F-5.13.27***). The Bird *et al*. (***Reference 5.13.181***) study used mechanical modelling to test three potential causes of the Wegener stress anomaly:

- lateral variations in density moment;
- resistance of unbroken lithosphere to plate rotation;
- stress concentration ahead of the crack tip of the East African Rift zone.

Modelling showed that resistance of the plates to rotation made the best fit to the Wegener stress anomaly data.

The strain rate map predicted by the preferred model has high rates along the East Africa Rift curving at 12°S into a western arc through the western margin of southern Africa. The study concluded that although southern Africa is surrounded by spreading ridges, most of it is not in a state of horizontal compression (from ridge push), but instead is generally in a state of horizontal extension because its high elevations lead to density moments exceeding those of spreading ridges. They note that while the northwest-southeast–directed most compressive horizontal principal stress (the Wegener stress anomaly) is real, in many places it is actually caused by northeast-southwest extensional tectonic stress related to the resistance of unbroken lithosphere to the plate rotation of the incipient Somalian Plate away from the Africa Plate.

The preferred model, which assumes there are no master faults separating Somalian Plate oceanic crust from Africa Plate oceanic crust, predicts higher and differently oriented stresses in the stronger oceanic lithosphere offshore. There could be coast-parallel extensional tectonic stress close to the continental margin and coast-parallel compressional stress further offshore. Unpublished exploration data of A. Logue shows north/northwest orientation of maximum horizontal compressive stress on the continental shelf offshore of the site (***Reference 5.13.197***).

© Eskom 2026/Rev 0a

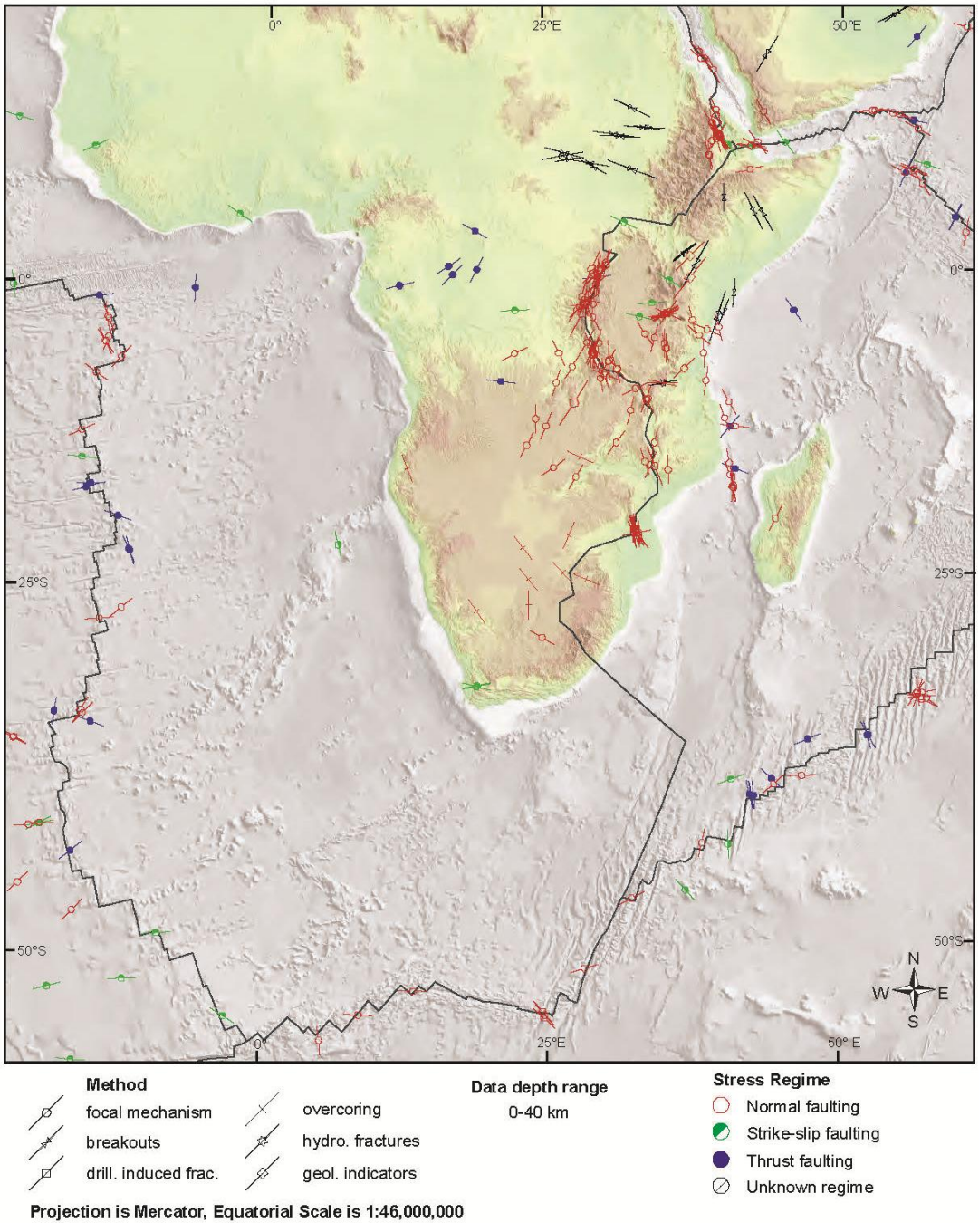


Figure 5.13-27
Southern Africa Stress Data from World Stress Map
(*Reference 5.13.196*)

© Eskom 2026/Rev 0a

Calais *et al.* (***Reference 5.13.182***) used GPS data to study the potential for microplates within the East African Rift zone. GPS data from 14 sites and slip vectors from 53 earthquakes were compared to two- and three-plate inversion models to find the best fit. Using a new kinematic model and mantle flow directions interpreted from seismic anisotropy measurements, Calais *et al.* (***Reference 5.13.182***) proposed that regional asthenospheric upwelling and locally focused mantle flow may influence continental deformation in East Africa. They noted that the proposed model, although consistent with the data, does not account for widespread seismicity observed west of the Western rift, where earthquake slip vectors show a consistent northwest-southeast trend.

Hartnady (***Reference 5.13.184***) interpreted this seismicity as delineating an additional microplate (Transgariep block on ***Figure F-5.13.25***). However, a GPS station located on that potential microplate does not show any significant relative motion with respect to Nubia. These observations suggest that if there is relative motion of the Zambian craton with respect to Nubia, it must happen at very slow rates (e.g., less than 1–2 mm/yr). Calais *et al.* (***Reference 5.13.182***) further speculate that southward-dipping asthenospheric flow associated with the East African Rift zone may also explain seismicity belts with minor or incipient normal faults that bound cratonic domains in southern Africa (Kaapvaal, Zimbabwe, Zambia cratons).

More recent analysis of South African GPS data compiled from 34 TRIGNET sites by Calais (***Reference 5.13.198***) showed that strain rates for all but the north-eastern corner of South Africa are not significant at the 95% confidence level (***Figure F-5.13.28***). Results of the analysis showed the following:

- Velocities at the best-quality TRIGNET sites are very well fit by a single angular rotation.
- Deviations from rigid plate behaviour do not exceed 0.4 mm/yr on average (maximum 1.1 mm/yr at site TDOU).
- Strain rates in the western part of the Western Cape and in the Eastern Cape are $2 \pm 4 \times 10^{-9}\text{yr}^{-1}$ on average and less than $6 \times 10^{-9}\text{yr}^{-1}$.
- Although strain rates from Delaunay triangulation are not significant at the 95% confidence level, the region of the Kango Fault indicates slight extension.

© Eskom 2026/Rev 0a

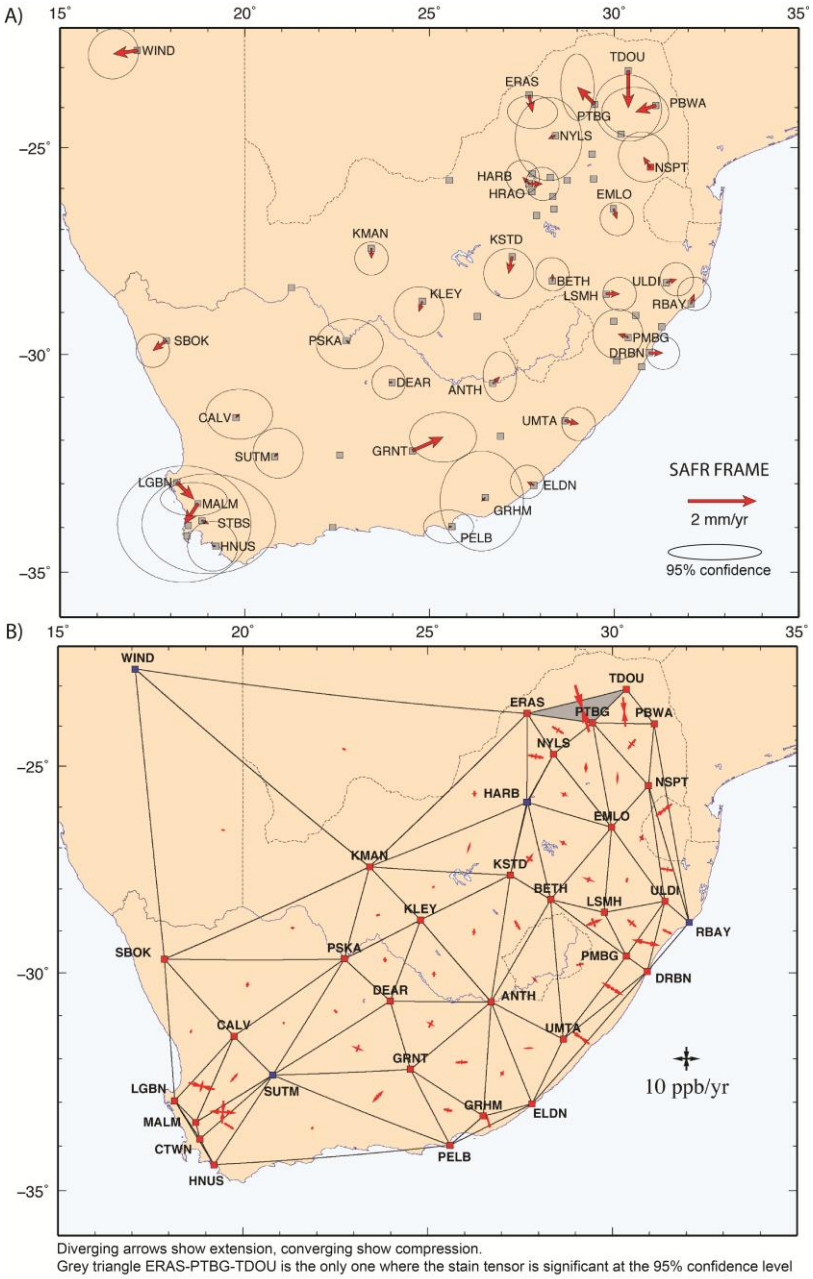


Figure 5.13-28
(a) Residual Velocities with Respect to a Frame Defined by All TRIGNET Stations for the 34 Best Sites.
(b) Map of Principal Horizontal Strain Rate Tensors Computed for a Delaunay Triangulation of the Best TRIGNET Sites (*Reference 5.13.19)*

© Eskom 2026/Rev 0a

The study by Calais (***Reference 5.13.198***) did not find evidence for higher strain rates wrapping around the Kaapvaal Craton as hypothesised by Bird *et al.* (***Reference 5.13.181***). There are also differences in the direction and rates for some stations, as shown by Calais *et al.* (***Reference 5.13.182***). The more recent analysis of Calais (***Reference 5.13.198***), which is based on more observational data and was focused on evaluating strain within the study region, is judged more reliable than earlier studies. Hartnady (***Reference 5.13.199***) notes that the continental strain rates presented by Bird *et al.* (***Reference 5.13.181***) are governed by heat-flow pattern (affecting lithospheric strength) and do not take into account hot-spot pre-weakening.

Calais (***Reference 5.13.198***) notes that although this recent analysis of geodetic data in the Thyspunt region shows no evidence of strain at statistically significant levels, the errors are large due to the relatively short period of observation and may not be a reliable measure for assessing earthquake recurrence.

Another approach to assessing the tectonic stress regime is the interpretation of stresses derived from focal mechanisms of instrumental earthquakes. As discussed in detail in ***Section 5.14*** (Seismic Hazard Analysis), the total number of high-quality mechanisms is limited in the site region due to the relatively low levels of seismicity and the rather broad seismic station distribution. Nevertheless, there are sufficient numbers of events to develop a regional sense of the tectonic regime across the southern part of Africa, away from the influence of the East African Rift. A set of 21 earthquakes were selected based on using the best-quality focal mechanisms and selecting a preferred mechanism for those few events having more than one reference,. ***Table T-5.13.4*** summarises the strike, dip, and rake angles of the fault plane solution for each earthquake in the data set. ***Table T-5.13.5*** summarises the azimuth and plunge of the P-axis (maximum compression) and T-axis (minimum compression) for each of those events.

A linear inversion algorithm and nonparametric bootstrap statistics were input into the software program SLICK (***Reference 5.13.215***) to derive regional stress tensors from the combined data set. The results are shown on ***Figure F-5.13.29***, and the derived regional stress tensors for the entire data set are presented below:

- P-axis – azimuth 320°/ plunge 60°.
- B-axis – azimuth 127°/ plunge 15°.
- T-axis – azimuth 220°/ plunge 5°.

© Eskom 2026/Rev 0a

Table 5.13.4
Summary of South African Focal Mechanism Information

Event	TM	ID	Reference	Φ(°)	δ(°)	λ(°)	SoF	Method
1969-09-29 Ceres Mainshock	T	1a	***5.13.200*** Fairhead & Girdler (1971)	131 [42]	82 [82]	~0	SS	First-motion polarities of teleseismic P and PKP phases. Main fault plane selected based on strike of aftershock distribution from Green & Bloch (***Reference 5.13.249*** 1971).
		1b	***5.13.201*** Green & McGarr (1972)	317-321	~90	~0	SS	First-motion P-wave polarities of 42 WWSSN long-period seismograms; main fault plane selected based on strike of aftershock distribution from Green & Bloch (1971).
		1c	***5.13.202*** Maasha & Molnar (1972)	44 133	82 81	~0	SS	First motion polarities and P-wave spectra for seismic moment determination
		1d	***5.13.203*** Shudofsky (1985)	310	82	180	SS	Rayleigh-wave inversion and body-wave modelling
		1e	***5.13.204*** Wagner & Langston (1988)	124 217	88 89	~0	SS	Waveform inversion and fitting of digitised long-period WWSSN data. Use both P and SH waves.
		1f	***5.13.205*** Foster & Jackson (1998)	305 [215]	87 [87]	3 [177]	SS	Waveform inversion and fitting using WWSSN body-wave data . Use both P and SH waves.
		1g	***5.13.206*** Krüger *et al.* (2011)	305	78	1.2	SS	Moment tensor inversion using scanned and digitised WWSSN data. Use both body- and surface waves
1970-04-14 Ceres Aftershock	T	2	***5.13.203*** Shudofsky (1985)	61	88	219	SS	Rayleigh-wave inversion and body-wave modelling
1976-07-01 Koffiefontein	T	3a	***5.13.207*** Fairhead & Stuart (1972)	2 18	70 20	'-	NM	First-motion polarities of P-waves

© Eskom 2026/Rev 0a

Event	TM	ID	Reference	Φ(°)	δ(°)	λ(°)	SoF	Method
		3b	***5.13.203*** Shudofsky (1985)	300	63	219	NO	Rayleigh-wave inversion and body-wave modelling
		3c	***5.13.208*** Jensen (1991)	308	22	-86	NM	Body-wave inversion of long-period WWSSN data. Uses both P and SH waves
1986-10-05 Matatiele	T	4	***5.13.209*** Dziewonski et al. (1987)	168 348	47 53	-90 -90	NM	Harvard Centroid Moment Tensor Solution
1990-09-26 Free State Gold Mines	M	5	***5.13.210*** Dziewonski et al. (1991)	11 153	45 52	-61 -115	NM	Harvard Centroid Moment Tensor Solution
1994-10-30 Free State Gold Mines	M	6a	***5.13.211*** Fan & Wallace (1991)	345	14	-105	NM	Regional moment tensor solution
		6b	***5.13.212*** Bowers (1997)	190	45	-70	NM	Global moment tensor inversion using broadband data
1997-09-25 Far West Rand	M	7	***5.13.213*** Brandt & Saunders (2011)	354 167	49 41	-86 -95	NM	Regional moment tensor solution using SASE waveforms
1998-04-24 Augrabies	T	8	***5.13.214*** Mangongolo (2012)*	132	80	18	SS	First-motion P-wave polarities of SASE data analysed using FPFIT
1998-06-22 Three Sisters	T	9	***5.13.214*** Mangongolo (2012)*	19	41	-121	NO	First-motion P-wave polarities of SASE data analysed using FPFIT
1998-09-06 Lesotho	T	10	***5.13.214*** Mangongolo (2012)*	148	48	-67	NM	First-motion P-wave polarities of SASE data analysed using FPFIT
1998-10-05 Fraserburg	T	11	***5.13.214*** Mangongolo (2012)*	9	67	-19	SS	First-motion P-wave polarities of SASE data analysed using FPFIT

References followed by an asterisk correspond to unpublished CGS data (see ***Reference 5.13.1***, chapter 6 for details).

TM is a flag indicating whether events are mining-related (M) or tectonic (T).

ID identifies the solution in ***Reference 5.13.1*** Figure 6.11. In the case of multiple solutions for the same event, the preferred solution is indicated in bold.

Φ, λ and δ are the strike, dip and rake angles of the fault plane solution, respectively, in degrees.

SoF is a flag indicating the style of faulting: SS=strike-slip, NM=normal, NO=normal-oblique.

© Eskom 2026/Rev 0a

Table 5.13.5
P-axes and T-axes for Earthquakes Having Focal Mechanisms (see ***Table T-5.13.4***)

Event	TM	ID	Φ(°) P	δ(°) P	Φ(°) T	δ(°) T
1969-09-29 Ceres Mainshock	T	1g (1)	260	8	169	9
1970-04-14 Ceres Aftershock	T	2 (2)	293	28	188	25
1976-07-01 Koffiefontein	T	3c (3)	31	67	215	23
1986-10-05 Matatiele	T	4	78	88	258	2
1990-09-26 Free State Gold Mines	M	5	1	70	261	4
1994-10-30 Free State Gold Mines	M	6b (6)	183	76	86	2
1997-09-25 Far West Rand	M	7	299	85	81	4
1998-04-24 Augrabies	T	8	264	5	356	20
1998-06-22 Three Sisters	T	9	200	69	311	8
1998-09-06 Lesotho	T	10	130	73	222	1
1998-10-05 Fraserburg	T	11	329	29	237	4
1998-12-05 Far West Rand	M	12	348	23	246	26
1999-02-04 Fauresmith	T	13a (13)	129	32	220	2
1999-07-03 Koffiefontein	T	14	287	26	26	18
2007-03-11 Leeu-Gamka	T	15	161	3	68	39
2010-11-21 Augrabies	T	16	335	15	233	37
2010-12-25 Augrabies (18:29)	T	17	330	15	229	36
2010-12-25 Augrabies (23:28)	T	18	326	17	224	34
2010-12-28 Augrabies	T	19	325	16	223	36
2011-01-04 Augrabies	T	20	334	10	237	35
2011-12-18 Augrabies	T	21b (21)	210	23	302	6

TM is a flag indicating whether events are mining-related (M) or tectonic (T).

ID identifies the solution on ***Table T-5.13.4***. The ID in brackets indicates the corresponding number as plotted in stress orientation.

Φ and δ are the azimuth, plunge angles of the p- and t-axes, respectively, in degrees.

© Eskom 2026/Rev 0a

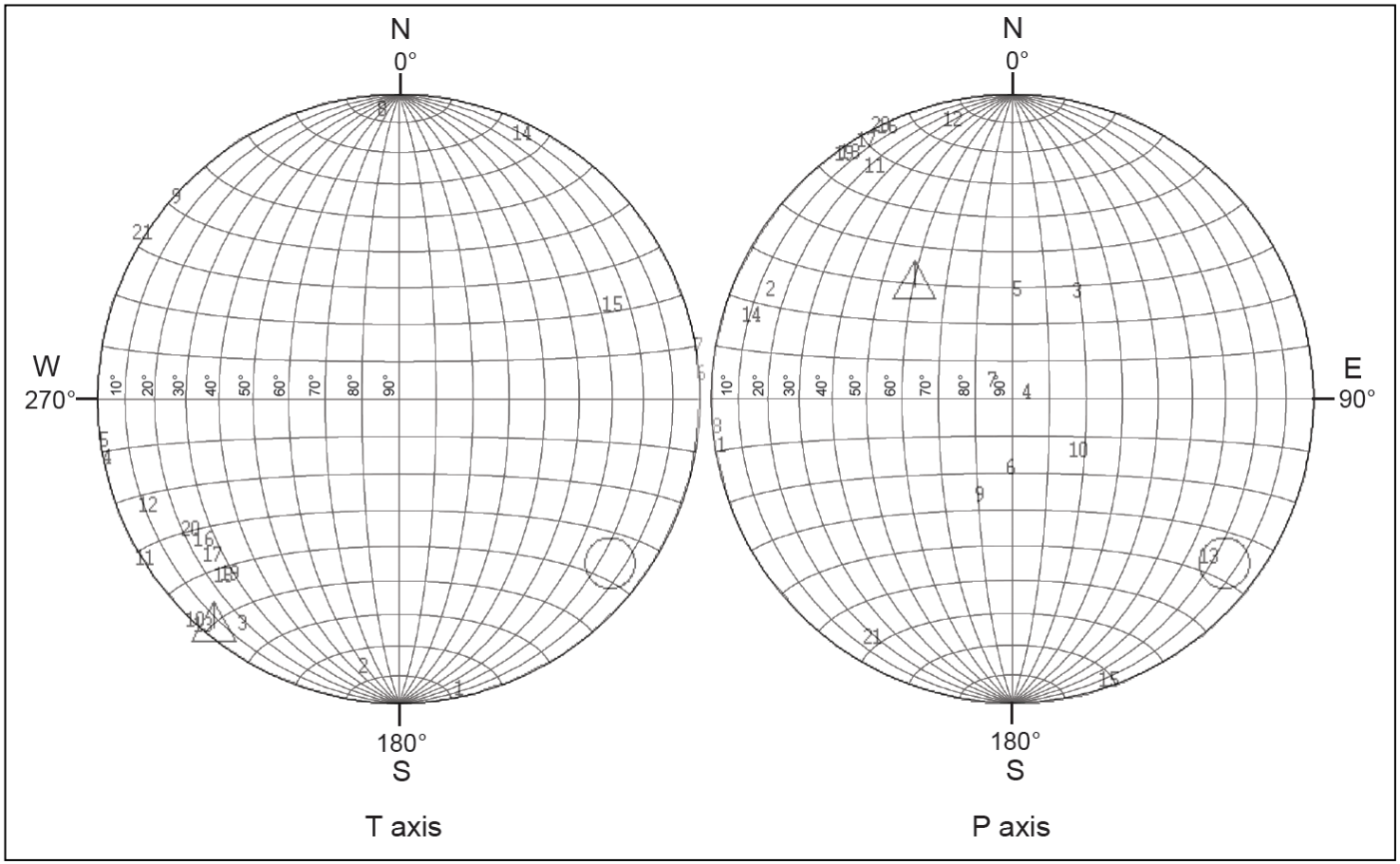


Figure 5.13-29
Stereonet Plots of P-Axes and T-Axes of the Earthquakes Having Focal Mechanisms in Table T-5.13.5. The stress tensors for the entire data set are shown with triangles for the P- and T-axes, and the B-axis is shown with a circle.

© Eskom 2026/Rev 0a

These regional stress indicators can be used to infer the tectonic regime. The exact cut-off values defining the tectonic regime categories are subjective. Zoback (***Reference 5.13.216***) used the broadest possible categorisation consistent with actual P-, B-, and T-axes values in ***Table T-5.13.6***. The choice of axes used to infer the maximum horizontal stress direction (S_H) orientation is also displayed in the table. For example, the S_H orientation is taken as the azimuth of the B-axis in case of a pure normal faulting regime (NF) and as the azimuth of the T-axis + 90° in the NS case, when the B-axis generally plunges more steeply than the T-axis.

The criteria given in ***Table T-5.13.6*** were used to derive stress tensors for the region that suggest that the overall tectonic regime is normal faulting, with some tendency toward normal strike-slip (*i.e.,* the plunge of the P-axis does not greatly exceed 52°). This is clearly in accord with the mix of normal and strike-slip focal mechanisms derived for the region (discussed in ***Section 5.14*** – Seismological Database) and with observations of Brandt & Saunders (***Reference 5.13.213***).

Table 5.13.6
Tectonic Regime Assignment (*Reference 5.13.216*) for Given Plunges of the P-, B-, and T-Axes in Degrees

P-axis	B-axis	T-axis	Regime	S_H-azimuth
pl > 52		pl < 35	NF	azim. of B-axis
40 < pl < 52		pl < 20	NS	azim. of T-axis + 90°
pl < 40	pl > 45	pl < 20	SS	azim. of T-axis + 90°
pl < 20	pl > 45	pl < 40	SS	azim. of P-axis
pl < 20		40 < pl < 52	TS	azim. of P-axis
pl < 35		pl > 52	TF	azim. of P-axis

NF: Normal faulting
NS: Normal strike-slip
SS: Strike-slip
TS: Thrust strike-slip
TF: Thrust faulting
S_H: Maximum horizontal compressive stress

Based on criteria in the study by Zoback (***Reference 5.13.216***), the azimuth of maximum horizontal compression S_H is 127° or northwest-southeast. This compressive stress direction is comparable to that derived from other indicators of maximum horizontal stress directions such as borehole breakouts.

Geological information also has been reviewed to assess the current stress regime in the Thyspunt study region. Geological studies of jointing and fractures along the south coast of South Africa between Alexander Bay and Port Elizabeth show little evidence of recent deformation (***Reference 5.13.24***). De Beer (***Reference 5.13.24***) observed little evidence of joints propagating through the Pliocene to late Pleistocene Bredasdorp Group, indicating low levels of neotectonic stress.

The Kango Fault, the northernmost of the Cape Fold Belt structures to have been reactivated during the Mesozoic extensional stress regime (***Figure F-5.13.3***), is the only fault in South Africa with definitive evidence of Quaternary surface faulting (see ***Subsection 5.13.5.1.(d) v*** – Cenozoic Structures). Palaeoseismic trenching and geomorphic mapping along the Kango Fault indicate that the style of Quaternary reactivation has been normal slip (***References 5.13.217***, ***5.13.218***, ***5.13.14***, and ***5.13.54***). These studies also documented that three latest Pleistocene to Holocene surface-faulting events have occurred along the reactivated Kango Fault, and these surface-rupturing earthquakes were preceded by a long period (tens of thousands of years) of relative quiescence (***Reference 5.13.54***).

The low cumulative displacements and apparent temporal clustering of events observed along the Quaternary-reactivated Kango Fault are typical of the long-term behaviour of recognised active faults in other stable continental regions that are characterised by episodes of activity separated by quiescent intervals of at least 10–100 kyr (commonly) or more (***Reference 5.13.219***). The Kango Fault may be in such a period of activity based on the evidence for repeated late Pleistocene and Holocene surface rupturing events recognised along the eastern part of the fault zone. However, long-term rates of erosion inferred from cosmogenic nuclide (CN) analysis of stream sediments from drainage basins throughout the study region (both north and south of the Kango Fault) are relatively uniform and low (average 4.5 ± 0.9 m/Myr; area-weighted average of 5.4 m/Myr) (***Reference 5.13.51***; see ***Subsection 5.13.5.1.(d) i*** – Uplift and Denudation Rates). These low rates of erosion argue for low rates of erosionally driven rock uplift and are consistent with the characterisation of the region as a stable continental region.

Uplift and Denudation Rates

The African continent has an atypically high-elevation craton when compared to other continents. About 500 m of positive residual elevation, referred to as the “African Superswell”, covers eastern Africa, southern Africa (including the Kalahari craton), and an area of the south-eastern Atlantic Ocean basin southwest of the African continent (***Reference 5.13.190*** and ***Figure F-5.13.30***).

Numerous studies have addressed both the timing and mechanisms of uplift leading to the development of the Superswell. There is a growing body of evidence that suggests that significant uplift occurred in the Cretaceous post-rift period, and some researchers attribute the significant unroofing that occurred in this time to igneous processes (significant igneous intrusions due to possible mantle upwelling) (***References 5.13.220***, ***5.13.221***, and ***5.13.95***). There may also be a component of isostatic adjustment to erosion that would give rise to patterns of higher uplift near the Great Escarpment and coastal regions (***References 5.13.222***, ***5.13.223***, ***5.13.224***, ***5.13.225***, and ***5.13.226***). Others favour various models and configurations of mantle convection leading to buoyancy in either the upper mantle or deeper mantle as the major cause of the high elevation (***References 5.13.190***, ***5.13.189***, ***5.13.191***, ***5.13.227***, ***5.13.228***, ***5.13.229***, and ***5.13.230***).

© Eskom 2026/Rev 0a

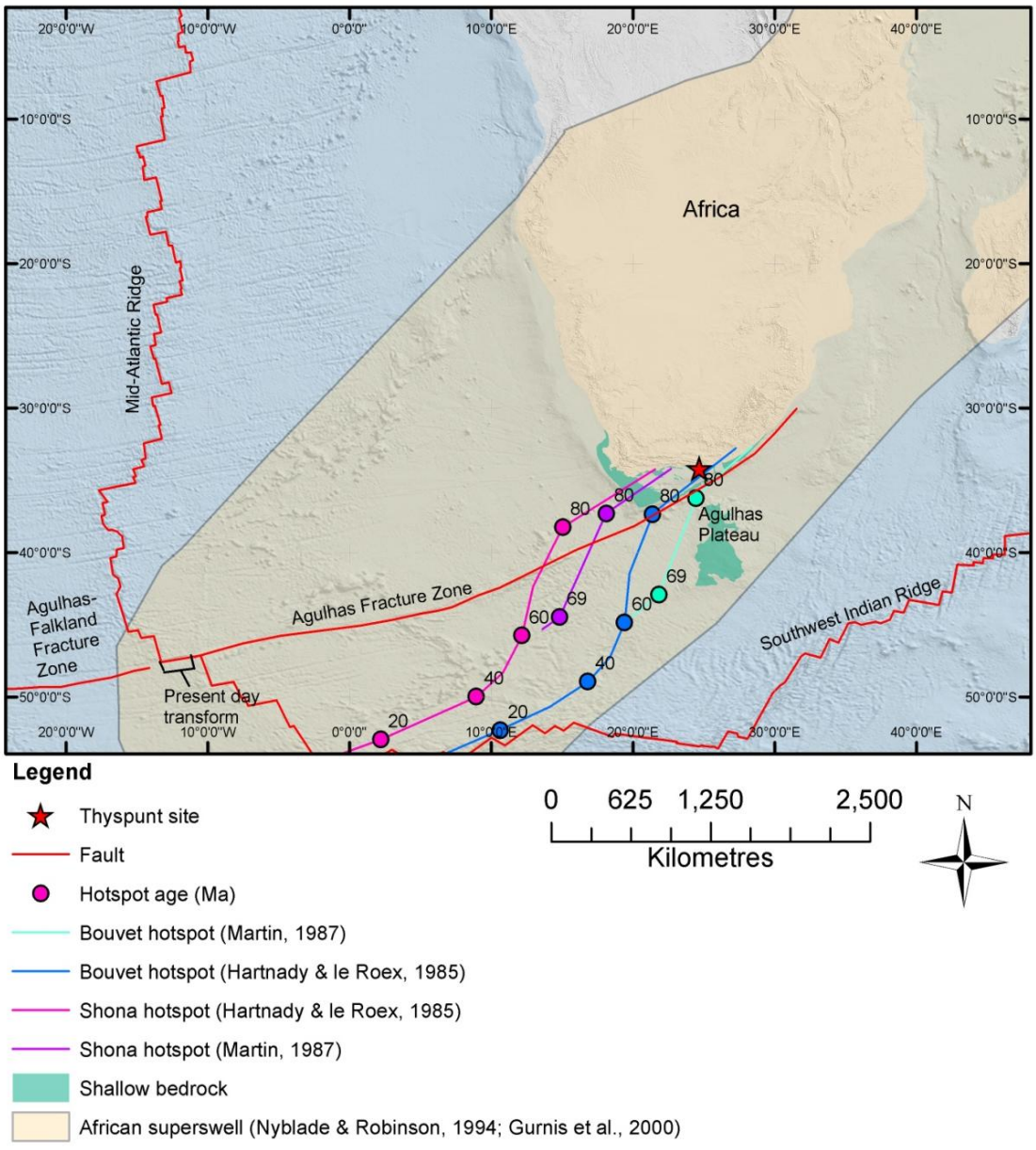


Figure 5.13-30
Map of African Superswell and Inferred Hotspot Tracks

Brandt *et al.* (***Reference 5.13.192***) conclude that deep mantle processes are likely to be the cause of the high Kalahari elevation, and consequently, for much of the anomalous elevation of the African Superswell, at least across southern Africa.

More pertinent to the assessment of seismic hazards in the study region are long-term average Cenozoic rates of uplift and information pertaining to contemporary stress and strain patterns. Many recent studies have documented evidence for slower and more uniform rates of erosion in the Cenozoic (***References 5.13.231***, ***5.13.232***, ***5.13.227***, ***5.13.233***, ***5.13.234***, ***5.13.235***, ***5.13.236***, ***5.13.221***, ***5.13.237***, and ***5.13.238***) than were previously suggested by King (***Reference 5.13.239***) and Partridge & Maud (***Reference 5.13.152***). Slow erosion and uplift rates are inferred from dating surfaces using cosmogenic nuclides, and from determining cooling rates associated with uplift and denudation using fission track analysis. Reconstruction of the palaeo topography of the African continent using seismic tomography and geological data showed that the topography was already high during the Cretaceous and that there is no need to invoke high rates of Cenozoic uplift to explain the modern topography (***Reference 5.13.240***).

Locations of recent studies documenting long-term uplift and denudation rates in southern Africa are shown on ***Figure F-5.13.31***; a summary of the key observations from these studies is provided in Hanson *et al.* 2012a, Appendix A (***Reference 5.13.58***).

In the Southern Cape, denudation of 2.5–3.5 km during the mid- to Late Cretaceous was followed by less than 1 km of Cenozoic denudation along the southern coast (***Reference 5.13.221***). Tinker *et al.* (***Reference 5.13.221***) sampled outcrops for AFT on a north-south profile from Marysdale to Oudtshoorn and supplemented these data with samples from four boreholes. Tinker et al. (***Reference 5.13.221***) splits Cretaceous erosion into two pulses of denudation (140–120 Ma and 100–80 Ma). The earlier period of denudation is evident landwards of the escarpment and the later denudation period seawards of the escarpment. From 136 Ma to 120 Ma, a large volume of sediment was deposited off the coast of the Southern Cape (***Reference 5.13.237***); coincident with the earlier period of denudation. This volume of sediment is not large enough to account for all of the denudation predicted by AFT analysis (***Reference 5.13.237***). In the later period, 2.5–3.5 km of denudation occurred at a rate of 15–175 m/Myr (***Reference 5.13.221***). Rates of basin deposition were an order of magnitude lower in the Cenozoic than in the Cretaceous.

© Eskom 2026/Rev 0a

D

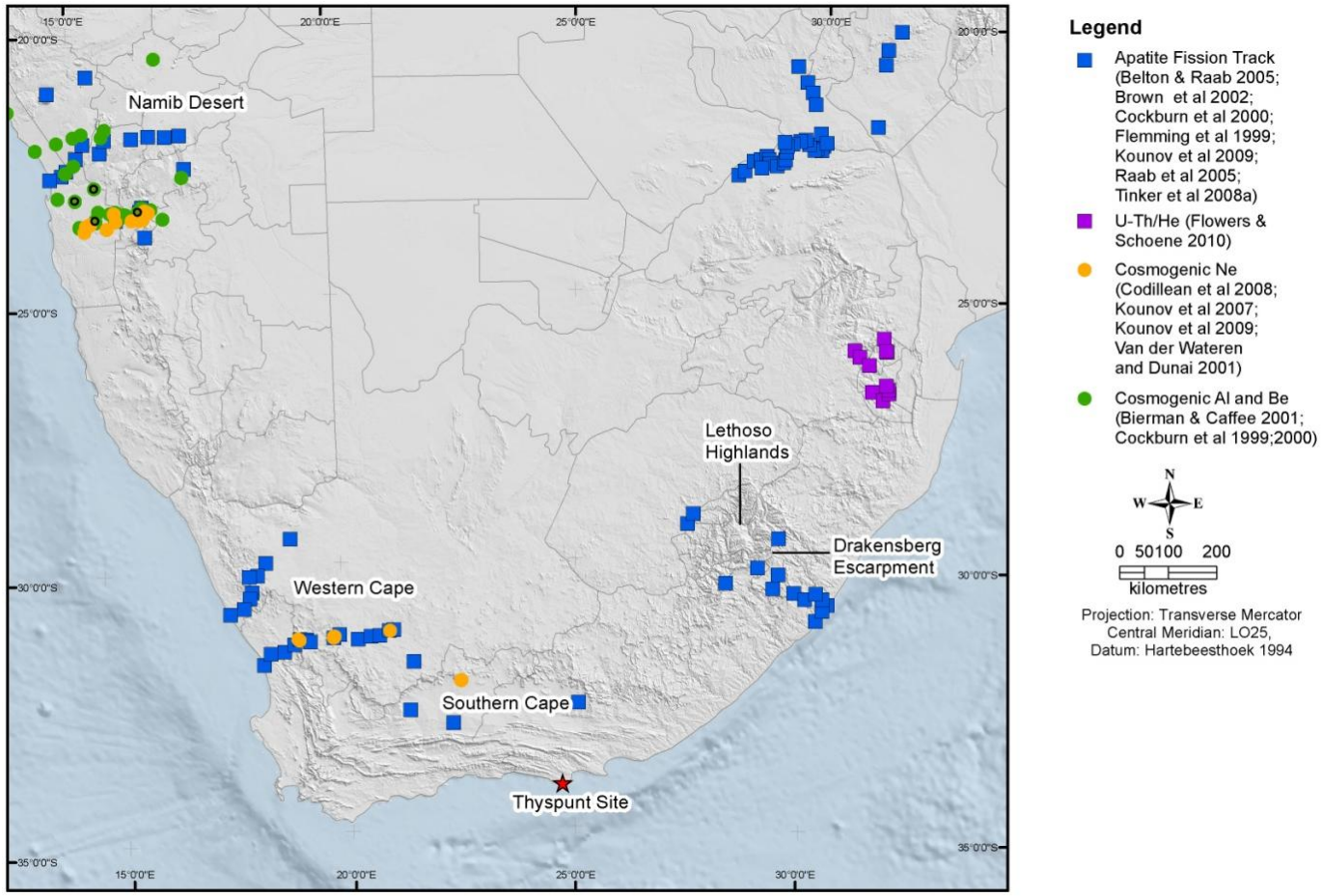


Figure 5.13-31
Locations of Data Points of Studies of Erosion and Uplift Rates in Southern Africa

© Eskom 2026/Rev 0a

Bierman (***Reference 5.13.51***) analysed the ^{10}Be content of eight sand samples collected from rivers draining to the Indian Ocean along the southern coast of South Africa (six of which are from different river systems) to estimate basin-wide denudation rates (***Figure F-5.13.32***). The results of this analysis indicate that the land surface in south central South Africa is eroding at a rate of about 5.4 m/Myr (area-weighted average). This very slow erosion rate, which is similar to rates assessed by Scharf *et al.* (***Reference 5.13.241***) in the Cape region to the west (***Figure F-5.13.32***), is consistent with those measured in other nontectonically active areas around the world (***Reference 5.13.242***). Bierman (***Reference 5.13.51***) noted that there is no statistically significant relationship between basin-scale erosion rates and physical properties of the sampled watersheds, including area, elevation range, mean elevation, mean slope, and mean annual precipitation. The lack of any relationship between basin-scale erosion rates and mean basin slope is consistent with steady base level and, thus, an absence of differential uplift.

Studies of river terraces along the Sundays River by Hattingh (***Reference 5.13.170***) and Erlanger *et al.* (***Reference 5.13.172***) interpret incision rates of less than 20 m/Ma with a trend of lower rates towards the present. Erlanger *et al.* (***Reference 5.13.172***) calculated river incision rates of 16.1 ± 1.3 m/Myr over the last 4 Myr and an average palaeo-erosion rate of 6.62 ± 1.1m/My.

As described in this subsection above, the study region is characterised by low rates of seismicity and low strain rates inferred from analysis of GPS data in the region south of Latitude 23°S. New cosmogenic data gathered as part of the Thyspunt geological investigations (***Reference 5.13.51***) and results of recent studies outlined above suggest that south-central South Africa is a geomorphically stable region. Erosion rates, and thus rates of isostatic uplift, are very low. Overall, south-central South Africa is an exceptionally stable landscape.

Regional and Local Earthquakes

This section provides an overview of the seismicity surrounding the Thyspunt site, starting from a regional summary and then homing in on the site.

A description of the earthquake catalogue developed for the project is provided in ***Section 5.14*** (Seismic Hazard Analysis), and the earthquake catalogue report is included in Appendix 5 to the Thyspunt PSHA report (***Reference 5.13.1***).

© Eskom 2026/Rev 0a

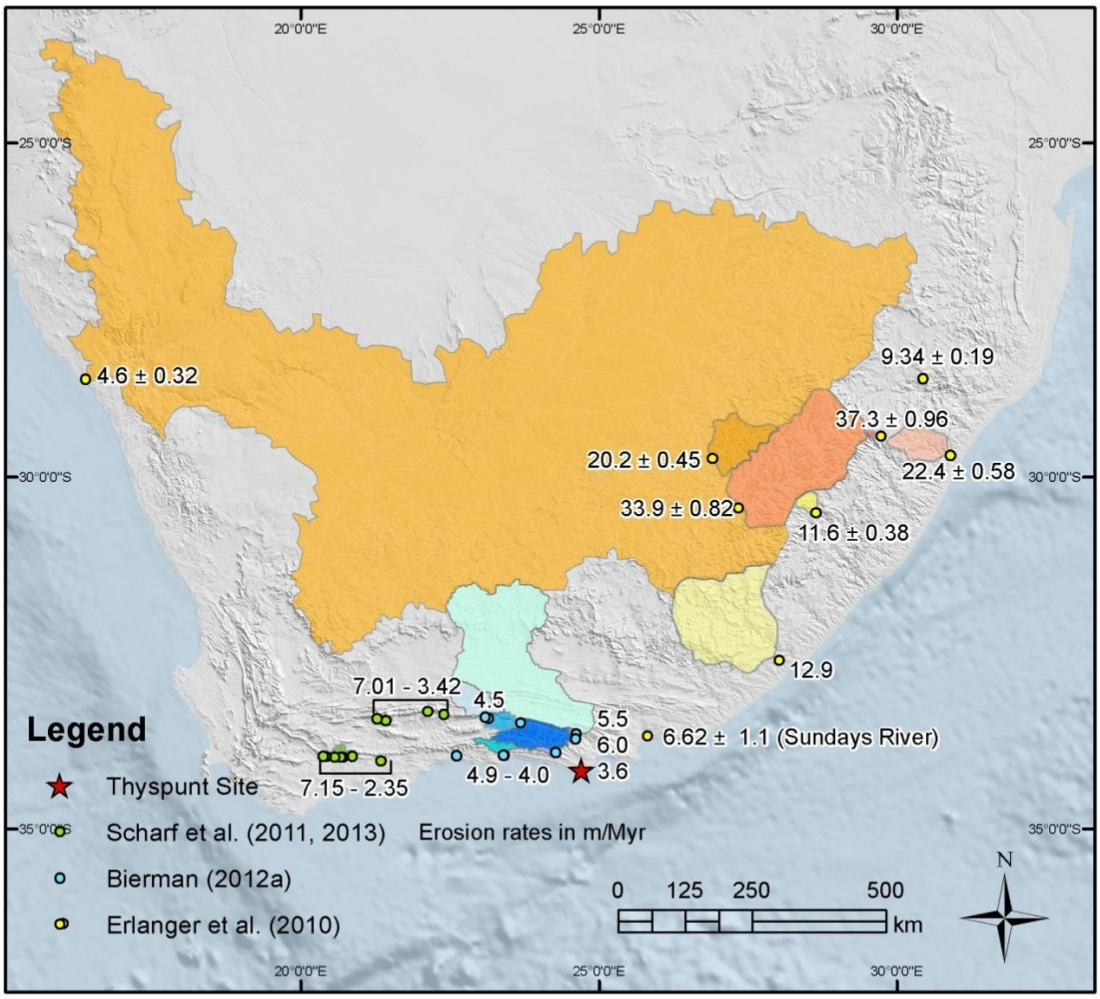


Figure 5.13-32
Compilation of Basin Erosion Rates in the Southern Coastal Region of South Africa. Coloured polygons map the locations of drainage basins sampled for erosion rates (*Reference 5.13.1*)

Seismicity in sub-Saharan Africa is concentrated mainly in the eastern part of the continent, along the western and eastern branches of the East African Rift System (*e.g.*, ***References 5.13.205*** and ***5.13.243***). Away from the well-delineated branches of the Rift System, seismicity is diffuse, as shown on ***Figure F-5.13.33***, which depicts the catalogue compiled for the southern and eastern African regional study undertaken by Midzi *et al.* (***Reference 5.13.243***) as part of the Global Seismic Hazard Assessment Project (GSHAP).

© Eskom 2026/Rev 0a

The seismicity of the whole of this region is characterised by the relative rarity of large (Mw ≥ 7.0) events. There are no events of this magnitude in the Global Large Historical Earthquake Catalogue (GLHECAT; ***Reference 5.13.244***) covering the years 1000–1903, developed as a global reference catalogue as part of the Global Earthquake Model (GEM) project. While the relatively shorter recorded history of Africa may be a contributor to this, the rarity of large events is confirmed by the instrumental record. That record includes only three events with Mw on the order of 7.0 or above since the inception of instrumental seismology in 1900, global catalogues being complete at this level:

- the 13 December 1910 event in the Rukwa region of Tanzania (M_S 7.4 according to ***Reference 5.13.245*** and M_w 6.9, according to ***Reference 5.13.246***);
- the 20 May 1990 event in southern Sudan (M_w 7.2, according to ***Reference 5.13.246***); and
- the 22 February 2006 main shock of the earthquake sequence in southern Mozambique (M_w 7.0, according to ***Reference 5.13.247***).

Seismicity in South Africa is characterised by diffuse patterns, as shown on ***Figure F-5.13.34***. Concentrations of small-to-moderate events in Gauteng and the Welkom region of the Free State are related to deep gold-mining activity. Natural seismicity is found to be slightly more prominent along the Namaqua-Natal Mobile Belt between Namaqualand and the KwaZulu-Natal coast via Lesotho.

The following discussion focusses on the seismicity in the region south of the 28°S parallel, in accordance with the spatial extent of the seismic source characterisation (SSC) model developed in the Thyspunt study (***Reference 5.13.1***).

The seismic history of South Africa includes a small number of events that were large enough to be widely felt and, in some cases, cause slight to moderate damage locally. The magnitudes of these events are generally in excess of M_w 5.5; however, there are only three events with magnitudes greater than M_w 6.0. A concentration of such events can be found in the south-western Cape (which boasts the longest earthquake record, dating back to the 17th century).

© Eskom 2026/Rev 0a

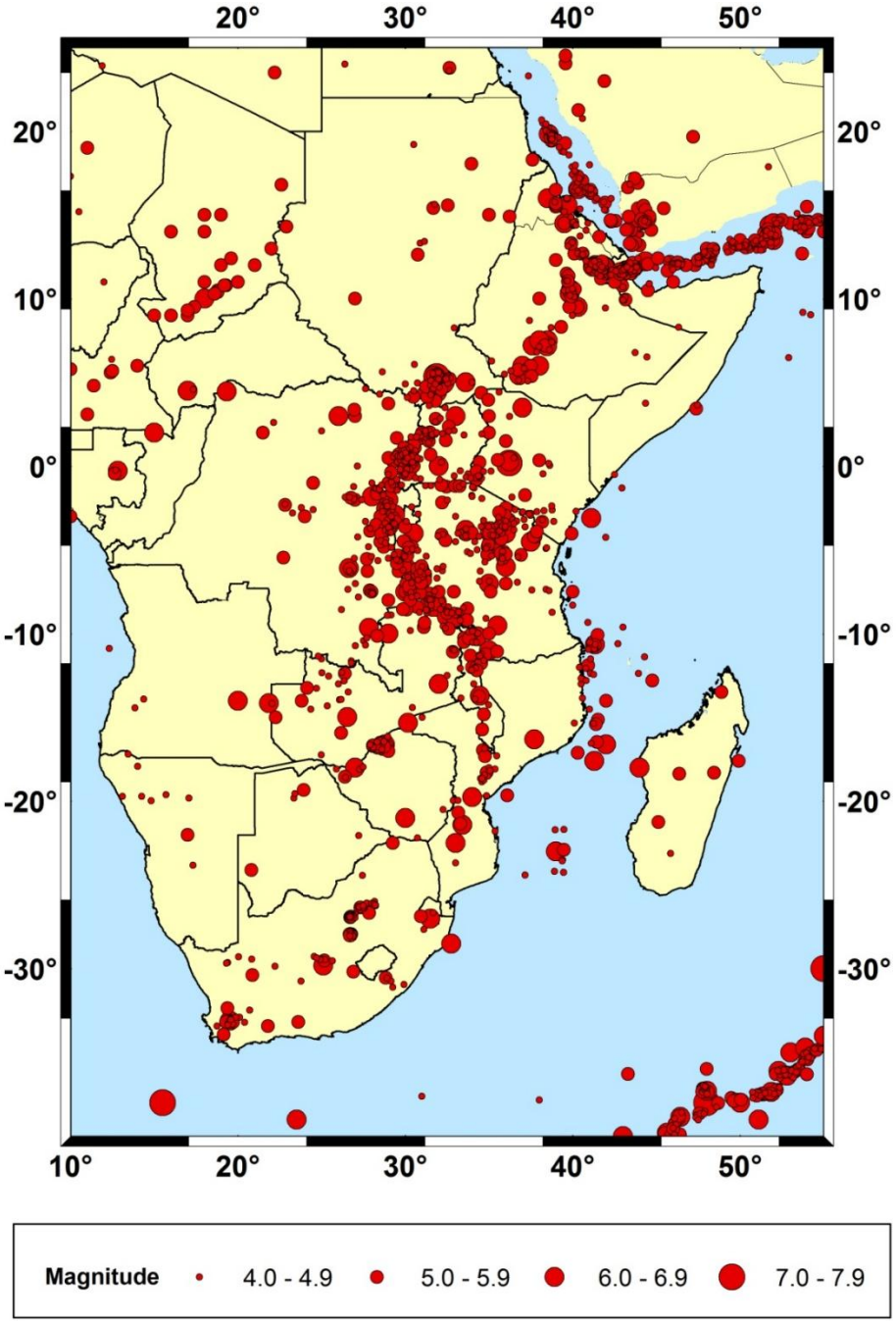


Figure 5.13-33
Seismicity of Southern and Eastern Africa as Compiled in the Global Seismic Hazard Assessment (GSHAP) Regional Study (*Reference 5.13.243*). Magnitudes are expressed in terms of surface-wave magnitude, MS

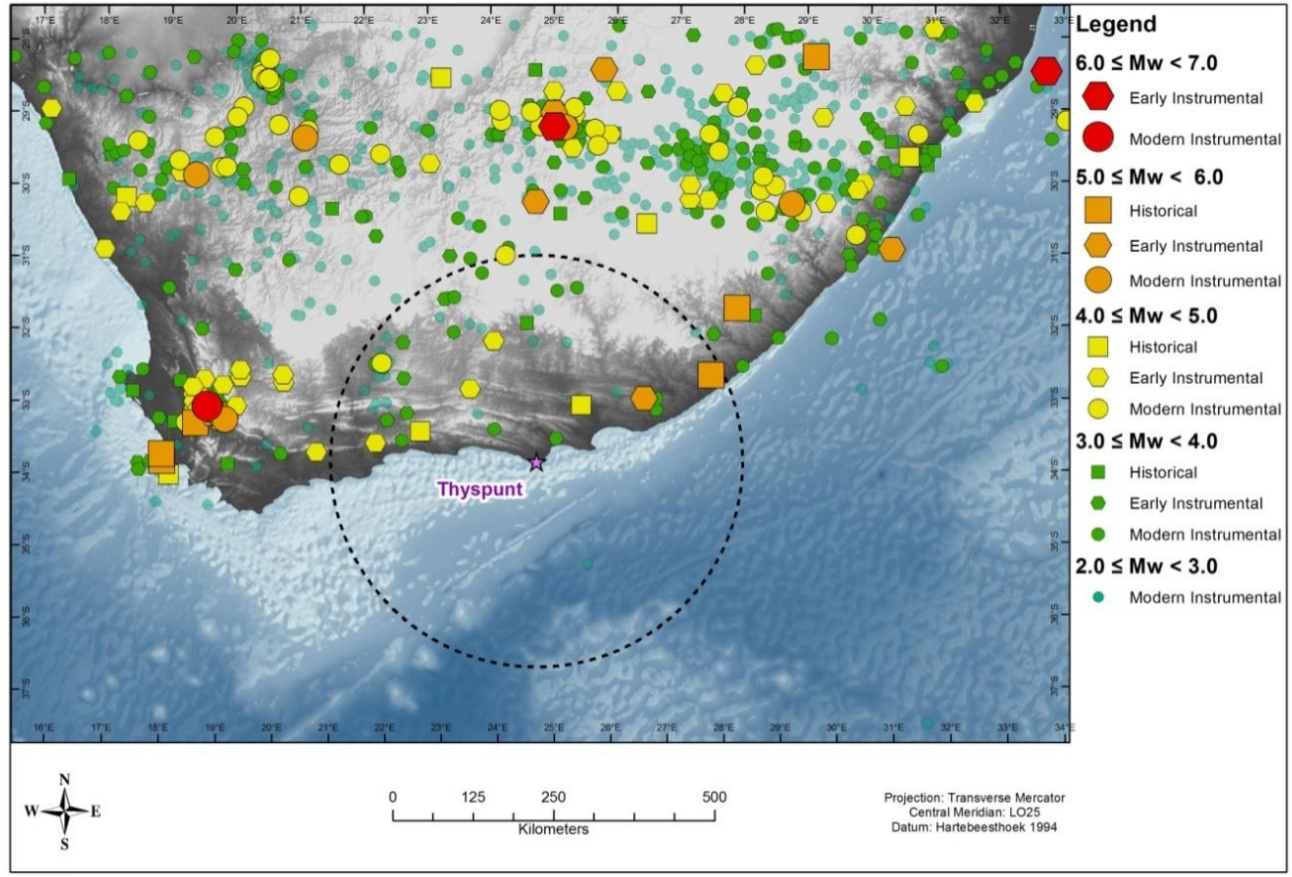


Figure 5.13-34
South African Seismicity for the Region South of the 28°S Parallel. The dashed circle indicates the 320 km radius around the Thyspunt site. Only events with Mw ≥ 2.0 are shown (*Reference 5.13.1*)

© Eskom 2026/Rev 0a

The catalogue for this region includes an earthquake that occurred in the Cape Town area on 4 December 1809, which was followed by a large number of aftershocks, another event that was felt over the south-western Cape on 14 August 1857, as well as the M_w 6.2 earthquake that affected the Ceres-Tulbagh region on 29 September 1969. The latter was also accompanied by an extensive aftershock sequence, which continued through the 1970s and 1980s.

Another region repeatedly visited by moderate-to-large earthquakes is the Koffiefontein region of the Free State, where an M_w 6.2 event occurred on 20 February 1920, as well as an M_w 5.8 event on 1 July 1976 and numerous smaller events.

Events with magnitudes in excess of M_w 5.0 can also be found in and around Lesotho, with the most recent occurring on 5 October 1986 (M_w 5.3) in the Matatiele region, as well as in the Poffadder and Springbok regions of the Northern Cape. Isolated events of this size have also occurred in the eastern part of the Eastern Cape.

Offshore seismicity is mostly confined to the region off the KwaZulu-Natal coast, linking up with a concentration of seismicity along the axis of the Mozambique Channel.

A large event occurred on 31 December 1932 off Cape St. Lucia, which was felt over the whole of the eastern part of the country. Another large event occurred south of South Africa on 4 December 1920, which was felt along the southern coast from Cape Town to Port Elizabeth. It should be noted that, because of the lack of nearby seismograph stations, offshore events with smaller magnitudes are difficult to detect away from the coastlines.

The diffuse patterns of seismicity are accompanied in some localities by episodes of swarm-like activity. Examples include the swarm that affected the Sutherland region of the Western Cape in early 1952, repeated small-magnitude events in the Kokstad region of the Eastern Cape, and the recent earthquake swarm that affected the Augrabies region of the Northern Cape in 2010 and 2011.

Seismicity in the region surrounding the Thyspunt site is generally very low, and does not include any $M_w \geq 6.0$ events, as shown on ***Figure F-5.13.35***. Within a radius of 320 km of the site, there are only two $M_w \geq 5.0$ events, both of which occurred to the east of the site, and six $M_w \geq 4.0$ events documented in the catalogue. Historical seismicity in the Eastern Cape region is documented continuously from about 1820, with an abundance of high-quality local sources, as presented in the study undertaken by Albini (***Reference 5.13.248***) for the Thyspunt project.

© Eskom 2026/Rev 0a

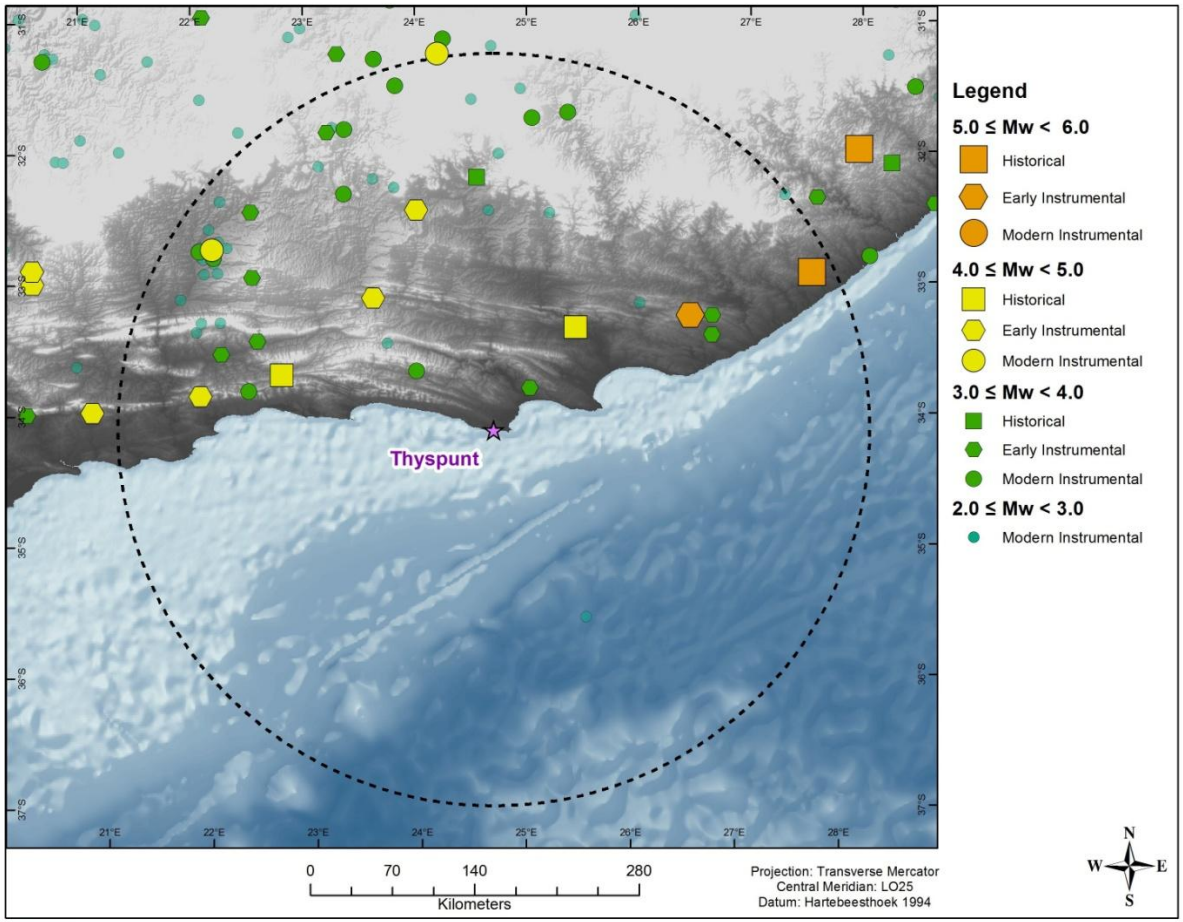


Figure 5.13-35
Seismicity for Region Surrounding the Thyspunt Site. The dashed circle indicates the 320 km radius (*Reference 5.13.1*)

© Eskom 2026/Rev 0a

Reference 5.13.248 confirms, in particular, the genuinely low level of seismicity of the region, demonstrating that the absence of significant historical events can be linked to the non-occurrence of such events, rather than to information gaps.

The Albini (***Reference 5.13.248***) study also reassessed larger individual events of the historical and early instrumental periods. The earliest of these events occurred on 21 May 1850 and was previously located at Grahamstown, on the basis of a single intensity observation. The collection of additional primary source materials allowed the development of a macroseismic intensity distribution showing that this event had been felt as far as George, to the west, and as far as the Pietermaritzburg/Durban region, to the east.

As a result, the reappraised location of this event is near 32°S, 28°E between Queenstown and Umtata, 200 km to the northeast of the original location. The magnitude of this event has been assessed to be M_w 5.7, somewhat larger than the previous estimate of M_L 5.0. A slightly smaller event (M_w 5.1) occurred on 15 October 1867 in the King William's Town–East London area, and was felt as far as Somerset East and Colesberg.

The most prominently featured event in the seismic histories developed by Albini (***Reference 5.13.248***) at 12 major towns surrounding the Thyspunt site is the 9 August 1932 Grahamstown event (M_w 5.7), which contributed the highest intensities observed at these localities over the time period 1820–1936. There is no record of higher intensities or larger events occurring in the vicinity of the Thyspunt site, based on the instrumental portion of the catalogue. It is noteworthy that seismicity appears to be confined onshore, although, as noted previously, this could also be influenced by completeness issues at the moderate magnitudes considered.

ii Regional Geophysical Data

Regional gravity and magnetic survey maps are important data sets that in conjunction with regional seismic profile surveys have been used to decipher major structural and rheological boundaries within the basement underlying the site region.

Gravity and Magnetic Survey Data and Maps

Figure F-5.13.36 shows the South African national gravity data covering the onshore areas, combined with the Gravity Recovery and Climate Experiment (GRACE) map for the offshore areas.

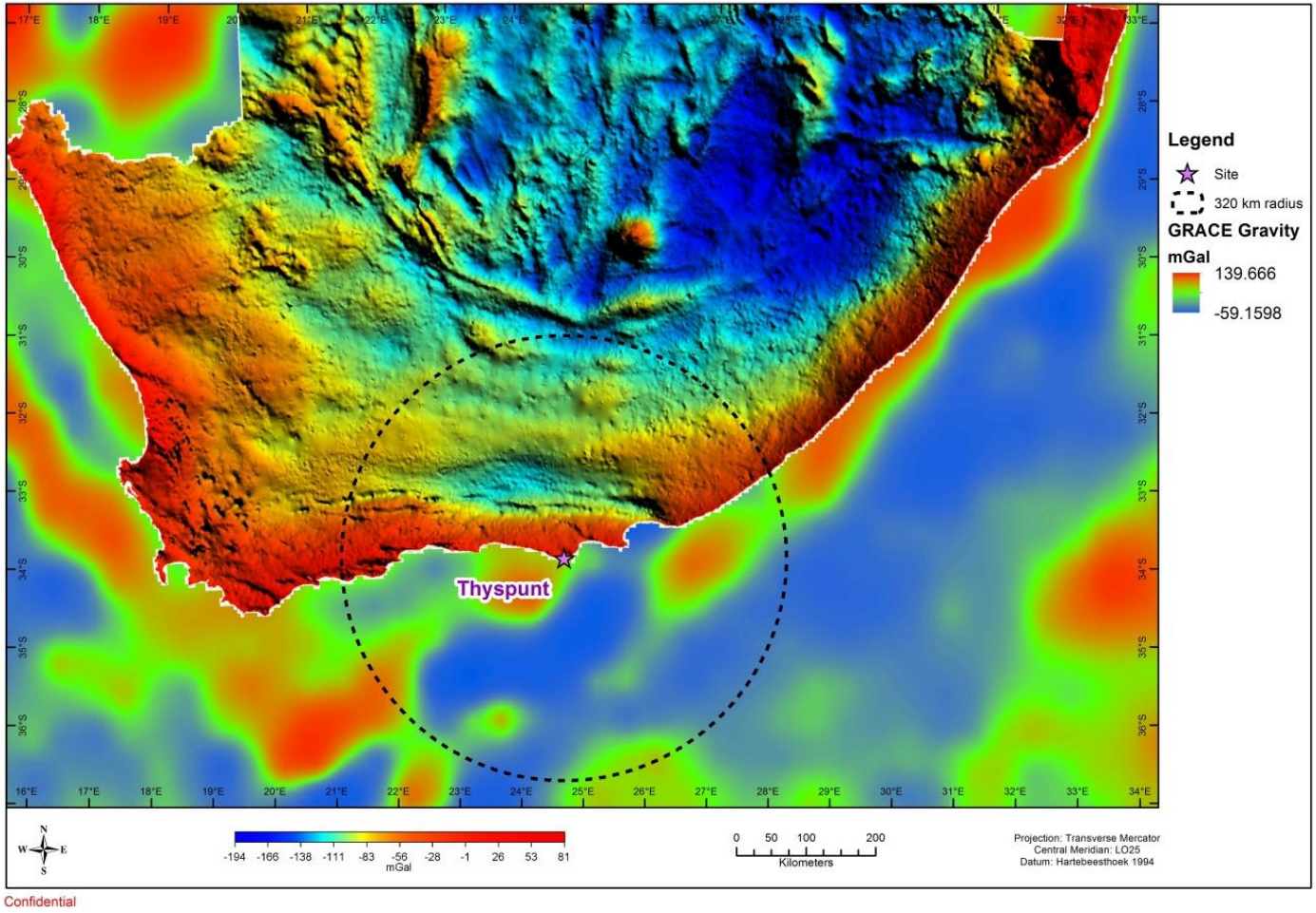


Figure 5.13-36
South African National Gravity Data (Onshore) and GRACE Data (Offshore) with Thyspunt Site and the 320 km radius.

© Eskom 2026/Rev 0a

Gravity data for the entire South Africa onshore areas have been collected during the last few decades of the twentieth century. A total of 98,237 gravity measurement points covers the country amounting to one measurement roughly every 12 km^2. Data were first collected along roads, but later in-filled to obtain a more regular grid. Measurements were tied in to a network of base stations, which were in turn tied in to absolute gravity values at stations in Paarl and Silverton. ***Figure F-5.13.37*** shows the distribution of the gravity stations, base stations and the two absolute gravity stations. Measurements were conducted with La Coste and Romberg gravimeters and elevations were determined using micro-barometers. Bouguer anomaly values were calculated assuming a mean density of 2670 kg/m^3. The measurements were tied to the International Gravity Standardisation Net values and were referred to the gravity formula based on the 1967 geodetic reference system (***Reference 5.13.250***).

Magnetic data is shown in ***Figure F-5.13.38*** and consists of the South African national magnetic data covering the onshore area combined with the World Digital Magnetic Anomaly Map (WDMAM) covering the offshore area.

The WDMAM is a result of an international effort to create the first global compilation from the large volume of magnetic anomaly information derived over 50 years of aeromagnetic surveys (land areas), including research vessel magnetometer traverses (at sea) and observations from earth-orbiting satellites. The GFZ German Research Centre for Geoscience at Potsdam has been involved in the compilation of this map and has built its own version of the map that can be downloaded from their website (http://ftp.gtk.fi/WDMAM2007/).

The national aeromagnetic survey for South Africa was conducted between the years 1958 and 1997 (***Reference 5.13.251***). It was flown in two primary sections – the Karoo survey, done between 1976 and 1982 and covering almost half of the country; and the rest, which was surveyed by various contractors over a period of more than 30 years, starting in 1958 and ending in 1997.

Magnetic and gravity anomalies identified in these data are described below.

An extensive positive magnetic anomaly, parallel to the South African south coast and more than 1,000 km long (***Reference 5.13.252***), has been reported immediately to the north of the Cape Fold Belt (CFB; ***Figure F5.13.38***). This is the so-called Beattie Magnetic Anomaly (BMA), and it has been studied by several investigators (*i.e.,* ***References 5.13.101***, ***5.13.253***, ***5.13.111***, and ***5.13.254***).

© Eskom 2026/Rev 0a

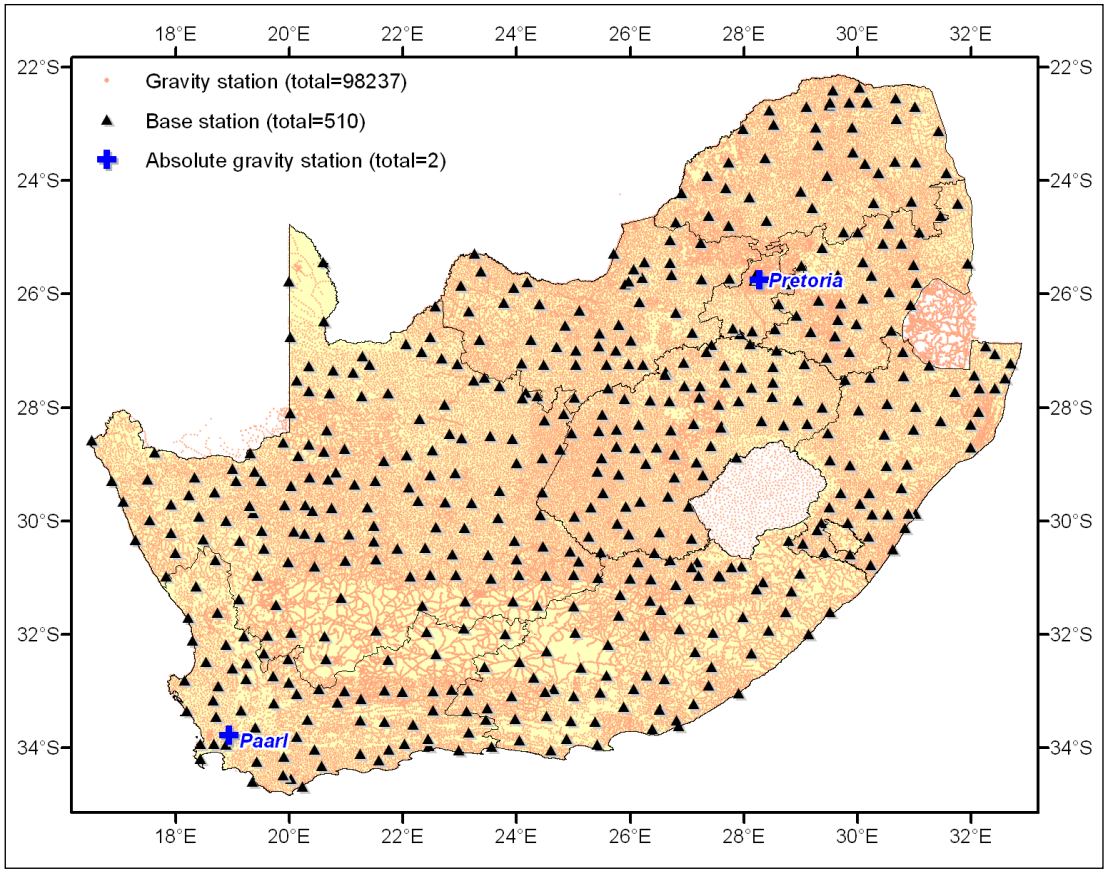
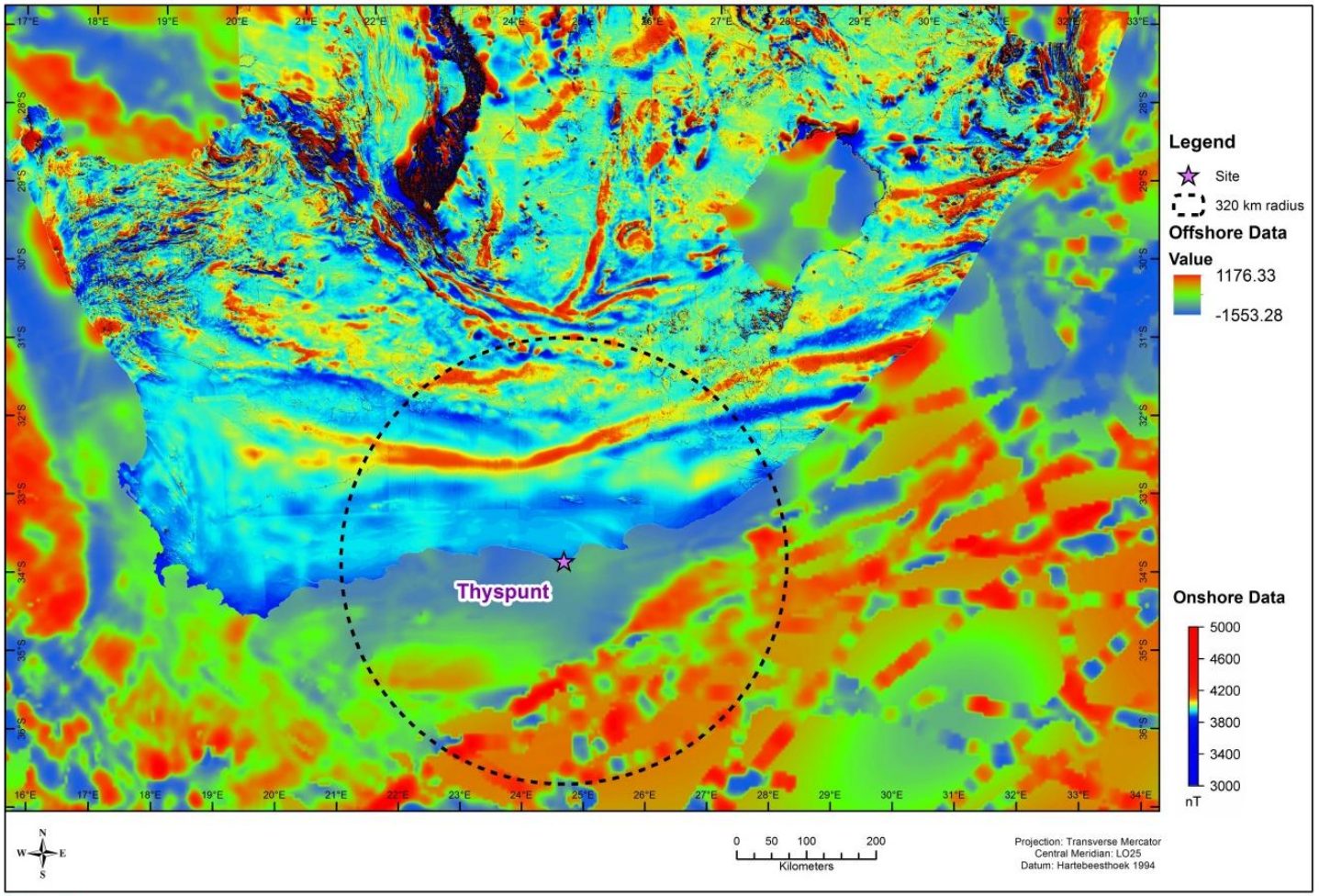


Figure 5.13-37
Distribution of the Gravity Stations, Base Stations, and Absolute Gravity Stations Used for the Collection of the National Gravity Data.



Confidential

Figure 5.13-38
South African National Magnetic Data (Onshore) and WDMAM Data (Offshore)

© Eskom 2026/Rev 0a

The BMA, which stands out from the magnetically neutral Karoo crust, is the largest terrestrial and electrically conductive anomaly in the world (***References 5.13.255***, ***5.13.253***, ***5.13.111***, and ***5.13.254***). In general, the BMA runs in the east-west direction within the Great Karoo province. However, in the eastern part of the zone, this anomaly swings in the northeast direction parallel to the structural grain of the Namaqua-Natal Mobile Belt. The BMA in the mid-crust is present at depths between 7 km and 15 km with a thickness of about 6 km (***Reference 5.13.112***).

There have been lengthy debates regarding the origin of the BMA and different models include a Neoproterozoic palaeosuture represented by a steeply dipping ophiolite (***Reference 5.13.255***), two wide and highly magnetised sheet-like prisms situated at depths of 10–20 km in the mid-crust (***Reference 5.13.254***) and a Namaqua-like stratabound and massive sulphide ore body (***Reference 5.13.112***). Weckmann et al. (***Reference 5.13.111***) suggested that the conductors below the axis of the BMA may be Mesoproterozoic structures.

A zone of electrically conductive material in the crust or upper mantle, now known as the Southern Cape Conductive Belt (SCCB), was discovered in the southern Cape following a magnetometer array study (***Reference 5.13.256***). This 140 km wide and 1,000 km long zone (***References 5.13.253*** and ***5.13.111***) is located at depths of approximately 46–52 km beneath the southern Karoo Basin and frontal CFB (***Reference 5.13.257***).

Some studies suggested that there may be a link between the SCCB and the BMA (***References 5.13.258*** and ***5.13.106***), and that they may share a common source in the form of deep serpentinised palaeo-oceanic crust (e.g., ***References 5.13.106*** and ***5.13.107***). However, Weckmann et al. (***References 5.13.253*** and ***5.13.111***) demonstrated that a common source for these two anomalies is unlikely, although its origin is still unresolved (***Reference 5.13.112***).

In the eastern part of the Great Karoo, Karoo-related dykes that intruded as ring structures appear on the magnetic susceptibility map as positive magnetic highs. These are especially observed north of the BMA.

In the offshore, the Agulhas Fracture Zone, which is mapped at the base of the continental slope, coincides with the northern edge of prominent magnetic anomalies inferred to represent oceanic crust (***Figure F-5.13.38***).

A negative gravity anomaly, the Cape Isostatic Anomaly, has been reported between the southern escarpment of the Eastern Cape and the southern coast (Hales & Gough, 1960). It forms an east-west-oriented belt that is approximately

© Eskom 2026/Rev 0a

80 km wide (***References 5.13.259*** and ***5.13.107***) and diminishes to the west so that it is largely restricted to the eastern part of the Eastern Cape (***Figure F-5.13.36***). This anomaly is unrelated to surface geology and underlies exposures of both the Cape Supergroup and the southern part of the Karoo Supergroup, being centred at S33.6° E25.8° (***Reference 5.13.260***), approximately 50 km to 60 km north of the Kango-Baviaanskloof Fault trace (***Reference 5.13.25***). It is interpreted to be low density, thickened crust that represents the isostatic, uncompensated root of the once higher CFB (***References 5.13.259*** and ***5.13.107***).

Regional Seismic Profiles

The Agulhas-Karoo Geoscience Transect, which was completed as part of the *Inkaba yeAfrica* framework project (***Reference 5.13.261***), is an onshore-offshore transect crossing the southern continental margin of South Africa starting in the Karoo Province, passing through the Cape Fold Belt (CFB), the Agulhas Bank, the Agulhas-Falkland Fracture Zone (AFFZ) and the Agulhas Plateau (***Figure F-5.13.39***). A variety of data sets, including seismic reflection and refraction, magnetotelluric, petrological, geological, and geophysical methods, were applied to address many objectives, such as the following:

- Onshore—identification of the sources of the Beattie Magnetic Anomaly (BMA) and the Southern Cape Conductivity Belt (SCCB) and explanation of the history of the CFB.
- Offshore—the structure and formation of the AFFZ and adjacent basins, and the evolution of the Agulhas Plateau and its crustal structure including its volume, age, and magmatic source.

Seismic refraction/wide-angle reflection data along two combined onshore-offshore (GRA-AWI-20050200 and FRA-AWI-20050100) profiles (referred to as the eastern and western profiles) across the southern continental margin of South Africa were acquired as part of this research program (***Figures F-5.13.39***, ***F-5.13.40***, and ***F-5.13.41)***. Discussions of the data acquisition, processing, and interpretations of the profiles are presented in a series of reports and publications (***References 5.13.262***, ***5.13.69***; ***5.13.147***; ***5.13.77***, ***5.13.263***, and ***5.13.130***).

Conclusions about crustal properties and the nature and timing of related tectonic/geodynamic processes based on interpretations of these profiles, summarised in ***Reference 5.13.77***, are described in the following paragraphs.

Both profiles cross continental, stretched continental, transitional and oceanic crust. Average velocities of the crust (without the sedimentary layer) along the eastern profile with interpretation are shown on ***Figure F-5.13.41, Part A***.

© Eskom 2026/Rev 0a

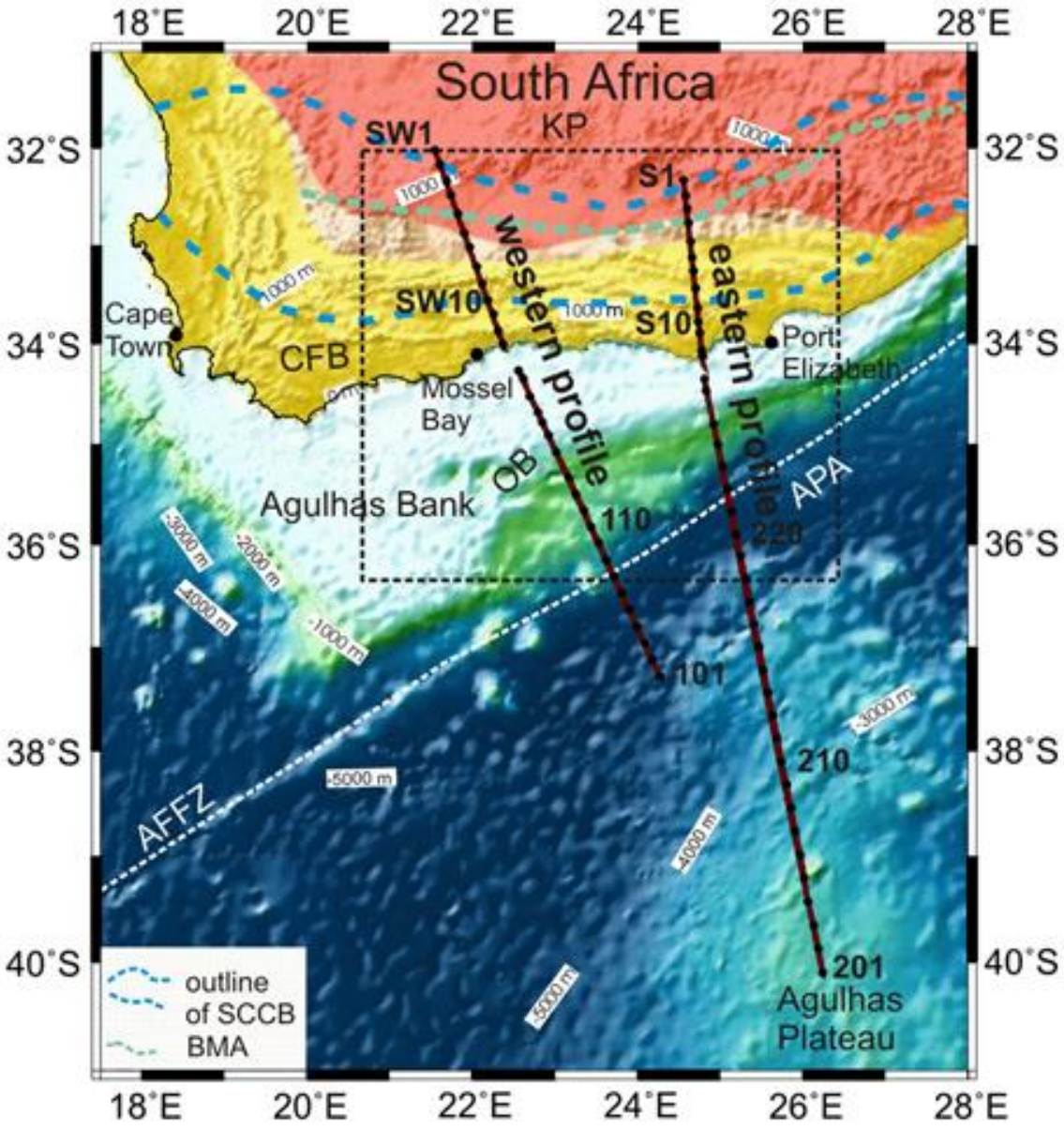


Figure 5.13-39
Overview Map Showing the Location of Two Combined Onshore-Offshore Seismic Profiles of the Agulhas-Karoo Geoscience Transect. The dashed box shows the extent of Figure F-5.13.40 (*Reference 5.13.77*)

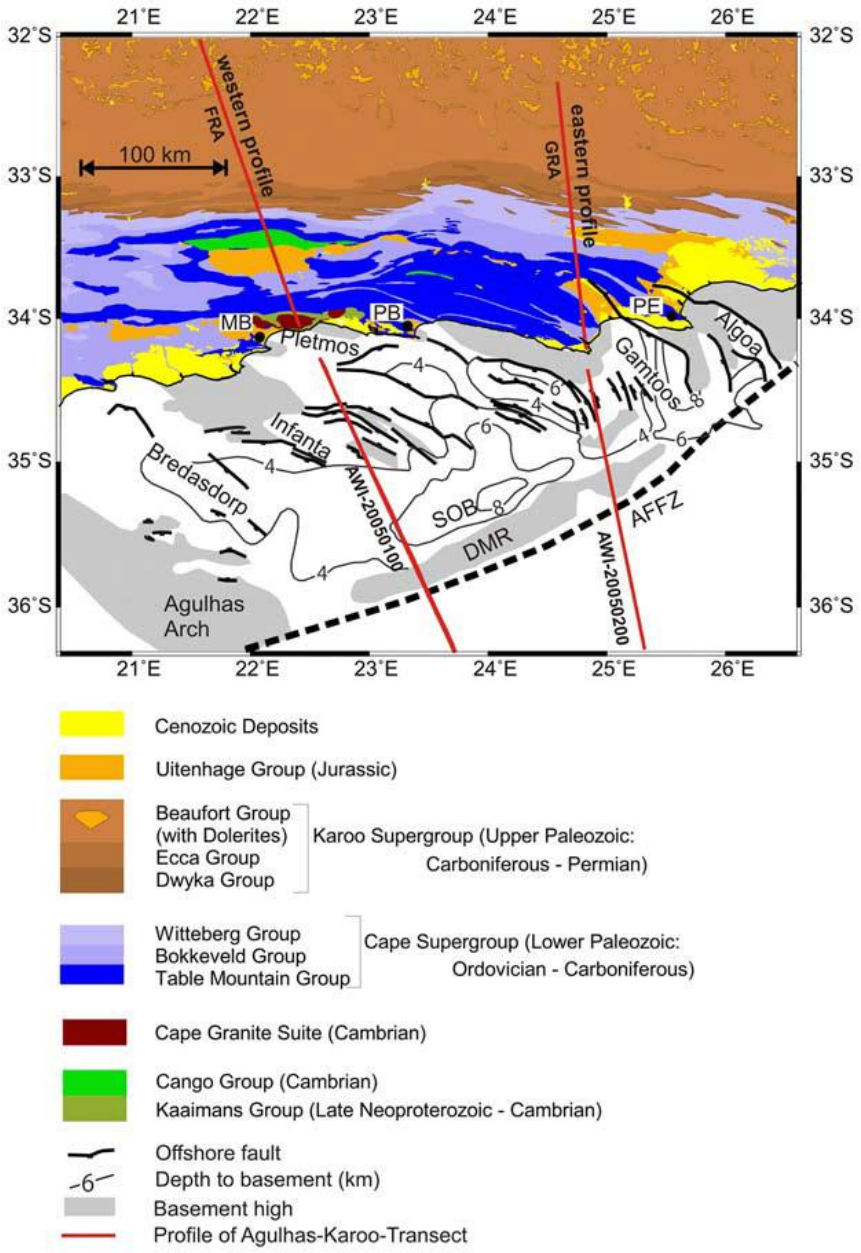


Figure 5.13-40
Detailed Map of the Onshore Geology and Structure of the Offshore Basins. The dashed line marks the position of the Agulhas-Falkland Fracture Zone (AFFZ). DMR = Diaz Marginal Ridge; MB = Mossel Bay; PB = Plettenberg Bay; PE = Port Elizabeth; SOB = Southern Outeniqua Basin (*Reference 5.13.77*)

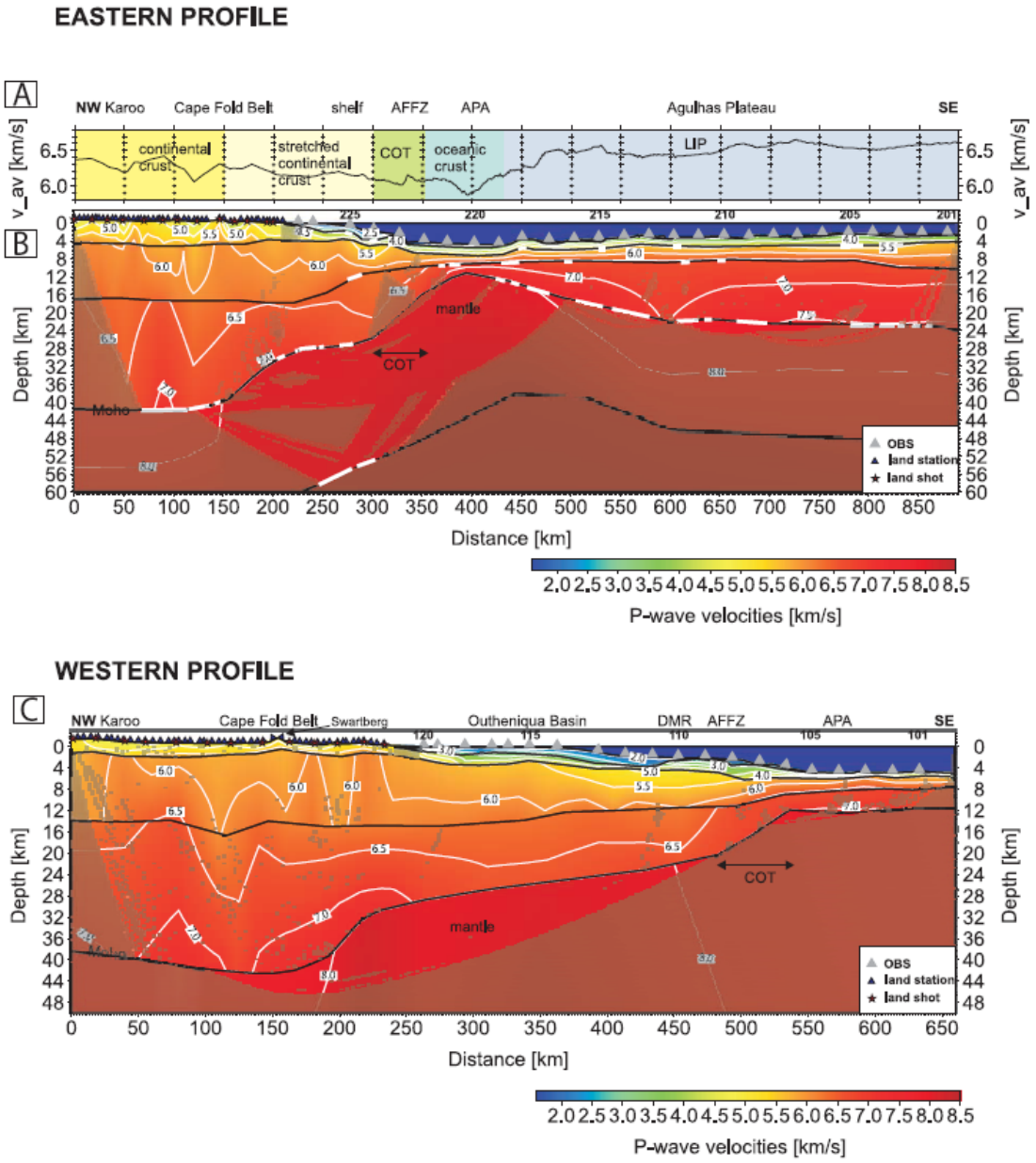


Figure 5.13-41
Seismic P-Wave Velocity-Depth Model for the Eastern and Western Seismic Profiles, with the Lowermost Solid Line Representing the Moho (*Reference 5.13.77*)

Seismic P-wave velocity-depth models of the eastern (GRA-AWI-20050200) and western (FRA-AWI-20050100) profiles are shown on ***Figure F-5.13.41, Parts B and C***, respectively. According to the velocity-depth models crustal thicknesses (including sedimentary layers) vary from approximately 42 km beneath the CFB, to approximately 28 km beneath the shelf, approximately 8 km in the Agulhas Passage, and approximately 20 km on the Agulhas Plateau.

The AFFZ coincides with a 50 km wide transitional zone between continental and oceanic crust. The oceanic crust south of the AFFZ exhibits relatively low average crustal velocities (~6.0 km/s), which have been attributed crustal thinning and intrusive/extrusive processes associated with the transform-ridge intersection and the thermal effects of the adjacent continental crust during formation.

Crustal stretching factors derived from the velocity-depth models imply that extension in the Outeniqua Basin acted on regional as well as local scales (***Figure F-5.13.42)***. Two episodes of crustal extension are recognised. An initial episode influenced the entire Outeniqua Basin and the conjugate Falkland Plateau Basin (see ***Figure F-5.13.16***), and is attributed to stresses associated with the breakup between Africa and South America during the rift stage. A second stretching episode, possibly related to shear motion along the AFFZ, only impacted the southern half of the Outeniqua Basin and Falkland Plateau Basin. Crustal velocities directly beneath the Outeniqua Basin are consistent with the interpretation of Cape Supergroup rocks underlying most parts of the basin and the Diaz Marginal Ridge, a sub-cropping ridge bounding the southern margin of the Outeniqua Basin.

The formation of the Diaz Marginal Ridge is attributed to either a transpressional episode along the Agulhas-Falkland Transform, or more likely to thermal uplift accompanying the passage of the spreading ridge to the south.

A detailed deep crustal section (IyA-200501; ***Figures F-5.13.43*** and ***F-5.13.44***) from the northern part of the western Agulhas-Karoo Geoscience Transect profile was constructed from the joint interpretation of (1) archive data comprising surface geology, aeromagnetic data, nearby deep boreholes, teleseismic receiver function and regional seismic reflection profiles, and (2) the newer high-resolution geophysical data consisting of near vertical seismic reflection data, shallow P- and S-wave velocity data, wide angle refraction data, high resolution magnetotelluric data and impedance spectroscopy measurements on borehole samples (***References 5.13.264***,***5.13.265***, ***5.13.112***, and ***5.13.266***).

© Eskom 2026/Rev 0a

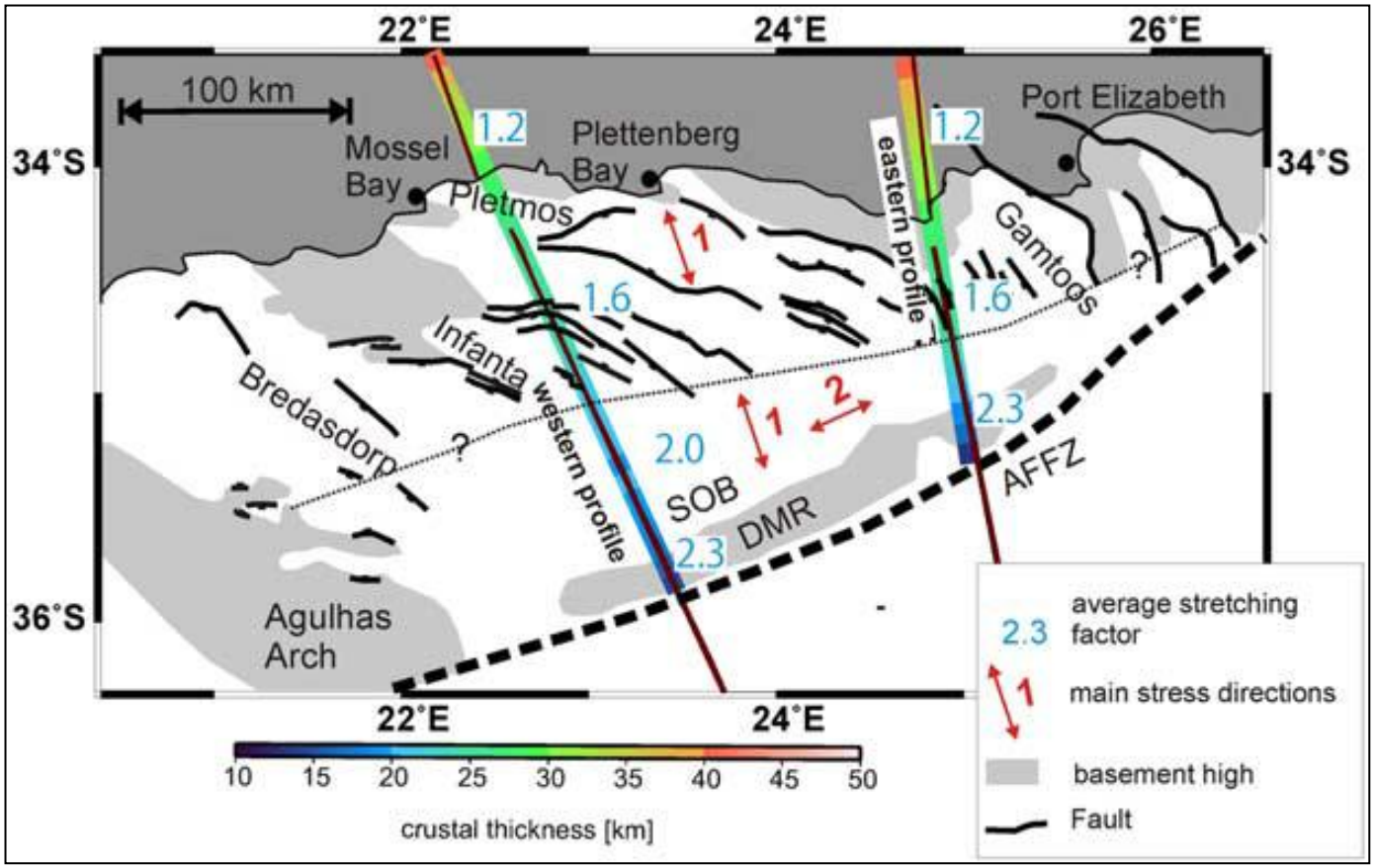


Figure 5.13-42
Map of the Outeniqua Basin with Colour-Coded Crustal Thicknesses Along the Seismic Profiles and Average Stretching Factors. Red arrows show the approximate stress directions DMR = Diaz Marginal Ridge. SOB = Southern Outeniqua Basin (*Reference 5.13.77*)

© Eskom 2026/Rev 0a

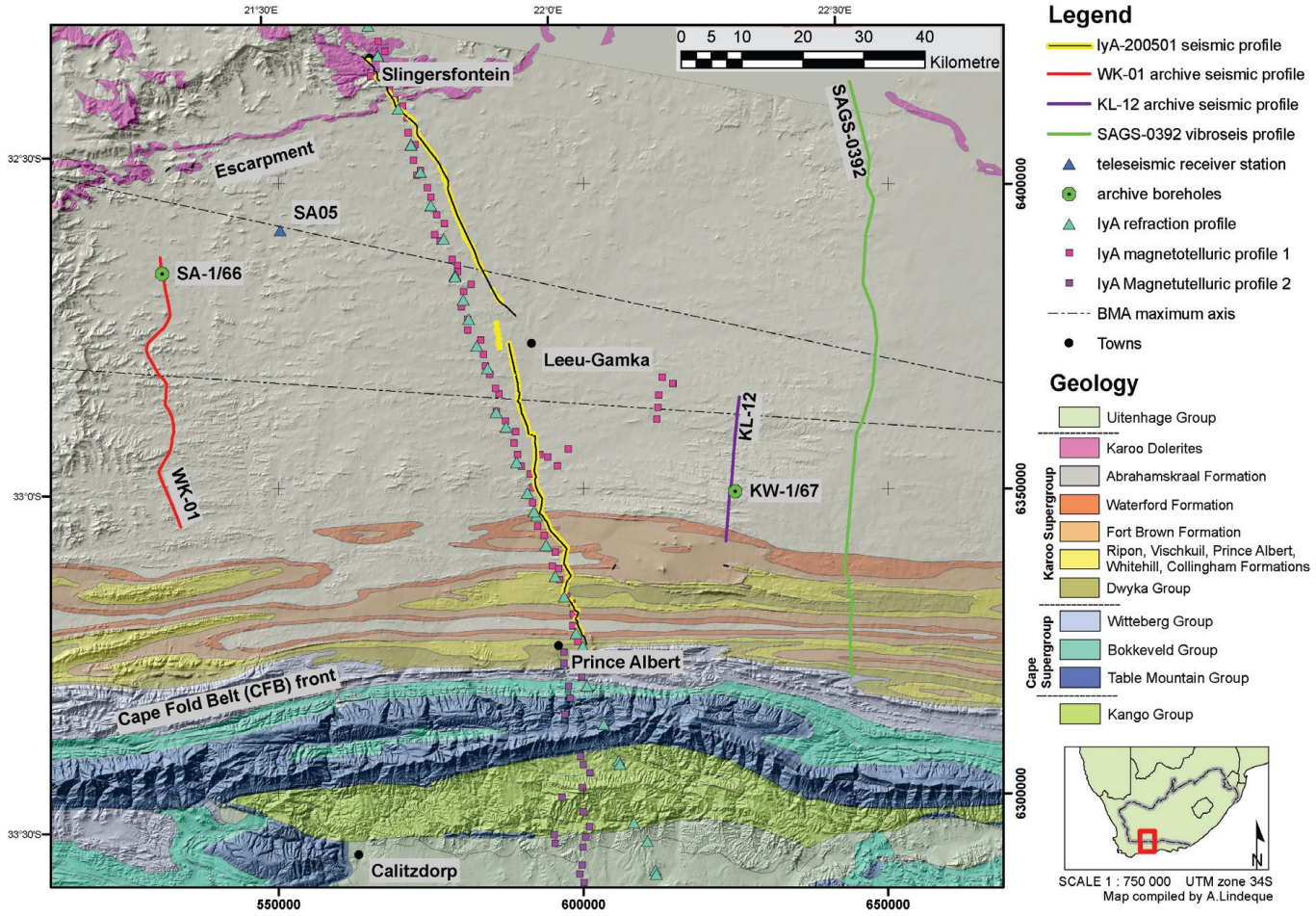


Figure 5.13-43
Geological Map Showing Location of Profile lyA-200501 (*Reference 5.13.112*)

© Eskom 2026/Rev 0a

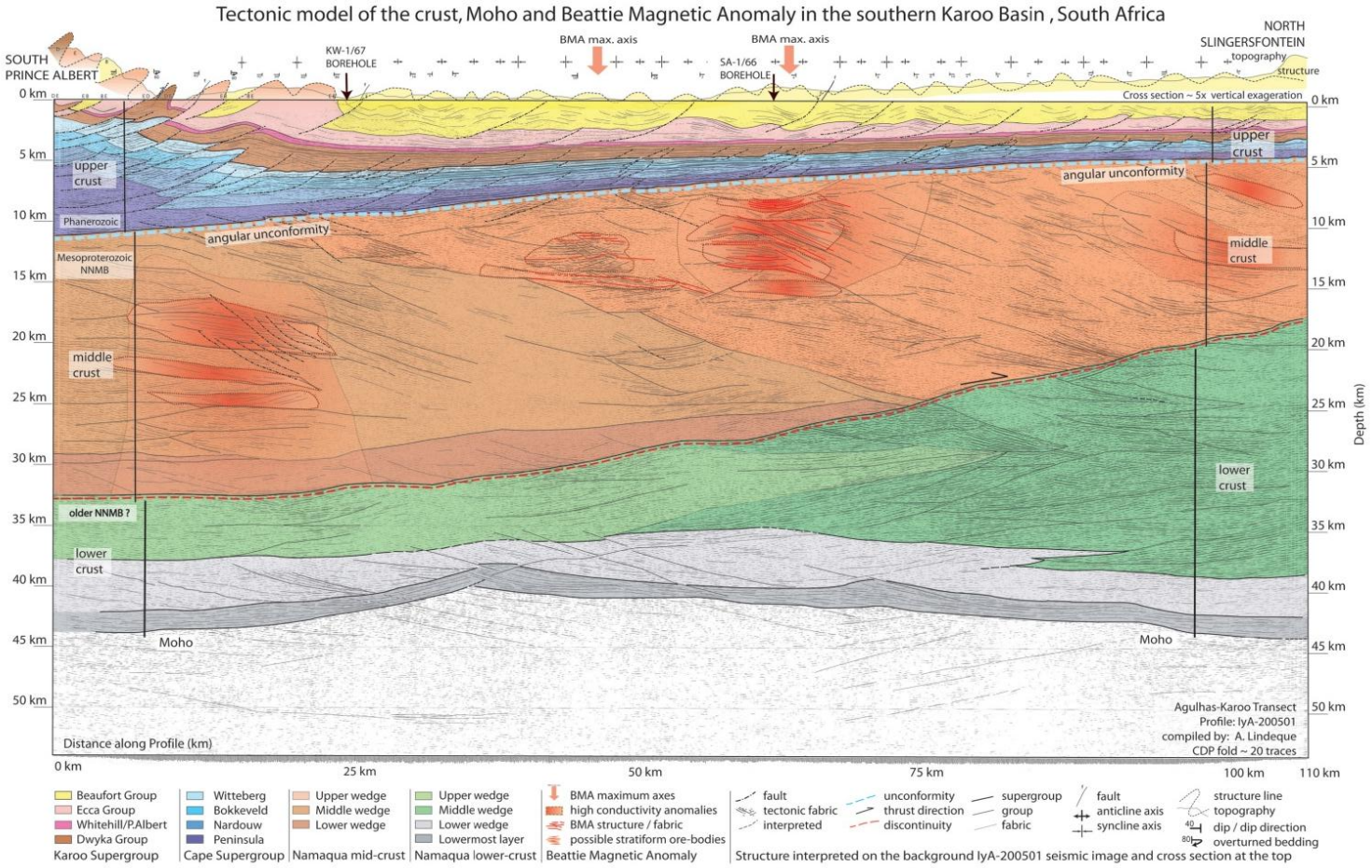


Figure 5.13-44
Deep Crustal Model (*Reference 5.13.112*)

© Eskom 2026/Rev 0a

The resulting deep crustal model (***Figure F-5.13.44*** and ***Reference 5.13.112***) differentiates four components in the upper 45 km thick crust:

- An approximately 2–5 km thick folded Karoo Supergroup is disrupted by low-angle faults rooted in a zone of local décollements. This component rests on the Cape Supergroup wedge.

- The continuous undeformed sub-horizontal wedge of the Cape Supergroup extends from the escarpment in the north, where it has a thickness of 1.5 km, to the tectonic front of the CFB in the south, where it achieves a thickness of 10 km and rests on an unconformity that dips about 3° to the south. This unconformity separates the wedge from the mid-crust.

- The approximately 13–21 km mid-crust displays a north-dipping seismic fabric and is interpreted as the Mesoproterozoic, Namaqua-Natal Mobile Belt (NNMB) crust. A south-dipping mid-crustal detachment, interpreted as a ductile thrust zone, separates the mid-crust from thick lower crust.

- A highly reflective, approximately 10–24 km thick lower crust is interpreted to be an older Palaeoproterozoic section of the NNMB (or possibly Archaean cratonic basement). It is bounded by an approximately 2–5 km thick highly reflective bottom layer that subparallels the underlying Moho. This bottom layer is interpreted as a mafic underplate, metasomatic reaction zone, or lower-crust-to-mantle transition zone. The NNMB mid-crustal layer is interpreted to contain the source for the BMA. The seismic-reflection and -refraction data are interpreted to show that the NNMB continues below the CFB tectonic front up to the continental margin and the Agulhas Fracture Zone, suggesting a thin-skinned tectonic thrust model for the evolution of the CFB without significant foredeep stratigraphic thickening in the Karoo Basin (***Reference 5.13.112***).

iii Palaeozoic Tectonic Structures, Faults and Folds in the Cape Fold Belt

The CFB formed in the Permo-Triassic and is exposed as a mountain chain of 1,200 km along the west and south coasts of South Africa (***References 5.13.267*** and ***5.13.136***). The on-land width of the southern branch is about 200 km, and the western branch, about 150 km. Deformation during the Permian-Triassic Cape Orogeny formed the CFB (***Reference 5.13.268***), while the associated crustal loading created the Karoo Basin to the north (***References 5.13.124*** and ***5.13.112***). The CFB dominates the structural configuration of southern South Africa and is generally considered to have formed part of a larger mountain chain that formed along the southern margin of Gondwana from the Sierra de la Ventana in Argentina to the Pensacola

© Eskom 2026/Rev 0a

Mountains of the Trans-Antarctic Mountains (***References 5.13.269*** and ***5.13.123***).

Controls on the geometry of the Permian-Triassic CFB at depth are largely derived from fold geometries at the surface. Underlying these folds, Paton *et al.* (***Reference 5.13.131***) interpret that a series of moderately shallow, south-dipping thrust faults coalesce at depth onto a common decollement somewhere below the Cape Supergroup and within the Pre-Cape Group with a minor detachment existing within the Upper Devonian. To further constrain the geometry and to quantify horizontal shortening across the CFB, two regional-scale cross sections were constructed by Paton *et al.* (***Reference 5.13.131***; ***Figure F-5.13.45***). The two sections have been restored to three structural time frames that include modern-day geometry (***Figure F-5.13.46, Profile 1A***), restoration of the compressional CFB through removal of extensional structures (***Figure F-5.13.46, Profile 1B***), and a restored section to pre-CFB deformation (***Figure F-5.13.46, Profile 1C***). Paton *et al.* (***Reference 5.13.131***) interpret northern and southern structural domains that differ in the amount of shortening across the CFB (***Figure F-5.13.46***).

Profile 1 is a north-south cross section that extends from the coast near Plettenberg Bay and ends approximately 120 km to the north where the foreland of the CFB transitions into the Karoo Basin (***Figure F-5.13.45***). Profile 2 is a southwest-northeast-oriented profile extending from the coast 50 km west of Cape St Francis and ends approximately 120 km to the northeast near the intersection of the Algoa Basin, the CFB foreland, and the Karoo Basin.

The northern structural domain is confined to a 25 km and 35 km section of Profile 1 and Profile 2, respectively. The structure in this domain is dominated by foreland thrusting with northward-verging and asymmetric folds. Paton *et al.* (***Reference 5.13.131***) report that while some of these faults reach the surface, most of them have very little displacement in outcrops and no more than 3 km in the subsurface. The shortening accommodated by folding in this domain is lower in amplitude than in the southern domain, and folds are more frequent and smaller in wavelength. Paton *et al*. (***Reference 5.13.131***) calculated the Palaeozoic horizontal shortening to be 5 km along Profile 1 and 7.5 km along Profile 2 in this domain.

The southern domain forms the dominant topography of the CFB with elevations up to 1500 m. This is positioned south of a relatively short (~10–15 km) transitional domain characterised as a zone of negligible shortening. The southern domain extends for approximately 80 km in both Profiles 1 and 2.

© Eskom 2026/Rev 0a

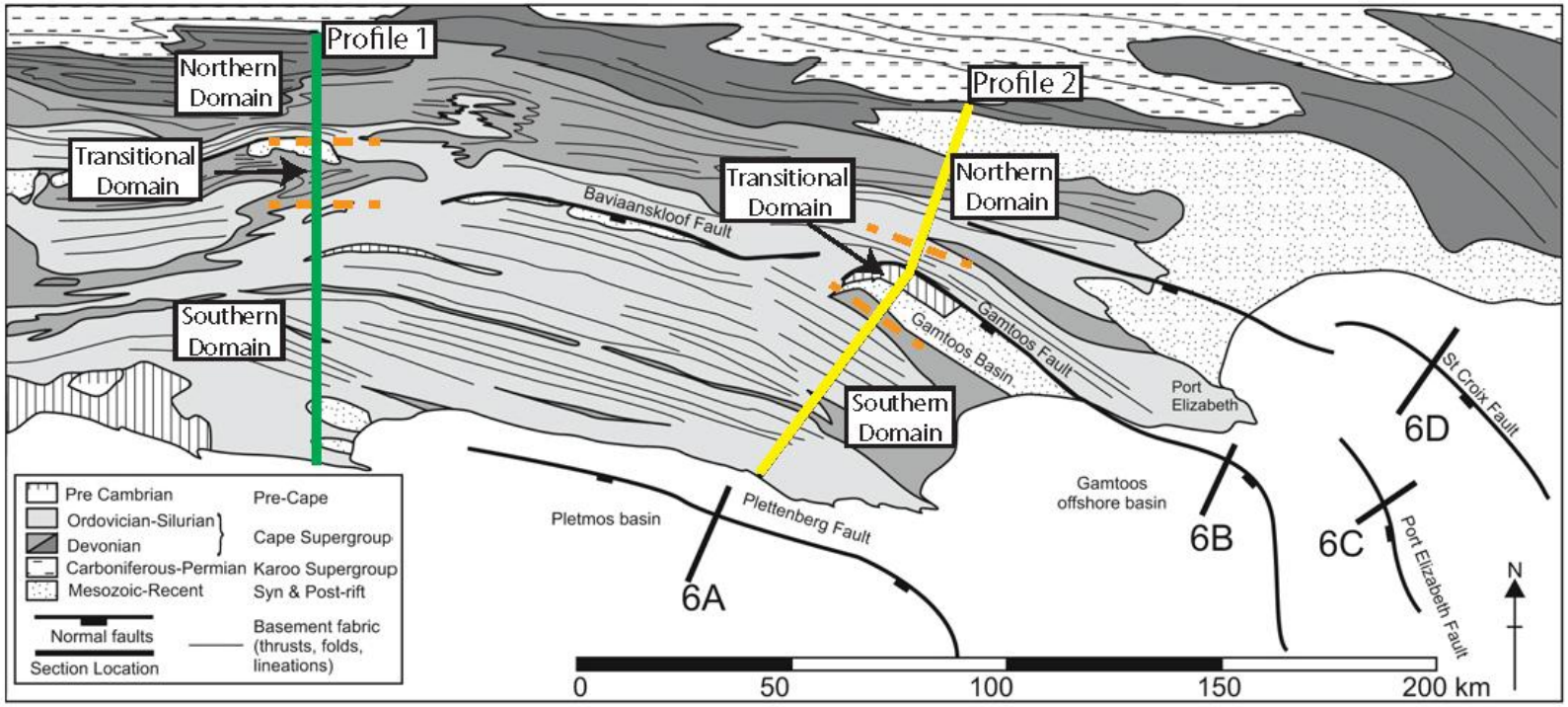


Figure 5.13-45
Geological Map Showing Locations of Profiles 1 and 2. The transitional zone between structural domains is indicated by orange dashed line. (Modified from *Reference 5.13.131*)

© Eskom 2026/Rev 0a

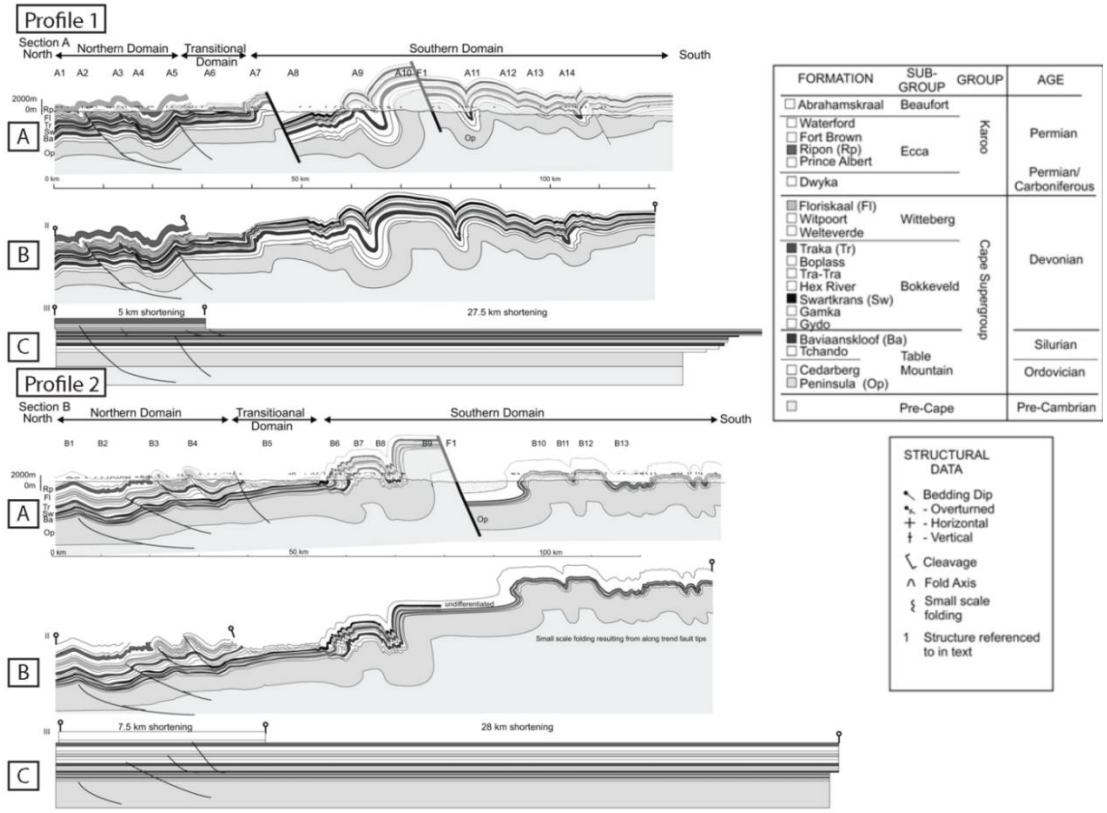


Figure 5.13-46
Regional Cross Sections Across the Cape Fold Belt Showing Three Stages of Deformation Across the Zone. For each section: (A) Present-day geometry with topography and structural data plotted. (B) Shows the restoration of the Cape Fold Belt through the removal of extensional faults. (C) Restored sections to pre-Cape Fold Belt deformation. (Modified from *Reference 5.13.131*)

© Eskom 2026/Rev 0a

The structure in this domain comprises a series of approximately 8 km wavelength box folds. The genesis of these box folds is attributed to motion on underlying high angle (>45) reverse faults (***Reference 5.13.131***). Paton *et al.* (***Reference 5.13.131***) calculated the Palaeozoic horizontal shortening to be 27.5 km along Profile 1 and 28 km along Profile 2 in this domain. The Mesozoic extensional structures that reactivated near and along many of the Palaeozoic reverse faults are contained within the southern domain. The cross sections suggest that the northernmost extension is near the transitional domain on Profile 1 (fold A7) and near fault F1 in Profile 2 within the southern domain.

In a more regional study of the CFB tectogenesis, Hälbich (***Reference 5.13.118***) subdivided the crust into six zones to measure the relative shortening from south to north along a 310 km transect between longitude 22° and 23°. In contrast to the detailed profiles of Paton *et al.* (***Reference 5.13.131***), the cross section was not fault specific, and the crust was represented in the form of a block strain model displaying the progressive development of the CFB. The total shortening presented in this work suggests a total of 127 km of horizontal shortening. The southern zones 6, 5, and 4, (comparable to the southern domain described above) include the southern CFB, are shown to have accommodated 70%, 30%, and 35% horizontal shortening, respectively. Northern zones 3, 2, and 1, (comparable to the northern domain described above) containing the CFB foreland and the Karoo Basin are shown to have accommodated far less at 35%, 7.5%, and <5% shortening, respectively. These values suggest a culmination of shortening followed by a significant decrease in shortening from south to north similar to those in Paton *et al.* (***Reference 5.13.131***)**.**

The strong correlation in orientation between compressional and extensional structures in the CFB suggests the thrust faults were likely reactivated in the Mesozoic as normal faults. The normal faults in both of the cross sections by Paton *et al.* (***Reference 5.13.131***) occur in a structurally consistent location immediately to the south of the northern limb of major anticlinal folds.

iv Mesozoic Tectonic Structures

Extension during continental breakup of Gondwana, resulted in the reactivation of pre-existing fold-belt compressional faults (References 5.13.142, 5.13.150, 5.13.140, and 5.13.144) to form a number of onshore and offshore graben and half-graben rift basins. In addition to the smaller onshore basins, the large offshore Outeniqua Basin consists of a series of smaller sub-basins, including the Bredasdorp, Pletmos, Gamtoos, and Algoa Basins (Figures F-5.13.3 and F-5.13.40). Major faults within the site region, especially those more proximal to the Thyspunt site that were evaluated as potential fault sources for the PSHA

© Eskom 2026/Rev 0a

(see ***Section 5.14*** – Seismic Hazard Analysis), are described below (from north to south).

Ceres-Kango-Baviaanskloof-Coega Fault System

Complex and extensive Mesozoic faults in the site region extend from east to west across southern South Africa. The northernmost onshore component of these faults is referred to as the Ceres-Kango-Baviaanskloof-Coega (CKBC) fault system that can be traced from Cape Town to near Port Elizabeth (***Figure F-5.13.47***). The onshore CKBC fault system traverses the southern Cape Fold Belt for about 600 km before extending offshore. The offshore trace of the fault is known as the St Croix Fault and extends for about 110 km. The Kouga Fault, directly to the south also appears to be kinematically linked to the CKBC.

The CKBC formed as a major extensional fault system beginning in the Early Jurassic (~180 Ma) when a general increase in tectonic activity was followed by the linkage of fracture systems across Gondwana (***Reference 5.13.143***). Together this system of faults represents the northernmost Mesozoic crustal extension in southern Africa. At its eastern end, the fault system takes on a southeast orientation towards the coastline where the onshore Coega Fault becomes the offshore St Croix Fault. Various authors (***References 5.13.270***, ***5.13.271***, and ***5.13.70***) suggested that these curvatures may be the result of the crust of African Plate being dragged along the Agulhas-Falkland Fracture Zone (AFFZ).

The CKBC fault system formed as individual faults that are structurally related due to their continuity, geometry, and sense of movement. Further, the faults have similar histories through time, reactivating as south-dipping normal faults in the Mesozoic along pre-existing thrust faults. The Kouga Fault is positioned directly south of the Baviaanskloof Fault and is linked to the CKBC by a series of northeast-striking cross faults referred to as the Paul Sauer Faults (***Reference 5.13.26*** and ***Figure F-5.13.48***).

The Ceres Fault is the westernmost segment of the CKBC system, extending from a point southeast of Touws River (***Reference 5.13.13***), near the western end of the Kango Fault, to the town of Ceres in the west. The fault terminates where the east-west trend of the southern branch of the Cape Fold Belt coalesces with the north-northwest-trending western branch in the Cape syntaxis (***Reference 5.13.134***). The syntaxis is situated in the Western Cape province and is characterised by complex faulting and folding positioned well out of the site region (***Reference 5.13.133***). Field reconnaissance by Goedhart (***Reference 5.13.14***) along the Ceres Fault suggests a steepening in the fault

© Eskom 2026/Rev 0a

dip relative to the eastern section of the CKBC system. Further, there has been no evidence to suggest Neotectonic reactivation of this fault.

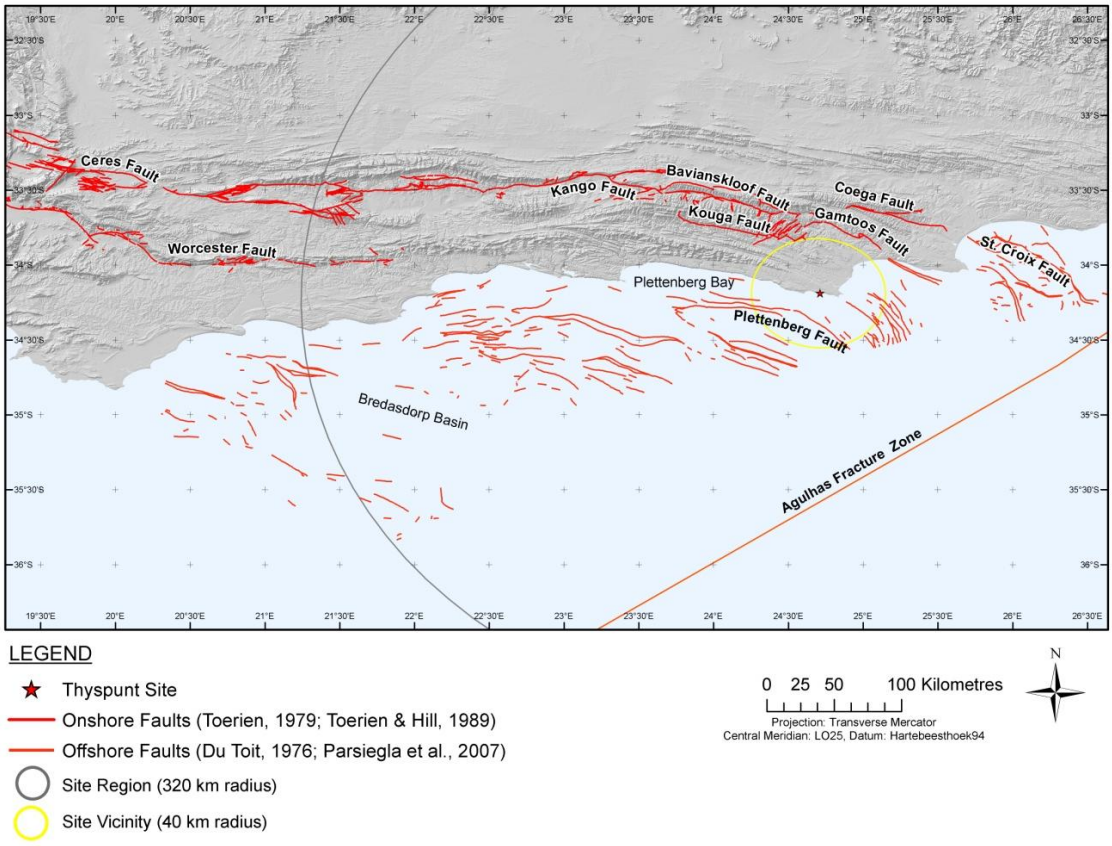


Figure 5.13-47
Map Showing Major Onshore Offshore Faults in the Site Region; the Mesozoic Normal Faults Onshore Generally Dip to the South

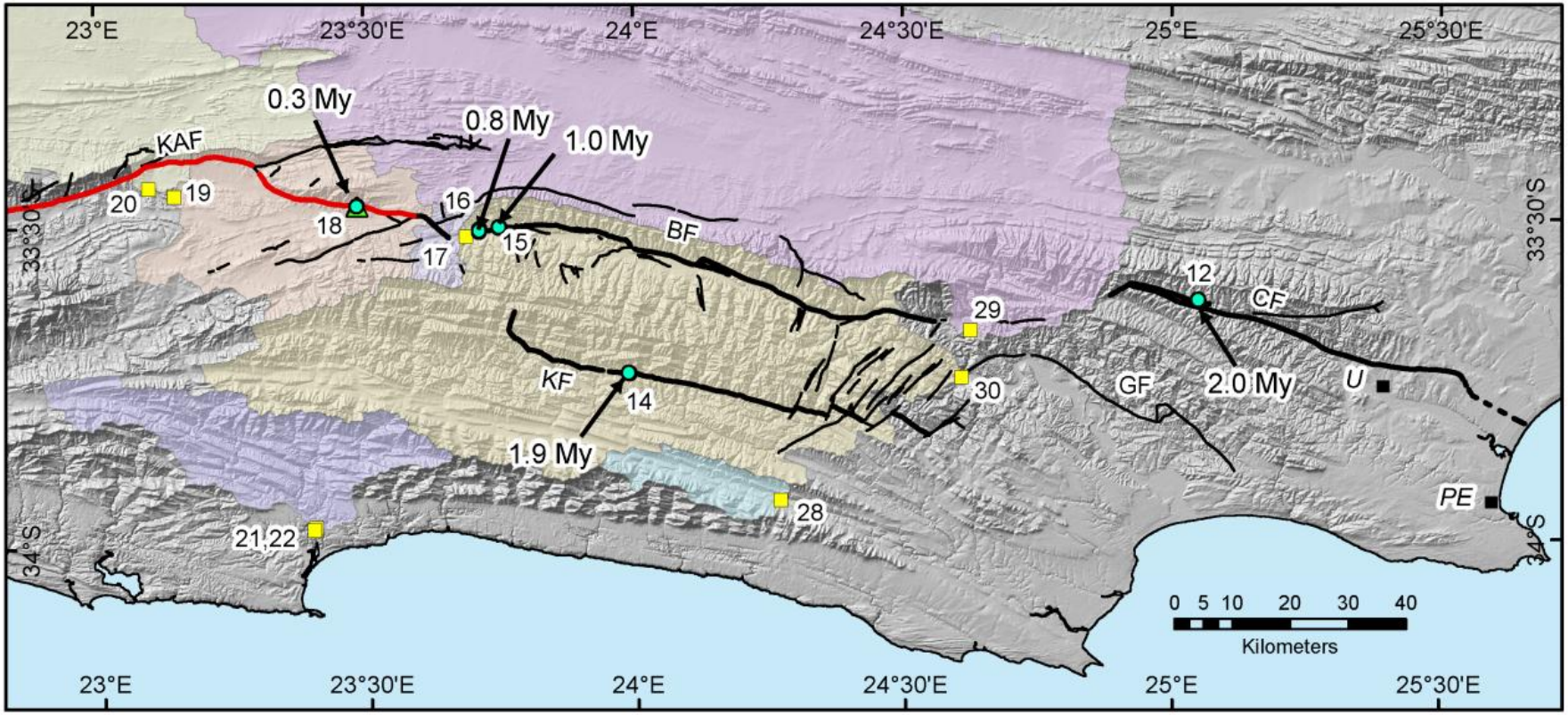


Figure 5.13-48
Sample Location Map with Minimum Limiting Ages for Pediment Samples (Green Circles) and Erosion Rates for River Samples (Yellow Boxes). TSP sample sites identified by number. BF = Baviaanskloof Fault, CF = Coega Fault, GF = Gamtoos Fault, KAF = Kango Fault, KF = Kouga Fault, PE = Plettenberg Fault, U = Uitenhage

© Eskom 2026/Rev 0a

The Kango Fault is positioned west of a 10 km step-over from the Ceres Fault and neighbours the Baviaanskloof Fault to the east. The east-west-striking fault has a total length of 320 km and is south dipping, extending to at least 10–12 km in the subsurface (***Reference 5.13.263***). This fault is unique within the CKBC fault system because the eastern ~100 km shows evidence of Quaternary reactivation. Discussion of the Cenozoic movement on this portion of the Kango Fault is discussed in ***Subsection 5.13.5.1.(d) v*** (Kango Fault Zone).

The Baviaanskloof Fault extends 110 km from the eastern end of the Kango Fault where a geomorphic step coincides with a south-easterly change in strike of the fault system (***Reference 5.13.54***). In the west, the Baviaanskloof Fault intersects multiple high-level pediment surfaces that are capped by gravels that are mapped as the Tertiary Grahamstown (Tg) Formation. These gravel deposits are cemented by pedogenic processes and are now lithified as silcretes and ferricretes. Following the fault trace to the east the Tg surfaces become non-existent and the fault is observed as a range-front escarpment that juxtaposes Ordovician-age quartzites against Jurassic basin-filling deposits (Enon Formation). As part of the Geological Investigations for the PSHA study (***Reference 5.13.1***), observations of no apparent vertical offset of the Tg silcrete surface where remnants cross the fault were documented at five sites (***Reference 5.13.17***). Geochronology samples (TSP16 and TSP15) collected from the silcrete surfaces at two of these sites indicate that the exposed surfaces have been stable for a minimum of 0.8–1.0 Myr or have experienced maximum erosion rates of 0.32–0.51 m/Myr, based on cosmogenic nuclide dating (***Reference 5.13.51*** and ***Figure F-5.13.48***). Observations and information related to the mapping at specific sites is documented in Prasad & Claassen (***Reference 5.13.17***).

The Coega Fault is a bounding fault of the Algoa Basin half-graben. The Coega Fault is characterised by two sections. The western 30 km consists of two subparallel northwest-striking, south-dipping fault traces that juxtapose quartzite of the Palaeozoic Table Mountain Group in mountainous terrain. There are many locations along the western portion of the fault where remnants of silcrete-mantled pediment surfaces (Tg) at elevations of approximately160 m above the valley floor overlie the mapped fault. Geochronology samples collected from the Tg surface at sample site TSP12 indicate that the exposed undeformed surface at this site has been stable for a minimum of 2.0–3.7 Myr or has experienced a maximum erosion rate of 0.11–0.21 m/Myr, based on cosmogenic nuclide dating (***Reference 5.13.51***).

The transition zone between the western and eastern Coega fault sections is situated northwest of Uitenhage (***Reference 5.13.18***) and marks a change in

strike orientation for the Coega Fault. Here the Coega Fault juxtaposes more competent Cape Supergroup rocks to the north against softer Cretaceous sediment south of the fault; which results in an escarpment with a relative relief of 200 m (***Reference 5.13.272***). Within the transition zone, the two traces comprising the Coega fault are locally connected by northeast-striking *en-echelon* cross-faults (***Reference 5.13.18***).

The eastern Coega fault zone comprises the section of the fault zone south of Uitenhage to the Ngqura Harbour at the mouth of the Coega River (***Reference 5.13.19***). The Eastern Coega Fault Zone generally lies within the Uitenhage Group (Cretaceous Kirkwood and Sundays River Formations). Locally, the fault juxtaposes quartzite of the Peninsula Formation (Table Mountain Group) against softer sedimentary rocks of the Uitenhage Group. This section of the fault, however, is buried under younger Tertiary to Recent sediments and is not exposed or geomorphically well expressed at the surface.

Because of the general buried nature of the fault, the precise location and geometry of the Eastern Coega Fault Zone are uncertain. The fault, as mapped by the CGS and verified through geophysical data collected by private companies (***References 5.13.273*** and ***5.13.274***), is traced ~300 m south of Coega Kop. These studies suggest that the onshore segment of the Coega Fault may not be a uniform, steeply dipping and inclined fault plane, as suggested by W.C. le Roux (***Reference 5.13.273***), but rather consists of a zone of elongated and subparallel horst-and-graben structures. The fault corridor defined for the Thyspunt PSHA Geological Investigations work encompassed the general location of the main traces of the Eastern Coega fault zone as inferred from previous studies (***Reference 5.13.19***).

Secondary faulting associated with the Coega Fault was previously identified in the vicinity of Coega Kop, where north-easterly trending splay faults, in the shape of a horse-tail are present. Goedhart & Hattingh (***Reference 5.13.275***) reported two incidences of reverse faulting, with displacement of 0.5 m and 1 m, respectively, from a trench dug at the Motherwell township This trench was inferred to overly the Coega Fault and was interpreted to be possible evidence for Neogene compressive reactivation of the fault. However, viable nontectonic mechanisms (e.g., decompression, resulting from over consolidation (shrinkage) and subsequent decompression (swelling) of the Cenozoic sediments) are considered more likely given the setting and nature of bedrock units in the area (***Reference 5.13.19***).

Mitha et al. (***Reference 5.13.19***) compiled and evaluated a subsurface database comprised from over 500 borings and shallow trench pit logs that provided information on the location and activity of the Coega Fault

© Eskom 2026/Rev 0a

(***Reference 5.13.19***). Although small deformation features and a previously unrecognised splay from the Coega fault zone were identified in this study, there was no evidence to indicate neotectonic reactivation of the fault zone. Marine terrace platforms ranging in age from middle Pleistocene (minimum of 330 ka) to early Pliocene (~4 Ma) appear to be continuous and undeformed across the Coega fault zone, as previously mapped by the CGS (***Reference 5.13.19***).

South of the Baviaanskloof and Coega Faults, the Kouga Fault runs approximately 80 km and parallel to the CKBC fault system along its entire length before terminating against a series of northeast-striking cross-faults called the Paul Sauer Faults. The Paul Sauer Faults offset the Kouga Fault right-laterally as the fault system steps eastward to the faults bounding the Gamtoos and Coega Basins. Both the Kouga and Paul Sauer Faults, contained in the Palaeozoic bedrock, intersect a series of overlying Tg surfaces. The Kouga Fault is similar in geomorphic and structural characteristics to the Baviaanskloof and western Coega Faults in that it juxtaposes Palaeozoic quartzite rocks and it is common to observe Tg silcrete surfaces overlying the bevelled quartzite pediments. Cosmogenic analysis of samples from an undeformed Tg surface across the Kouga Fault (TSP16, ***Figure 5.13.48***) indicates that the exposed surface has been stable for a minimum of 1.9 Myr or has experienced very slow erosion at maximum rates of 0.14–0.20 m/Myr (***Reference 5.13.51***).

Gamtoos Fault

The Gamtoos Fault is the main basin-bounding fault along the eastern margin of the Gamtoos Basin, one of four major depocentres on the southern South Africa continental margin formed during the early stages of Mesozoic rifting (***Figure F-5.13.49***; ***Subsection 5.13.5.1.(b) ii***). The Gamtoos Basin forms part of the larger Outeniqua Basin and is separated from the Pletmos and Algoa Basins by local structural highs, the St Francis and Recife Arches, respectively. The broad-scale structural and sedimentological evolution of the Gamtoos Basin is described in several publications (*e.g.*, ***References 5.13.270***, ***5.13.162***, and ***5.13.73***). Thomson (***Reference 5.13.144***) describes the evolution of the Gamtoos Basin as a complex process linked to the breakup of Gondwana, pre-existing basement structure, and transitory effects of mantle plumes.

The Gamtoos Fault is approximately 47 km from the Thyspunt site at its closest approach (***Figure F-5.13.49***). The geometry of the offshore structure is well known from interpretation of offshore seismic data (*e.g.*, ***References 5.13.162***, ***5.13.73***, ***5.13.276***, ***5.13.137***, and ***5.13.45***; ***Figures F-5.13.50***, ***F-5.13.51***, and ***F-5.13.52***). The Gamtoos Fault trends northwest–southeast onshore and bends

© Eskom 2026/Rev 0a

to a more north–south trend approximately 10 km south of Cape Recife (***References 5.13.277***, ***5.13.278***, and ***5.13.162***).

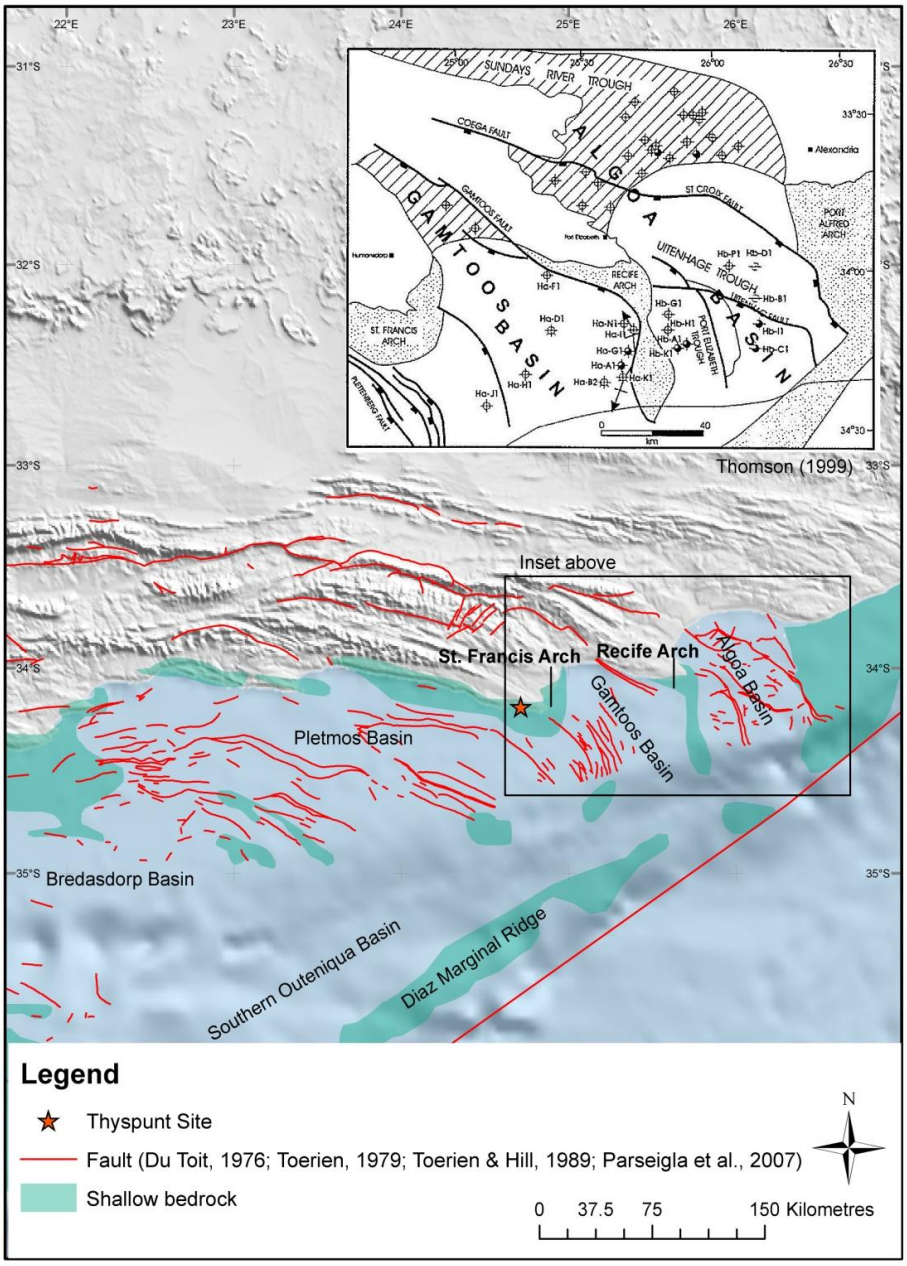


Figure 5.13-49
Map of the Outeniqua Basin Showing the Major Structural Elements and Sub-Basins and Enlargement of the Gamtoos and Algoa Basins (Modified from *Reference 5.13.144*)

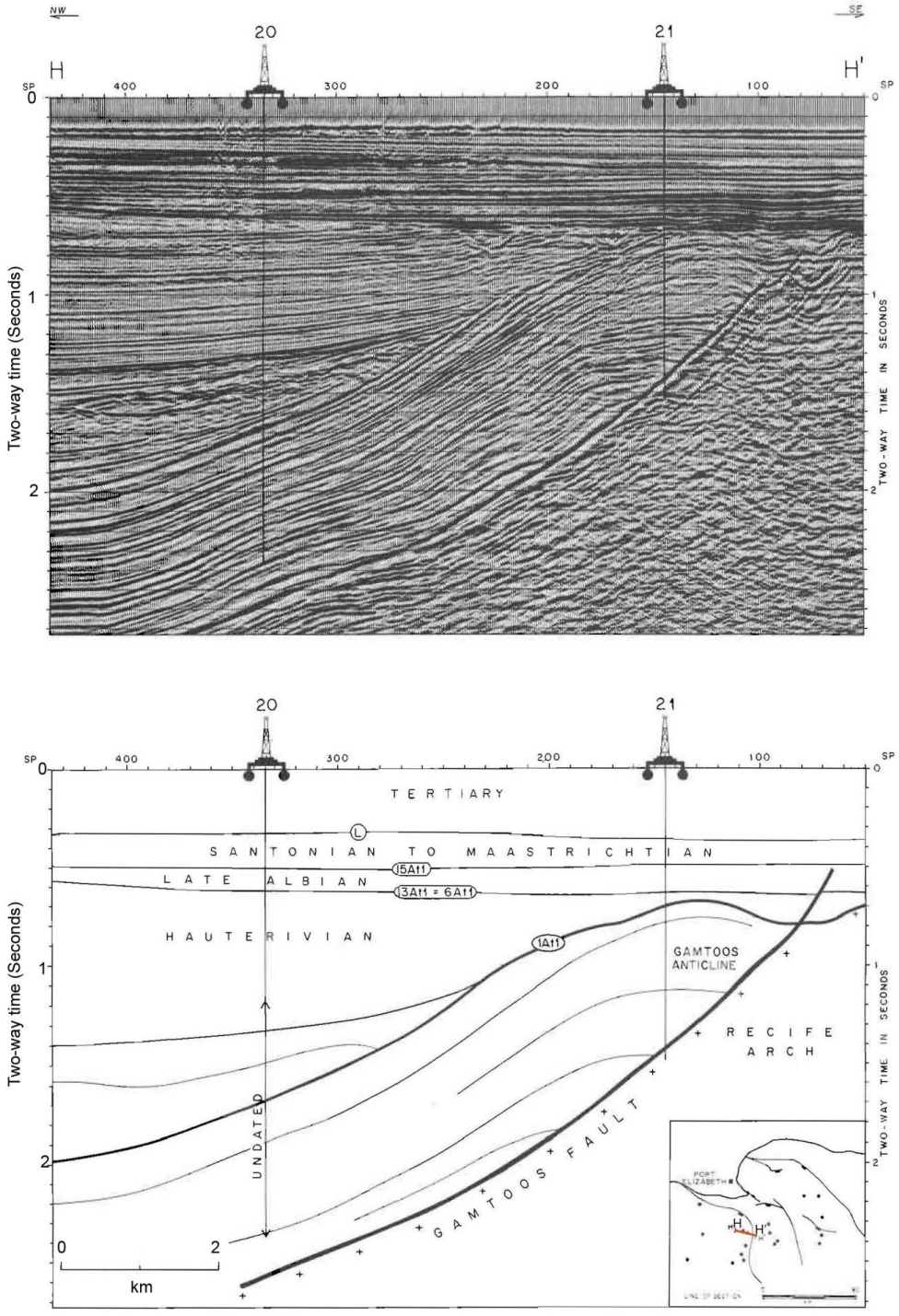


Figure 5.13-50
Seismic Profile H-H′ and Geological Interpretation Across the Southern Gamtoos Basin (*Reference 5.13.162*)

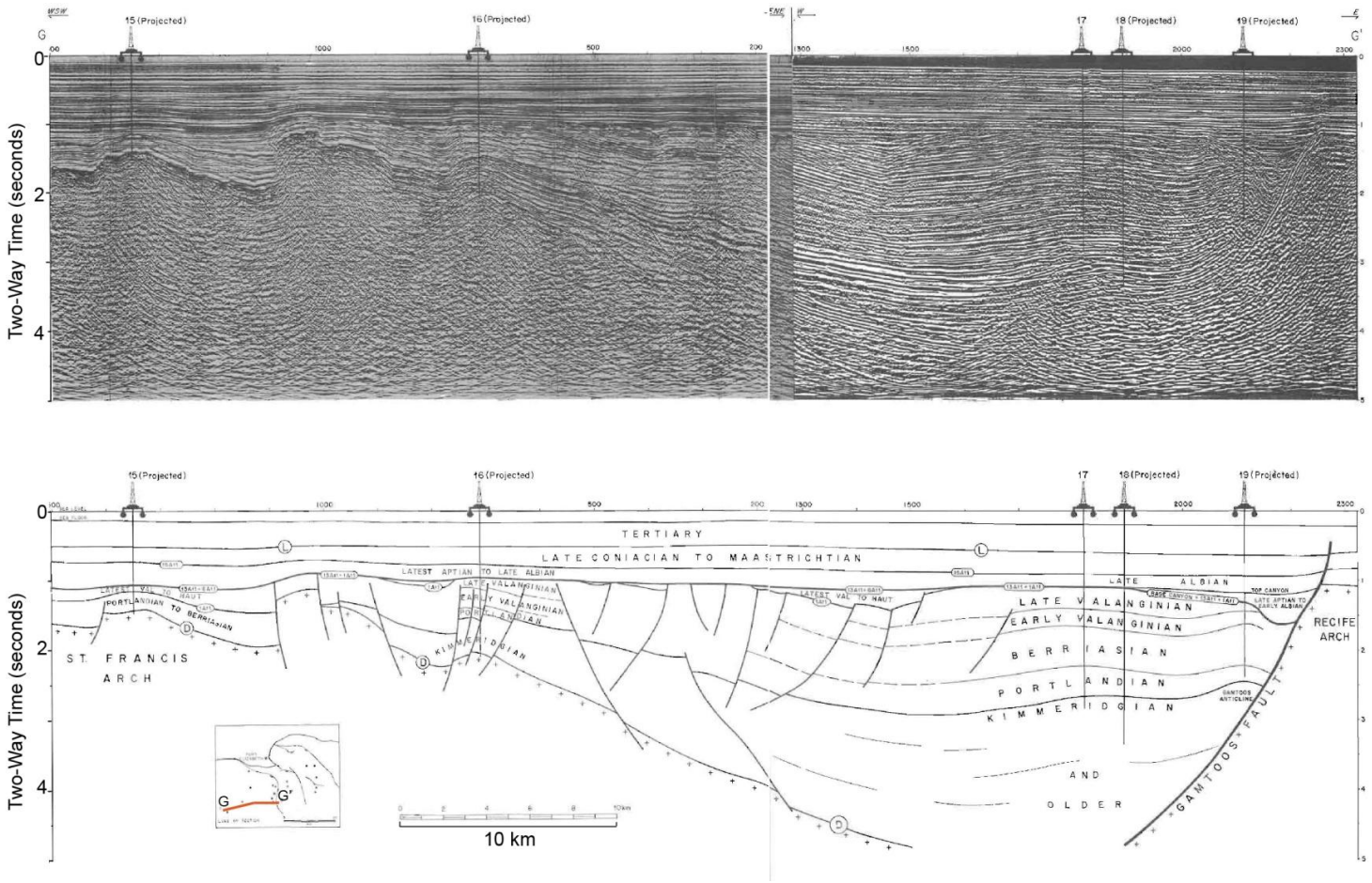


Figure 5.13-51
Seismic Profile G-G′ and Geological Interpretation Across the Southern Gamtoos Basin (*Reference 5.13.162*)

© Eskom 2026/Rev 0a

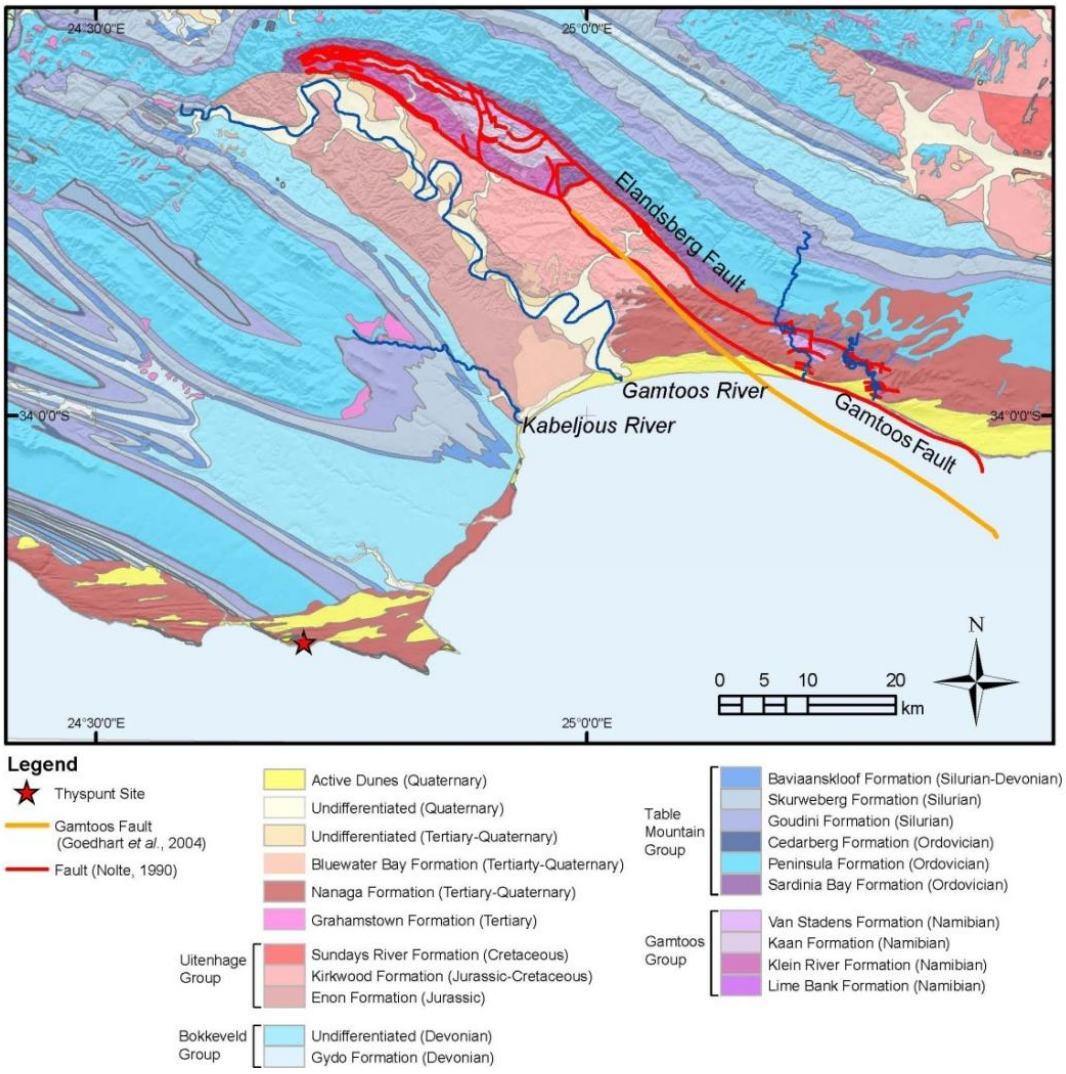


Figure 5.13-52
Geology Along the Gamtoos Fault (Modified from *Reference 5.13.91*)

The observed (minimum) total length of the Gamtoos Fault is 170 km, including both onshore (90 km) and offshore (80 km) reaches (***Reference 5.13.137***).

Onshore, the Gamtoos Fault runs parallel to, and 3–5 km to the southwest of, the Elandsberg Fault (***Figure F-5.13.52***). The onshore portion of the fault zone

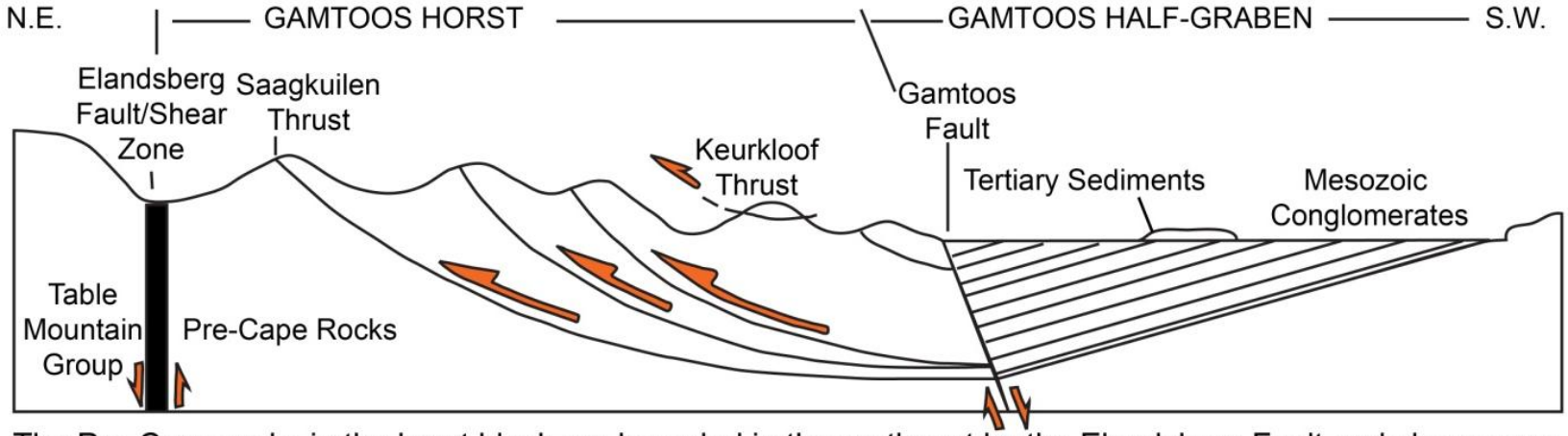
has been studied by Nolte (***Reference 5.13.278***), Shone *et al.* (***Reference 5.13.113***), and Booth & Shone (***Reference 5.13.150***). The fault zone comprises a complex cropping out of Mesozoic, Cape Supergroup, and Pre-Cape strata. The contacts between the three units are fault-bound, with the Gamtoos Fault containing Mesozoic syn-rift strata in its hanging wall and Pre-Cape strata in its footwall (***Figure F-5.13.53***). The Elandsberg Fault has Pre-Cape strata in its footwall and Table Mountain Group (Cape Supergroup) strata in its hanging wall. Between the faults is a horst block of deformed Proterozoic sedimentary rocks of the Gamtoos Group (***References 5.13.278*** and ***5.13.113***).

The horst block is bounded and cut by northeast-southwest-trending faults, which offset the Elandsberg Fault but not the Gamtoos Fault; this indicates that the Elandsberg Fault was not reactivated during Mesozoic extension when the transfer faults were formed (***Reference 5.13.278***). The Pre-Cape Group appears to have undergone multiple phases of deformation, with the most prominent deformation fabric being associated with the late Palaeozoic Cape Orogeny. The older structures have the same trend as the Gamtoos Fault, which is considered to have reactivated a Cape Fold Belt fault (***References 5.13.113*** and ***5.13.137***).

Onshore, the throw on the Gamtoos Fault is 15 km; offshore, the fault exhibits a throw of 16.5 km (***Reference 5.13.131***) and is traced to a depth of 11–12 km (***References 5.13.162***, ***5.13.131***, and ***5.13.130***). Most, if not all, of this offset is interpreted to have occurred in the Mesozoic to early Tertiary (***References 5.13.162*** and ***5.13.131***).

The onshore trace of the Gamtoos Fault is generally obscured by Quaternary sedimentation, especially near the coast, where active and stabilised dunes are present (***References 5.13.137*** and ***5.13.58***; ***Figures F-5.13.52*** and ***F-5.13.54***). The Cenozoic sediments at the coast cover the Gamtoos Fault for at least half of its onshore length (***Figure F-5.13.52***), but its location has been inferred from aeromagnetic data, as discussed in Goedhart *et al.* (***Reference 5.13.13***). Where not obscured, the fault is traced based on the difference in lithologies of the Proterozoic Gamtoos Group and younger sediments on the downthrown block (***Reference 5.13.278***). Offshore, the fault is traced on seismic reflection profiles (References 5.13.277, 5.13.162, and 5.13.73).

© Eskom 2026/Rev 0a



The Pre-Cape rocks in the horst block are bounded in the northeast by the Elandsberg Fault and shear zone, and in the southwest by the Gamtoos Fault. Imbricate thrusts in Pre-Cape strata dip to the south. Folds in the Cape and Pre-Cape are diagrammatic. Section shows present-day topography with more-resistant Table Mountain quartzite (Cape Supergroup) forming high ground in the northeast of the section

Figure 5.13-53
Simplified Cross Section Across the Gamtoos Horst Block in the Onshore Region (Modified from *Reference 5.13.113*)

© Eskom 2026/Rev 0a

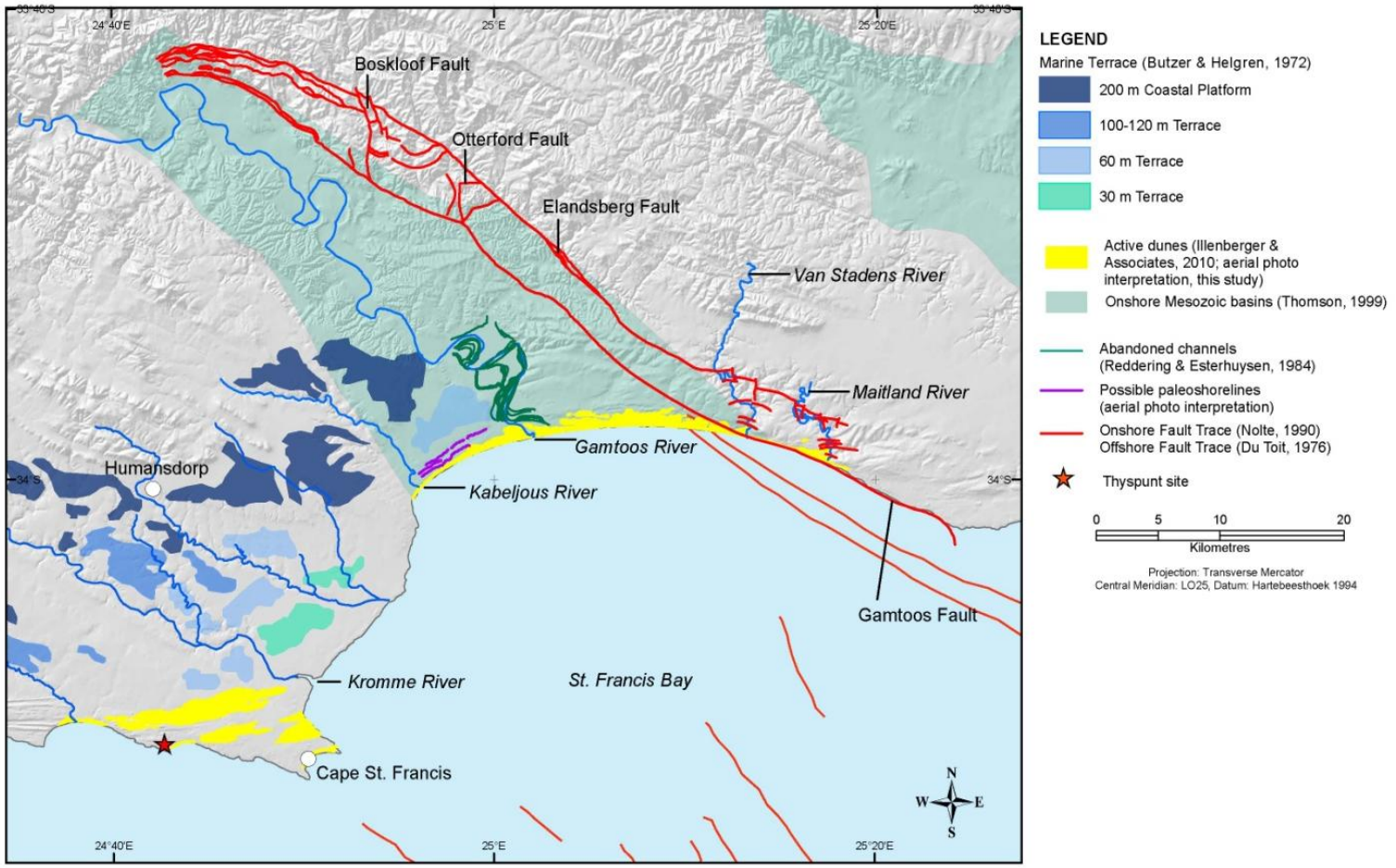


Figure 5.13-54
Compilation Map Showing Generalised Quaternary Geology and Locations of Onshore and Offshore Traces of the Gamtoos and Elandsberg Faults (Modified from *Reference 5.13.58*)

© Eskom 2026/Rev 0a

Although the Gamtoos Fault changes trend from approximately northwest–southeast to north–south, the cross-sectional geometry of the fault demonstrates a continuous, linear and nonsegmented fault plane; this suggests that the fault is not made up of multiple en-echelon configured segments (***References 5.13.276*** and ***5.13.137***). Paton & Underhill (***Reference 5.13.276***) also demonstrate that the complex interplay between compression and extension postulated by previous workers is not needed to explain the fold deformation observed along the fault. Rather, this deformation may be a consequence of the accommodation of extension by the unusual plan-view trace of the fault inherited from underlying strata. The Gamtoos Fault displays a listric geometry in many, but not all, subsurface images (***References 5.13.144*** and ***5.13.130***).

The dip of the fault ranges from ~26 degrees to the southwest onshore (***Reference 5.13.130***) to 34 degrees on the northwest-trending portion of the offshore fault (***Reference 5.13.137***). However, alternative interpretations of the data suggest that the fault could be much steeper (60 degrees) down to seismogenic depth (***Reference 5.13.1***).

The following evidence for neotectonic inactivity of the Gamtoos is cited in published literature and site specific studies:

- Seismic lines along the southern part of the fault zone (the more northerly trending part of the fault) are interpreted to show evidence of no displacement of the Upper Cretaceous 15At1 horizon and overlying Tertiary strata (***Reference 5.13.162*** and ***Figure F-5.13.50***).
- Based on compilation of regional marine terrace data, there is no apparent change in uplift across the fault zone of terraces inferred to be Pliocene in age (*e.g.*, the 60 m and 30 m terraces) (***Reference 5.13.58*** and ***Figure F-5.13.7***). Davies (***Reference 5.13.88***) reports estuarine deposits along the Gamtoos River (hanging wall) at a height of approximately 18 m. At Cape Recife and in the vicinity of the Coega River on the footwall (east of the mapped traces of the fault), Davies (***Reference 5.13.88***) also identified beach and estuarine deposits, respectively, at ~18 m.
- There is no obvious geomorphic expression (lineaments, scarps, etc.) in aerial photographs, GoogleEarth imagery, or available DEM data (10 m resolution) to suggest Quaternary reactivation of the Gamtoos Fault although aeolian sands may cover any expression near the coast (***References 5.13.24*** and ***5.13.58***).
- Paton (***Reference 5.13.137***) states that there is no bathymetric expression of the Gamtoos Fault. This observation is supported by the new high-resolution bathymetry data set compiled by De Wet ***Reference 5.13.59***. As

shown on ***Figure F-5.13.52***, the large scarps interpreted from the seismic profiles (***Reference 5.13.45***) are not apparent in the topographic profiles.

Plettenberg Fault

The Plettenberg Fault is a Cape Fold Belt thrust reactivated as a normal fault during Mesozoic extension (***References 5.13.142***, ***5.13.162***, and ***5.13.137***). The Plettenberg Fault is the main basin-bounding fault along the eastern margin of the Pletmos Basin (***Figure F-5.13.55***).

The fault likely originated as a thrust fault during the Permo-Triassic Cape Orogeny. The Pletmos Basin, which is one of the major sub-basins of the larger Outeniqua Basin, is bounded on the northeast by the St Francis Arch and on the southwest by the Infanta Embayment. Major events and phases of deformation in the Pletmos Basin are summarised on ***Figure F-5.13.17.***

The Plettenberg Fault trends approximately east–west from approximately 50 km southeast of Plettenberg Bay to approximately 15 km off Oyster Bay, where it bends to a more northwest-southeast trend along the western flank of the St Francis Arch (***References 5.13.277*** and ***5.13.72***; ***Figure F-5.13.55***). The Plettenberg Fault is 20 km from the Thyspunt site at its closest approach (***Reference 5.13.1***). The total length of the fault is approximately 160 km (***References 5.13.277***, ***5.13.137***, and ***5.13.45***). Although it has been speculated that the Plettenberg Fault possibly links up onshore with the Worcester Fault zone (***Reference 5.13.24***) or that the fault may continue onshore south of the Worcester fault and west of Plettenberg Bay, where it may be associated with Mesozoic sediments along Plettenberg Bay, published maps and figures limit the fault to the offshore (including figures in ***Reference 5.13.137***). The fault is traced on seismic reflection lines and as the contact between Mesozoic basin sediments and basement rocks. Sediment thickness in the Pletmos Basin is up to 11,000 m thick in depocentres adjacent to basin-bounding faults (***Reference 5.13.73***).

The Plettenberg Fault is well imaged in offshore seismic data (***References 5.13.72***, ***5.13.162***, ***5.13.137***, and ***5.13.131***; ***Figure F-5.13.56***). The Plettenberg Fault is imaged to a depth of at least 12,000 m to 13,000 m in 2-D seismic reflection sections, in Paton *et al.* ***Reference 5.13.131***) and Paton (***Reference 5.13.137***), respectively. The downdip geometry of the Plettenberg Fault is interpreted from seismic lines to be planar and dipping at 65 degrees to the southwest on the northwest-southeast-trending portion, and at 50 degrees to the west on the north-south-trending portion (***References 5.13.137*** and ***5.13.131***).

© Eskom 2026/Rev 0a

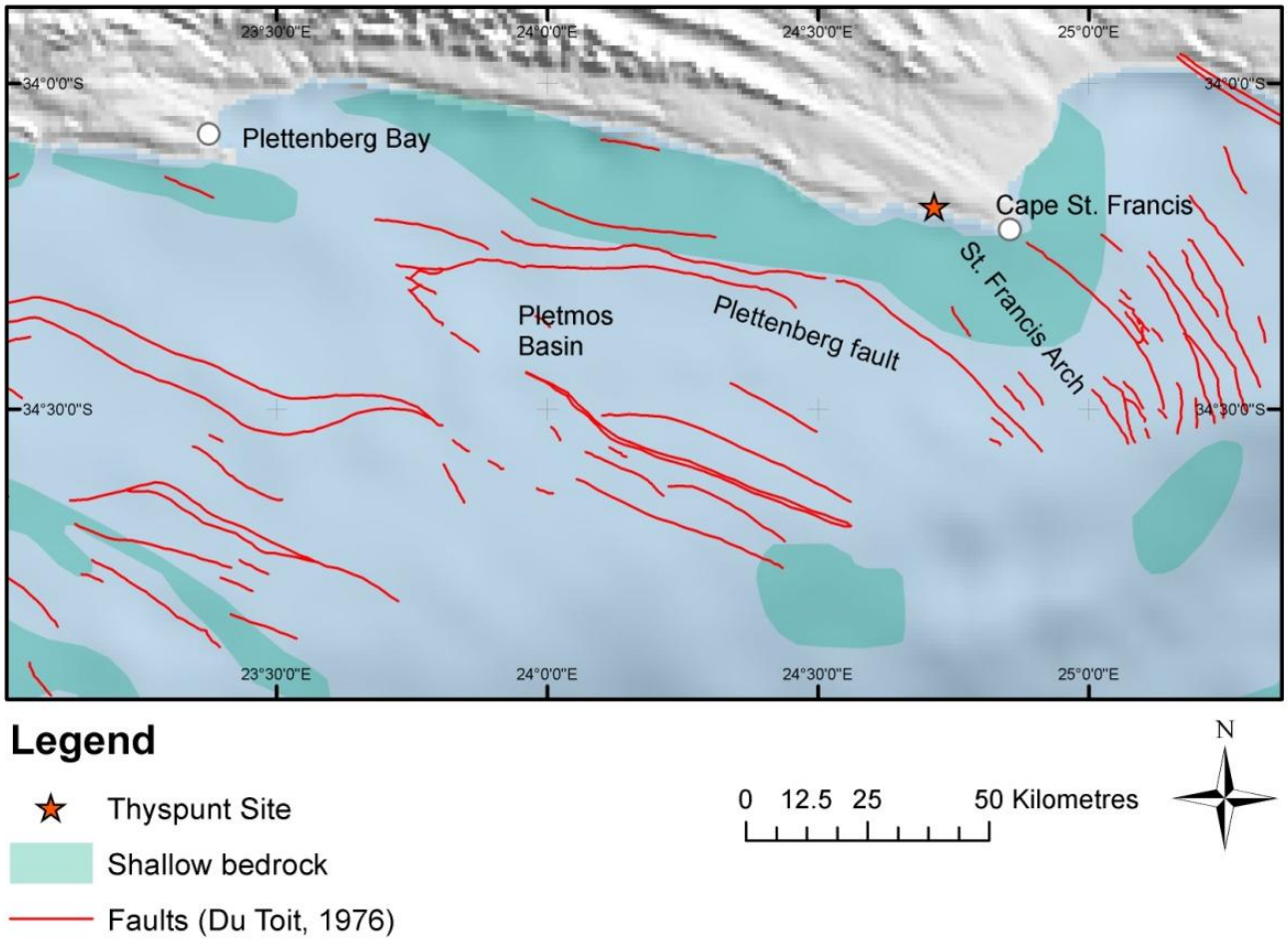


Figure 5.13-55
Map Showing Location of Plettenberg Fault (Modified from *Reference 5.13.72*). Base topography: *Reference 5.13.279*

© Eskom 2026/Rev 0a

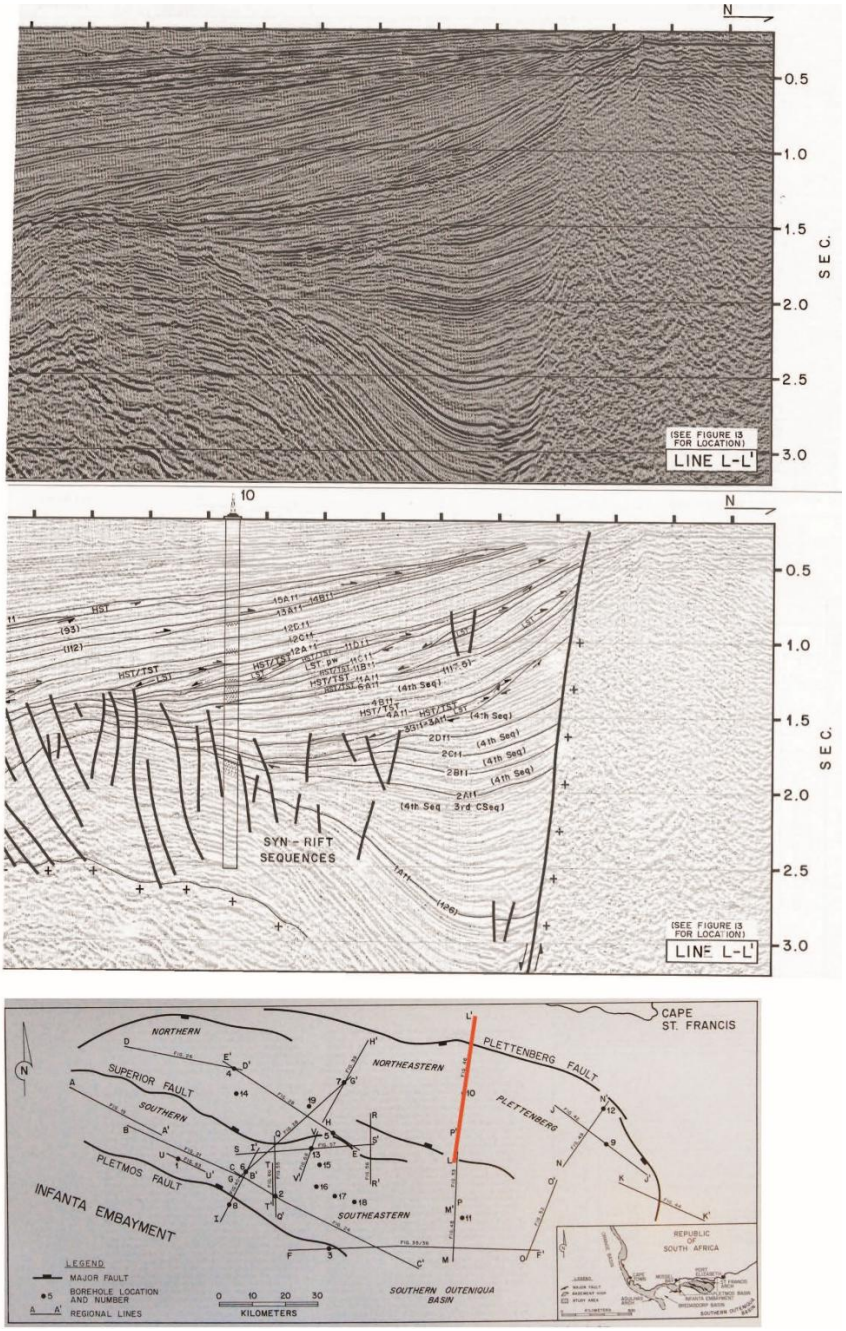


Figure 5.13-56
Seismic Section L-L′ (Uninterpreted and Interpreted) Across the Plettenberg Fault (Offshore) (Modified from *Reference 5.13.72*)

Published interpretations of seismic lines across the Plettenberg Fault (*e.g.*, ***Figure F-5.13.56***) do not show the fault extending up to the seafloor (***References 5.13.72*** and ***5.13.137***). Interpretations of seismic lines across the fault presented at the Thyspunt PSHA SSHAC Workshop 1 (***Reference 5.13.45***), however, do show the fault extending to the seafloor and locally being associated with possible minimum post-Cretaceous (post-22At1 sequence boundary) displacements of up to 22 m (***Figures F-5.13.61*** and ***F-5.13.62***).

It was noted by Roux (***Reference 5.13.45***) that apparent displacements observed in the offshore data may be due to nontectonic mechanisms such as decompaction of sediments on the downthrown side or isostatic restoration due to major erosion on the upthrown side of faults. It was also acknowledged in the presentation that the 2-D seismic data are not geared towards evaluating neotectonic activity and that the resolution of the data is not sufficient to evaluate shallow fault displacements. In addition, wave erosion during fluctuations of sea level across the continental shelf may diminish or remove evidence of Tertiary and recent faulting. Finally, Roux (***Reference 5.13.45***) concluded that the entire offshore region is tectonically stable and not expected to be influenced by major tectonic activity.

Paton (***Reference 5.13.137***) states that there is no bathymetric expression of the Plettenberg Fault. This observation is further supported by inspection of a recently processed high-resolution bathymetry data set compiled by De Wet (***Reference 5.13.59***) from single-beam bathymetric data collected from shiptrack data and gridded at a resolution of approximately 1 m. There are no seafloor scarps associated with the post-Cretaceous offsets interpreted from the seismic data, and there is not a continuous scarp along the trace of the fault that would suggest latest Pleistocene to Holocene (post-LGM transgression) displacement of the seafloor (***Reference 5.13.1*** Plate A2.6 and ***Figure F-5.13.57***).

In summary, the majority, if not all, tectonic displacement on the Plettenberg Fault occurred during Mesozoic extension related to the breakup of Gondwana (***Reference 5.13.137***). Little tectonic activity has occurred since 80 Ma (***Reference 5.13.72***). The Plettenberg Fault exhibits downthrow towards the south or southwest (***References 5.13.142*** and ***5.13.162***), and the possible evidence for Tertiary displacement on the fault reported by Roux (***Reference 5.13.45***) is down to the southwest. New high-resolution bathymetric data by De Wet (***Reference 5.13.59***) does not show displacement along the fault in the areas mapped by Roux (***Reference 5.13.45***). There are no alignments of microseismicity or associated moderate- to large-magnitude

© Eskom 2026/Rev 0a

earthquakes (***Subsection 5.13.5.3.(b)***) to indicate that the Plettenberg Fault is seismogenic in the contemporary tectonic regime (***Reference 5.13.1***).

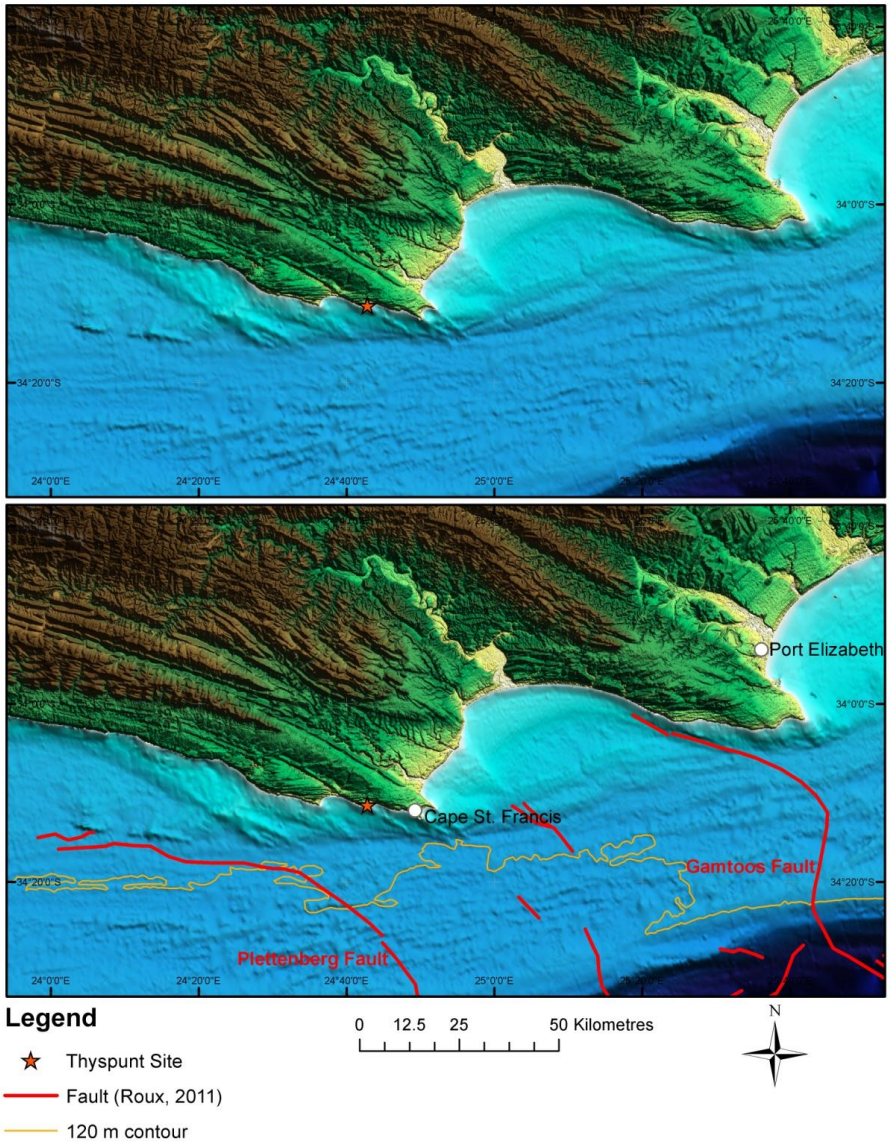


Figure 5.13-57
High-Resolution Bathymetric Map Showing Geomorphology Along the Offshore Plettenberg Fault:
(A) Uninterpreted (*Reference 5.13.59*; Topography from *Reference 5.13.280*).
(B) with Post-Cretaceous Faults as Mapped by Roux (*Reference 5.13.45*)

Cape St Francis Fault

The Cape St Francis Fault is entirely offshore and has an approximate mapped length of 40 km. This fault sits within the site region and comes within 17 km of the Thyspunt site (***Figure F-5.13.58*** and ***Reference 5.13.1***).

The Cape St Francis Fault and associated faults along the Cape St Francis Arch are northwest–southeast extensional faults with tectonic age and style similar to that of the major onshore faults, such as the Ceres-Kango-Baviaanskloof-Coega and Kouga Faults (***Reference 5.13.26***).

The position of the offshore fault is constrained by a number of seismic reflection profiles that image the St Francis Arch from offshore petroleum exploration surveys (***References 5.13.142***, ***5.13.162***, and ***5.13.45***). The mapped horizons from the survey data locate the fault trace within Cretaceous stratigraphy. A published interpretation of seismic profiles across the faults within the St Francis Arch indicates there is no offset of Tertiary units (***Reference 5.13.142*** and ***Figure F-5.13.59***). McMillan *et al.* (***Reference 5.13.162***) interpret seismic sections over the southern end of the fault complex along the hinge of the St Francis Arch and also concludes that the southern north-northwest to south-southeast segment of the Cape St Francis Fault was last active at approximately 116.5 Ma (***Figure F-5.13.60***).

Roux (***Reference 5.13.45***) presents a set of time-horizon maps that show the relationship between faults interpreted to cut the base of Cretaceous (1At1 unconformity) versus the fault traces that extend upwards into Tertiary reflectors (post 22At1 unconformity) or to the seafloor (***Figure F-5.13.61***). Possible post-Cretaceous displacement is only observed on two short faults (5 km and 10 km long) within the Gamtoos Basin positioned northeast of the Cape St Francis Fault and along short segments in the southern part of the fault zone (***Figure F-5.13.59***). In the interpreted seismic profile line A (***Figure 5.13.62***) of Roux (***Reference 5.13.45***) the western trace is shown to truncate the 22At1 unconformity. The eastern fault is traced to the seafloor in the uplifted and eroded part of the Cape St Francis arch where sediments at the seafloor are inferred to be pre-Cretaceous syn-rift sediments. Both faults are projected to the seafloor and possible scarps associated with the faults are estimated to be less than 10 m in height. Roux (***Reference 5.13.45***) acknowledges that the fault traces that are postulated to be post-Cretaceous are poorly imaged at shallow depths, and his general conclusions are that the offshore region is tectonically stable and that the seafloor scarp(s) could have formed by nontectonic processes such as current-driven differential erosion at the fault trace.

© Eskom 2026/Rev 0a

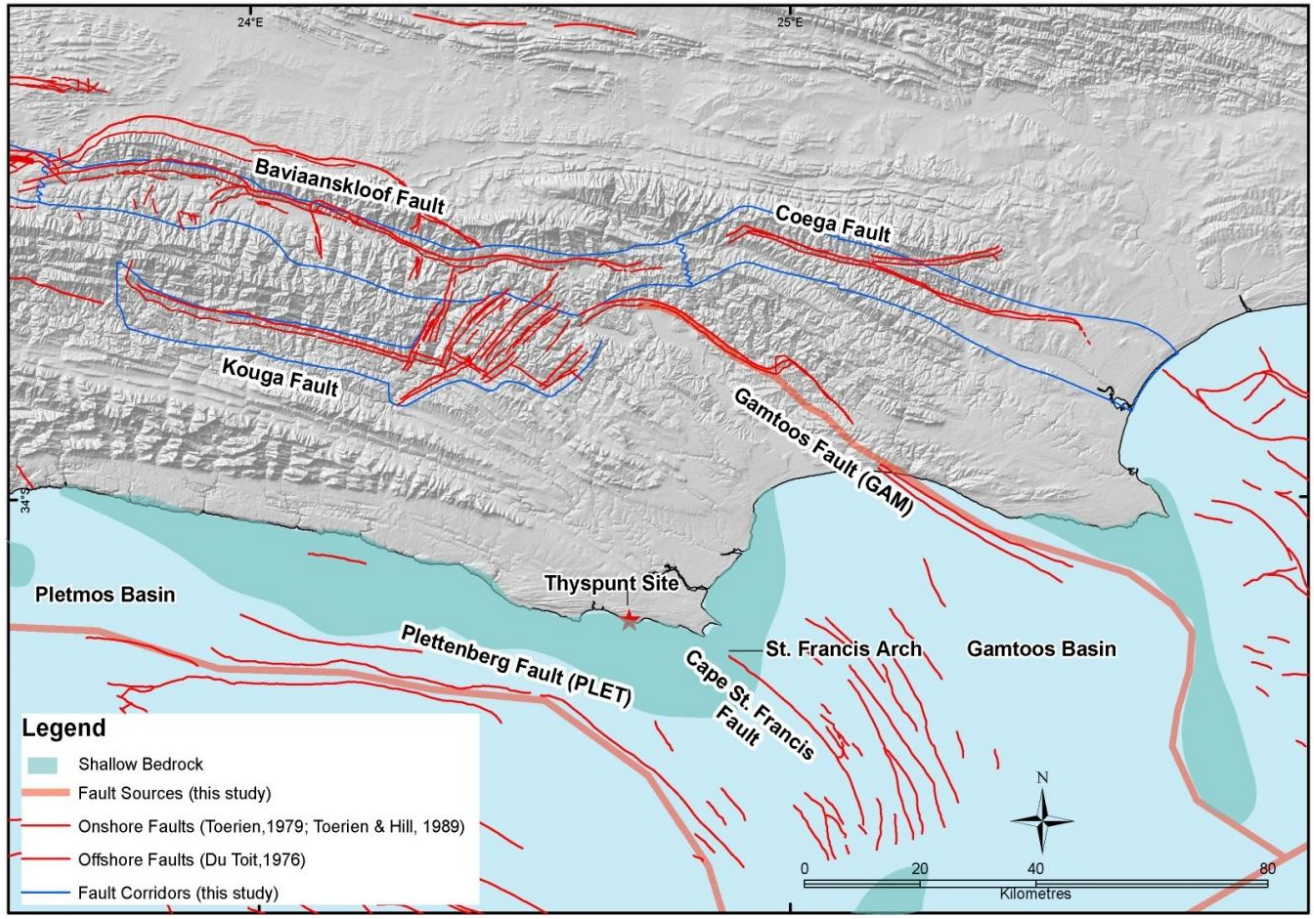


Figure 5.13-58
Map Showing Location of the Cape St Francis Fault and Associated Fault Traces from Du Toit (*Reference 5.13.277*)

© Eskom 2026/Rev 0a

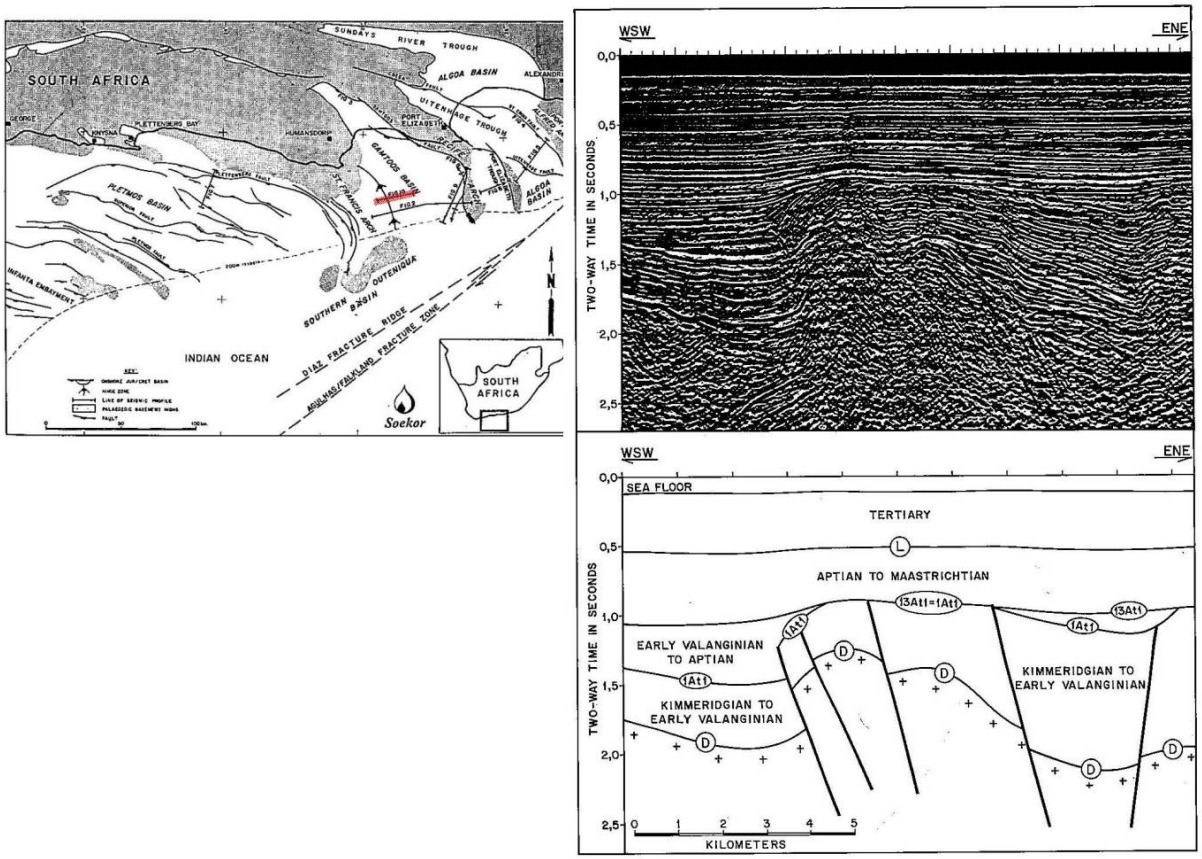


Figure 5.13-59
Seismic Profile Across the Cape St Francis Fault Showing No Offset Across the Cretaceous (1At1) Horizon. The location of the profile shown is highlighted in red on the map (upper left) (Modified from *Reference 5.13.142*)

© Eskom 2026/Rev 0a

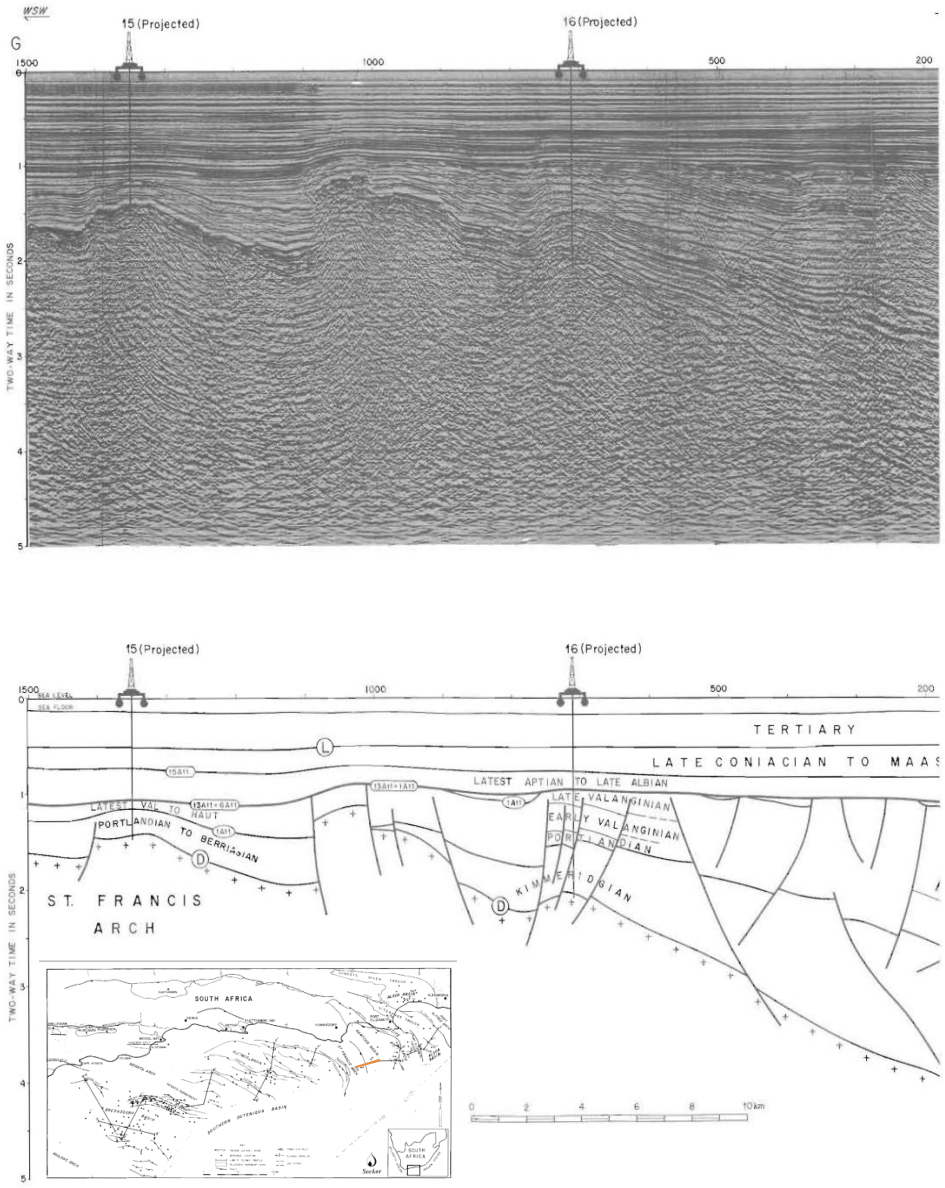


Figure 5.13-60
Seismic Profile with Interpretation Showing Evidence of No Apparent Offset of Aptian (109.5–108 Ma) and Overlying Upper Cretaceous and Tertiary Section (*Reference 5.13.162*). The location of the profile is highlighted by the orange line in the inset map

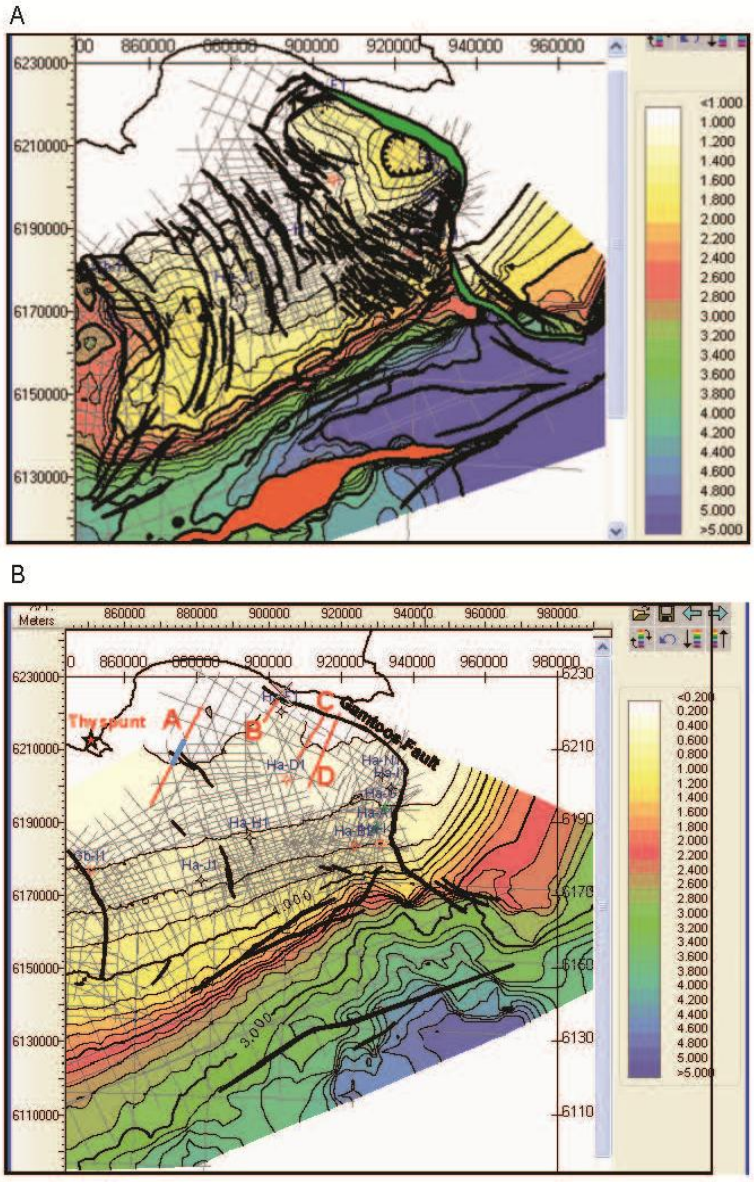


Figure 5.13-61
(A) Two-way Travel Time (TWT) Map to the Top of Synrift Deposits (1At1 Unconformity) Showing Faults That Displace the Base of Cretaceous as Seen in Seismic Data. (B) TWT Map to the Base of Tertiary (22At1 Unconformity) Showing Interpreted Post-Cretaceous Faults and Locations of Interpreted Seismic Lines Presented by Roux (*Reference 5.13.45*). The portion of Line A shown on Figure F-5.13.62 is highlighted in blue (Modified from *Reference 5.13.45*)

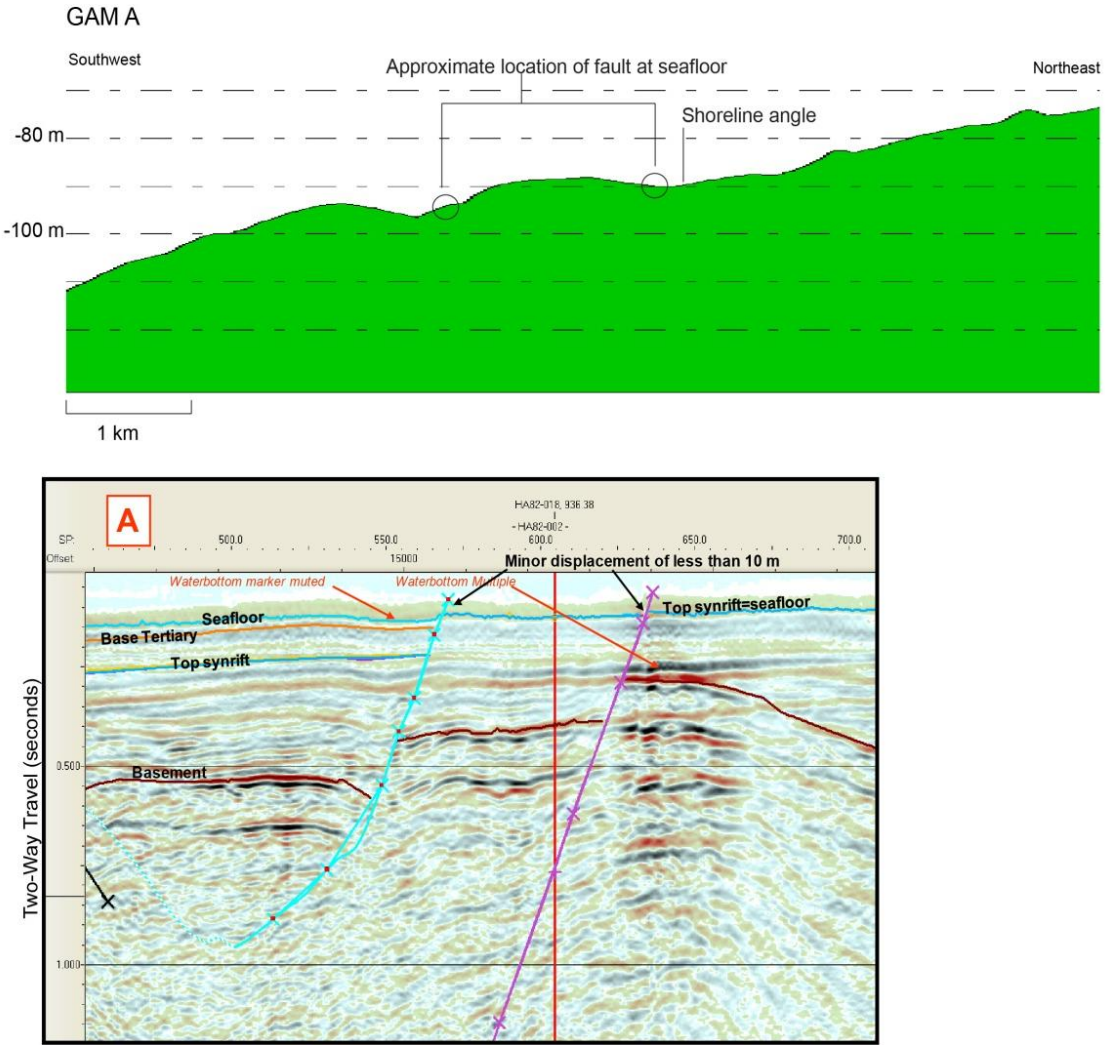


Figure 5.13-62
Upper Panel Displays Bathymetric Profile from De Wet (*Reference 5.13.59*) That Is Approximately Scaled (Horizontal Axis) to the Seismic Profile in the Lower Panel Interpreted by Roux (*Reference 5.13.45*) Across Minor Fault Within the Gamtoos Basin

© Eskom 2026/Rev 0a

The resolution of the industry seismic profiles near the seafloor is considered to be of poor quality, especially in attempting to quantify offset at a metre-scale.

Recently collected high-resolution bathymetry of the offshore region of the seafloor (***Reference 5.13.59***) provides an independent data set with which to evaluate possible seafloor scarps that may be associated with the post-Cretaceous (post-22At1 unconformity) faults interpreted by Roux (***Reference 5.13.45*** and ***Figure F-5.13.60***). Topographic profiles extracted from the digital elevation model (DEM) allow closer investigation of geomorphic features along the seafloor.

Analysis of multiple profiles across the Cape St Francis fault zone showed that the escarpments that roughly coincide with the northern parts of the post-Cretaceous faults mapped by Roux (***Reference 5.13.45***) are coincident with back edges of submerged terraces based on the observation that the scarps are shore-parallel rather than fault-parallel features (***Reference 5.13.1***). The profiles show evidence of a palaeoshoreline at a water depth of approximately 125 m. This submerged shoreline is likely correlative with the Last Glacial Maximum (LGM) shoreline that formed at approximately 22–20 ka at 125 ± 4 m below present sea level (see discussion of the LGM in Hanson *et al*. (***Reference 5.13.58*** Appendix A). Benches at a water depth of approximately 90 m that are observed in several profiles appear to be related to a submerged terrace of unknown age that trends perpendicular to the faults. There is no indication that either a submerged shoreline at approximately –125 m (inferred to have formed during the LGM lowstand at approximately 22–20 ka) or a submerged shoreline a -90 m is displaced across the post-Cretaceous faults identified by Roux (***References 5.13.45*** and ***5.13.1***).

The relief on the continental shelf at and seaward of the LGM shoreline appears to be related to linear aeolianite ridges that subparallel the LGM shoreline. Some of the linear ridges below the LGM shoreline may pre-date the LGM and could be as old as Pliocene. There are no apparent scarps or lineaments crossing the ridges, which can be traced for distances of kilometres to tens of kilometres.

A possible onshore extension of the Cape St Francis Fault is discussed by Goedhart (***Reference 5.13.26***), who postulated that, because of the gap in the data set in the nearshore, the use of the offshore survey data alone is not sufficient to preclude an onshore extension of the fault at Cape St Francis Bay. A detailed marine terrace mapping programme was conducted in the Oyster Bay to Cape St Francis study area (***Reference 5.13.58***) that addressed the seismogenic probability of potential onshore extensions of the Cape St Francis Fault and other structures within the Cape St Francis fault zone, as well as minor northeast-trending secondary faults documented by onshore bedrock

© Eskom 2026/Rev 0a

mapping and interpretation of offshore seismic data (***References 5.13.281***, ***5.13.282***, and ***5.13.46***). The onshore marine terrace study in the 8 km region around the Thyspunt site indicated that a 13 ± 1 m shoreline angle can be mapped and correlated from Oyster Bay to Seal Point near Cape St Francis (***Reference 5.13.58***). The 13 ± 1 m shoreline angle is correlated to the MIS 11 sea level, indicating an age of approximately 400 ka. There is no indication that terraces inferred to be Pliocene in age are deformed across the onshore projected trends of any of the faults within the Cape St Francis fault zone (***Reference 5.13.1***).

Worcester Fault

The east–west oriented portion of the Worcester Fault is a Cape Fold Belt thrust fault reactivated in the Mesozoic as a steep normal fault south side down (***References 5.13.140*** and ***5.13.24***). The throw of the Worcester Fault is reported to be a minimum of 3,811 m (12,500 feet) (***Reference 5.13.283***) up to 6 km in the syntaxis of the Cape Fold Belt near Worcester (***Reference 5.13.24***). The majority, if not all, of this displacement occurred during Mesozoic extension (Middle Jurassic to Middle Cretaceous time). De Beer (***Reference 5.13.24***) reports that faulting of the Jurassic-Cretaceous Uitenhage Group sediments deposited in depocentres along the Worcester Fault may have occurred until the Late Cretaceous. The fault appears to have remained an important structural weakness until Late Cretaceous to early Cenozoic times, as shown by its association with plugs of olivine melilitite observed locally (***Reference 5.13.24***).

The Worcester Fault is approximately 269 km from the site at its closest approach (***Figure F-5.13.63***). It consists of a series of faults trending north–south in the Western Cape and east–west in the Eastern Cape, meeting in a broad bend at the syntaxis (***Figure F-5.13.63*** and ***F-5.13-64***). Evidence for the fault becomes difficult to discern to the east, near the coast, but the trend is possibly towards the offshore Plettenberg Fault (***Reference 5.13.24*** and ***Figure F-5.13.47***). Although De Beer (***Reference 5.13.24***) suggests that the fault could extend to the coastline east of Mossel Bay and perhaps link up with the offshore Plettenberg Fault, the fault is not shown as a continuous structure on geological maps (***References 5.13.284*** and ***5.13.167***; ***Figures F-5.13.47*** and ***F-5.13.65***). The eastern endpoint of the Worcester Fault is designated as the eastern end of the relatively continuous fault as shown by De Beer (***Reference 5.13.24***) and on the Ladismith 1:250 000 geological map (***Reference 5.13.284***; ***Figures F-5.13.63*** and ***F-5.13.65***, respectively). ***Figure F-5.13.65*** shows that the fault does not displace extensive Tg pediment remnants farther to the east.

© Eskom 2026/Rev 0a

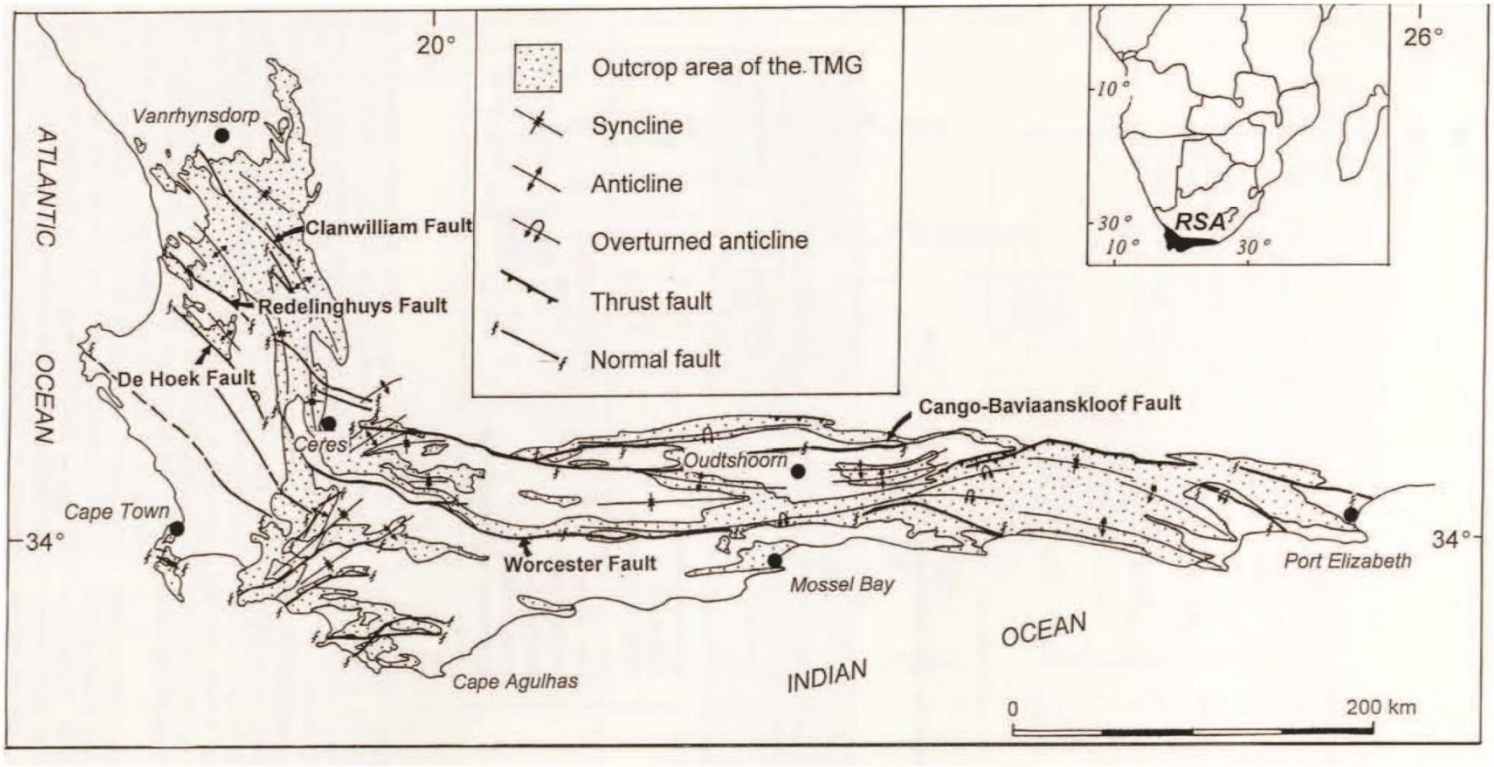


Figure 5.13-63
Map Showing Extent of Worcester Fault (*Reference 5.13.24*)

© Eskom 2026/Rev 0a

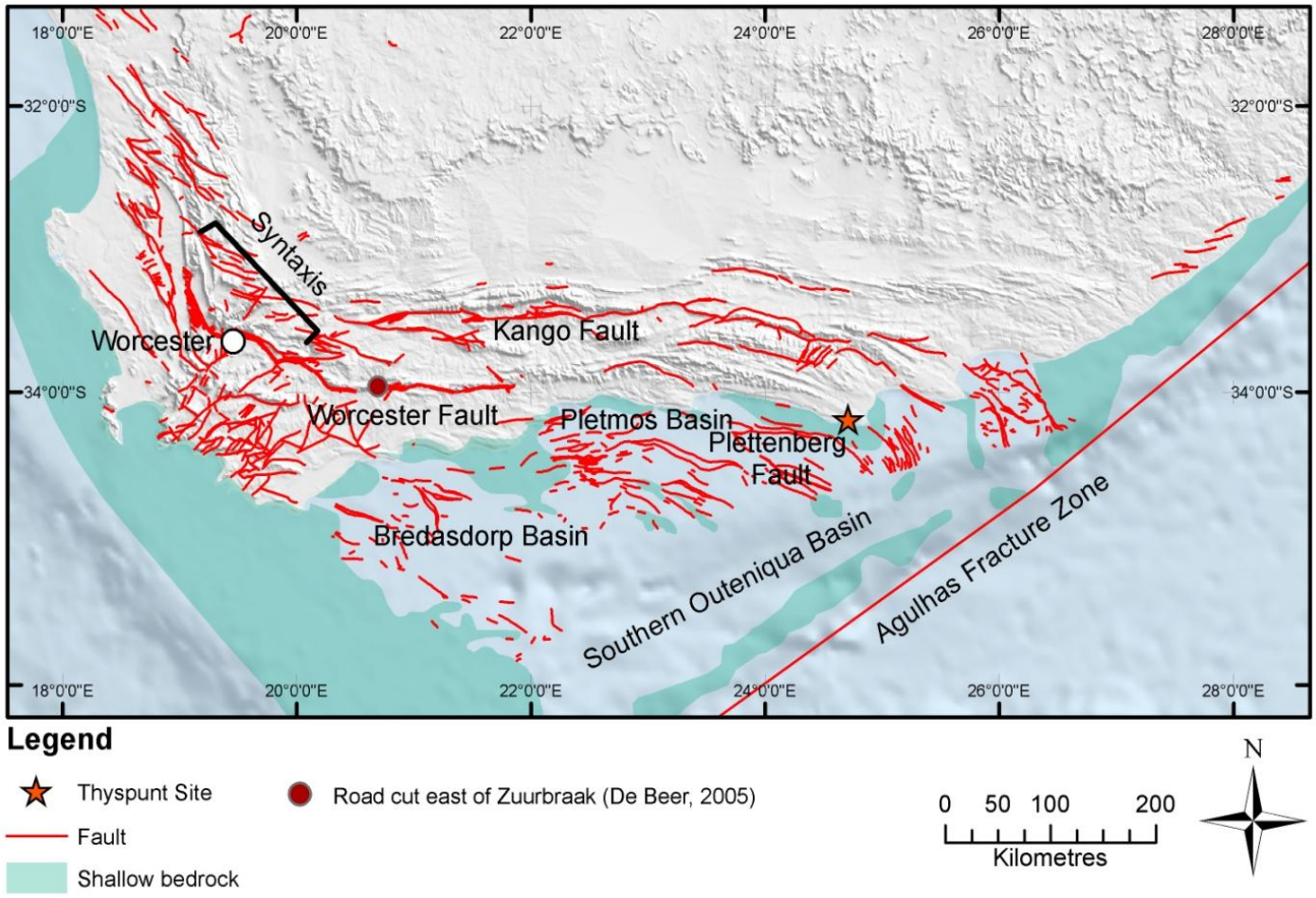


Figure 5.13-64
Map Showing Worcester Fault Relative to Offshore Faults and the Syntaxis Region of the Cape Fold Belt

© Eskom 2026/Rev 0a

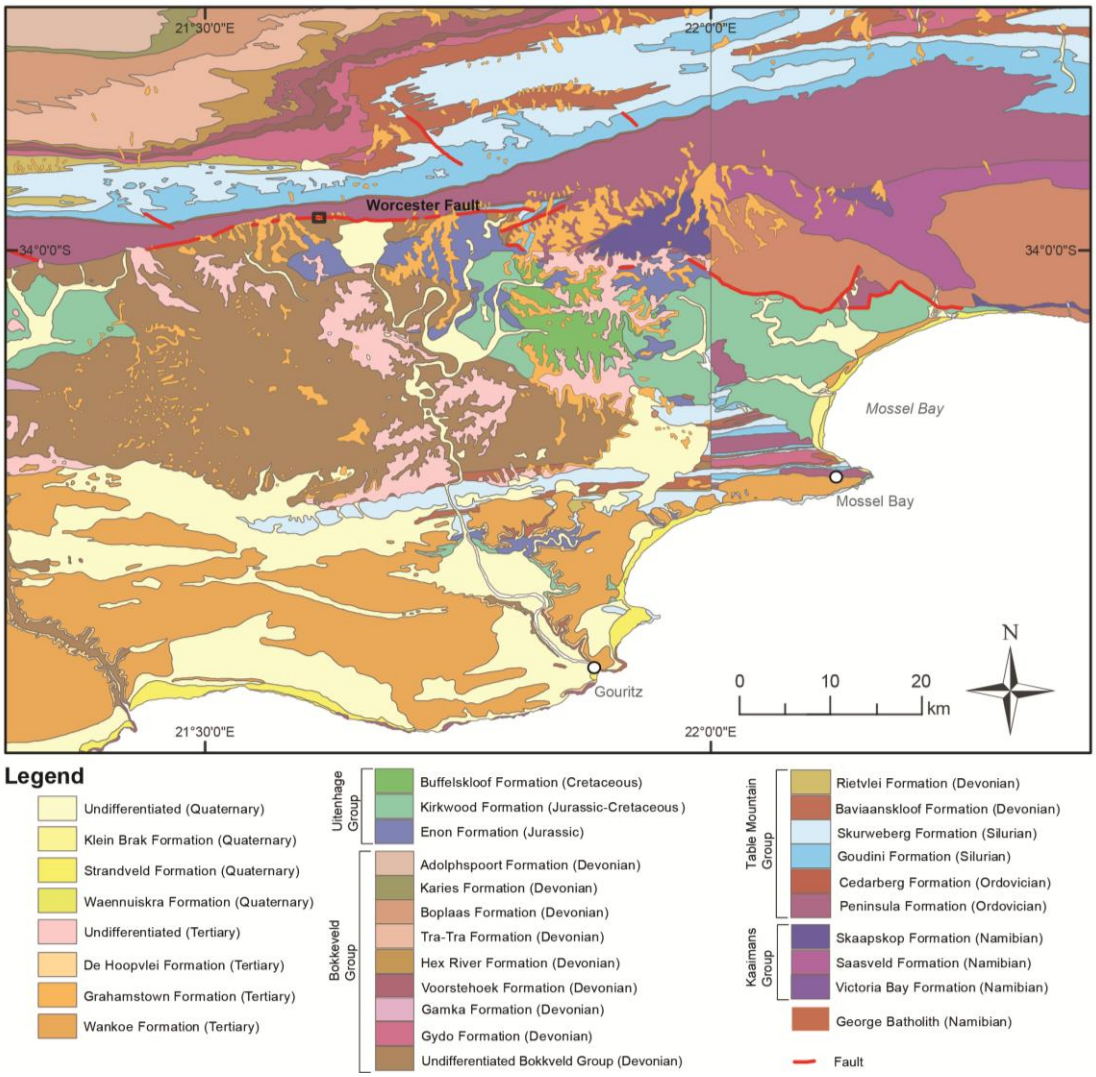


Figure 5.13-65
Geological Map Showing Unfaulted Grahamstown Formation (Tg) Surfaces Inferred to Be Miocene in Age Mapped Across the Worcester Fault (Modified from *References 5.13.284*; *5.13.167* and *5.13.287*). Black box indicates area of *Figure F-5.13.68*

There is a possible association between the Worcester Fault zone and seismicity in the Ceres area. Near Ceres, the Groenhof Fault, which is considered a possible source for the 1969 Mw 6.2 Ceres earthquake, may be the structural step-over between the Worcester and De Hoek Faults (***References 5.13.249*** and ***5.13.24***; see ***Figures F-5.13.63*** and ***F-5.13.66***).

Evidence of possible neotectonic reactivation—two small faults each with down-to-the-south displacement of 0.5 m—was reported by J. Viljoen in a road cut east of Swellendam (***Reference 5.13.24*** and ***Figure F-5.13.67***). De Beer (***Reference 5.13.24***) notes that these faults do not displace the unconformity between the locally described units A and B. Unit A is a channel-fill cut into the Mid-Early Cretaceous (pre-drift onset, 126 Ma) Kirkwood Formation. Unit B is composed of gravel and cobbles overlying a terrace cut into unit A (***Figure F-5.13.67***). The ages of units A and B are unknown. Unit A may be related to the alluvial plain of the palaeo-Tradouw River and its west-flowing tributary at the foot of the Langeberg Mountains. Assuming this is the case, some 20 m of further incision of the course of the Tradouw River into Bokkeveld Group rocks has occurred since deposition of unit A. Using broad estimates of the long-term average rate of incision of the modern Tradouw River into the coastal platform in post-Miocene time (at a rate of ~80 m in 5.3 Ma), De Beer (***Reference 5.13.24***) estimates that 20 m of incision would have taken at least 1.3 Myr, and that the most recent period of faulting could not have been younger than middle Pleistocene. Reconnaissance investigation of 1:10 000–scale colour aerial photographs also failed to indicate a recent fault scarp along the expected lateral continuation of the faults observed in the road cut (***Reference 5.13.24***).

Low rates of denudation and inferred rock uplift for the region encompassing the Worcester Fault are consistent with the long period of inactivity (1.3 Myr or longer) inferred for the road-cut exposure of the fault near the Tradouw River as described by De Beer (***Reference 5.13.24***). Denudation rates and geomorphic evolution of the Cape Fold Belt determined through the use of in situ–produced cosmogenic ^{10}Be show similarity between catchment-averaged denudation rates (determined from river sediment samples) and denudation rates on interfluves (determined from bedrock samples) (***References 5.13.241*** and ***5.13.94***). ^{10}Be-based denudation rates of the Cape Fold Belt fall between 1.98 ± 0.23 m/Myr and 7.95 ± 0.90 m/Myr; these rates are among the lowest in the world (***Reference 5.13.94***). Sample locations in the vicinity of the Tradouw River near the road-cut locality described by De Beer (***Reference 5.13.24***) yielded denudation rates of 6.13 ± 0.68 m/Myr and 4.72 ± 0.54 m/Myr (***Reference 5.13.241***; comparable to the average rate of 5.4 m/Myr) measured for drainage basins farther to the east by Bierman (***Reference 5.13.51*** and ***Figure F-5.13.32***).

© Eskom 2026/Rev 0a

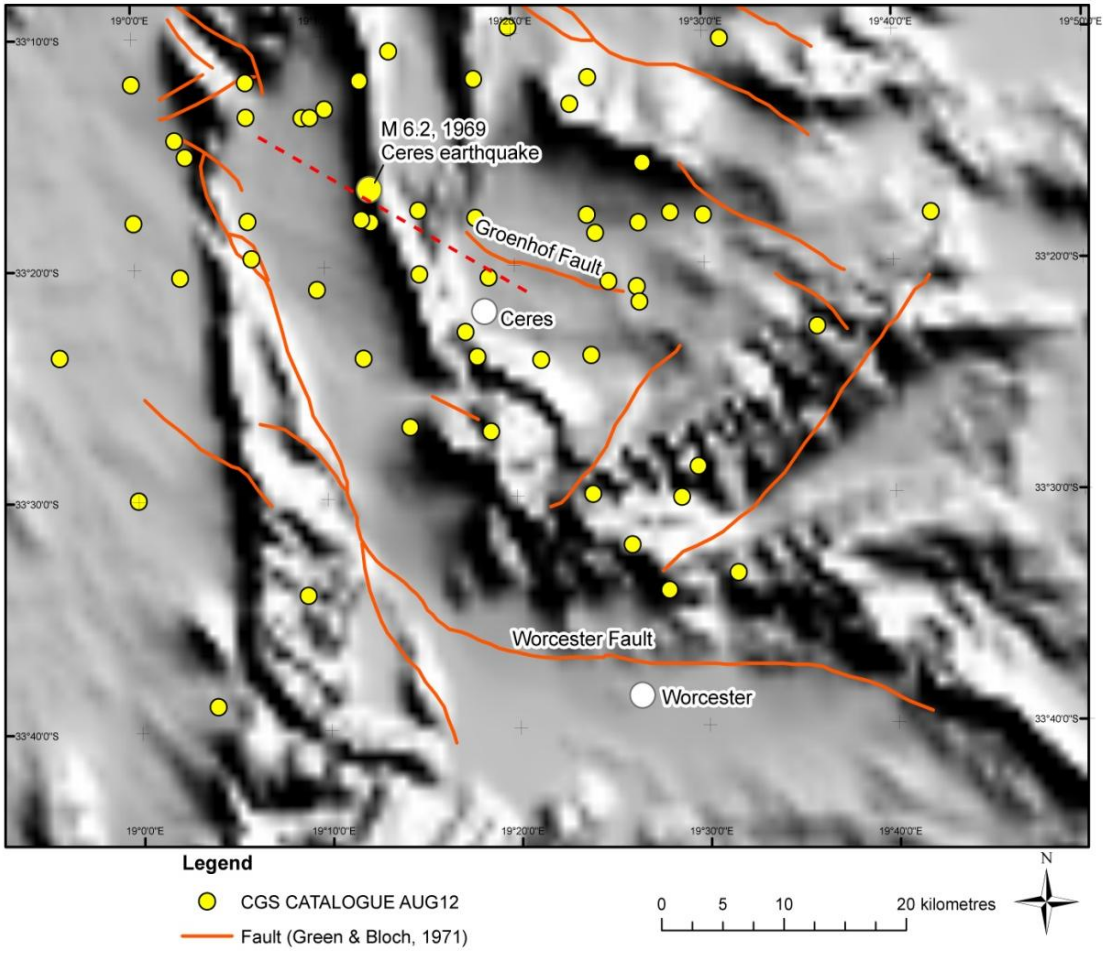
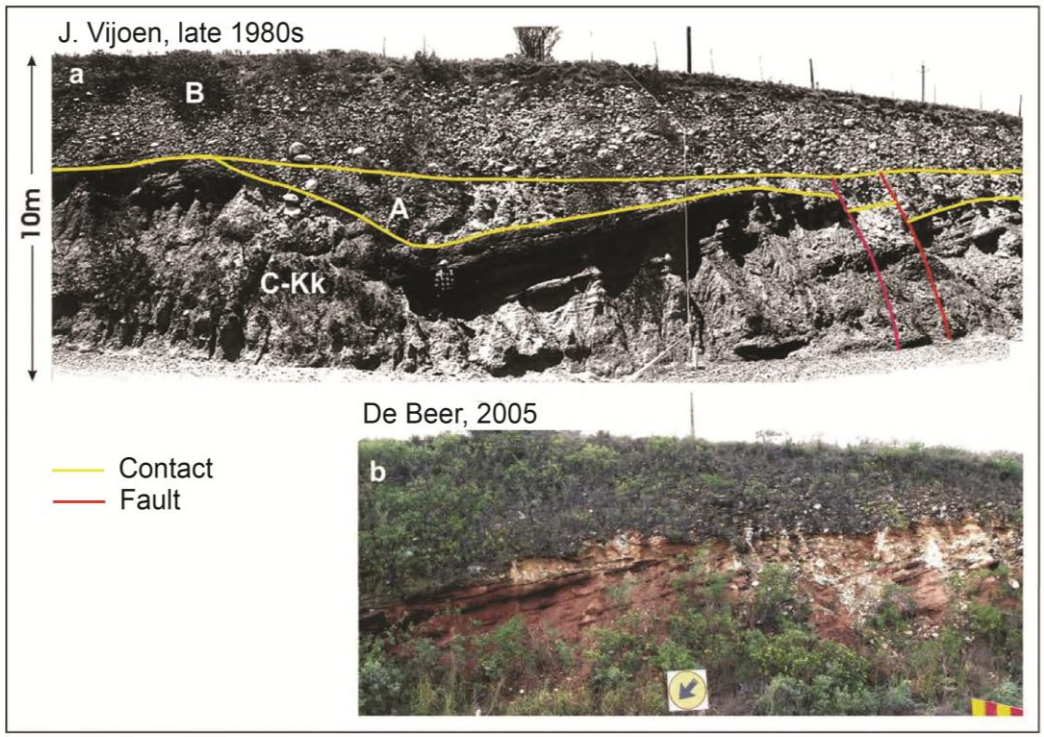


Figure 5.13-66
Location of 1969 Ceres Aftershocks (Red Dashed Line) Relative to the Groenhof and Worcester Faults (Modified from *Reference 5.13.249*)



C-Kk = Kirkwood Formation mudstones, A = gritty conglomerate deposited in a channel, and B = gravel- and cobble-containing unit overlying unit A with a horizontal unconformity. The two subvertical red solid lines depict faults that affected the Kirkwood and unit A, but not unit B

Figure 5.13-67
Road Cut East of Zuurbraak Showing Evidence of Neotectonic Reactivation of the Worcester Fault:
(a) Mosaic Compiled by J. Viljoen in the Late 1980s.
(b) Photograph of the Road Cut as Viewed by De Beer (*Reference 5.13.24*)

Bierman (***Reference 5.13.51***) calculates that the long-term average erosionally driven isostatic rock uplift rate in the Eastern Cape is approximately 4.4 m/Myr.

Thick, consolidated alluvial scree deposits covering the Worcester Fault in another road cut at the foot of the Langeberg Mountains north of Riversdale also showed no evidence of faulting (***Reference 5.13.24***). The age of the scree deposits is unknown.

© Eskom 2026/Rev 0a

High geomorphic surfaces (possible pediments locally overlain by Grahamstown Formation [Tg]) in the eastern part of the mapped Worcester Fault appear unfaulted based on interpretation of aerial photographs and GoogleEarth images, which shows no evidence (lineaments or scarps) of surface faulting (***Figure F-5.13.68***). It is not certain whether these surfaces are underlain by alluvial deposits or whether they are stripped bedrock erosional surfaces. Drainages on either side of the high geomorphic surface shown on ***Figure F-5.13.68*** are incised approximately 50 m to 100 m below the surface. Van Zyl (***Reference 5.13.285***) groups unfaulted surfaces directly east of the end of the mapped Worcester Fault with other extensive flat erosional surfaces as part of the "terrestrial African surface." Following Partridge & Maud (***Reference 5.13.152***) and Maud (***Reference 5.13.286***), Van Zyl (***Reference 5.13.285***) interprets these surfaces as relicts of topography that existed prior to the drop in sea level in the Miocene at approximately 18 Ma. Hagedorn (***Reference 5.13.92***) reports preliminary results of two electron spin resonance tests that indicated ages of 7.3 Ma and 9.4 Ma, respectively, for two samples of the silcrete caps on pediment remnants in the Little Karoo. According to these ages, the pediments date from the upper Miocene, but they could be even older if their formation was not synchronous with the silcretisations.

Along the coast near the hypothesised trend of the Worcester Fault zone, regional marine terrace data sets do not indicate any deviations from the regional data to suggest Pliocene or Quaternary deformation. In particular, the regional marine terrace compilation does not indicate any significant vertical deformation across the projected trends of the Worcester Fault to the coastline (***References 5.13.58*** Plate A2.3 and ***5.13.1***).

Faults in the Bredasdorp Basin

The Bredasdorp Basin sits southwest of Mossel Bay and is filled with Upper Jurassic and Lower Cretaceous and Cenozoic divergent margin rocks (***Reference 5.13.72*** and ***Figure F-5.13.69***). The basin is bounded on the west and southwest by the Agulhas Arch and opens south-eastward to connect with the Southern Outeniqua Basin, which is terminated on the southeast by the Agulhas-Falkland Fracture Zone (AFFZ; ***Reference 5.13.72***).

© Eskom 2026/Rev 0a

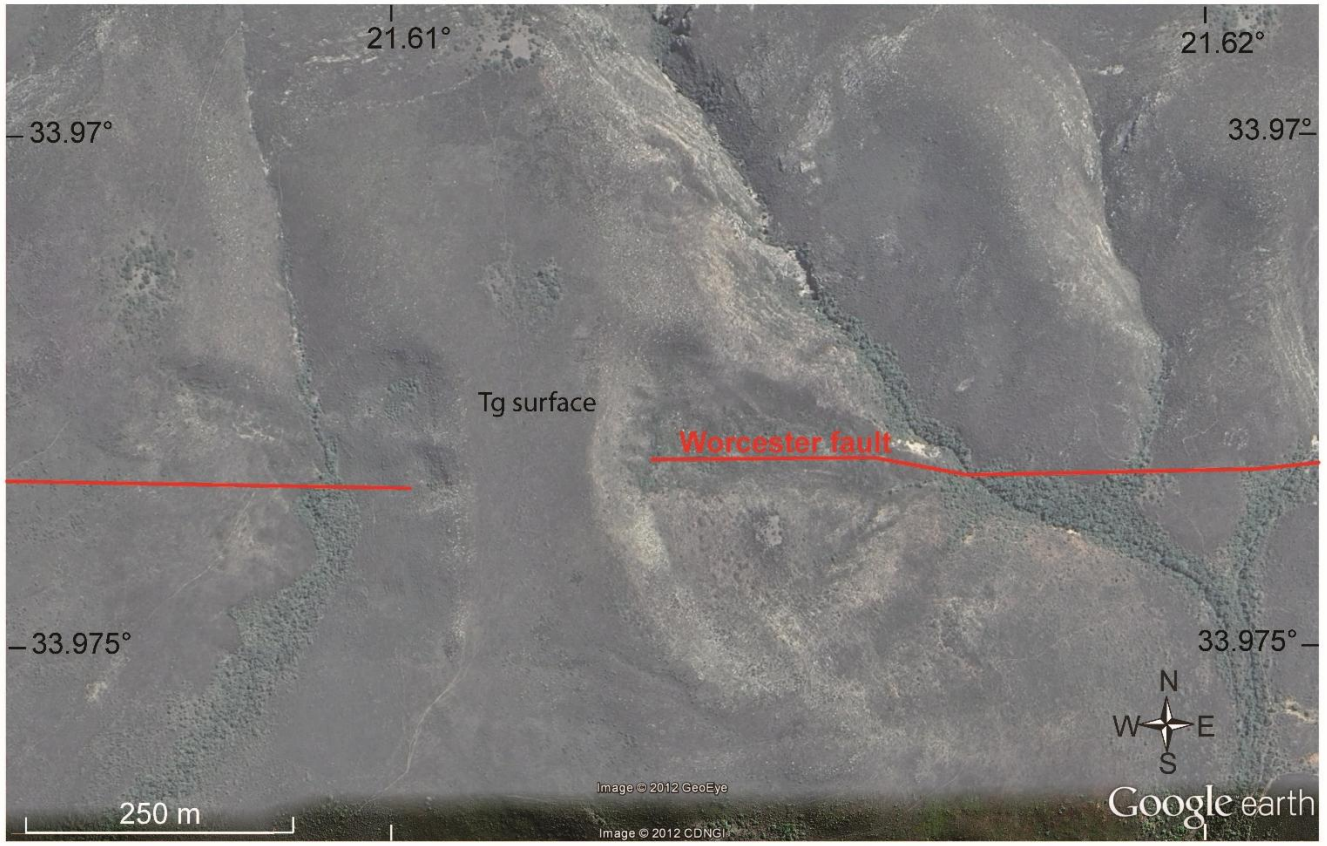


Figure 5.13-68
GoogleEarth Image Showing Unfaulted Geomorphic Surface (Pediment or Eroded Pediment) Across the Mapped Trace of the Worcester Fault (as Mapped by Theron, *Reference 5.13.284*) (Figure from *Reference 5.13.1*)

© Eskom 2026/Rev 0a

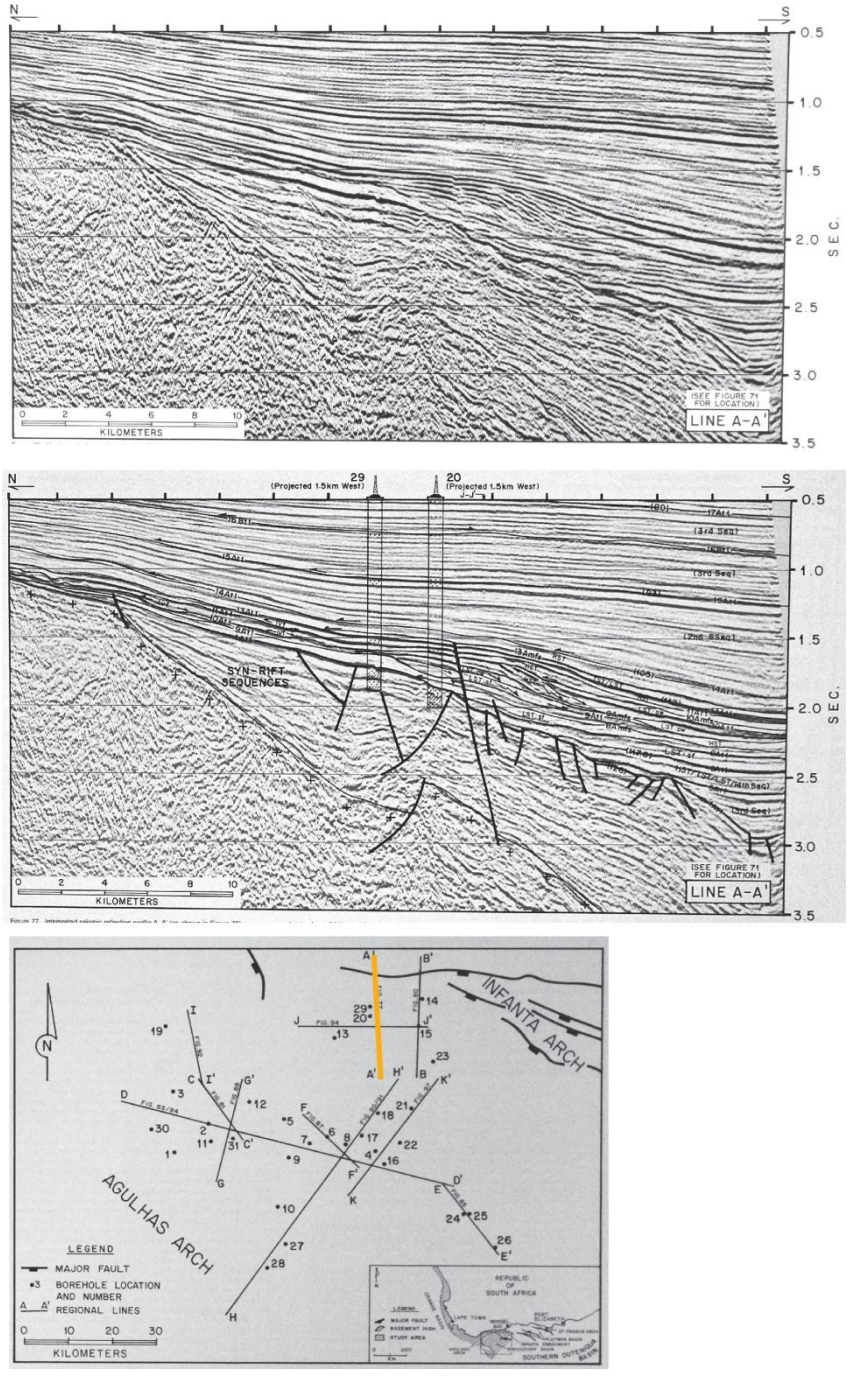


Figure 5.13-69
Seismic Line Across the Infanta Arch and Bredasdorp Basins
(*Reference 5.13.72*)

To the northwest the Bredasdorp Basin is bounded by a series of Cretaceous age normal faults. These faults run along the southern edge of the Infanta Arch (***Figure F-5.13.69*** and ***Reference 5.13.72***). The basin is 200 km long and 80 km wide (***Reference 5.13.74***). It occurs mainly offshore of the modern coastline.

Agulhas Fault Zone

The Agulhas-Falkland transform (now represented by the Agulhas-Falkland Fracture Zone, or AFFZ) is an approximately 1,200 km right-lateral strike-slip fault zone (ridge-ridge offset) (***Figure F-5.13.30***). The AFFZ evolved between the South American and African Plates during the Early Cretaceous breakup of West Gondwana (***Reference 5.13.68***). Along southern Africa it now forms the boundary between continental and oceanic crust.

The portion of the AFFZ south of the African continent, referred to herein as the Agulhas Fracture Zone, is embedded in a 50 km wide transitional zone between continental and oceanic crust (***Reference 5.13.77***; ***Figures F-5.13.70*** and ***F-5.13.71***) and consists of a zone of faults between the edge of the continental shelf and the base of the continental slope (***Figures F-5.13.72*** and ***F-5.13.73***). The crust thins across this transition zone from 30 km beneath the continental shelf to 7 km in the deep sea (***Reference 5.13.69***). The Agulhas Fracture Zone, as defined in ***Reference 5.13.68*** as a relatively narrow arcuate zone. At its northeast extent, south of Durban, the fracture zone begins less than 15 km from the shoreline. The continental shelf spans between the Agulhas Fracture Zone and the South African coast as the coastline curves away from the fracture zone (***Figure F-5.13.70***).

The Agulhas Fracture Zone is approximately 91 km from the site at its closest approach (***Figure F-5.13.70***). Faults within the Agulhas Fracture Zone have steep to near-vertical dips; some faults within the zone dip approximately 70 degrees, based on seismic profile data (***References 5.13.77*** and ***5.13.83***; ***Figures F-5.13.72*** and ***F-5.13.73***).

Ben-Avraham *et al.* (***Reference 5.13.68***) divide the Agulhas Fracture Zone off the coast of South Africa into four segments (***Figure F-5.13.70***) that are inferred to be largely inherited from Middle to Late Jurassic rifts and oceanic embayments. The two segments nearest to the Thyspunt site are the Mallory Trough segment (segment 1) and the Diaz Ridge segment (segment 2) (***Figure F-5.13.70***).

© Eskom 2026/Rev 0a

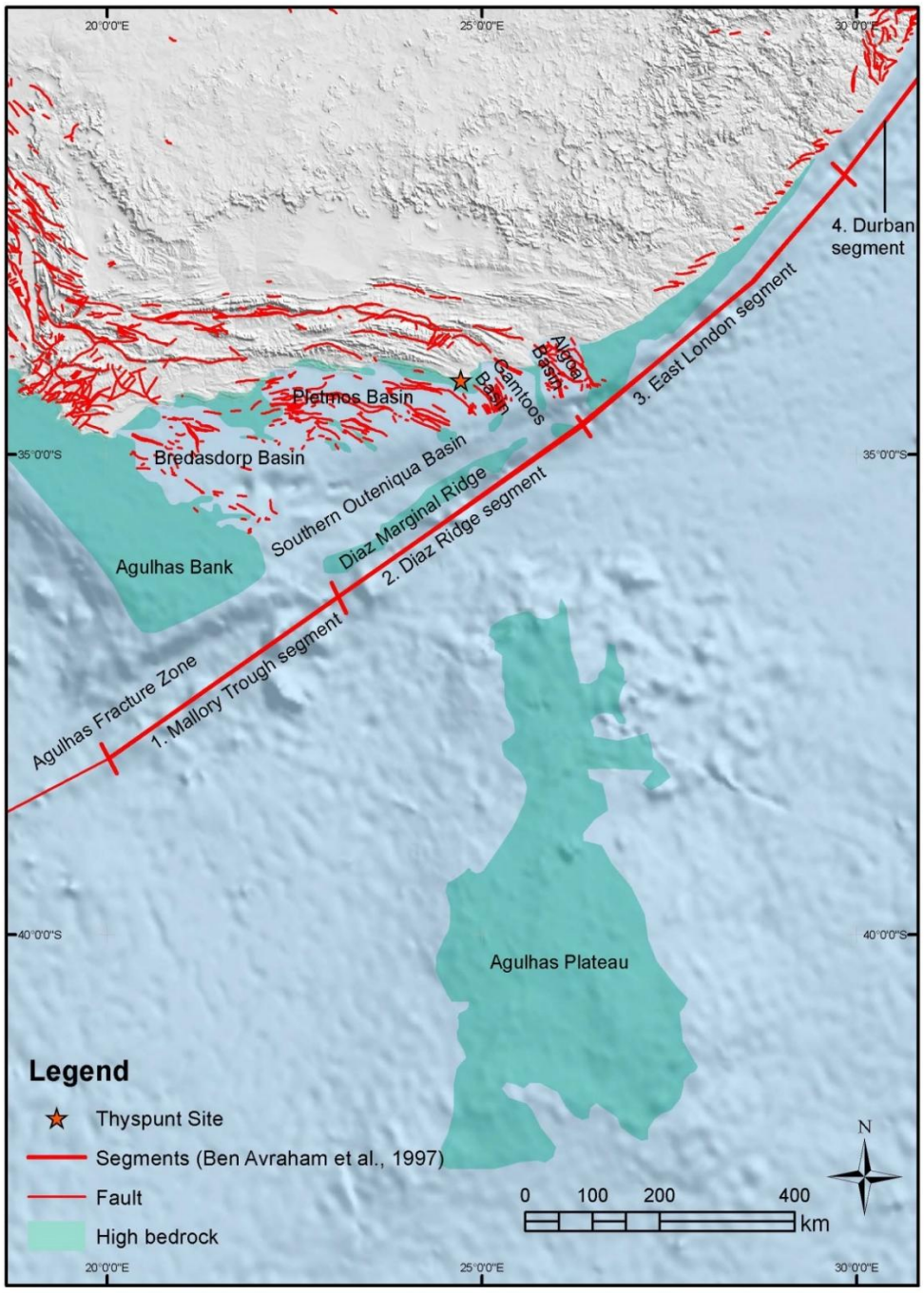
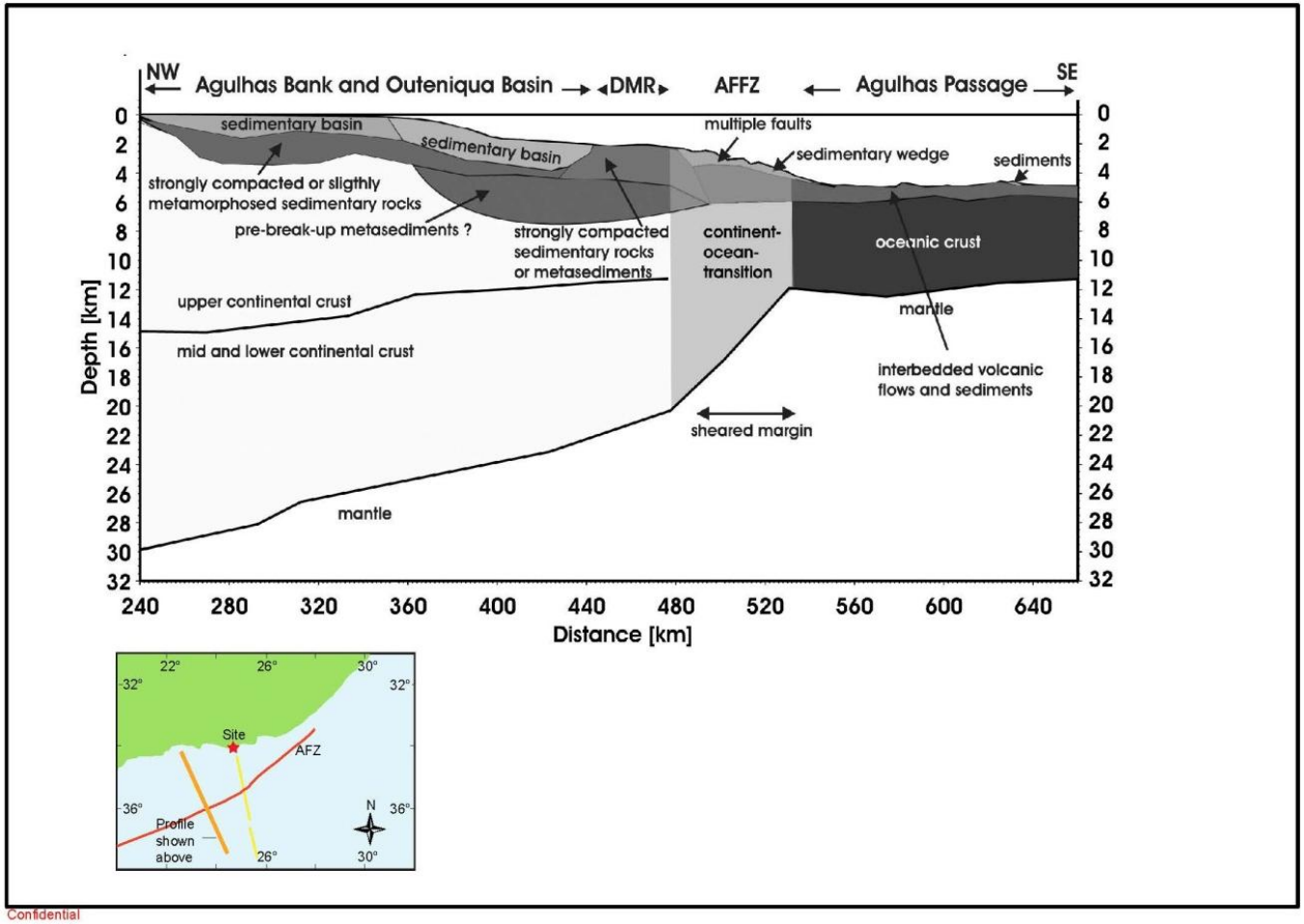


Figure 5.13-70
Map of Agulhas Fracture Zone Marginal to the Southern African Continent, Illustrating Fourfold Segmentation (*Reference 5.13.68*)



Confidential

Figure 5.13-71
Interpreted Structure of the South African Continent Margin (*Reference 5.13.69*). DMR = Diaz Marginal Ridge; AFFZ = Agulhas-Falkland Fracture Zone

© Eskom 2026/Rev 0a

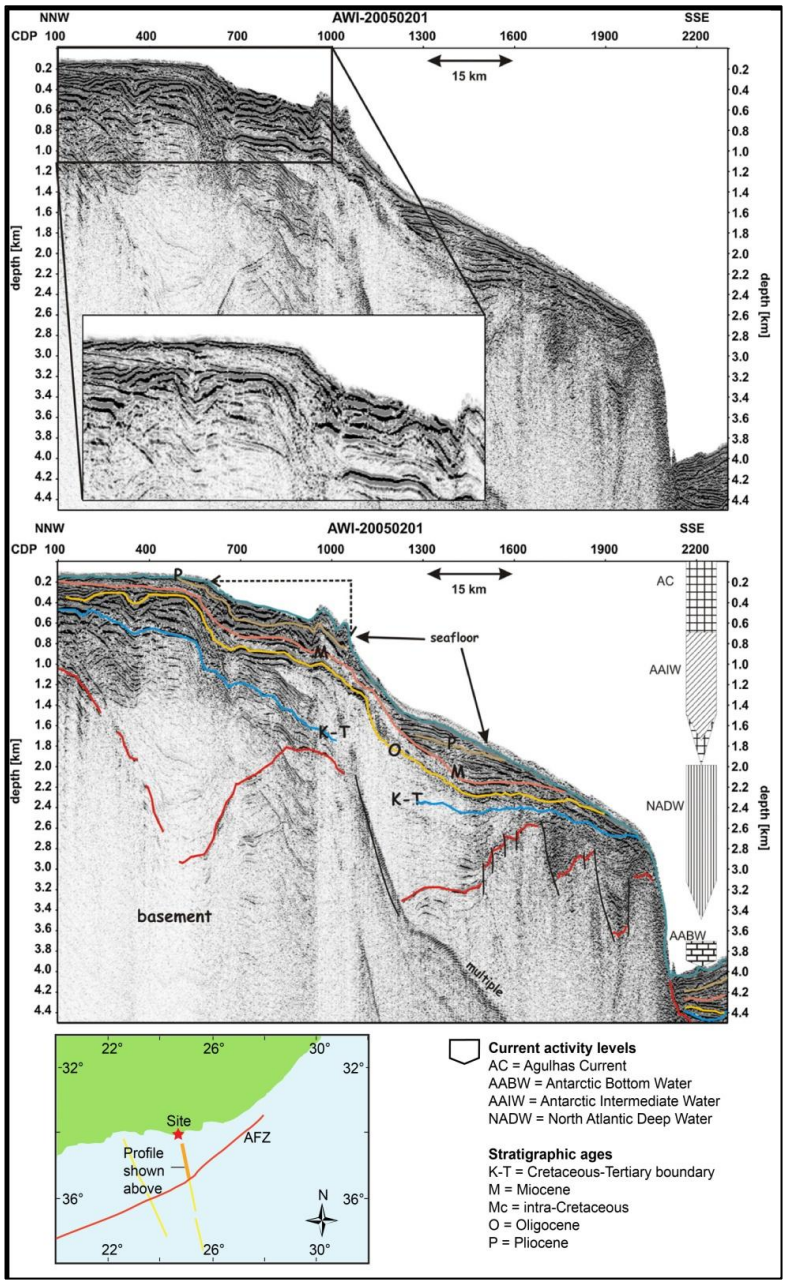


Figure 5.13-72
Profile AWI-20050201 Showing the Shelf and Continental Shelf into Agulhas Passage. The hatched blocks show the activity levels of the various currents (*Reference 5.13.83*)

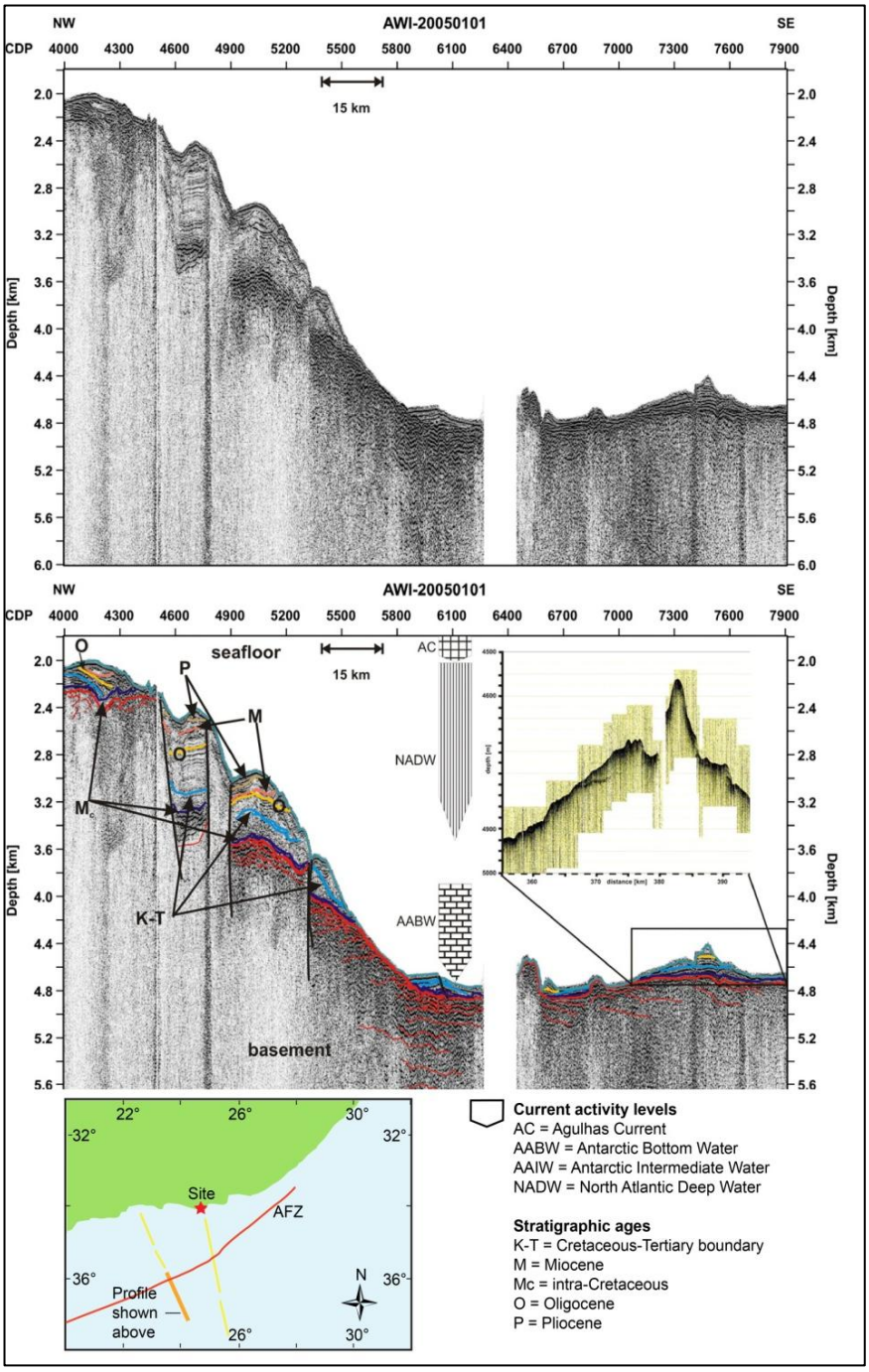


Figure 5.13-73
Profile AWI-20050101 Showing the Continental Rise and Agulhas Passage. The hatched blocks show the activity levels of various currents (*Reference 5.13.83*)

Evidence for possible neotectonic reactivation of the Agulhas Fracture Zone comes from seismic profiles and evidence of recent volcanism. Ben-Avraham (***Reference 5.13.288***) interpreted evidence for disturbance of the seafloor along the Agulhas Fracture Zone in some sections (south of Port Elizabeth) but not in others, Parsiegla et al. (***Reference 5.13.69***) and Uenzelmann-Neben & Huhn (***Reference 5.13.83***) also interpret evidence for reactivation of faults in the Agulhas Fracture Zone based on the regional seismic reflection profile (AWI-20050101). Uenzelmann-Neben & Huhn (***Reference 5.13.83***) interprets some of these faults to disturb an early Pliocene marker horizon. In addition, Ben-Avraham (***Reference 5.13.288***) describes young volcanic rocks in the Agulhas Plateau and Mozambique Ridge.

The evidence for reactivation of the AFZ is not conclusive, and several observations suggest that there is little or no compelling evidence for neotectonic reactivation. Although some seismic lines across the Agulhas Fracture Zone are interpreted to have evidence of reactivated faults, others are not (***References 5.13.288*** and ***5.13.83***). Uenzelmann-Neben & Huhn (***Reference 5.13.83***) report evidence for significant erosion by the Antarctic Bottom Water current at water depths of interpreted seismic disturbance. This indicates that erosion rather than fault activity may have formed the observed features. The largest apparent vertical offsets (up to 600 m) of the early Pliocene marker horizon across an individual fault trace (***Figure F-5.13.73***) imply a rate of vertical displacement that does not appear to be consistent with onshore Pliocene to Quaternary uplift rates (***Reference 5.13.1***). The relationship of the Agulhas Fracture Zone to possibly young basaltic intrusions and volcanic glass samples dredged from the Mozambique Ridge and Agulhas Plateau areas is not known. Volcanism may be related to the diffuse Lwandle-Nubian plate boundary (***References 5.13.289*** and ***5.13.199***) rather than the Agulhas Fracture Zone.

v Cenozoic Structures

Geological information has been reviewed to assess the current stress regime and evidence for neotectonic deformation in the Thyspunt study region. Evidence for palaeoseismic-neotectonic deformation in onland Neogene to Quaternary sediments between Alexander Bay and Port Elizabeth was compiled and evaluated in a series of office-based and field reconnaissance studies conducted by the CGS as summarised in De Beer (***References 5.13.16***, ***5.13.24***, and ***5.13.25***).

The results of these investigations showed that only the Kango Fault, the northernmost of the Cape Fold Belt structures to have been reactivated during the Mesozoic extensional stress regime, exhibits definitive evidence for

© Eskom 2026/Rev 0a

neotectonic deformation and Quaternary reactivation (see discussion below in ***Subsection 5.13.5.1.(d) v***).

Geological studies of jointing and fractures along the south coast of South Africa between Alexander Bay and Port Elizabeth show little evidence of recent deformation (***Reference 5.13.24***). De Beer (***Reference 5.13.24***) observed little evidence of joints propagating through the Pliocene to late Pleistocene Bredasdorp Group, indicating low levels of neotectonic stress. In addition, De Beer (***Reference 5.13.24***) concluded that most lineaments identified in Pleistocene sediments on aerial photographs were palaeostrandlines and palaeodune-morphology-based when examined in the field. Also, little evidence of neotectonic activity was found in the region based on the examination of natural exposures, roadcuts, and cuts in quarries.

De Beer (***Reference 5.13.25***) and Roberts (***Reference 5.13.50***) note that the development and general continuity of prominent, well-defined coastal terraces at similar levels about sea level along extensive stretches of the southern coast region and the repeated reoccupation of some terraces during many millions of years are evidence of a particularly stable continental margin.

Geological investigations completed as part of the Thyspunt PSHA further documented the absence of Quaternary deformation on major faults within the Thyspunt site region (***References 5.13.17***, ***5.13.18***, ***5.13.19***, and ***5.13.58***).

Kango Fault Zone

The Kango Fault is the only recognised Quaternary fault in South Africa (***References 5.13.217***, ***5.13.218***, and ***5.13.14***). Palaeoseismic investigations by Goedhart (***References 5.13.14*** and ***5.13.15***) provided preliminary information regarding the size, timing, and extent of the most recent surface-faulting event on the Kango Fault. Additional palaeoseismic investigations completed as part of the Geological Investigations programme for the Thyspunt PSHA (***Reference 5.13.54***) were conducted at several sites to provide additional information to quantify the magnitude and recurrence of surface-faulting events on the Kango Fault.

The length, segmentation, and geometry of the Kango Fault are largely inherited from structures initially formed during the Permo-Triassic Cape Orogeny and were reactivated during the breakup of Gondwana in the Mesozoic and subsequent rifting of the South Atlantic. During the Mesozoic, the Cape Fold Belt underwent negative structural inversion, resulting in the superposition of a Mesozoic extensional system on the fold belt (***References 5.13.117***, ***5.13.290***, ***5.13.137***, and ***5.13.131***). The most recent extensional (normal) faulting during the Tertiary and Quaternary likewise

© Eskom 2026/Rev 0a

reflects the geometry, dip, and segment lengths inherited from the Mesozoic extension (***References 5.13.217***, ***5.13.13***, and ***5.13.137***).

The location and extent of the Kango Fault are variously defined. Goedhart & Booth (***Reference 5.13.291***), Goedhart & De Klerk (***Reference 5.13.292***), and Goedhart (***Reference 5.13.293***) describe the Kango Fault as a 320 km long east-west-striking, southward-dipping crustal-scale tectonic structure that extends to a depth of at least 10–12 km (***Figures F-5.13.74*** and ***F-5.13.75***).

Goedhart (***References 5.13.13*** and ***5.13.293***) places its western boundary near the town of Touws River, where there appears to be a 10 km gap between the south-dipping Kango Fault and the near-vertical Ceres Fault to the west. The eastern end of the Kango Fault, which is the western end of the Baviaanskloof Fault, located slightly south and west of the town of Willowmore, is placed at a geomorphic step that also coincides with a change in strike of the fault system. Paton (***Reference 5.13.137***) shows discontinuous normal faulting at the eastern end of the Kango fault and describes the Kango and Baviaanskloof Faults as having an en-echelon, right-stepping relationship, corresponding to a nonbreached relay ramp. Field- and office-based studies conducted by Goedhart (***References 5.13.13***, ***5.13.14***, and ***5.13.15***) revealed no evidence for Quaternary reactivation across the en-echelon stepover to the Baviaanskloof Fault.

Paton (***Reference 5.13.137***) identifies a number of fault arrays within the >480 km long Mesozoic extensional system of South Africa, the onshore portion of which includes the Kango, Baviaanskloof, and Gamtoos Faults. The longest of the fault arrays is the Kango Fault, with a total length of 240 km from its western end at Ladismith (approximately 85 km east of the Touws River endpoint favoured by Goedhart (***Reference 5.13.13***) to its eastern end near Willowmore. Paton (***Reference 5.13.137***) describes the inherited Mesozoic rift structures along the Kango Fault as a series of coalesced segments that have a linear rather than en-echelon trend. Paton (***Reference 5.13.137***) uses plan-view geometry and the presence of intrabasin highs along strike to subdivide the Kango Fault into five segments that have lengths (from west to east) of 70 km, 100 km, 30 km, 20 km, and 20 km.

© Eskom 2026/Rev 0a

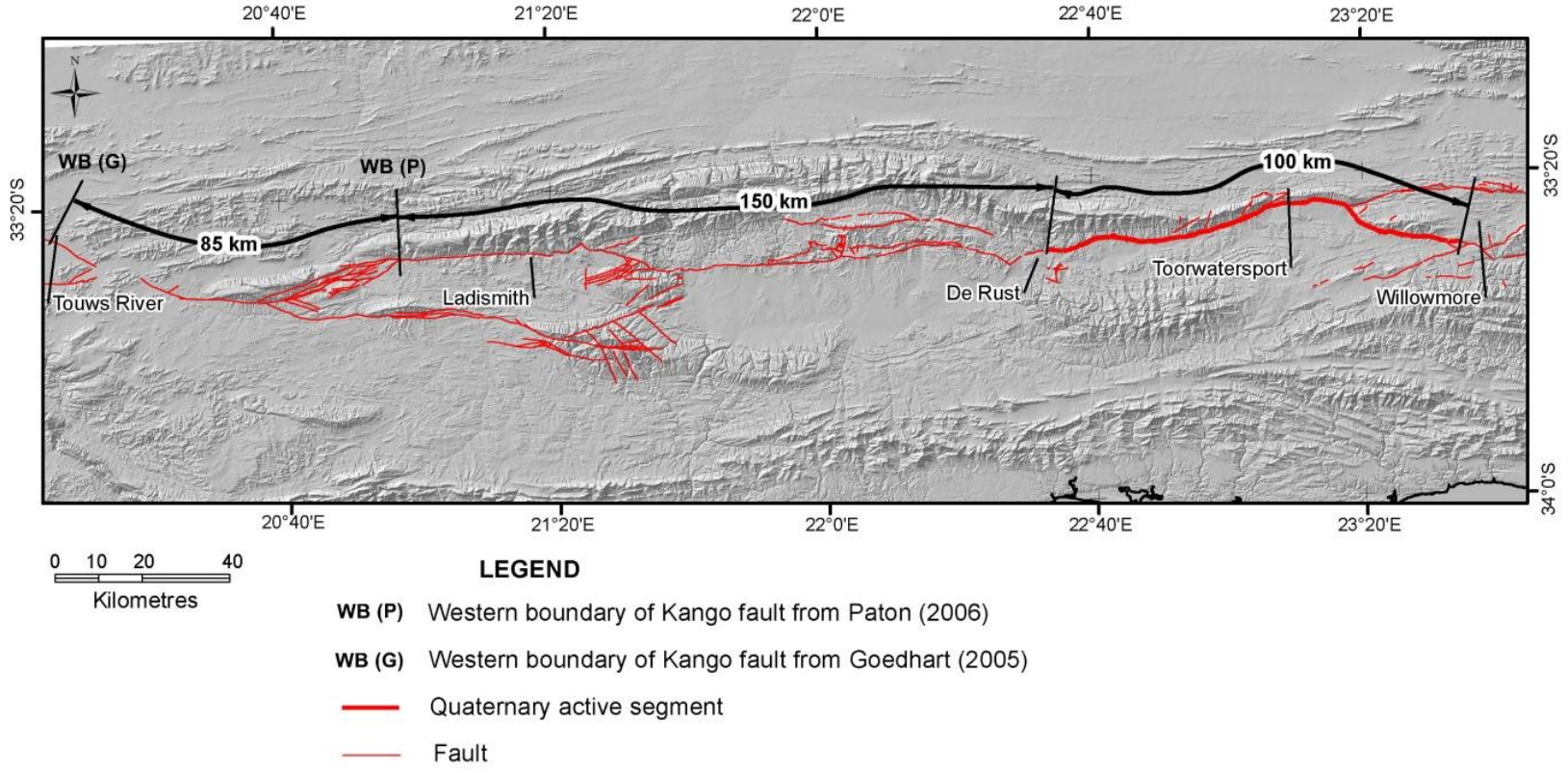


Figure 5.13-74
Alternative Western Boundary of the Kango Fault (*Reference 5.13.54*)

© Eskom 2026/Rev 0a

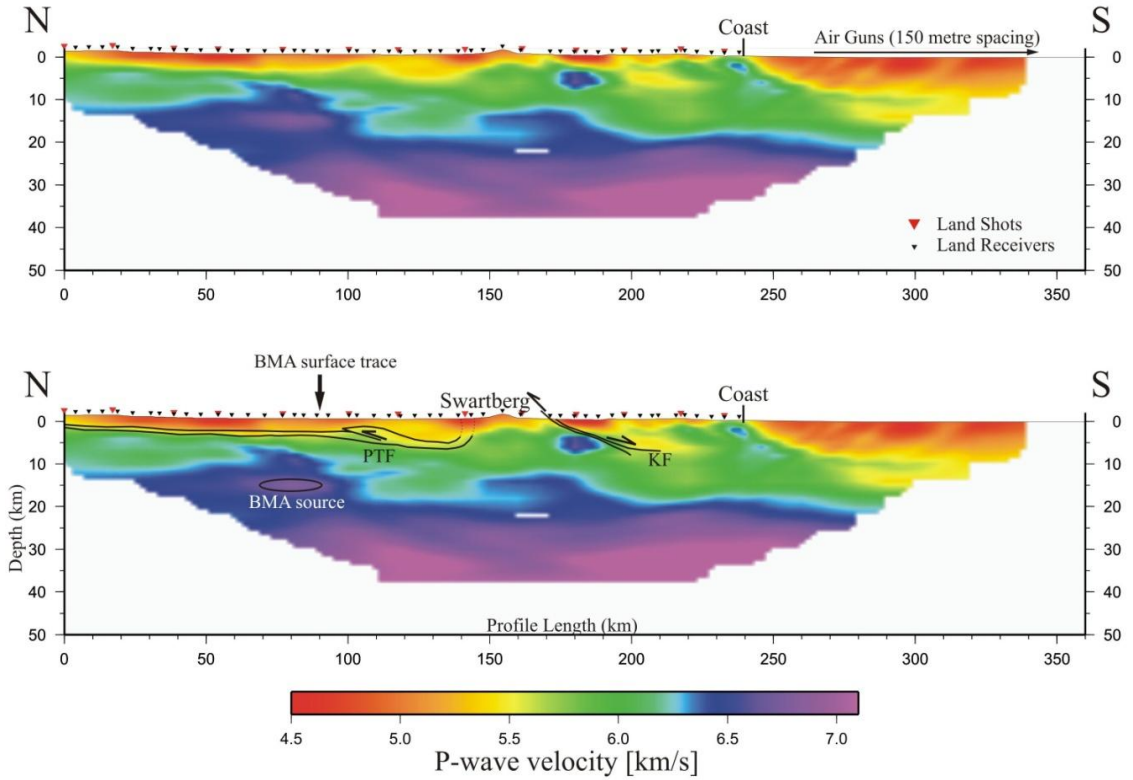


Figure 5.13-75
P-Wave Velocity Model for the Western Profile in Figure F-5.13.40. The upper panel shows just the model, the lower panel includes interpretations. Northernmost deformation of the Cape Supergroup has been marked by an arrow (PTF). Farther south, the geometry of the normal listric Kango Fault (KF; surfacing at 170 km) has been drawn. A high-velocity anomaly most likely related to the Beattie Magnetic Anomaly (BMA) has been indicated with an ellipse at a depth of ~15 km, at profile km 80 (*Reference 5.13 263*)

© Eskom 2026/Rev 0a

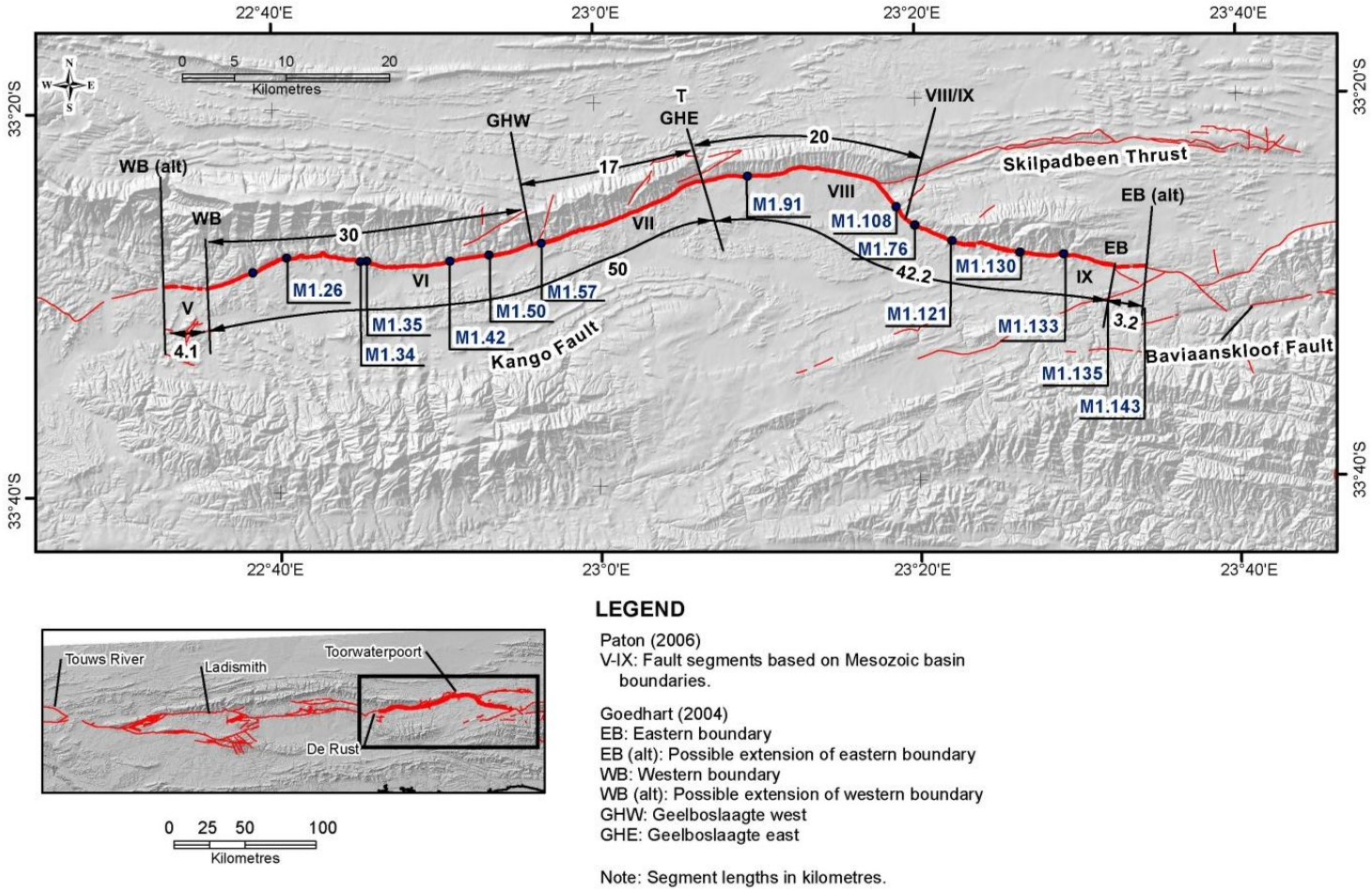


Figure 5.13-76
Field Localities and Possible Segment Boundaries Along the Quaternary-Reactivated Kango Fault (*Reference 5.13.54* Table 7)

© Eskom 2026/Rev 0a

The 92–101 km long eastern segment of the Kango Fault east of De Rust appears to be unique among faults within the Ceres-Kango-Baviaanskloof-Coega Fault system (***Figure F-5.13.47***) in that it shows evidence of repeated normal-slip surface-faulting events during the Quaternary (***References 5.13.14***, ***5.13.14***, and ***5.13.54***). No evidence of Quaternary faulting along the Kango Fault west of De Rust has been reported, based on reconnaissance studies conducted by Goedhart (***Reference 5.13.14***) and De Beer (***Reference 5.13.16***). Field localities and postulated segment boundaries along the Quaternary-reactivated segment of the Kango Fault discussed below, are shown on ***Figure F-5.13.76***.

The eastern part of the Kango Fault that shows evidence for reactivation in the contemporary tectonic setting includes the three eastern structural segments defined by Paton (***Reference 5.13.137***). Goedhart (***References 5.13.13***, ***5.13.14***, and ***5.13.15***) defines the total length of the reactivated Kango Fault as 84 km and suggests that it comprises only two segments: a western segment (45 km long) and an eastern segment (39 km long) (***Figure F-5.13.76***).

Hanson *et al.* (***Reference 5.13.54***) recognised that there is uncertainty in how fault segments are defined and describe possible segment boundaries along the Quaternary-reactivated Kango Fault based on behavioural, structural, geologic, and geometric data (see Table 7 in ***Reference 5.13.54***). The observations summarised by Hanson *et al.* (***Reference 5.13.54***) suggest that this reactivated portion of the Kango Fault, which they consider to range from 92 km to 100 km in length, may be further subdivided into smaller segments as short as 20–30 km to as long as 50–54 km (***Figure F-5.13.76***).

The downdip geometry of the Kango Fault inferred from several geophysical onshore and offshore experiments, including interpretation of crustal-scale seismic refraction data, is shown as a low-angle (<20°) fault that becomes listric at approximately 8–12 km (***References 5.13.265***, ***5.13.130***, ***5.13.263***, and ***Figure F-5.13.75***). In the near-surface trench exposures, the main fault dips steeply (67°S; ***Reference 5.13.15***). Based on the subsurface information from resistivity survey and borings collected at the M1.42 site (***Reference 5.13.292***), the dip of the fault at depths up to approximately 70 m is approximately 50 degrees to the south (***Reference 5.13.54***; also see Plate A2.12 in ***Reference 5.13.1***).

Data from palaeoseismic investigations along the Kango Fault pertaining to possible rupture segments, rupture areas, and displacements per event may be used to estimate the magnitude of prehistoric surface ruptures along the reactivated Kango Fault (Table 8 in ***Reference 5.13.54***). These data suggest that the expected M_{char} earthquake on the reactivated Kango Fault ranges from a minimum of approximately M_w 6.6 to a maximum of M_w 7.6.

© Eskom 2026/Rev 0a

The Kango Fault lies within a seismically quiescent region of South Africa, but has evidence for three latest Pleistocene to Holocene surface-faulting events preceded by a long period of several tens of thousands of years of no activity (***Reference 5.13.54***). The occurrence of three latest Pleistocene to Holocene surface-faulting events along the reactivated Kango Fault—two surface-rupturing events in the past 10–15 kyr along the western part of the fault, and at least one latest Pleistocene event between 22.6 ka and 25.4 ka along the eastern part—indicates that the Kango Fault may be within a period of higher activity.

The available ages for the oldest deposits in the two trenches along the western part of the fault (~74 ka from M1.26 trench T1; 63 ka or 123 ka from M1.42; ***Figure F-5.13.76***) indicate that the two most recent events (MREs) documented at both sites were preceded by a long period of several tens of thousands of years of no activity (***Reference 5.13.54***).

Low cumulative neotectonic displacement on the reactivated Kango Fault also suggests that the recent rate of activity is not typical of the long-term behaviour of the fault. Cumulative net vertical separation of erosional surfaces (pediment or strath terraces) formed on the top of bedrock in the hanging wall and footwall of the fault zone at the M1.42 site ranges from 26 m to 33.4 m (***Reference 5.13.54***). This cumulative displacement appears to postdate 2.5 ± 0.6 Ma.

The low cumulative displacements and apparent temporal clustering of events observed along the Kango Fault are typical of the long-term behaviour of recognised active faults in other stable continental regions that are characterised by episodes of activity separated by quiescent intervals of at least 10,000 to (commonly) 100,000 years or more (***References 5.13.294***, ***5.13.295***, and ***5.13.219***)

Variations in total vertical separation across the fault between the western and eastern halves of the reactivated fault, as well as the timing of the most recent surface ruptures at the M1.133 site (eastern half) relative to the M1.26 and M1.42 sites (western half), suggest that there have been long-term differences in the slip history of these two reaches of the reactivated Kango Fault.

As reported by Hanson *et al.* (***Reference 5.13.54***), palaeoseismic investigations at sites in the western part (M1.42 and M1.26 sites) and eastern part (M1.133 site) of the Quaternary-reactivated Kango Fault, provide the best constraints on the timing and rate of recurrence of surface-rupturing earthquakes on the Kango Fault.

© Eskom 2026/Rev 0a

Palaeoseismic studies at the M1.26 site, combined with new OSL ages and reanalysis of the M1.42 trench log in light of these results, demonstrate that two surface-faulting events have likely occurred along the western part of the reactivated Kango Fault in latest Pleistocene to Holocene time (***Reference 5.13.54***). This interpretation updates the previous conclusion that the M1.42 trench recorded a single surface-rupturing event approximately 10 ka (***Reference 5.13.15***). The penultimate event (PE) occurred between 15 ka and 10 ka (most likely between 13 ka and 10.3 ka), and the MRE occurred between 7 ka and 4 ka. Given offset of sedimentary layers of 2–3 m documented at these sites, a Holocene vertical slip rate estimated from the M1.26 and M1.42 site data (2–3 m/10–15 kyr) ranges from 0.13 millimetre per year (mm/yr) to 0.3 mm/yr.

Remnants of the Tertiary Grahamstown Formation (Tg) pediment remnants are displaced along the eastern part of the reactivated Kango Fault segment. At the M1.133 site (***Figure F-5.13.76***) the MRE is estimated to have occurred between 22.6 ka and 25.4 ka. This estimated age is based on cosmogenic nuclide (CN) analysis of a series of samples taken from the scarp face at this site (***Reference 5.13.51***). It is not known whether the net vertical separation of 2–3.5 m across the youngest zone of faulting at this site occurred during this MRE only or whether it is the result of more than one event. A latest Pleistocene vertical slip rate based on data from the M1.133 site (2–3.5 m/22.6–25.4 kyr) ranges from 0.08 mm/yr to 0.13 mm/yr.

The available ages for the oldest deposits in the two trenches (~74 ka from M1.26 trench T1, 63 or 123 ka from M1.42) indicate that the two MREs at these sites were preceded by a long period of several tens of thousands of years of no activity.

CN burial ages for the unconformity at the contact between sediments and bedrock at the M1.42 site on both the hanging-wall and footwall blocks allow for assessment of a long-term slip rate at this site (***Reference 5.13.54***). The resistivity survey and confirmatory drilling programme conducted at the M1.42 site indicate a cumulative net vertical separation of a basal unconformity (on top of bedrock) across the fault zone of between 26 m and 33.4 m (see Plate A2.12 in ***Reference 5.13.1***). CN burial ages for basal gravel overlying this unconformity on the hanging wall range from 2.2 Ma to 3.2 Ma. Cobbles directly overlying the unconformity on the footwall block yielded a CN age of approximately 2.1 Ma. Within the uncertainties of the CN burial method, these results suggest the unconformities are of similar age. A long-term Quaternary slip rate ranging from 0.008 mm/yr to 0.018 mm/yr is estimated from these data (26–33.4 m/2,100–3,200 kyr).

© Eskom 2026/Rev 0a

There are no known localities along the eastern part of the reactivated Kango Fault, where the displacement of the unconformity at the top of bedrock/base of Tg deposits has been measured. At the M1.133 site on the eastern end of the reactivated segment, cumulative net vertical separation of the present Tg surface across the youngest zone of faulting and two possible older degraded fault scarps is approximately 7 ± 2 m. A minimum limiting exposure age of 360–380 kyr, based on boulders embedded in the silcrete surface above and below the youngest zone of faulting has been measured for the disrupted Tg surface at this site. Given the cumulative displacement of the fault zone provided above this yield a likely long-term slip rate of 0.012–0.025 mm/yr. This slip rate is not well controlled because the CN results provide either a minimum limiting exposure age or a maximum surface erosion rate (1.6 ± 0.2 m/Myr). This is impeded by the fact that the age of the Tg surfaces are not well constrained. Cosmogenic analyses conducted on various Tg silcretes (***Reference 5.13.54***) throughout the study region yielded minimum-limiting exposure ages of 1–4 Ma, which suggest that long-term slip rate at site M1.133 may be as low as 0.001–0.01 mm/yr. However, Hagedorn (***Reference 5.13.92***) reported preliminary electron spin resonance ages of 7.3 and 9.4 Ma for the Tg silcrete in the Oudtshoorn Basin. If it is assumed that the cumulative slip of the Kango fault postdates the formation of caprock across the entire fault zone, the long-term slip rate at the M1.133 site would be as low as 0.0007–0.001 mm/yr (7 ± 2 m/7.3–9.4 Ma) (***Reference 5.13.54***).

5.13.5.2 Site Geology

Geology is discussed at three levels of detail within the site vicinity (40 km radius) (***Subsection 5.13.5.2.(a)***), site area (8 km radius) (***Subsection 5.13.5.2.(b)***), and site location (1 km radius) (***Subsection 5.13.5.2.(c)***).

a) Site Vicinity (40 km Radius)

The site vicinity covers an area of approximately 5,000 km^2. Discussion of the site vicinity is done on a 1:50,000-scale basis. The majority of the area is situated offshore on a gently dipping, relatively broad continental shelf. The onshore area is represented by a seaward-sloping coastal plain situated on the St Francis Arch, a bedrock high between two Mesozoic extensional basins, the Pletmos Basin to the west and the Gamtoos Basin to the east (***Figure F-5.13.49***). The Kareedouw and Suuranys Mountains of the Cape Fold Belt rise above the coastal plain, separating the coastal platform from the interior and forming the northern boundary of the South African south coast (***Figures F-5.13.77*** and ***F-5.13.78***). The site vicinity includes the towns of Humansdorp, and Jeffreys Bay and other smaller villages such as Cape St Francis, St Francis Bay, Oyster Bay, Kruisfontein and Clarkson.

© Eskom 2026/Rev 0a

i Physiography and Topography

In general, the current-swept continental shelf in the site vicinity dips gently (0.5 to 2.5 degrees (***Reference 5.13.83***) to the south and lacks significant physiographic features (e.g., canyons or islands) (***References 5.13.296***, ***5.13.281***, and ***5.13.59***). There are several smaller topographic features present in the site vicinity. The site vicinity contains several embayments including portions of St Francis Bay, Seal Bay, Thys Bay, and Oyster Bay. These bays are typically bounded by headlands of more-resistant units of the Table Mountain Group. On the continental shelf, evidence for palaeoshorelines is interpreted at water depths of –27 to –30 m, –34 to –38 m, –45 ± 3 m, –70 m, –78 to –79 m, –103 ± 2 m, and –107 m (+1, –3) in the site area (***Reference 5.13.58***). The submerged shorelines are interpreted to have formed during lowered Pleistocene sea levels.

© Eskom 2026/Rev 0a

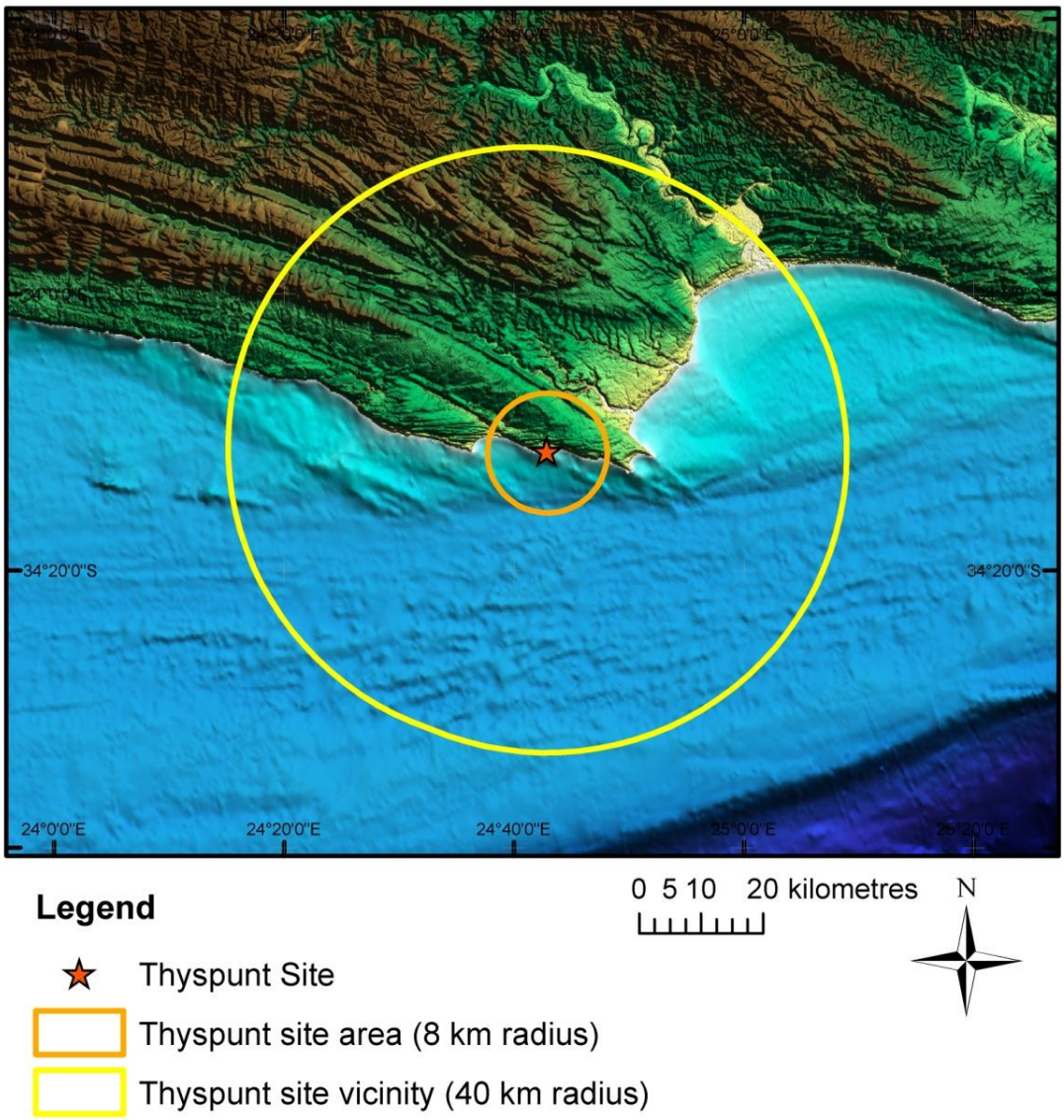


Figure 5.13-77
Digital Elevation Model of the Site Vicinity (40 km Radius)
(Onshore Data from *Reference 5.13.280*; Offshore Data from *Reference 5.13.59*)

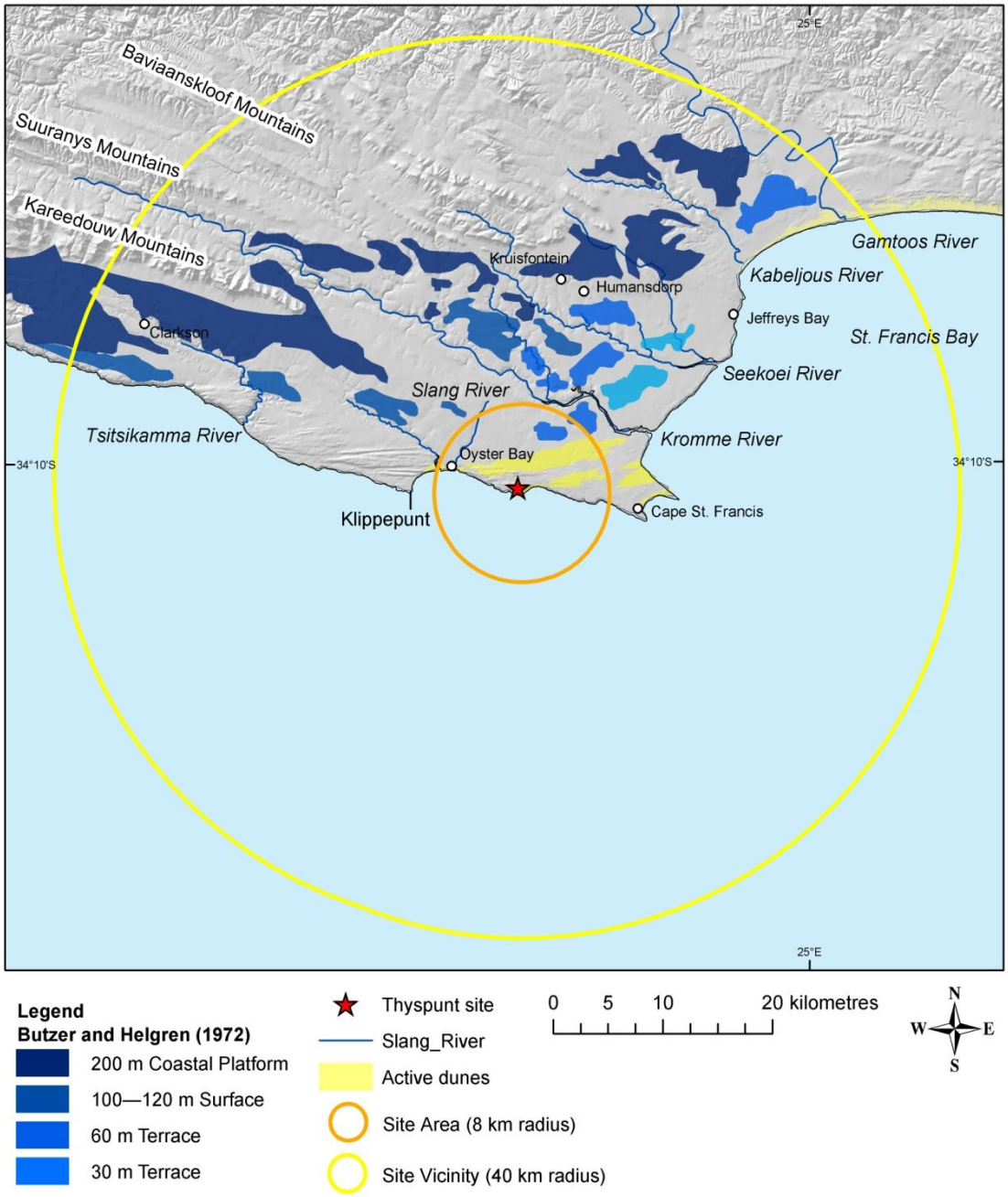


Figure 5.13-78
Digital Elevation Model of the Site Vicinity (40 km Radius) and Site Area (8 km Radius) and Map of Coastal Terraces

In addition to erosional palaeoshorelines, relict and sometimes cemented dunes also appear to be present on the continental shelf as remnant depositional systems (***Reference 5.13.58***). Geomorphic features on the seafloor bottom (linear ridges) that sub-parallel isobaths at water depths of approximately 90–130 m are most likely remnant ridges of aeolianite possibly modified by erosion or sedimentation during Pleistocene sea-level fluctuations (***Figure F-5.13.77***). Acoustic characteristics of these features identified on geophysical data sets are comparable to similar structures which have been sampled and extensively studied along other parts of the South African continental shelf (***References 5.13.297*** and ***5.13.298***). The age of these features is unknown, but correlation to local and global sea level curves suggests that they may have formed during the regression from the MIS 5a highstand (~80 ka) to the Last Glacial Maximum (LGM) lowstand (~21 ka), which is universally recognised as having a water depth of ~120 m (***Reference 5.13.58*** Appendix A). However, some of these features lie at greater depth, beyond the minimum expression of Late Quaternary base level, and could possibly be much older (Neogene).

The site vicinity around Thyspunt is characterised by a dual-trending coastline. A northwest-southeast-trending, south-facing, relatively straight and rocky coastline extending from Nature's Valley (beyond the boundary of the site vicinity) to Cape St Francis reflects the trend of the underlying folded Palaeozoic rocks of the Table Mountain Group. North of St Francis, the coastline exhibits a southwest-northeast-trending, southeast-facing undulating coastline underlain by Devonian-aged rocks of the Bokkeveld Group and the Mesozoic aged Uitenhage Group rocks. The coastline morphology and bedrock topography are in part the consequence of the variation in lithological units and the process of differential weathering that lead to the formation of alternating headlands and log spiral embayments. The prominent Cape St Francis and Klippepunt headlands and surrounding rocky coastline are the result of the resistant nature of sandstone and quartzitic bedrock units of the Skurweberg and Peninsula Formations, whereas the development of the Cape St Francis and Slangbaai embayments are the consequence of the less erosion-resistive nature of the thinly bedded sandstones, shales, and mudstones of the Goudini, Cedarberg, Gydo, and Baviaanskloof Formations. North of Jeffreys Bay, the development of a log spiral bay can be attributed to the erodible nature of the Bokkeveld and Uitenhage Group rocks underlying the area. Similarly, topographic highs and mountain ranges within the interior of the site vicinity are associated with erosion-resistant and competent quartzitic sandstone–bearing geological units such as the Peninsula and Skurweberg Formations that produce hills and prominent ridges.

© Eskom 2026/Rev 0a

The onshore geomorphology of the site vicinity includes a relatively broad, flat-lying to gently seaward-sloping coastal platform, the maximum elevation of which is approximated to 200 m asl. The coastal margins of this platform are irregularly overlain by Cenozoic marine and aeolian deposits. Modern linear east-west-trending unconsolidated dunes that form part of the Oyster Bay–St Francis headland bypass dune field and dune fields near the mouth of the Gamtoos River, bury the older marine and aeolian deposits (***Reference 5.13.27***). As discussed above in ***Subsection 5.13.5.1.(a)***, a flight of lower marine terraces of Pliocene and Pleistocene age also are present in a narrow strip along the coastline.

The landward extent of the transgressive Miocene marine planation event which arguably led to the development of the coastal platform is marked by a palaeo-sea cliff, a sharp break in slope situated at the southern foot (~260–280 m asl) of the interior Cape Fold Mountains (***Reference 5.13.153*** and ***Figure F-5.13.79***), northwest of Humansdorp near the town of Kruisfontein. These mountain areas (Kareedouw, Suuranys, and Kareedouw Mountains) reach maximum elevations of over 750 m asl. The marine-planed surface is incised by post-planation rivers that expose inclined bedrock. The interior of the site vicinity is drained by four major rivers that discharge into the Indian Ocean. These rivers generally follow the northwest-southeast geological trend of underlying geological formations. Towards the northeast, areas are drained by the Gamtoos River, and towards the south of Hankey and Loerie, by the Seekoei River. North of Sea Vista, the surrounding area is drained by the Kromme River, and west of Oesterbaai, roughly 15 km from Clarkson, the area is drained by the Tsitsikamma River (***Reference 5.13.27***). Other smaller rivers and streams, such as the Slang River, also drain the site vicinity.

On the Cape St Francis headland, two active large-scale headland-bypass dune corridors are recognised; the Oyster Bay dunefield (locally referred to as the Sand River) and the Thysbaai dunefield (***Figure F-5.13.80*** and ***Reference 5.13.302***). The Oyster Bay dunefield, which varies in width from about 500 to 1,200 m, is currently active over a length of about 13–14 km. Transverse dune height varies from 40 m in the upwind (western) end of the dunefield to 5 m at the downwind (eastern) end. The smaller Thysbaai dunefield has a maximum length of about 6 km, a maximum width of about 1,000 m, and average transverse dune height within the field of about 11 m (***Reference 5.13.299***). A third dunefield, the Santareme dunefield, which occurred along the downwind (eastern) seaboard of the headland, was completely stabilised during the 1970s and 1980s to enable development of a holiday resort suburb in the area.

© Eskom 2026/Rev 0a

A small headland-bypass system, about 200 m wide and 700–800 m long, crosses the easternmost cape (Cape St Francis) (***References 5.13.300***, ***5.13.301***, and ***5.13.86***).



Figure 5.13-79
The Landward Extent of the Transgressive Miocene Marine Planation Event Which Led to the Development of the Platform Is Marked by a Palaeosea Cliff, a Sharp Break in Slope Situated at the Southern Foot (~300 m asl) of the Interior Cape Fold Mountains, Northwest of Humansdorp near the Town of Kruisfontein

© Eskom 2026/Rev 0a

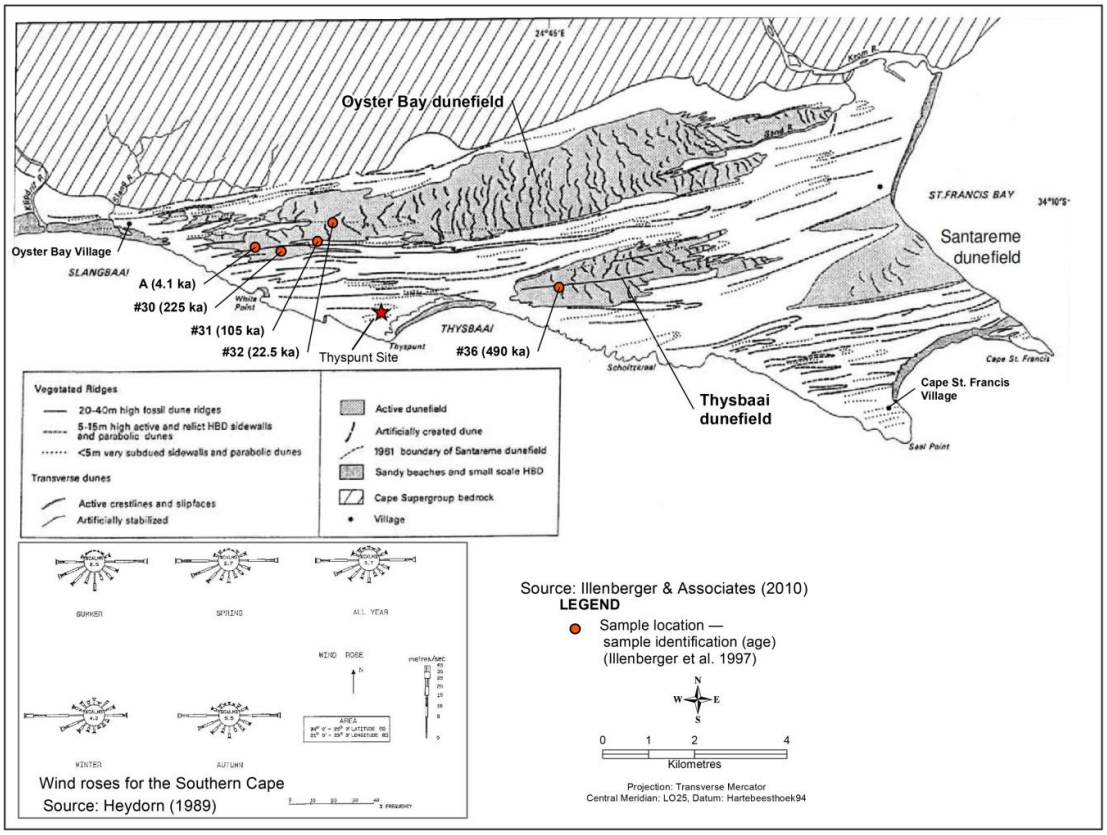


Figure 5.13-80
Dunefields near the Thyspunt Site (Modified from *References 5.13.299* and *5.13.302*)

Older (fossil) dunes are recognised in the Cape St Francis headland area (***Figure F-5.13.80***) as well as elsewhere along the entire South African coast. Luminescence dating of fossil dune ridges at the windward (western) end of the Oyster Bay dunefield confirmed dune activity associated with Late Pleistocene interglacials. Weathered dune rock from a ridge flank was dated at 105 ka, and case-hardened aeolianite from the downwind nose of another ridge was dated at 225 ka. Iron-enriched sands found on the flanks of the fossil ridges were dated to 225 ka (Oyster Bay dunefield) and 490 ka (Thysbaai dunefield) (***References 5.13.303*** and ***5.13.86***). These ages correspond to major dune-building activity on sea level regressions for this part of the coast.

ii Stratigraphy

The geology of the site vicinity is characterised by two distinct sedimentary sequences of Palaeozoic and Cenozoic age (***Table T-5.13.7***). The area is entirely underlain by northwest-southeast-striking Palaeozoic bedrock of the Table Mountain and Bokkeveld Groups, which underwent deformation during the Permo-Triassic Cape Orogeny and now forms part of the Cape Fold Belt. The bedrock is irregularly overlain along coastal margins by unconsolidated to semiconsolidated clastic nearshore-marine and coastal aeolian-derived Cenozoic deposits of the Algoa Group. These predominantly aeolian deposits form part of the Oyster Bay–St Francis bypass dune field, which, near Cape St Francis, extends approximately 10 km into the hinterland (***Figure F-5.13.81***).

A lithostratigraphic summary of rock types within the Site vicinity, in accordance with the nomenclature of the South African Committee for Stratigraphy (***Reference 5.13.160***), is provided in ***Table T-5.13.7***.

Table Mountain Group

The Table Mountain Group represents the basal group of the Cape Supergroup and is unconformably underlain by basement rocks of the Gamtoos Group. The Palaeozoic lithostatigraphy of the site vicinity comprises five clastic sedimentary formations: the Peninsula, Cedarberg, Goudini, Skurweberg, and Baviaanskloof Formations. The lithological character and thicknesses of these formations are indicated on ***Figure F-5.13.82***. The occurrence of the formations within the site vicinity is indicated on ***Figure F-5.13.81***. The interpreted subsurface occurrence of formations beneath Cenozoic Algoa Group in the Cape St Francis area is portrayed on ***Figure F-5.13.83***). See ***Subsections 5.13.5.2.(b) ii*** and ***5.13.5.2.(c) ii*** for the interpreted subsurface occurrence of formations closer to Thyspunt.

© Eskom 2026/Rev 0a

Table 5.13.7
Lithostratigraphic Summary of Rock Types in the Site Vicinity
(*References 5.13.160* and *5.13.27*)

Age		Super-group	Group	Formation	Lithological Description
Cenozoic	Holocene		Algoa	Schelm Hoek	Aeolian sand, soil horizons, and middens
	Pleistocene			Nahoon	Aeolian calcareous sandstone, palaeosols, and subordinate calcrete
				Salnova	Marine and/or estuarine calcareous sandstone, siltstone, coquinite, and basal gravels
				Nanaga	Calcareous sandstone (aeolianite), palaeosols, subordinate, and calcrete,
	Miocene–Pliocene			Alexandria	Calcareous sandstone, semi-consolidated conglomerate, coquinite, and basal gravels
	Palaeocene –Miocene			Grahamstown	Pedogenic silcrete
Mesozoic	Cretaceous		Uitenhage	Kirkwood	Sandstone interbedded mudstone
	Jurassic			Enon	Conglomerate, subordinate interbedded sandstone, and mudstone
Palaeozoic	Devonian	Cape	Bokkeveld	Gydo	Black to brown shale, subordinate siltstone
	Silurian		Table Mountain	Baviaanskloof	Impure feldspathic sandstone, subordinate shale
				Skurweberg	Quartzitic sandstone, medium- to course-grained, cross-bedded, subordinate shale
				Goudini	Brown-weathering thinly bedded siltstone, mudstones, quartzitic sandstone
	Ordovician			Cedarberg	Black shale, laminated
				Peninsula	Quartzitic sandstone, massive and laminar, and cross-bedded, medium- to coarse-grained
Proterozoic	Namibian		Gamtoos		Quartzites, conglomerate, phyllite, shale, limestone

Note: The Gamtoos Group does not crop out in the area, but is included in this lithostratigraphic summary because it forms the basement in the site vicinity.

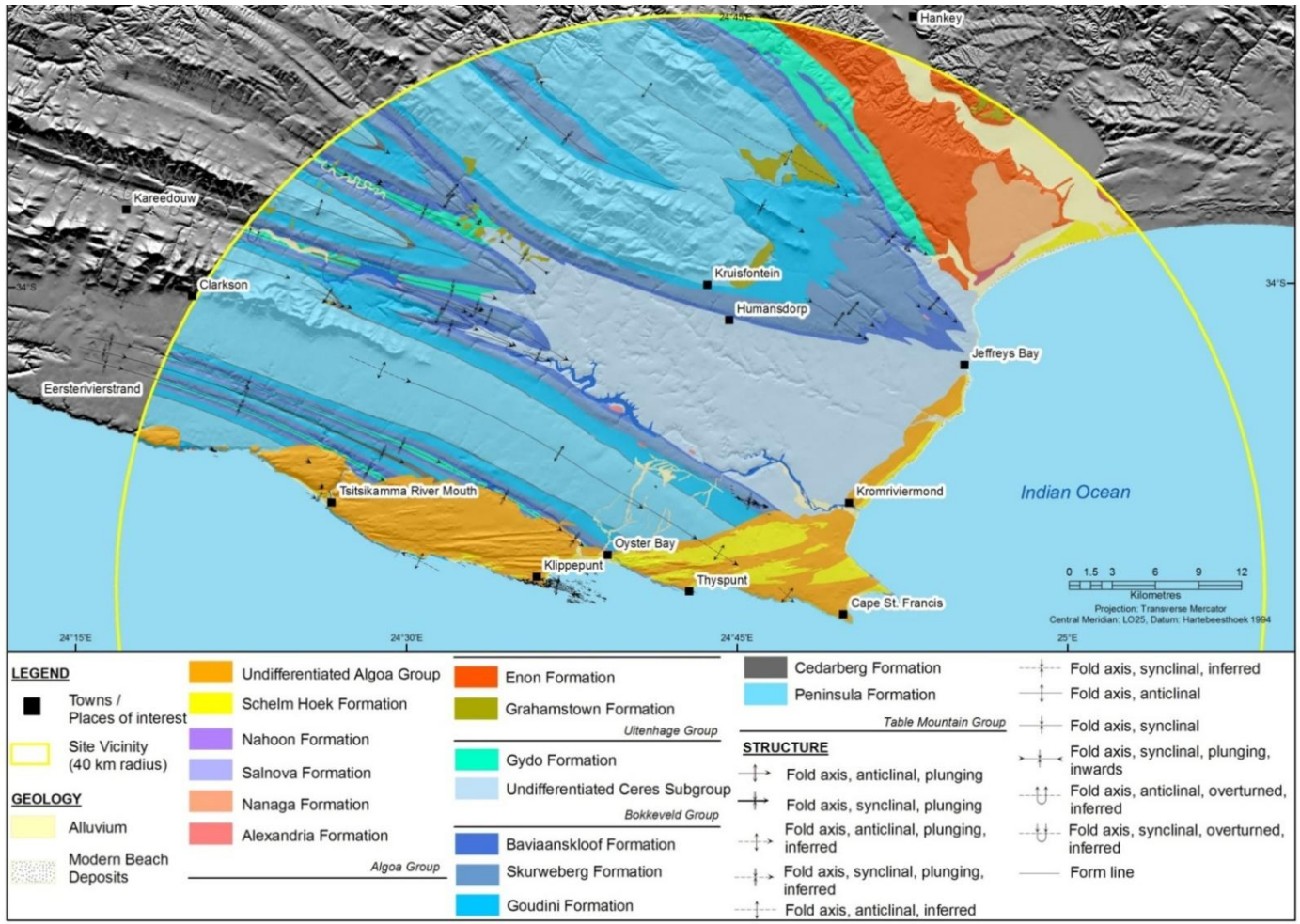


Figure 5.13-81
Geology of the Site Vicinity (Modified from *Reference 5.13.27*)

© Eskom 2026/Rev 0a

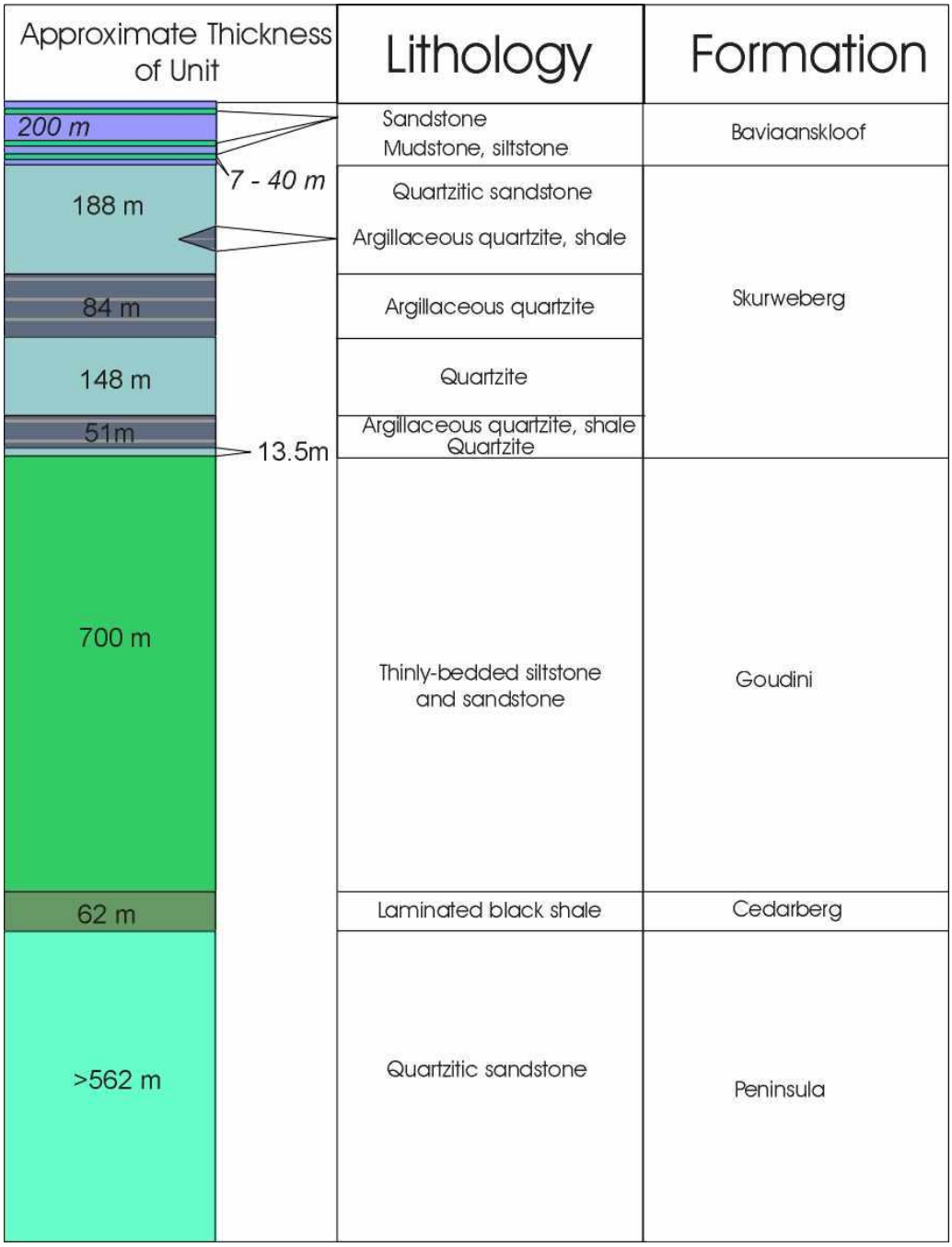


Figure 5.13-82
Approximate Thicknesses and Lithology of the Formations of the Table Mountain Group Present Within the Site Vicinity (Figure Not to Scale; Modified from *Reference 5.13.27*)

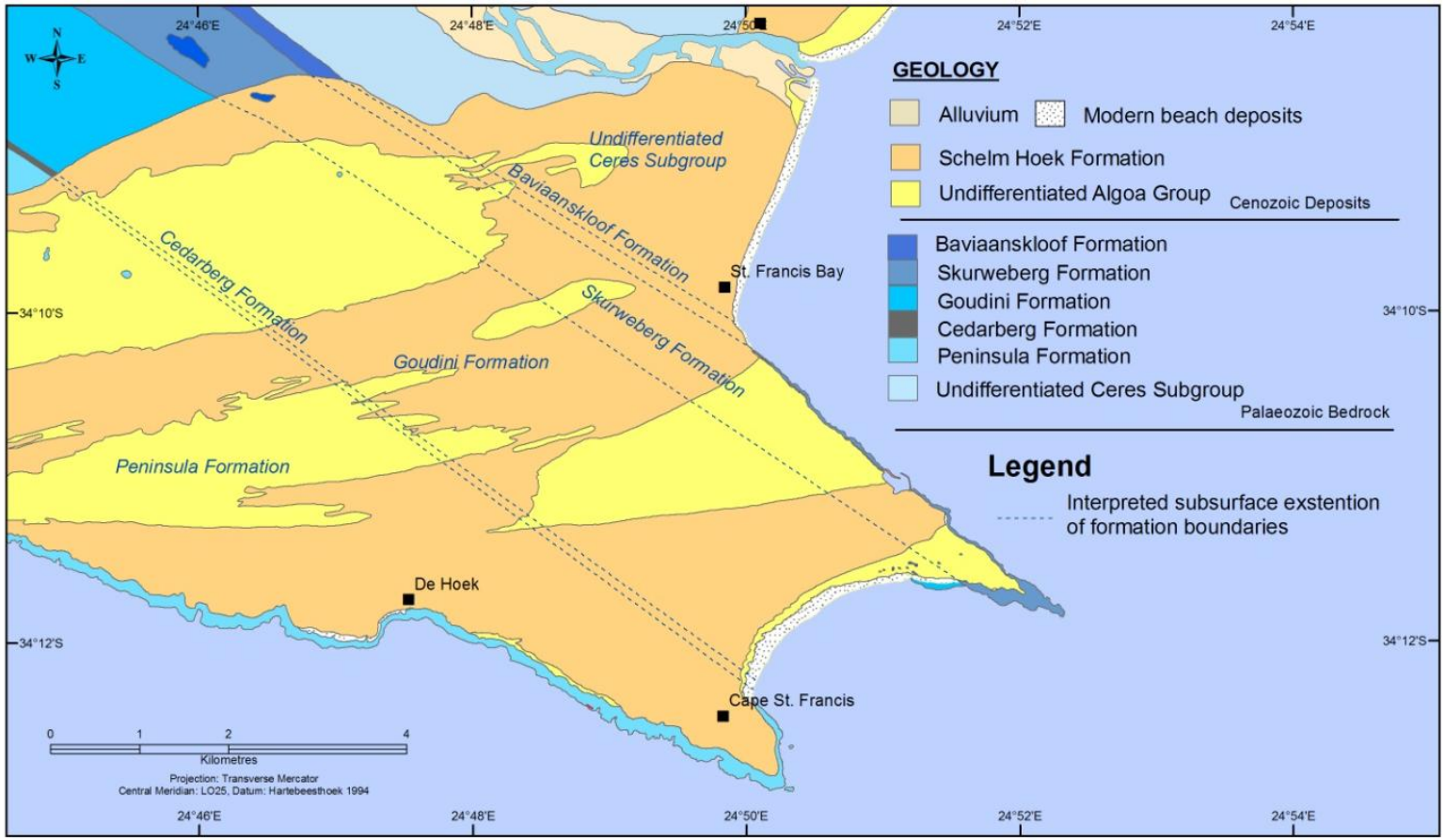


Figure 5.13-83
Interpreted Subsurface Occurrence of the Formations of the Table Mountain Group Beneath the Cenozoic Algoa Group Along the North-eastern Limb of the Main Cape St Francis Anticline in the Cape St Francis Area

© Eskom 2026/Rev 0a

Peninsula Formation

The Ordovician Peninsula Formation is aerially, stratigraphically, and topographically the most prominent formation within the site vicinity. Expression of the formation within the landscape takes the form of west-northwest/east-southeast-trending mountainous exposures in the Kareedouw and Suuranys mountains west of Humansdorp, as linear ridges or topographic relative highs within the interior and as a rugged coastline between Thysbaai and Seal Point.

The Peninsula Formation comprises the basal unit of the Table Mountain Group and is composed of light grey, supermature, and medium-grained massive to well-bedded quartzitic sandstones. The sandstones are frequently stained pink or red by iron oxides and infrequently interbedded with thin (>1 m) argillaceous (mudrock or phyllite) horizons (***Figure F-5.13.84a***). The thickness of the formation in the vicinity of Thyspunt is >562 m (***Reference 5.13.27***).

Sedimentary structures documented in the site vicinity (***Reference 5.13.27***) include large-scale trough and planar cross bedding, cross-lamination, horizontal lamination channel structures and soft sediment deformation (***Figure F-5.13.84b***; ***References 5.13.304*** and ***5.13.27***). Sedimentary structures indicate that sandstone of the Peninsula Formation was deposited in a predominantly shallow marine environment (***Reference 5.13.305***). The Peninsula Formation is conformably overlain by the Cedarberg Formation.

Cedarberg Formation

The laterally persistent Ordovician Cedarberg Formation has varying thickness, ranging between 50–150 m within the site vicinity (***References 5.13.27***, ***5.13.305***, and ***5.13.119***). Goedhart et al. (***Reference 5.13.27***) indicated a thickness of 62 m in the vicinity of Thyspunt (***Figure F-5.13.83***) and attributed the variation in thickness to the formation's argillaceous nature that forms a structurally favourable detachment zone along the limbs of large folds, causing it to either be partially smeared out or seemingly absent. This lithostratigraphically incompetent unit consists of black, thinly laminated, fine-grained carbonaceous shale (***Figure F5.13.85a***), often containing pyrite (***Reference 5.13.304***) and infrequently containing thinly bedded siltstone. The formation weathers negatively to produce lengthy linear landscape depressions. Weathered exposures appear grey, greenish grey, and yellow (***Figure F-5.13.85b***), as documented south of the Kouga Dam (***Reference 5.13.27***). The Cedarberg Formation is poorly exposed within the site vicinity.

© Eskom 2026/Rev 0a

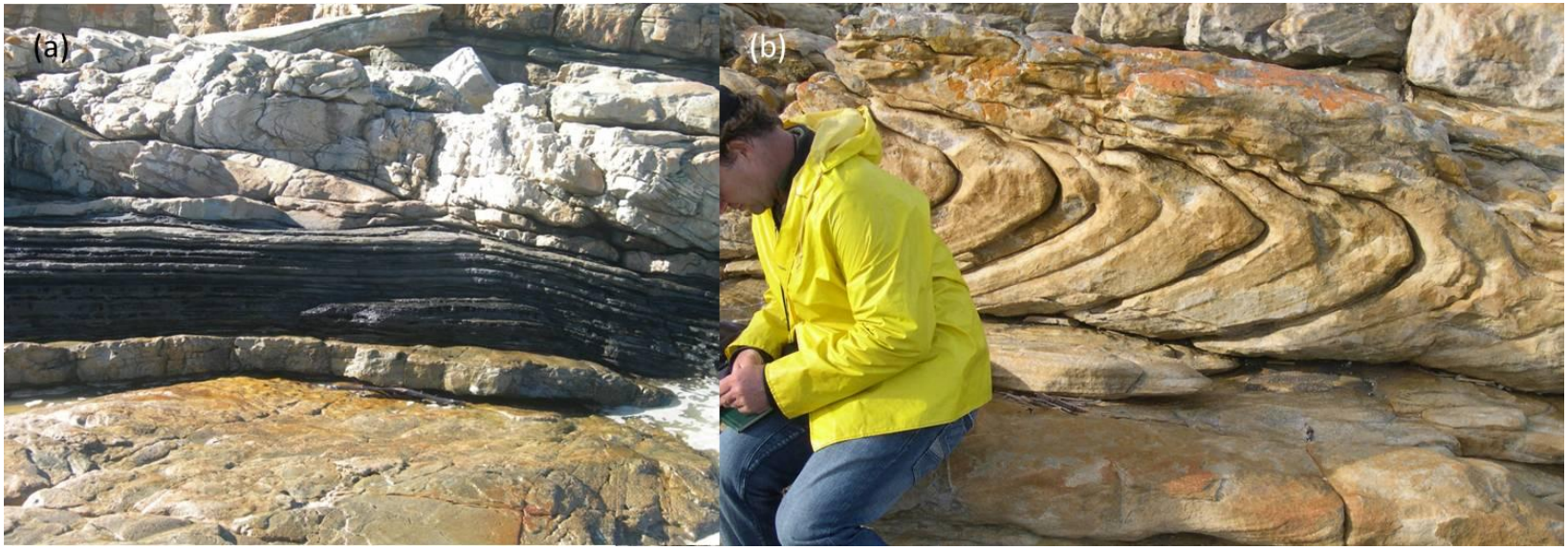


Figure 5.13-84
(a) A Coastal Exposure of Competent Quartzitic Sandstone of the Peninsula Formation, Interbedded with Subordinate Dark Grey Mudrock (1.4 m in thickness) West of De Hoek. Location of Photo: 34°11′48.1″ S, 24°47′39.0″ E.
(b) Soft Sediment Deformation in Quartzitic Sandstone of the Peninsula Formation Along Coastal Exposures East of Thys Bay. Location of Photo: 34°11′20.6″ S, 24°44′34.1″ E

© Eskom 2026/Rev 0a

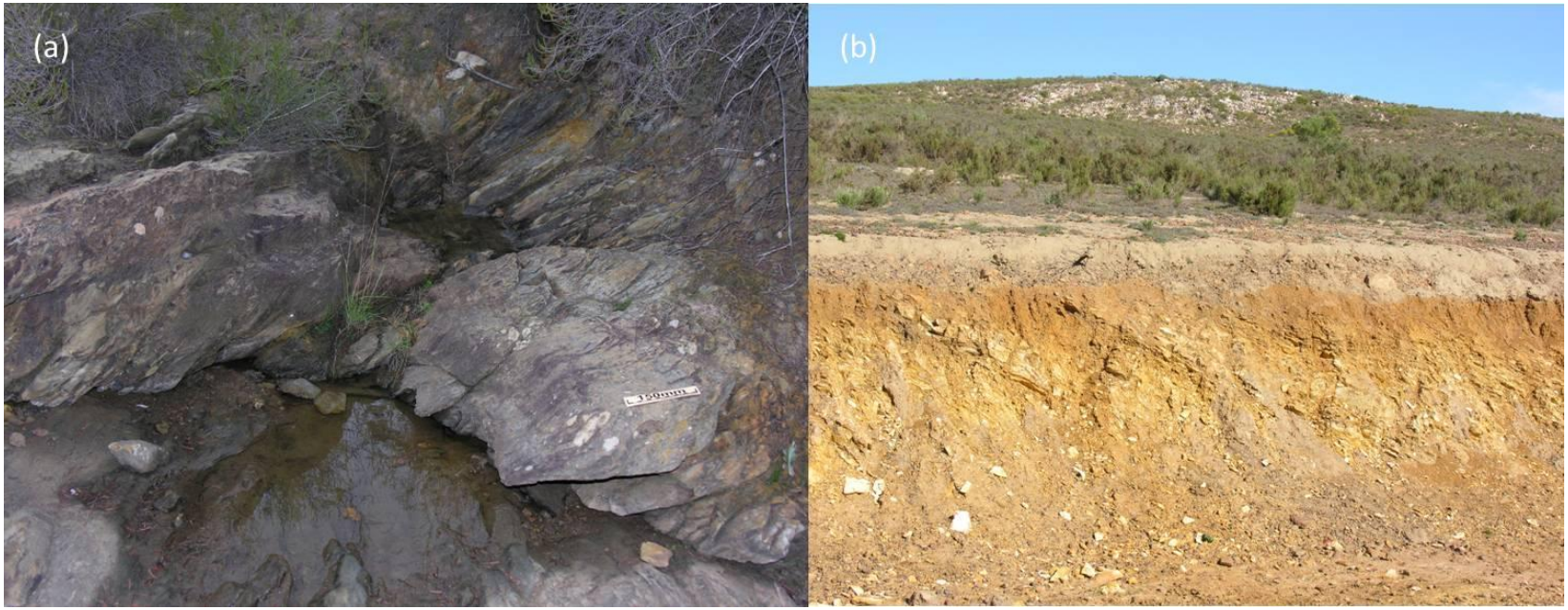


Figure 5.13-85
(a) Rarely Exposed Dark Grey to Blackish, Fine-Grained Argillaceous Cedarberg Formation Visible at the Base of a Valley, South of the Kouga Dam (33°51′44.5″ S, 24°35′42.1″ E). (b) Light Brown to Yellowish Brown Weathered Shale and Siltstone Exposure of the Cedarberg Formation Situated Within a Topographic Low Within the Landscape. Note the Elevated Quartzitic Ridge of the Peninsula Formation in the Background (33°52′13.0″ S; 24°36′35.1″ E). Photos Sourced from *Reference 5.13.27*

© Eskom 2026/Rev 0a

The subsurface occurrence of the Cedarberg Formation near Cape St Francis is confirmed by three geophysical surveys (***References 5.13.42***, ***5.13.306***, and ***5.13.44***) and borehole CSF-14 (***Reference 5.13.58***) and is indicated on ***Figure F-5.13.86***. Survey lines indicate that the thickness of the Cedarberg Formation in the area of Cape St Francis is approximately 120 m.

Goudini Formation

The Silurian Goudini Formation is composed of immature, medium-grained, pale grey, unweathered and brownish to reddish weathered quartzitic sandstone with subordinate mudstone/shale and siltstone (***Reference 5.13.119***; ***Figure F-5.13.87***). The Goudini Formation sandstone is a medium-grained quartz arenite (***Reference 5.13.49***) and is commonly cross-bedded and less commonly laminated (***Reference 5.13.22***). These tabular sandstone units are thickly bedded and may be siliceous in places. Finer-grained sandstone is generally more massive (***Figure F-5.13.88***) and shows evidence of bioturbation (***Reference 5.13.22***). Subordinate mudstone/shale and siltstone is thinly bedded and is generally structureless or contains horizontal lamination. Generally, bedding consistently shows rapid lithological changes.

The Goudini Formation shows great variation in thickness within the site vicinity. Goedhart et al. (***Reference 5.13.27***) indicated an approximate thickness of 700 m (***Figures F-5.13.81*** and ***F-5.13.82***) whilst Malan et al., (***Reference 5.13.270***) calculated a thickness of 230 m ± 30 m in the areas northwest of Humansdorp. The lithologically incompetent formation is well exposed east of Humansdorp and northwest of Kruisfontein, where it forms prominent low-relief areas adjacent to topographic highs of the more erosion resistant Skurweberg Formation. Selective erosion of near-vertically inclined beds of this Formation along coastal exposures, such as those within the Huisklip Nature Reserve (***Figure F-5.13.88***), west of Klippepunt, produced jagged ledges. Deposition of the Goudini Formation strata occurred in a shoreline environment on a shallow stable shelf (***References 5.13.91*** and ***5.13.270***).

Skurweberg Formation

The Silurian Skurweberg Formation, which is similar in age to the Goudini Formation, is composed of tabular, grey to pale grey, mature quartzitic sandstone (***Figure F-5.13.89 a&b***) interbedded with subordinate and infrequent immature argillaceous shale units (***References 5.13.307*** and ***5.13.30***) and conglomerate stringers. The sandstones and shales are generally medium- to thick-bedded, while the conglomerates are, on average, a metre in thickness (***References 5.13.28*** and ***5.13.308***).

© Eskom 2026/Rev 0a

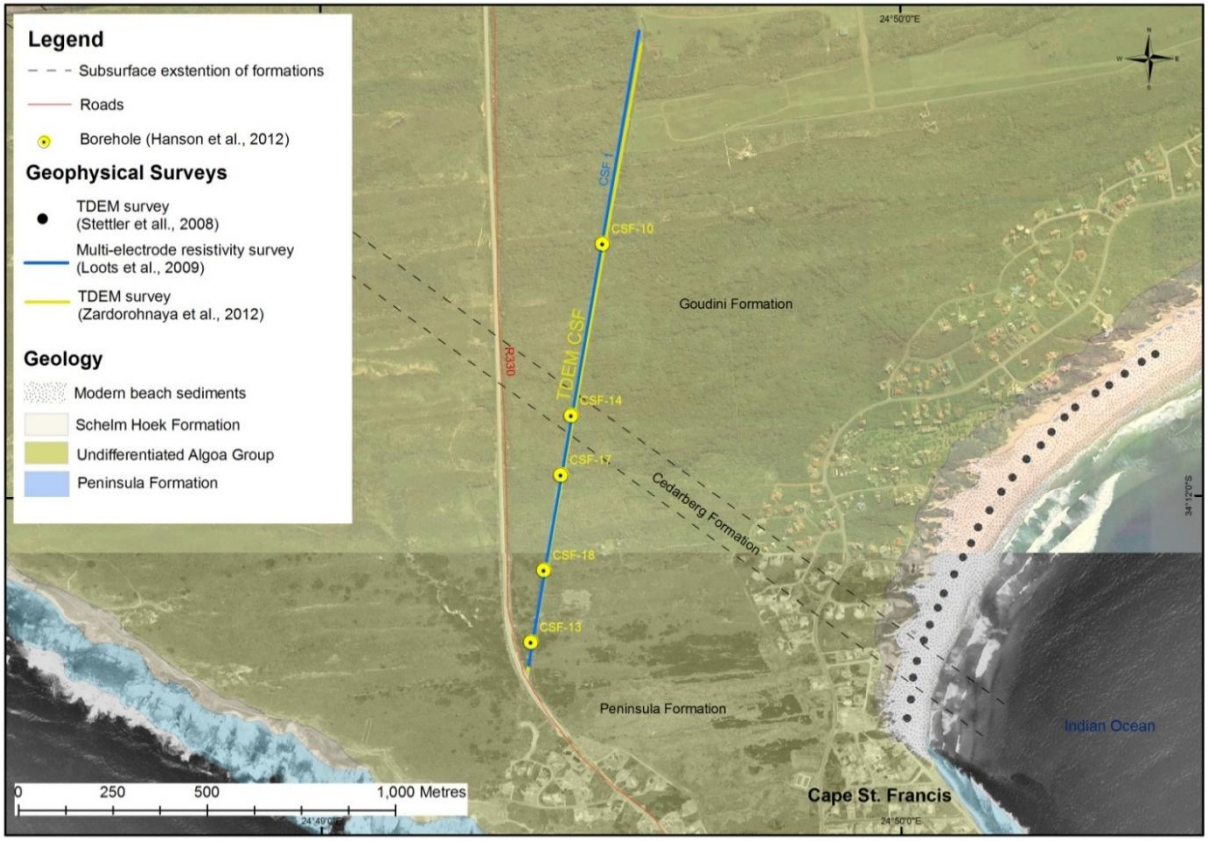


Figure 5.13-86
The Subsurface Occurrence of the Cedarberg Formation near Cape St Francis Interpreted from Geophysical Ground Surveys (*References 5.13.42*, *5.13.306*, and *5.13.44*) and Borehole Data (*Reference 5.13.58*)

© Eskom 2026/Rev 0a



Figure 5.13-87
Alternating Shale and Dirty Sandstone of the Goudini Formation Seen in Borehole CSF-10 Between 40.90 m and 54.25 m Below Ground (34°11′38.2″ S, 24°49′29.3″ E). The Red Arrow Indicates the Contact Between the Cenozoic Algoa Group Sediments and the Palaeozoic Goudini Formation

© Eskom 2026/Rev 0a



Figure 5.13-88
Sandstone of the Goudini Formation Is Well Exposed Along the Coast Within the Huisklip Nature Reserve. Location of Photo: 34°8′25.4″ S, 24°26′30.3″ E

© Eskom 2026/Rev 0a



Figure 5.13-89
(a) Coastal Exposures of the Skurweberg Formation Composed of Grey to Pale Grey, Mature Quartzitic Sandstone Dipping Approximately 50° S at 34°11′23.6″ S, 24°41′54.2″ E Near Tony's Bay.
(b) A Weathered Exposure of Immature Sandstone Within the Skurweberg Formation, 13 km west of Kruisfontein (33°59′40.2″ S, 24°34′50.6″ E)

© Eskom 2026/Rev 0a

Sandstone is moderately sorted and medium- to course-grained. Beds are apparently massive but, upon close inspection trough cross-bedding is a frequent occurrence. Shale beds are very micaceous, often bioturbated and carbonaceous and frequently appear structureless or horizontally laminated. In some cases shale bands appear clayey (almost kaolinitic). Close to the contact between the Skurweberg and Goudini Formations, the number of shale bands within the Skurweberg Formation increases and shale beds appear darker and more carbonaceous (***References 5.13.28*** and ***5.13.308***). In the site vicinity the formation approximate thickness is approximately 484 m (***Reference 5.13.27*** and ***Figures F-5.13.81*** and ***F-5.13.82***).

Deposition of the texturally mature Skurweberg Formation took place in a shallow, nearshore marine environment such as a coastal plain (***References 5.13.309*** and ***5.13.109***).

Baviaanskloof Formation

The Silurian to Devonian aged Baviaanskloof Formation is the uppermost unit of the Table Mountain Group within the site vicinity (***Table T-5.13.7***). The formation consists of immature sandstone, mature feldspathic sandstone, minor rhythmite, mudstone, and siltstone (***Reference 5.13.310***). The immature argillaceous sandstone (***Figure F-5.13.90a***) is identifiable by its medium to dark grey colour, fine- to very fine-grained seemingly massive appearance, and commonly siliceous nature. Subordinate interbedded dark grey to black horizons of siltstone, structureless to lenticular-bedded silty mudrock, and laminated rhythmite are also present. The sandstone units vary in thickness from 7 m to 40 m (***Reference 5.13.27***). More argillaceous micaceous or carbonaceous units are <4 m thick. Siltstones and dirty sandstones are often bioturbated and contain invertebrate casts, shells, crinoids, and horizontal tube-like burrows. Sedimentary structures within the Baviaanskloof Formation sandstones include horizontal lamination, wavy bedding, micro-cross-lamination, rare cross-bedding, and ripple marks (***Reference 5.13.310***).

Within the site vicinity near the Kouga Dam, the Baviaanskloof Formation attains a thickness of 200 m (***Reference 5.13.310***).

The Baviaanskloof Formation represents sediments deposited in a shallow-marine environment. Thicker sandstone units in the middle part of the formation represent shoreface and foreshore environments (***Reference 5.13.119***). The formation conformably overlies the Skurweberg Formation (***Figure F-5.13.90b***).

© Eskom 2026/Rev 0a

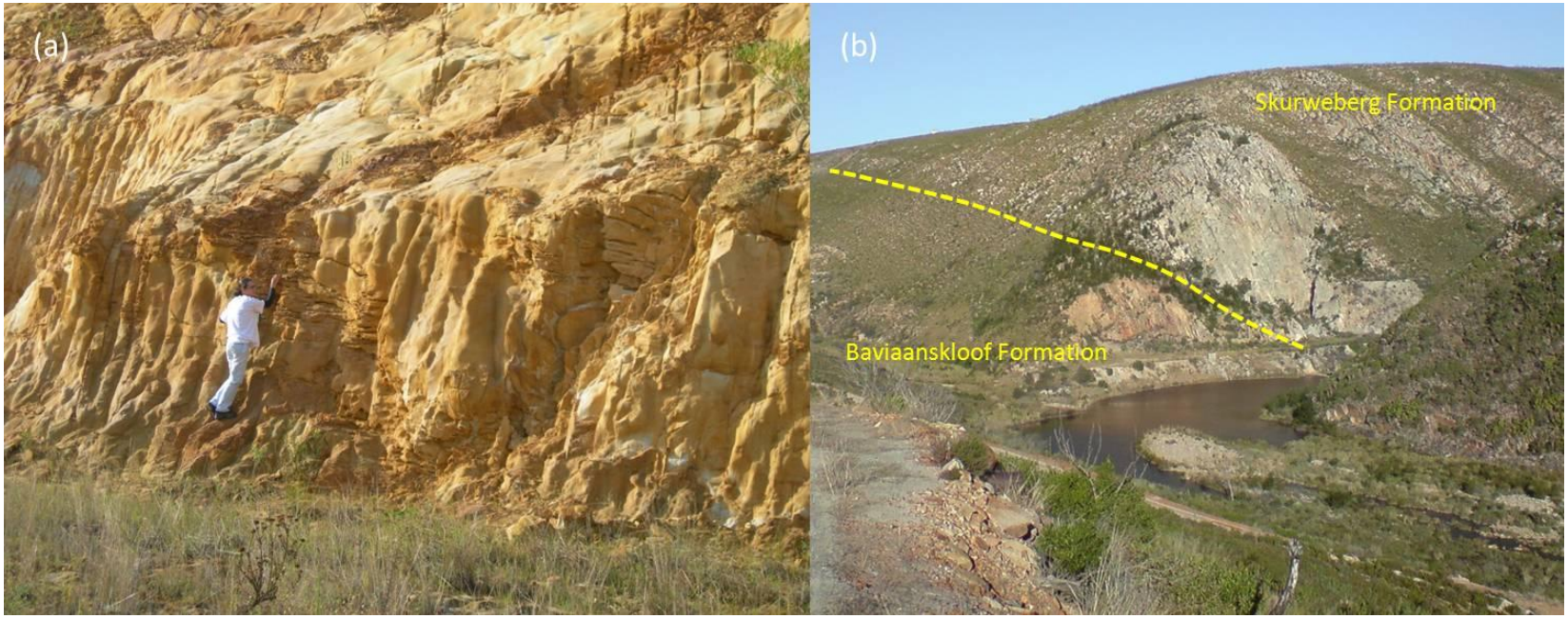


Figure 5.13-90
(a) Immature Argillaceous Sandstone of the Baviaanskloof Formation near Sunnyside Dam, Northeast of Humansdorp (34°00′45.6″ S, 24°51′33.5″ E).
(b) Along a River Section East of the Churchill Dam, the Contact Between Quartzitic Sandstone of the Skurweberg Formation (upper right) and the Immature Sandstone of the Baviaanskloof Formation (lower left) Can Be Seen (34°00′08.6″ S, 24°29′46.9″ E)

© Eskom 2026/Rev 0a

Bokkeveld Group

The Devonian Bokkeveld Group (***Figure F-5.13.81***) is subdivided into the Traka and Ceres Subgroups, of which only the latter outcrops in the site vicinity (***Figure F-5.13.81***) where it conformably overlies the Table Mountain Group as an off-lapping succession. The Bokkeveld Group comprises an upward-coarsening cyclic alternation of fine-grained sandstone and dark-grey mudstone and shale (***Reference 5.13.311***). In the Eastern Cape, east of 21°E the group attains a 1,700 m thickness (***Reference 5.13.119***).

The incompetent group produces unpronounced topography within the landscape with a low frequency of exposures within the site vicinity. Exposures can be fossiliferous, containing mainly invertebrate fossils.

The Bokkeveld Group accumulated as a southward-prograding clastic wedge composed of laterally merged arcuate deltas (***Reference 5.13.312***). Deeper-water deposition took place as shale accumulated in a prodelta–shelf setting. Shallower-water sandstone was deposited as tidal- and wave-reworked delta-front sand deposits. Repeated cycles of mudrock-dominated units overlain by sandstone-dominated units make up the Bokkeveld Group. Together with the overall upwards-coarsening trend in the Group, this is interpreted to represent a progradational (seaward building) stacking pattern of repeated transgression-regression cycles (***Reference 5.13.119***).

Gydo Formation and Undifferentiated Ceres Sub-Group

The Gydo Formation forms the basal unit of the Ceres Subgroup in the site vicinity and consists of a 600 m thick succession of mudrock/shale (***Figure F-5.13.91 a&b***), siltstone, and lesser immature sandstone.

Although the Gydo Formation's basal contact with the Baviaanskloof Formation is easily defined, lack of good exposure within the site vicinity prohibits the identification of its upper contact with the overlying Gamka Formation. Lack of exposure also hampers the delineation of other formations (Voorstehoek, Hex River, Tra-Tra, and Boplaas) within the Ceres Subgroup. Therefore, sediments of the Bokkeveld Group are largely mapped (***Reference 5.13.27***) as undifferentiated Ceres Subgroup (***Figure F-5.13.81***).

© Eskom 2026/Rev 0a



Figure 5.13-91
(a) Weathered Mudstone of Ceres Subgroup, Possible Gydo Formation Showing Slaty Cleavage Approximately 9 km East of the Churchill Dam (33°59′25.1″ S, 24°35′23.1″ E). (b) Bioturbated Dark Grey Shale of the Gydo Formation Along the Hankey Pass, Approximately 8 km Southwest of the Hankey (33°53′28.2″ S, 24°50′08.1″ E). The Exposure Shows Burrow Orientation Approximately Parallel to Bedding Laminations

© Eskom 2026/Rev 0a

Uitenhage Group

Sediments of the Uitenhage Group were deposited in the Late Jurassic to Early Cretaceous in the northwest-southeast-trending asymmetrical Gamtoos Basin (***Reference 5.13.161***). The Gamtoos Basin is located along the north-eastern boundary margins of the site vicinity and can be described as a half-graben of which the Gamtoos Fault (not located within site vicinity) forms the northern to north-eastern boundary (***References 5.13.30*** and ***5.13.27***).

The Uitenhage Group is comprised of three lithologically distinct units; the Enon, Kirkwood and Sundays River Formations. The Sundays River Formation does not occur in close proximity to the site vicinity and is thus not discuss below. Although the Kirkwood Formation is not observed within the area covered by the site vicinity either it represents a geologically significant formation in very close proximity to the site vicinity boundary and, so is included in the discussed here.

Strata of the Uitenhage Group were deposited in a structural basin during the period of crustal extension at the time preceding and including the Gondwana breakup (***Reference 5.13.161***). These deposits present a local influence of inversion of an earlier thrust zone of the Cape Fold belt (***Reference 5.13.274***). The deposition of large volumes of quartzitic gravel (now lithified conglomerate) associated with the Enon Formation (***Figure F-5.13.81***) in mountain eastward-draining river valleys occurred in response to the breakup of Gondwana. As the Gamtoos Valley widened and deepened, a river system with a gentler gradient occupied its confines and deposited river deposits of the Kirkwood Formation.

Enon Formation

The Enon Formation is the lowermost unit of the Uitenhage Group (***Figure F-5.13.81***) and consists of reddish brown to orange-yellow conglomerate with infrequent lenticular interbedded sandstone and mudstone. The conglomerate is comprised of large sub-rounded, discoidal to spherical quartzitic cobbles and pebbles tightly packed together with a silty/sandy matrix and red limonitic cement that acts as a cohesive agent for the entire formation (***Reference 5.13.161*** and ***Figure F5.13.92a***).

Exposures show that most clasts themselves are also coated with limonite (hematite and goethite), the presence of which is responsible for the colour variation within the formation. Clasts are derived from the arenaceous Table Mountain Group in the surrounding areas north of the Gamtoos Basin. The formation appears massive, but often shows imbricated and graded layers (***Reference 5.13.313*** and ***Figure F-5.13.92a***).

© Eskom 2026/Rev 0a

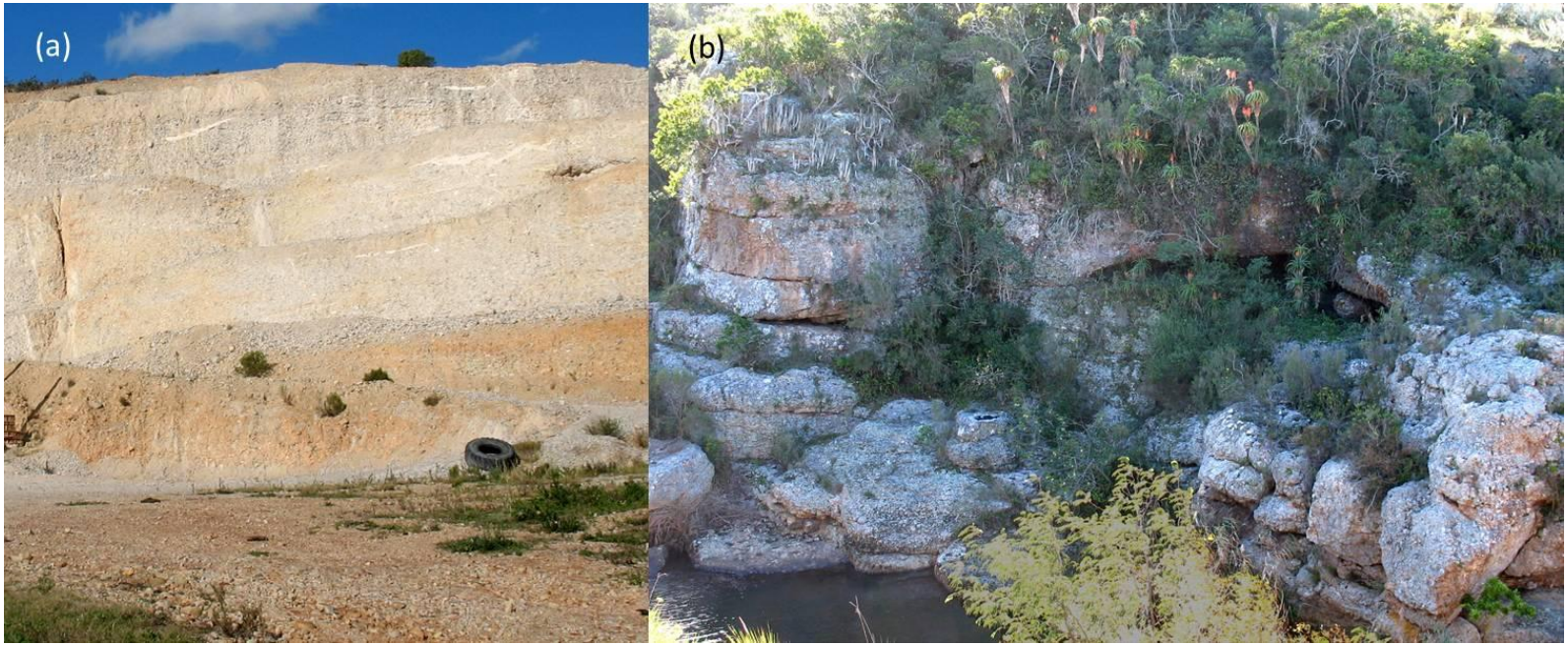


Figure 5.13-92
(a) Conglomerate and Sandstone Lenses of the Enon Formation Exposed in a Series of Benches at the Hankey Pass Quarry (33°52′ 09.6″ S, 24°51′ 12.3″ E). The Conglomerate Displays Crudely Graded Bedding.
(b) Conglomerate and Pebbly Sandstone of the Enon Formation Exposed Along the Kabeljous River Showing Shallow Cave Development due to Weathering of Poorly Consolidated Conglomerate (33°58′15.2″ S, 24°54′30.1″ E)

© Eskom 2026/Rev 0a

Formation thickness within the site vicinity is difficult to ascertain, but is known to exceed the 150 m documented at exposures. A borehole on the Mauritskraal farm situated near the coast within the Gamtoos Basin, showed the Enon Formation to be 1980 m thick (***Reference 5.13.75***).

Within the confines of the Gamtoos Basin the Enon Formation is exclusively underlain by Palaeozoic bedrock. The unconformable, gradual, and interfingering (***Reference 5.13.161***) contact zone between the Enon Formation and argillaceous rocks of the Ceres Subgroup is well exposed in the Hankey Pass west of Hankey. In addition, exceptional exposures of the Enon Formation occur in the Gamtoos valley between Hankey and Andrieskraal (***Reference 5.13.27***). Along the banks of the Kabeljous River cave development (***Figure F-5.13.92b***) and honeycombing of cliff-face exposures of the Enon Formation is quite prevalent as the result of weathering of conglomerate matrix and cement.

Kirkwood Formation

The Kirkwood Formation outcrops on the boundary margins of the site vicinity, near the Gamtoos River estuary. Here, the arenaceous Kirkwood Formation is composed of prominently cross-bedded and medium-grained, cream-coloured sandstone with interbedded siltstone and orange-red mudstone arranged in lenticular bedsets. Grey weathering, normally-graded conglomerate beds are infrequent and generally grade upward into interfingering sandstone (***Figure F-5.13.93 a&b***). Thickness of the formation near the site vicinity is unknown; however (***Reference 5.13.313***) indicates a 2000 m thickness in parts of the Algoa Basin.

Based on microfossil evidence, an Early Cretaceous age has been assigned to the Kirkwood Formation (***References 5.13.314*** and ***5.13.315***).

Grahamstown Formation

The Grahamstown Formation overlies Palaeozoic bedrock and is identified within the site vicinity as thin 1–3 m thick scattered remnants of grey, whitish-cream to yellow, light brown or red silcrete. The Formation is considered to represent remnant pediment surfaces that originally formed as more continuous broad pediplains in front of the mountains. The silcrete itself can be described as a siliceous accumulation of superficial or near-surface material consisting of various particle sizes and shapes and ranging from pieces of silcrete, gravel, and sand. Locally the silcrete exposures are generally smooth; however, its surface is frequently hummocky due to irregularly weathered pits (***Figure F-5.13.94***).

© Eskom 2026/Rev 0a

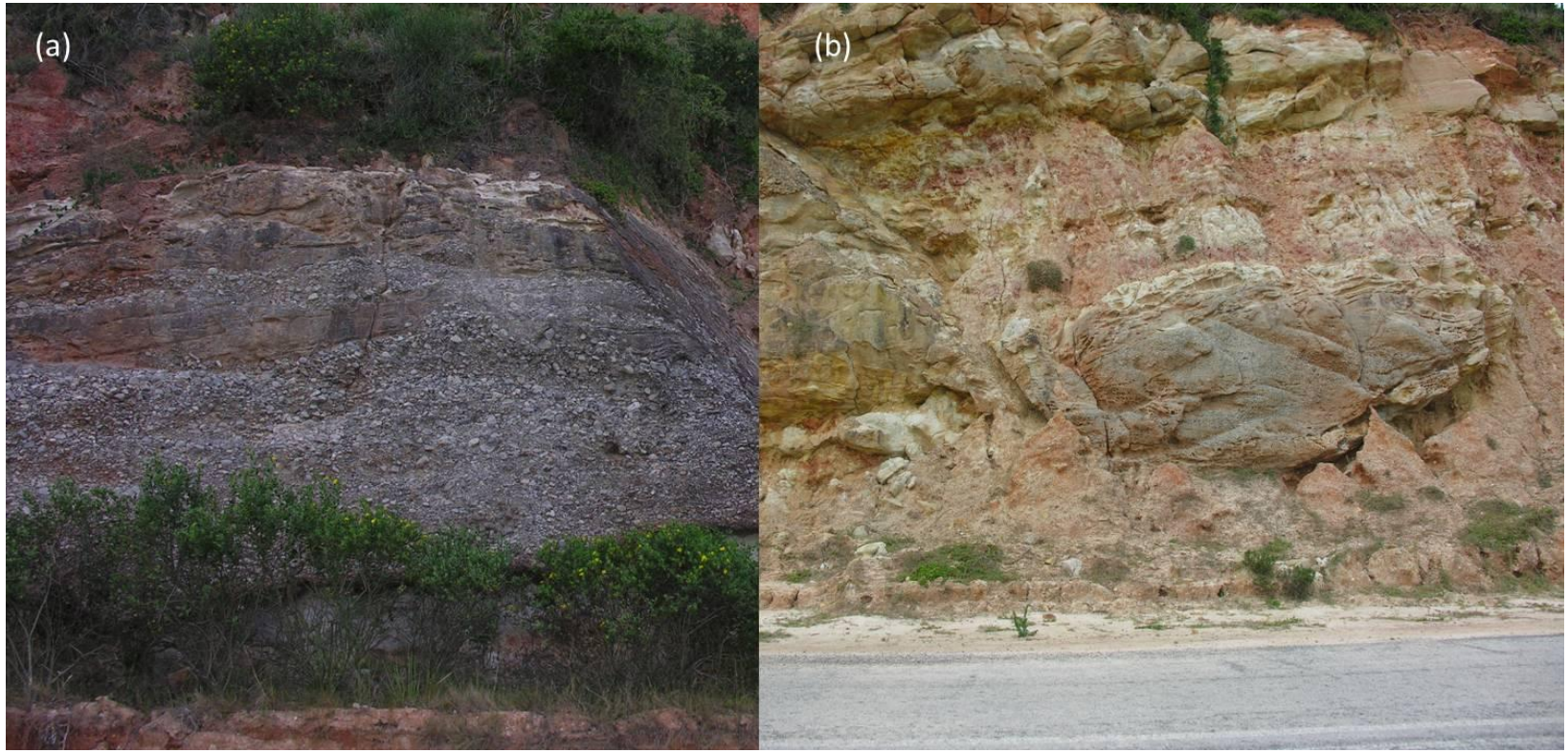


Figure 5.13-93
(a) A 4 m Exposure of Grey-Weathered Normally Graded Kirkwood Formation Conglomerate, Grading Upward into Interfingering Sandstone Located Near the Gamtoos River Estuary (33°54′ 22.7″ S, 25°01′ 22.1″ E).
(b) Weathered Orange-Red Mudstone and Cream-Coloured Sandstone of the Kirkwood Formation (33°54′ 17.9″ S, 25°01′ 20.9″ E)

© Eskom 2026/Rev 0a



Figure 5.13-94
Weathered, Pebbly, Ferruginous Silcrete of the Grahamstown Formation on the ThabaManzi Farm (33°57′44.3″ S, 24°34′17.9″ E)

© Eskom 2026/Rev 0a

The Grahamstown Formation (Tg) and underlying pediment surface at the bedrock alluvium contact are generally considered to be Miocene in age or older. Hagedorn (***Reference 5.13.92***) reports preliminary results of two electron spin resonance (ESR) tests that indicated ages of 7.3 and 9.4 Ma, respectively, for two samples of the silcrete caps on pediment remnants in the Little Karoo just north of the site vicinity. According to these ages, the pediments date from the upper Miocene, but they could be older if the planation was not synchronous with the silcretisations. Another unknown in inferring the age of the pediments is the time required for the formation of about 10 m thickness of the silcrete caps observed in this region.

Concentrations of beryllium-10 (^{10}Be) in outcropping boulders embedded in silcrete from the Tg surface can be interpreted as minimum limiting exposure ages or maximum limiting erosion rates. Cosmogenic nuclide (CN) analyses of boulders and clasts from unfaulted Tg surfaces overlying the Baviaanskloof, Kouga, and Western Coega faults northwest of the site vicinity, suggest that either these surfaces have been stable for relatively long periods of time (i.e., average minimum limiting ages of 1.0 Myr, 1.9 Myr, and 2.0 Myr, respectively) or maximum limiting erosion rates have been 0.11–3.2 m/Myr (median = 0.54 m/Myr; ***Reference 5.13.51***).

Algoa Group

Clastic nearshore-marine and coastal aeolian formations of the Late Cenozoic Algoa Group were deposited along coastal margins and toward the immediate hinterland. The formations within the Algoa Group are directly related to sediment supply associated with variations in sea level from the Eocene to present (***Reference 5.13.163*** and ***Figure F-5.13.81***). Where possible within the site vicinity, the Algoa Group was subdivided into its component formations. Where large tracts of coastal forest or extensive agricultural lands did not allow for sufficient exposure of individual formations, the Cenozoic sediments were mapped as 'undifferentiated Algoa Group' (***Figure F-5.13.81***).

The Algoa Group shows a clear trend in thickness distribution between Oyster Bay and Cape St Francis. Across the southern to northern extent of the mapped Algoa Group outcrop (***Reference 5.13.27***), borehole data (***References 5.13.28***, ***5.13.308***, ***5.13.316***, ***5.13.317***, ***5.13.318***, ***5.13.319***, ***5.13.60***, ***5.13.61***, ***5.13.62***, and ***5.13.58***) indicate that the thickness of sediments is zoned. The zonation is in part attributed to the Algoa Group's approximate distance from the present-day coastline and underlying landscape surface. Variation in lithological units of underlying Palaeozoic bedrock and the process of differential weathering within the palaeo-landscape influenced the uneven nature of the antecedent substrate. This trend in thickness in the site area is discussed further in ***Subsection 5.13.5.2.(b) ii***. A somewhat similar trend in

thickness distribution is observed in boreholes (***References 5.13.28***, ***5.13.308***, ***5.13.316***, ***5.13.317***, ***5.13.318***, and ***5.13.58***) near Cape St Francis and De Hoek (***Figure F-5.13.95***). These maximum thicknesses near Cape St Francis are associated with the presence of a palaeo-valley cut into incompetent Palaeozoic bedrock formations of the Goudini and Cedarberg Formations, as evident by bedrock elevation of as low as –11.52 m and –9.44 m below sea level (***Reference 5.13.58***). A similar trend in the thickness distribution of the Algoa Group sediments is expected to occur west of Oyster Bay, but due to limited borehole data this is only speculation.

Alexandria Formation

The Miocene- to Pliocene-aged sediments (***Reference 5.13.320***) of the Alexandria Formation rest unconformably on a narrow, planar, seaward sloping marine platform that is cut into older Palaeozoic or Mesozoic successions.

Sediments of the Alexandria Formation consist of calcareous sandstone, imbricated conglomerates composed of disc to roller shaped clasts in the pebble to large cobble size class within a fine-grained matrix and coquinite (***Reference 5.13.321***). The formation is typically up to 10 m thick, and preserved within the site vicinity as a thin veneer of discontinuous marine deposit (***Reference 5.13.322***) commonly overlain by palaeodunes of the Nanaga Formation (***Reference 5.13.323***).

The composition of the Alexandria Formation is largely dependent on underlying lithologies. The Formation can be considered calcareous where it is underlain by impermeable strata; however, within the site vicinity the substrate is porous in nature, and therefore the formation can be considered relatively noncalcareous (***Figure F-5.13.96b***; ***References 5.13.322***, ***5.13.324***, and ***5.13.27***).

Within the site vicinity, the Alexandria Formation is present as two types of deposit:

- Weathered residual consisting of thin, discontinuous veneer of conglomerate lags overlying the resistant Table Mountain Group. Goedhart & Hattingh (***Reference 5.13.275***) have ascribed weathered remnants of the formation to surficial pedogenic regolith (***Figure F-5.13.96a***).
    1. Thick conglomerate overlying the resistant Skurweberg and Peninsula Formations (***Figure F-5.13.96b***).

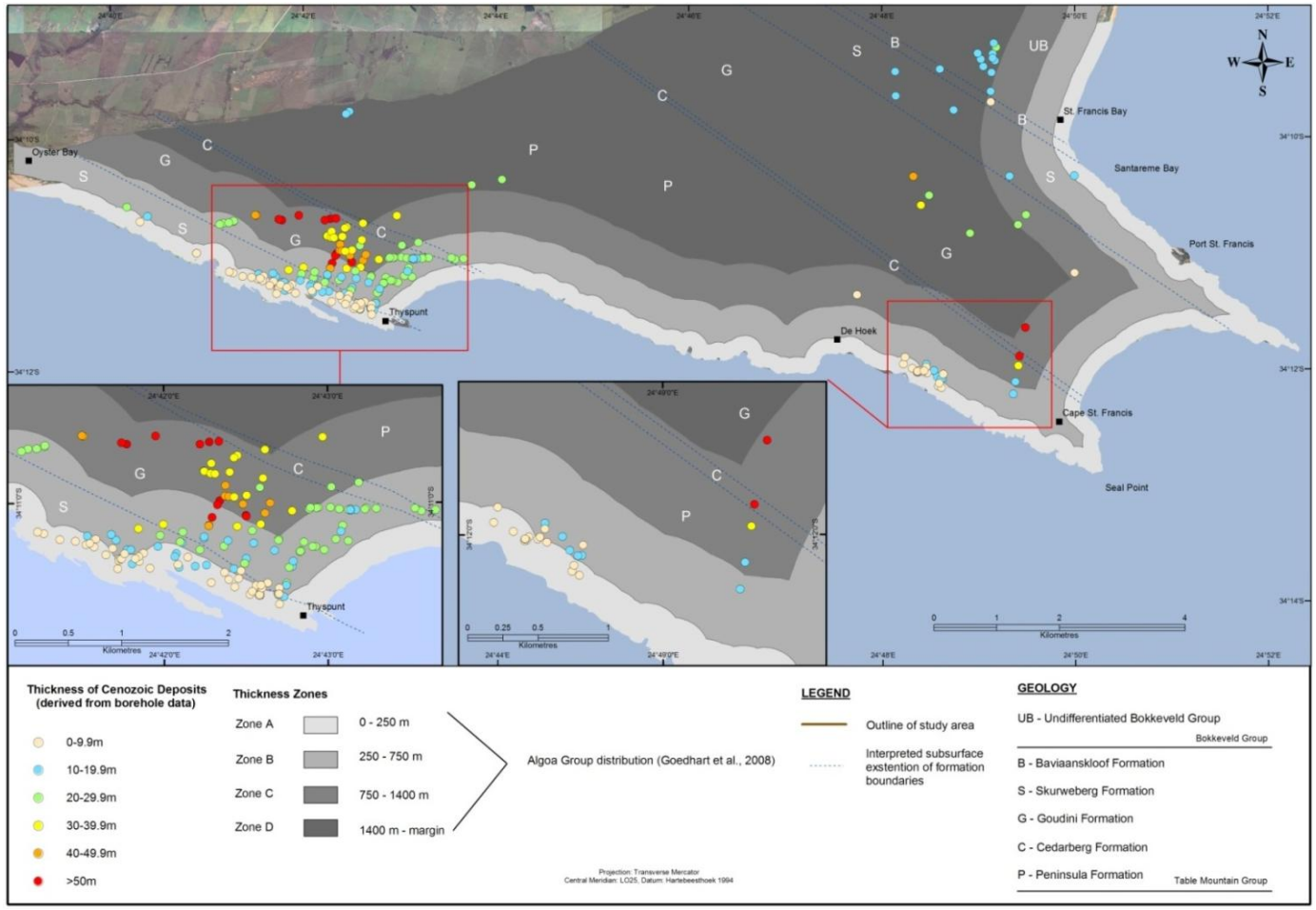


Figure 5.13-95
Cenozoic Overburden (Algoa Group) Thicknesses in the Thyspunt, De Hoek, Cape St Francis, and St Francis Areas Within the Site Vicinity

© Eskom 2026/Rev 0a

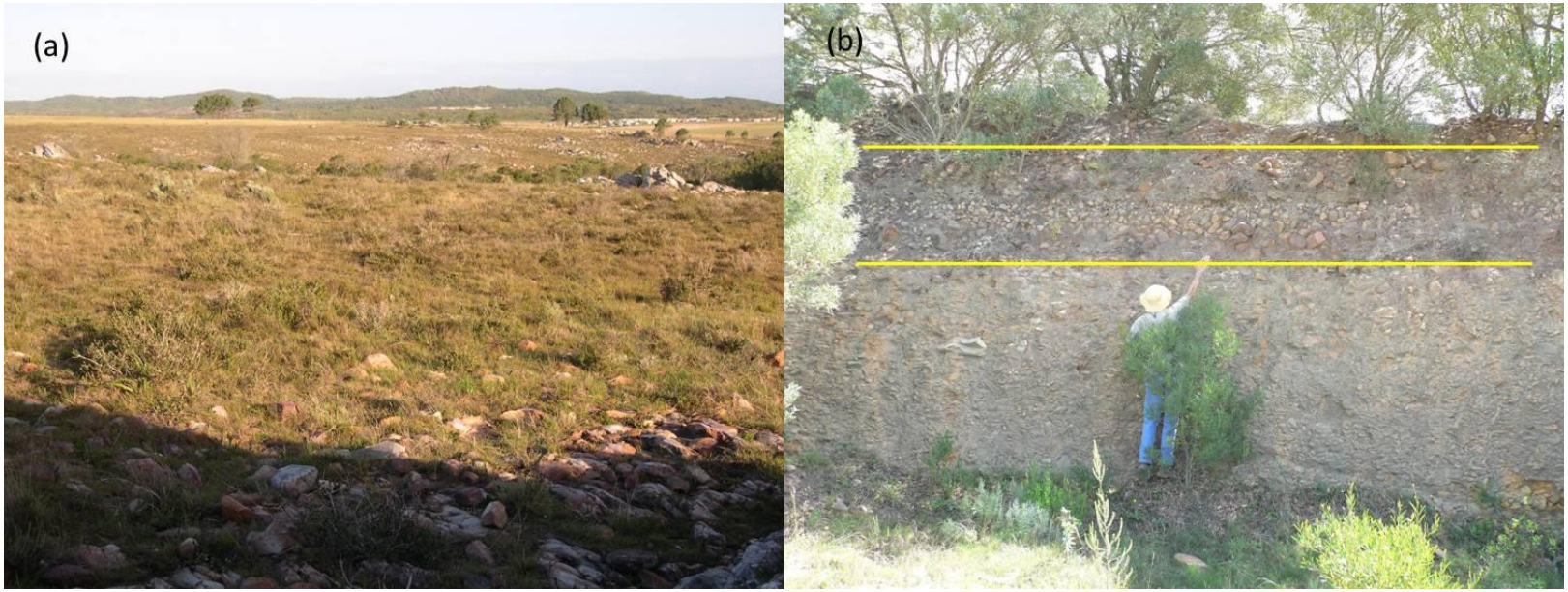


Figure 5.13-96
(a) Quartzitic Sandstone of the Peninsula Formation Overlain by a Thin Discontinuous Cobble Lag of the Alexandria Formation (seen in the foreground of the photo). Location of Photo: 34°09′ 06.6″ S, 24°39′ 31.8″ E).
(b) Deeply Weathered Conglomerate of the Alexandria Formation Exposed in a Quarry Located Northeast of Oyster Bay (34°07′ 48.0″ S, 24°42′ 47.4″ E)

© Eskom 2026/Rev 0a

Sedimentary structures such as horizontal lamination and low angle bedding, in conjunction with biogenic structures and fossil assemblages within the Alexandria Formation, indicate a range of marine depositional environments from upper shoreface to foreshore to lagoonal and/ or estuarine (***References 5.13.322*** and ***5.13.324***). Deposition of the Alexandria Formation occurred during regressive periods where shelly, sand-dominated sediments were deposited along the shore face on the coastal platform and during periods of stable seas where gravel-dominated sediments were deposited along linear slope breaks along the beach ridge shoreline.

These deposits have been correlated with similar deposits in the Western Cape and Kwa-Zulu Natal (***Reference 5.13.325***).

Nanaga Formation

The late Miocene to early Pliocene palaeodune deposits of the Nanaga Formation unconformably overlie the Alexandria Formation and form smooth, rounded hills with undulating ridges (***Reference 5.13.326***). Within the site vicinity the formation may be overlain by the younger aeolian Schelm Hoek Formation. Within the site vicinity the formation frequently attains a thickness of 50 m, and – exceptionally– a thickness of 100 m (***Reference 5.13.27***).

The Nanaga Formation is predominately comprised of fine-grained, well-sorted, grey-white to yellowish, predominantly calcareous sands that is largely unconsolidated, but also may be semi- to well-consolidated to form calcareous sandstone. This variation in consolidation is due to the mobility of calcium carbonate cement within these palaeodune deposits. In the upper portions of the formation, the original calcareous shell fragments have been leached by groundwater producing karst weathering and a red clay soil (***Reference 5.13.325***).

Large-scale aeolian planar cross-bedding is common in the formation and undulating topography is a typical geomorphic feature of the formation in the coastal hinterland. The formation may show signs of local weathering and redistribution. In places, surface calcrete is overlain by a grey to reddish-brown residual soil.

The Nanaga Formation on the 1:250 000 geological map of Port Elizabeth (***Reference 5.13.91***) lies in an area between Sandbaai and Slangbaai. Middle Pleistocene linear, 60–80 m high fossil dune ridges between Slangbaai and the Tsitsikamma River mouth have been described by Illenberger & Burkinshaw (***Reference 5.13.86***).

© Eskom 2026/Rev 0a

The aeolianites of the Nanaga Formation accumulated in coastal dunefields along late Cenozoic shorelines as coastlines receded; they become progressively younger from the inland margin of the palaeodune field toward the coast as a function of progradation on subsequent sea-level transgressions. These deposits can be traced along the southern African coastline (***References 5.13.325*** and ***5.13.153***).

Salnova Formation

The marine and estuarine deposits of the Salnova Formation are overlain either by recent windblown sands of the Schelm Hoek Formation (***Figure F-5.13.97***), the consolidated aeolianites of the Nahoon Formation, soil layers, or calcrete. The formation generally ranges in thickness from 1.5 m to 6.5 m and is characterised by a rich invertebrate fossil assemblage that gives the formation its 10–60 weight percentage of calcium carbonate. This high calcium carbonate content and the upper inland limit of occurrence of 18 m above sea level allows the formation to be distinguished from older deposits (***Reference 5.13.327***), while the absence of terrestrial deposits makes it distinguishable from younger overlying formations (***Reference 5.13.27***).

The late Pleistocene sediments of the Salnova Formation include fine- to coarse-grained calcareous sandstone, shelly limestone, and coquinite; or unconsolidated fine- to coarse-grained calcareous sand, gravel, coquina, and conglomerate (***Reference 5.13.327***).

The Salnova Formation is exposed to the west of Cape St Francis in a continuous pavement that is exposed in interdune hollows near the western edge of the bypass dune field (***Figure F-5.13.97***).

The Salnova Formation was deposited on a previous glacio-eustatic sea-level highstand and lies on wave-cut surface that truncates the underlying Palaeozoic units in the site vicinity (***Reference 5.13.27***). Although exposed as a discontinuous remnant on land (***References 5.13.323*** and ***5.13.325***), the formation is likely to be present in the offshore environment (***Reference 5.13.328***).

Nahoon Formation

The palaeodunes of the middle to late Pleistocene Nahoon Formation consist of well-consolidated dune rock (aeolianite) (***Figure F-5.13.98 a***) composed of calcareous sandstone, interbedded palaeosols, and isolated thin calcrete layers (***Reference 5.13.166***). The humic palaeosol component of the formation is semi-consolidated and varies in colour from greyish-yellow to light olive grey.

© Eskom 2026/Rev 0a



Figure 5.13-97
A Partial Remnant Exposure of the Salnova Formation Located in the Interdune Areas West of Cape St Francis Below 18 m asl (34°11′34.5″ S, 24°50′ 58.6″ E). Unconsolidated and Partially Vegetated Dunes of the Schelm Hoek Formation is Seen in the Background

© Eskom 2026/Rev 0a

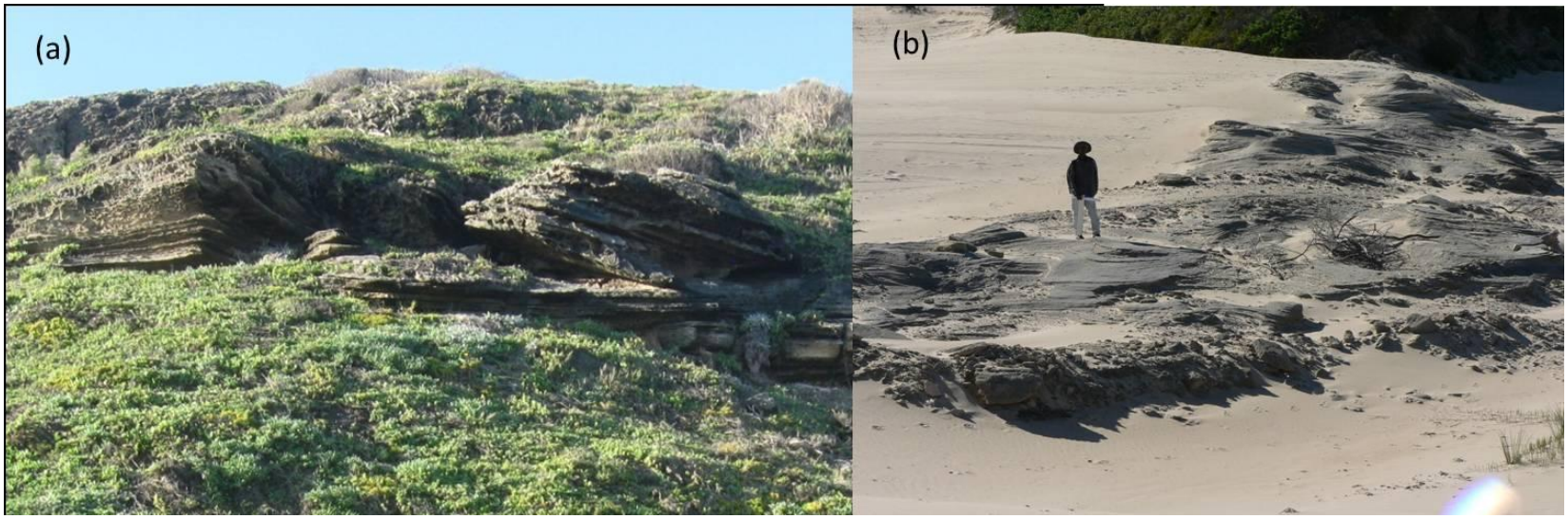


Figure 5.13-98
(a) An Exposure of Aeolianite of the Nahoon Formation near Oyster Bay.
(b) Aeolianite of the Nahoon Formation Exposed along the Western Edge of the St Francis Headland Bypass Dunefield, Mantled by Unconsolidated Mobile Sand of the Schelm Hoek Formation (34°11′31.5″ S, 24°51′10.9″ E). Photo Taken from the Database of Goedhart et al. (Reference 5.13.27)

© Eskom 2026/Rev 0a

The calcareous component varies in colour from grey-yellow to yellow-brown and is composed of fine- to medium-grained structureless or crossbedded dune sand. Ripple marks, disturbed bedding and slumping may be present locally (***Reference 5.13.166***).

The formation in the site vicinity varies in thickness from 6 m to 15 m and was formed in response to a sea level regression (***Reference 5.13.166***) and often underlies vegetated backshore dunes aligned obliquely to the present shoreline. The Nahoon Formation is visually distinct, but is largely obscured by soil horizons, calcrete and younger unconsolidated sand of the Schelm Hoek Formation (***Reference 5.13.27***).

In the site vicinity, the Nahoon Formation aeolianites form the core of the larger coastal dunes a few kilometres inland of Cape St Francis (***Reference 5.13.166***) Isolated remnant exposures of the formation are located adjacent to, and seaward of, the active dunes of the Schelm Hoek Formation (***Figure F-5.13.98 b***). Noticeable exposures occur near Oyster Bay and in an area surrounding the Tsitsikamma River mouth.

Large tracts of sandy seafloor exposed during a glacio-eustatic fall in sea level from the peak of the Last Interglacial were reworked by prevailing south westerly and south easterly winds that deposited the calcareous sands onshore. These coastal dunefields were deposited disconformably on the marine/ beach deposit of the Salnova Formation and unconformably on pre-Cenozoic strata (***Reference 5.13.166***); deposits later underwent cementation by calcareous recrystallisation. The Nahoon Formation is correlated with similar units in the Western Cape and KwaZulu Natal (***Reference 5.13.325***).

Schelm Hoek Formation

The Holocene deposits of the Schelm Hoek Formation disconformably overlie the Nahoon or Salnova Formations (***Reference 5.13.329***) and formations of the Table Mountain Group. The dunes of this formation are easily distinguished from the older, consolidated deposits and are composed of calcareous and unconsolidated aeolian sands (***Figure F-5.13.99 a***) derived from the adjacent sandy beaches and are contained within the Oyster Bay and Thys Bay coastal dunefields. Dunes on average attain a height of 30 m to 45 m and may contain midden horizons, poorly developed soils, palaeosols, and wetlands (***Figure F-5.13.99b***).

The dunes consist of fine-grained and well-sorted quartz grains, with a 20% to 40% calcareous component derived from shell fragments, foraminifera, echinoid spines, and isolated land snail shells. Wind ripples and high-angled planar aeolian cross bedding may be present (***Reference 5.13.174***).

© Eskom 2026/Rev 0a

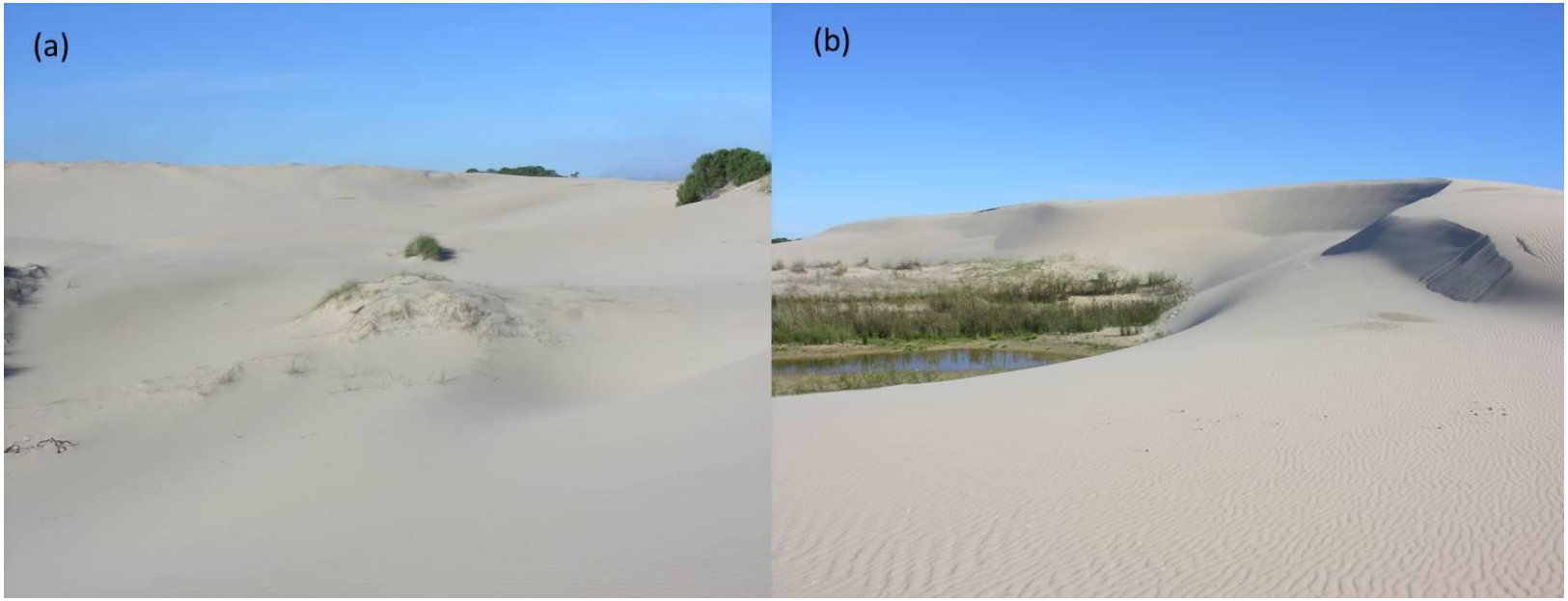


Figure 5.13-99
(a) Unconsolidated Mobile Dune Sand of the Schelm Hoek Formation that Form Part of the Oyster Bay Dunefield (34°10′14.1″ S, 24°44′11.0″ E).
(b) Ephemeral Wetlands are Common in the Thys Bay and Oyster Bay Dunefields, Forming in Between Dune Depressions or at the Base of Dune Slopes. Location of Photo: 34°10′20.2″ S, 24°44′16.0″ E

© Eskom 2026/Rev 0a

At Thyspunt, dunes of the Schelmhoek Formation occur up to 4 km inland where the oldest dunes are stabilised by a dense vegetation of eastern-Cape bush, shrubs, and fynbos (***Reference 5.13.28***). Although most dunes are vegetated, active sand accumulation and deposition continues (***References 5.13.329*** and ***5.13.27***). There are no identified actively migrating dunes close to the Thyspunt site.

Modern Beach Deposits

Longshore currents flow predominantly eastwards, but may vary locally around headlands due to wave refraction changing the wave propagation direction. The local interaction of the predominant southwesterly wind, wave sets, and currents in the nearshore and beach environment results in a complex assemblage of bedforms and sedimentary structures that include convolute lamination, near horizontal lamination, trough cross-bedding, trough cross-lamination, sale structures, and cross-bedding from berm overwash.

Within the site vicinity, the beach sediment consists of cobbles to boulders and medium- to coarse-grained sand (***Figure F-5.13.100a***). Within protected bays, the sand is well sorted and is composed of 60% to 70% quartz grains, 30% to 38% carbonate shell fragments and minor heavy minerals (***Figure F-5.13.100***). Quartzite gravel clast accumulations representing storm deposits occur on berms in the back beach area, while shell lag deposits occur in the swash zone. Thick storm beach deposits can be found along the Tsitsikamma coast northwest of Thyspunt (***Reference 5.13.27***).

The beach deposits are laterally interfingered with the estuarine deposits of the Gamtoos, Kabeljous, Seekoei, and Kromme Rivers (***References 5.13.330***, ***5.13.331***, ***5.13.332***, and ***5.13.333***). The deposition of sediment is largely influenced by the physical characteristic of these rivers. The mud-dominated Gamtoos estuary has a narrow intertidal zone; this is in contrast to the Kromme River estuary which has a well-developed intertidal flat area. The smaller Kabeljous River estuary is a periodically blocked inlet that is occasionally influenced by tides, while the Seekoei River estuary is highly disrupted (***References 5.13.330*** and ***5.13.331***). The result is that estuarine deposits within the sandy beach environments are highly variable.

Alluvium, River Terrace and Colluvium Deposits

Alluvial deposits comprise coarse-grained gravel and finer-grained sand and silt deposits. Gravel deposits consist of angular to rounded boulders, cobbles, or pebbles, or a combination of the above in areas proximal to areas of steep slopes. Sand, silt, and mud deposits are present in areas more distal to the stream source.

© Eskom 2026/Rev 0a

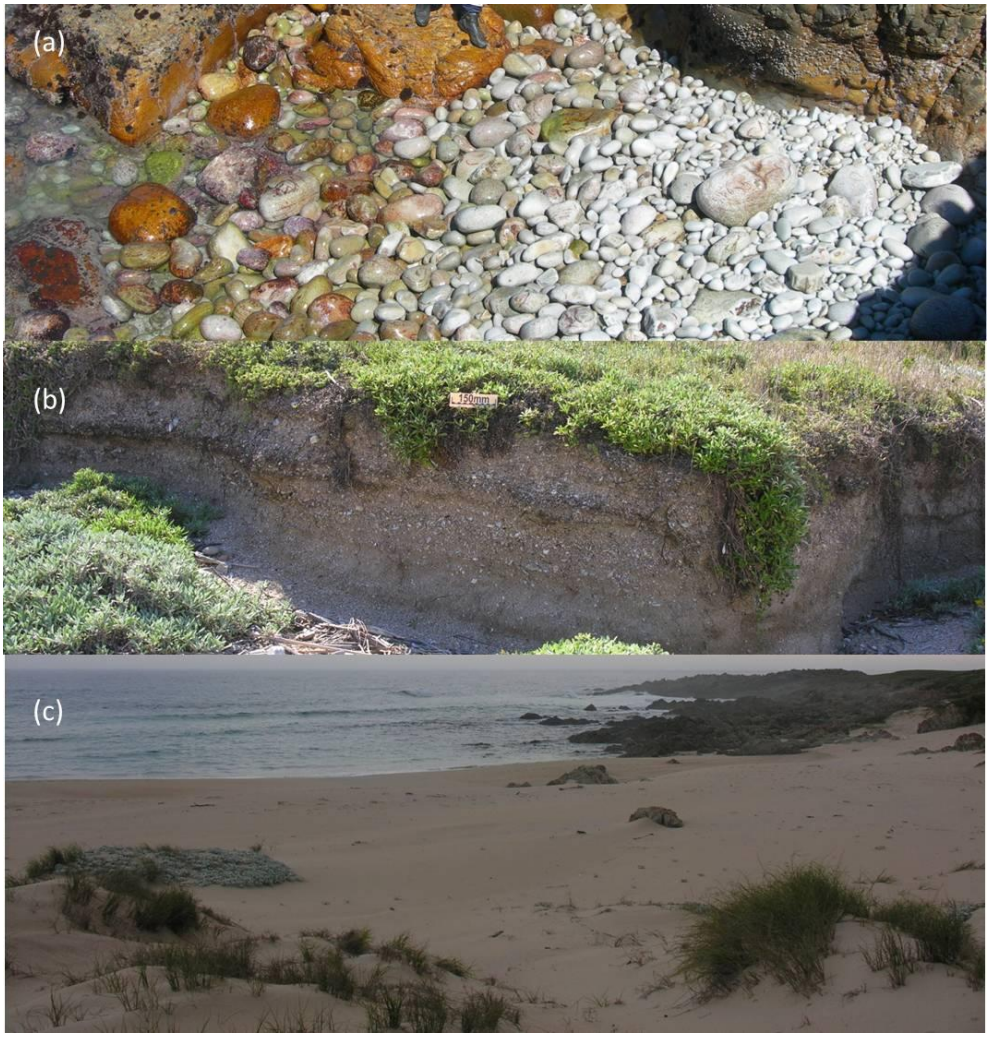


Figure 5.13-100
(a) A Coastal Inlet with Cobbles and Boulder Deposits, Near Cape St Francis. These Deposits are a Frequent Occurrence Northwest of Seal Point.
(b) Stratified, Shell Rich Beach Deposits of Granule Size Exposed in a Beach Terrace, Approximately 300 m From the Coastline and 3 km Northwest of Seal Point Lighthouse (34°11′26.3″ S, 24°45′01.1″ E).
(c) Unconsolidated Modern Beach Sands Deposited in an Embayment Southeast of Oyster Bay (34°10′59.7″ S, 24°41′08.4″ E)

© Eskom 2026/Rev 0a

These deposits may contain weakly developed and horizontally extensive pedogenic profiles (***Reference 5.13.332***). Major alluvial deposits occur in the Gamtoos Basin where the Gamtoos River has a meandering channel deeply eroded into a wide floodplain (***Reference 5.13.332***). Other minor alluvial accumulations in the site vicinity may be found at the Kabeljous River northeast of Jeffreys Bay and within minor streams.

Fluvial deposits associated with modern rivers vary between 2 m and 4 m thick (***Reference 5.13.27***) and in places appear to cover extensive areas of the lower Kromme Valley (***Figure F-5.13.101***).

Terraces in the lower Kromme Valley, as well as in the Klipdrift River and Slang River valleys, are sandy but do contain rounded and well-sorted small cobble- to large pebble-sized clasts. Deposits consist of predominantly unconsolidated medium- to fine-grained sand and silt units with subordinate gravel and coarse-grained sand layers. The primary depositional structure is planar bedding and shallow channel structures (***Reference 5.13.27***).

Colluvial sediments are derived from the forces of gravitation, soil wash and soil creep. Colluvium within the site vicinity is an incoherent, poorly sorted, structureless mass of unconsolidated rock debris consisting of boulder- to pebble-sized clasts of Skurweberg and Peninsula Formation quartzite and smaller sand to silt-sized particles. Well-rounded quartzite clasts of the Alexandria Formation may be present. The thickness of the colluvium within the site area is approximately 10 m to 15 m thick (***Reference 5.13.27***). The colluvium is generally unstratified, but where stratification is present it may be a result of interfingering of the colluvium with alluvium, piedmont gravels, and gravel deposits of older river terraces.

Pedogenic Deposits

Pedogenic horizons within the site vicinity include calcrete, tufa and silicified gravels. Soils in the site vicinity are predominantly calcareous although soft-plinthic ferricrete soil horizons may be present locally. A high level of silcrete also occurs.

© Eskom 2026/Rev 0a



Figure 5.13-101
Extensive Alluvial Deposits Along the Banks of the Lower Kromme River

© Eskom 2026/Rev 0a



Figure 5.13-102
A 3 m Thick Tufa Deposit West of De Hoek (34°10′59.7″ S, 24°41′08.4″ E). The Deposit is Located at the Interface Between the Palaeozoic and Cenozoic Strata

© Eskom 2026/Rev 0a

Calcrete and tufa (***Figure F-5.13.102***) occur mainly in the coastal region to the east of Thyspunt and is characterised by hard, irregular, sub-horizontal, calcareous laminae surrounded by crumbly chalky carbonate. The calcrete occurs either as nodules in the soil developed on the Uitenhage Group or as laterally extensive sheets beneath the soil covering Late Cenozoic Algoa Group sediments. The calcrete is formed by the evaporation of groundwater that carried calcium carbonate in solution from the underlying deposits. In places, calcrete formed near palaeodune surfaces or along bedding planes of large-scale cross-beds. Calcrete formation may still be active (***Reference 5.13.27***).

Scattered occurrences of approximately 0.5 m thick silicified gravel deposits may be found in the site vicinity. The gravels consist of indurated river gravel of pebble- to boulder-sized Peninsula Formation quartzite.

Iii Structural Geology

The structural geology of Palaeozoic rocks within the site vicinity is the result of northerly directed intercontinental compression associated with four paroxysm phases during the Permo-Triassic Cape Orogeny 280-230 Ma (***References 5.13.30*** and ***5.13.142***). The compressional events led to the northward-directed shortening of the basement and accompanying sedimentary rocks, which resulted in the development of folds, thrust, and décollement in the upper stratigraphic units (***References 5.13.101*** and ***5.13.334***) which can be observed in the site vicinity today (***Table T-5.13.8***). The deformation of the Cape Fold Belt ceased during the Triassic. Subsequent extension associated with the breakup of Gondwana, resulted in inversion of the compressional faults resulting in the development of large normal faults such as those responsible for the formation of the Gamtoos and Algoa Basins (***Reference 5.13.142***). Sea-level fluctuations from the Late Cretaceous to the present day resulted in the development of well-planed, seaward-sloping erosional platforms incised into Palaeozoic rocks, which formed a base for the deposition of clastic nearshore marine and coastal aeolian-derived deposits (***Reference 5.13.335***).

Refer to ***Figure F-5.13.103*** for structural features as mapped by Goedhart *et al.* (***Reference 5.13.27***).

Deformation effects as a result of the Permo-Triassic Cape Orogeny are greatest in the south and diminish northwards in the direction of the Karoo Basin. The lithological character of formations influenced deformation. Incompetent units, such as the Goudini or Baviaanskloof Formations, deform to produce mostly asymmetrical tight isoclinal folds; northward-verging, late-stage single folds with occasional conjugate kink folds. More competent formations such as the Peninsula and Skurweberg Formations develop thrust

© Eskom 2026/Rev 0a

faults. In addition, these competent units also frequently display tension gashes, typically rotated en-echelon along conjugate fracture sets (***References 5.13.30***, ***5.13.37***, ***5.13.26***, and ***5.13.27***).

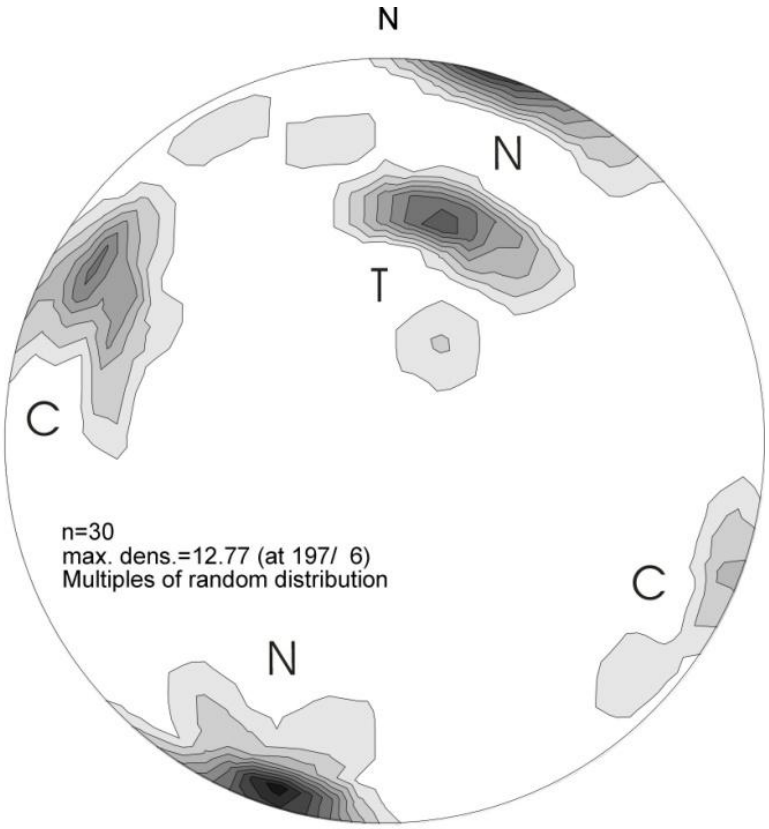


Figure 5.13-103
Distribution of Poles to Fault Planes Within the Site Vicinity
(*Reference 5.13.27*)

Table 5.13.8
The Four Compressional Paroxysms of the Permo-Triassic Cape Orogeny and Their Resultant Effect on Strata (Modified from *References 5.13.101*, *5.13.336*, and *5.13.337*)

Event & Time	Type of Deformation	Resultant Deformation from Event
First Paroxysm ± 278 Ma	Folding	● Major mechanism of deformation is flexure slip folding ● Asymmetrical folding
	Cleavage	● S_1 cleavage development
Second Paroxysm ± 258 Ma	Folding	● Isoclinal, almost recumbent folds
	Cleavage	● S_2 cleavage develops
Third Paroxysm ± 247 Ma	Folding	● Refolding of asymmetrical folds
	Faults	● Development of thrusts
	Cleavage	● S_3 cleavage develops
Fourth Paroxysm ± 230 Ma	Folding	● Listric folding ● Kink bands develop
	Faults	● Listric thrusting ● Minor shears
	Cleavage	● Fanning axial plane solution cleavage

Faulting

Norman *et al.* (***Reference 5.13.338***), Raubenheimer *et al.* (***Reference 5.13.28***), and Goedhart *et al.* (***Reference 5.13.27***) recognised and documented a variety of faults within the site vicinity:

- *High-angle cross-faults*: North-northeast/south-southwest- to northeast-southwest-trending faults that dip steeply towards the southeast and show a small variation in strike and dip. Downward displacement is both to the southeast and northwest and consequently produces small horst-and-graben structures. These faults tend to be localised and short in length and appear to have been formed either to accommodate undulations and competency along fold lengths during their formation or by later oblique extension related to Mesozoic extension (***Reference 5.13.27***).

© Eskom 2026/Rev 0a

- *Strike faults*: Northwest-southeast-trending faults that are near-vertical to steeply dipping and frequently have a down-to-the-south sense of displacement. These are the dominant type of faults within the site vicinity.
- *Thrust faults*: Northwest-southeast-striking thrust faults generally form parallel to the bedding of the titled Cape Supergroup and show a strong association with bedding-parallel normal faults (***Reference 5.13.27***).

Normal Faulting

The most prominent onland fracture zone associated with normal faulting within the site vicinity, the 'Klippepunt Fault', is situated 6 km west of Thyspunt and passes 2.5 km south of Thyspunt in the offshore. The fracture zone was identified by AEC investigators (***References 5.13.33***, ***5.13.21***, ***5.13.22***, and ***5.13.338***) and was initially described as a northwest-southeast-striking approximately 200 m wide and 80 km long fault which shows apparent rotation along its fault plane. The fracture zone was then interpreted to be connected to the Trawler-Bay and Huisklip fracture zones and in addition was interpreted to continue offshore along a south-eastward trend, joining the Cape St Francis fault family much further offshore. This conclusion was based on interpretation of a medium sensitivity aeromagnetic survey (***References 5.13.33*** and ***5.13.34***) and the presence of breccia in drill core (***References 5.13.28*** and ***5.13.308***).

Detailed re-investigation (***References 5.13.30***, ***5.13.35***, ***5.13.36***, ***5.13.26***, and ***5.13.46***) of the interpreted Klippepunt fault, in particular along its southern onshore margin (***Reference 5.13.27***), led to a reinterpretation of the fracture zone. Evidence collected along the highly structurally deformed zone favours the presence of an overturned (***Figure F-5.13.104***), tight non-coaxial anticlinal fold that developed in the northern root zone of a large recumbent fold rather than a fault zone. Breccia documented in borehole core (***Reference 5.13.28***) and observed during field investigations (***Reference 5.13.27***) is associated with isolated shearing that appears to run southwards and south-westwards into thrust faulted bedding across the steeply overturned (***Figure F-5.13.105 a &b***) westward-plunging fold hinge. Goedhart *et al.* (***Reference 5.13.27***) described these crushed zones within the Skurweberg Formation as narrow discontinuous en-echelon breccia lenses (***Figure F-5.13.106 a &b***) of >1 m to 9 m wide. Deformation of the area is intensified by the presence of pervasive axial planar cleavage and jointing (***Figure F-5.13.107***).

The offshore occurrence of the Klippepunt fracture zone was investigated by Horwood (***Reference 5.13.46***); he could find no conclusive evidence for a fault zone at Klippepunt.

© Eskom 2026/Rev 0a

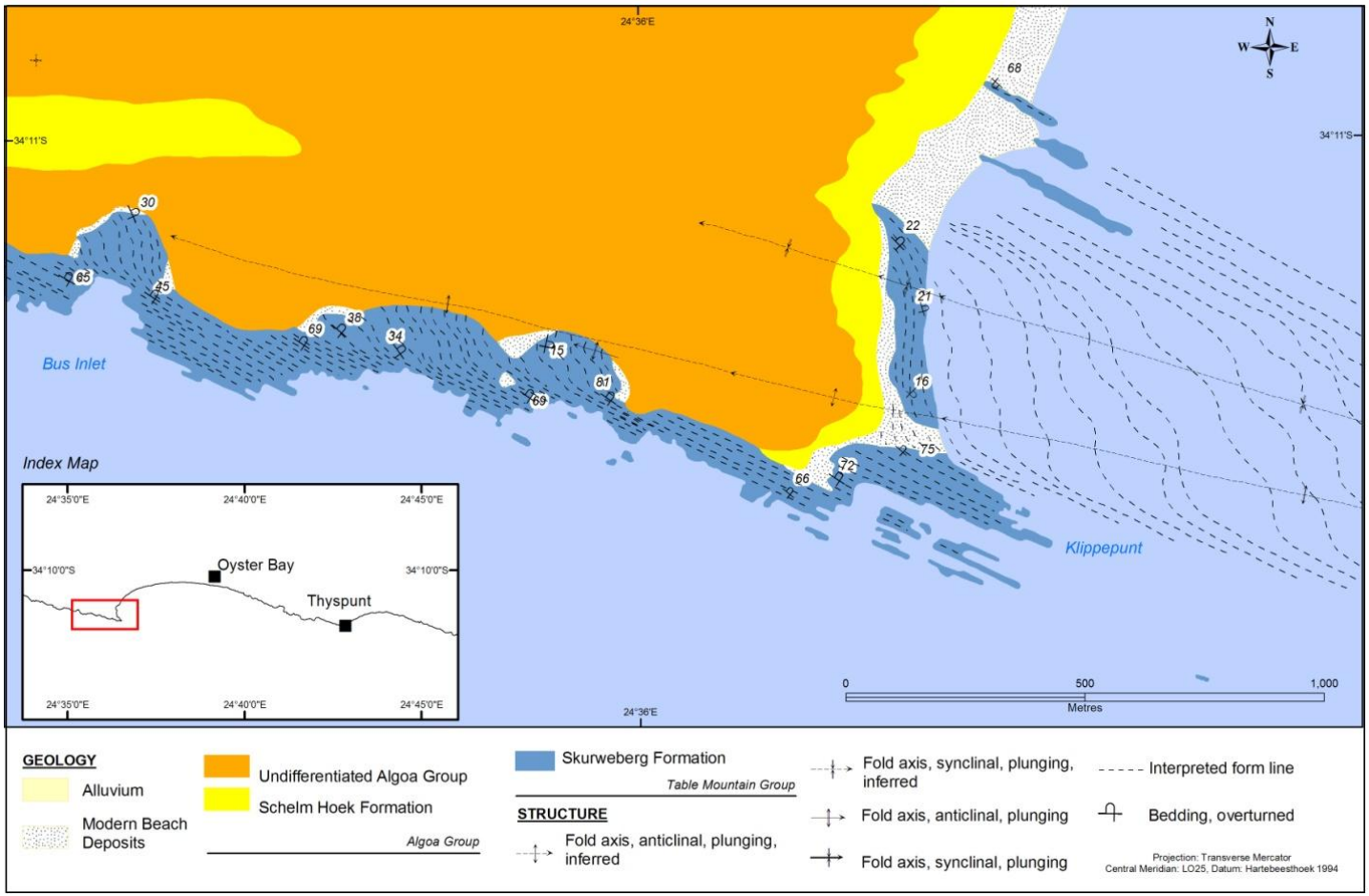


Figure 5.13-104
Structural Interpretation of the Klippepunt Area (Modified from *Reference 5.13.27*)

© Eskom 2026/Rev 0a

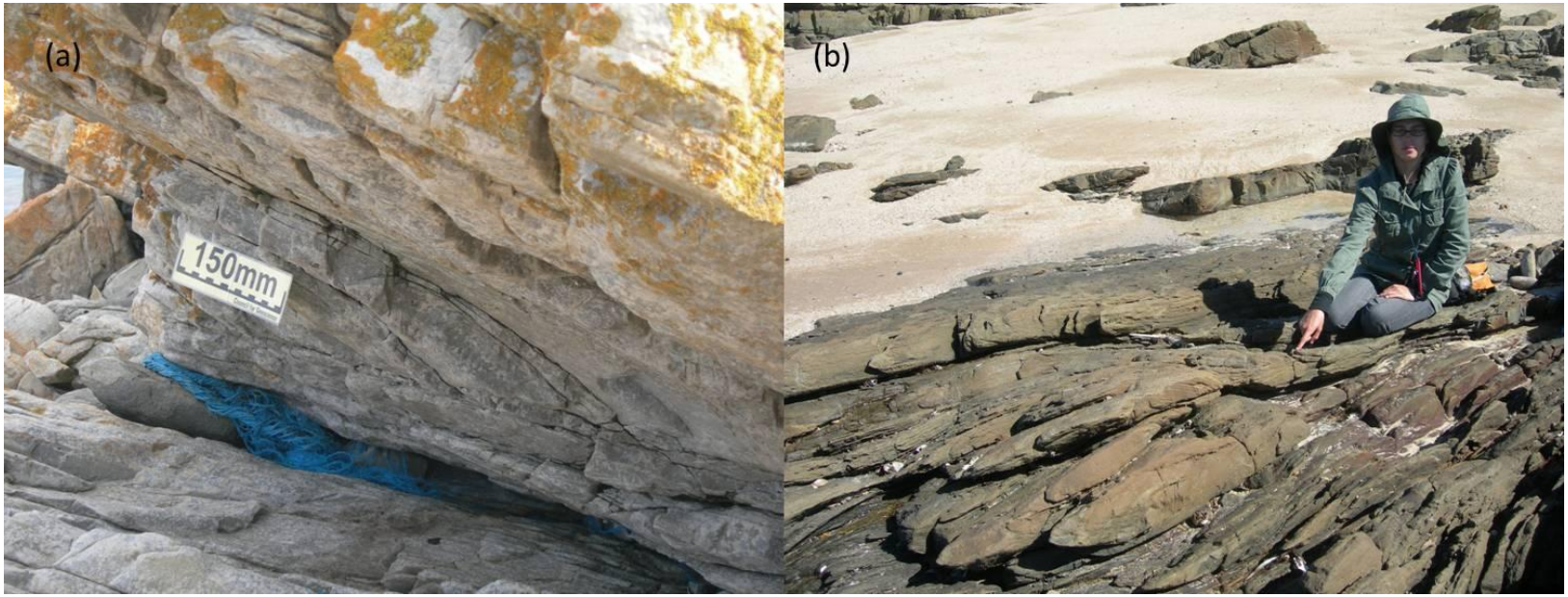


Figure 5.13-105
(a) Overturned Convex Cross-Beds in Quartzitic Sandstone of the Skurweberg Formation Immediately West of Klippepunt (34°11′12.3″, 24°35′45.1″).
(b) Overturned Convex Shallow Channel in Sandstone of the Baviaanskloof Formation (34°11′07.2″, 24°36′21.3″)

© Eskom 2026/Rev 0a



Figure 5.13-106
(a) A 3 m Wide Crushed Lens of Overturned Skurweberg Formation Quartzite West of Klippepunt; View Is Eastwards (34°11′15.4″, 24°35′47.1″).
(b) A View West of the Same Crushed Lens Seen in Figure (a), Showing a Yellow-Brown Mylonised Brecciated Lens (Indicated by the Yellow Line)

© Eskom 2026/Rev 0a



Figure 5.13-107
Intensely Fractured Skurweberg Formation Showing Pervasive Axial Planar Cleavage and Jointing Situated Between Two Adjacent Less-Fractured Beds Northwest of Klippepunt (34°11′14.8″, 24°35′44.1″)

© Eskom 2026/Rev 0a

The sequence of deformation that led to the Klippepunt's structural characteristics is outlined by Goedhart *et al.* (***Reference 5.13.27***) as follows:

- Regional folding and overturned bedding; followed or accompanied by ***Figure F-5.13.105 a &b***.
- Low-angle bedding-parallel to sub-parallel northward-directed thrusting.
- Secondary folding that rippled the thrust planes.
- Fold tightening and intense shearing, some of which traversed the bedding-parallel thrusts at a high angle, but which also flatten along their length to run laterally north-westwards into shattered bedding to produce isolated en-echelon shear or brecciated zones (***Figure F-5.13.106 a &b***) not related to Mesozoic right-lateral strike-slip faulting (***Reference 5.13.22***).
- In a last phase of deformation, a late compressional stage produced cross-cutting conjugate sets of joints and en-echelon tension gashes.

A series of north-northeast-trending high-angle faults are indicated on Atomic Energy Corporation (AEC) maps (***References 5.13.28***, ***5.13.308***, and ***5.13.34***) in the Thyspunt and Cape St Francis areas. Their apparent presence was inferred from a broad-resolution airborne geophysical study (***Reference 5.13.34***), but were not included on their site location maps of Cape St Francis and De Hoek areas.

The validity of these faults was investigated by Goedhart *et al.* (***Reference 5.13.27***) who described the presence of these faults as "problematic". The presence of these faults could not be verified in the field or by high-resolution geophysical surveys (***References 5.13.35*** and ***5.13.40***). The offshore portion of the faults could not be confirmed by Davidson & Smith (***Reference 5.13.281***) as it does not include the De Hoek area. A more recent review of borehole data (***References 5.13.28***, ***5.13.316***, ***5.13.317***, ***5.13.318***, ***5.13.319***, ***5.13.60***, and ***5.13.61***) only indicate the interception of highly fractured, but not brecciated strata that is more likely associated with high-frequency jointing areas or shatter zones (***References 5.13.28*** and ***5.13.27***), rather than faulting.

Thrust Faulting

Within the site vicinity, the most prominent interpreted thrust faulting initially described to occur as a series of interconnected northwest-southeast coastline-parallel-trending thrusts, west of Oyster Bay between Klippepunt and the Tsitsikamma River mouth (***References 5.13.339***, ***5.13.340***, ***5.13.23***, ***5.13.22***, ***5.13.338***, ***5.13.21***, and ***F-5.13.108***) were reinvestigated by Goedhart *et al.* (***Reference 5.13.27***) in an attempt to determine the validity of their presence. The presence of these thrusts was interpreted based on a medium sensitivity

© Eskom 2026/Rev 0a

aeromagnetic survey (***Reference 5.13.33***) and only very limited field work. Ascertaining the occurrence and extent of these thrusts is difficult because of limited exposure along coastal margins, which are predominately covered by thick Cenozoic overburden that extends up to 8 km into the hinterland. In addition, high-resolution aeromagnetics was not able to confirm thrust faulting (***Reference 5.13.35***).

The most westerly reported thrust fault within the site vicinity, the Tsitsikamma River mouth thrust (***Figure F-5.13.108***) or Huisklip Fault, is interpreted (***Reference 5.13.27***) to be an out-of-limb thrust fault, produced from an overturned north-verging syncline in the incompetent Goudini Formation. The fold is situated at the northern extent of a series of tightly overturned anticlines and synclines that were compressed from southwest to northeast against and perhaps partly over the hinge area of the underlying southeast-plunging anticline, exposed at the Tsitsikamma River mouth.

The presence of the Tsitsikamma River mouth thrust is confirmed by a 20 m wide crushed zone and a 2–5 m brecciated horizon at the mouth of the Tsitsikamma River (***Figure F-5.13.109*** and ***Reference 5.13.27***). The thrust is inferred to continue offshore northwest along the coast to pass along the southwest flank of a large anticline exposed in the surf zone near the river mouth. Its eastward extent under thick Cenozoic dune over could not be determined in the field or by high-resolution aeromagnetics (***Reference 5.13.35***).

Along coastal exposures west of the Thyspunt Site Area, but east of Morgan's Bay, the Wreck Point thrust was interpreted to occur at the contact between the steeply south-dipping overturned Skurweberg Formation to the north and the moderately northward-dipping underlying Goudini Formation to the south (***Reference 5.13.27***). Small isolated intraformational zones of crushed rock, described as breccia (***References 5.13.339*** and ***5.13.340***), were indicated at the base of the Skurweberg Formation near the Wreck Point thrust fault and interpreted by Goedhart *et al.* (***Reference 5.13.27***) to be associated with either a local competency contrast in bedding, another possible small thrust fault, or a local compressional fault along a locally dominated joint direction (***Reference 5.13.27***).

Goedhart *et al.* (***Reference 5.13.27***) did not exclude the possibility that the interpreted Wreck Point thrust fault may be connected to the Tsitsikamma River mouth thrust at the inferred contact between the above mentioned formations.

© Eskom 2026/Rev 0a

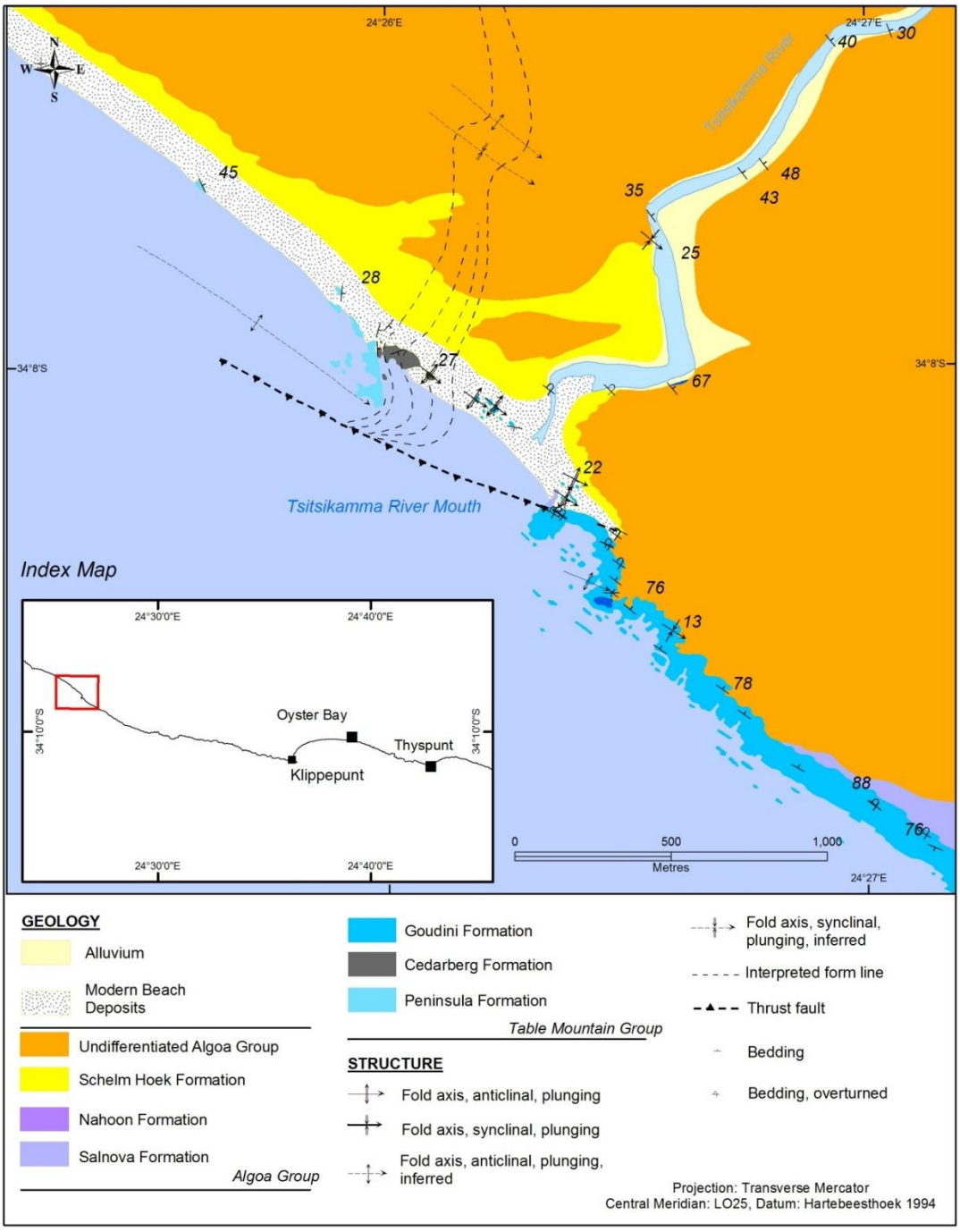


Figure 5.13-108
Interpreted Location of the Tsitsikamma Thrust Fault, near the Tsitsikamma River Mouth (Modified from *Reference 5.13.27*)



Figure 5.13-109
A 2 m Wide Breccia Horizon, Partly Overlain by Boulders Indicating the Tsitsikamma River Mouth Fault as Viewed Due East. The Breccia Horizon Is Bounded by Tightly Folded Overturned Goudini Formation at Angles That Changes Abruptly to Open Folded East-Southeast and Southeast-Dipping Beds on the Nose of the Broad Anticline (*Reference 5.13.27*; 34°08′15.5″, 24°26′21.9″)

The structural feature is interpreted to have formed during the time of Cape Fold Belt deformation and not from deformation associated with movement along the Agulhas Fault Fracture Zone. The location of these and other thrusts within the area beneath Cenozoic cover is speculative and could not be confirmed by high-resolution aeromagnetics (***Reference 5.13.35***).

The AEC Trawler Bay fault system as described by Norman *et al.* (***References 5.13.23*** and ***5.13.22***) was inferred to occur to the west of Klippepunt based on a becciated zone, midway between the latter promontory

© Eskom 2026/Rev 0a

and Morgan's Bay and reportedly outcrop in an inter-tidal zone near Trawler Bay. This position contrasts with that of Van Wyk (***Reference 5.13.21***), who inferred it to occur 500 m north of the bay. Norman et al. (***Reference 5.13.23***) conceded that the zones of shattered rocks do not equal those seen at Klippepunt and that no lateral tangential vector component occurs on the fault. Goedhart *et al.* (***Reference 5.13.27***) investigated the validity of these faults and could not confirm their presence along coastal exposes, whilst stating that tidal reach may not have been low enough at the time to confirm the presence of the these faults.

Mesozoic Faulting

In the north-eastern area of the site vicinity, the Jurassic Kirkwood and Enon Formations were deposited in the 80 km wide Mesozoic Gamtoos Basin bounded to the east by the spoon-shaped half-graben Gamtoos Fault with a southerly downthrow of several kilometres (***Reference 5.13.142***). Both the Kirkwood and Enon Formations display several minor intraformational northwest-southwest- and east-west-trending faults exposed in a road cut, approximately 2 km from the Gamtoos River estuary on the road (***Figure F-5.13.110 a&b***) between Humansdorp and Hankey (***References 5.13.24*** and ***5.13.27***). Along this section of the road, tan-coloured sandstone interbedded with pale mudstone lie in faulted contact with red sandstone (***Figure F-5.13.110a***). A faulted 3 m conglomerate bed is also documented along this road cut (***Figure F-5.13.110b***). Faults show a 45–75 degree inclination. Faulting took place after the formation had undergone diagenesis, but no faults within the Gamtoos Basin are documented to pass upwards into, or displace, younger overlying Cenozoic deposits that cap these Mesozoic outcrops (***References 5.13.23*** and ***5.13.27***). In addition, the Gamtoos Fault in general is regarded as a fault that has not been active since latest Cenozoic times (***Reference 5.13.24***), not affecting sediments younger than middle Tertiary age (***Reference 5.13.341***).

© Eskom 2026/Rev 0a



Figure 5.13-110
(a) A 4 m Exposure of the Kirkwood Formation Showing a Faulted Contact Between Orange-Red Mudstone Interbedded with Isolated Sandstone and Grey Weathering Conglomerate (33°54′22.7″, 25°01′22.1″).
(b) A 3 m Exposure of the Kirkwood Formation Showing a Faulted Contact Between Orange-Red Mudstone and Tan-Coloured Sandstone (33°54′28.0″, 25°01′24.4″)

© Eskom 2026/Rev 0a

Fold Trends

Folding within the site vicinity is the result of northerly directed compression associated with four phases of paroxysm during the Permo-Triassic Cape Orogeny, which led to the development of folds with generally asymmetrical northeast-verging folding and décollement occurring in the upper stratigraphic units (***References 5.13.101*** and ***5.13.334***). The upper hinge areas are often dragged over northwards to form upward north-curving axial planes (***References 5.13.101*** and ***5.13.334***). Within the site vicinity fold axes are northwest-southeast-striking, parallel to the bedding trend (***Figure F-5.13.111a***) with a dominant southeast plunge direction and a subordinate northwest plunge direction (***Figure F-5.13.111b***), often reflected as double-plunging (***Reference 5.13.27***) indicative of cross-folding. The amplitude and wavelength of folds are linked to the competency and bed thicknesses of the various formations. Incompetent plastic formations, such as the Goudini, Cedarberg, Baviaanskloof, and Gydo Formations, tend to produce asymmetrical to tight isoclinal folds that are smaller in size and more closely spaced, which in turn leads to the formation of intense cleavage, substantial shortening, and volume reduction. This is clearly seen in strata of the Baviaanskloof Formation in the areas north of Jeffrey's Bay and northwest of Humansdorp. The incompetent Cedarberg Formation forms a structurally favourable detachment zone along the limbs of large folds, especially in the northern regions of the site vicinity and is thus frequently smeared out, absent or preserved in tight fold noses. Competent, brittle units such as the Skurweberg and Peninsula Formations are more likely to produce large-scale broad and open folds (***Figure F-5.13.112 a&b***) and thrust faults. Slip along bedding planes (***Figure F-5.13.113 a&b***), together with possible stacking of bedding planes along small thrust ramps are thought to have facilitated differential movement during folding.

Large regional synclines and anticlines can be described as anticlinoriums or synclinoriums, showing numerous smaller secondary folds on its flanks (***Reference 5.13.27***). These folds reflect a gentle curvature of folds along strike, bounded by more steeply dipping bedding. Goedhart *et al.* (***Reference 5.13.27***) described the presence of low-lying undulations along the broad hinge zones that are localised zones of more intense jointing, which are often associated with small dislocations that are representative of the various lithological competencies.

Apart from the coaxial folding described above, infrequent non-coaxial and kink folding was also observed within the site vicinity, but on a much smaller scale (***Figure F-5.13.114 a&b***). Tight non-coaxial folding occurs in exposures of the

© Eskom 2026/Rev 0a

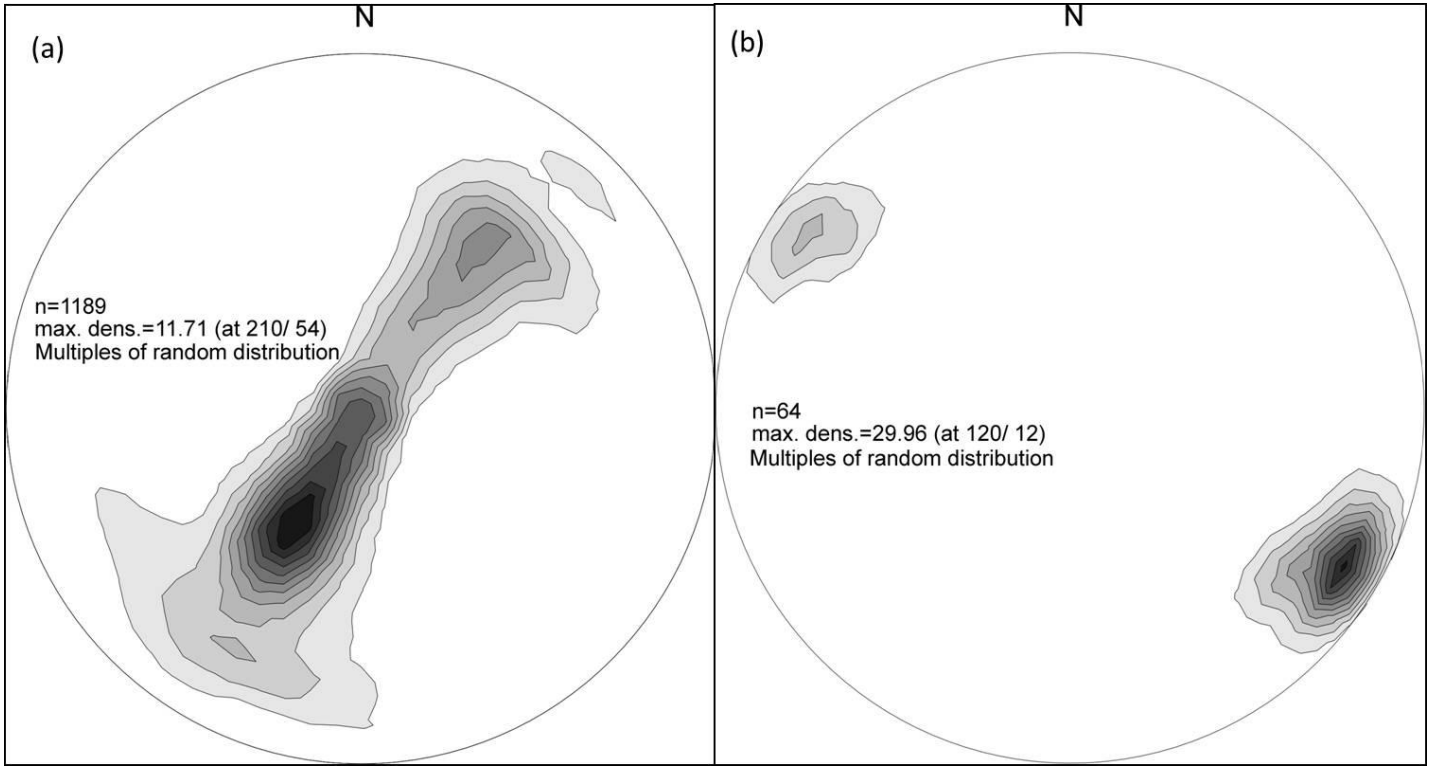


Figure 5.13-111
(a) Stereonet Showing Poles to Palaeozoic Bedding Within the Site Vicinity; The Folded Nature of the Bedrock Rocks Is Clearly Reflected (*Reference 5.13.27*).
(b) Stereonet of Fold Axes Documented Within the Site Vicinity. A Dominant Shallow Southeast Plunge and a Subordinate Shallow Northwest Plunge Direction Is Recorded and Reflects the Presence of Double Plunging Folding (*Reference 5.13.27*)

© Eskom 2026/Rev 0a



Figure 5.13-112
(a) A Low-Amplitude Anticline in Incompetent Quartzitic Sandstone of the Peninsula Formation Exposed Northwest of De Hoek Along Coastal Exposures (34°11′47.1″, 24°46′35.3″).
(b) An Overturned North-Verging Fold, in Sandstone of the Table Mountain Group, near Churchill Dam (34°00′02.3″, 24°29′40.3″)

© Eskom 2026/Rev 0a

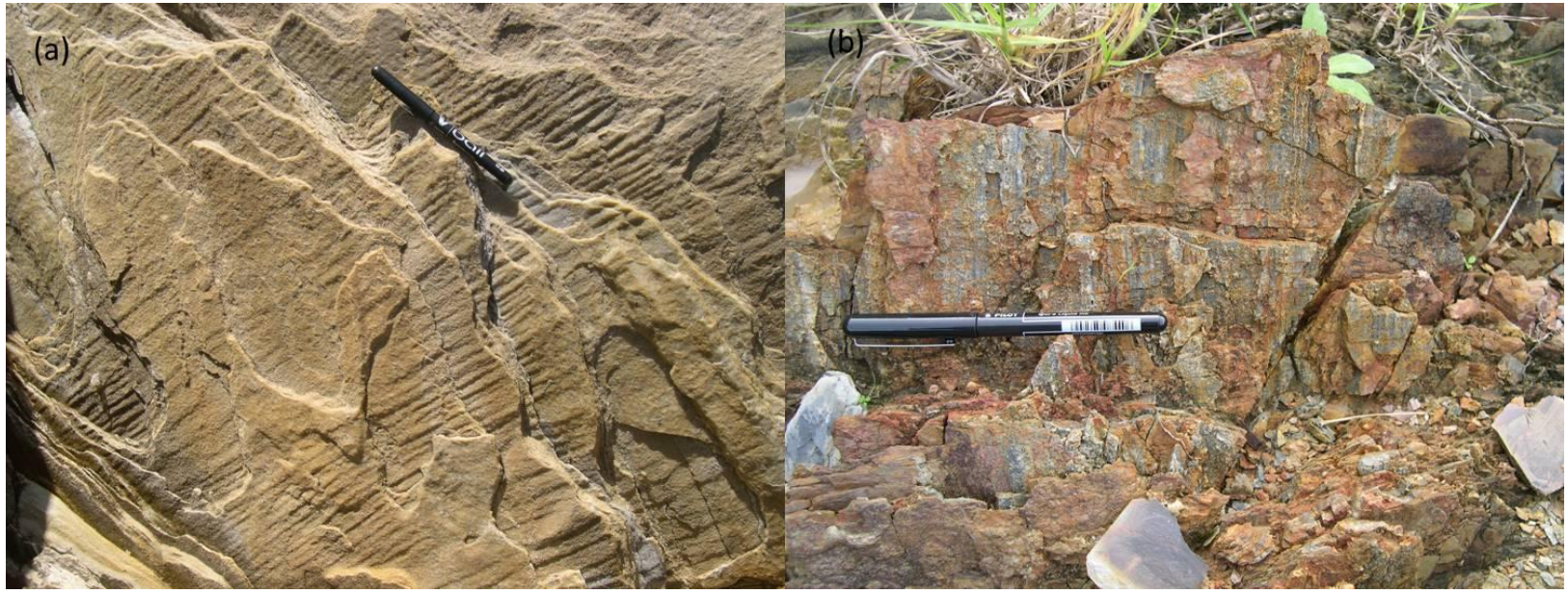


Figure 5.13-113
(a) Slickensides Along Quartzitic Sandstone of the Peninsula Formation Bedding Planes West of Thys Bay (34°11′16.9″, 24°44′23.0″).
(b) Slickensides Along Bedding Planes in Strata of the Undifferentiated Bokkeveld Group 7 km Northwest of Paradise Beach. These Slickensides Are Indicative of Movement Along Bedding Planes to Facilitate Folding (34°04′34.9″, 24°49′19.4″)

© Eskom 2026/Rev 0a



Figure 5.13-114
(a) Kink Folding Observed in a Sandstone Exposure of the Goudini Formation on the Northern Flank of an Overturned North-Verging Anticline Along the Banks of the Tsitsikamma River (34°07′47.2″, 24°26′33.1″).
(b) Kink Folding Observed in Coastal Quartzitic Sandstone Exposures of the Peninsula Formation Southeast of De Hoek (34°12′19.6″, 24°48′49.5″)

© Eskom 2026/Rev 0a

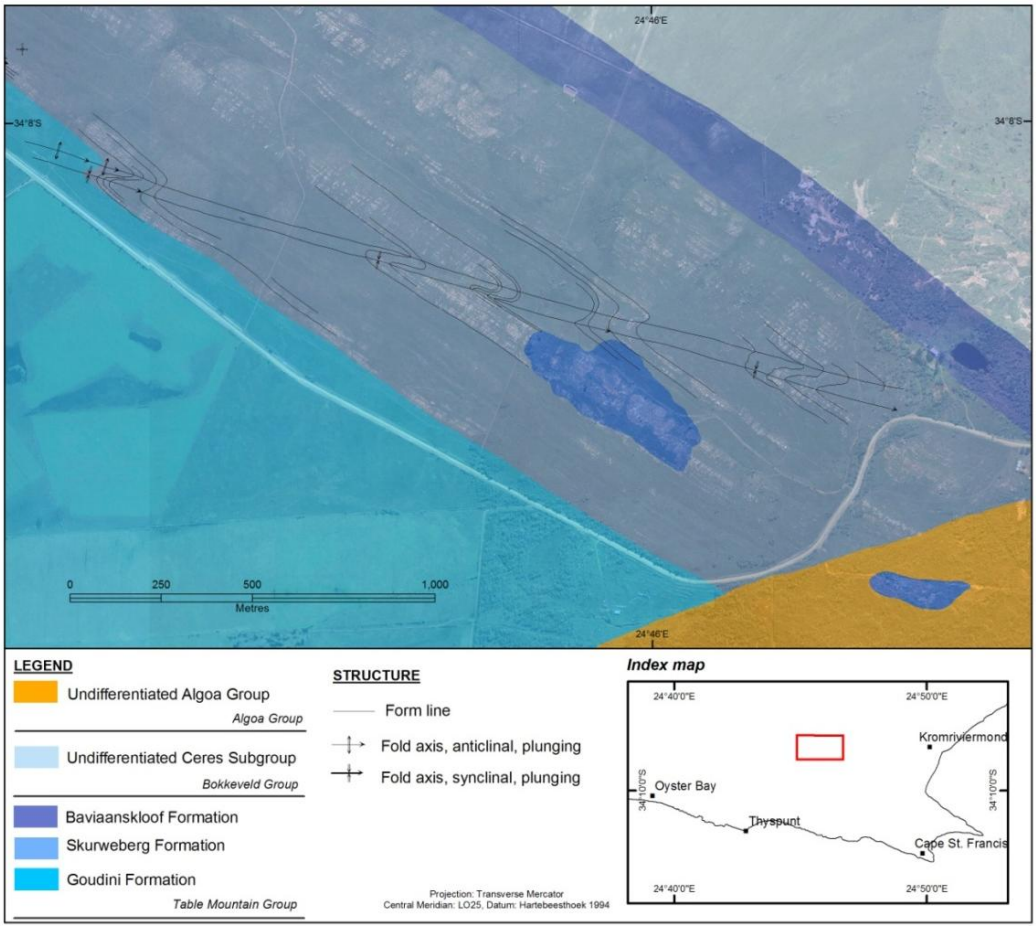


Figure 5.13-115
An Aerial View of Non-coaxial Folding Observed in Exposures of the Skurweberg Formation on the Northern Limb of the Main Cape St Francis Anticline (Modified from *Reference 5.13.27*)

Skurweberg Formation on the northern limb of the main Cape St Francis anticline (***Figure F-5.13.115***).

Here the folds plunge south-eastwards with fold hinges striking between 275 and 95 degrees (***Reference 5.13.27***). The continuation of these folds could not be traced out into the adjacent, underlying, incompetent Goudini Formation. Similar non-coaxial folding is documented at Klippepunt.

© Eskom 2026/Rev 0a

Kink folding within the site vicinity, which is documented in more lithologically competent units, occurs as micro- to meso-scale structural features that are regarded as late stage deformation features.

The most prominent folding structure between Cape St Francis and Oyster Bay is the regional northwest-southeast-striking, southeast-plunging Cape St Francis anticline. The fold axis of the anticline trends parallel to the northwest-southeast bedding strike and verges to the north with quartzitic sandstone of the Peninsula Formation occupying the core of the fold. Bedding inclination is mostly controlled by this anticline and the parallel distance away from its fold axis. Near the fold axis, around the broad fold hinge area, bedding inclination is shallow, with dip values ranging from 5 to 20 degrees. With increasing distance away from the fold axis, dip values show a steady increase from the shallow 5–20-degree grouping to a steeper inclination of between 30 and 40 degrees west of De Hoek (where the fold axis is interpreted to occur along coastal exposures) and east near Cape St Francis. Closer to Thyspunt towards the west, bedding inclination reaches a maximum of between 50 and 65 degrees. Greater dip values are documented, but are rare and localised. Steeper-dipping bedding near Thyspunt compared to Cape St Francis is indicative of a steeper-dipping south-westerly fold limb and a shallower-dipping north-easterly fold limb The Cape St Francis anticline trends parallel to semi-parallel to folding associated with the Cape Fold Belt and is thus of similar age (***Reference 5.13.27***).

Reinterpretation of the structural context of the Klippepunt area (***Reference 5.13.27***) suggests a large recumbent fold occurs mainly above the erosion surface at the headland, west of Oyster Bay with only its inverted lower limbs remaining. Beds are highly sheared around the southern flexure, whilst further north, strata display localised gently westward-plunging parasitic folding. The interpreted northern fold closure occurs roughly 1 km northwest of Klippepunt and is marked by the near-vertical north-facing remnant exposures of the Baviaanskloof Formation (***Reference 5.13.27***).

Joints

The structural imprint most prevalent within the site vicinity area rocks is from joints, the formation of which is the result of Permo-Triassic deformation and in places Mesozoic extension (170–140 Ma). These features are described by Goedhart *et al.* (***Reference 5.13.27***) as old features within the landscape. As joint sets formed in response to local compressive stresses during folding of Table Mountain Group strata that took place during the Cape Orogeny, some joints developed along incipient conjugate shears, some of which may have experienced localised incremental slip at the time (***Reference 5.13.27***).

© Eskom 2026/Rev 0a

Joint sets are described in detail by numerous authors (***References 5.13.23***, ***5.13.338***, ***5.13.28***, ***5.13.308***, ***5.13.30***, ***5.13.36***, and ***5.13.27***). The dominant joint set direction, J1, is northeast-southwest; perpendicular to the bedding trend of northwest-southeast. J2, the subordinate joint set strikes east-northeast/west-southwest. Together, joint sets J1 and J2 form conjugate set X. Joint set J3 has a northwest-southeast trend, parallel to bedding direction. The final J4 set strikes west-northwest and east-southeast. Joint sets J3 and J4 produce conjugate set Y (***Figure F-5.13.116***; ***Table T-5.13.9***; and ***Reference 5.13.27***). Locally, joint sets may vary in orientation and some subordinate sets may be dominant. Joint sets dip vertically to near-vertically.

Joint and fracture openings are either empty or filled with rusty brown iron precipitate or milky white quartz (***Figure F-5.13.117 a&b***). Formations like Skurweberg and Peninsula frequently show quartz fillings (***Figure F-5.13.117a***). Quartz veins are typically a millimetre to a centimetre in width, but veins as wide as a metre have been documented (***Reference 5.13.27***).

Along coastal exposures, areas with a high joint frequency produce zones of weakness also referred to as ‘shatter zones’ (***References 5.13.28*** and ***5.13.27***). Such zones weather negatively and are associated with deep gullies and surge channels, with a cross-cutting relationship parallel and perpendicular to strike (***Figure F-5.13.118 a&b***). These zones are indicative of regions where the expression of compressional stress was most pronounced. Gullies that form parallel to strike, can often be attributed to erosion of softer inter-bedded units rather than joint-related ‘shatter zones’ (***Reference 5.13.27***).

A similar trend is observed within the interior landscape where highly jointed areas of rock produce deep and narrow valleys within the landscape and are often exploited by river flow.

Goedhart *et al.* (***Reference 5.13.27***) documented several micro-faults along coastal exposures within the site vicinity that formed in response to small centimetres to metre displacement along joint planes. Isolated cases of a few hundred metre displacements are noted by Goedhart *et al.* (***Reference 5.13.27***).

© Eskom 2026/Rev 0a



Figure 5.13-116
The Strike Direction of Joints Recorded Within the Site Vicinity (*Reference 5.13.27*). The Main Joint Direction J1 Is Northeast-Southwest

Table 5.13.9
Summary of Joint Set Directions at the Thyspunt Site (*Reference 5.13.27*)

Joint Set	Conjugate Set	Occurrence	Direction	Strike/Dip
J1	X	Dominant	NE-SW	30° ± 20°/ 85°–90° NW, SE
J2	X	Subordinate	ENE-WSW	45°–80°/ 75°–80° NW
J3	Y	Subordinate	NW-SE	110°–150°/ 80° NE
J4	Y	Weak/other	WNW-ESE	300°–330°/ 75°–90° E

© Eskom 2026/Rev 0a

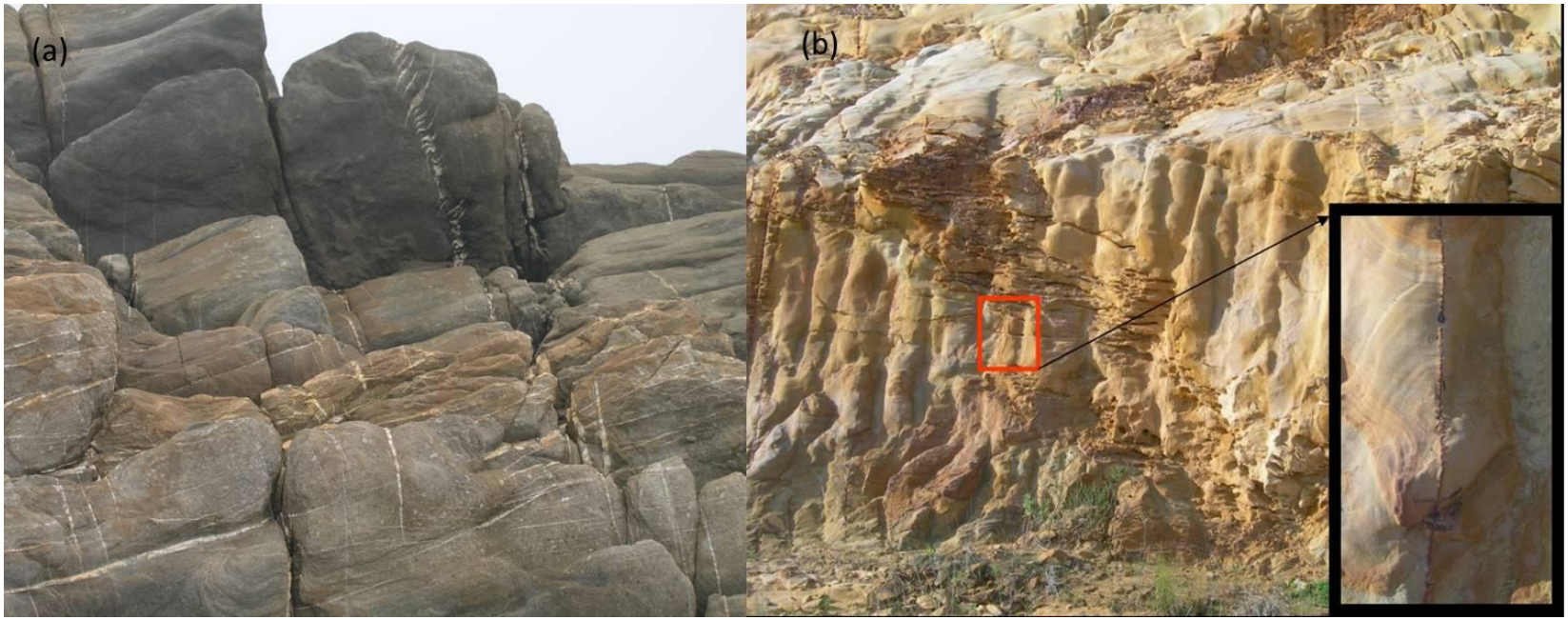


Figure 5.13-117
(a) Quartz-Filled Joints and Fractures in Quartzitic Sandstone of the Skurweberg Formation; Notice the Quartz-Filled Tension/Echelon Gashes (34°11′23.0″ 24°36′23.5″).
(b) Fractures and Veins Filled with Iron Precipitate in Weathered Sandstone of the Baviaanskloof Formation

© Eskom 2026/Rev 0a



Figure 5.13-118
(a) Cross-Cutting Gullies Formed Parallel and Perpendicular to Skurweberg Formation Bedding in Response to Intensely Closely Spaced Jointing in the Area Northwest of Tony's Bay (34°11′11.9″, 24°41′17.2″).
(b) An Aerial View of Gully Formation Observed in the Peninsula Formation, Just East of Thys Bay. Gullies Form in Areas Where the Joint Frequency and Thus Deformation Is Greatest, Creating Zones of Weakness, Which Are Exploited by Erosional Power of Wave Action. Gully Trends Match Joint Trends Found in the Area

© Eskom 2026/Rev 0a

b) Site Area (8 km Radius)

The site area covers a region of approximately 200 km^2 and encompasses the small seaside village of Oyster Bay located near the western perimeter of the site area boundary. The majority of the site area is situated offshore on a gently dipping broad continental shelf. The onland portion of the site area is largely covered by undulating east-west trending Cenozoic dune deposits of the Algoa Group.

i Physiography and Topography (8 km Radius)

The site area is situated along a northwest-southeast-trending, south-facing, relatively straight and rocky coastline. Intermittent steep narrow inlets or gullies cross cut perpendicular to the coastline; the formation of these geomorphic features is attributed to the selective erosion of joint sets. The rugged coastline is interrupted by two prominent embayments: Thys Bay to the east and Slang Bay to the west. The development of these log spiral sandy beach embayments is the consequence of the less erosion-resistant nature of certain of the underlying, formations of the Table Mountain Group. Smaller localised embayments such as Tony's Bay, located approximately 1.5 km northwest of Thyspunt, form as a result of an underlying incompetent lithological unit within the predominately competent quartzitic sandstone of the Skurweberg Formation. Locally, bedrock lithology and geological structure also influence the topographic morphology of the site area interior. Topographic highs are associated with the competent quartzitic sandstone of the Peninsula Formation, which occurs within the apex of the Cape St. Francis anticline and is expressed in the landscape as a linear northwest-southeast-trending convex ridge (***Figure F-5.13.119*** and ***Reference 5.13.27***).

A steady progression of increasing surface elevation is observed from coastal margins toward the interior of the site area (***Figure F-5.13.119***). The portion of the site area blanketed by Cenozoic dune cover is characterised by undulating topography; a consequence of alternating east-west-trending dune ridges and troughs.

The site area is underlain by folded northwest-southeast-trending Palaeozoic Table Mountain Group rocks, the majority of which are covered along coastal margins by Cenozoic marine and aeolian deposits, including modern linear east-west-trending dunes that form part of the Oyster Bay–St Francis headland bypass dunefield (***Figure F-5.13.120)***. These dunefields are generally stabilised by dense vegetation; however, large sections of exposed dunes with active sand accumulation and deposition still occur (***References 5.13.329***, ***5.13.86***, and ***5.13.27***).

© Eskom 2026/Rev 0a

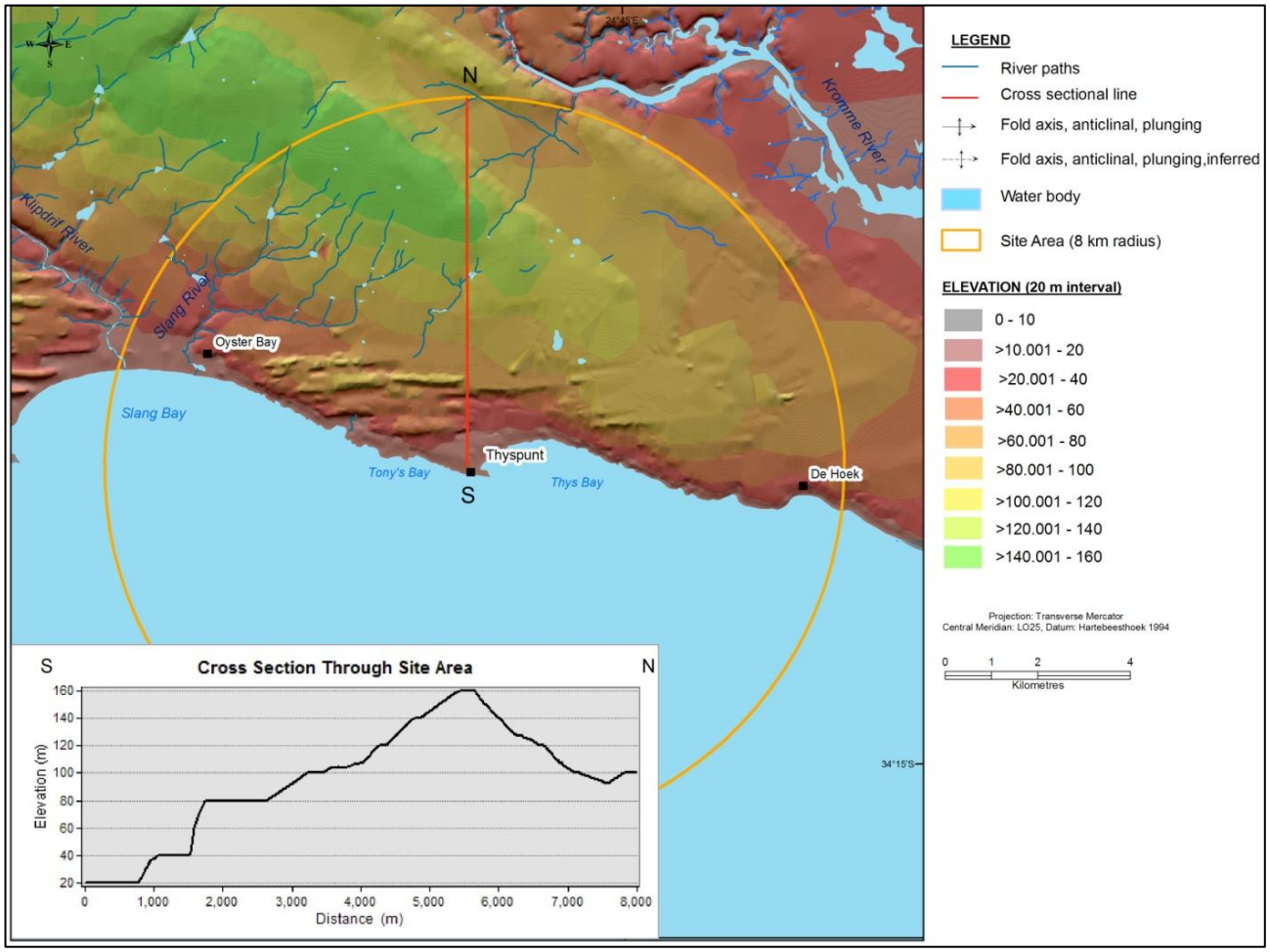


Figure 5.13-119
A 20 m Interval DEM of the Site Area, Showing a South-North Topographical Profile Across the Onland Portion of the 8 km Radius Region

© Eskom 2026/Rev 0a

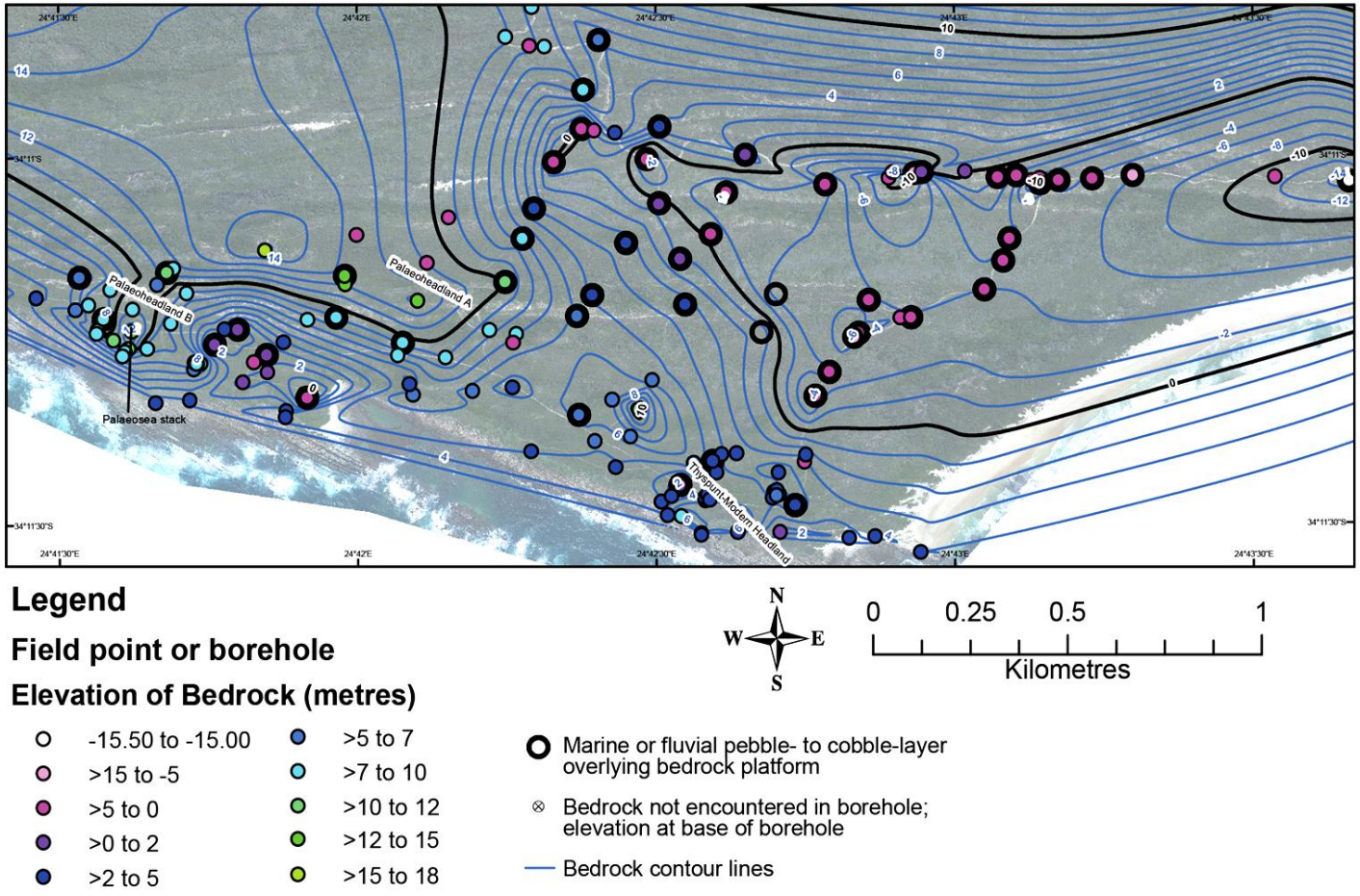


Figure 5.13-120
Figure Showing Bedrock Elevations Beneath Cenozoic Cover in the Thyspunt Area (Source: *Reference 5.13.58*)

© Eskom 2026/Rev 0a

Two specific dunefields are recognised within the site area: the Oyster Bay dunefield and the Thysbaai dunefield (see ***Figure F-5.13.121*** and ***Subsection 5.13.5.2.(a) i*** for greater detail). No active dune migration is occurring within 2 km of Thyspunt (***Reference 5.13.27***).

In the site area, three main southeast-flowing rivers (***Figure F-5.13.119***) drain into the Indian Ocean. All three are either located at or close to the site area boundary. The largest of these rivers, the perennial Kromme River, drains the northern perimeter of the 8 km site area boundary and cuts into argillaceous bedrock of the Bokkeveld Group to the north and east. Two ephemeral rivers, the Klipdrif and Slang Rivers, drain the south-western perimeter region of the site area. The Klipdrif River is predominately cut into argillaceous bedrock of the Baviaanskloof Formation. The river mouth is situated approximately 2 km west of the village of Oyster Bay along the Oyster Bay embayment. The smallest river situated close to Thyspunt is the Slang River. The river flows into Oyster Bay at the village of Oyster Bay. Along the shoreline, a narrow strip (<40 m) of freshwater springs and marshy sediment occur at irregular intervals at the coastal contact between Cenozoic dune cover and coastal rock exposures. Ephemeral wetlands are also a common occurrence within the more northern regions of the Oyster Bay–St Francis headland bypass dunefield.

Beneath Cenozoic overburden, the subsurface topography and geomorphology of the Palaeozoic bedrock are partly controlled by its lithology and the formation of seaward-sloping, flat to gently undulating probably Neogene- to Quaternary-aged marine terrace platforms that were cut into bedrock as step-like sequences of various ages and elevations (***Reference 5.13.58***).

Cross sections developed from subsurface data reveal that, beneath Cenozoic cover, bedrock elevations associated with competent rock units (such as the Skurweberg Formation along the coast) occur at higher elevations than bedrock towards the north-eastern portion of the Thyspunt site area, where the incompetent Goudini Formation occurs (***Figures F-5.13.120*** and ***F-5.13.121***; ***Reference 5.13.58***, Appendix D). This depression in elevation towards the northeast is attributed to the presence of a gently sloping palaeovalley identified along cross sections 2, 6, A, B,C, D, E, and F (***Figure F-5.13.121***; see ***Reference 5.13.58*** Appendix Figures D-4, D-8, D-14, D-15, D-16, D-17, D-18, and D-19) that shares a trend similar to that of Thys Bay.

Boreholes THY-MR12 and THY-MR11-M3 (***Figure F-5.13.121***; ***References 5.13.58*** and ***5.13.60***) record bedrock elevations as low as 15 m below sea level that appears to reflect fluvial channel incision.

© Eskom 2026/Rev 0a

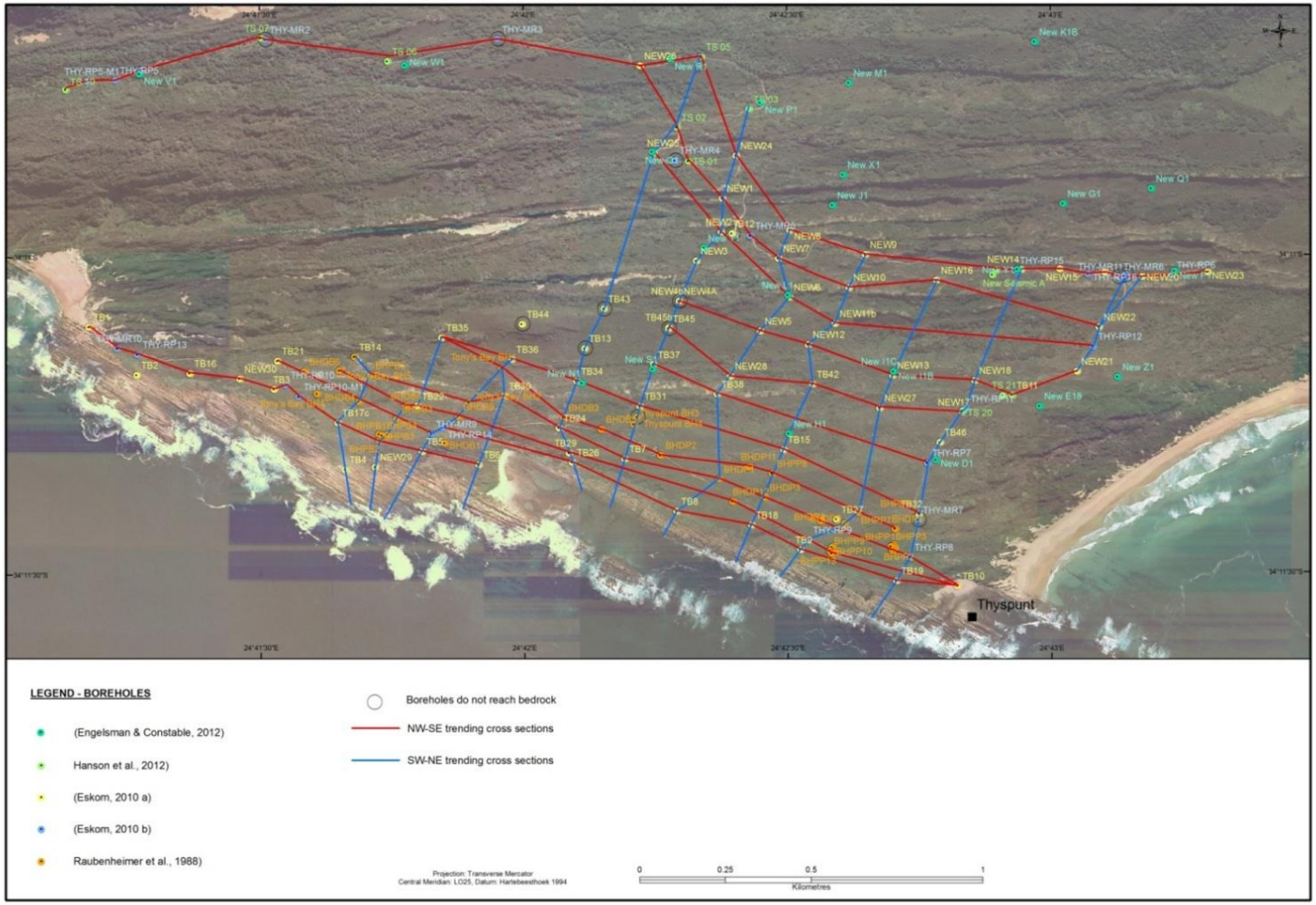


Figure 5.13-121
Map Showing Locations of Cross Sections Based on Subsurface Boring Data at Thyspunt (Modified from *Reference 5.13.58*). Cross Sections in *Reference 5.13.58*, Appendix D

© Eskom 2026/Rev 0a

Highest bedrock elevations beneath dune cover are recorded 300 m north of Tony's Bay (***Figure F-5.13.121***, on cross section 9; see ***Reference 5.13.58*** Appendix D, Figure D-12) in boreholes TB35 (15 m amsl) and TB36 (13 m amsl) situated on the Skurweberg Formation (***Reference 5.13.61***), and inland 1.5 km northwest of Tony's Bay in boreholes THY-RP5 and THY-RP5-M1 (18 m amsl; ***Figure F-5.13.121***, cross section K; see ***Reference 5.13.58*** Appendix D, Figure D-25) and TS-10 (20 m amsl) situated on the Goudini Formation (***References 5.13.58***, ***5.13.60***, and ***5.13.61***).

Marine Terraces

A detailed field mapping programme to identify and correlate marine terraces was conducted between Oyster Bay and Cape St Francis (***Reference 5.13.58***). Maps and shore-parallel profiles that show locations of field localities, topographic profiles, top of bedrock elevations, and geochronology samples and correlation of terraces are provided in Appendix 2 (Plates A2.1, A2.2, A2.4, and A2.5) of ***Reference 5.13.1***. Simplified versions of the map for the Thyspunt site and the shore parallel profile showing terrace correlations are provided on ***Figures F-5.13.122, F-5.13.123***, and ***F-5.13.124*.**

The results of studies in this area (***Reference 5.13.58***), which includes the Thyspunt site, address the capability of offshore faults (i.e., the Cape St Francis fault zone, see ***Subsection 5.13.5.1.(d) iv***) and minor northeast-trending secondary faults documented by onshore bedrock mapping and interpretation of offshore seismic data and the potential for surface deformation at the site (see ***Subsection 5.13.5.3***). The following general observations and conclusions have been made:

- OSL ages (***Reference 5.13.55***) provide information on ages of dune deposits and limiting ages for underlying wave-cut platforms or fluvial strath terraces, but do not provide good constraints on the actual ages of the bedrock surfaces.

Cosmogenic dating analysis provides a method of estimating older ages and hence provides better information on the ages of marine terrace platforms in the study area (***Reference 5.13.52***). Burial ages for clasts and top of bedrock from core samples appear to provide the most reliable ages. Although surface samples generally provide consistent relative ages (increasing age with increasing shoreline angle elevation), the cosmogenic total history ages for the older higher platforms (~15–30 m) in particular seem too young in relation to regional data regarding overall long-term uplift. ***Figure F-5.13.125*** shows an example of a marine terrace profile and sample locations.

© Eskom 2026/Rev 0a

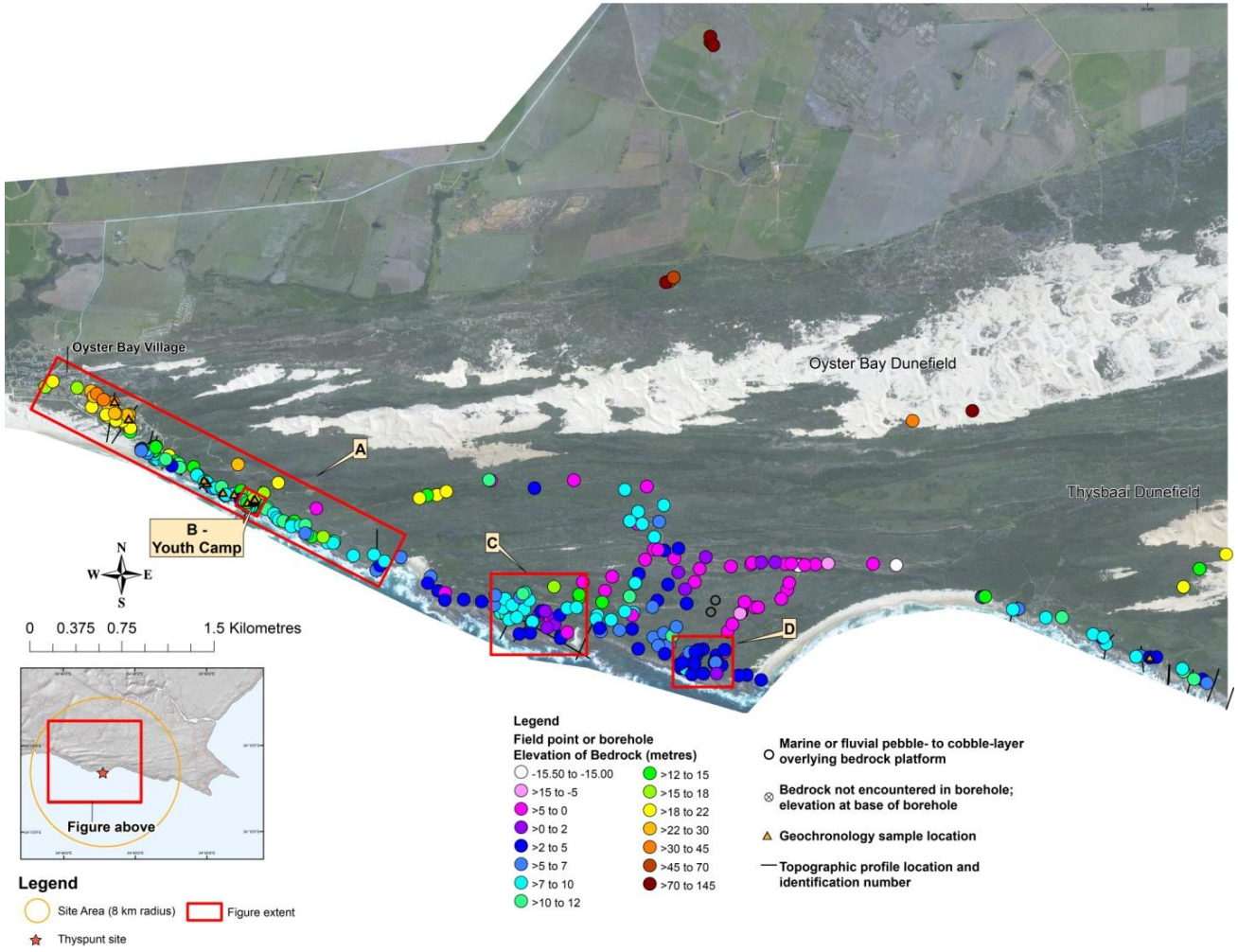


Figure 5.13-122
Elevation of Bedrock at the Thyspunt Site

© Eskom 2026/Rev 0a

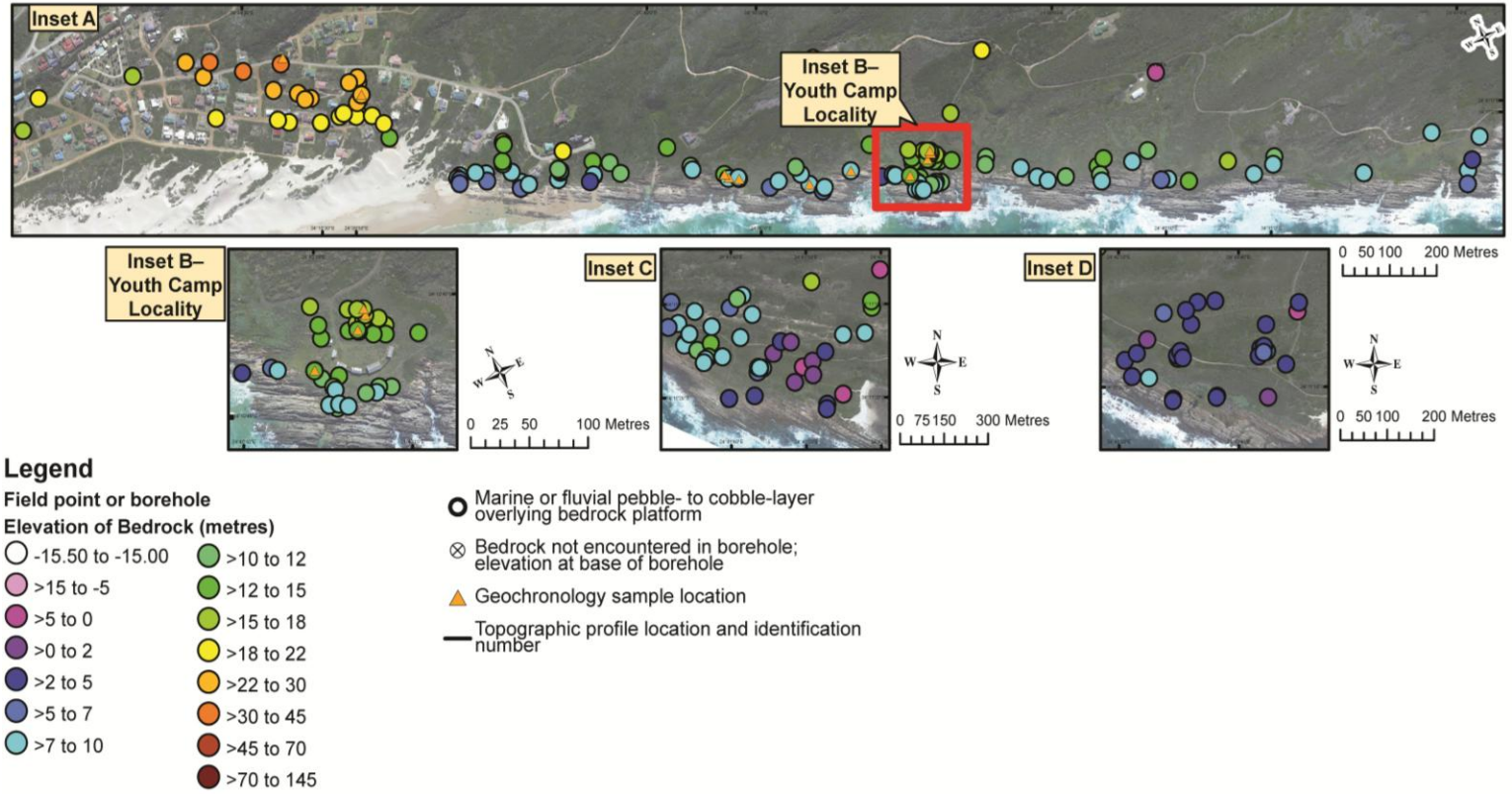


Figure 5.13-123
Detailed Maps of Elevation of Bedrock West of Thyspunt Site (see insets on Figure F-5.13.122)

© Eskom 2026/Rev 0a

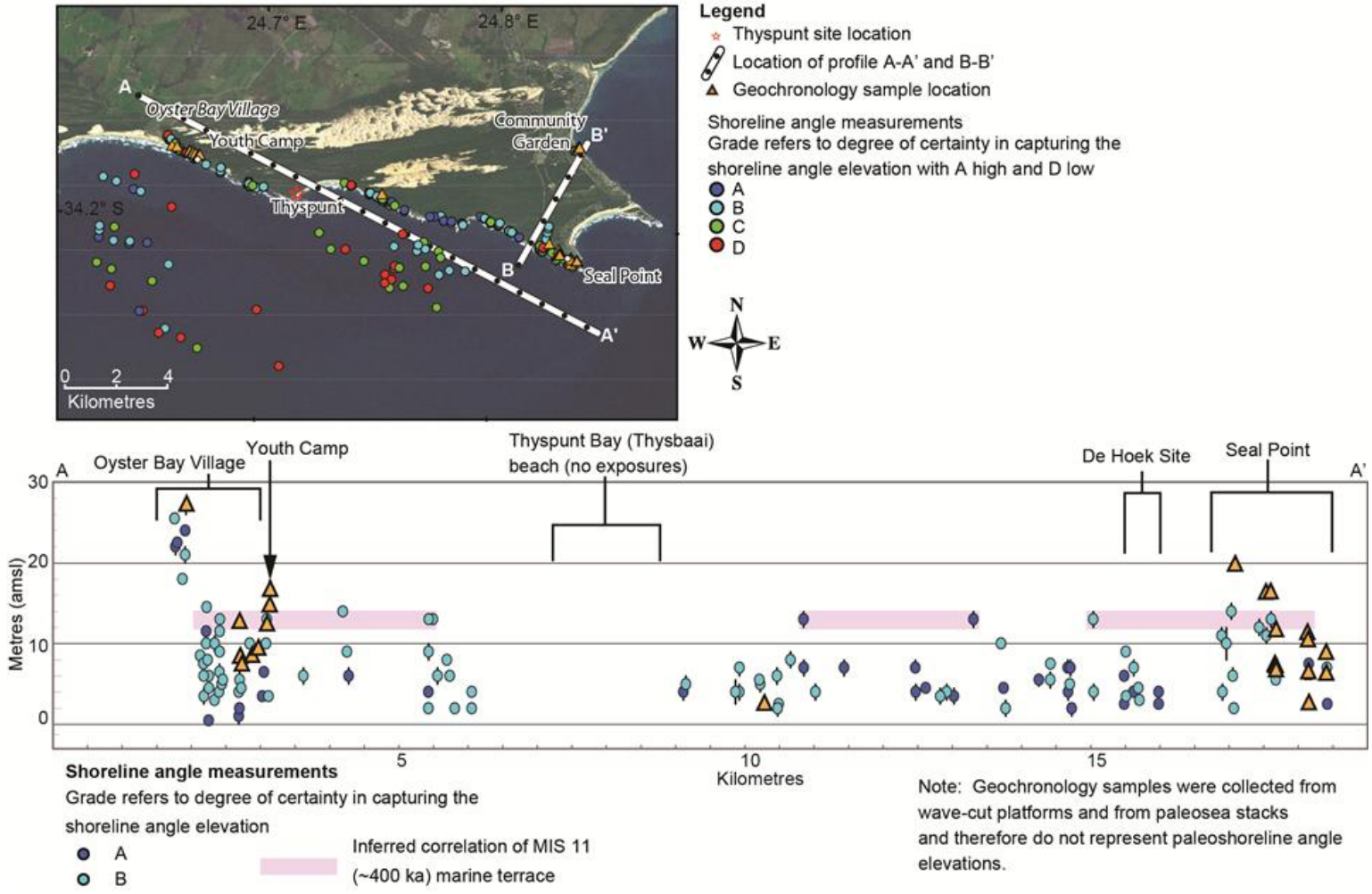


Figure 5.13-124
Correlation of Marine Terraces near the Thyspunt Site

© Eskom 2026/Rev 0a

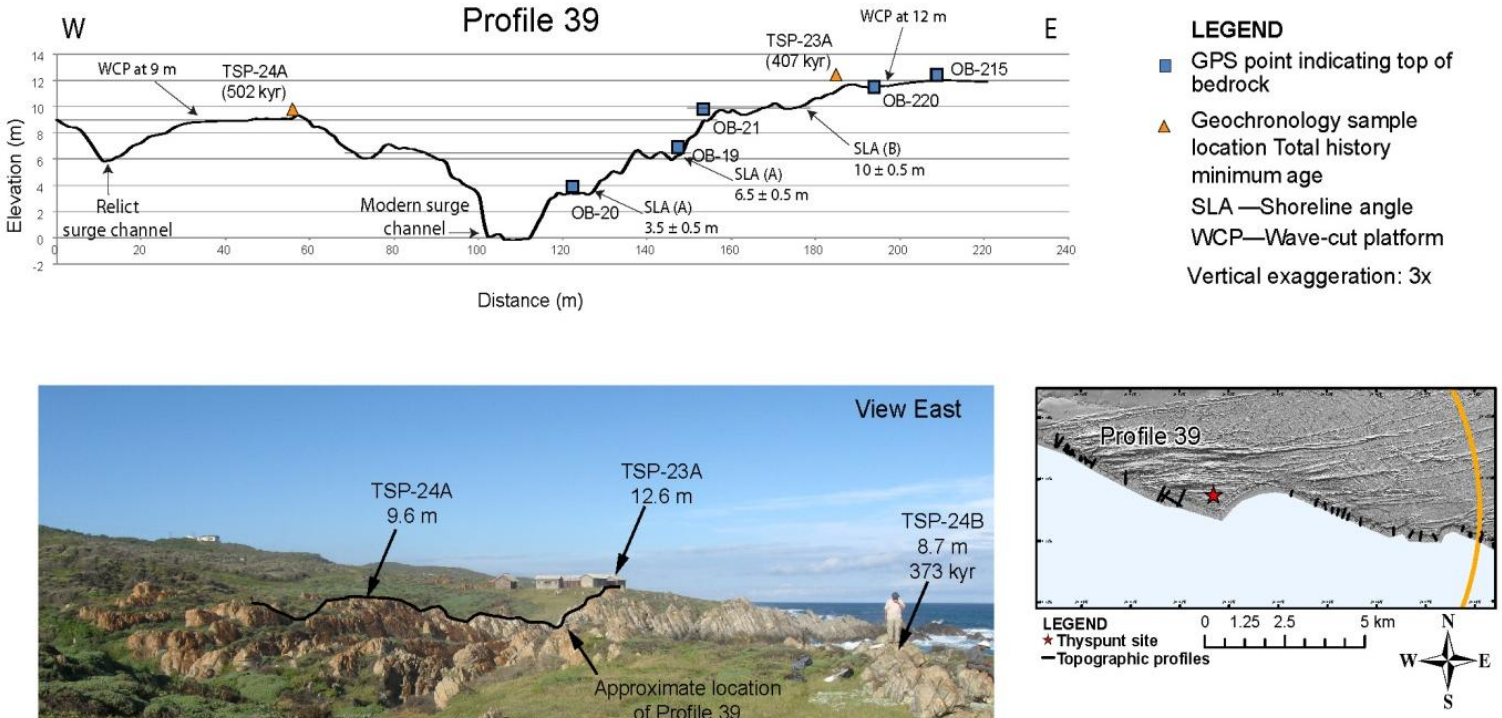


Figure 5.13-125
Example of Marine Terrace Study Topographic Profile and Sampling Locations

© Eskom 2026/Rev 0a

- Based on comparison with other regional marine terrace studies, the highest platforms exposed in the Thyspunt site area likely correlate with the mid-Pliocene warm-interval (3.3–3.0 Ma) sea-level highstands.
- Although the shoreline angle for the highest marine platform (at an elevation of approximately 30 m) is not exposed, the similarity in the elevation of the seaward edge of the platform exposed at both the eastern and western ends of the Oyster Bay to St Francis Bay area suggests that there has been no apparent vertical deformation of this platform since it was formed initially (***Figure F-5.13.124***).

The oldest ages (~1.1–1.7 Ma) for terraces in the site area obtained by cosmogenic analysis are burial ages for platforms at or close to modern sea level (±1.5 m) (TSP-16 and TSP-14, respectively; ***Reference 5.13.52***).

These platforms lie in a large palaeobay behind the Thyspunt headland. Shoreline angles for these platforms are not well defined, and the relatively low relief in this palaeobay could be the result of reoccupation of the seaward parts of older terraces by younger highstands and fluvial incision and erosion during lowstands. Assuming palaeosea level was above –10 m during the formation of these platforms, these data are not inconsistent with a low, long-term isostatic rock uplift rate of approximately 4.4 m/Myr suggested by cosmogenic analysis of stream sediment samples. The inferred uplift rate for the six paired samples (marine terrace bedrock/overlying beach gravel) is 5.0 ± 0.7 m/Myr (***Reference 5.13.52***):

- The consistency between the minimum exposure time and burial times for the paired samples of clasts and bedrock from the underlying platforms (*e.g.*, TSP-NEW 14 and TSP-NEW 16 cosmogenic samples) indicates that the ages for these samples are more reliable than the samples collected from the higher marine terraces at the surface, which may have a more complex history (***Reference 5.13.52***).
- The Pleistocene total history age of 1.04 Ma for sample TSP-26 (elevation of 26.7 m) in Oyster Bay is likely a minimum limiting age for this platform (***Reference 5.13.52***).
- Intermediate elevation terraces (shoreline angle elevations of 15–20 m) yielded middle Pleistocene ages of 560–680 ka, which are also judged to be minimum limiting ages (***Reference 5.13.52***).
- Minimum exposure history ages obtained for cosmogenic samples suggest that the 13 ± 1 m and 7–7.5 m terraces identified in the Thyspunt site area correlate with the Pleistocene MIS 11 and possibly MIS 9, respectively (***Figure F-5.13.124***). The correlation with MIS 9 is judged to be less reliable than the correlation of the higher platform with MIS 11.

Offshore Physiography

Seven offshore landscape feature zones were broadly identified by Davidson & Smith (***Reference 5.13.281***) within the site area (***Figure F-5.13.122***). Rocky Table Mountain Group quartzitic sandstone outcrops slope to the southeast at angles of generally less than 0.5 degree are interpreted on either side of a central sediment-filled basin slope. These rugged outcrops form ridges and pinnacles up to 1–7 m high. The sediment basin contains narrow furrow structures interpreted to be associated with sediment slumping. Further discussion of the formation of features from either slumping or erosion is found in ***Subsection 5.13.5.4*** Tsunamigenic Sources. Minor rock outcrop also occurs towards the south. Rocky outcrops along the western portions of the site are intermittently covered with sediment. A sediment filled basin is also identified along the eastern margins of the site area (***Figure F-5.13.126***).

A series of offshore topographic profiles developed from 1 m MBES data DEM through areas of bedrock outcrop, indicate several possible submerged wave-cut platforms and associated palaeoshorelines (***Figure F-5.13.127*** and ***Reference 5.13.58***). Profiles reveal that platforms in the offshore region generally exhibit very low gradient slopes of approximately 0.005 degree. A prominent palaeoshoreline and associated platform approximately 1,000 m wide at elevations of approximately –45 ± 3 m, appears along the western bedrock outcrop (***Figures F-5.13.126*** and ***F-5.13.127***; also see ***Reference 5.13.58*** Profile O1 to O4, Appendix Figures C-28 and C-29). Shoreline angles at similar elevations occur along the eastern offshore bedrock outcrops. Higher platforms and possible shoreline angles are interpreted along offshore outcrops, at elevations of –34 m to –38 m (***Figure F-5.13.127***) and –27 m to –30 m. Upper offshore platforms within the site location are relatively broad (1,000–2,000 m) and have bevelled the tops of more-resistant beds and lower areas or swales of less-resistant rock. The width and low gradients of these platforms indicate that they likely resulted from reoccupation during multiple transgressions and regressions (***Reference 5.13.58***).

Other offshore profiles indicate shoreline angles at –63 m, with lower platforms with shoreline angles identified at –70 m and –78 m to –79 m, with the lowest possible terrace back edges identified at –103 ± 2 m and –107 + 1, –3 m along Profile O-10 (see ***Reference 5.13.58***, Appendix C, Figure C-32).

© Eskom 2026/Rev 0a

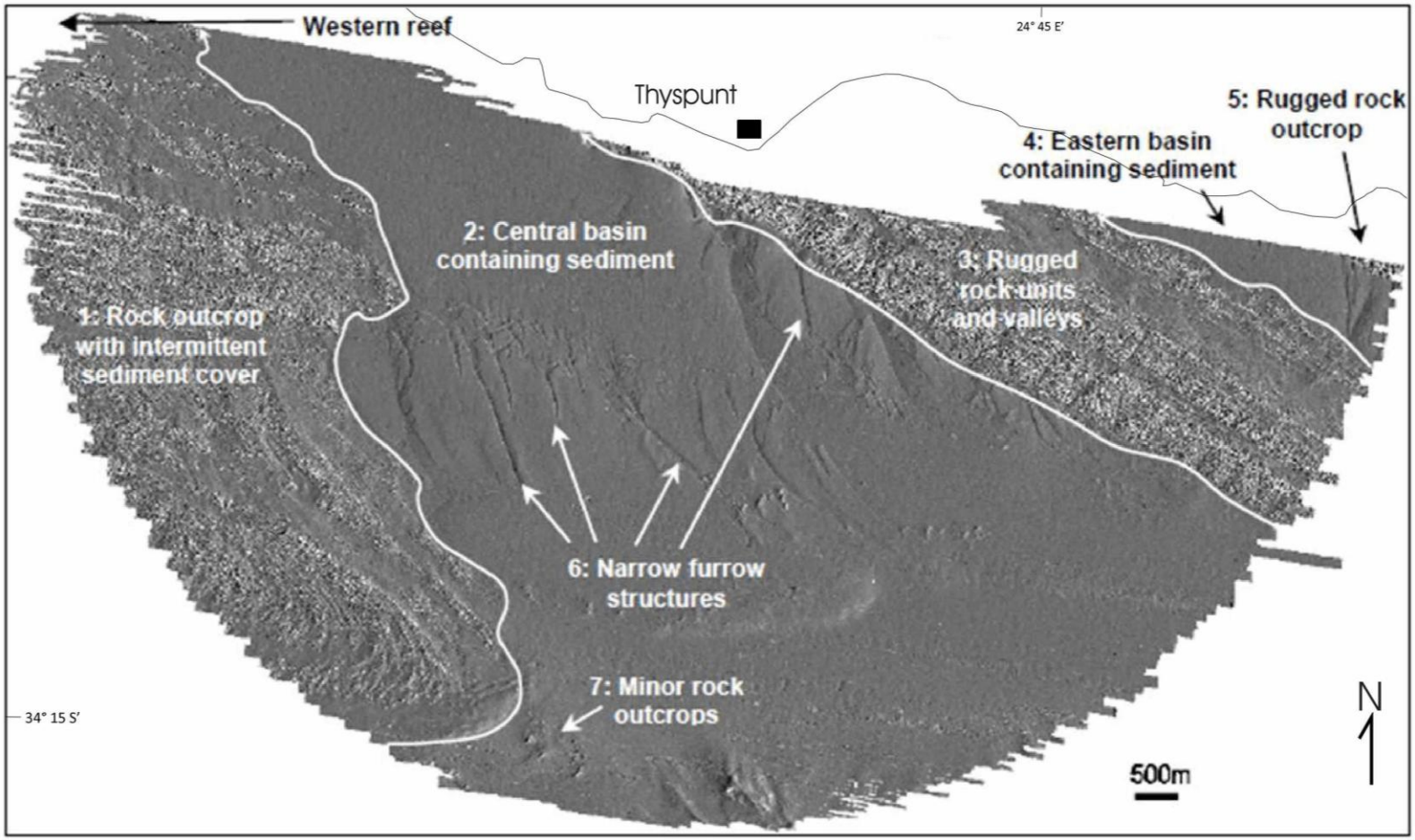


Figure 5.13-126
Grey-Scale Offshore MBES Bathymetry Data for the 8 km Site Area (from *Reference 5.13.281*)

© Eskom 2026/Rev 0a

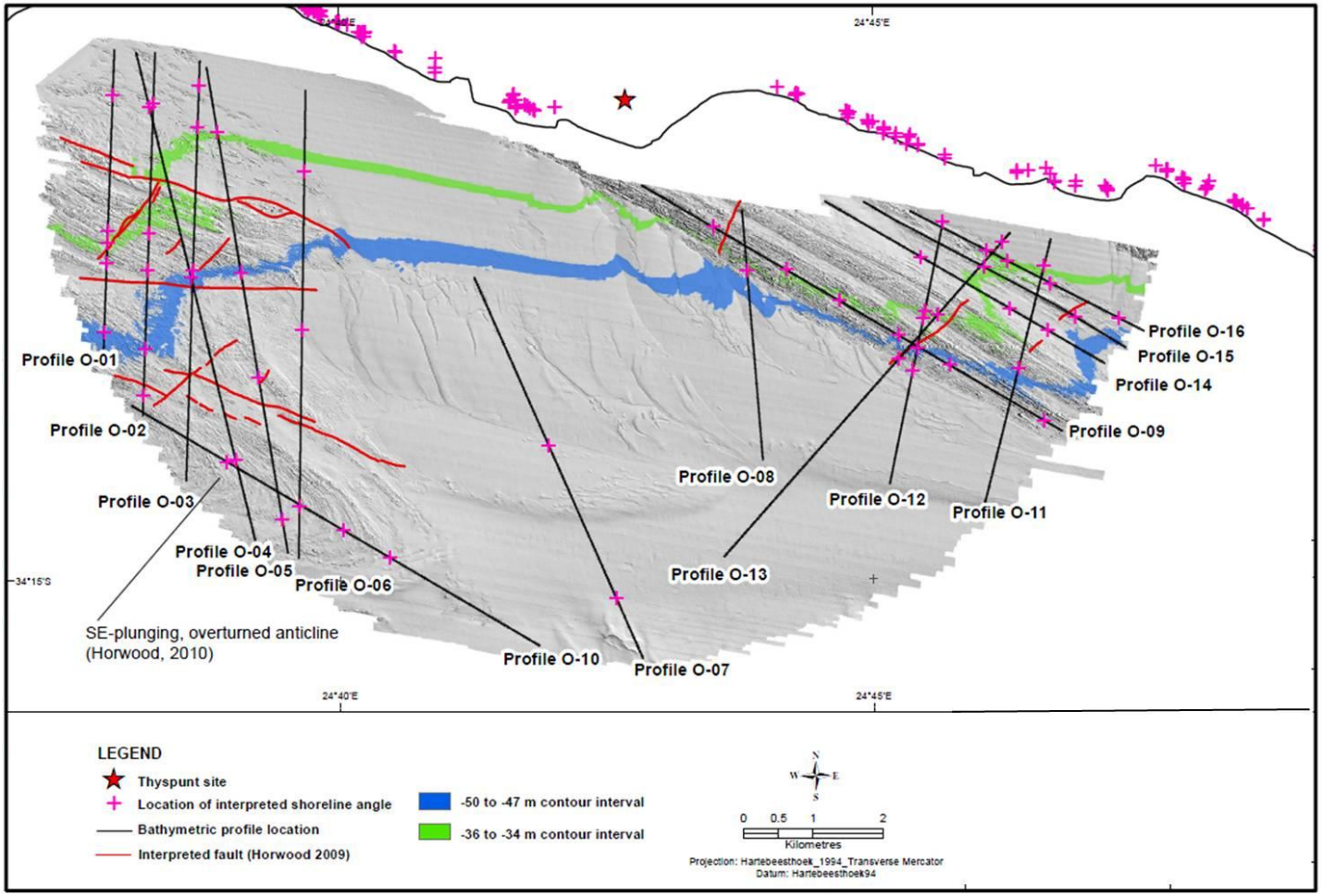


Figure 5.13-127
Offshore Topographic Profiles Developed from 1 m MBES Data DEM Through Areas of Bedrock Outcrop (from *Reference 5.13.58*)

© Eskom 2026/Rev 0a

ii Stratigraphy (8 km Radius)

In the site area, the northwest-southeast-striking Palaeozoic strata comprise two stratigraphic groups, the Palaeozoic Bokkeveld and Table Mountain Groups. These are predominately exposed along the coastal margins and are overlain by the unconsolidated to semiconsolidated clastic nearshore-marine and coastal aeolian-derived Cenozoic Algoa Group sediments (***Figure F-5.13.128*** and ***Table T-5.13.10***).

Table 5.13.10
Lithostratigraphic Summary of Rock Units Within the Site Area (8 km Radius)

Age		Super-group	Group	Formation	Lithological Description
Cenozoic	Holocene		Algoa	Schelm Hoek	Aeolian sand, soil horizons, and shell middens
	Pleistocene			Nahoon	Aeolian calcareous sandstone, palaeosols, and subordinate calcrete
				Salnova	Marine and/or estuarine calcareous sandstone, siltstone, coquinite, and basal gravels
				Nanaga	Calcareous sandstone (aeolianite), palaeosols, and calcrete
	Pliocene Miocene			Alexandria	Calcareous sandstone, semiconsolidated conglomerate, coquinite, and basal gravels
Palaeozoic	Devonian	Cape	Bokkeveld	Gydo	Black to brown shale, subordinate siltstone.
	Silurian		Table Mountain	Baviaanskloof	Impure feldspathic sandstone, subordinate shale
				Skurweberg	Quartzitic sandstone, medium- to course-grained, profusely cross-bedded, subordinate shale
				Goudini	Brown-weathered thinly bedded siltstone, mudstones, quartzitic sandstone
	Ordovician			Cedarberg	Black shale, laminated
				Peninsula	Quartzitic sandstone, massive and laminar and cross-bedded, medium- to coarse-grained

© Eskom 2026/Rev 0a

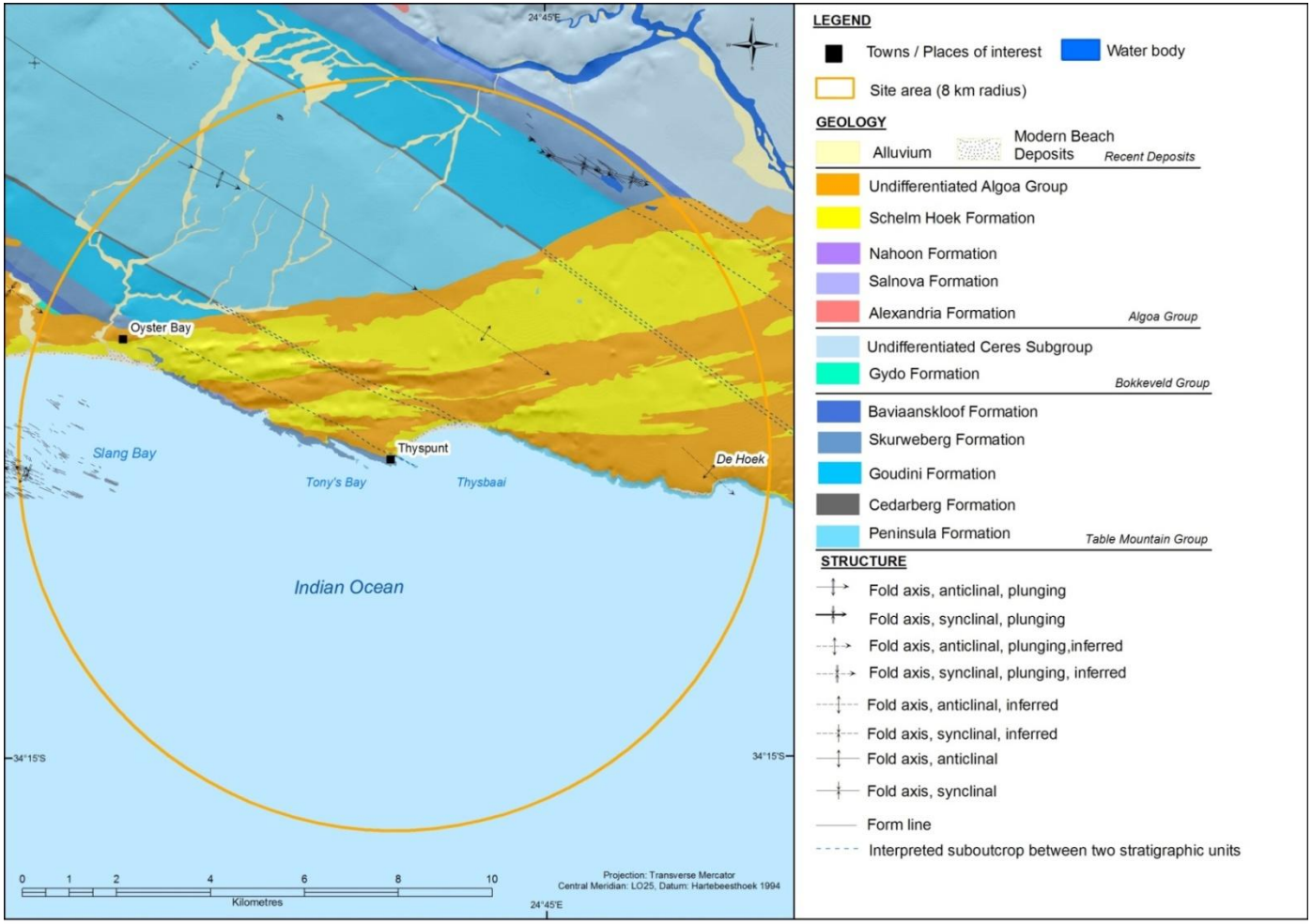


Figure 5.13-128
Geology of the Site Area (Modified from *Reference 5.13.27*)

© Eskom 2026/Rev 0a

Palaeozoic Bedrock

For detailed lithostratigraphic descriptions and depositional setting of Palaeozoic bedrock, refer to ***Subsection 5.13.5.2.(a) i***.

The Ordovician Peninsula Formation, the basal unit of the Table Mountain Group, is composed of light grey, supermature, and medium-grained massive to well-bedded quartzitic sandstones that form a stratigraphically and topographically, very prominent formation within the interior and subsurface. Within the site area the Peninsula Formation is contained within the crest of the main Cape St. Francis northwest-southeast-trending anticline and exposed along a thin 11 km strip of rugged coastline east of Thys Bay towards Cape St. Francis. Small isolated exposures also occur south of Buffelsbos, outcropping beneath the younger aeolian sediments (***Reference 5.13.27***) of the Oyster Bay dunefield (***Figure F-5.13.128***). Overlying units of the Table Mountain Group outcrop north and south of the site area. The sandstones of the Peninsula Formation are frequently stained pink or red by iron oxides and infrequently interbedded with thin (>1 m) argillaceous (mudrock or phyllite) horizons, as documented along coastal exposures west of De Hoek (***Figure F-5.13.129 a&b***). Further inland (250 m north of De Hoek) coastal exposures and borehole data (***References 5.13.28*** and ***5.13.308***) indicate the presence of shale units up to 3 m thick.

The approximate thickness of the Peninsula Formation (***Figure F-5.13.82***) in the vicinity of Thyspunt exceeds 560 m (***Reference 5.13.27***). The Peninsula Formation is conformably overlain by the Cedarberg Formation and this contact is inferred from the combined results obtained from a time domain electromagnetic study (***Reference 5.13.42***), a ground magnetic traverse (***Reference 5.13.35***) along Thys Bay, and borehole data (***References 5.13.28***, ***5.13.308***, ***5.13.60***, ***5.13.61***, and ***5.13.62***). Geophysical results place the boundary between the two formations approximately 425 m west of the last Peninsula Formation exposure along Thys Bay (***Figure F-5.13.128***).

The overlying Ordovician Cedarberg Formation is approximately 62 m thick (***Figure F-5.13.129*** and ***Reference 5.13.27***), but may vary in local thickness.

This laterally persistent (***References 5.13.305*** and ***5.13.119***), lithostratigraphically thin unit consists of black, finely laminated carbonaceous shale, often containing pyrite (***Reference 5.13.304***).

© Eskom 2026/Rev 0a



Figure 5.13-129
(a) Coastal Exposure of Competent Quartzitic Sandstone of the Peninsula Formation, Interbedded with Three Subordinate Dark Grey Mudrock Layers West of De Hoek. Location of photo: 34°11′48.4″ S, 24°47′38.3″ E.
(b) Quartzitic Sandstone of the Peninsula Formation in Borehole NEW 30 (*Reference 5.13.61*) from 93 m to 99 m Below Ground Level, Approximately 1 km Northwest of Tony's Bay (34°11′11.5″ S, 24°41′27.7″ E)

Within the site area, there are no exposures of the Cedarberg Formation; however, its presence in the subsurface along the south-western limb of the main Cape St. Francis anticline beneath Cenozoic cover is confirmed by borehole data (***References 5.13.28***, ***5.13.60***, ***5.13.61***, ***5.13.62***, and ***5.13.58***) and geophysical data (***References 5.13.35***, ***5.13.42***, and ***5.13.44***) and is indicated on ***Figure F-5.13.128***.

The Cedarberg Formation's lower contact with the Peninsula Formation is sharp, whereas the upper contact with the Goudini Formation is gradational (***Reference 5.13.342*** and ***5.13.305***).

The Silurian Goudini Formation is composed of medium-grained, pale grey, unweathered to brownish weathered quartzitic sandstone with subordinate mudstone/shale and siltstone (***Figure F-5.13.130***; ***References 5.13.119*** and ***5.13.27***). The Goudini Formation sandstone is a medium-grained quartz arenite (***Reference 5.13.49***) and is commonly cross-bedded (***References 5.13.23*** and ***5.13.22***).

Fine-grained sandstone of the Goudini Formation is generally more massive and shows evidence of bioturbation (***References 5.13.23*** and ***5.13.22***). Bedding is thin and consistently shows rapid lithological changes. Exposures of the lithologically incompetent formation within the site area are not frequent, but are documented along a small, still uneroded strip towards the western end of Thys Bay and small exposures in the interior. The formation produces unpronounced bedrock topography within the site area interior and subsurface and the formation of the Thys Bay embayment is attributed to the lithologically incompetent formation's susceptibility to erosion. Subsurface occurrence of the formation beneath Cenozoic overburden within the site area is indicated on ***Figure F-5.13.128***).

The competent Skurweberg Formation (as described in ***Subsection 5.13.5.2.(a) i***) overlies the Goudini Formation (***Figure F-5.13.131 a&b***) and crops out on both the eastern and western sides of the dominant, southward-plunging Cape St. Francis anticline.

The Skurweberg Formation is well exposed as the prominent rocky coastline between Oyster Bay and Thyspunt and expressed in the landscape as parallel topographic highs as a function of linear bedding. In the vicinity of the Thyspunt site, the formation thickness reaches approximately 700 m (***Reference 5.13.27***). The Skurweberg Formation is conformably overlain by the Baviaanskloof Formation.

No onshore exposures of the Devonian- to Silurian-aged incompetent Baviaanskloof Formation occur within the 8km site area. Outcrops are mapped



Figure 5.13-130
The Medium-Grained, Pale Grey Quartzitic Sandstone with Subordinate Mudstone/Shale and Siltstone of the Goudini Formation as Observed in Borehole NEW12 (*Reference 5.13.61*) (34°11′08.3″ S, 24°42′32.4″ E) from 30.49 m to 43.34 m Below Ground Level. Bedding Is Thin and Shows Consistent Rapid Lithological Change.

© Eskom 2026/Rev 0a



Figure 5.13-131
(a) Coastal Exposures of the Skurweberg Formation Composed of Grey to Pale Grey Mature Quartzitic Sandstone Dipping Approximately 50° S at 34°11′23.6″ S, 24°41′54.2″ E near Tony's Bay.
(b) Unweathered Quartzitic Sandstone of the Skurweberg Formation Seen in Borehole NEW 29 (*Reference 5.13.61*) from 69.43 m to 76.69 m Below Ground Level

© Eskom 2026/Rev 0a

on either side of the main northwest-southeast trending anticline west of Oyster Bay and southwest of the Kromme River (***Reference 5.13.27*** and ***Figure F-5.13.128***). The Baviaanskloof Formation consists of immature sandstone, mature feldspathic sandstone, minor rhythmite, mudstone and siltstone (***Reference 5.13.310***) and is conformably overlain by the Gydo Formation or directly overlain by Cenozoic sediments where exposed along the coastal margin. This formation produces relative topographic lows within the landscape. A stratotype for the Baviaanskloof Formation located within the site vicinity near the Kouga Dam showed the thickness of the formation to be 200 m (***Reference 5.13.310***).

The argillaceous Silurian aged Gydo Formation is the lowermost unit of the Bokkeveld Group Ceres Subgroup, and consists of mudrock, shale, siltstone, and lesser immature sandstone producing an unpronounced topography. Within the site area, it outcrops west of Oyster Bay, where the majority of the formation is overlain by the Cenozoic Algoa Group.

Cenozoic Deposits

For detailed lithostratigraphic descriptions and depositional setting of Cenozoic overburden, refer to ***Subsection 5.13.5.2.(a) i***.

Along coastal margin of the study area, the bedrock is predominately overlain by unconsolidated to semi-consolidated clastic nearshore-marine and coastal aeolian-derived Cenozoic deposits constituting the Algoa Group (***Figure F-5.13.128***). Cenozoic sediments rest on a broad, seaward-sloping, probably Neogene-aged series of flat to gently undulating wave-cut platforms that extend northward to the base of the hinterland mountains (***References 5.13.168*** and ***5.13.58***). The results of marine terrace investigations (***Reference 5.13.58***), have constrained ages and correlations of marine terraces at the Thyspunt site (*see* ***Subsection 5.13.5.2.(b) i***).

The Algoa Group sediments are subdivided into the Alexandria, Nanaga, Salnova, Nahoon, and Schelm Hoek Formations (***Table T-5.13.10***). Differentiation between these formations within the site area is complex. This complexity does not necessarily arise from the subdivision of marine versus aeolian sediments, but rather as a function of obstruction of vast areas by coastal vegetation. Goedhart *et al*. (***Reference 5.13.27***) were only able to differentiate between formations in certain areas, and thus classified large regions within the site area as ‘undifferentiated Algoa Group’ (***Figure F-5.13.128***) in regions where specific formations could not be identified.

The thickness of the Algoa Group within not only the site area, but also the site location, is in part correlated with its approximate distance from the present day

coastline and the landscape topography prior to deposition of the Algoa Group strata (see cross-sections in Appendix D of ***Reference 5.13.58*** and ***Figure F-5.13.121***). The latter of these two factors is strongly influenced by the variation in lithological units and the process of differential weathering of underlying bedrock that may lead to the formation of alternating headlands and embayments along the modern coastline and prominent topographic highs or depressions within the palaeo-landscape.

The general trend in thickness of the undifferentiated Algoa Group, treated here as a composite unit, is characterised by progressive thickening for the first few hundred meters from the coast, peaking towards a zone of maximum thickness, followed by a thinning of units that occurs on the landward margin of the deposit (***Figures F-5.13.95***, ***F-5.13.132***, and ***F-5.13.133***). This trend is observed at Thyspunt in a coast-parallel-trending zonation referred to as A-D and shown graphically in ***Figure F-5.13.132***. The Algoa Group sediments along the south coast generally young in a seaward direction as a result of progradation on successive sea-level highstands. The most recently deposited sediments of the Algoa Group (within Zone A) extend inland from the coastal margin for approximately ~250 m. *Zone A* (***Figures F-5.13.132*** and ***F-5.13.133***) shows sediment thicknesses ranging from a minimum of 3 m in borehole TB8 near the shoreline to a maximum of 14 m in borehole TB32 m from the coast (***Reference 5.13.61***) with average thicknesses ranging from 3 m to 9 m. (***Figure F-5.13.132***).

In accordance with the model of sediment accretion at Thyspunt, a steady increase in thickness is documented to occur in Zone B, which extends into the hinterland between a narrow ~250–750 m band oriented semiparallel to the coastline (Zone B, ***Figure F-5.13.132***). Here the sediments range in thickness from 10 m to 20 m with isolated boreholes such as THY-PR7 (***Reference 5.13.60***) revealing sediment thicknesses of up to 23 m. Towards the north into Zone C, the influence of antecedent palaeotopography becomes evident where the average sediment thickness range escalates significantly (Zone C, ***Figure F-5.13.132***) to between 34 m and 54 m. This area of maximum thickness of the Algoa Group is associated with an incised palaeo-channel that follows the same trend as the Thys Bay embayment. The formation of the embayment and relatively lower bedrock topography within the hinterland is the result of preferred erosion along the lithologically incompetent Goudini Formation. Evidence supporting the presence of a palaeochannel or palaeovalley is derived from bedrock elevations of –6 m amsl towards the western side of Thys Bay and are as deeply incised as –15 m amsl towards the eastern extent of Thys Bay (***Reference 5.13.58***; see Plate A2.1 in Appendix 2 of ***Reference 5.13.1***).

© Eskom 2026/Rev 0a

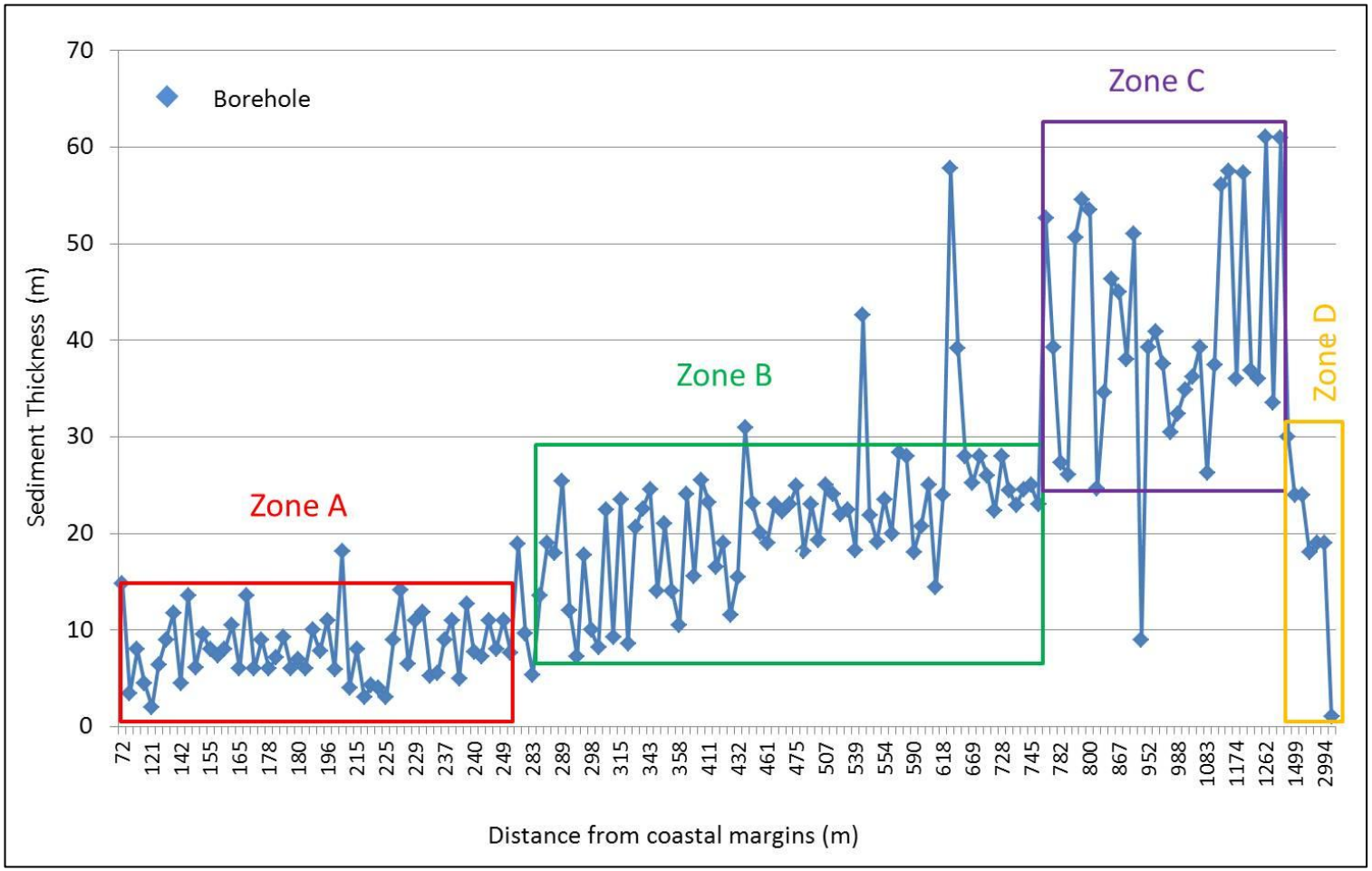


Figure 5.13-132
Borehole Thickness of the Cenozoic Algoa Group Within the Site Area Plotted Against Their Distance Away from Coastal Margins. Four Thickness Zones, A to D, Can Be Identified

© Eskom 2026/Rev 0a

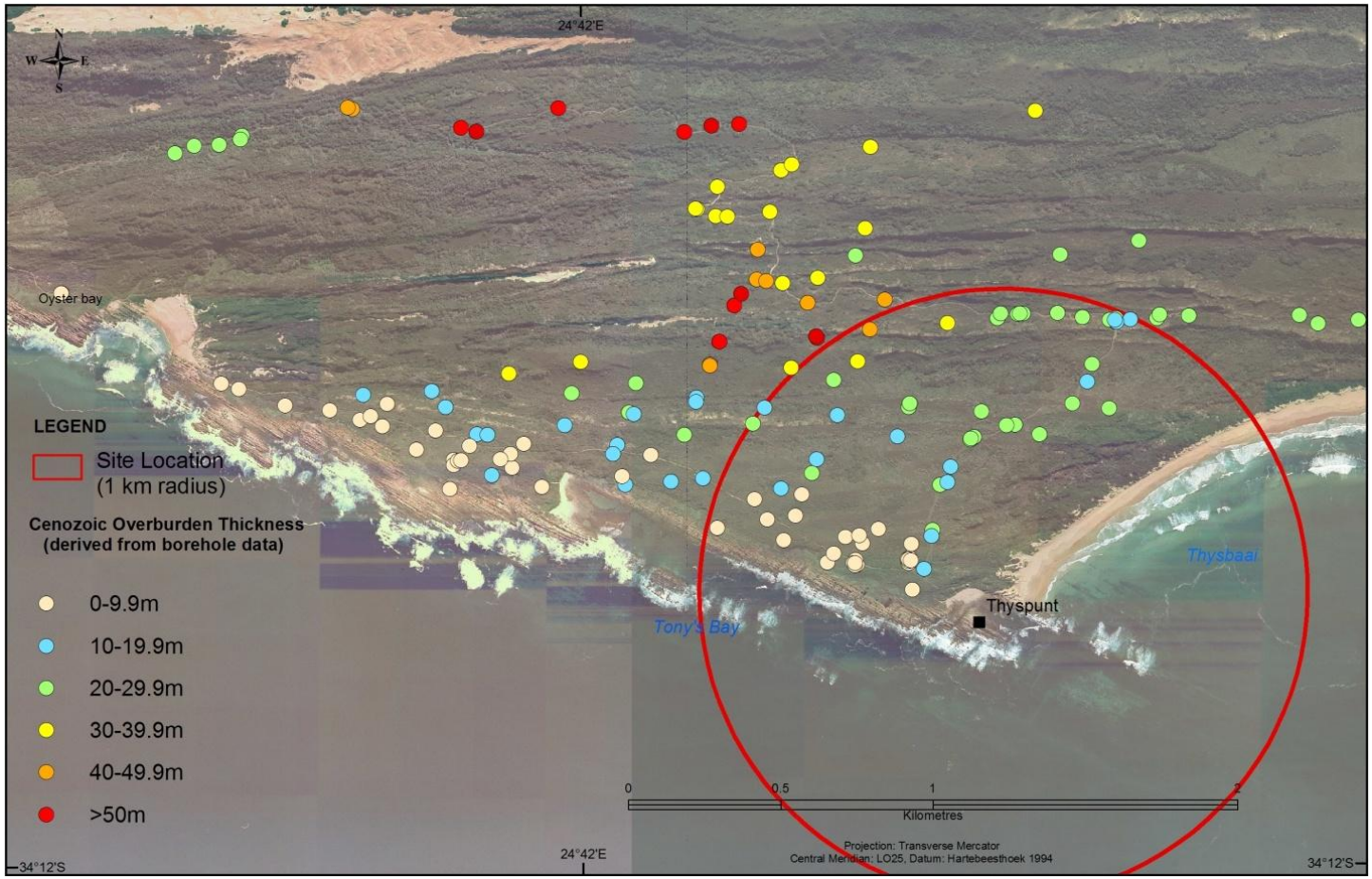


Figure 5.13-133
Cenozoic Overburden Thicknesses at Thyspunt as Derived from Borehole Data (*References 5.13.28*, *5.13.308*, *5.13.60*, *5.13.61*, *5.13.58*, and *5.13.62*). The Site Location (1 km Radius) is also indicated

© Eskom 2026/Rev 0a

Associated borehole logs are interpreted as fluvial and alluvial deposits indicative of a palaeochannel incised into bedrock. The Algoa Group reaches its maximum recorded thickness of 61 m in borehole NEW L1 (***Figure F-5.13.121***; ***Reference 5.13.62***). Near the northern marginal (Zone D, refer to ***Subsection 5.13.5.2.(a) ii***) extent of the mapped Algoa Group (***Reference 5.13.27***), thicknesses have an average range of between 17 m and 25 m. Zone D lies approximately 1,450–3,000 m inland of the coastline.

Dune cordons may have complex origins, with younger phases being stacked upon an older core, but the relative age of aeolian deposits is typically inferred from their proximity to the coast (***References 5.13.174***; ***5.13.175***, ***5.13.85***, and ***5.13.176***). Luminescence ages for dune deposits of the Algoa Group in the Oyster Bay and Thysbaai dunefields range from Holocene to early-middle Pleistocene (>490 ka) (***Reference 5.13.303*** and ***Figure F-5.13.80***). OSL ages for samples of core collected at the Thyspunt site ranged in age from 25 ka to >130 ka (***Reference 5.13.55***).

The lowermost unit of the Algoa Group, the Alexandria Formation, is not exposed within the site area, but may be present in the subsurface overlying higher bedrock platforms (elevations of ≥18–30 m amsl) along the northern margins of the mapped Algoa Formation within the site area.

The Nanaga Formation (***Figure F-5.13.134***), which overlies the Alexandria Formation elsewhere in the site vicinity, accumulated in coastal dunefields along Late Miocene to Early Pleistocene's receding shorelines and likely is present in the subsurface in the northern areas of mapped Algoa Formation in the site area. Outside the site area, the formation is composed of unconsolidated to semiconsolidated, medium-grained, cross-bedded, calcareous dune sand and calcretes (see ***Subsection 5.13.5.2.(a) ii***).This formation is generally overlain by the younger unconsolidated mobile dunes of the Schelm Hoek Formation ***Figure F-5.13.135***. In addition, the Nanaga Formation is sporadically overlain by the younger marine deposits of the Salnova Formation or by the Nahoon Formation (***Figure F-5.13.136***). The Nahoon Formation consists of a well cemented aeolianite, generally less than 15 m in thickness, composed of calcareous sandstone, interbedded with palaeosols and isolated, very thin calcrete layers that formed in response to a sea-level regression (***Reference 5.13.166***) during the late Pleistocene. The upper contact with the Schelm Hoek Formation in both aerial view and subsurface borehole information within the site area is difficult to ascertain and is typically inferred.

The Salnova Formation deposits are situated on relatively lower wave-cut surfaces (elevations of ≥18–30 m amsl) and are thought to represent highstands of sea level during one or more of the Quaternary interglacials.

© Eskom 2026/Rev 0a



Figure 5.13-134
Calcareous Light Grey to Greyish-Yellow Unconsolidated to Semiconsolidated Dune Sand Associated with the Nanaga Formation Observed in Borehole TS-07 (*Reference 5.13.58*) from 12.45 m to 27.15 m Below Ground Level (34°10′31.1″ S, 24°41′38.2″ E)

© Eskom 2026/Rev 0a

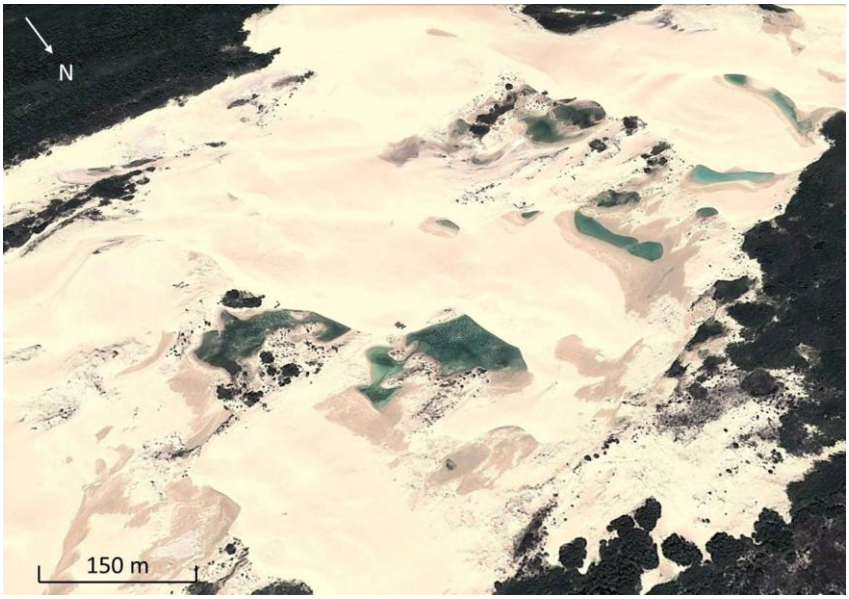


Figure 5.13-135
Unconsolidated Aeolian Dune Sands of the Schelm Hoek Formation Within the Oyster Bay Dunefield. Note the Development of Wetlands Within Dune Depressions



Figure 5.13-136
Nahoon Formation Palaeodune Rock Partly Overlain by Mobile Dune Sand of the Schelm Hoek Formation (34°10′31.1″ S, 24°41′38.2″ E)

© Eskom 2026/Rev 0a

These sediments were deposited in an intertidal zone environment ranging from sandy beaches to rocky shores (***Reference 5.13.166***). Much like the Alexandria Formation, the lithology of the formation consists of unconsolidated fine- to coarse-grained calcareous sand, calcareous sandstone, shelly limestone, coquina and basal gravel often described as conglomerate (***Reference 5.13.166***). The formation rarely exceeds 20 m in thickness. The determination of ages at of the top of the underlying bedrock and clasts welded onto marine terraces is discussed in ***Subsection 5.13.5.2.(b) i***. Within the site area, the Salnova Formation is stratigraphically overlain by the Nahoon Formation, but is more frequently buried by the semi-consolidated to unconsolidated aeolian sands of the Schelm Hoek Formation.

Basal gravel deposits stratigraphically correlative with either the Alexandria Formation or the Salnova Formation (***Reference 5.13.58***), overlying bedrock within the site area, are not laterally persistent and spatially show great thickness variation (***Figure F-5.13.137*** and ***Table T-5.13.11***).

Table 5.13.11
Maximum and Average Thicknesses of Basal Gravel Deposits Above Bedrock Stratigraphically Correlated to Either the Alexandria or Salnova Formation Within the Site Area

Area	Thickness of Basal Gravel Deposit	
	Maximum (m)	**Average (m)**
Oyster Bay	6.2	Only one borehole contained basal gravel layer
Thyspunt	11.5	0.2–5 with an increase in average thickness to 5–10 in some areas such as the palaeovalley where some of the thicker deposits may be fluvial channel gravel
Tony's Bay	8.9	0.5–3
De Hoek	4	0.5–1.5 on average, but basal gravel layer not extensive

Note: Thicknesses derived from borehole data (***References 5.13.28***, ***5.13.308***, ***5.13.58***, and ***5.13.62***).

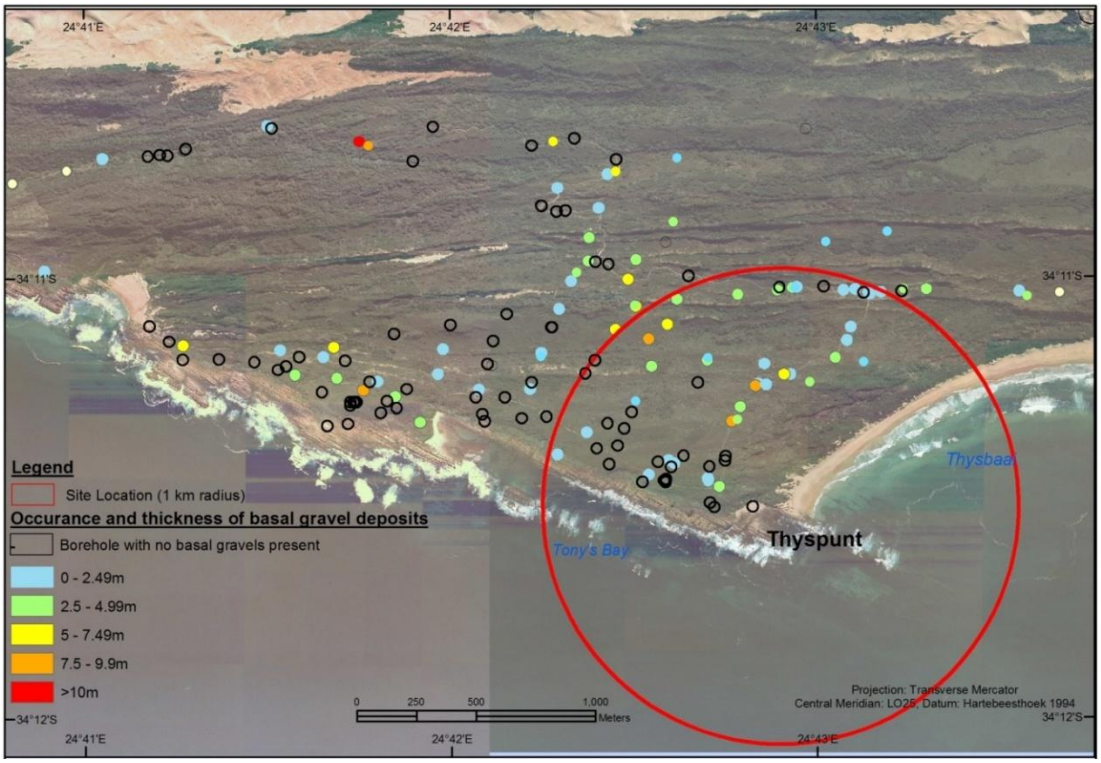


Figure 5.13-137
Distribution of the Basal Gravel Deposits Stratigraphically Either Correlated to the Alexandria or Salnova Formation at Thyspunt as Derived from Borehole Data (*References 5.13.28*, *5.13.308*, *5.13.60*, *5.13.61*, *5.13.58*, and *5.13.62*). The Site Location (1 km Radius) is also indicated.

These basal gravel deposits are composed of highly calcareous light grey to yellowish grey, medium- to fine-grained, and moderately to well-sorted sandstone and conglomerate composed of imbricated, disc- to roller-shaped clasts of pebble to cobble size set in a fine- to medium-grained sandy matrix (***Figure F-5.13.138***). The composition of the conglomerate depends on the underlying source materials, and in the greater site vicinity, clasts consist predominately of Table Mountain Group quartzite. The maximum thickness of basal gravels recorded from subsurface data (***References 5.13.28***, ***5.13.60***, ***5.13.61***, ***5.13.58***, and ***5.13.62***) at Thyspunt is 11.5 m in borehole TS-06, 1.5 km northwest of Tony's Bay. Average thickness is calculated between 0.5 m and 5 m, with occasional 5–10 m thicknesses (***Figure F-5.13.137*** and ***Table T-5.13.11***).

© Eskom 2026/Rev 0a

The basal gravel deposits act as a conduit for groundwater movement in the area, which enhances in-situ weathering of the underlying bedrock, especially in bedrock topographic lows. Thus the contact zone between the basal gravel and sand deposits (inferred to be Alexandria or Salnova Formation) and the bedrock can be described as a weathered contact (***Figure F-5.13.138***).

Offshore Stratigraphy

The continental shelf and coastal pain form the submerged and emergent portions of a seamless feature, exposed or inundated by fluctuating sea levels. Onshore units of the Table Mountain Group thus extend onto the adjacent continental shelf which forms the offshore site area.

Davidson & Smith (***Reference 5.13.281***) used marine geophysical data and the onshore geological maps to interpret marine outcrops as sandstones of the Table Mountain Group. Consistent with the onshore rocks, these units are jointed and faulted and cover 35% of the offshore survey area. See ***Figure F-5.13.139*** for a map showing the location of bedrock outcrops and sediment cover.

Unlithified and partially lithified sediments are interpreted to be Pliocene to Quaternary in age (***Reference 5.13.281***). The sediment is interpreted to be composed of silty, fine sand, and shell fragments and may belong to the Nanaga Formation based on field relations and acoustic signature (***Reference 5.13.281***). At the landward extent of the survey off Thys Bay is an area of gravel and coarse sediment (0.6% of the surveyed area). Approximately one-quarter (24%) of the sediment is rippled. Partially lithified sediment is found mainly in the center of the survey area.

© Eskom 2026/Rev 0a



Figure 5.13-138
The Miocene to Early Pliocene Alexandria Formation or Early Quaternary Salnova Formation Conglomerate (Highlighted in White) Composed of Imbricated, Disc- to Roller-Shaped Clasts of Pebble to Cobble Size Set in a Fine- to Medium-Grained Sandy Matrix Observed in Borehole NEW12 (*Reference 5.13.61*; 34°11′08.3″ S, 24°42′32.4″ E) Between 13.50 m and 30.49 m Below Ground Level. The basal gravel deposits act as a conduit for groundwater movement in the area, which enhances in-situ weathering of the underlying bedrock, especially in bedrock topographic lows for up to as much as 30 cm. Thus, the contact zone between the basal gravel and sand deposits can be described as a weathered contact (highlighted in red)

© Eskom 2026/Rev 0a

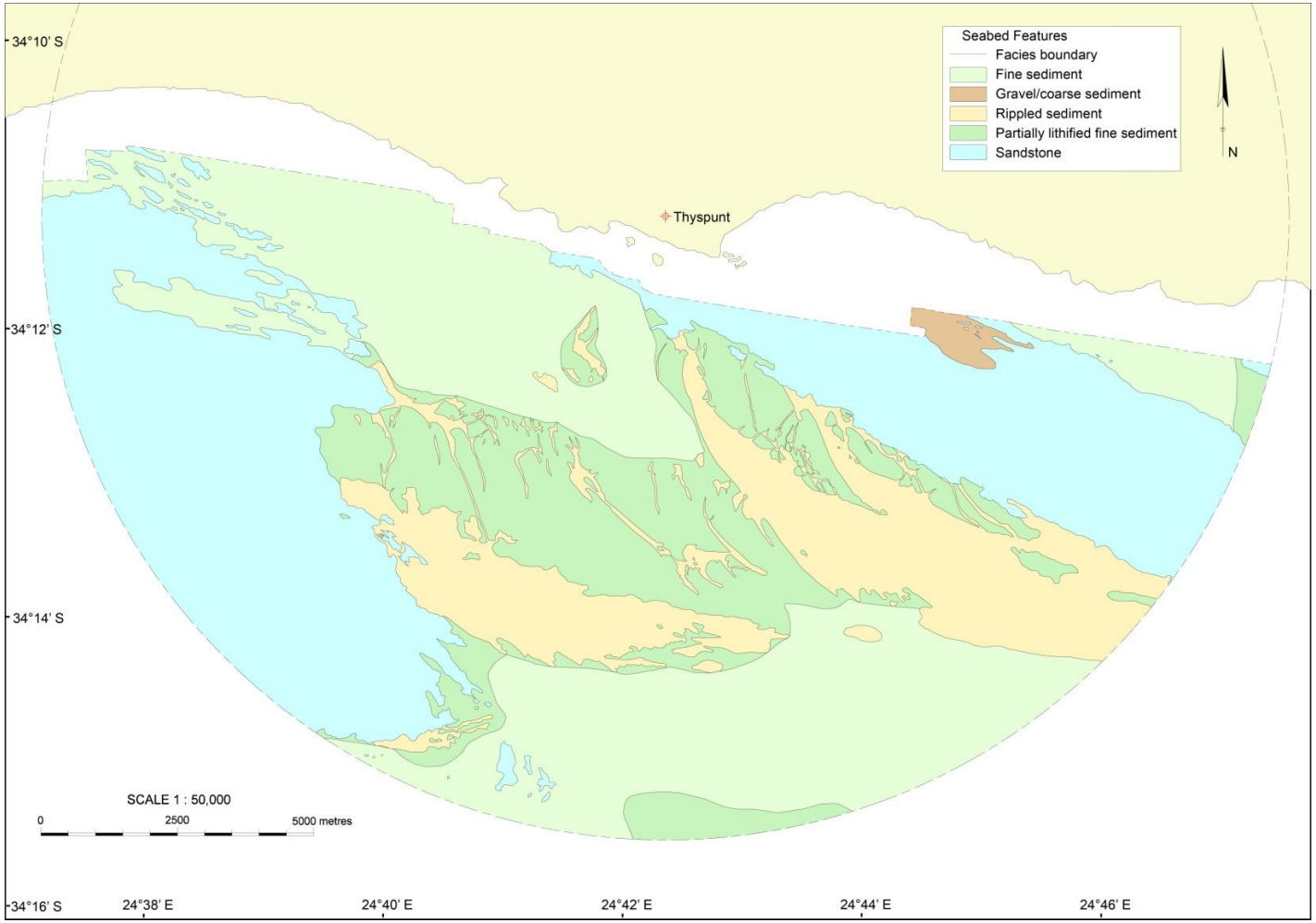


Figure 5.13-139
Offshore Lithological Seabed Features (Modified from *Reference 5.13.281*)

Sub-bottom profiling into the fine-grained sediment indicated two units in some locations. The upper unit is approximately 1–12 m thick and the lower unit is 2.8 m or more thick. Total sediment thickness was measured at 12–14 m. As The imaging methods has a maximum detection limit of approximately 14 m thickness, which means that sediment is possibly thicker at some locations.

iii Structural Geology (8 km Radius)

This section provides a description of the geologic structures within the site area.

Onshore Structure

The site area encompasses both the southwestern and northeastern limbs of the regional-scale northwest-southeast-striking, southeast-plunging asymmetrical Cape St Francis anticline (***Figure F-5.13.128***). Goedhart *et al.* (***Reference 5.13.27***) describes this anticline as an anticlinorium with numerous smaller secondary folds on its flanks and the presence of low-lying undulations along a broad hinge zone that are localised zones of more intense jointing, often associated with small dislocations representative of the various lithological competencies. The fold axis of the Cape St Francis anticline trends parallel to the northwest-southeast bedding strike and verges to the north. The fold axis is interpreted to terminate its on land occurrence near De Hoek from where it continues further offshore. The trend of the anticline is parallel to semiparallel to folding associated with the Cape Orogeny and is therefore considered to be of a similar age.

Bedding inclination within the site area is mostly controlled by this anticline and the parallel distance away from its fold axis. Near the fold axis, bedding inclination is shallow, with dip values ranging from 5 to 20 degrees. With increasing distance away from the fold axis dip values show a steady increase from the shallow 5–20-degree grouping to a steeper inclination of between 30 and 40 degrees west of De Hoek. Along the Thyspunt coast, bedding inclination reaches a maximum of between 50 and 65 degrees. Greater dip values are documented, but are rare and localised.

Northeastward-directed compression that led to the formation of the Cape St Francis anticline, also led to the predominantly brittle deformation in the competent quartzitic rocks of the Skurweberg and Peninsula formations within the site area. Less competent, more argillaceous sandstone and shaley beds (Goudini Formation) underwent more ductile deformation, with some apparent ductile deformation being achieved by small-scale brittle deformation (***Reference 5.13.27***). It is these competency differences and continued folding along the Cape St Francis anticline that led to the development of variable

compression and shortening of beds and ultimately local spatial corrections (***Reference 5.13.27***). Towards the south and southwest of the Cape St Francis anticline, this is clearly evident from the fold style where the large body of competent Peninsula Formation quartzitic sandstone that forms the core of the anticline acts as a structural buttress to compression.

Folds in thinner-bedded formations are piled up tightly against the anticline's southern limb, rupturing in places to form small east-southeast thrusts (***Figure F-5.13.140***) oblique to the main Cape St Francis fold axis.

Deformation is also manifested by overfolding of beds (***Figure F-5-13.141***), late-stage kink bands and movement along bedding planes. Beds are intensely jointed and sheared along thrust planes and where the dip angle increases significantly the beds are frequently folded. Folding in these areas ranges from open to tight isoclinal folds. Some of these fold limbs were cut off and displaced by further progressive movement (***Reference 5.13.27***).

Joints sets within the site area reflect trends indicated for joint sets in ***Subsection 5.13.5.2.(a) iii***. Goedhart *et al.* (***Reference 5.13.27***) noted that within the site area joint sets often disappear or show a change in strike when penetrating strata with different competency. Joint frequency within not only the site area, but also the greater site vicinity appears to be variable. Zones of closely or moderately spaced joints are separated by areas of tens or hundreds of metres of very sparsely spaced jointing. Areas of high frequency jointing are often referred to as shatter zones and generally weather negatively to form gullies along coastal exposures as seen between Cape St Francis and Oyster Bay (***References 5.13.12***, ***5.13.22***, ***5.13.338***, ***5.13.28***, and ***5.13.30***.

Both minor normal left-lateral and right-lateral displacements occur along joint planes (***Figure F-5.13.142***). Movement is typically on the order of a few centimetres, but rare hundred-metre movements have been documented and are regarded as space-accommodating minor faulting during folding.

A series of high-angle faults were indicated on Atomic Energy Cooperation (AEC) maps (***References 5.13.28***, ***5.13.308***, and ***5.13.33***) in the area between Oyster Bay and De Hoek based on a broad-resolution airborne geophysical study (***Reference 5.13.33***). The validity of these faults was investigated by Goedhart *et al.* (***Reference 5.13.27***), who concluded that these faults could not be verified in the field. In addition, high-resolution geophysical surveys (***References 5.13.35*** and ***5.13.40***) could not verify their existence.

© Eskom 2026/Rev 0a



Figure 5.13-140
Possible Thrust Ramps Seen in Coastal Exposures of the Peninsula Formation Quartzitic Sandstone Immediately East of Thys Bay (34°11′15.9″ S, 24° 44′21.7″ E)

© Eskom 2026/Rev 0a



Figure 5.13-141
Z-Shaped Folding and Overfolding Resulting in Bedding Shortening Seen in Strata of the Peninsula Formation in the Area Immediately East of Thys Bay. Overfolding May Have Been Accompanied by Thrusting Semiparallel to the Cape St Francis Fold Axis, with Folded Dismembered Fold Limb Stacked Against More Competent Beds (34°11′16.9″ S, 24°44′23.0″ E; *Reference 5.13.27*)

© Eskom 2026/Rev 0a



Figure 5.13-142
Small-Scale Localised Microfaults Develop Along Joint or Fracture Planes. At This Locality (34°11′26.6″ S, 24°44′52.4″ E) Along the Coast a 15 cm Displacement of a Light Green-Grey Shale Unit in the Peninsula Formation is seen

© Eskom 2026/Rev 0a

Borehole data (***References 5.13.28***, ***5.13.317***, ***5.13.318***, and ***5.13.319***) did intercept what was interpreted as brecciated zones, but these could not be traced through to coastal exposures. Rather, they are interpreted to coincide with high-frequency jointing areas (shatter zones).

West of Oyster Bay, a structural feature referred to as the 'SV1' lineament was defined by Cole & Naudé (***Reference 5.13.35***) during airborne geophysical surveys conducted in the area. SV1 was interpreted to be a 15.4 km long northeast-southwest-trending lineament with a 600 m displacement and a probable fault. Subsequent investigation by Goedhart & Cole (***Reference 5.13.36***) suggests that SV1 is not a fault for its entire length and with only a small offset possibly occurring in the Cedarberg Formation at its western end. This was confirmed by ground geophysical investigations by Raath & Cole (***Reference 5.13.40***) that showed offset only at the western end of the feature, and no strata displacement or disruption along the remaining eastern end. SV1 is not presumed to be a fault, but rather, it coincides with an area subjected to high-frequency jointing that adheres to the already-documented jointing pattern in the site area where minimal movement has occurred along joint planes (***Reference 5.13.36***).

Offshore Structure

The offshore and nearshore morphology of the seafloor within the site area is characterised by a sediment-filled central basin bounded by outcrops of bedrock on the western and eastern margins (***Reference 5.13.281*** and ***5.13.343***). The bedrock consists predominantly of Table Mountain sandstones that are folded, steeply bedded, and highly fractured. Sandstone ridges have relief of up to 7 m (***Reference 5.13.58***). Horwood (***Reference 5.13.46***) identified a prominent fold in the southwestern part of the offshore site area. The dominant northwest/west-northwest bedding trend is displaced by smaller northeast-trending fractures which are interpreted to be younger normal faults. These faults display a dip-slip motion with downthrow to the southeast (***Reference 5.13.46***).

c) Site Location (1 km Radius)

The site location covers an area of approximately 3 km^2. The onshore portion of the site location is almost exclusively covered by east-west trending dune deposits of the Algoa Group. The largest portion of the site location is situated offshore.

© Eskom 2026/Rev 0a

i Physiography and Topography (1km Radius)

Within the site location area (***Figure F-5.13.143***), Thyspunt is separated into a northwest-southeast-trending, southwest-facing, relatively straight and rocky coastline to the west and the sandy beach log-spiral embayment of Thys Bay to the east.

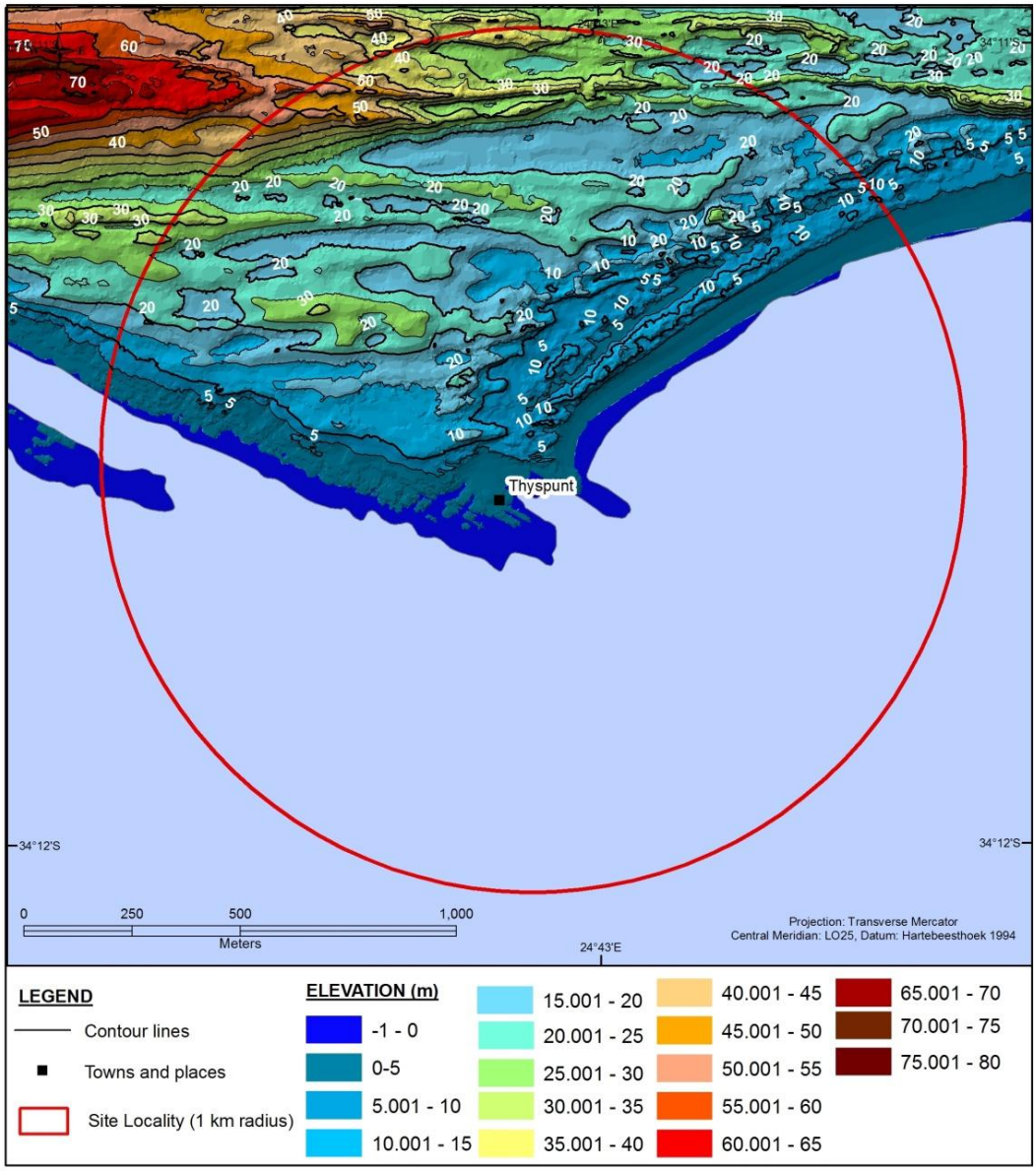


Figure 5.13-143
Digital Elevation Model of the Site Location

The rocky coastline reflects the underlying bedrock geology. The coastline morphology is in part the consequence of the distribution and lithology of underlying geological formations and their differential resistance to weathering that led to the development of alternating headlands and embayments. The Thyspunt headland and surrounding rocky coastline reflects the erosion-resistant nature of the quartzitic sandstone of the Skurweberg Formation. The development of Thys Bay is the consequence of the less erosion-resistive nature of the thinly bedded sandstones, shales, and mudstones of the underlying Goudini and Cedarberg Formations. Except for rocky coastal exposures, the entire site locality is blanketed by stable, vegetated Cenozoic Algoa Group dune deposits. A narrow strip of modern linear east-west-trending active dunes of the Thys baai dunefield still occur to the north of modern beach deposits at Thys Bay (also see ***Subsection 5.13.5.2.(b) i***).

Elevation increases away from coastal margins in a steady but undulating nature (***Figure F-5.13.144***) associated with the rolling dune geography. Elevation highs are associated with dune ridges whilst topographic lows are related to dune troughs. Three prominent east-west-trending dune ridges occur within the site locality, the most elevated of which occurs along the north-western boundary of the site locality at between 50 and 55 m asl (***Figure F-5.13.143***). Refer to ***Subsection 5.13.5.2.(b) i*** for bedrock topography and information regarding marine terraces within the site location.

The site location is not drained by any rivers; however, a number of coastal seeps do occur along southwest-facing coastal margins at the base of dunes, above the high water mark. These seeps lead to the formation of numerous wetlands distributed in patches along the coast in a narrow >40 m band along the coast. The seeps form as rainwater infiltrate and filter through porous dune cover to reach less porous bedrock from where the water flows downgradient to reach rocky coastal exposures as a spring.

Refer to ***Subsection 5.13.5.2.(b) i*** for offshore physiography and topography.

ii Stratigraphy (1km Radius)

The site location is characterised by northwest-southeast-trending; southwest-dipping bedrock of the Ordovician Goudini and Silurian Skurweberg Formations (***Figure F-5.13.145***). Within the site location, the incompetent Goudini Formation forms the majority of the bedrock.

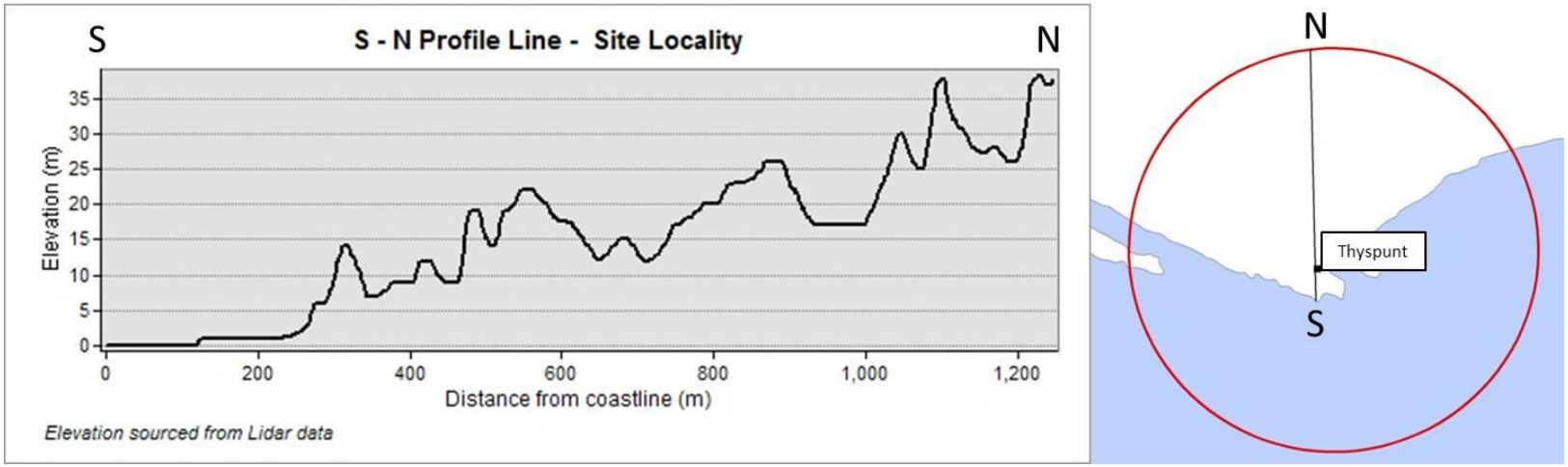


Figure 5.13-144
Elevation Shows a Steady Increase away from Coastal Margins in a Northerly Direction

© Eskom 2026/Rev 0a

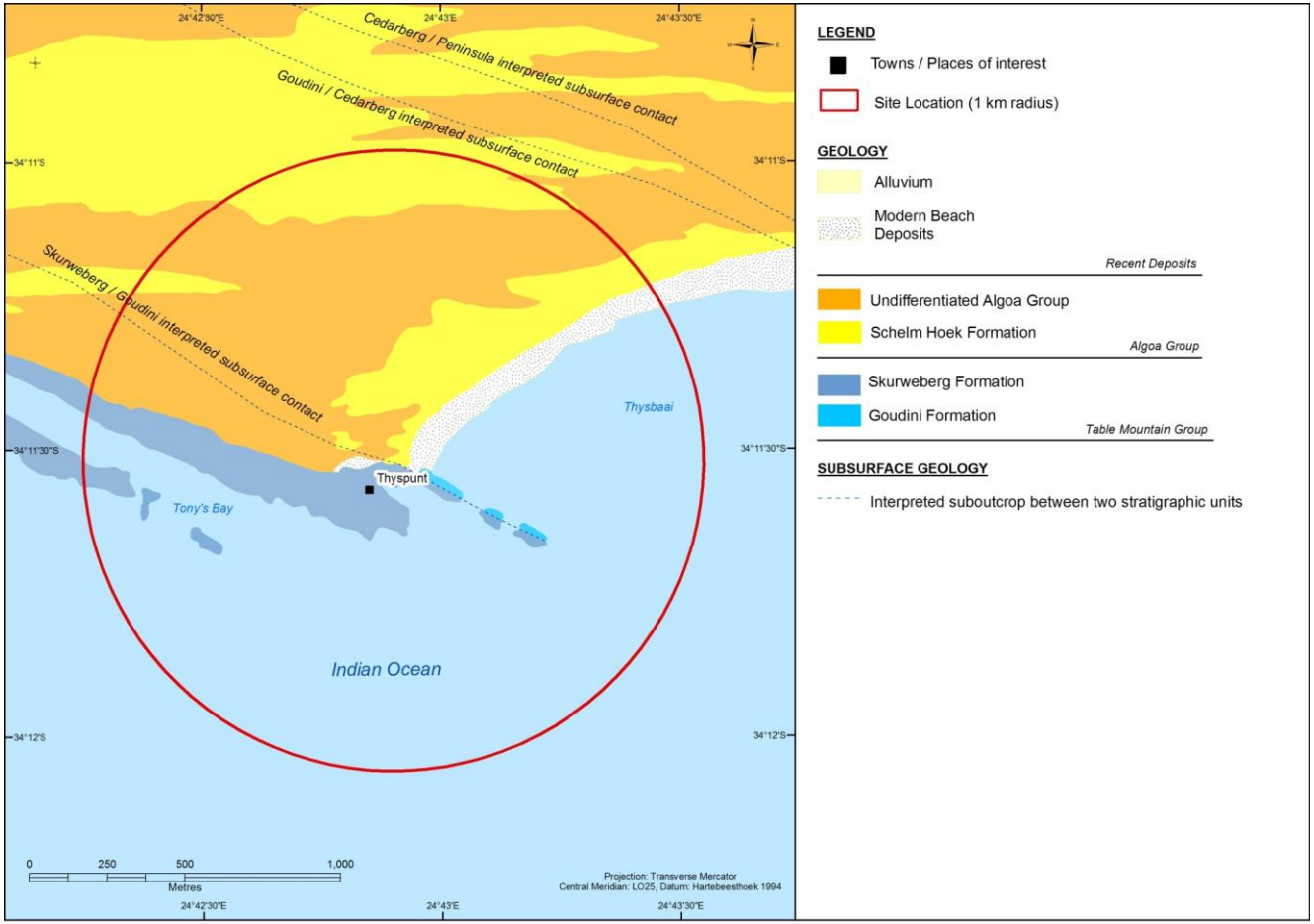


Figure 5.13-145
Geology of the Site Location (1 km Radius) (Modified from *Reference 5.13.27*)

© Eskom 2026/Rev 0a

The Goudini and Skurweberg Formations are partly exposed along a narrow 80–200 m wide northwest-southeast rocky coastline near Thyspunt, but predominantly overlain inland by unconsolidated to semiconsolidated clastic nearshore-marine and coastal aeolian-derived Cenozoic sediments of the Algoa Group (***Figure F-5.13.145***). Descriptions of these units are provided in ***Subsections 5.13.5.2.(a) i*** and ***5.13.5.2.(b) ii***. Seismic site characterisation of shear-wave velocity within the Goudini Formation as a function of depth at multiple locations across the site is provided in ***Section 5.14*** (Seismic Hazard Analysis).

An unweathered, narrow 50 m wide strip of the incompetent Goudini Formation sandstone is exposed at Thyspunt (***Figure F-5.13.145***) and it is here where the Goudini Formation's upper contact with the Skurweberg Formation is mapped along coastal exposures, as transitional over at least 25 m (***Reference 5.13.27***). Close to the contact between the Skurweberg and Goudini Formations, the number of shale bands within the Skurweberg Formation increases, with shale beds appearing darker and more carbonaceous (***References 5.13.28*** and ***5.13.308***). The subsurface contact between these formations beneath Cenozoic sediments is interpreted from borehole data (***References 5.13.28***, ***5.13.60***, ***5.13.61***, ***5.13.62***, and ***5.13.58***) and is indicated on ***Figure F-5.13.145***.

The interface between the bedrock and Cenozoic sediments of the Algoa Group is often described as a sharp, but weathered, contact and is characterised by either the absence or presence of marine deposits stratigraphically correlative with either the Alexandria (***Reference 5.13.321***) or the Salnova Formations (***Reference 5.13.58***). These deposits consist of sand and/or gravels on a number of well-planed, seaward-sloping platforms in shoreface and foreshore to lagoonal and/or estuarine depositional settings (see ***Subsection 5.13.5.2.(b) ii***).

Sediments of the Algoa Group can stratigraphically be subdivided into the Alexandria, Nanaga, Salnova, Nahoon, and Schelm Hoek Formations (see ***Subsection 5.13.5.2.(a) ii***), only the latter of which is exposed within the site location as small, isolated, unconsolidated sand exposures, not yet overgrown by dense coastal vegetation. Differentiation between formations, not only within the site location, but also the greater site vicinity is problematic, due to limited exposure. Goedhart *et al.* (***Reference 5.13.27***) were able to identify only the Schelm Hoek Formation within the site location, and thus chose to define the remaining areas as undifferentiated Algoa Group (***Figure F-5.13.145***). The presence of the Salnova Formation within the subsurface is, however, confirmed by borehole data (***References 5.13.28***, ***5.13.60***, ***5.13.61***, ***5.13.62***, and ***5.13.58***). Also refer to the discussion in ***Subsection 5.13.5.2.(b) ii***.

© Eskom 2026/Rev 0a

The Algoa Group's maximum documented thickness within the site location is 54 m in borehole NEW L1 (***Reference 5.13.62***) and 50 m in borehole NEW 6 (***Reference 5.13.61***) along the north-northwestern boundary margin of the site location (***Figure F-5.13.133***), an area associated with the presence of a palaeochannel. Bedrock elevations are close to or below sea level within much of the site location, which is located along the same trend as the Thys Bay embayment (***Reference 5.13.38***). Refer to the discussion in ***Subsection 5.13.5.2.(b) ii***.

The Algoa Group is overlain by fine-grained sandy soil containing less than 6 percent clay. These soils are grey to dark brown in colour (***Figure F-5.13.146***).

Further inland, with increasing distance away from coastal margins, soils become darker grey due to the accumulation of organic matter in the A horizon. The dune soils, which may contain shell middens, can reach thicknesses in excess of 3 m (***Reference 5.13.344***).

iii Structural Geology (1km Radius)

Within the site location (***Figure F-5.13.147***), Palaeozoic bedrock of the Skurweberg and Goudini Formations is situated along the western limb of the regional northwest-southeast-striking, southeast-plunging Cape St Francis anticline described in ***Subsection 5.13.5.2.(b) iii***. A narrow strip of southeast-dipping coastal exposures indicates moderately steep bedding inclinations, dipping on average between 40 and 50 degrees, with a maximum of 60 degrees documented 200 m northeast of Thyspunt (***Figure F-5.13.147***).

Although the majority of bedrock is overlain and buried by Cenozoic deposits, bedding inclination further north within the site location is assumed to be within the above-mentioned range, based on hinterland inclinations and the distance from the Cape St Francis anticlinal fold axis (***References 5.13.28***, ***5.13.308***, and ***5.13.27***).

No normal faults or thrust faults are recognised within the site location (***References 5.13.28***, ***5.13.308***, and ***5.13.27***).

The jointing patterns within the site location reflect those discussed in ***Subsections 5.13.5.2.(a) iii*** and ***5.13.5.2.(b) iii***.

5.13.5.3 Surface Faulting Evaluation

This subsection describes the evidence used to evaluate the potential for future surface faulting and related capable tectonic deformation at the Thyspunt site and surrounding site area.

© Eskom 2026/Rev 0a



Figure 5.13-146
Brown to Dark Brown, Fine-Grained Organic Sand Forms the Top Soil Within the Site Location. The Topsoil Thickness in Borehole TB32 (34°11′24.4″ S, 24°42′45.0″ E), Located Approximately 300 m from Thyspunt, Is 2.05 m (Highlighted in Green). The Topsoil Is Underlain by Undifferentiated Algoa Group Sediments

© Eskom 2026/Rev 0a

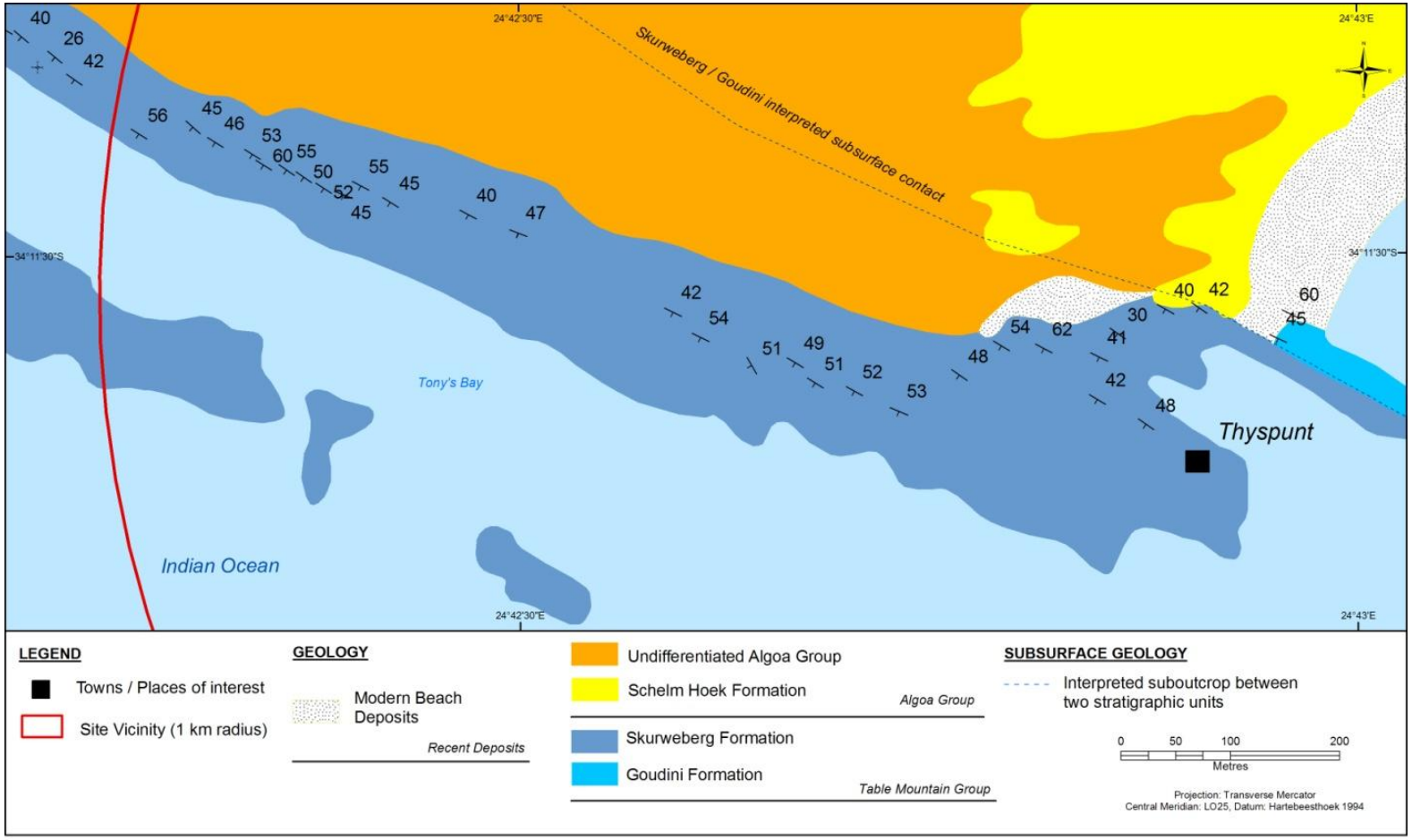


Figure 5.13-147
Moderately Steep Bedding Inclinations Along the Northwest-Southeast-Trending Coastline of the Site Locality

© Eskom 2026/Rev 0a

The approach to assessing the potential for surface deformation related to surface faulting hazard follows the guidance provided in US NRC Regulatory Guide 1.208 (***Reference 5.13.8***) and the IAEA guidance in SSG-9 (***Reference 5.13.5***). The following aspects of the geology and seismicity of the site region are discussed:

- Geological, seismological, and geophysical investigations (***Subsection 5.13.5.3.(a)***).
- Geological evidence of surface deformation or lack thereof (***Subsection 5.13.5.3.(b)***).
- Earthquakes associated with capable tectonic sources (***Subsection 5.13.5.3.(c)***).
- Ages of most recent deformation (***Subsection 5.13.5.3.(d)***).
- Relationship between tectonic structures in the site area and regional tectonic structures (***Subsection 5.13.5.3.(e)***).
- Characterisation of identified capable tectonic sources (***Subsection 5.13.5.3.(f)***).
- Designation of zones of Quaternary deformation in the site region (***Subsection 5.13.5.3.(g)***).
- Potential for surface tectonic deformation at the site (***Subsection 5.13.5.3.(h)***).

Results of the surface faulting evaluation indicate that there is evidence of no Quaternary tectonic surface faulting or fold deformation at the Thyspunt site. The closest approach to the site of a known Quaternary active fault, the Kango Fault, is 129 km. Other nearby structures that were active in the Mesozoic, such as the Plettenberg and Gamtoos Faults, which lie at distances of 20 km and 47 km, respectively, at closest approach, are assessed to not be capable tectonic sources. For purposes of the probabilistic seismic hazard analysis (***Reference 5.13.1***), these faults were assessed to have a low probability of being seismogenic (p[S] = 0.2] in the present tectonic regime, but were included as potential seismic sources that could generate vibratory ground motions at the site. However, from the standpoint of a deterministic surface faulting evaluation and applying the criteria given in international regulatory guidance, these faults are not assessed to be capable of generating surface faulting at the site (***Subsection 5.13.5.3.(f)***). As discussed in ***Subsection 5.13.5.3.(e)*** below, even if the Plettenberg Fault is assumed to generate a large-magnitude earthquake, secondary rupture at the site during such an event would be negligible.

This subsection is specifically focused on the assessment of surface faulting due to tectonic mechanisms. The consideration of surface displacement due to

© Eskom 2026/Rev 0a

nontectonic mechanisms such as geotechnical soil failure, is given in ***Section 5.15*** (Geotechnical Characterisation).

a) Geological, Seismological and Geophysical Investigations

Published and unpublished literature and data on structures and tectonics in the Thyspunt site region and vicinity as discussed in ***Subsections 5.13.5.1*** and ***5.13.5.2*** provide information on the timing of tectonic deformation in the site region and site vicinity, respectively.

Geological, seismological, and geophysical site characterisation studies that provide additional information that can be used to assess the potential for surface faulting are summarised in ***Table T-5.13-1***. These include early site selection studies (*e.g.,* ***References 5.13.12***, ***5.13.23***, and ***5.13.28***), as well as site characterisation studies (geophysical investigations and geological mapping) conducted by the Council for Geoscience in the time period 2007–2008 (***References 5.13.37***, ***5.13.35***, ***5.13.40***, ***5.13.36***, ***5.13.41***; ***5.13.26***, and ***5.13.27***).

Subsurface information from other geotechnical site characterisation reports (***References 5.13.28***, ***5.13.60***, and ***5.13.61***) were used in the mapping and assessment of the geology and geomorphology of the site as outlined in Hanson *et al.* (***Reference 5.13.58***). A more complete discussion of the available subsurface data and geotechnical conditions at the Thyspunt site is presented in ***Section 5.15***.

Geological investigations conducted in support of the PSHA (***Section 5.14***) included mapping and age-dating of the marine terrace sequence within the site area and portions of the surrounding site vicinity (***Reference 5.13.58***). These studies, used in conjunction with detailed subsurface investigations to assess the geotechnical conditions of the site location (see ***Section 5.15***), provided basic data and information to assess the stability of the site location and the potential for tectonic surface faulting.

b) Geological Evidence of Surface Deformation or the Lack Thereof

A review of published literature and maps, offshore investigations, and field reconnaissance indicates that there are no major faults within the site area, and none of the smaller faults or deformation features identified in onshore bedrock exposures or from interpretation of offshore data within 8 km of the site show evidence for displacement of Quaternary (2.6 Ma) deposits or landforms (***Subsection 5.13.5.2.(b) iii***). Although previous studies mapped faults within site vicinity (40 km radius), no evidence was found for Quaternary fault activity (***Subsection 5.13.5.2.(a) iii***).

Earlier site characterisation studies during the 1980s were followed up by further geophysical investigations in 2007 (***References 5.13.35***, ***5.13.40***, ***5.13.36***, and ***5.13.41***). The latter investigations covered a significant part of the site vicinity (onshore) and the site area (onshore and offshore). They were later verified in the field (***Reference 5.13.27***), but no evidence of faulting or strong ground motion could be found in the Cenozoic-age cover rocks. This confirms the earlier AEC and CGS findings (***References 5.13.12***, ***5.13.23***, ***5.13.26***, and ***5.13.37***). Furthermore, practically all of the linear features were found to be related to old joint patterns (***Reference 5.13.27***).

Several geophysical techniques were employed to investigate the possible north-west extension of the Cape St Francis offshore fault into the site area, but no single method could confirm the potential presence of such an extension. The mapped trace of the fault comes within 17 km of the site (***Reference 5.13.1***), but tracing it further is complicated by the difficulty of identifying bedding-parallel faults in steeply dipping strata. The TDEM studies completed in 2008 (see ***Reference 5.13.42***) precluded three of the potential locations for the onshore extension of the Cape St Francis Fault. A subsequent reinterpretation of the TDEM results in conjunction with geological observations (see Addendum in ***Reference 5.13.43***) proposed a model with the Cape St Francis Fault dying out before reaching the onshore.

Interpretation of drilling data along an additional TDEM survey (***Reference 5.13.44***) across the previously projected trend of the Cape St Francis Fault provided additional information to evaluate possible extensions of the Cape St Francis Fault onshore. The physical condition of core recovered during the 2012 Cape St Francis drilling program (***Reference 5.13.58***, Appendix B) suggests that it is unlikely that a fault runs adjacent to the Cedarberg Formation. The possibility that anomaly D identified by Zadorozhnaya *et al.* (***Reference 5.13.44***) represents a fault (possibly the Cape St Francis Fault), however, cannot be excluded when viewed in conjunction with the evidence presented by Stettler *et al.* (***Reference 5.13.43***) and in Appendix F of Hanson *et al.* (***Reference 5.13.58***). However, lack of evidence of surface deformation in the site area (summarised in ***Subsection 5.13.5.3.(h)***) and St Francis coast, including along the projected trends of the Cape St Francis Fault, indicates that even if the Mesozoic fault extends onshore, it has not displaced Quaternary deposits or geomorphic surfaces (***Reference 5.13.58***).

The Plettenberg Fault, a large Mesozoic basin-bounding offshore fault whose closest approach to the site is 20 km, was examined for evidence of Cenozoic deformation. Published interpretations of seismic lines across the Plettenberg Fault (*e.g.*, ***Figure F-5.13-56***) do not show the fault extending up to the seafloor

© Eskom 2026/Rev 0a

(***References 5.13.72*** and ***5.13.137***). Subsequent interpretations of seismic lines (***Reference 5.13.45***), showed that while there is evidence for no post-Cretaceous activity on some seismic profiles across the Plettenberg Fault, there is equivocal evidence for Tertiary displacement on other lines (***Reference 5.13.45***). The origin and timing of possible Tertiary displacement observed in the seismic data is not well-constrained. The apparent vertical displacement observed on some lines may have occurred in the early Tertiary or may be due to nontectonic processes (***Reference 5.13.45***).

Inspection of a recently processed high-resolution bathymetry data set compiled by De Wet (***Reference 5.13.59***) from single-beam bathymetric data collected from shiptrack data and gridded at a resolution of approximately 1 m (***Figure F-5.13-57***) reveal evidence of no late Quaternary faulting. For example, there are no geomorphic features associated with the post-Cretaceous offsets interpreted from the seismic data, and there is not a continuous scarp along the trace of the fault that would suggest latest Pleistocene to Holocene (post-LGM transgression) displacement of the seafloor (***Reference 5.13.1***). Based on a review of these data, the Plettenberg Fault is assessed to have a low probability of being seismogenic in the probabilistic seismic hazard analysis (***Reference 5.13.1***).

Dunefields in the site area range from active to Pleistocene in age (see ***Subsection 5.13.5.2.(a) i***). Stabilised and lithified dunes were examined using LiDAR data processed into a shaded relief model (1 m resolution, ***Figure F-5.13.148***) and aerial photographs (pixel size of 15 cm for individual frames; composite image pixel resolution of 1 m). No linear features cutting or displacing the dunes were identified in the study area. In addition, there is no obvious geomorphic expression (lineaments, scarps, etc.) in aerial photographs, GoogleEarth imagery, or available DEM data (10 m resolution) to suggest Quaternary reactivation of the Gamtoos Fault (***References 5.13.24*** and ***5.13.58***).

c) Earthquakes Associated with Capable Tectonic Sources

There have been no historically reported earthquakes or alignments of earthquakes within 40 km of the site that can be associated with a mapped bedrock fault (see ***Section 5.14*** – Seismic Hazard Analysis). No earthquakes larger than M_w 3.0 are identified in the site vicinity (***Figure F-5.13-35***).

d) Ages of Most Recent Deformation

The major deformation on bedrock structures in the site vicinity appears to have occurred during the Mesozoic and most faults in the region are believed to have

been inactive since late Mesozoic to early Cenozoic time, at least 30 million years ago (***Subsections 5.13.5.1.(b)***, ***5.13.5.1.(d) i*** and ***5.13.5.1.(d) iv***).

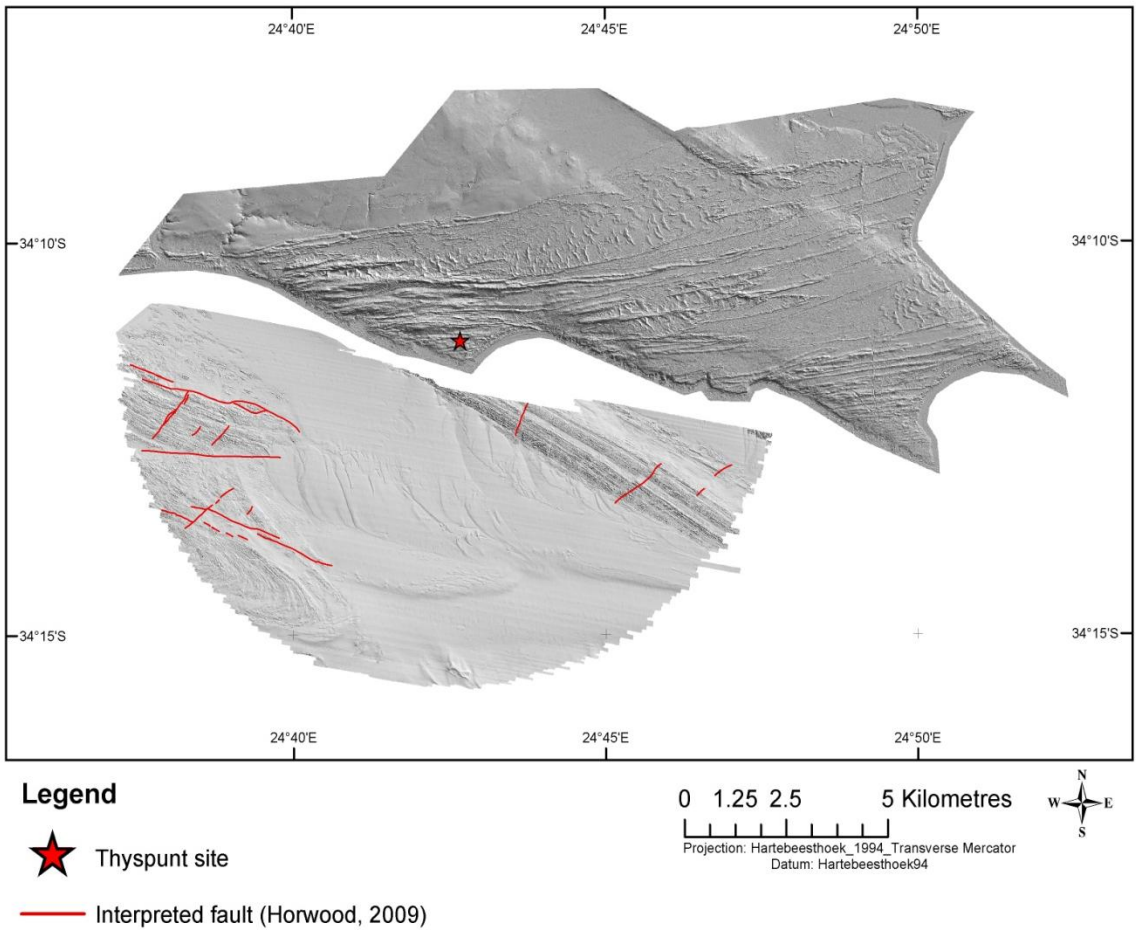


Figure 5.13-148
Onshore LiDAR and Offshore Bathymetric Data Presented as Hillshade DEMs (Interpreted Fault Data from *Reference 5.13.46*)

A detailed marine terrace field mapping programme was conducted in the Oyster Bay to Cape St Francis study area (***Reference 5.13.58***). Maps and shore-parallel profiles that show locations of field localities, topographic profiles, top of bedrock elevations, and geochronology samples and correlation of marine terraces are provided in Appendix 2 of ***Reference 5.13.1*** (Plates A2–5.2-2 through A2–5.2-5). The results of studies in this area (***Reference 5.13.58***), which includes the Thyspunt site, demonstrate that offshore faults (*i.e.*, the Cape St Francis fault zone) and minor northeast-trending secondary faults documented by onshore bedrock mapping and interpretation of offshore seismic data show no evidence of deformation in the past 400 ka to possibly 3.0 Ma.

This conclusion is based on the following general observations and conclusions:

- Age constraints of Quaternary marine terrace platforms and cover sediments in the site area and site vicinity inferred from optically stimulated luminescence (OSL) and cosmogenic nuclide (CN) analyses (***References 5.13.55*** and ***5.13.52***, respectively) support regional correlations.
- Based on comparison with other regional marine terrace studies, the highest platforms exposed in the Thyspunt Site Area likely correlate with the mid-Pliocene warm-interval (3.3–3.0 Ma) sea-level highstand and regressional shorelines from that highstand. Although the shoreline angle for the highest marine platform (at an elevation of approximately 30 m) is not exposed, the similarity in the elevation of the seaward edge of the platform exposed at both the eastern and western ends of the Oyster Bay to St Francis Bay area suggests that there has been no apparent vertical deformation of this platform across the projected trends of offshore faults (*e.g.*, Cape St Francis or secondary northeast-trending faults) since it was formed initially.
- The oldest ages (~1.1–1.7 Ma) for terraces in the site area obtained by cosmogenic nuclide analysis are burial ages for marine platforms at or close to modern sea level (±1.5 m) (TSP-16 and TSP-14, respectively; ***Reference 5.13.52***). The consistency between the minimum exposure time and burial times for the paired samples of clasts and bedrock from the platforms (*e.g.*, TSP-NEW 14 and TSP-NEW 16 cosmogenic nuclide dating samples) indicates that the ages for these samples are more reliable than the samples collected from the higher marine terraces at the surface, which may have a more complex history (***Reference 5.13.52***). These platforms lie in a large palaeobay behind the Thyspunt headland. Shoreline angles for these platforms are not well-defined, and the relatively low relief in this palaeobay could be the result of reoccupation of the seaward parts of older terraces by younger highstands and fluvial incision and erosion during

© Eskom 2026/Rev 0a

lowstands. Assuming palaeosea level was above –10 m during the formation of these platforms, these data are not inconsistent with a low, long-term isostatic rock uplift rate of approximately 4.4 m/Myr suggested by cosmogenic nuclide analysis of stream sediment samples. The inferred uplift rate for the six paired samples (marine terrace bedrock/overlying beach gravel) is 5.0 ± 0.7 m/Myr (***Reference 5.13.52***).

- The Pleistocene total history age of 1.04 Ma for sample TSP-26 (elevation of 26.7 m) in Oyster Bay is likely a minimum limiting age for this platform (***Reference 5.13.52***).
- Intermediate elevation terraces (shoreline angle elevations of 15–20 m) yielded middle Pleistocene ages of 560–680 ka, which are also judged to be minimum limiting ages (***Reference 5.13.52***).
- Minimum exposure history ages for cosmogenic dating samples suggest that the 13 ± 1 m and 7–7.5 m terraces identified in the Thyspunt site area correlate with the Pleistocene Marine Isotope Stage MIS 11 (~400 ka) and possibly MIS 9 (~320 ka), respectively. The correlation with MIS 9 is judged to be less reliable than the correlation of the higher platform with MIS 11.
- Marine terraces identified and mapped as part of the Geological Investigations programme correlate with regional marine terrace sequences based on elevation and altitudinal spacing (***Reference 5.13.58***). No disruptions or evidence of vertical offset of the marine terrace sequences was observed. The 13 ± 1 m terrace observed at several locations in the study area between Oyster Bay to St Francis Bay appears to correlate with the well-dated MIS 11 (400 ka) terrace (up to ~14 m) identified at several locations in the Mossel Bay region (***Reference 5.13.345***); this conclusion is based on cosmogenic nuclide ages of bedrock platforms in the study area, width and geomorphic expression of the marine terrace as a prominent feature, and general similarities in marine terrace sequences identified regionally (***Reference 5.13.58***).

e) Relationship Between Tectonic Structures in the Site Area and Regional Tectonic Structures

Mapped surface bedrock faults within the site area (8-km radius) are primarily related to the Mesozoic extensional deformation. With the exception of the Kango Fault, which is approximately 129 km at closest distance, there is no new information to suggest that the faults associated with the Mesozoic basins in the site region are capable tectonic structures as defined by Regulatory Guide 1.208 (Appendix D; ***Reference 5.13.8***). Evidence for no surface deformation of high surfaces underlain by Grahamstown Formation (Tg) that cross the surface traces of the Kouga, Coega, and Baviaanskloof Faults (***References 5.13.20***, ***5.13.18***, and ***5.13.17***) demonstrate that these faults have not experienced surface rupturing earthquakes in the past 1–4 million years,

and in some cases, the past estimated 8–10 million years or longer time period (see ***Subsection 5.13.5.1.(d) iv***).

As discussed in ***Section 5.14*** (Seismic Hazard Analysis), the Plettenberg Fault is assessed for purposes of the probabilistic seismic hazard analysis to have a low probability of being seismogenic (p[S] = 0.2). For purposes of the surface faulting evaluation, the potential for a coseismic rupture on the Plettenberg Fault, which at its closest approach lies 20 km away, to generate secondary faulting at the site was assessed. As part of a probabilistic fault displacement hazard analysis approach developed for normal faults, Youngs *et al.* (***Reference 5.13.346***) compiled and analysed data on the width of the zone of secondary faulting associated with observed normal-faulting earthquakes. The width was measured as a function of whether the secondary faults lay on the hanging-wall or the footwall side of the primary coseismic fault, and the magnitude of the earthquake giving rise to the surface faulting. The Thyspunt site lies on the footwall side of the Plettenberg Fault. The footwall data generally show a narrower zone of secondary faults than the hanging-wall side, and the width of the zone of secondary faults generally is larger with increasing magnitude. In general, the expected width of the zone secondary faulting on the footwall for large-magnitude (M > 7) earthquakes is less than 10 km, and the widest zone in the data set was 15 km.

Based on these data and given the 20 km closest distance to the Plettenberg Fault, it is concluded that even if the Plettenberg Fault is assumed to generate a large-magnitude earthquake, the probability that surface faulting will occur at the site due to secondary faulting is essentially zero.

f) Characterisation of Identified Capable Tectonic Sources

A “capable tectonic source”, as defined by Regulatory Guide 1.208 (***Reference 5.13.8***), is described by at least one of the following characteristics:

- Presence of surface or near-surface deformation of landforms or geological deposits of a recurring nature within the last approximately 500,000 years, or at least once in the last approximately 50,000 years.
- A reasonable association with one or more large earthquakes or sustained earthquake activity that usually is accompanied by significant surface deformation.
- Structural association with a capable tectonic source having characteristics of list item 1 above, such that movement on one could reasonably be expected to be accompanied by movement on the other.

No capable faults are present in the site area (8-km radius) based on observations of mapped structures and timing of most recent deformation

discussed above in ***Subsections 5.13.5.3.(b)*** and ***5.13.5.3.(d)***. Consideration of the other criteria used to assess fault capability (*i.e.*, association with seismicity or structures with a capable tectonic source), does not indicate that structures in the site vicinity are capable tectonic sources. There is an absence of moderate-to-large earthquakes or alignments of seismicity in the site vicinity (see ***Subsection 5.13.5.3.(c)***) that could suggest the presence of a capable tectonic source. Very few earthquakes have been observed within the site region (***Section 5.14*** – Seismic Hazard Analysis) and, with the exception of the Quaternary-reactivated Kango Fault, there is no known evidence for palaeoearthquakes in the site region. Significant tectonic deformation on structures in the Eastern Cape region (*i.e.*, Mesozoic rift basins and related secondary faults) occurred in the late Mesozoic (***References 5.13.74*** and ***5.13.162***; see ***Subsection 5.13.5.3.(d)***).

g) Designation of Zones of Quaternary Deformation in the Site Region

No zones of Quaternary deformation that would require additional investigation are identified within the Thyspunt site region. Palaeoseismic investigations conducted along the Kango Fault, the only recognised Quaternary fault, in the site region provided sufficient information to characterise the Kango Fault as a seismic source in the PSHA (***Reference 5.13.1***).

h) Potential for Surface Tectonic Deformation at the Site

The potential for tectonic deformation at the Thyspunt site is assessed to be negligible. This conclusion is based on the following observations and criteria:

- The results of geological investigations have demonstrated that mapped faults within the site area are not capable faults. ***Subsection 5.13.5.2.(b) iii*** discusses these results in detail.
- Bedrock geological mapping in the site vicinity (***Reference 5.13.27***; ***Figure F-5.13.81***) identified no evidence for surface faulting or deformation that would suggest capable faults in the Thyspunt site area.
- The absence of geomorphic features indicative of Quaternary deformation as reported in the previous siting reports and literature and inferred from the results of marine terrace and field studies conducted as part of the Thyspunt GI programme.

The floors and walls of excavations for all safety-related structures for the Thyspunt nuclear facilities will be mapped in detail, and the NNR will be notified immediately if previously unknown geological features that could represent a hazard to the proposed facilities are identified. Following US NRC Regulatory Guide 1.208 (***Reference 5.13.8***), any potential deformation feature identified in

© Eskom 2026/Rev 0a

the excavations will be characterised to assess surface deformation or ground-motion-generating potential.

5.13.5.4 Tsunamigenic Sources

This section provides a summary of the tsunamigenic sources that have the potential to affect the site. The descriptive information provided in this section may be used to develop input parameters for the characterisation of tsunamigenic sources as described in ***Section 5.9*** (Oceanography and Coastal Engineering) of this SSR. That section discusses the modelling of the size, nature, and local effect, and flooding characteristics of tsunamis at the site.

The candidate potential near-field and far-field tsunamigenic sources are to be assessed according to the characteristics identified in the guidance given in US NRC NUREG/CR-6966 (***Reference 5.13.11***) as well as IAEA guidance (***Reference 5.13.347***), including:

- Earthquakes;
- submarine landslides;
- subaerial landslide (additional parameters to those given above for submarine landslides);
- volcanoes (pyroclastic flow); and
- volcanoes (caldera collapse).

The historical and geological record of tsunamis along the South African coast is very sparse. In Okal *et al.* (***Reference 5.13.348***), five sources of significant tsunamigenic capacity (*i.e.*, cosmic impact, submarine seismic events, submarine slides and slumps, volcanic activity, and terrestrial landslides or rockfalls) were considered for southern Africa. Of the five sources, cosmic impact and volcanic eruptions and pyroclastic flows were determined not to be significant sources of tsunamis for southern Africa (***Reference 5.13.66***). ***Section 5.9.8.9*** (Tsunami) provides the probable maximum tsunami generated by identified tsunamigenic sources. Potential sources for tsunami hazard to the site, including far-field subduction zone earthquakes and volcanic edifice collapse, as well as more proximal submarine landslides, are discussed in this section.

Rapid displacement along submarine faults can induce large and damaging tsunamis, while other sources, such as submarine slumps or terrestrial landslides are also often triggered by seismic events. The southern African coastline is a stable intraplate, trailing edge passive margin, which is characterised by general seismic quiescence, although low-frequency, low-intensity background seismicity prevails (***Reference 5.13.1***).

© Eskom 2026/Rev 0a

a) Far-Field Sources

The two types of far-field sources of tsunamis, i.e. teleseismic (subduction zone earthquakes) and volcanic-edifice (collapse), are considered in this section.

i Teleseismic Sources

Three subduction zones have been identified as having the capability of generating a tsunami that could be destructive in South Africa: the South Sandwich, the Makran, and the Sumatra subduction zones (***Figure F-5.13.149***). Because southern Africa has stable, quiescent plate boundaries, large tsunamis generated at other plate margins are considered.

Historically, tsunamis generated on far-field subduction zones have been recorded in South Africa. For example, the 1960 Chilean tsunami was recorded in Mossel Bay (***Reference 5.13.349***). In addition, the 2004 Indian Ocean tsunami was recorded in many locations along the South African coast including damaging waves in the Port Elizabeth harbour (***Reference 5.13.350***). ***Section 5.9.8.9*** discusses historical tsunamis recorded in Port Elizabeth.

The South Sandwich Island or Scotia subduction zone is geographically the closest active subduction zone at over 4,000 km from the site. Historically, the region has had many M 7+ earthquakes with the largest being a M 8.3 normal faulting earthquake in 1929. The 1929 event was not on the subduction zone but rather in the South Atlantic Plate (***Reference 5.13.351***). To determine the tsunami hazard to Africa from the South Sandwich Island subduction zone, Okal & Hartnady (***Reference 5.13.351***) modelled tsunamis generated by the 1929 event and similar magnitude thrust events on the subduction zone. Using a 32-year instrumental earthquake record, Kijko *et al.* (***Reference 5.13.65***) calculated a maximum magnitude of 7.64 ± 0.24 for an earthquake on the South Sandwich Island subduction zone. However, Okal & Hartnady (***Reference 5.13.351***) conclude that the post-1962 instrumental record does not characterise the range of events that can occur on the South Sandwich Islands subduction zone and that there is a high potential for larger and more frequent events than recorded historically. In addition, Lynner & Long (***Reference 5.13.352***) concluded that the Scotian subduction zone, although it is slightly shorter, shares many similar features to the Caribbean subduction zone, which has been assessed to have a small probability of M 9 earthquakes in hazard studies (*e.g.*, ***Reference 5.13.353***).

The Makran subduction zone is located in the Arabian Sea near Oman, Iran and Pakistan. The largest historical event was an M 8.1 thrust earthquake in 1945 (***Reference 5.13.354***).

© Eskom 2026/Rev 0a

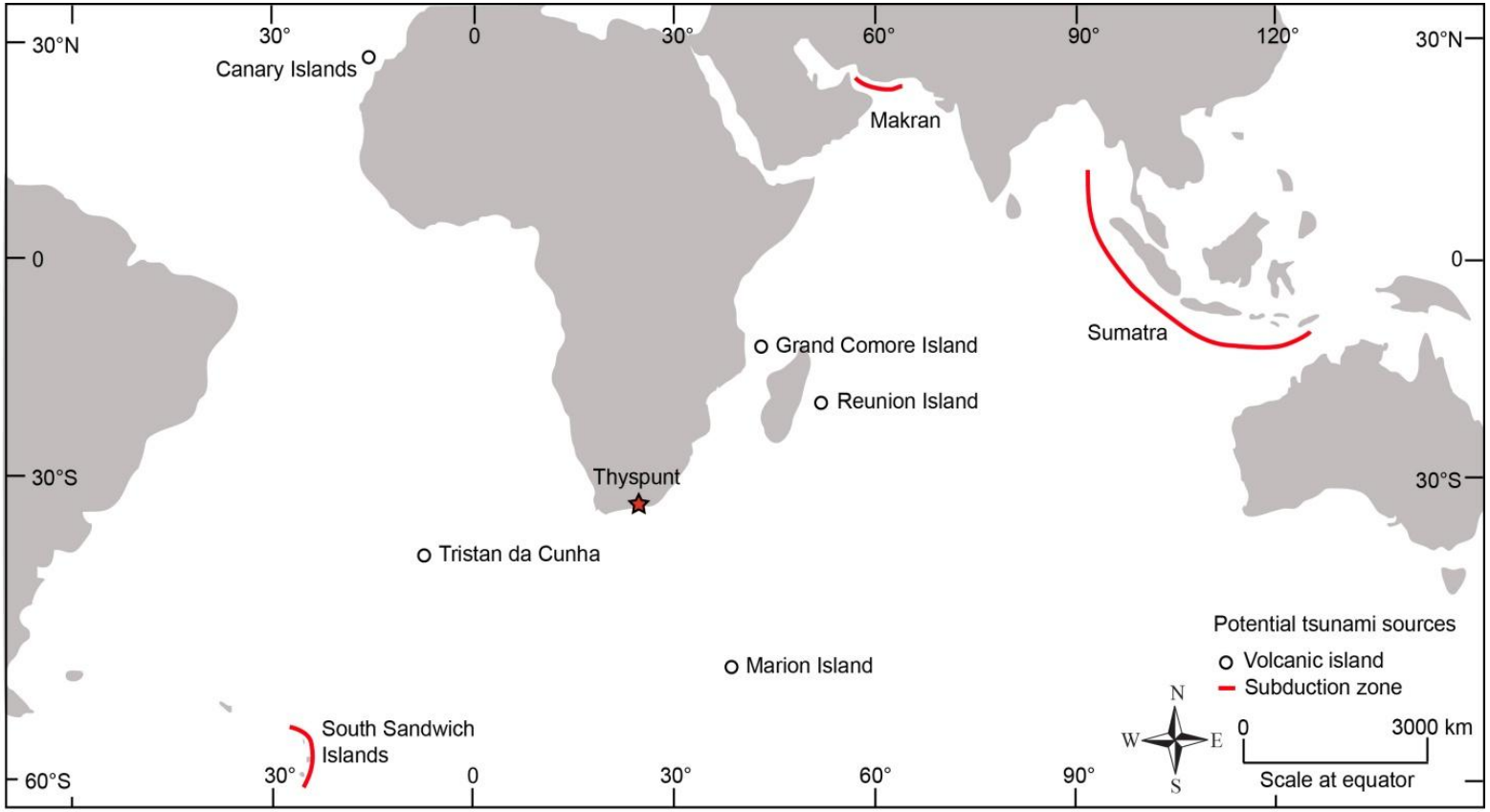


Figure 5.13-149
Subduction Zones and Volcanic Islands Determined to Have the Potential to Create Damaging Tsunamis in South Africa

© Eskom 2026/Rev 0a

The 1945 earthquake generated a large (5–10 m) local tsunami (***Reference 5.13.355***). The highest waves of the tsunami occurred hours after the earthquake, indicating that either the waves were generated by a submarine landslide (***Reference 5.13.355***) or the bathymetry of the continental shelf trapped the tsunami wave energy (***Reference 5.13.356***). For the Makran subduction zone, Kijko *et al.* (***Reference 5.13.65***) calculated a maximum earthquake magnitude of 8.44 ± 0.29 based on a 570-year historical and instrumental record. More recently, Smith *et al.* (***Reference 5.13.357***) calculated a maximum range of M 8.7 to M 9.2 based on the geometry of the subduction zone. Other recent studies (***References 5.13.358*** and ***5.13.359***) calculate Mmax between 8.1 and 8.2.

The Sumatra subduction zone was the source of the 2004 Indian Ocean earthquake and tsunami. The 2004 tsunami had a wave height of more than 2.7 m in Port Elizabeth (***Reference 5.13.350***). Using a 32-year earthquake catalogue, Kijko *et al*. (***Reference 5.13.65***) calculated a maximum credible earthquake magnitude of 9.20 for the Sumatra subduction zone. Modelling of potential sources along this subduction zone indicates tsunami waves along the South African coast, could be larger than the 2004 event if the tsunami is generated by earthquakes farther south on the subduction zone (***Reference 5.13.360***).

ii Volcanic Edifice Sources

Large landslides have been mapped on the flanks of many volcanic islands including the Hawaiian Islands (***Reference 5.13.361***), Canary Islands (***Reference 5.13.362***), Réunion Island (***References 5.13.363*** and ***5.13.364***), Tristan da Cunha Islands (***Reference 5.13.362***), Marion Island (***Reference 5.13.365***), and Mayotte and Comoro Islands (***References 5.13.366*** and ***5.13.367***; and ***Figure F-5.13.149***). These large-scale failures (up to 5,000 km^3 of material (***Reference 5.13.361***) are typically debris avalanches but slumps are also mapped. One of the potential tsunami sources for the site, Réunion Island, has four large (>100 km^3) mapped landslides, two of which occurred in the last 2 Myr, and many smaller mapped landslides (***Reference 5.13.364***). Modelling indicates that submarine slides generate larger tsunamis than slumps (***Reference 5.13.368***).

In the Canary Islands, the landslide deposits are interpreted as having accumulated during multiple slope-failure events and events with more than one depositional phase (***Reference 5.13.369***). Locat & Lee (***Reference 5.13.370***) list possible factors in the initiation of large volcanic flank landslides to include magma near the surface, the physical properties of layered volcanic rocks, and changes in magma and gas pressure associated with the volcano. Although no historical flank failures of the magnitude of mapped

© Eskom 2026/Rev 0a

prehistorical events have occurred on intraplate volcanoes, such failures are believed to generate large tsunamis. Modelling of volcanic-landslide (500 km^3) sourced tsunamis indicates local wave run-up of potentially hundreds of meters and far-field run up of tens of meters or less based on a Canary Island example (***Reference 5.13.371***).

The islands of Grand Comore and Réunion off the southern African east coast (***References 5.13.65*** and ***5.13.366***), and Marion Island in the southern Indian Ocean (***Figure F-5.13.149***) were considered potential sources of tsunamis in South Africa as a result of volcanism/edifice collapse.

b) Local Sources

Local tsunami sources include potential sources along the coast and continental margin of South Africa. These tsunami sources include faults and submarine landsides. No historical tsunamis in South Africa have been linked conclusively to these sources.

ii Active Faults

Mapped submarine faults in the site region include the Gamtoos Fault, Cape St Francis Fault, Plettenberg Fault, and Agulhas fracture zone (***Figure F-5.13.150***). None of these faults has had a historical earthquake large enough to generate a tsunami and all are unlikely to be seismically active (***Reference 5.13.1***). The Gamtoos Fault, Plettenberg Fault, and Agulhas fracture zones were determined to have seismogenic potential based on their similar orientations and settings to the Quaternary-active Kango Fault (***Reference 5.13.1***). However, the assessment of all available seismicity, geologic, and geophysical data for these faults resulted in the assessment that the seismogenic probability for these faults is very low (0.2). In a deterministic analysis, therefore, these faults are judged to be inactive and not capable of generating coseismic displacements. Therefore, the tsunamigenic capabilities of these faults have not been considered further.

ii Landslides

Historical evidence for tsunamis that may have been induced by offshore slumping along the South African coast is sparse, offshore deposits display periods of higher slumping rates in the late Mesozoic (148 Ma to 65 Ma), early to late Tertiary (65 Ma to 1.8 Ma) and possibly Quaternary (1.8 Ma to present; ***Reference 5.13.66***). Two potential submarine slump-generated tsunamis occurred in 1969 and 2008 (***Reference 5.13.66***). Recently, these events have been hypothesised to have been atmospherically induced waves known as meteotsunamis (***References 5.13.66*** and ***5.13.372***).

© Eskom 2026/Rev 0a

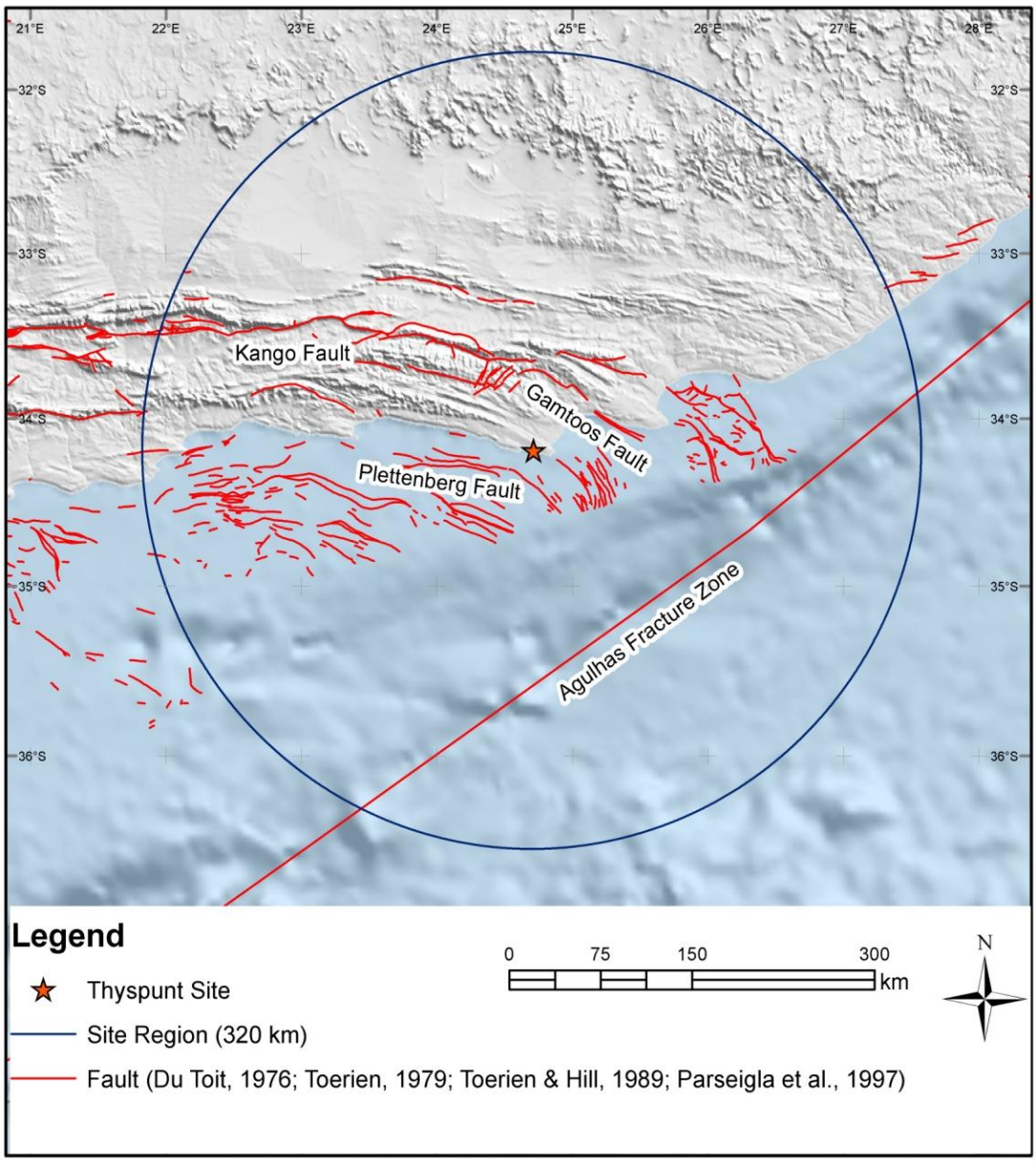


Figure 5.13-150
South African Faults in the Thyspunt Site Region. Most Faults Show Evidence of Mesozoic Activity, but Only the Kango Fault Is Known to Have Evidence of Quaternary Reactivation

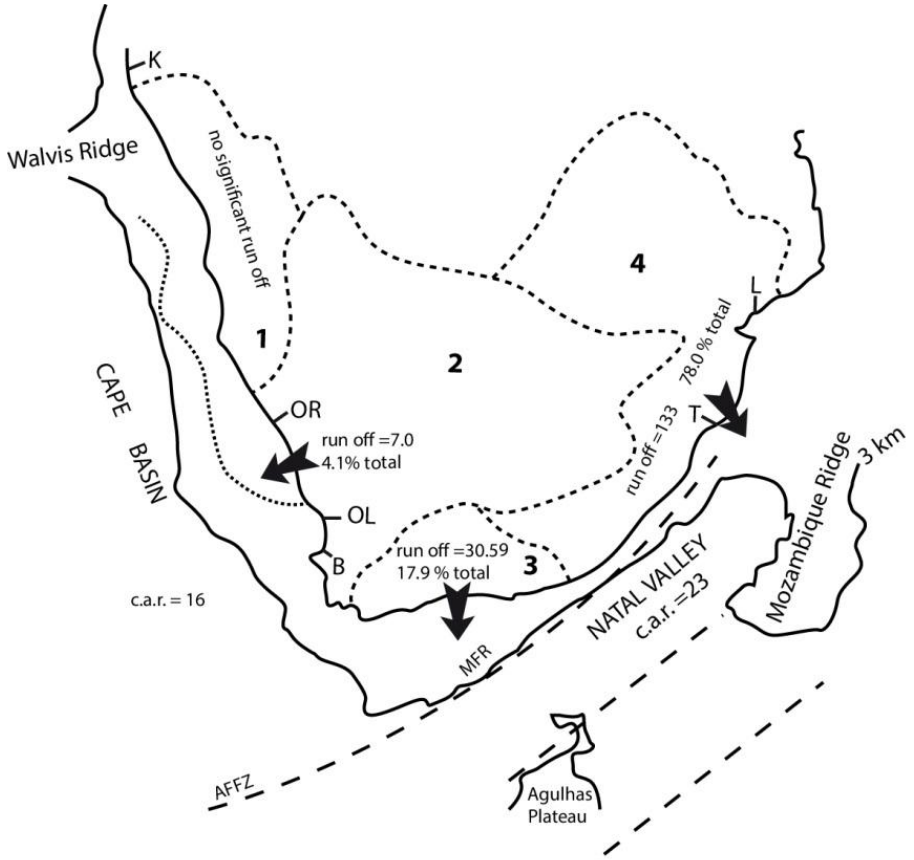
Locat & Lee (***Reference 5.13.370***) list 10 common causes of submarine failures:

- oversteepening;
- seismic loading;
- storm-wave loading;
- rapid accumulation and underconsolidation;
- gas charging;
- gas hydrate disassociation;
- low tides;
- seepage;
- glacial loading; and
- yolcanic island growth.

Of these, only the first 3 are likely to be sources of submarine failure in the site region. Oversteepening along the continental slope could occur due to erosion by currents (***Reference 5.13.83***). Seismic and storm-wave loading are also considered potential sources (***References 5.13.373***, ***5.13.66***, and ***Reference 5.13.372***). The remainder of the causes of submarine failures are unlikely in the site region. The low (~2 cm/ka) sedimentation rate on the continental slope (***Reference 5.13.83***) makes rapid sedimentation and underconsolidation unlikely (***Figure F-5.13.151***). While gas hydrates are present along the western margin of South Africa (***Reference 5.13.374***) and natural gas leakage has been described by Boyd et al. (***Reference 5.13.375***) in the Orange Basin, they have not to date been reported from the southern coast. The site region is not currently subject to the changes in temperature and pressure that are commonly associated with destabilizing gas hydrates (***Reference 5.13.370***). In addition, the southern shelf and slope do not have a recent history of a large tidal range, glaciation or volcanism, all of which are linked to destabilizing slopes (***Reference 5.13.370***).

The gradual dip (0–2.5 degrees) of the continental shelf (***Reference 5.13.83***) reduces the landslide risk in this area. Although shelf sediments have the potential to liquefy due to strong shaking during earthquakes, the low gradient of the continental shelf in the vicinity of the Agulhas Bank makes it unlikely that the sediment will begin to flow and evolve into a slide (***Reference 5.13.377***). Sediment strength will decline during strong shaking in areas with slopes of 0 degrees; the sediment will not fail or flow far in absence of a slope. Some areas of the continental shelf have higher slopes but typically these sites are small or do not consist of unconsolidated sediment (***Reference 5.13.281***). The shelf region near the Thyspunt site does not have any steep-walled submarine canyons, which can be sources of failures.

© Eskom 2026/Rev 0a



Drainage areas and fluvial sediment yields in southern Africa.
1 = between Kunene and Orange rivers - no significant runoff; 2 = west coast: Orange, Olifants and Berg rivers; 3 = southern Cape; 4 = east coast, including Tugela and Limpopo rivers. Runoff yields is in x 10^6 m^3/yr.
Abbreviations: c.a.r. = Cenozoic sediment accumulation rate/area within the 0,5 km isopachyte in $m^3/km^2/yr$; AFFZ = Agulhas-Falkland Fracture Zone; MFR = marginal fracture ridge.
Rivers - K = Kunene, OR = Orange, OL=Olifants, B = Berg, T = Tugela, L = Limpopo

Figure 5.13-151
Rates of Terrestrial Sediment Input into the Marine System in Southern Africa (*Reference 5.13.376*)

In addition, the low sedimentation rate on the continental slope and shelf in the site region (***Reference 5.13.83***) reduces the likelihood of landslides (***References 5.13.378*** and ***5.13.379***).

Potential slump deposits were mapped by Fugro South Africa (Pty), Ltd (FPSAL) (***Reference 5.13.281***) in their detailed mapping of the seafloor in the site area (***Figure F-5.13.152***). The bathymetry contains furrows 1–2 m deep and about 20 m wide that typically occur in partially consolidated sediment in 50–60 m water depth. The longer furrows are typically parallel to slope with some shorter, cross-cutting furrows. The slope of the shelf is approximately 0.6 degrees parallel to the long furrows and 0.04 degrees to the east, perpendicular to the furrows. Measured sediment thickness in this area is 0–14 m. FPSAL (***Reference 5.13.281***) interpreted these features as evidence of slumping, with the furrows opening up as the intervening blocks slid. Based on this model, the age of these events would be post-Pliocene or Holocene depending on the age of the sediments.

The Davidson & Smith model (***Reference 5.13.281***) proposes that the sediment blocks exhibit wide-scale fracturing and slumping and that the asymmetrical furrows are the surface expression of the planes along which slumping occurred. They also propose that these planes are faults, extending to greater depths within the sediment curving towards the west, and that erosive processes subsequently deepened the furrows. Horwood (***Reference 5.13.46***), however, interpreted these offshore features to be erosional channels as opposed to slumps, generated by current activity in the area.

Cawthra (***Reference 5.13.380***) speculates that the sediment represented by the yellow facies in ***Figure F-5.13.152*** (“rippled sediment”) may underlie the positive features (“partially lithified fine sediment” in ***Figure F-5.13.152***), suggesting that the furrows are exposed remnants of an underlying gravel pavement. In this case, the top of this unit (‘rippled sediment’) likely marks a sequence boundary which formed during the regression from the Last Interglacial to Last Glacial Maximum. Similar features and this model of continental shelf sedimentation has been described along the mid-shelf of the South African east coast (***References 5.13.381*** and ***5.13.382***). As sea level fell and the clastic shoreline retreated, this surface was rapidly buried by migrating dunes. The dune sediments may have been partially cemented in places by meteoric water, but were not completely or uniformly cemented across the facies, accounting for the geophysical signature of the “partially lithified fine sediment” of ***Figure F-5.13.152***. The present sediment mounds may thus be partially preserved sedimentary bedforms, sculpted by the prevailing currents, bounded by higher, exposed bedrock on both the inshore and offshore. The

asymmetry of the sediment mounds, with stoss slopes on the western margin, suggests an eastward flow direction.

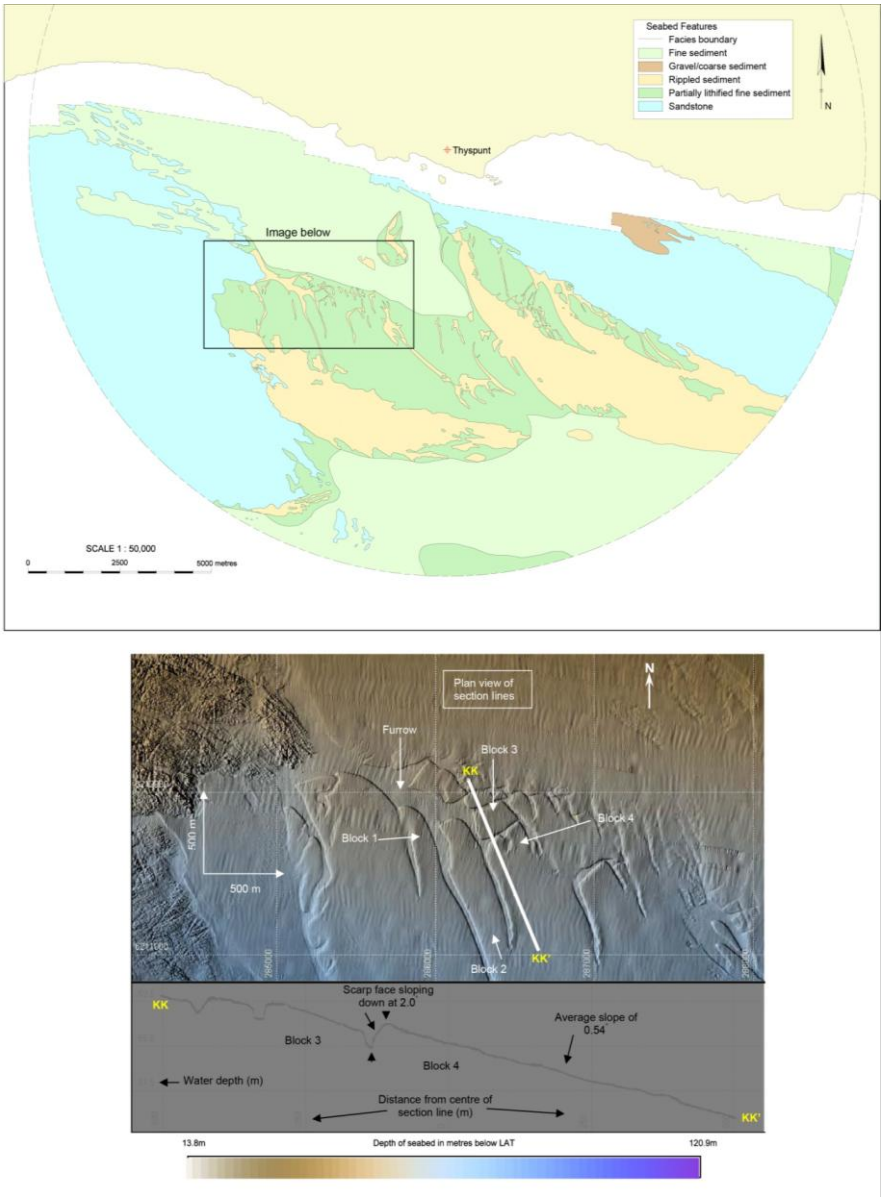


Figure 5.13-152
Top: Geology from the Site Area Offshore of the Site. Bottom: Detailed Bathymetry off the Coast of the Thyspunt Site and Topographic Profile Across Features Alternatively Interpreted to Be the Result of Slumping and Erosion. Modified from *Reference 5.13.281*

The current thus may be a countercurrent rather than the core of the Agulhas Current, which flows westward. Hanson *et al.* (***Reference 5.13.58***), based on these arguments, concluded that the features were not slump-induced.

Potential sources of tsunamis along the southern African coast are mass failures along the shelf edge and continental slope. Dingle (***Reference 5.13.373***) mapped a large failure, the Agulhas Slump, along the shelf edge between East London and Cape Agulhas (***Figure F-5.13.153***), although the origin of this feature as a single massive slope failure has been disputed (***Reference 5.13.83***). The Agulhas slump as mapped by Dingle (***Reference 5.13.373***), using single beam bathymetric and seismic data, is 750 km wide and up to 106 km long. The age of the slump was determined to be post Pliocene based on the age of included sediments and the “fresh” appearance of the slide, although Dingle (***Reference 5.13.373***) concluded that the “fresh” morphology could be enhanced through erosion by the Agulhas Current.

Off the coast of East London, within the mapped Agulhas slump, later work mapped a narrow belt of possibly Quaternary slumping (***Reference 5.13.383***). Uenzelmann-Neben & Huhn (***Reference 5.13.83***) documented greater evidence for erosion along the mapped Agulhas Slump. Using two high resolution seismic lines the study did not find evidence for a glide plane or fissured zone as interpreted by Dingle (***Reference 5.13.373***) on the upper slope or at the western end of the mapped slump.

Some evidence for mass transport deposition was found on the lower continental slope on their eastern profile. Uenzelmann-Neben & Huhn (***Reference 5.13.83***) concluded that much of Dingle’s (***Reference 5.13.373***) evidence for the Agulhas Slump was instead the result of erosion of the seafloor and lack of deposition due to strong oceanic currents including the Agulhas Current, Antarctic Intermediate Water, North Atlantic Deep Water, and Antarctic Bottom Water.

The eastern coast of South Africa has higher rates of sediment input (***Figure F-5.13.151***) than the southern and western coasts (***References 5.13.373*** and ***5.13.366***; ***Figure F-5.13.153***) and may be subject to tsunamigenic landsliding (***Reference 5.13.366***). Hartnady (***Reference 5.13.372***) refers to this region, which includes the northern end of the Agulhas slump as mapped by Dingle (***Reference 5.13.373***) as the Wild Coast slump. The formation of the slump is linked to slope instability created by erosion related to the onset of the North Atlantic Deep Water in the early Pliocene (***Reference 5.13.372***). Interpretation of seismic lines offshore of Port St Johns show the region exhibits pervasive slumping (***Reference 5.13.384***) rather than a single slump. In addition, north of

© Eskom 2026/Rev 0a

Port St Johns, associated with the mouths of major rivers, is a zone of large, mapped slumps.

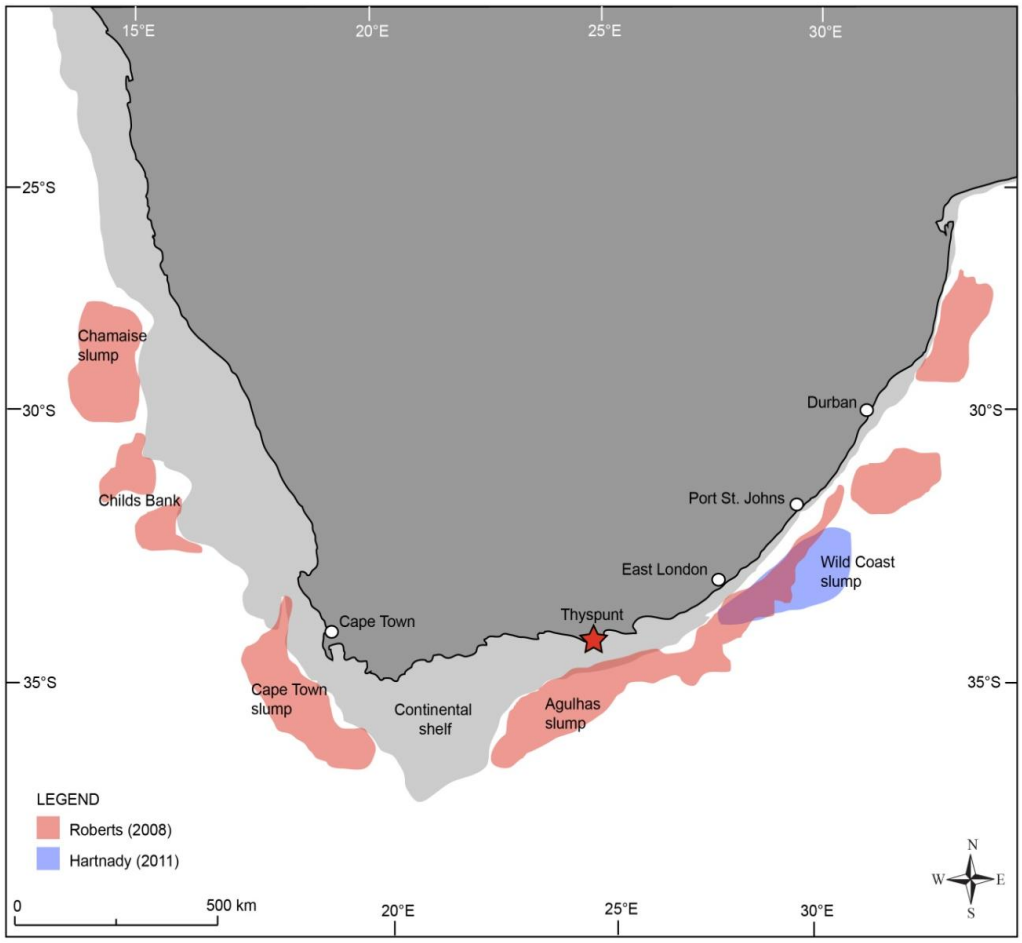


Figure 5.13-153
Mapped Slumps along the South African Margin

Along the western coast of South Africa three zones of slumping have been mapped (***Reference 5.13.376***). From north to south the zones are the Chamaise, Childs Bank, and Cape Town/Cape Canyon. The Cape Town slump is the closest of these features to the site region. It is approximately120 km wide and 400 km long (***Reference 5.13.385***). The slump is associated with the late Tertiary submarine Cape Canyon. The canyon may have originally transported the sediments of the joined Orange and Olifants Rivers. The higher than modern sedimentation rate may have led to conditions conducive to large slumps. The slump contains Pliocene sediments, and therefore may be

Quaternary in age (***Reference 5.13.385***) or even the last 120 kyr (***Reference 5.13.386***).

5.13.6 Monitoring

From the standpoint of the geology of the site, the monitoring of the site consists of ongoing monitoring of earthquake activity in the region and the incorporation of new geological information derived from the geological investigations conducted for the PSHA.

5.13.6.1 Seismic Monitoring

Seismic monitoring in South Africa occurs routinely as part of the South African National Seismological Network (SANSN), operated by the Council for Geoscience. Decisions to enhance the network with the installation of additional seismograph stations have been initiated and conducted to provide the information required for the PSHA (***Section 5.14***). These enhancements were made to facilitate the collection and analysis of as much site-specific seismic data as possible before the PSHA concluded.

The data related to seismic monitoring was assembled and compiled into an earthquake catalogue for use in the PSHA. The results of this monitoring are summarised in ***Section 5.14*** (Seismic Hazard Analysis) of the SSR and include the earthquake catalogue, as well as the following data:

- Site-specific seismic monitoring (Eskom client network), including previous microseismic monitoring investigations.
- Routine monitoring by the SANSN.

The earthquake catalogue developed for the PSHA (***Section 5.14***) includes earthquakes monitored up to and including December 2011. Because seismic monitoring is a routine activity, there is no expectation that the results of ongoing seismic monitoring will have a major effect on either the assessment of seismic hazards (***Section 5.14*** – Seismic Hazard Analysis) or the assessment of site suitability (***Section 6*** – Evaluation of External Events).

5.13.6.2 Incorporation of New Information

Throughout the time that the investigations for the PSHA were being conducted, results and data were being updated on a regular basis to ensure that the results, conclusions, and/or outcomes derived during that period are based on the latest facts. For example, as described in ***Section 5.14*** (Seismic Hazard Analysis), a number of geological investigations were conducted with the specific purpose of providing new information for use in the PSHA. These

© Eskom 2026/Rev 0a

investigations were conducted, completed, and documented in a timely manner for their use as input information for the PSHA.

The impact of all this information on the outcome of the seismic hazard analysis is assessed in ***Section 5.14***.

5.13.7 Management of Uncertainties

The identification and treatment of uncertainties in geological and geophysical data and interpretations is a function of the particular application to which the data were applied. The uncertainty that has impact on vibratory ground-motion hazard from earthquakes is dealt with explicitly in the PSHA in ***Section 5.14*** of this SSR. The data, models, and uncertainties associated with the assessment of surface faulting are dealt with explicitly in ***Subsection 5.13.5.5*** (Surface Faulting Evaluation).

Other assessments of geological hazards, tsunami hazard, or geotechnical design considerations may require assessments of the uncertainties in the geological data. As needed, the uncertainties will be provided and incorporated into the analyses by the relevant specialists, and documented in the applicable sections of the SSR where those hazard analyses are documented.

5.13.8 Management System

The activities carried out in ***Section 5.13*** (Geology), the links between the inputs discussed in ***Section 5.13*** (Geology) and the other SSR sections and chapters, and the quality control requirements are listed in ***Table T-5.13.12***.

Geological data described and used in this SSR were gathered over a period of about 25 years and thus incorporate historical data that were not gathered in accordance with latest quality regulations. However, the use of those data in analyses, such as the PSHA, is controlled by quality procedures that are now in place.

© Eskom 2026/Rev 0a

Table 5.13.12
Summary of Activities, Links, and Quality Requirements

Activity	Links		Quality Requirements
	Inputs	Outputs	
Geological Fieldwork	Input from geological fieldwork	***Sections 5.9***, ***5.11***, ***5.13***, ***5.14***, and ***5.15***. Geological data collected by fieldwork forms important input to oceanography & coastal engineering, geohydrology, geology, seismic hazard, and geotechnical investigations.	Work done according to Eskom-approved QMS appropriate for the classification of the activity.
Geophysics	Geophysical interpretations of geology and stratigraphic units	***Sections 5.13***, ***5.14***, and ***5.15***. Interpretation of the geophysical surveys provides key input to geological interpretations, geotechnical properties, lithologies, and structural interpretation of faults for seismic hazard analysis.	Work done according to Eskom-approved QMS appropriate for the classification of the activity.
Drilling	Input data from geotechnical and geohydrological drilling programme	***Sections 5.13***, ***5.14***, and ***5.15***. Lithological logs and other geological information resulting from drilling are used as key input into the interpretations of subsurface geology, geotechnical properties, and site response characteristics for seismic hazard analysis.	• Selection of suppliers from Approved List. • Rationale for drilling methods used. • Risk assessment. • Method statement. • Health, safety and environmental management plan. • Peer review.
Dating	Ages of various geological units	***Sections 5.13***, ***5.14***, and ***5.15***. The results of age determination analyses of geological layers are used to interpret the geology, geotechnical layers, and rates of fault slip for the seismic hazard analysis.	• Selection of suppliers from Approved List. • Established selection criteria for laboratories

Activity	Links		Quality Requirements
	Inputs	Outputs	
Seismic Monitoring	Recordings of local and regional earthquakes	***Section 5.14***. The monitoring data are used to develop the earthquake catalogue.	Work done according to internal CGS quality standards.
Development of Earthquake Catalogue	Historical and instrumental records of earthquakes	***Sections 5.13*** *and* ***5.14***. Earthquake catalogue used in seismic source characterisation model in ***Section 5.14***.	Work done according to Eskom-approved QMS appropriate for the classification of the activity.
Monitoring		***Section 5.2***.	Monitoring protocol

The Integrated Management System (IMS) for the current geological investigations of the proposed site is described in this subsection, with reference to the overall IMS for the SSR, addressed in ***Section 10*** (Quality Management) of the Thyspunt SSR.

The geological investigations undertaken in support of the PSHA entail a wide variety of activities, including:

- desktop study;
- site investigations;
- receipt/use of data from other SSR investigations;
- data analysis and reporting;
- use of computer software, in particular, Excel spread sheets and GIS, for collating, interpreting, and presenting data; and
- mapping and creation of a GIS database and data management system.

Each of these activities has a different effect on the safety of a nuclear installation. All these data collecting activities were classified in terms of their safety impact using Eskom's safety classification methodology (***Reference 5.13.387***) and the relevant controls and checks were implemented. The classification of tasks and the technical procedures are described in ***Reference 5.13.388***.

© Eskom 2026/Rev 0a

An appropriate IMS (***Reference 5.13.389***), was established, as stipulated in the National Nuclear Regulator document RD-0034 (***Reference 5.13.390***) to control the execution of these activites implemented. Before the data gathering for the PSHA began, the following documents were compiled and approved by Eskom to assist in quality assurance and ensure that work was carried out safely:

- Project Execution Plan (***Reference 5.13.391***).
- Project Quality Plan (***Reference 5.13.392***).
- Risk Register Methodology (***Reference 5.13.393***).
- Compliance Matrix (***Reference 5.13.394***).
- Safety Culture Enhancement Program (***Reference 5.13.395***).

The regulatory compliance matrix for ***Section 5.13*** is shown in ***Table T-5.13-1***.

Subsequently the IMS was revised and resulted in two new documents ***References 5.13.395*** and ***5.13.396*****.** While revising some of the above mentioned documents, new revisions were also released, in line with continuous improvement. The CGS Nuclear Geohazards Group's (NGG) IMS is ISO-9001 accredited. Therefore, the work in this section was performed under an integrated management system in line with that described in ***Section 10*** (Quality Management) of this SSR.

5.13.9 Conclusions

This subsection sets out the main findings of this section of this SSR, including conclusions regarding the adequacy of the geological knowledge base, use of the geological information for seismic hazard analysis, surface faulting potential, and identification of tsunamigenic sources.

5.13.9.1 Adequacy of Geological Knowledge Base

Geological investigations that contribute to the knowledge base for the Thyspunt site have been conducted over more than the last 25 years. These studies include geological mapping, onshore and offshore geophysical studies, geochronological analyses, geomorphic studies, palaeoseismic studies, and geotechnical investigations. These studies were conducted as part of early screening studies to evaluate multiple nuclear sites, specific studies conducted by the CGS for the Thyspunt site, and geological investigations conducted specifically to address key issues of importance to the seismic hazard analysis.

© Eskom 2026/Rev 0a

Consistent with all existing NNR guidance and international regulatory guidance and standards, the full range of methods and tools were exercised and the investigations included the recommended increasing levels of specificity ranging from the site region, site vicinity, and site area, to the site location. As is also recommended in the existing regulatory guidance, the results of the investigations conducted for the site were integrated with studies conducted by a large number of investigators within the geological community and published in the professional literature.

The net result of integrating all the geological studies conducted with the interpretations offered by members of the community in technical publications is a strong, complete geological knowledge base for the site region, site vicinity, site area, and site location. Because the bulk of the studies were conducted according to international best practices for nuclear facilities according the regulatory guidance of the IAEA and the U.S. NRC, the knowledge base is commensurate with the geological knowledge base at other nuclear facilities worldwide. As a result, the subsequent disciplines that rely on the geological knowledge base as inputs to their analyses are provided with the information and data that they require.

The onshore and offshore regional geology and tectonics at the site are well understood. The shoreline and coastal plain at the site area and location represent an old and stable landscape. From an erosional point of view, the resistant rocks that establish this rugged coastline provide a stable base for the construction of nuclear installations. Significant changes in the geological environment (*e.g.*, large rock falls) are therefore extremely unlikely. Given the silica-rich (sandstones and siltstones) nature of the Palaeozoic-age bedrock underlying the site location, there is no risk of solution cavities forming beneath the site.

The presence of thick sediment cover and groundwater aquifers may pose a secondary threat to the site, and the deep excavations that are expected to be made for the nuclear installation foundations during construction may pose a man-made slope failure threat. Geotechnical design solutions should mitigate these hazards, as discussed in ***Section 5.15*** (Geotechnical Characterisation).

5.13.9.2 Seismic Hazard Analysis

The most important potential hazard at the site for which geological information given in ***Section 5.13*** provides input, is seismic hazard, both vibratory ground motion hazard (described in ***Section 5.14***) and surface faulting hazard (described in ***Subsection 5.13.5.3***). The probabilistic seismic hazard analysis (PSHA) was conducted using methodologies that are recommended in U.S. NRC regulatory guidance (see Regulatory Compliance Matrix ***Table T-5.13.1***).

The geological data and knowledge documented in this section are the primary basis for the seismic source characterisation conducted for the PSHA. The development of the data, and their use in the PSHA, has been conducted in compliance with NNR and international regulations and regulatory guidance. From that standpoint, the available geologic, seismologic, and geophysical data in the site region, vicinity, area, and location are sufficient and adequate for purposes of assessing both the seismic hazard at the site and, the suitability of the site. The results of the PSHA are documented in ***Section 5.14*** (Seismic Hazard Analysis) and will be used in assessing the suitability of the site from the standpoint of external events such as earthquakes (***Section 6*** – Evaluation of External Events).

5.13.9.3 Surface Faulting Evaluation

The evaluation of the potential for surface faulting at the site is based on all the available information, including investigations conducted in the site region, vicinity, area, and location (see ***Subsection 5.13.5.3***). Based on a detailed evaluation of all available data, and following the regulatory guidance given in U.S. NRC for assessing the potential for surface faulting, it is concluded that there is no evidence for capable tectonic deformation at the Thyspunt site location and that the potential for tectonic deformation is negligible. This conclusion is based on the following lines of evidence. The results of geological investigations have demonstrated that mapped faults within the site area are not capable faults (see ***Subsection 5.13.5.2.(b) iii***). Bedrock geological mapping in the site vicinity identified no evidence for surface faulting or deformation that would suggest capable faults in the Thyspunt site area. The basis for this conclusion is the absence of geomorphic features indicative of Quaternary deformation, as reported in the previous siting reports and literature, and inferred from the results of marine terrace and field studies conducted as part of the Thyspunt geological investigations programme.

It is assumed that, following the Regulatory Guide 1.208 (***Reference 5.13.8***), the floors and walls of excavations for all safety-related structures for the Thyspunt nuclear facilities will be mapped in detail, and that the NNR will be notified immediately if previously unknown geological features that could represent a hazard to the proposed facilities are identified. Any potential deformation feature identified in the excavations will be characterised to assess surface deformation or ground-motion-generating potential.

5.13.9.4 Tsunamigenic Sources

This section provides a summary of the tsunamigenic sources that have the potential to affect the site. The descriptive information provided in this section is used to develop input parameters for the characterisation of tsunamigenic

© Eskom 2026/Rev 0a

sources as described in ***Section 5.9*** (Oceanography and Coastal Engineering) of this SSR. That section discusses the modelling of the size, nature, and local effect, and flooding characteristics of tsunamis at the site.

The candidate potential near-field and far-field tsunamigenic sources are to be assessed according to the characteristics identified in the guidance given in U.S. NRC NUREG/CR-6966 (***Reference 5.13.11***) and IAEA guidance (***Reference 5.13.347***), including earthquakes, submarine landslides, subaerial landslides, volcanoes (pyroclastic flow), and volcanoes (caldera collapse).

The tsunami hazard is being evaluated, taking into consideration all potential tsunamigenic sources such as distant subduction zone sources, local seismic sources, and local sources from slumping or landslides. The results of the tsunami hazard analysis and the associated probable maximum tsunami for consideration in design are given in ***Section 5.9*** (Oceanography and Coastal Engineering).

© Eskom 2026/Rev 0a

5.13.10 References

5.13.1) Bommer, J.J., Coppersmith, K.J., Coppersmith, R.T., Hanson, K.L., Mangongolo, A., Neveling, J., Rathje, E.M., Rodriguez-Marek, A., Shelembe, R., Scherbaum, F., Stafford, P.J., & Strasser, F.O. (2013), **Probabilistic Seismic Hazard Analysis for the Thyspunt Nuclear Site, South Africa**. Report 2013-0190, 900 pp. Pretoria, Council for Geoscience.

5.13.2) Department of Energy, Republic of South Africa (2011), **The Regulations on Licensing of Sites for New Nuclear Installations**. Government Gazette No. 34735, Regulation 927. Pretoria.

5.13.3) National Nuclear Regulator (2012), PP-0014: **Considerations of External Events for New Nuclear Installations**. Rev. 0 (Draft). Centurion.

5.13.4) International Atomic Energy Agency (2003), **Site Evaluation for Nuclear Installations**. Safety Requirements No. NS-R-3. Vienna.

5.13.5) International Atomic Energy Agency (2010), **Seismic Hazards in Site Evaluation for Nuclear Installations**. Safety Standards Series, Specific Safety Guide SSG-9. Vienna.

5.13.6) International Atomic Energy Agency (2004), **Geotechnical Aspects of Site Evaluation and Foundations for Nuclear Power Plants**. Safety Guide NS-G-3.6. Vienna.

5.13.7) U.S. Nuclear Regulatory Commission (2007), **10 CFR 100, Geologic and Seismic Siting Criteria**. Section 100.23 of Title 10, Code of Federal Regulations Part 100, Reactor Site Criteria. Issued in Federal Register Notice 72 FR 57447, Oct. 9, 2007.

5.13.8) U.S. Nuclear Regulatory Commission (2006), **Performance-Based Approach to Define the Site-Specific Earthquake Ground Motion**. Regulatory Guide 1.208. Washington DC

5.13.9) U.S. Nuclear Regulatory Commission (2003), **Site Investigations for Foundations of Nuclear Power Plants**. Regulatory Guide 1.132. Washington DC.

5.13.10) American National Standards Institute/American Nuclear Society (2008), **Criteria for Investigations of Nuclear Facility Sites for Seismic Hazard Assessments**. Standard ANSI/ANS-2.27-2008. La Grange Park, Illinois, American Nuclear Society.

5.13.11) U.S. Nuclear Regulatory Commission (2009), **Tsunami Hazard Assessment at Nuclear Power Plant Sites in the United States of America**. NUREG/CR-6966. Washington DC.

© Eskom 2026/Rev 0a

5.13.12) Norman, N.G., Andersen, N.J.B., & Faurie, J.N. (1986), **A Preliminary Assessment of Regional and Coastal Geology from Cape St. Francis to the Tsitsikamma River with the View to the Selection of Candidate Sites for a Nuclear Power Station. Nuclear Siting Investigation in the Eastern Cape, Parts A, B, C**. Progress Report No. 5. NSIP-EC-005760#P1-59. Pretoria, Atomic Energy Corporation of South Africa, Ltd., Department of Geotechnology.

5.13.13) Goedhart, M.L. (2004), **A Geological Investigation of Neotectonic Reactivation Along the Ceres-Kango-Baviaanskloof-Coega Fault System in the Southern and Eastern Cape, South Africa**. **Desk Study Report.** CGS Report No. 2004-0189, NSIP-SHA-013852#P1-153. Pretoria, Council for Geoscience.

5.13.14) Goedhart, M.L. (2005), **A Geological Investigation of Neotectonic Reactivation Along the Ceres-Kango-Baviaanskloof-Coega Fault System in the Southern and Eastern Cape, South Africa**. **Field Reconnaissance Report**. CGS Report No. 2005-0084. NSIP-SHA-013852#P1-133. Pretoria, Council for Geoscience.

5.13.15) Goedhart, M.L. (2006), **A Geological Investigation of Neotectonic Reactivation Along the Ceres-Kango-Baviaanskloof-Coega Fault System in the Southern and Eastern Cape, South Africa**. **Trench Report.** CGS Report No. 2006-0185, NSIP-SHA-018229#P1-286. Pretoria, Council for Geoscience.

5.13.16) de Beer, C.H. (2004), **Investigation into Evidence for Neotectonic Deformation Within Inland Neogene to Quaternary Deposits Between Alexander Bay and Port Elizabeth**. Desk Study Report. CGS Report No. 2004-0226, NSIP-SHA-014382#P1-187. Pretoria, Council for Geoscience.

5.13.17) Prasad, K. & Claassen, D. (2012), **Report on the Baviaanskloof Fault Segment of the Ceres-Kango-Baviaanskloof-Coega Fault System. Neotectonic Studies for Evidence for Possible Post-Tertiary Grahamstown Formation (Tg) Reactivation of the Fault**. CGS Report No. 2012-0177, Rev. 0, 36 pp. Pretoria, Council for Geoscience.

5.13.18) Reddering, J.S.V., Claassen, D., & Coppersmith, R. (2012), **An Investigation into the Western Coega Fault for Seismic Source Characterization of the Proposed Thyspunt Nuclear Site, Eastern Cape, South Africa**. CGS Report No. 2012-0030, 52 pp. Pretoria, Council for Geoscience.

5.13.19) Mitha, V.R., Hanson, K.L., & Roberts, D.L. (2013), **Subsurface Neotectonic Investigation of the Eastern Part of the Coega Fault Corridor, Eastern Cape, South Africa**. CGS Report No. 2012-0029, Rev. 0, 90 pp. Pretoria, Council for Geoscience.

5.13.20) McCalpin, J.P. (compiler) (2009), **Field Reconnaissance and Seismic Source Characterisation of the Kouga, "Paul Sauer", Kango, and**

Baviaanskloof Fault Zones, Cape Fold Belt, Republic of South Africa. CGS Report No. 2009-0235, Rev. 0. Pretoria, Council for Geoscience.

5.13.21) Van Wyk, J.H. (1987), **Eskom Eastern Cape Nuclear Siting Project: Geological Map of the Coastal Strip Between Tsitsikamma River Mouth and Cape St. Francis**. Compiled by the Department of Geotechnology, Atomic Energy Corporation of South Africa Ltd. Pretoria.

5.13.22) Norman, N.G., Raubenheimer, E., Muller, A., Andersen, N.J.B., Faurie, J.N. (1987), **Final Report on the Geology of the Area between Cape St. Francis and the Tsitsikamma River Mouth, Eskom Eastern Cape Project – Investigations for the Siting of Nuclear Power Stations**, Progress Report No. 15, Vol 1: Geological Description of the Project Area. PIN-988(B/R), GEA 730, NSIP-EC-005620#P1–27. Pretoria, Atomic Energy Corporation of South Africa, Ltd., Department of Geotechnology.

5.13.23) Norman, N.G., Joubert, W.R., Hambleton-Jones, B.B., Toens, P.D. (1986), **Appraisal of Faulting in the Project Area – Investigations for the Siting of Nuclear Power Stations**, Progress Report No. 12. PIN-964(B/R), GEA 701, NSIP-EC-006290-#P1-27. Pretoria, Atomic Energy Corporation of South Africa, Ltd., Department of Geotechnology.

5.13.24) de Beer, C.H. (2005), **Investigation into Evidence for Neotectonic Deformation within Inland Neogene to Quaternary Deposits between Alexander Bay and Port Elizabeth – South Coast Report**. CGS Report No. 2005-0180, NSIP-SHA-016311#P1-197. Pretoria, Council for Geoscience.

5.13.25) de Beer, C.H. (2006a), **Investigation into Evidence for Neotectonic Deformation Within Onland Neogene to Quaternary Deposits Between Alexander Bay and Port Elizabeth – Executive Summary Report**. CGS Report No. 2006-0065. Rev. 0. 209 pp. Pretoria, Council for Geoscience.

5.13.26) Goedhart, M.L. (2007b), **Potential Onshore and Offshore Geological Hazards for the Thyspunt Nuclear Site, Eastern Cape, South Africa: A Review of the Latest Airborne and Marine Geophysical Data and Their Impact on the Existing Geological Model for the Site Vicinity Area**. CGS Report No. 2007-0274, Rev. 0. 59 pp. Pretoria, Council for Geoscience.

5.13.27) Goedhart, M.L., Reddering, J.S.V., Kilian, D., Mitha, V., Bosch, P.J.A., & Black, D. (2008), **Surface Geology and Update of Onland Geological Hazards for the 40-km Site Vicinity and 8-km Site Area Around the Proposed Thyspunt Nuclear Power Plant, Eastern Cape, South Africa**. CGS Report No. 2008-0222, 218 pp. Pretoria, Council for Geoscience.

© Eskom 2026/Rev 0a

5.13.28) Raubenheimer, E., Hambleton-Jones, B.B., & Toens, P.D. (1988), **Detailed Geology of De Hoek, Thyspunt and Tony's Bay. Volume 1: Geological Description. Eskom Southern Cape Project. Investigations for the Siting of Nuclear Power Stations**. Progress Report No. 20, GEA 801, NSIP-N002557. Pretoria, Atomic Energy Corporation of South Africa, Ltd., Department of Geotechnology.

5.13.29) Mountain, M.J. and Partners (1988), **Report on Engineering Geological Investigations of Aspects of the Surficial Deposits and Bedrock at De Hoek, Tony's Bay and Thyspunt Sites, Escom Eastern Cape Nuclear Siting Project**, Consultation Report to Atomic Energy Corporation of South Africa, Ltd., Pretoria. Report Ref. 294/D/9, NSIP-EC-006597#P1–99.

5.13.30) de Beer, C.H. (2000), **Geology and Tectonics of the Thyspunt Site, Humansdorp**. Internal Report to the Seismology Unit, 21 pp. Pretoria, Council for Geoscience.

5.13.31) Andersen, N.J.B., Muller, J.A., & Faurie, J.N. (1986), **A Geological Interpretation of the Detailed Aeromagnetic Survey Carried out South of Humansdorp**. Escom Eastern Cape project, Progress Report No. 9. PIN-937 (B/R) GEA 61. Pretoria, Atomic Energy Corporation of South Africa, Ltd., Department of Geotechnology.

5.13.32) Cole, J. (2008), **Interpretation of Regional Geophysical Data in the Site Vicinity of Thyspunt**. CGS Report No. 2008-0222. Pretoria, Council for Geoscience.

5.13.33) Muller, J.A., Andersen, N.J.B., Hambleton-Jones, B.B., & Toens, P.D. (1986), **The Detection of the Klippepunt Low Angle Strike Fault by a Medium Sensitivity Aeromagnetic Survey – Investigations for the Siting of Nuclear Power Stations**. Progress Report No. 11. PIN-963(B/R), GEA 700, NSIP-EC-06155#P1–13. Pretoria, Atomic Energy Corporation of South Africa, Ltd., Department of Geotechnology.

5.13.34) Muller, J.A., Andersen, N.J.B., Hambleton-Jones, B.B., & Toens, P.D. (1986), **Results and Geophysical Interpretation of the Detailed Aeromagnetic Survey Conducted in the Coastal Area of the Humansdorp District – Investigations for the Siting of Nuclear Power Stations**. Progress Report No. 14. PIN-982(B/R), GEA 721, NSIP-EC-006157#P1–19. Pretoria, Atomic Energy Corporation of South Africa, Ltd., Department of Geotechnology.

5.13.35) Cole, J. & Naudé, C. (2007), **Final Report: Airborne Survey of Thyspunt**. CGS Report No. 2007-0006, NSIP-NSI-019039#P1-67. Pretoria, Council for Geoscience.

5.13.36) Goedhart, M.L. & Cole, J. (2007), **Nuclear Siting Investigation Program: Remote Sensing Assessment of the Length of Aeromagnetic Lineament SV1, Thyspunt**. CGS Report No. 2007-0211, NSIP-NSI-020327#P1-29. Pretoria, Council for Geoscience.

© Eskom 2026/Rev 0a

5.13.37) Goedhart, M.L. (2007a), **Onshore and Offshore Geohazards for the Thyspunt Nuclear Power Plant: A Summary of New Airborne and Marine Geophysical Data, and Existing Offshore Seismic Reflection Data**. CGS Report No. 2007-0257, Rev. 0, 16 pp. Pretoria, Council for Geoscience.

5.13.38) Muller, J. A., Andersen, N.J.B., & Hennop, F. (1986), **A Reconnaissance Gravity Survey of Selected Sites Between Cape St. Francis and the Tsitsikamma River – Geological Investigations for the Siting of Nuclear Power Stations**. Progress Report No. 4. PIN-919(B/R), GEA 656, NSIP-EC-006286#P1–27. Pretoria, Atomic Energy Corporation of South Africa, Ltd., Department of Geotechnology.

5.13.39) Faurie, J.N., Muller, J.A., Andersen, N.J.B., & Hennop, F. (1986), **Gravity and Seismic Refraction Surveys on Thyspunt, Morgan's Bay and Brakkeduinen**. Progress Report 7, PIN-935 (B/R). GEA-669, NSIP-EC-006594#P1-42. Atomic Energy Corporation of South Africa, Ltd., Department of Geotechnology, Pretoria.

5.13.40) Raath, C.J. de W. & Cole, J. (2007), **Ground Geophysical Survey Investigating a Feature Identified during the Airborne Geophysical Study of the Area Around Thyspunt**. CGS Report No. 2007-0198, Rev. 1, 11 pp. NSIP-NSI-020068#P1-11. Pretoria, Council for Geoscience.

5.13.41) Cole, J. & Cole, P. (2007), **Geophysical Interpretation of the Marine Magnetic Data Collected in the Offshore Site Area (8 km Radius) of Thyspunt**. CGS Report No. 2007-0189, NSIP-NSI-020268#P1-12. Pretoria, Council for Geoscience.

5.13.42) Stettler, E.H., Zadorozhnaya, V.Y., & Goedhart, M.L. (2008), **Results of a Time Domain Electromagnetic Survey Over Four Possible Fault Positions Signifying the Landward Continuation of the Cape St. Francis Fault, Cape St. Francis and Oyster Bay, Eastern Province**. CGS Report No. 2008-0171, 30 pp. Pretoria, Council for Geoscience.

5.13.43) Stettler, E.H., Zadorozhnaya, V.Y., & Goedhart, M.L. (2008), **Results of a Time Domain Electromagnetic Survey Over Four Possible Fault Positions Signifying the Landward Continuation of the Cape St. Francis Fault, Cape St. Francis and Oyster Bay, Eastern Province**. CGS Report No. 2008-0171 – Addendum, 30 pp. Pretoria, Council for Geoscience.

5.13.44) Zadorozhnaya, V., Eberle, D., & Claassen, D. (2012), **Results of a Time Domain Electromagnetic Survey Conducted at Cape St. Francis with the Intent of Locating the Bedrock Surface Buried Beneath Cenozoic Cover, Eastern Cape, South Africa**. CGS Report No. 2012-0152, Rev. 0, 15 pp. Pretoria, Council for Geoscience.

5.13.45) Roux, J. (2011), **Offshore Geophysical Data**. PowerPoint presentation (given by A. Davids on behalf of the author) at SSHAC Workshop 1, April 16, Cape Town.

© Eskom 2026/Rev 0a

5.13.46) Horwood, S. (2009), **Thyspunt 8 km Radius Marine Survey: Structural Geology Report**. CGS Report No. 2009-0027, Rev. 0, 11 pp. Pretoria, Council for Geoscience.

5.13.47) Fugro Survey Africa (2007), **Thyspunt Nearshore Final Report, Cape Town**. NSIP-NSI-020579#P1-113.

5.13.48) Fugro Survey Africa. (2007), **Final Report for the Offshore Geophysical Survey at Thyspunt**. NSIP-NSI-019130#P1-206. Cape Town.

5.13.49) Brynard, H.J., Hambleton-Jones, B.B., & Toens, P.D. (1988), **Report on Mineralogical Investigation of Samples from Thyspunt and De Hoek near Humansdorp – Investigations for the Siting of Nuclear Power Stations**. Progress Report No. 21, PIN-1078(B/R), GEA 805, NSIP-EC-006255#P1–5. Pretoria, Atomic Energy Corporation of South Africa, Ltd., Department of Geotechnology.

5.13.50) Roberts, D.L. (2006), **Dating and Preliminary Correlation of Raised Marine and Estuarine Terraces on the Western and Southern Coast of South Africa**. **Final Report**. CGS Report No. 2006-0186. NSIP-SHA-018230#P1-206. Pretoria, Council for Geoscience.

5.13.51) Bierman, P.R. (2012a), **Report #1, Cosmogenic Geochronology, Southern Africa Fault Corridor Investigation**. Appendix B.3 in Hanson, K., Slack, C., & Coppersmith, R., Thyspunt Geological Investigations – Kango Fault Study. CGS Report No. 2012-0035, Rev. 0. Pretoria, Council for Geoscience.

5.13.52) Bierman, P.R. (2012b), Report #2, **Cosmogenic Geochronology, Southern Africa Southern Coast Marine Terraces**. Appendix E.1 in Hanson, K.L., Glaser, L., Coppersmith, R., Roberts, D.L, Claassen, D., & Black, D.E., Thyspunt Geological Investigations – Marine Terrace Studies. CGS Report No. 2012-0034, Rev. 0. Pretoria, Council for Geoscience.

5.13.53) Forman, S.L. (2012b), **Optical Ages for Displaced and Deposited Sediments Associated with the Kango Fault, Western Cape, South Africa**. Appendix B.2 in Hanson, K., Slack, C., & Coppersmith, R. (2012b), Thyspunt Geological Investigations – Kango Fault Study. CGS Report No. 2012-0035, Rev. 0. Pretoria, Council for Geoscience.

5.13.54) Hanson, K., Slack, C., & Coppersmith, R. (2012b), **Thyspunt Geological Investigations – Kango Fault Study**. CGS Report No. 2012-0035, Rev. 0. Pretoria, Council for Geoscience.

5.13.55) Forman, S.L. (2012a), **Optical Ages for Aeolian and Littoral Sediments from Drill-Core, Eastern Cape, South Africa**. Appendix E.2 in Hanson, K.L., Glaser, L., Coppersmith, R., Roberts, D.L, Claassen, D., & Black, D.E. (2012a), Thyspunt Geological Investigations – Marine Terrace Studies. CGS Report No. 2012-0034, Rev. 0. Pretoria, Council for Geoscience.

© Eskom 2026/Rev 0a

5.13.56) Roberts, D.L. (2004**), Dating and Correlation of Raised Marine and Estuarine Terraces on the Western and Southern Coasts of South Africa**. **Literature Review Report**. CGS Report No. 2004-0047, NSIP-SHA-012662#P1-55. Pretoria, Council for Geoscience.

5.13.57) Roberts, D.L. (2005), **Dating and Preliminary Correlation of Raised Marine and Estuarine Terraces on the Western and Southern Coast of South Africa**. CGS Report No. 2005-0183, Rev. 1, NSIP-SHA-016344#P1-141. Pretoria, Council for Geoscience.

5.13.58) Hanson, K.L., Glaser, L., Coppersmith, R., Roberts, D.L, Claassen, D. & Black, D.E. (2012a), **Thyspunt Geological Investigations – Marine Terrace Studies**. CGS Report No. 2012-0034, Rev. 0. Pretoria, Council for Geoscience.

5.13.59) de Wet, W.M. (2012), **Bathymetry of the South African Continental Shelf**. MSc Thesis, University of Cape Town.

5.13.60) Eskom (2010a), **Exploration Borehole Data and Logs**. In Thyspunt Site Safety Report, Section 5.11, Geohydrology, Appendix A-5.11.D, Draft Report, June.

5.13.61) Eskom (2010b), **Borehole Logs**. In Thyspunt Site Safety Report, Section 5.15, Geotechnical Characterization, Appendix A-5.15.B, Draft Report, June.

5.13.62) Engelsman, B. & Constable, B. (2012), **Thyspunt Shear Wave Velocity Measurements**. Report No. 449376, SRK Consulting Ltd.

5.13.63) Park, C. (2011), **Seismic Site Characterization in Thyspunt Area by Active and Passive MASW Surveys: Data Processing Results**. CGS Report No. 2011-0196, Rev. 0. Pretoria, Council for Geoscience.

5.13.64) Rathje, E.M., Cichowicz, A., & Birch, D. (2012), **Seismic Site Characterization for the Thyspunt Nuclear Siting Project**. CGS Report No. 2012-1036, Rev. 1. Pretoria, Council for Geoscience.

5.13.65) Kijko, A, Midzi, V, Ramperthap, J., Singh, M. (2008**), A Probabilistic Tsunami Hazard Assessment for Coastal South Africa from Distant Tsunamogenic Areas**. CGS Report No. 2008-0156. Pretoria, Council for Geoscience.

5.13.66) Roberts, D.L. (2008), **Potential Sources of Tsunami Along the South African Coast**. CGS Report No. 2008-0220, Rev. 2. Pretoria, Council for Geoscience.

5.13.67) Uenzelmann-Neben, G., Schluter, P., & Weigelt, E. (2007), **Cenozoic Oceanic Circulation Within the South African Gateway: Indications from Seismic Stratigraphy**. South African Journal of Geology 110, 275-294.

5.13.68) Ben-Avraham, Z., Hartnady, C.J.H., & Kitchin, K.A. (1997), **Structure and Tectonics of the Agulhas-Falkland Fracture Zone**. Tectonophysics 282, 83-98.

© Eskom 2026/Rev 0a

5.13.69) Parsiegla, N., Gohl, K., & Uenzelmann-Neben, G. (2007), **Deep Crustal Structure of the Sheared South African Continental Margin: First Results of the Agulhas-Karoo Geoscience Transect**. South African Journal of Geology 110, 393-406.

5.13.70) Ben-Avraham, Z., Hartnady, C.J.H., & Malan, J.A. (1993), **Early Tectonic Extension Between the Agulhas Bank and the Falkland Plateau due to the Rotation of the Lafonia Microplate**. Earth and Planetary Science Letters 117, 43-58.

5.13.71) Martin, A.K. & Flemming, B.W. (1986), **The Holocene Shelf Sediment Wedge off the South and East Coast of South Africa**. In: Knight, R.J. & McLean, J.R. (eds.), Shelf Sands and Sandstones, pp. 27-44, Canadian Society of Petroleum Geologists Memoir 11.

5.13.72) Brown, L.F., Benson, J.M., Brink, G.J., Doherty, S., Jollands, A., Jungslager, E.H.A., Keenan, J.H.G., Muntingh, A., & van Wyk, N.J.S. (1995), **Sequence Stratigraphy in Offshore South African Divergent Basins: An Atlas on Exploration for Cretaceous Lowstand Traps by Soekor (Pty) Ltd**. AAPG Studies in Geology #41, 184 pp.

5.13.73) Broad, D.S., Jungslager, E.H.A., McLachlan, I.R., & Roux, J. (2006), **Offshore Mesozoic Basins**. In: Johnson, M.R., Anhaeusser, C.R., & Thomas, R.J. (eds.), The Geology of South Africa, pp. 553-572. Johannesburg, Geological Society of South Africa / Pretoria, Council for Geoscience.

5.13.74) Broad, D.S., Jungslager, E.H.A., McLachlan, I.R., Roux, J., & Van der Spuy, D. (2012), **South Africa's Offshore Mesozoic Basins**. In: Roberts, D.G. & Bally, A.W. (eds.), Phanerozoic Passive Margins, Cratonic Basins and Global Tectonic Maps, pp. 535-564. Rotterdam, Elsevier.

5.13.75) Dingle, R.V., Siesser, W.G., & Newton, A.R. (1983), **Mesozoic and Tertiary Geology of Southern Africa**. Rotterdam, A.A. Balkema, 375 pp.

5.13.76) Malan, J.A. & Viljoen, J.H.A. (2008), **Southern Cape Geology: Evolution of a Rifted Margin**. AAPG International Conference and Exhibition FIELD EXCURSION FT07 GUIDEBOOK 30, October–3 November, 60 pp.

5.13.77) Parsiegla, N., Stankiewicz, J., Gohl, K., Ryberg, T., & Uenzelmann-Neben, G. (2009), **Southern African Continental Margin: Dynamic Processes of a Transform Margin**. Geochemistry, Geophysics, Geosystems 10(3), 1-20.

5.13.78) Gentle, R.I. (1987), **The Geology of the Inner Continental Shelf and Agulhas Arch: Cape Town to Port Elizabeth**. Joint Geological Survey / University of Cape Town Bulletin 20.

5.13.79) Birch, G.F. (1979), **Nearshore Quaternary Sedimentation off the South Coast of South Africa**. Marine Geoscience Unit Technical Report No. 11, Progress Reports for the Year 1978, pp. 127-146. Joint Geological Survey / University of Cape Town.

© Eskom 2026/Rev 0a

5.13.80) De Decker, R.H. (1983), **The Sediments of Plettenberg Bay and the Submerged Robberg Spit**. Joint Geological Survey / University of Cape Town Marine Geoscience Group Technical Report No. 14, pp. 255-265.

5.13.81) Flemming, B.W. (1978), **Underwater Observations Along a High-Energy, Cliffed Coastline (Tsitsikamma)**. Joint Geological Survey/ University of Cape Town Marine Geoscience Group Technical Report No. 11, pp. 57-146.

5.13.82) Bird, E.C.F., 2008, **Coastal Geomorphology: An Introduction**, 2nd Ed., 411 pp. Chichester, John Wiley.

5.13.83) Uenzelmann-Neben, G. & Huhn, K. (2009), **Sedimentary Deposits on the Southern South African Continental Margin: Slumping Versus Non-deposition or Erosion by Ocean Currents?** Marine Geology 266, 65-79.

5.13.84) Partridge, T.C., Dollar, E.S.J., Moolman, J., & Dollar, L.H. (2010), **The Geomorphic Provinces of South Africa, Lesotho and Swaziland: Physiographic Subdivision for Earth and Environmental Scientists**. Transactions of the Royal Society of South Africa 65(1), 1-47.

5.13.85) Roberts, D.L., Bateman, M.D., Murray-Wallace, C., Carr, A.S. & Holmes, P.J. (2009), **West Coast Dune Plumes: Climate Driven Contrasts in Dunefield Morphogenesis Along the Western and Southern South African coasts**. Palaeogeography, Palaeoclimatology, Palaeoecology 271, 24-38.

5.13.86) Illenberger, W. & Burkinshaw, J. (2007), **The Cape St. Francis Headland Bypass Dune System and Beach Erosion at St. Francis Bay, and Sediment Accumulation in the Kromme Estuary**. Description for Heritage Center, December 2001, 6 pp., unpublished report. (Update of December 2001 report).

5.13.87) Davies, O. (1971), **Pleistocene Shorelines in the Southern and South-Eastern Cape Province (Part 1)**. Annals of the Natal Museum 21 (1), 183 223.

5.13.88) Davies, O. (1972), **Pleistocene Shorelines in the Southern and South-Eastern Cape Province (Part 2)**. Annals of the Natal Museum 21 (2), 225 279.

5.13.89) Davies, O. (1973), **Pleistocene Shorelines in the Western Cape and South-West Africa**. Annals of the Natal Museum 21 (3), 719-765.

5.13.90) Toerien, D.K. (1979), Explanation: **The Geology of the Oudtshoorn Area (Sheet 3322, scale 1:250 000)**. Pretoria, Geological Survey of South Africa, 13 pp.

5.13.91) Toerien, D.K. (compiler; 1991), **The Geology of the Port Elizabeth Area (Sheet 3324, scale 1:250 000)**. Pretoria, Geological Survey of South Africa.

5.13.92) Hagedorn, J. (1988), **Silcretes in the Western Little Karoo and Their Relation to Geomorphology and Palaeoecology**. Palaeoecology of Africa 19, 371-375.

5.13.93) Hälbich, I.W. (1983c), **Disharmonic Folding, Detachment and Thrusting in the Cape Fold Belt**. In: Söhnge, A.P.G. & Hälbich, I.W. (eds.), Special

Publication 12, Geodynamics of the Cape Fold Belt: A Contribution to the National Geodynamics Programme, ch. 10, pp. 115-123. Johannesburg, Geological Society of South Africa.

5.13.94) Scharf, T., Codilean, A.T., de Wit, M., Jansen, J.D., & Kubik, P.W. (2013), **Strong Rocks Sustain Ancient Postorogenic Topography in Southern Africa**. Geology 41, 331-334.

5.13.95) Flowers, R.M. & Schoene, B. (2010), **(U-Th)/He Thermochronometry Constraints on Unroofing of the Eastern Kaapvaal Craton and Significance for Uplift of the Southern African Plateau**. Geology Boulder 38(9), 827-830.

5.13.96) Catuneanu, O., Wopfner, H., Eriksson, P.G., Cairncross, B., Rubidge, B.S., Smith, R.M.H., & Hancox, P.J. (eds.) (2005), **The Karoo Basins of South-Central Africa**. Journal of African Earth Sciences 43(1–3), 211-253.

5.13.97) de Wit, M.J., Roering, C., Hart, R.J., Armstrong, R.A., De Ronde, C.E.J., Green, R.W.E., Tredoux, M., Peberdy, E., & Hart, R.A. (1992), **Formation of an Archaean Continent**. Nature 357, 553-562.

5.13.98) Jacobs, J., Pisarevsky, S., Thomas, R.J., & Becker, T. (2008), **The Kalahari Craton during the Assembly and Dispersal of Rodinia**. Precambrian Research 160(1-2), 142-158.

5.13.99) Jacobs, J. & Thomas, R.J. (1994), **Oblique Collision at About 1.1 Ga Along the Southern Margin of the Kaapvaal Continent, Southeast Africa**. Geologische Rundschau 83(2), 322-333.

5.13.100) de Wit, M.J. & Ransome, I.G.D. (1992), Regional Inversion Tectonics Along the Southern Margin of Gondwana. In: de Wit, M.J. & Ransome, I.G.D. (eds.), Inversion Tectonics of the Cape Fold Belt, Karoo and Cretaceous Basins of Southern Africa, pp. 15-21. Rotterdam, A.A. Balkema.

5.13.101) Hälbich, I.W. (1983a), **A Geodynamic Model for the Cape Fold Belt (CFB)**. In: Söhnge, A.P.G. & Hälbich, I.W. (eds.), Special Publication 12, Geodynamics of the Cape Fold Belt: A Contribution to the National Geodynamics Programme, ch. 15, pp. 177-184, Johannesburg, Geological Society of South Africa.

5.13.102) Cornell, D.H., Thomas, R.J., Moen, H.F.G., Reid, D.L., Moore, J.M., & Gibson, R.L. (2006), **The Namaqua-Natal Province**. In: Johnson, M.R., Anhaeusser, C.R., & Thomas, R.J. (eds.), The Geology of South Africa, pp. 325-379. Johannesburg, Geological Society of South Africa / Pretoria, Council for Geoscience.

5.13.103) Eglington, B.M., Harmer, R.E., & Kerr, A. (1989), **Isotope and Geochemical Constraints on Proterozoic Crustal Evolution in Southeastern Africa**. Precambrian Research 45, 159-174.

5.13.104) Eglington, B.M. & Armstrong, R.A. (2003), **Geochronological and Isotopic Constraints on the Mesoproterozoic Namaqua-Natal Belt: Evidence from**

Deep Borehole Intersections in South Africa. Precambrian Research 125, 179-189.

5.13.105) Eglington, B.M. (2006), **Evolution of the Namaqua-Natal Belt, Southern Africa – A Geochronological and Isotope Geochemical Review**. Journal of African Earth Sciences 46, 93-111.

5.13.106) de Beer, J.H. (1978), **The Relationship Between the Deep Electrical Resistivity Structure and Tectonic Provinces in Southern Africa: Part 2**. Results obtained by magnetometer array studies, Transactions of the Geological Society of South Africa 81, 143-154.

5.13.107) Pitts, B.E., Maher, M.J., de Beer, J.H., & Gough, D.I. (1992), **Interpretation of Magnetic, Gravity and Magnetotelluric Data Across the Cape Fold Belt and Karoo Basin**. In: de Wit, M.J. & Ransome, I.G.D. (eds.), Inversion Tectonics of the Cape Fold Belt, Karoo and Cretaceous Basins of Southern Africa, pp. 27-32. Rotterdam, A.A. Balkema.

5.13.108) Eglington, B.M., de Beer, J.H., Pitts, B.E., Meyer, R., Geerthsen, K., & Maher, M.J. (1993), **Geological, Geophysical and Isotopic Constraints on the Nature of the Mesoproterozoic Namaqua-Natal Belt of Southern Africa**. In: Peters, J.W., Kesse, G.O., & Acquah, P.C. (eds.), Proceedings of the 9th International Geological Conference of the Geological Society of Africa, pp. 114-135. Accra, Geological Society of Africa.

5.13.109) Tankard, A.J., Jackson, M.P.A., Eriksson, K.A., Hobday, D.K., Hunter, D.R., & Minter, W.E.L. (1982), **Crustal Evolution of Southern Africa**. New York, Springer-Verlag, 523 pp.

5.13.110) Harvey, J.D., de Wit, M.J., Stankiewicz, J., & Doucouré, C.M. (2001), **Structural Variations of the Crust in the Southwestern Cape, Deduced from Seismic Receiver Functions**. South African Journal of Geology 104, 231-242.

5.13.111) Weckmann, U., Ritter, O. Jung, A., Branch, T., & de Wit, M. (2007), **Magnetotelluric Measurements Across the Beattie Magnetic Anomaly and the Southern Cape Conductive Belt, South Africa**. Journal of Geophysical Research 112(B05416), 10 pp.

5.13.112) Lindeque, A., de Wit, J., Ryberg, T., Weber, M., & Chevallier, L. (2011), **Deep Crustal Profile Across the Southern Karoo Basin and Beattie Magnetic Anomaly, South Africa: An Integrated Interpretation with Tectonic Implications**. South African Journal of Geology 114(3/4), 265-292.

5.13.113) Shone, R.W., Nolte, C.C., & Booth, P.W.K. (1990), **Pre-Cape Rocks of the Gamtoos Area – A Complex Tectonostratigraphic Package Preserved as a Horst Block**. South African Journal of Geology 93 (4), 616-621.

5.13.114) Barnett, W., Armstrong, R., & de Wit, M.J. (1997), **Stratigraphy of the Upper Neoproterozoic Kango and Lower Paleozoic Table Mountain Group of the Cape Fold Belt Revisited**. South African Journal of Geology 100(3), 237-250.

5.13.115) Gresse, P.G., Von Veh, M.W., & Frimmel, H.E. (2006), **Namibian (Neoproterozoic) to Early Cambrian Successions**. In: Johnson, M.R., Anhaeusser, C.R., & Thomas, R.J. (eds.), The Geology of South Africa, pp. 395-420. Johannesburg, Geological Society of South Africa / Pretoria, Council for Geoscience.

5.13.116) Gresse, P.G. (1983), **Lithostratigraphy and Structure of the Kaaimans Group**. In: A.P.G. Söhnge, A.P.G. & Hälbich, I.W. (eds.), Special Publication 12, Geodynamics of the Cape Fold Belt: A Contribution to the National Geodynamics Programme, pp. 177-184. Johannesburg, Geological Society of South Africa.

5.13.117) Le Roux, J.P. (1983), **Structural Evolution of the Kango Group**. In: Söhnge, A.P.G. & Hälbich, I.W. (eds.), Special Publication 12, Geodynamics of the Cape Fold Belt: A Contribution to the National Geodynamics Programme, ch. 5, pp. 47-56. Johannesburg, Geological Society of South Africa.

5.13.118) Hälbich, I.W. (1983b), **A Tectonogenesis of the Cape Fold Belt (CFB)**. In: Söhnge, A.P.G. & Hälbich, I.W. (eds.), Special Publication 12, Geodynamics of the Cape Fold Belt: A Contribution to the National Geodynamics Programme, ch. 14, pp. 165-175. Johannesburg, Geological Society of South Africa.

5.13.119) Thamm, A.G. & Johnson, M.R. (2006), **The Cape Supergroup**. In: Johnson, M.R., Anhaeusser, C.R., & Thomas, R.J. (eds.), The Geology of South Africa, pp. 443-460. Johannesburg, Geological Society of South Africa / Pretoria, Council for Geoscience.

5.13.120) Martini, J.E.J. (1974), **On the Presence of Ash Beds and Volcanic Fragments in the Graywackes of the Karoo System in the Southern Cape Province (South Africa)**. Transactions of the Geological Society of South Africa 77, 113-116.

5.13.121) Lock, B.E. (1980), **Flat-Plate Subduction and the Cape Fold Belt of South Africa**. *Geology* 8, 35-39.

5.13.122) Catuneanu, O., Hancox, P.J., & Rubidge, B.S. (1998), **Reciprocal Flexural Behaviour and Contrasting Stratigraphies: A New Basin Development Model for the Karoo Retroarc Foreland System, South Africa**. Basin Research 10, 417-439.

5.13.123) Dalziel, I.W.D., Lawver, L.A., & Murphy, J.B. (2000), **Plumes, Orogenesis, and Supercontinental Fragmentation**. Earth and Planetary Science Letters 178, 1-11.

5.13.124) Johnson, M.R., Van Vuuren, C.J., Visser, J.N.J., Cole, D.I, Wickens, H. de V., Christie, A.M.D., Roberts, D.L., & Brandl, G. (2006), **Sedimentary Rocks of**

the Karoo Supergroup. In: Johnson, M.R., Anhaeusser, C.R., & Thomas, R.J. (eds.), The Geology of South Africa, pp. 461-500. Johannesburg, Geological Society of South Africa / Pretoria, Council for Geoscience.

5.13.125) Milani, E.J. & de Wit, M.J. (2008), **Correlations Between the Classic Paraná and Cape Karoo Sequences of South America and Southern Africa and Their Basin Infills Flanking the Gondwanides: du Toit Revisited**. In: Pankhurst, R.J., Trouw, R.A.J., Brito Neves, B.B., & de Wit, M.J. (eds.), West Gondwana: Pre-Cenozoic Correlations Across the South Atlantic Region, pp. 319-342, Special Publications 294. London, Geological Society.

5.13.126) Kingsley, C.S. (1981), **A Composite Submarine Fan-Delta-Fluvial Model for the Ecca and lower Beaufort Groups of Permian Age in the Eastern Cape Province, South Africa**. Transactions of the Geological Society of South Africa 84, 27-40.

5.13.127) Winter, H. de la R. (1984), **Tectonostratigraphy, as Applied to Analysis of South African Phanerozoic Basins**. Transactions of the Geological Society of South Africa 87, 169-179.

5.13.128) Ramos, V.A. (1986), **Discussion on 'Tectonostratigraphy as Applied to Analysis of South African Phanerozoic Basins', by H. de la R. Winter**. Transactions of the Geological Society of South Africa 89, 427-429.

5.13.129) Hälbich, I.W. & Swart, J. (1983), **Structural Zoning and Dynamic History of the Cover Rocks of the Cape Fold Belt**. In: Söhnge, A.P.G. & Hälbich, I.W. (eds.), Special Publication 12, Geodynamics of the Cape Fold Belt: A Contribution to the National Geodynamics Programme, pp. 75-100. Johannesburg, Geological Society of South Africa.

5.13.130) Stankiewicz, J., Ryberg, T., Schulze, A., Lindeque, A., Weber, M.H., & de Wit, M.J. (2007), **Initial Results from Wide-Angle Seismic Refraction Lines in the Southern Cape**. South African Journal of Geology 110, 407-418.

5.13.131) Paton, D.A., Macdonald, D.I.M., & Underhill, J.R. (2006), **Applicability of Thin or Thick Skinned Structural Models in a Region of Multiple Inversion Episodes: Southern South Africa**. Journal of Structural Geology 28(11), 1933-1947.

5.13.132) de Villiers, J. (1944), **A Review of the Cape Orogeny**. Annals of the University Stellenbosch 22(10), 183-208.

5.13.133) Söhnge, A.P.G. (1983), **The Cape Fold Belt – Perspective**. In: Söhnge, A.P.G. & Hälbich, I.W. (eds.), Special Publication 12, Geodynamics of the Cape Fold Belt: A Contribution to the National Geodynamics Programme, pp. 1-6. Johannesburg, Geological Society of South Africa.

5.13.134) de Beer, C.H. (1990), **Simultaneous Folding in the Western and Southern Branches of the Cape Fold Belt**. South African Journal Geology 93(4), 583-591.

5.13.135) de Beer, C.H. (1998), **Structure of the Cape Fold Belt in the Ceres Arc**. Council for Geoscience Bulletin 123, 93 pp.

5.13.136) de Beer, C.H. (2002b), **The Stratigraphy, Lithology and Structure of the Table Mountain Group**. In: Pietersen, K. & Parsons, R. (eds.), A Synthesis of the Hydrogeology of the Table Mountain Group – Formation of a Research Strategy, pp. 8-18, Water Research Commission, WRC Report No. TT 158/01.

5.13.137) Paton, D.A. (2006), **Influence of Crustal Heterogeneity on Normal Fault Dimensions and Evolution: Southern South Africa Extensional System**. Journal of Structural Geology 28(5), 868-886.

5.13.138) de Beer, C.H. (1995), **Fold Interference from Simultaneous Shortening in Different Directions: The Cape Fold Belt Syntaxis**. Journal of African Earth Sciences 21(1), 157-169.

5.13.139) Hälbich, I.W., Fitch, F.J., & Miller, J.A. (1983), **Dating the Cape Orogeny**. In: Söhnge, A.P.G. & Hälbich, I.W. (eds.), Special Publication 12, Geodynamics of the Cape Fold Belt: A Contribution to the National Geodynamics Programme, ch. 13, pp. 149-164. Johannesburg, Geological Society of South Africa.

5.13.140) Gresse, P.G., Theron, J.N., Fitch, F.J., & Miller, J.A. (1992), **Tectonic Inversion and Radiometric Resetting of the Basement in the Cape Fold Belt**. In: de Wit, M.J. & Ransome, I.G.D. (eds.), Inversion Tectonics of the Cape Fold Belt, Karoo and Cretaceous Basins of Southern Africa, pp. 217-228. Rotterdam, A.A. Balkema.

5.13.141) de Beer, J.H. & Meyer, R. (1984), **Geophysical Characteristics of the Namaqua-Natal Belt and Its Boundaries**. South Africa, Journal of Geodynamics 1, 473-494.

5.13.142) Bate, K.J. & Malan, J.A. (1992), **Tectonostratigraphic Evolution of the Algoa, Gamtoos and Pletmos Basins, Offshore South Africa. In Inversion Tectonics of the Cape Fold Belt, Karoo and Cretaceous Basins of Southern Africa**. In: de Wit, M.J. & Ransome, I.D.G. (eds.), Proceedings, Conference on Inversion Tectonics of the Cape Fold Belt, Cape Town, 2–6 December, 1991, pp. 61-73. Rotterdam, A.A. Balkema.

5.13.143) Watkeys, M.K. (2006), **Gondwana Break-up: A South African Perspective**. In: Johnson, M.R. Anhaeusser, C.R. & Thomas, R.J. (eds.), The Geology of South Africa, pp. 531-540. Johannesburg, Geological Society of South Africa / Pretoria, Council for Geoscience.

5.13.144) Thomson, K. (1999), **Role of Continental Break-Up, Mantle Plume Development and Fault Reactivation in the Evolution of the Gamtoos Basin, South Africa**. Marine and Petroleum Geology 16, 409-429.

5.13.145) Fairhead, J.D. (1988), **Mesozoic Plate Tectonic Reconstructions of the Central South Atlantic Ocean: The Role of the West and Central African Rift Systems**. Tectonophysics 155, 181-191.

© Eskom 2026/Rev 0a

5.13.146) Hartnady, C.J.H. & le Roex, A.P. (1985), **Southern Ocean Hotspot Tracks and the Cenozoic Absolute Motion of the African, Antarctic, and South American Plates**. Earth and Planetary Science Letters 75, 245-257.

5.13.147) Parsiegla, N., Gohl, K., & Uenzelmann-Neben, G. (2008), **The Agulhas Plateau: Structure and Evolution of a Large Igneous Province**. Geophysical Journal International 174, 336-350.

5.13.148) König, M. & Jokat, W. (2006), **The Mesozoic Breakup of the Weddell Sea**. Journal of Geophysical Research 111(B12102), doi:10.1029/2005JB004035.

5.13.149) Conrad, C.P. & Gurnis, M. (2003), **Seismic Tomography, Surface Uplift, and the Breakup of Gondwanaland: Integrating Mantle Convection Backwards in Time**. Geochemistry, Geophysics, Geosystems 4(3).

5.13.150) Booth, P.W.K. & Shone, R.W. (1999), **Complex Thrusting at Uniondale, Eastern Sector of the Cape Fold Belt, Republic of South Africa: Structural Evidence for the Need to Revise Lithostratigraphy**. Journal of African Earth Sciences 29, 125-133.

5.13.151) Martin, A.K. & Hartnady, C.J.H. (1986), **Plate Tectonic Development of the Southwest Indian Ocean: A Revised Reconstruction of East Antarctica and Africa**. Journal of Geophysical Research 91 (B5), 4767-4786.

5.13.152) Partridge, T.C. & Maud, R.R. (1987), **Geomorphic Evolution of Southern Africa Since the Mesozoic**. South African Journal of Geology 90, 179-208.

5.13.153) Roberts, D.L., Botha, G.A. Maud, R.R., & Pether, J. (2006), **Coastal Cenozoic Deposits**. In: Johnson, M.R., Anhaeusser, C.R., & Thomas, R.J. (eds.), The Geology of South Africa, pp. 605-628. Johannesburg, Geological Society of South Africa / Pretoria, Council for Geoscience.

5.13.154) Johnson, M.R. (1976), **Stratigraphy and Sedimentology of the Cape and Karoo Sequences in the Eastern Cape Province**. Ph.D. Thesis, Rhodes University, Grahamstown, South Africa, 336 pp.

5.13.155) Hill, R.S. & Nolte, C.C. (1989), **Gamtoos Group**. In: Johnson, M.R. (ed.), Catalogue of South African Lithostratigraphic Units, Volume 1, 2 pp. South African Committee for Stratigraphy.

5.13.156) Scheepers, R. & Schoch, A.E. (2006), **The Cape Granite Suite**. In: Johnson, M.R., Anhaeusser, C.R., & Thomas, R.J. (eds.), The Geology of South Africa, pp. 421-432. Johannesburg, Geolological Society of South Africa / Pretoria, Council for Geoscience.

5.13.157) Smith, R.M.H., Eriksson, P.G., & Botha, W.J. (1993), **A Review of the Stratigraphy and Sedimentary Environments of the Karoo-Aged Basins of Southern Africa**. Journal of African Earth Sciences (and the Middle East) 16(1–2), 143-169.

© Eskom 2026/Rev 0a

5.13.158) Reeves, C. (2000), **The Geophysical Mapping of Mesozoic Dyke Swarms in Southern Africa and Their Origin in the Disruption of Gondwana**. Journal of African Earth Sciences 30(3), 499-513,

5.13.159) Hill, R.S. (1992), **Suurberg Group Including the Slagboom, Coerney and Mimosa Formations (Karoo Sequence)**. In: Johnson, M.R. (ed.), Catalogue of South African Lithostratigraphic Units, Volume 4. South African Committee for Stratigraphy.

5.13.160) South African Committee for Stratigraphy (1980), **Stratigraphy of South Africa. Part 1: Lithostratigraphy of the Republic of South Africa, South West Africa/Namibia and the Republics of Bophuthatswana, Transkei and Venda**. In: Kent, L.E. (comp.), Handbook Geological Survey of South Africa, vol. 8, 690 pp.

5.13.161) Shone, R.W. (2006), **Onshore Post-Karoo Mesozoic Deposits**. In: Johnson, M.R., Anhaeusser, C.R., & Thomas, R.J. (eds.), The Geology of South Africa, pp. 541-552. Johannesburg, Geological Society of South Africa / Pretoria, Council for Geoscience.

5.13.162) McMillan, I.K., Brink, G.I., Broad, D.S., & Maier, J.J. (1997), **Late Mesozoic Sedimentary Basins off the South Coast of South Africa**. In: Selley, R.C. (ed.), African Basins, vol. 3 in Sedimentary Basins of the World series, pp. 319-376. Amsterdam, Elsevier.

5.13.163) Le Roux, F.G. (1990), **Algoa Group**. Catalogue of South African Lithostratigraphic Units, Vol. 1, South African Committee for Stratigraphy, 2 pp.

5.13.164) Partridge, T.C., Botha, G.A., & Haddon, I.G. (2006), **Cenozoic Deposits of the Interior**. In: Johnson, M.R., Anhaeusser, C.R., & Thomas, R.J. (eds.), The Geology of South Africa, pp. 585-604. Johannesburg, Geological Society of South Africa / Pretoria, Council for Geoscience.

5.13.165) Mountain, E.D. (1980), **Grahamstown Peneplain**. Transactions of the Geological Society of South Africa. 83, pp. 47-53

5.13.166) Le Roux, F.G. (1989), **Lithostratigraphy of the Nahoon Formation**. Lithostratigraphic Series No. 9, South African Committee for Stratigraphy, 14 pp.

5.13.167) Malan, J.A. (compiler) (1987), **Riversdale Quadrant Geological Map, 1:250 000 Scale**. Compiled from mapping by Siegfried, H.P., Viljoen, J.H.A., Wickens, H. de V., Toerien, D.K., & Malan, J.A. Council for Geoscience map 3420. Also available: map explanation by Malan, J.A. & Viljoen, J.H.A. (1994), 63 pp.

5.13.168) Butzer, K.W. & Helgren, D.M. (1972), **Late Cenozoic Evolution of the Cape Coast Between Knysna and Cape St. Francis, South Africa**. Quaternary Research 2(2), 143-169.

© Eskom 2026/Rev 0a

5.13.169) Marker, M.E. (1987), **A Note on Marine Benches of the Southern Cape**. South African Journal of Geology 90, 120-123.

5.13.170) Hattingh, J. (2001), **Late Cenozoic Drainage Evolution in the Algoa Basin with Special Reference to the Sundays River Valley**. Council for Geoscience Bulletin 128, 103 pp.

5.13.171) Erlanger, E.D. (2010), **Rock Uplift, Erosion, and Tectonic Uplift of South Africa Determined with Cosmogenic ^{26}Al and ^{10}Be**. MSc Thesis, Purdue University, 196 pp.

5.13.172) Erlanger, E.D., Granger, D.E., & Gibbon, R.J. (2012), **Rock Uplift Rates in South Africa from Isochron Burial Dating of Fluvial and Marine Terraces**. Geology 40, 1019-1022.

5.13.173) Hattingh. J. (1996), **Late Cenozoic Drainage Evolution in the Algoa Basin, with Special Reference to theSundays River Valley, Eastern Cape**. Unpublished Ph.D. thesis, University of Port Elizabeth, 181pp.

5.13.174) Illenberger, W.K. (1996), **The Geomorphologic Evolution of the Wilderness Dune Cordons, South Africa**. Quaternary International 33, 11-20.

5.13.175) Roberts, D.L., Bateman, M.D., Murray-Wallace, C.V., Carr, A.S., &Holmes, P.J. (2008), **Last Interglacial Fossil Elephant Trackways Dated by OSL/AAR in Coastal Aeolianites, Still Bay, South Africa**. Palaeogeography, Palaeoclimatology, Palaeoecology 257, 261-279.

5.13.176) Bateman, M.D., Carr, A.S., Dunajko, A.C., Holmes, P.J., Roberts, D.L., McLaren, S.J., Bryant, R.G., Marker, M.E., & Murray-Wallace, C.V. (2011), **The Evolution of Coastal Barrier Systems: A Case Study of the Middle-Late Pleistocene Wilderness Barriers, South Africa**. Quaternary Science Reviews 30, 63-81.

5.13.177) Birch, G.F., Du Plessis, A. & Willis, J.P., 1978, **Offshore and Onland Geological and Geophysical Investigations in the Wilderness Lakes Region**. Transactions of the Geological Society of South Africa 81, 339-352.

5.13.178) Bremner, J.M. & Day, R.W. (1991), **Acoustic Stratigraphy and Late Cenozoic Sediments in Algoa Bay**. In Algoa Bay – Marine Geoscientific Investigations, Geological Survey Bulletin 100, pp. 123-163.

5.13.179) Du Plessis, A. & Glass, J.G.K. (1991), **Geology of the Sea Floor in the Vicinity of Jahleel and St Croix Islands, Algoa Bay, in Algoa Bay – Marine Geoscientific Investigations**. Geological Survey Bulletin 100, pp. 95-122.

5.13.180) Ebinger, C.J., Yemane, T., Harding, D.J., Tesfaye, S., Kelley, S. & Rex, D. (2000), **Rift Deflection, Migration and Propagation: Linkage of the Ethiopian and Eastern Rifts, Africa**. Geological Society of America Bulletin 112(2), 163-176.

© Eskom 2026/Rev 0a

5.13.181) Bird, P., Ben-Avraham, Z., Schubert, G., Andreoli, M., & Viola, G. (2006), **Patterns of Stress and Strain Rate in Southern Africa**. Journal of Geophysical Research 111, B08402, doi:10.1029/2005JB003882, 14 pp.

5.13.182) Calais, E., Ebinger, C., Hartnady, C., & Nocquet, J.M. (2006), **Kinematics of the East African Rift from GPS and Earthquake Slip Data**. In: Yirgu, G., Ebinger, C.J., & Maguire, P.K.H. (eds.), The Afar Volcanic Province Within the East African Rift System, pp. 9-22, Geological Society of London, Special Publication 259.

5.13.183) Hartnady, C.J.H. (2003), **Recent Motion of the African Plates**. Unpublished manuscript, 26 pp.

5.13.184) Hartnady, C.J.H. (2002), **Earthquake Hazard in Africa: Perspectives on the Nubia-Somalia Boundary**. South African Journal of Science 98, 425-428.

5.13.185) Horner-Johnson, B.C., Gordon, R.G., & Argus, D.F. (2007), **Plate Kinematic Evidence for the Existence of a Distinct Plate Between the Nubian and Somalian Plates Along the Southwest Indian Ridge**. Journal of Geophysical Research 112, B05418.

5.13.186) DeMets, C., Gordon, R.G., & Argus, D.F. (2010), **Geologically Current Plate Motions**. Geophysical Journal International 181, 1-80.

5.13.187) Stamps, D.S., Flesch, L.M., & Calais, E. (2010), **Lithospheric Buoyancy Forces in Africa from a Thin Sheet Approach**. International Journal of Earth Sciences 99(7), 1525-1533.

5.13.188) Morgan, W.J. (1983), **Hotspot Tracks and Early Rifting of the Atlantic**. Tectonophysics 94(1-4), 123-139.

5.13.189) Burke, K. (1996), **The African Plate**. South African Journal of Geology 99(4), 341-409.

5.13.190) Nyblade, A.A. & Robinson, S.W. (1994), **The African Superswell**. Geophysical Research Letters 21, 765-768.

5.13.191) Lithgow-Bertelloni, C. & Silver, P.G. (1998), **Dynamic Topography, Plate Driving Forces and the African Superswell**. Nature 395, 269-272.

5.13.192) Brandt, M.B.C., Grand, S.P., Nyblade, A.A., & Dirks, P.H.G.M. (2011), **Upper Mantle Seismic Structure Beneath Southern Africa: Constraints on the Buoyancy Supporting the African Superswell**. Pure and Applied Geophysics 169(4), 595-614.

5.13.193) Bilham, R., Bendick, R., Larson, K., Mohr, P., Braun, J., Tesfaye, S., & Asfaw, L. (1999), **Secular and Tidal Strain Across the Main Ethiopian Rift**. Geophysical Research Letters 26(18), 2789-2792.

5.13.194) Bird, P., Liu, Z., & Rucker, W.K. (2008), **Stresses That Drive the Plates from Below: Definitions, Computational Path, Model Optimization, and Error**

Analysis. Journal of Geophysical Research 113(B11), doi:10.1029/2007JB005460.

5.13.195) Reinecker, J., Heidbach, O., Tingay, M., Connolly, P., & Muller, B. (2004), **The 2004 Release of the World Stress Map**.

5.13.196) Heidbach, O., Tingay, M., Barth, A., Reinecker, J., Kurfess, D., & Müller, B. (2008), **The World Stress Map Database Release 2008**. <http://dc-app3-14.gfz-potsdam.de>.

5.13.197) Andreoli, M.A.G. (2012), **Implications of Neotectonic Evidence in the Eastern Cape Region**. PowerPoint presentation, at SSHAC Level 3 Workshop 2, January 17.

5.13.198) Calais, E. (2009), **Present-Day Strain Rates in South Africa from the Analysis of a Continuous GPS Network (TRIGNET)**. CGS Report No. 2009-0233, Rev. 0, 21 pp. Pretoria, Council for Geoscience.

5.13.199) Hartnady, C. (2012), **Seismotectonic Model for Southern Africa and Implications of Tectonic Features To Seismic Hazard**. PowerPoint presentation at SSHAC Level 3 Workshop 2, 16 January 2012, Cape Town.

5.13.200) Fairhead, J.D. & Girdler, R.W. (1971), **The Seismicity of Africa**. Geophysical Journal of the Royal Astronomical Society 24, 271-301.

5.13.201) Green, R.W.E. & McGarr, A. (1972), **A Comparison of the Focal Mechanism and Aftershock Distribution of the Ceres, South Africa Earthquake of September 29, 1969**. Bulletin of the Seismological Society of America 62, 869-871.

5.13.202) Maasha, N. & Molnar, P. (1972), **Earthquake Fault Parameters and Tectonics in Africa**. Journal of Geophysical Research 77(29), 5731-5743.

5.13.203) Shudofsky, G.N. (1985), **Source Mechanisms and Focal Depths of East African Earthquakes Using Rayleigh-Wave Inversion and Body-Wave Modelling**. Geophysical Journal International 83, 563-614.

5.13.204) Wagner, G.S. & Langston, C.A. (1988). **East African Earthquake Body Wave Inversion with Implications for Continental Structure and Deformation**. Geophysical Journal International 94(3), 503-518.

5.13.205) Foster, A.N. & Jackson, J.A. (1998), **Source Parameters of Large African Earthquake: Implications for Crustal Rheology and Regional Kinematics**. Geophysical Journal International 134, 422-448.

5.13.206) Krüger, F., Reichmann, S., & Scherbaum, F. (2011). **Moment Tensor Solution for the 29.9.1969 Ceres Earthquake**. Presentation at Thyspunt Nuclear Siting Project Workshop 1, April.

5.13.207) Fairhead, J.D. & Stuart, G.W. (1982), **The Seismicity of the East African Rift System and Comparison with Other Continental Rifts**. In: Pálmason, G.

(ed.), Continental and Oceanic Rifts, 41-61. Washington, D.C., American Geophysical Union.

5.13.208) Jensen, B.L. (1991), **Source Parameters and Seismotectonics of Three Earthquakes in the Stable Continental Interior of Africa**. MSc thesis, Memphis State University.

5.13.209) Dziewonski, A.M., Ekström, G., Woodhouse, J.H., & Zwart, G. (1987). **Centroid-Moment Tensor Solutions for October–December 1986**. Physics of the Earth and Planetary Interiors 48, 5-17.

5.13.210) Dziewonski, A.M., Ekström, G., Woodhouse, J.H. & Zwart, G. (1991), **Centroid-Moment Tensor Solutions for July–September 1990**. Physics of the Earth and Planetary Interiors 67, 211–220.

5.13.211) Fan, G. & Wallace, T. (1995), **Focal Mechanism of a Recent Event in South Africa: A Study Using a Sparse Very Broadband Network**. Seismological Research Letters 66, 13-18.

5.13.212) Bowers, D. (1997), **The October 30, 1994, Seismic Disturbance in South Africa: Earthquake or Large Rock Burst?** Journal of Geophysical Research 102(B5), 9843-9857.

5.13.213) Brandt, M.B.C. & Saunders, I. (2011), **New Regional Moment Tensors in South Africa**. Seismological Research Letters 82(1), 69-80, doi:10.1785/gssrl.82.1.69.

5.13.214) Mangongolo, A. & Strasser, F. (2012), **Focal Depth Estimation: Part 1: Instrumental Data**. PowerPoint presentation at SSHAC Level 3 Working Meeting 2, 27-30 March. Pretoria.

5.13.215) Michael, A.J. (1984), **Determination of Stress from Slip Data: Faults and Folds**. Journal of Geophysical Research 89, 11517-11526.

5.13.216) Zoback, M.L. (1992), **First- and Second-Order Patterns of Stress in the Lithosphere: The World Stress Map Project**. Journal of Geophysical Research 97, 11703-11728.

5.13.217) Hill, R.S. (1988), **Quaternary Faulting in the South-Eastern Cape Province**. South African Journal of Geology 91(3), 399-403.

5.13.218) Partridge, T.C. (1995), **A Review of Existing Data on Neotectonics and Palaeoseismicity to Assist in the Assessment of Seismic Hazard at Possible Nuclear Power Station Sites in South Africa**. Report to the Environmental, Engineering and Marine Science Division, Council for Geoscience, Pretoria, 34 pp. (Confidential).

5.13.219) Clark, D., McPherson, A., & Collins, D.C.N. (2011), **Australia's Seismogenic Neotectonic Record: A Case for Heterogeneous Intraplate Deformation**. Record 2011/11. Geoscience Australia, Canberra.

© Eskom 2026/Rev 0a

5.13.220) de Wit, M. (2007), **The Kalahari Epeirogeny and Climate Change: Differentiating Cause and Effect from Core to Space**. South African Journal of Geology 110, 367-392.

5.13.221) Tinker, J., de Wit, M. & Brown, R. (2008b), **Mesozoic Exhumation of the Southern Cape, South Africa, Quantified Using Apatite Fission-Track Thermochronology**. Tectonophysics 455(1–4), 77-93.

5.13.222) Ollier, C.D. & Marker, M.E. (1985), **The Great Escarpment of Southern Africa**. Zeitschrift für Geomorphologie, Supplementband 54, 37-56.

5.13.223) Summerfield, M.A. (1985), **Plate Tectonics and Landscape Development on the African Continent**. In: Morisawa, M. & Hack, J.T. (eds.), Tectonic Geomorphology: Proceedings of the 15th Annual Binghamton Geomorphology Symposium, September 1984, ch. 2, pp. 27-51. Boston, Allen & Unwin.

5.13.224) Gilchrist, A.R. & Summerfield, M.A. (1991), **Denudation, Isostasy and Landscape Evolution**. Earth Surface Processes and Landforms 16(6), 555-562.

5.13.225) Gilchrist, A.R., Summerfield, M.A., & Cockburn, H.A.P. (1994), **Landscape Dissection, Isostatic Uplift and the Morphologic Development of Orogens**. Geology 22(22), 963-966.

5.13.226) Brown, R.W., Gallagher, K., Gleadow, A.J.W., & Summerfield, M.A. (2000), **Morphotectonic Evolution of the South Atlantic Margins of Africa and South America**. M.A. Summerfield, ed., Geomorphology and Global Tectonics, pp. 255-280. New York, John Wiley.

5.13.227) Gurnis, M., Mitrovica, J.X., Ritsema, J., & van Heijst, H.-J. (2000), **Constraining Mantle Density Structure Using Geological Evidence of Surface Uplift Rates: The Case of the African Superplume**. Geochemistry, Geophysics, Geosystems 1, Paper No. 1999GC000035.

5.13.228) Simmons, N.A., Forte, A.M., & Grand, S.P. (2007), **Thermochemical Structure and Dynamics of the Africa Superplume**. Geophysical Research Letters 34(2), doi:10.1029/2006GL028009.

5.13.229) Dobson, K.J., McDonald, R., Brown, R.W., Gallagher, K., & Stuart, F.M. (2010), **Dating the Emergence of the African Superswell: A Window into Mantle Processes Using Combined (U-Th)/He and AFT Thermochronology**. Geophysical Research Abstracts 12 EGU 2010-5167.

5.13.230) Moucha, R. & Forte, A.M. (2011), **Changes in African Topography Driven by Mantle Convection**. Nature Geoscience 4, 707-712.

5.13.231) Fleming, A., Summerfield, M.A., Stone, J.O., Fifield, L.K., & Cresswell, R.G. (1999), **Denudation Rates for the Southern Drakensberg Escarpment, SE Africa, Derived from in-situ–Produced Cosmogenic (super 36) Cl: Initial Results**. Journal of the Geological Society of London 156, 209-212.

© Eskom 2026/Rev 0a

5.13.232) Cockburn, H.A.P., Seidl, M.A., & Summerfield, M.A. (1999), **Quantifying Denudation Rates on Inselbergs in the Central Namib Desert Using in situ–Produced Cosmogenic ^{10}Be and ^{26}Al**. Geology Boulder 27 (5), 399-402.

5.13.233) Bierman, P.R. & Caffee, M.W. (2001), **Slow Rates of Rock Surface Erosion and Sediment Production Across the Namib Desert and Escarpment, Southern Africa**. American Journal of Science 301(4-5), 326-358.

5.13.234) Brown, R.W., Summerfield, M.A., & Gleadow, A.J.W. (2002), **Denudational History Along a Transect Across the Drakensberg Escarpment of Southern Africa Derived from Apatite Fission Track Thermochronology**. Journal of Geophysical Research 107(B12), 2350, doi:10.1029/2001JB000745, 18 pp.

5.13.235) Dimas, V.-A. & Brown, R.W. (2003), **Evolution of the South African Drakensberg High-Elevation Passive Margin: New Insights from Low-Temperature Thermochronologic Data from Deep Boreholes**. Abstract Series 70 from 17th Victorian Universities Earth Sciences Conference, September 5, Monash University, Melbourne, Australia.

5.13.236) Luft, F.F., Luft, J.L., Jr., Chemale, F., Jr., Lelarge, M.L.M.V., & Avila, J.N. (2005), **Post-Gondwana Break-Up Record Constraints from Apatite Fission Track Thermochronology in NW Namibia**. Radiation Measurements 39(6), 675-679.

5.13.237) Tinker, J., de Wit, M., & Brown, R. (2008a), **Linking Source and Sink: Evaluating the Balance between Onshore Erosion and Offshore Sediment Accumulation Since Gondwana Break-Up, South Africa**. Tectonophysics 455(1–4), 94-103.

5.13.238) Kounov, A., Viola, G., de Wit, M., & Andreoli, M.A.G. (2009), **Denudation Along the Atlantic Passive Margin: New Insights from Apatite Fission-Track Analysis on the Western Coast of South Africa**. Geological Society, London, Special Publications 324(1), 287-306.

5.13.239) King, L.C. (1962), **The Morphology of the Earth: A Study and Synthesis of World Scenery**. Edinburgh, Oliver & Boyd.

5.13.240) Doucouré, C.M. & de Wit, M.J. (2003), **Old Inherited Origin for the Present near Bimodal Topography of Africa**. Journal of African Earth Sciences 36, 371-388.

5.13.241) Scharf, T., Codilean, A.T., de Wit, M.J., & Kubik, P.W. (2011), **Denudation Rates and Geomorphic Evolution of the Cape Fold Belt, Determined Through the Use of in-situ Produced Cosmogenic ^{10}Be**. Poster presentation at Geosynthesis 2011, Integrating the Earth Sciences, 8th Annual Inkaba Workshop, August 28–2 September, Cape Town.

5.13.242) Portenga, E.W. & Bierman, P. (2011), **Understanding Earth's Eroding Surface with ^{10}Be**. GSA Today 21(8), 4-10.

5.13.243) Midzi, V., Hlatiwayo, D.J., Chapola, L.S., Kebede, F., Atakan, K., Lombe, D.K., Turyomurugyendo, G., & Tugume, F.A. (1999), **Seismic Hazard Assessment in Eastern and Southern Africa**. Annali di Geofisica 42(6), 1067-1083.

5.13.244) Albini, P., Musson, R.M.W, Gomez Capera, A.A., Locati, A., Rovida, A., Stucchi, M., & Vigáno, D. (2012), **Tools for Compiling the Global Earthquake History. GEM Project Presentation, Global Earthquake Model**. Available from <http://www.nexus.globalquakemodel.org/global-earthquake-history>.

5.13.245) Ambraseys, N.N. & Adams, R.D. (1991), **Reappraisal of Major African Earthquakes, South of 20°N, 1900–1930**. Natural Hazards 4, 389-419.

5.13.246) Ayele, A. & Kulhánek, O. (2000), **Reassessment of Source Parameters for Three Major Earthquakes in the East African Rift System from Historical Seismograms and Bulletins**. Annali di Geofisica 43(1), 81-94.

5.13.247) Fenton, C.H. & Bommer, J.J. (2006), **The M_w 7 Machaze, Mozambique, Earthquake of 23 February 2006**. Seismological Research Letters 77(4), 426-439.

5.13.248) Albini, P. (2012), **Investigating the Past Seismicity of the Eastern Cape Province, South Africa**. CGS Report No. 2012-0099, Rev. 0. Pretoria, Council for Geoscience.

5.13.249) Green, R.W.E. & Bloch, S. (1971), **The Ceres, South Africa, Earthquake of September 29, 1969: I. Report on Some Aftershocks**. Bulletin of the Seismological Society of America 61(4), 851-859.

5.13.250) Cole, J. & Stettler, R.H. (2012). **A review of the gravity processing procedures and data.** Report No. 2012-1146. Pretoria, Council for Geoscience.

5.13.251) Ledwaba, L., Dingoko, O.W., Cole, P., & Havenga, M. (2009). **Compilation of Survey Specifications for All the Old Regional Airborne Geophysical Surveys Conducted over South Africa**. CGS Report No. 2009-0130, 45 pp. Pretoria, Council for Geoscience.

5.13.252) Beattie, J.C. (1909), **Report of a Magnetic Survey of South Africa**. Royal Society of London Publication, 235 pp. London, Cambridge University Press.

5.13.253) Weckmann, U., Jung, A., Branch, T., & Ritter, O. (2007), **Comparison of Electrical Conductivity Structures and 2D Magnetic Modelling Along Two Profiles Crossing the Beattie Magnetic Anomaly, South Africa**. South African Journal of Geology 110, 449-464.

5.13.254) Quesnel, Y., Weckmann, U., Ritter, O., Stankiewicz, J., Lesur, V., Mandea, M., Langlais, B., Sotin, C., & Galdéano, A. (2009), **Simple Models for the Beattie Magnetic Anomaly in South Africa**. Tectonophysics 478, 111-118.

5.13.255) de Beer, J., Van Zijl, J., & Gough, D. (1982), **The Southern Cape Conductive Belt, South Africa: Its Composition, Origin and Tectonic Significance**. Tectonophysics 83, 205-225.

© Eskom 2026/Rev 0a

5.13.256) Gough, D.I., de Beer, J.H., & Van Zijl, J.S.V. (1973), **A Magnetometer Array Study in Southern Africa**. Geophysical Journal of the Royal Astronomical Society 34, 421-433.

5.13.257) de Beer, J.H. & Gough, D.I. (1980), **Conductive Structures in Southernmost Africa: A Magnetometer Array Study**. Geophysical Journal of the Royal Astronomical Society 63, 479-495.

5.13.258) de Beer, J.H., van Zijl, J.S.V., & Bahnemann, F.K. (1974), **Plate Tectonic Origin for the Cape Fold Belt**. Nature 252, 675-676.

5.13.259) Hales, A.L. & Gough, D.I. (1960), **Isostatic Anomalies and Crustal Structure in the Southern Cape**. Geophysical Journal of the Royal Astronomical Society 3, 225-236.

5.13.260) Smit, P.J., Hales, A.L., & Gough, D.I. (1962), **The Gravity Survey of the Republic of South Africa**. Handbook 3, 486 pp. Pretoria, Geological Survey of South Africa.

5.13.261) de Wit, M. & Hornsfield, B. (2007), **Built on the Shoulders of Alfred Wegener and Alex du Toit to Apply German Precision Technology to the Geological Superlatives of South Africa**. South African Journal of Geology 110(2-3), 165-174.

5.13.262) **Stankiewicz, J.** (2011), **Shallow structure in the Karoo Basin, South Africa, inferred from a near-vertical reflection seismic profile.** South African Journal of Geology 114(3-4), 293-298**.**

5.13.263) Stankiewicz, J., Parsiegla, N., Ryberg, T., Gohl, K., Weckmann U., Trumbull, R., & Weber, M. (2008), **Crustal Structure of the Southern Margin of the African Continent: Results from Geophysical Experiments**. Journal of Geophysical Research 113(B10313), 15 pp.

5.13.264) Lindeque, A., Ryberg, T., Weber, M., & de Wit, M.J. (2006), **Understanding the Beattie Magnetic Anomaly, Karoo Basin and Deep Crustal Tectonics of Southernmost Africa: Near Vertical Seismic Reflection Data of the Inkaba yeAfrica Onshore-Offshore Agulhas-Karoo Geoscience Transect**. American Geophysical Union, EOS Transactions 87, 52.

5.13.265) Lindeque, A., Ryberg, T., Stankiewicz, J., Weber, M., & de Wit, M.J. (2007), **Deep Crustal Seismic Reflection Experiment Across the Southern Karoo Basin, South Africa**. South African Journal of Geology 110, 419-438.

5.13.266) Lindeque, A.S. & de Wit, M.J. (2009), **Revealing the Beattie Magnetic Anomaly and the Anatomy of the Crust of Southernmost Africa: Geophysics and Deep Subsurface Geology Where the Cape Fold Belt and Karoo Basin Meet**. 11th SAGA Biennial Technical Meeting and Exhibition, Swaziland, 16-18 September, 490-499.

5.13.267) Söhnge, A.P.G. & Hälbich, I.W. (1983), **Geodynamics of the Cape Fold Belt**. Special Publication, Geological Society of South Africa, 12, 184 pp. Johannesburg, Geological Society of South Africa.

5.13.268) Newton, A.R., Shone, R.W., & Booth, P.W.K. (2006), **The Cape Fold Belt**. In: Johnson, M.R., Anhaeusser, C.R., & Thomas, R.J. (eds.), The Geology of South Africa, pp. 521-530. Johannesburg, Geological Society of South Africa / Pretoria, Council for Geoscience.

5.13.269) Du Toit, A.L. (1937), **Our Wandering Continents: An Hypothesis of Continental Drifting**. London, Oliver and Boyd, 366 pp.

5.13.270) Malan, J.A., Theron, J.N., and Hill, R.S. (1989), **Lithostratigraphy of the Goudini Formation (Table Mountain Group)**. South African Committee for Stratigraphy (SACS), Lithostratigraphic Series, 2, 5 pp.

5.13.271) Durrheim, R.J. (1987), **Seismic Reflection and Refraction Studies of the Deep Structure of the Agulhas Bank**. Geophysical Journal of the Royal Astronomical Society 89, 395-398.

5.13.272) Ingram, B.A. (1998), **The Coega Fault and Table Mountain Group Rocks, Northwest of Uitenhage**. Unpublished MSc thesis, University of Port Elizabeth, 152 pp.

5.13.273) Le Roux, W.C. (2000), **Geology of the Area Immediately Adjacent to the Coega Fault in the Uitenhage Vicinity, Eastern Cape**. CGS Report No. 2000-0017, 41 pp & 6 map folders. Pretoria, Council for Geoscience.

5.13.274) Goedhart, M.L., Small, G.W., & Hulley, V. (2004), **Groundwater Targeting in the Algoa Bay Region, from Humansdorp to Alexandria, Eastern Cape, South Africa**. CGS Report No. 2004-1061, 261 pp. Pretoria, Council for Geoscience.

5.13.275) Goedhart, M.L. & Hattingh, J. (1997), **The Geology of the Coega River Mouth and Proposed Adjacent Industrial Development Zone**. CGS Report No. 1997-0008, 50 pp. Pretoria, Council for Geoscience.

5.13.276) Paton, D.A. & Underhill, J.R. (2004), **Role of Crustal Anisotropy in Modifying the Structural and Sedimentological Evolution of Extensional Basins: The Gamtoos Basin, South Africa**. Basin Research 16, 339-359.

5.13.277) Du Toit, S.R. (1976), **Mesozoic Geology of the Agulhas Bank, South Africa**. MSc Thesis, University of Cape Town, 182 pp.

5.13.278) Nolte, C.C. (1990), **Structure and Tectonostratigraphy of the Gamtoos Belt Between Tweewaters and Classen Point, Eastern Cape Province, R.S.A**. MSc Thesis, University of Port Elizabeth, 267 pp.

5.13.279) Amante, C. & Eakins, B.W. (2009), **ETOPO1 1 Arc-Minute Global Relief Model: Procedures, Data Sources and Analysis**. NOAA Technical Memorandum NESDIS NGDC-24, 19 pp. March.

© Eskom 2026/Rev 0a

5.13.280) Becker, J.J., Sandwell, D.T., Smith, W.H.F., Braud, J., Binder, B., Depner, J., Fabre, D., & 11 others (2009), **Global Bathymetry and Elevation Data at 30 Arc Seconds Resolution: SRTM30_PLUS**. Marine Geodesy 32(4), 355-371.

5.13.281) Davidson, A. & Smith, S. (2007), **Geophysical Survey Report for Thyspunt Eskom Site Surveys**. South Africa, Fugro Survey Africa (PTY) Ltd. Report No. MZ581za-01-RPT-03-01 (Client Reference: NSIP-NSI-019130#P1-215), prepared for Eskom Holdings Limited, South Africa, 85 pp. plus appendices.

5.13.282) Goedhart, M.L. (2008), **Potential Onshore and Offshore Geological Hazards for the Thyspunt Nuclear Site, Eastern Cape, South Africa: A Review of the Latest Airborne and Marine Geophysical Data and Their Impact on the Existing Geological Model for the Site Vicinity Area**. CGS Report No. 2007-0274, Rev. 1. 85 pp. Pretoria, Council for Geoscience.

5.13.283) Söhnge, A.P.G. (1934), **The Worcester Fault**. Transactions of the Geological Society of South Africa 37, 253-277.

5.13.284) Theron, J.N. (compiler) (1992), **Ladismith Quadrant Geological Map, 1:250 000 Scale**. Compiled from mapping by Wickens, H. de V., Whittingham, J.K., Theron, J.N., Hiller, N., Dunlevy, J.N., Siegfried, H.P., Le Roux, P.M., Grey, P.R, Gresse, P.G., & Toerien, D.K. carried out from 1974 to 1981; Council for Geoscience map 3320.

5.13.285) van Zyl, M. (1997), **Landscape Evolution of the Garden Route Between the Bloukrans River and Mossel Bay**. MSc Thesis, University of Port Elizabeth, 135 pp.

5.13.286) Maud, R.R. (1996), **The Macro-Geomorphology of the Eastern Cape**. In: Lewis, C.A. (ed.), The Geomorphology of the Eastern Cape, South Africa, pp. 1-18. Grahamstown, Grocott & Sherry.

5.13.287) Toerien, D.K. & Roby, D.J. (compilers) (1979), **Oudtshoorn Quadrant Geological Map, 1:250 000 Scale**. Compiled from 1:125 000 sheet Gamkapoort–Prince Albert, 1:148 752 sheet Mossel Bay, and from mapping by Rossouw, P.J., & Blignaut, J.J.G. (1939-40), Haughton, S.H., & Frommurze, H.F. (1930-3), Du Plessis, P.G. (1944-4), Marlow, A.G. (1973-74), Potgieter, C.T. (1946-47), Krynauw, J.R. (1975), and Gresse, P.G. (1974), and revised in part by Toerien, D.K. (1973-77); Council for Geoscience map 3322.

5.13.288) Ben-Avraham, Z. (1995), **Neotectonic Activity Offshore Southeast Africa and Its Implications**. South African Journal of Geology 98(2), 202-207.

5.13.289) Reznikov, M., Ben-Avraham, Z., Hartnady, C., & Niemi, T.M. (2005), **Structure of the Transkei Basin and Natal Valley, Southwest Indian Ocean, from Seismic Reflection and Potential Field Data**.Tectonophysics 397, 127-141

5.13.290) Booth, P.W.K. & Shone, R.W. (1992), **The Pre-Cape – Table Mountain Group Contact West of Port Elizabeth**. South African Journal of Geology 95 (1/2), 34-39.

© Eskom 2026/Rev 0a

5.13.291) Goedhart, M.L. & Booth, P.W.K. (2009), **Early Holocene Extensional Tectonics in the South-Eastern Cape Fold Belt, South Africa**. Paper presented at Ancient Rocks to Modern Techniques, 11th South African Geophysical Association (SAGA) Biennial Technical Meeting and Exhibition, Inkaba yeAfrica Phase II workshop, 16 September, Manzini, Swaziland.

5.13.292) Goedhart, M.L. & de Klerk, M. (2011), **A High-Resolution Multi-Electrode Resistivity Survey to Investigate a Neotectonic Rupture Along the Kango Fault, near Oudtshoorn, Southern Cape Fold Belt, South Africa**. Unpublished report by Kainos South Africa and Cape Geophysics submitted to the Council for Geoscience, Report No. KSA-2011-0003, 26 May.

5.13.293) Goedhart, M.L. (2012), **Palaeoseismic Characteristics of the Kango Fault and Associated Uncertainties, Coega Fault Style & Potential CFB SSZs**. PowerPoint presentation at SSHAC Level 3 Workshop 2, Cape Town, 15-18 January 2012.

5.13.294) Crone, A.J., Machette, M.N., & Bowman, J.R. (1997), **Episodic Nature of Earthquake Activity in Stable Continental Regions Revealed by Palaeoseismicity Studies of Australian and North American Quaternary Faults**. Australian Journal of Earth Sciences 44, 203-214.

5.13.295) Crone, A.J., De Martini, P.M., Machette, M.N., Okumura, K., & Prescott, J.R. (2003), **Paleoseismicity of Two Historically Quiescent Faults in Australia: Implications for Fault Behavior in Stable Continental Regions**. Bulletin of the Seismological Society of America 93(5), 1913-1934.

5.13.296) Martin, A.K. & Flemming, B.W. (1988), **Physiography, Structure and Geological Evolution of the Natal Continental Shelf**. In: Schumann, E.H. (ed.), Coastal Ocean Studies off Natal, South Africa: Lecture Notes on Coastal and Estuarine Studies, chap. 2, pp. 11-46. New York, Springer-Verlag.

5.13.297) Cawthra, H.C., Uken, R., & Oveckhina, M. (2012), **New Insights into the Geological Evolution of the Bluff Ridge and Adjacent Blood Reef, Durban, South Africa**. South African Journal of Geology 115(3), 291-308.

5.13.298) Cawthra, H.C. (2013), **Report on the First 'Ground-Truth' Survey of Mossel Bay, South Africa: Scuba Diving and Sediment Sampling Programme**.CGS Report No. 2013-0171, 23 pp. Cape Town, Council for Geoscience, Marine Geoscience Unit.

5.13.299) Illenberger & Associates (2010), **Environmental Impact Assessment for the Proposed Nuclear Power Station ('Nuclear 1') and Associated Infrastructure: Dune Geomorphology Impact Assessment**. Prepared for Arcus GIBB Pty Ltd on behalf of Eskom Holdings Ltd., October.

5.13.300) McLachlan, A., Illenberger, W.K., Burkinshaw, J.R., & Burns, M.E.R. (1994), **Management Implications of Tampering with Littoral Sand Sources**. Journal of Coastal Research 12 (Special Issue on Coastal Hazards), 51-59.

© Eskom 2026/Rev 0a

5.13.301) La Cock, G.D. & Burkinshaw, J.R. (1996), **Management Implications of Development Resulting in Disruption of a Headland-Bypass Dunefield and Its Associated River, Cape St Francis, South Africa**. Landscape and Urban Planning 34, 373-381.

5.13.302) Illenberger, W. Goedhart, M., & Hattingh, J. (1997), **Eastern Cape Coastal Excursion Guide**. SASQUA 13 Conference – Grahamstown, July.

5.13.303) Illenberger, W., Rust, I, Burkinshaw, J., Vogel, J. & Woodborne, S. (2005), **Luminescence Dating of Coastal Dunes of the Southern-Eastern Cape**. Paper presented at the South African Coast Paleoclimate, Paleoenvironment, Paleoecology, Paleoanthropology Project SACP4 Workshop, 5-6 November, Munro House, Dias Museum, Mossel Bay.

5.13.304) Shone, R.W. & Booth, P.W.K. (2005), **The Cape Basin, South Africa – A Review**. Journal of African Earth Sciences 43, 196-210.

5.13.305) Johnson, M.R., Theron, J.N., & Rust, I.C. (1999). **Table Mountain Group**. In: Johnson, M.R. (ed.). Catalogue of South African Lithostratigraphic Units 6, 6-43–6-45.

5.13.306) Loots, L., Chirenje, E., Claassen, D., & Black, D. (2009), **A Multi-electrode Resistivity Survey near Cape St. Francis and Thyspunt, Eastern Cape with the Intent to Locate the Position of Marine Terraces and Possible Faults Buried Under Cenozoic Cover**. CGS Report No. 2009-0211. Pretoria, Council for Geoscience.

5.13.307) Theron, J.N., Malan, J.A., & Hill, R.S. (1989), **Lithostratigraphy of the Skurweberg Formation (Table Mountain Group)**. South African Committee for Stratigraphy (SACS), Lithostratigraphic Series, 3, 6 pp.

5.13.308) Raubenheimer, E., Hambleton-Jones, B.B., & Toens, P.D. (1988), **Detailed Geology of De Hoek, Thyspunt and Tony's Bay. Volume 2: Geotechnical Maps. Eskom Southern Cape Project. Investigations for the Siting of Nuclear Power Stations**. Progress Report No. 20, GEA 801, NSIP-N002557. Pretoria, Atomic Energy Corporation of South Africa, Ltd., Department of Geotechnology.

5.13.309) Rust, I.C. (1967), **On the Sedimentation of the Table Mountain Group in the Western Cape Province**. D.Sc. Thesis, Stellenbosch University (unpublished).

5.13.310) Hill, R.S. (1991), **Lithostratigraphy of the Baviaanskloof Formation (Table Mountain Group), Including the Kareedouw Sandstone Member**. South African Committee for Stratigraphy, Lithostratigraphic Series No. 12, 6 pp.

5.13.311) Theron, J.N. & Loock, J.C. (1988), **Devonian Deltas of Cape Supergroup, South Africa**. In: McMillan, N.J., Embry, A.F., & Glass, D.J. (eds.), Devonian of the World, Volume 1: Regional Synthesis, Memoir 14, pp. 72-74. Canadian Society of Petroleum Geologists.

© Eskom 2026/Rev 0a

5.13.312) Tankard, A.J. & Barwis, J.H. (1982), **Wave-Dominated Deltaic Sedimentation in the Devonian Bokkeveld Basin of South Africa**. Journal of Sedimentary Petrology 52, 959-974.

5.13.313) Shone, R.W. (1976), **The Sedimentology of the Mesozoic Algoa Basin**. M.Sc. Dissertation, University of Port Elizabeth, 48 pp. (unpublished).

5.13.314) Winter, H. de la R. (1973), **Geology of the Algoa Basin, South Africa**. In: Blant, G. (ed.), Sedimentary Basins of the African Coasts, 2nd Part: South and East Coast, pp. 17-48. Paris, Association of African Geological Surveys.

5.13.315) McLachlan, I.R. & McMillan, I.K. (1976), **Review and Stratigraphic Significance of Southern Cape Mesozoic Palaeontology**. Transactions of the Geological Society of South Africa 79, 197-212.

5.13.316) Rosewarne, P.N. & Lomberg, C.R. (1989), **Groundwater Resource Evaluation at St. Francis**. SRK Consulting, Report No. 171719/3.

5.13.317) Maclear, M. (2002), **St Francis Bay Golf Estate: Groundwater Development, Exploration Phase**. SRK Consulting, Report No. 291491/1.

5.13.318) Maclear, M. (2005), **St. Francis Golf Links: Phase 2, Groundwater Development**. SRK Consulting, Report No. 344065.

5.13.319) Maclear, M. (2006), **St Francis Golf Links Groundwater Supply, Routine Groundwater Quality Monitoring**. SRK Consulting, Port Elizabeth, May 2006.

5.13.320) Dingle, R.V. (1981), **The Campanian and Maastrichtian Ostracoda of South–East Africa**. Annals of the South African Museum 85, 1–181.

5.13.321) Smuts, W.J. (1987), **The Sedimentology of the Alexandria Formation**. M.Sc. Thesis, University of Port Elizabeth (unpublished).

5.13.322) Le Roux, F.G. (1987a), **Lithostratigraphy of the Alexandria Formation**. South African Committee for Stratigraphy Lithostratigraphic Series No. 1. 18 pp.

5.13.323) Le Roux, F.G. (1989a), **The Lithostratigraphy of Cenozoic Deposits Along the South-East Cape Coast as Related to Sea-Level Change**. MSc Thesis, University of Stellenbosch, 247 pp.

5.13.324) Le Roux, F.G. (1987b), **Palaeontological Aspects of Tertiary Marine Deposits near Port Elizabeth**. South African Journal of Science 83, 508.

5.13.325) Maud, R.R. & Botha, G.A. (2000), **Deposits of the South Eastern and Southern Coasts**. In: Partridge, T.C. & Maud, R.R. (eds.). The Cenozoic of Southern Africa. Oxford Monographs on Geology and Geophysics, vol. 40, 19-32.

5.13.326) Le Roux, F.G. (1992), **Lithostratigraphy of the Nanaga Formation (Algoa Group)**. Lithostratigraphic Series No. 15, South African Committee for Stratigraphy, 9 pp.

© Eskom 2026/Rev 0a

5.13.327) Le Roux, F.G. (1991), **Lithostratigraphy of the Salnova Formation (Algoa Group)**. Lithostratigraphic Series No. 11, South African Committee for Stratigraphy, 20 pp.

5.13.328) Glass, J.G.K. & du Plessis, J. (1980), **Geological and Geophysical Investigation of the Area Between Jahleel Island and the Mainland**. CGS Report No. 1980-0211. Rev. 0. 27 pp. Pretoria, Council for Geoscience.

5.13.329) Illenberger, W.K. & Rust, I.C. (1988), **A Sand Budget for the Alexandria Coastal Dunefield, South Africa**. Sedimentology 35(3), 513-521.

5.13.330) Reddering, J.S.V. & Esterhuysen, K. (1983), **Sedimentation in the Kromme Estuary**. Research on Sedimentation in Estuaries (ROSIE) Report No. 6, University of Port Elizabeth, 92 pp.

5.13.331) Reddering, J.S.V. & Esterhuysen, K. (1984a), **Sedimentation in the Kabeljous Estuary**. Research on Sedimentation in Estuaries, Rosie (ROSIE) Report No. 8, University of Port Elizabeth, 42 pp.

5.13.332) Reddering, J.S.V. & Esterhuysen, K. (1984b). **Sedimentation in the Gamtoos Estuary**. Research on Sedimentation in Estuaries (ROSIE) Report No. 7, University of Port Elizabeth, 85 pp.

5.13.333) Esterhuysen, K. (1982), **The Seekoei Estuary: Example of a Disrupted Sedimentary Ecology**. Research on Sedimentation in Estuaries, Rosie Report No 5, University of Port Elizabeth, 54 pp.

5.13.334) Hälbich, I.W. (1992), **The Cape Fold Belt Orogeny: State of the Art 1970s–1980s.** In: de Wit, M.J. & Ransome, I.G.D. (eds.). Inversion Tectonics of the Cape Fold Belt, Karoo and Cretaceous Basins of Southern Africa, pp. 141-158. Rotterdam, Balkema.

5.13.335) Maud, R.R. (2008). **The Macro-geomorphology of the Eastern Cape**. In: Lewis, C.A. (ed.), Geomorphology of the Eastern Cape: South Africa (2nd Ed.), pp. 1-20. Grahamstown, NISC Publishers.

5.13.336) de Beer, C.H. (1992), **Structural Evolution of the Cape Folf Belt Syntaxis and Its Influence on Syntectonic Sedimentation in the SW Karoo Basin**, In: De Wit, M.J. & Ransome, I.G.D. (eds.), Inversion Tectonics of the Cape Fold Belt, Karoo and Cretaceous Basins of Southern Africa, pp. 197-206. Rotterdam, Balkema.

5.13.337) Brunsdon, G. (2006), **A Structural Study of Witteberg Group (Cape Supergroup) in the Cape Fold Belt, Steytlerville District**. M.Sc. Thesis, Eastern Cape, Nelson Mandela Metropolitan University, pp 193. (unpublished)

5.13.338) Norman, N.G., Raubenheimer, E., Muller, A., Andersen, N.J.B., Faurie, J.N. (1987), **Final Report on the Geology of the Area between Cape St. Francis and the Tsitsikamma River Mouth, Eskom Eastern Cape Project – Investigations for the Siting of Nuclear Power Stations**, Progress Report No. 15, Vol 2: Maps Showing Geology, Bedrock Elevation and Overburden

Thickness of De Hoek, Thyspunt, Tony's Bay, Klippepunt, Morgan's Bay and Brakkeduinen Sites. PIN-988(B/R), GEA 730, NSIP-EC-005620#P1–27. Pretoria, Atomic Energy Corporation of South Africa, Ltd., Department of Geotechnology.

5.13.339) Toerien, D.K. (1972), **1:50 000 Geological Field Sheet 3424AB Clarkson** (unpublished). Pretoria, Council for Geoscience.

5.13.340) Toerien, D.K. (1978), **1:50 000 Geological Field Sheet, 3424BA Kruisfontein** (unpublished). Pretoria, Council for Geoscience.

5.13.341) Malan, J.A. & Viljoen, J.H.A. (1990). **Mesozoic and Cenozoic Geology of the Cape South Coast**. Guidebook Geocongress '90. Geological Society of South Africa P03, 81 pp.

5.13.342) Toerien, D.K. & Hill, R.S. (1989), **The Geology of the Port Elizabeth Area: Explanation of Sheet 3324, scale 1:250 000**. 35 pp. Pretoria, Geological Survey of South Africa.

5.13.343) Steward, M. & Smith, H.S. (2007). **Geophysical Survey Report for Thyspunt Inshore Site Survey for Eskom, South Africa, Survey Period: 28 May to 25 June 2007**. Fugro Survey Africa (PTY), Ltd. Report No. MZ639za-01-RPT-03-01, Client Reference NSIP-NSI-010579#P1-113, prepared for Eskom Holdings Limited, South Africa, 51 pp. plus appendices.

5.13.344) Gertenbach, W.P.D. (2008), **A Study of the Vegetation of Portion 78 of the Farm Ongegunde Vryheid No. 746 (Rocky Coast Farm), Cape St. Francis.** Jeffrey's Bay, Gertenbach Ecological Consultation. 36 pp.

5.13.345) Roberts, D.L., Karkanas, P., Jacobs, Z., Marean, C.W., & Roberts, R.G. (2012), **Melting Ice Sheets 400,000 Years Ago Raised Sea Level by 13 m: Past Analogue for Future Trends**. Earth and Planetary Science Letters 357-358, 226-237.

5.13.346) Youngs, R.R., Arabasz, W.J., Anderson, R.E., Ramelli, A.R., Ake, J.P., Slemmons, D.B., McCalpin, J.P., Doser, D.I., Fridrich, C.J., Swan III, F.H., Rogers, A.M., Yount, J.C., Anderson, L.W., Smith, K.D., Bruhn, R.L., Knuepfer, P.L.K., Smith, R.B., dePolo, C.M., O'Leary, D.W., Coppersmith, K.J., Pezzopane, S.K., Schwartz, D.P., Whitney, J.W., Olig, S.S., & Toro, G.R. (2003), **A Methodology for Probabilistic Fault Displacement Hazard Analysis (PFDHA)**. Earthquake Spectra 19(1), 191-219.

5.13.347) International Atomic Energy Agency (2011), **Meteorological and Hydrological Hazards in Site Evaluation for Nuclear Installations**. Safety Standards Series, Specific Safety Guide SSG-17, 172 pp. Vienna.

5.13.348) Okal, E.A., Hartnady, C.J.H., & Hartmann, S. (2007), **Modeling the Tsunami Hazard to African Union States in the Western Indian Ocean from the Mentawai (Indonesia) Source Zone**. Workshop on Natural and Human-Induced Hazards and Disasters in Africa, Kampala (July 21-22), Uganda., 5 pp.

© Eskom 2026/Rev 0a

5.13.349) Van Dorn, W.G. (1984), **Some Tsunami Characteristics Deducible from Tide Records**. Journal of Physical Oceanography 14, 353–363.

5.13.350) Rabinovich, A.B. & Thomson, R. E. (2007), **The 26 December 2004 Sumatra Tsunami: Analysis of Tide Gauge Data from the World Ocean Part 1. Indian Ocean and South Africa**. Pure and Applied Geophysics 164, 261-308.

5.13.351) Okal, E.A. & Hartnady, C.J. (2009), **The South Sandwich Islands Earthquake of 27 June 1929: Seismological Study and Inference on Tsunami Risk for the South Atlantic**. South African Journal of Geology 112, 359-370.

5.13.352) Lynner, C. & Long, M.D. (2013), **Sub-slab Seismic Anisotropy and Mantle Flow Beneath the Caribbean and Scotia Subduction Zones: Effects of Slab Morphology and Kinematics**. Earth and Planetary Science Letters 361, 367-378.

5.13.353) Leonard, L.J., Rogers, G.C., & Mazzotti, S. (2012), **A Preliminary Tsunami Hazard Assessment of the Canadian Coastline**. Geological Survey of Canada, Open File Report 7201, 119 pp.

5.13.354) Byrne, D.E., Sykes, L.R., & Davis, D.M. (1992), **Great Thrust Earthquakes and Aseismic Slip Along the Plate Boundary of the Makran Subduction Zone**. Journal of Geophysical Research 97, 449-478.

5.13.355) Ambraseys, N.N. & Melville, C.P. (1982), **A History of Persian Earthquakes**. London, Cambridge University Press, 219 pp.

5.13.356) Neetu, S., Suresh, I., Shankar, R., Nagarajan, B., Sharma, R., Shenoi, S.S.C., Unnikrishnan, A.S., & Sundar, D. (2011), **Trapped Waves of the 27 November 1945 Makran Tsunami: Observations and Numerical Modeling**. Natural Hazards 59(3), 1609-1618.

5.13.357) Smith, G.L., McNeill, L.C., Wang, K., He, J., & Henstock, T.J. (2013), **Thermal Structure and Megathrust Seismogenic Potential of the Makran Subduction Zone**. Geophysical Research Letters 40(8), 1528-1533.

5.13.358) Deif, A. & El-Hussain, I. (2012), **Seismic Moment Rate and Earthquake Mean Recurrence Interval in the Major Tectonic Boundaries Around Oman**. Journal of Geophysics and Engineering 9, 773, doi:10.1088/1742-2132/9/6/773.

5.13.359) Rehman, S.U., Khalid, M., Ali, A., & Abd El-Aal, A.E.K. (2013), **Deterministic and Probabilistic Seismic Hazard Analysis for Gwadar City, Pakistan**. Arabian Journal of Geosciences 6(9). 3481-3492.

5.13.360) Okal, E.A. & Synolakis, C.E. (2008), **Far-Field Tsunami Hazard from Mega-Thrust Earthquakes in the Indian Ocean**. Geophysical Journal International 172, 995-1015.

5.13.361) Moore, J.G., Clague, D.A., Holcomp, R.T., Lipman, P.W., Normark, W.R., & Torresan, M.E. (1989). **Prodigious Submarine Landslides on the Hawaiian Ridge**. Journal of Geophysical Research 94, 17465-17484.

© Eskom 2026/Rev 0a

5.13.362) Holcomb, R.T. & Searle, R.C. (1991), **Large Landslides from Oceanic Volcanoes**. Marine Geotechnology 10, 19–32.

5.13.363) Lénat, J.-F., Vincent, P., & Bachélery, P. (1989), **The Off-Shore Continuation of an Active Basaltic Volcano: Piton de la Fournaise (Reunion Island, Indian Ocean); Structural and Geomorphological Interpretation from SEABEAM Mapping**. Journal of Volcanology and Geothermal Research 36(1–3), 1-36.

5.13.364) Oehler, J.-F., Lénat, J.-F. & Labazuy, P. (2008), **Growth and Collapse of the Reunion Island Volcanoes**. Bulletin of Volcanology 70, 717-742.

5.13.365) Chevallier, L. (1986), **Tectonics of Marion and Prince Edward Volcanoes (Indian Ocean): Result of Regional Control and Edifice Dynamics**. Tectonophysics 124(1–2), 155-175.

5.13.366) Hartnady, C.J.H. (2005), **Tsunami Potential on East African Coast, Western Indian Ocean Island States**. Disaster Reduction in Africa – ISDR Informs, Issue 5.

5.13.367) Audru, J.-C., Guennoc, P., Thinon, I., & Abellard, O. (2006), **Bathymay: La structure sous-marine de Mayotte révélée par l'imagerie multifaisceaux**. Comptes Rendus Geoscience 338(16), 1240-1249.

5.13.368) Grilli, S. & Watts, P. (2005), **Tsunami Generation by Submarine Mass Failure. I: Modeling, Experimental Validation, and Sensitivity Analyses**. Journal of Waterway, Port, Coastal, and Ocean Engineering 131(6), 283-297.

5.13.369) Wynn, R.B. & Masson, D.G. (2003), **Canary Islands Landslides and Tsunami Generation: Can We Use Turbidite Deposits to Interpret Landslide Processes?** In: Locat, J. & Mienert, J. (eds.), Submarine Mass Movements and their Consequences, Advances in Natural and Technological Hazards Research, v. 19, pp. 325-332. Dordrecht, the Netherlands, Kluwer Academic Publishers.

5.13.370) Locat, J. & Lee, H.J. (2002), **Submarine Landslides: Advances and Challenges**. Canadian Geotechnical Journal, 39, 193-212.

5.13.371) Mader, C. (2001), **Modeling the La Palma Landslide Tsunami**. Science of Tsunami Hazards 19(3), 150-170.

5.13.372) Hartnady, C.J.H. (2011), **Earthquake and Tsunami Impacts on Southern Africa**. ENHANS Workshop presentation, 21 January 2011.

5.13.373) Dingle, R.V. (1977), **The Anatomy of a Large Submarine Slump on a Sheared Continental Margin (SE Africa)**. Journal of the Geological Society of London 134; 293-310.

5.13.374) Ben-Avraham, Z., Reshef, M., & Smith, G. (2005), **Seismic Signature of Gas Hydrate and Mud Volcanoes on the South African Continental Margin**. In: Martinelli, G. & Panahi, P. (eds.), Proceedings of the NATO Advanced

Research Workshop on Mud Volcanism, Geodynamics and Seismicity Baku, Azerbaijan, 20-22 May 2003, pp. 17-27. The Netherlands, Springer.

5.13.375) Boyd, D., Anka, Z., di Primio, R., Kuhlmann, G., & and de Wit, M.J. (2011), **Passive Margin Evolution and Controls on Natural Gas Leakage in the Orange Basin, South Africa**. South African Journal of Geology 114, 415-432.

5.13.376) Dingle, R.V., Birch, G.F., Bremner, J.M., de Decker, R.H., du Plessis, A., Engelbrecht, J.C., Fincham, M.J., Fitton, T., Flemming, B.W., Gentle, R.I., Goodlad, S.W., Martin, A.K., Mills, E.G., Moir, G.J., Parker, R.J., Robson, S.H., Rogers, J., Salmon, D.A., Siesser, W.G., Simpson, E.S.W., Summerhayes, C.P., Westall, C.F., & Winter, A. (1987), **Deep-Sea Sedimentary Environments Around Southern Africa, South-East Atlantic and South-West Indian Oceans**. Annals of the South African Museum 98, 1–27.

5.13.377) ten Brink, U.S., Lee, H.J., Geist, E.L., & Twichell, D. (2009), **Assessment of Tsunami Hazards to the U.S. East Coast Using Relationships Between Submarine Landslides and Earthquakes**. Marine Geology 264, 65-73.

5.13.378) Biscontin, G. & Pestana, J.M. (2006), **Factors affecting Seismic Response of Submarine Slopes**. Natural Hazards and Earth System Sciences, 6, 97–107.

5.13.379) Tappin, D.R. (1987), **Mass Transport Events and Their Tsunami Hazard**. In: Mosher, D.C. et al. (eds.), Submarine Mass Movements and Their Consequences, pp. 667-684. Advances in Natural and Technological Hazards Research, Vol. 28.

5.13.380) Cawthra, H.C.C. (2012), **Depositional and Erosional Processes Occurring on the Continental Shelf and Slope: Implications to Causative Mechanisms and Origins of Seafloor Features**. PowerPoint presentation at SSHAC Level 3 Workshop 2, Stellenbosch, 16 January 2012.

5.13.381) Green, A.N. (2009), **Sediment Dynamics on the Narrow, Canyon-Incised and Current-Swept Shelf of the Northern KwaZulu-Natal Continental Shelf, South Africa**. Geo-Marine Letters 29, 201-219.

5.13.382) Cawthra, H.C., Neumann, F.H., Uken, R., Smith, A.M., Guastella, L., & Yates, A.M. (2012), **Sedimentation on the Narrow (8 km Wide), Oceanic Current-Influenced Continental Shelf off Durban, KwaZulu-Natal, South Africa**. Marine Geology 323-325, 107-122.

5.13.383) Dingle, R.V. & Robson, S. (1985), **Slumps, Canyons and Related Features on the Continental Margin off East London, SE Africa (SW Indian Ocean)**. Marine Geology 67, 37-54.

5.13.384) Niemi, T.M., Ben-Avraham, Z., Harnady, C.J.H. & Reznikov., M. (2000), **Post-Eocene Seismic Stratigraphy of the Deep Ocean Basin Adjacent to the Southeast African Continental Margin: A Record of Geostrophic Bottom Current Systems**. Marine Geology 162, 237-258.

5.13.385) Dingle, R.V. (1980), **Large Allochthonous Sediment Masses and Their Role in the Construction of the Continental Slope and Rise off Southwestern Africa**. Marine Geology 37, 333-354.

5.13.386) Wigley, R.A. & Compton, J.S. (2006), **Late Cenozoic Evolution of the Outer Continental Shelf at the Head of the Cape Canyon, South Africa**. Marine Geology 226, 1-23.

5.13.387) Eskom (2009), **Safety and Quality Classification of SSR Related Deliverables and Processes**. Report NSIP01432, Rev. A0, Draft 1. Johannesburg.

5.13.388) Hattingh, E., Neveling, J., Strasser, F.O., Cichwicz, A., Sebake, D., & Saunders, I. (2011), **Processes, Classification of Tasks and Technical Procedures**. CGS Report No. 2010-0171, Rev. 1. Pretoria, Council for Geoscience.

5.13.389) Flint, N.S., Hattingh, E., & Neveling, J. (2011), **Integrated Management System (IMS) Manual**. CGS Report No. 2010-0168, Rev. 1. Pretoria, Council for Geoscience.

5.13.390) National Nuclear Regulator (2008), **RD-0034, Quality and Safety Management Requirements for Nuclear Installations**. Rev. 0. Pretoria.

5.13.391) Neveling, J. & Hattingh, E. (2010), **Project Execution Plan (PEP) – Geological Investigations**. CGS Report No. 2010-0174, Rev. 0. Pretoria, Council for Geoscience.

5.13.392) Flint, N.S., Hattingh, E., & Neveling, J. (2011), **Project Quality Plan (PQP)**. CGS Report No. 2010-0170, Rev. 2. Pretoria, Council for Geoscience.

5.13.393) Hattingh, E. & Flint, N.S. (2012), **Risk Register Methodology**. CGS Report No. 2012-0009, Rev. 0. Pretoria, Council for Geoscience.

5.13.394) Hattingh, E. & Flint, N.S. (2011), **Compliance Matrix**. CGS Report No. 2010-0175, Rev. 1. Pretoria, Council for Geoscience.

5.13.395) Delport, F., Flint, N.S., Hattingh, E., & Neveling, J. (2011), **Safety Culture Enhancement Program (SCEP)**. CGS Report No. 2010-0192, Rev. 1. Pretoria, Council for Geoscience.

5.13.396) Van der Merwe, J.H.P., Graham, A. & Hattingh, E. (2013), **Nuclear Geo-Hazards Group Core Integrated Management System Manual**. CGS Report No. 2010-0168, Rev. 2. Pretoria, Council for Geoscience.

5.13.397) Van der Merwe, J.H.P., Graham, A., & Hattingh, E. (2013), **Nuclear Geo-Hazards Group Core Integrated Management System Procedures, Work Instructions, Forms and Checklists**. CGS Report No. 2013-0010, Rev. 0. Pretoria, Council for Geoscience

© Eskom 2026/Rev 0a